THE
PHYSICAL REVIEW

A journal of experimental and theoretical physics established by E. L. Nichols in 1893

SECOND SERIES, VOL. 79, No. 6 SEPTEMBER 15, 1950

Wide Angle Sprays Produced by Cosmic Radiation*

R. RONALD RAU AND G. G. HARRIS
Palmer Physical Laboratory, Princeton University, Princeton, New Jersey
(Received June 5, 1950)

New data are presented on the wide angle sprays produced by cosmic radiation which have been reported by Oppenheimer and Ney.

THE occurrence of wide angle sprays of minimum ionization particles produced in $\frac{1}{4}$-in. Pb plates in a cloud chamber sent to balloon altitudes has been reported by Oppenheimer and Ney.[1] The particles from these sprays only rarely penetrate another $\frac{1}{4}$ in. of Pb. We have also observed these events in cloud chambers and confirm the general conclusions of these authors.

In the present experiments a square cloud chamber with a transparent piston was used, allowing illumination of the chamber from the rear. The chamber contained three plates each 1 cm thick with effective dimensions of 10 by 20 cm. During one flight the three plates were Pb and during three others the top plate was Be and the lower two were Pb. A total of 1330 photographs, representing about 230 sec. sensitive time, were obtained above 70,000 ft. Twelve hundred of these were obtained at 90,000 ft. The chamber was expanded at 1-min. intervals inside a pressure-tight temperature-controlled gondola, which in turn was attached to a General Mills plastic balloon. About 3.5 g/cm² of material was immediately above the cloud chamber in addition to 20 g/cm² of atmosphere. These flights were made at 55°N geomagnetic latitude.

Table I is a tabulation of the statistics on the sprays we have observed. Our criteria for the selection of sprays were as follows: (a) at least six particles; (b) angular spread of event $>30°$; (c) event cannot be identified positively as an electromagnetic cascade event or a nuclear disintegration.

It is certainly true that some of the events listed in Table I, especially the smaller events, are electromagnetic in nature or are small nuclear disintegrations since our selection is not sharp enough to discriminate completely against such events. In particular, since the Pb plates are 1 cm thick, most heavily ionizing tracks from nuclear disintegrations will fail to get out of the Pb and we will see only the more penetrating, hence lower ionization particles.

Very few of the minimum ionization spray particles penetrated the 1-cm Pb plates. Approximately 500 of these particles were incident on the next Pb plate in a region of the plate where their penetration could be easily observed. The maximum number which penetrated is 50. This number is high since all tracks below the Pb plate were included which were in the expected penetration region. Some unrelated, yet space coincident, tracks are very likely included.

As Oppenheimer and Ney have pointed out, it is clear from the range of these spray particles in Pb that their mass is less than that of a μ-meson and therefore they are presumably electrons. The larger events contain between 30 and 100 particles, nearly all at minimum ionization, hence for these larger events a total energy of at least a few hundred Mev is involved. It is then rather difficult to associate these events with the ordinary electromagnetic cascade since, on the basis of our present knowledge, one would expect a number of associated energetic gamma-rays sufficient to make an observable cascade below the Pb plate.

It is difficult to determine the nature of the radiation which initiates these events. because of the large background of tracks in the cloud chamber. In Table I we have indicated 42 events initiated by ionizing particles and 88 by non-ionizing particles out of a total of 180 events, the initiating radiation being unknown for the remaining 50 events. It is certain that some of the events are started by non-ionizing radiation, since it does sometimes happen that a spray will be seen below

* Assisted by the joint program of the ONR and AEC.
[1] F. Oppenheimer and E. P. Ney, Phys. Rev. **76**, 1418 (1949).

TABLE I. Wide angle sprays of minimum ionization particles.

Total number of particles in event	6–9	10–14	15–25	>25	Total
Events of given number particles, including lower plate	78	59	34	9	180
Events of given number particles, excluding lower plate	45	35	20	5	100
Events of at least one particle >2×min., including lower plate	13	19	11	5	48
Events in which one or more particles penetrates 1-cm lead plate	11	10	4	4	29
Events initiated by an ionizing particle	19	14	7	2	42
Events initiated by a non-ionizing particle	45	24	15	4	88

Total number of frames = 1330
Total sensitive time = 230±50 sec.

a Pb plate when there are no tracks above the plate in the vicinity of the spray. On the other hand, identification of an ionizing track as the initiating particle is not as conclusive, due to the large number of random tracks in the chamber and the rather large probability that a random track will be nearly space related to the spray. The evidence in Table I found by stereoscopic viewing of the photographs indicates that both ionizing and non-ionizing radiation initiate spray events.

The question as to whether these events are produced in a single interaction or in a series of interactions in the Pb cannot be answered with the present data. It appears that for the smaller events the tracks in general can be traced back to a common origin (within a mm of each other). This origin is usually in the lower part of the Pb plate. For the large events it is not usually possible to localize the origin. One should remember that if these are electrons of a few Mev energy, the multiple scattering in the Pb would make determinations of the origin of the sprays by this geometric method meaningless.

It is possible that the large sprays are a result of a nearly horizontal electromagnetic cascade. However in that case we should observe a number of particles going upward comparable with the number going downward. In fact, only one event has been observed going upward and that was a small event containing six particles. Few events have more than one particle above the Pb plate in which the event originates. In Figs. 1 and 2 there are only two or three particles above the Pb plate which could be interpreted as going upward from the event, and some of these may be due to background. No spray events have been found originating in the Be plate, although 61 nuclear events have been observed in it. This is to be compared with the Pb plates in which the spray frequency is of the order of one-fifth of the nuclear disintegration frequency.

Figure 1 shows one of the two largest sprays which we have observed. The initiating particle is unknown

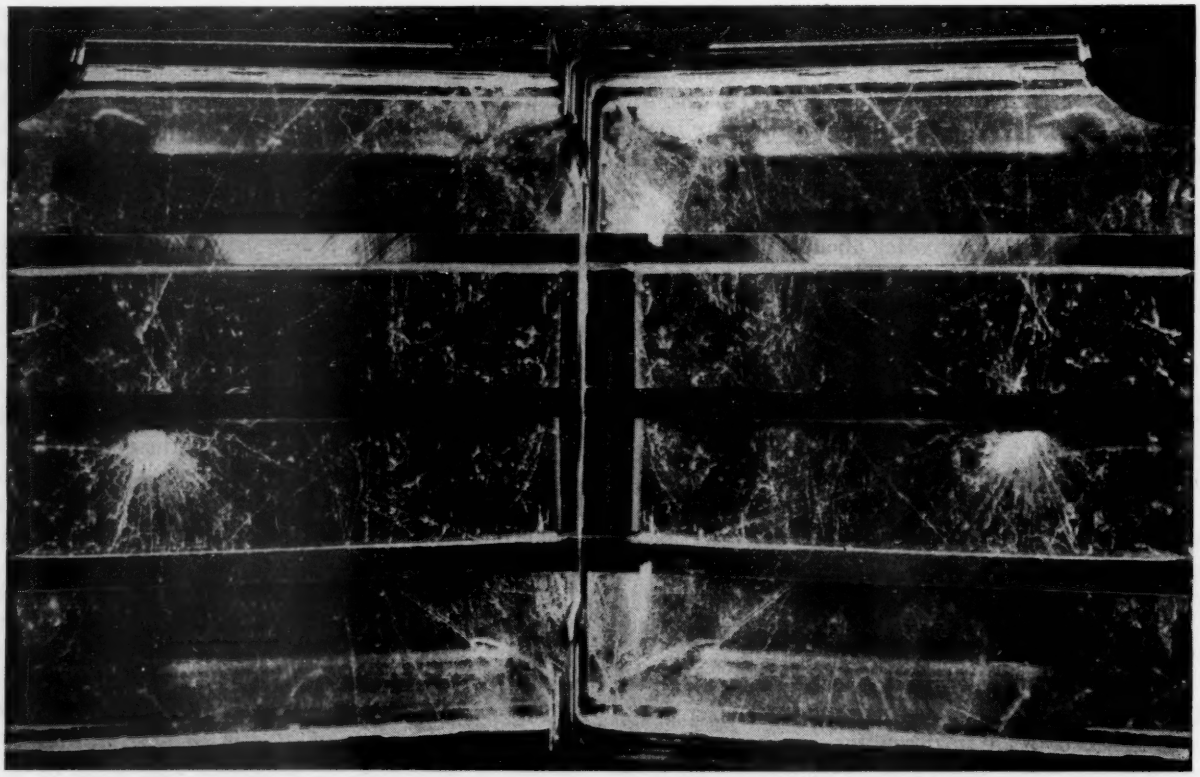

FIG. 1. A spray of minimum ionization particles occurring in the middle plate. The top plate is Be, the lower two are Pb. The left view is a mirror image for stereoscopic viewing. The angular width of the spray is about 130°.

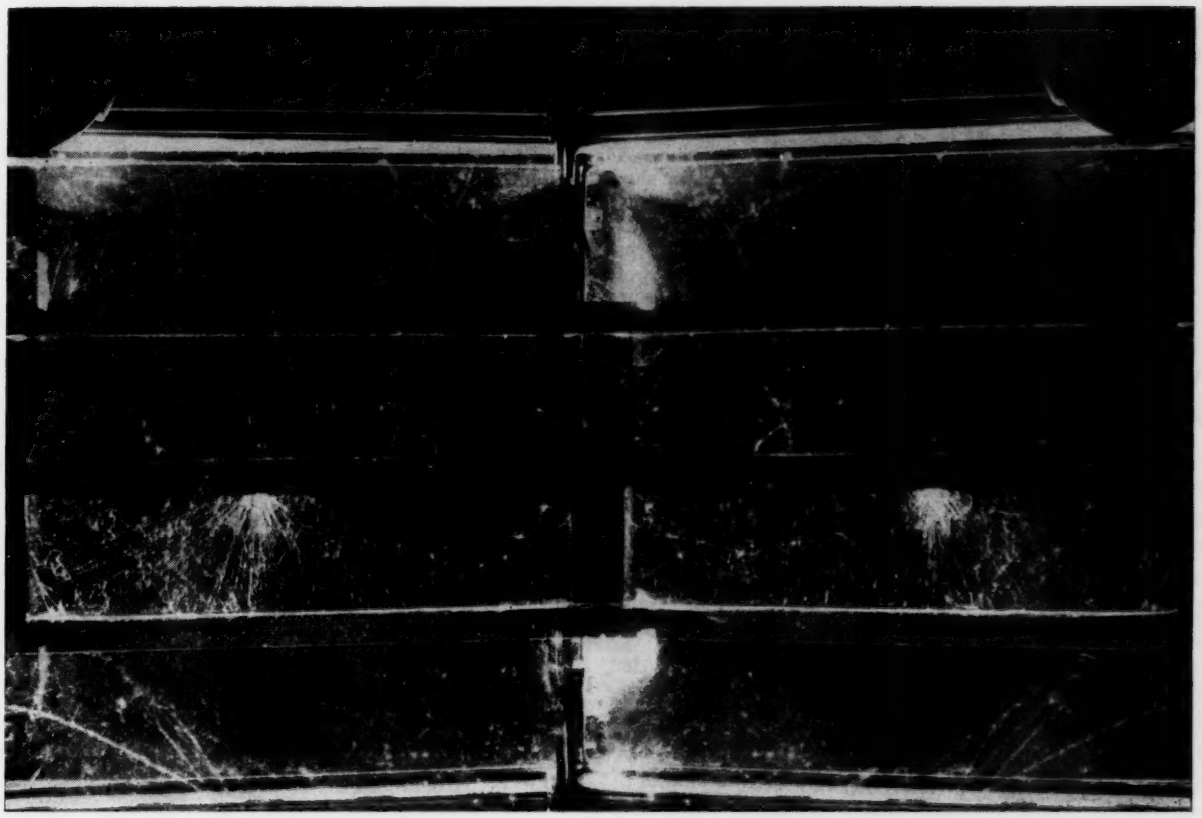

FIG. 2. A spray of minimum ionization particles occurring in the middle plate. The angular width of the spray is about 155°.

We have counted 50 tracks, but the density of tracks does not allow a complete count, and we estimate that there are at least 75 to 100 tracks in the event. At least one track has ionization greater than twice minimum. Thirty tracks are incident on the Pb plate below the origin, and a maximum of three penetrate the Pb plate. Two tracks above the Pb appear space and time related with the spray event.

Figure 2 shows the second large spray event. The initiating particle is again unknown. Sixty tracks have been counted, and it is estimated that the actual number is larger than 75. Forty tracks are incident on the Pb below, and a maximum of three penetrate. There are two tracks above the Pb plate that appear to be associated with the event.

In future flights we plan to use very thin Pb foils in the chamber to investigate the origin and range of the spray particles in greater detail.

On the Use of the Tomonaga Intermediate Coupling Method in Meson Theory*

KENNETH M. WATSON AND EDWARD W. HART
Radiation Laboratory, University of California, Berkeley, California
(Received April 21, 1950)

It is shown that the Tomonaga method for obtaining an intermediate coupling approximation in meson theory can be formulated very simply and will in general give accurate results in the limits of weak and strong coupling. The problem of nuclear forces in the charged scalar theory is studied. The ratio of ordinary to exchange forces is given as a function of the coupling strength. Photo-meson production is studied in the intermediate coupling region for both charged scalar and charged pseudoscalar theories. The method is seriously limited in that nucleon recoil is neglected.

I. INTRODUCTION

TOMONAGA[1] has given an intermediate coupling approximation for meson theory based on an Hartree approximation. In this method of treatment the mesons in the self-field of a nucleon are assumed to be in a finite set of orbital states, reducing the infinite number of degrees of freedom characteristic of field theory to a finite number. Rigorous results are obtained in the two extremes of weak and strong coupling.

The method is seriously limited in that it necessitates the neglect of nucleon recoil effects and requires the introduction of a finite "size" for the nucleons, making the theory non-relativistic. However, there exists no satisfactory theory for including the reactive effects of nucleon motion in a relativistically satisfactory manner: first, because the relativistic wave equation satisfied by free nucleons is not known; second, because the existing relativistically covariant meson theories involve divergent integrals which cannot be made finite even by renormalization of mass and mesonic charge, but must be handled by formal tricks;[2] third, the not-weak couplings between meson and nucleon in relativistic theories must be treated as if weak through the use of perturbation methods, casting considerable doubt on even the qualitative conclusions drawn from these theories. Whereas the Tomonaga method ignores the first two difficulties, it seems to permit at least a qualitative estimate of the effect of couplings which are neither strong nor weak. It may thus be of value in estimating the conditions under which perturbation theory will give untrustworthy results.

In the present paper the Tomonaga treatment will be reformulated in a manner which makes in particularly easy to apply. By way of illustration it will then be applied to the problem of nuclear forces in the charged scalar meson theory and to the problem of photo-meson production for charged scalar and charged pseudoscalar meson theories.

* This work was sponsored by the AEC.

[1] S. Tomonaga, Prog. Theor. Phys. 2, 6 (1947), and Sci. Pap. Inst. Phys. Chem. Research (Tokyo) 39, 247 (1941); T. Miyazima and S. Tomonaga, Sci. Pap. Inst. Phys. Chem. Research (Tokyo) 40, 21 (1942).

[2] J. Steinberger, Phys. Rev. 76, 1180 (1949).

II. FORMULATION OF THE METHOD

We consider the interaction of nucleons with a meson field characterized by a set of field variables $\phi_\lambda(x)$ $(\lambda=1, 2, \cdots n)$. We neglect relativistic effects pertaining to the nucleons, considering them to obey a Schrödinger equation. Associated with the field variables $\phi_\lambda(x)$, will be a set of canonical variables $\pi_\lambda(x)$ with the usual commutation relations

$$i[\pi_\sigma(x'), \phi_\lambda(x)]=\delta_{\lambda\sigma}\delta(\mathbf{x}'-\mathbf{x}), \tag{1}$$

all other combinations commuting.

The Schrödinger equation for the system consisting of N nucleons coupled to the meson field will be of the form[3]

$$[H_0+H_\mu+H']\Omega=i(\partial\Omega/\partial t), \tag{2}$$

where

$$H_0=\sum_{i=1}^{N} p_i^2/2M, \quad H_\mu=H_\mu(\pi, \phi),$$
$$H'=\sum_{i=1}^{N}\sum_{\lambda=1}^{n}\left[gO_\lambda\phi_\lambda(\mathbf{z}_i)+\sum_{k=1}^{3}\frac{g'}{\mu}O_{\lambda k}\frac{\partial}{\partial z_{ik}}\phi_\lambda(\mathbf{z}_i)\right]. \tag{3}$$

Here $\mathbf{p}_i$ is the momentum operator of the i'th nucleon, $\mathbf{z}_i$ is its space coordinate, and M is its mass. H_μ represents the Hamiltonian operator for free mesons, g and g' are coupling constants (of which one can in general be taken to be zero), and O_λ and $O_{\lambda k}$ are matrix operators. Letting μ represent the meson mass, we write

$$\omega^2\equiv\mu^2-\Delta, \tag{4}$$

and introduce the variables

$$U_\lambda(x)=1/\sqrt{2}[\omega^{\frac{1}{2}}\phi_\lambda(x)+i\omega^{-\frac{1}{2}}\pi_\lambda(x)],$$
$$U_\lambda^+(x)=1/\sqrt{2}[\omega^{\frac{1}{2}}\phi_\lambda(x)-i\omega^{-\frac{1}{2}}\pi_\lambda(x)], \tag{5}$$

which satisfy the commutation relations

$$[U_\lambda(x), U_\sigma^+(x')]=\delta_{\lambda\sigma}\delta(\mathbf{x}-\mathbf{x}'),$$
$$[U_\lambda(x), U_\sigma(x')]=[U_\lambda^+(x), U_\sigma^+(x')]=0. \tag{6}$$

In terms of these variables, H_μ and H' will have the form (for vector and pseudovector theories a somewhat

[3] We use units in which $\hbar=c=1$.

modified treatment is necessary)

$$H_\mu=\sum_{\lambda=1}^{n}\int d^3x U_\lambda^+(x)\omega U_\lambda(x), \tag{7}$$

(neglecting the vacuum fluctuation term) and

$$H'=\sum_{i=1}^{N}\sum_{\lambda=1}^{n}2^{-\frac{1}{2}}\omega^{-\frac{1}{2}}(z_i)\Big\{gO_\lambda[U_\lambda(z_i)+U_\lambda^+(z_i)] +\sum_{k=1}^{3}\frac{g'}{\mu}O_{\lambda k}\frac{\partial}{\partial z_{ik}}[U_\lambda(z_i)+U_\lambda^+(z_i)]\Big\}. \tag{8}$$

The field angular momentum in this representation is

$$\mathbf{M}=\sum_{\lambda=1}^{n}\int d^3x U_\lambda^+(x)[\mathbf{x}\times(1/i)\nabla]U_\lambda(x). \tag{9}$$

We now seek a unitary transformation, S, on Eq. (2) which diagonalizes $H_\mu+H'$, i.e.,

$$S_{q\alpha}[H_{\mu\alpha\beta}+H_{\alpha\beta}']S_{\beta q'}^{-1}=\delta_{qq'}\epsilon_q \tag{10}$$

in matrix form. Writing

$$\Omega_\alpha=\sum_{q'}S_{\alpha q'}^{-1}\Omega_{q'}',$$

Eq. (2) becomes

$$[(H_0+\epsilon_q)\delta_{qq'}+(q|S[H_0,S^{-1}]|q')]\Omega_{q'}'=i\partial\Omega_q'/\partial t. \tag{2'}$$

The quantity $S[H_0,S^{-1}]$ represents the effects of nucleon recoil. Even if S were known, this term would make a general solution of Eq. (2') difficult. However, if this term is considered to be small, it can be treated as first order perturbation and Eq. (2') becomes

$$\{H_0+\epsilon_0+S_{0\alpha}[H_0,S_{\alpha 0}^{-1}]\}\Omega_0'=i(\partial\Omega_0'/\partial t), \tag{2''}$$

where we represent the lowest eigenstate of Eq. (10) by $q=0$. For the problems which we are to consider the term $S_{0\alpha}[H_0,S_{\alpha 0}^{-1}]$ gives no contribution and will henceforth be dropped.

From Eq. (6) we see that a Fock[4] representation can be used for U_λ and U_λ^+. For instance, the operator

$$N_\lambda=\int d^3x U_\lambda^+U_\lambda \tag{11}$$

has integral eigenvalues and represents the number of mesons of "type λ" in the field. Let us now expand U_λ, U_λ^+ in a complete set of orthonormal functions, $\psi_\rho(x)$:

$$U_\lambda(x)=\sum_\rho a_{\lambda\rho}\psi_\rho(x),\quad U_\lambda^+(x)=\sum_\rho a_{\lambda\rho}^+\psi_\rho^*(x), \tag{12}$$

where it follows from Eqs. (6) and (11) that $a_{\lambda\rho}$ and $a_{\lambda\rho}^+$ are absorption and emission operators respectively for the state ρ and $n_{\lambda\rho}=a_{\lambda\rho}^+a_{\lambda\rho}$ is the occupation number of this state ρ by mesons of the type λ.

The essence of the Tomonaga method involves the determination of the functions $\psi_\rho(x)$ so that to a first approximation one can keep only a finite number of terms in Eq. (12), thus reducing the number of degrees of freedom to a finite number. Drawing a rough analogy to the case of atomic structure, we may expect that the mesons will show a tendency to be bound in that particular state ψ_{ρ_0} (or set of states if there is degeneracy) for which the energy of the system is a minimum for just one meson, since they obey Bose statistics. In particular, it would seem reasonable on this assumption to find these lowest states from lowest order perturbation theory and assume that the additional mesons appearing from higher order terms will be bound in these same states. We now show that this choice of states satisfies simultaneously the weak and strong coupling hypotheses.

Consider the self-energy of a single nucleon with coordinate $\mathbf{z}$ in the weak coupling case. Using a Fock[4] representation in which the coordinate of the i'th meson of type λ is $\mathbf{x}_i^\lambda$, we can write to lowest order in g, g' the eigenvalue equation

$$(H_\mu+H')\chi=\epsilon\chi, \tag{13}$$

as

$$\omega(x_1^\lambda)C_1(x_1^\lambda)+2^{-\frac{1}{2}}\Big\{gO_\lambda\omega^{-\frac{1}{2}}(x_1^\lambda)\delta(\mathbf{x}_1^\lambda-\mathbf{z}) -\sum_k\frac{g'}{\mu}O_{\lambda k}\omega^{-\frac{1}{2}}(x_1^\lambda)\frac{\partial}{\partial x_{1k}^\lambda}\delta(\mathbf{x}_1^\lambda-\mathbf{z})\Big\}C_0=0 \tag{14}$$

or

$$C_1(x_1^\lambda)=-2^{-\frac{1}{2}}\Big\{gO_\lambda\omega^{-\frac{1}{2}}(x_1^\lambda)\delta(\mathbf{x}_1^\lambda-\mathbf{z}) -\sum_k\frac{g'}{\mu}O_{\lambda k}\omega^{-\frac{1}{2}}(x_1^\lambda)\frac{\partial}{\partial x_{1k}^\lambda}\delta(\mathbf{x}_1^\lambda-\mathbf{z})\Big\}C_0, \tag{15}$$

where χ in Eq. (13) is the matrix $\{C_n\}$ with n representing the occupation number of the mesons in the field. From Eqs. (12) and (15) we see that the ground state eigenfunction $\psi_0(x)$ can be taken as

$$\psi_0(x)=L^{-\frac{1}{2}}\omega^{-\frac{1}{2}}(x)\delta(\mathbf{x}-\mathbf{z}), \tag{16}$$

if there is no gradient coupling. Here L is chosen to normalize ψ_0 to unity. For the term with the gradient coupling, we have from Eq. (15) three such states,

$$\psi_k(x)=-L_1^{-\frac{1}{2}}\omega^{-\frac{1}{2}}(x)(\partial/\partial x_k)\delta(\mathbf{x}-\mathbf{z}), \tag{17}$$

where L_1 is chosen to normalize ψ_k to unity.

Since the expressions for L and L_1 involve divergent integrals, we adopt the cut-off convention of expressing all divergent integrals in momentum space and replacing

$$\int_0^\infty f(k)dk \quad\text{by}\quad \int_0^{1/a}f(k)dk,$$

whenever the first integral diverges. It will be assumed that $a\mu\ll 1$.

According to Eqs. (16) and (17), the Tomonaga ap-

[4] V. Fock, Zeits. f. Physik 75, 622 (1932).

proximation involves rewriting Eq. (12) as

$$U_\lambda(x)=a_{\lambda 0}\psi_0(x)+\sum_{k=1}^{3}a_{\lambda k}\psi_k(x) \tag{18}$$

and the corresponding adjoint equation. Using Eqs. (7), (8), and (18), we write the Tomonaga approximation to Eq. (13) as

$$\sum_\lambda\left\{\frac{I}{L}a_{\lambda 0}{}^+a_{\lambda 0}+\sum_{k=1}^{3}\frac{I_1}{L_1}a_{\lambda k}{}^+a_{\lambda k}+g\frac{I}{(2L)^{\frac{1}{2}}}O_\lambda[a_{\lambda 0}+a_{\lambda 0}{}^+]\right.$$
$$\left.+\frac{g'}{\mu}\frac{I_1}{(2L_1)^{\frac{1}{2}}}\sum_{k=1}^{3}O_{\lambda k}[a_{\lambda k}+a_{\lambda k}{}^+]\right\}\chi=\epsilon\chi, \tag{19}$$

where

$$I=[\sqrt{L}\,\omega^{-\frac{1}{2}}(x)\psi_0(x)]_{x=z},$$
$$I_1=\left[\frac{1}{3}\sqrt{L_1}\sum_{k=1}^{3}\omega^{-\frac{1}{2}}\frac{\partial}{\partial x_k}\psi_k(x)\right]_{x=z}.$$

Defining canonical variables $q_{\lambda\alpha}$ and $p_{\lambda\alpha}$ ($\alpha=0, 1, 2, 3$) by

$$q_{\lambda\alpha}=2^{-\frac{1}{2}}(a_{\lambda\alpha}+a_{\lambda\alpha}{}^+),\quad p_{\lambda\alpha}=-i2^{-\frac{1}{2}}(a_{\lambda\alpha}-a_{\lambda\alpha}{}^+), \tag{20}$$

Eq. (19) becomes

$$\sum_\lambda\left\{\frac{I}{L}\frac{1}{2}(p_\lambda{}^2+q_\lambda{}^2-1)+g\frac{I}{\sqrt{L}}O_\lambda q_\lambda\right.$$
$$\left.+\sum_{k=1}^{3}\left[\frac{I_1}{L_1}\frac{1}{2}(p_{\lambda k}{}^2+q_{\lambda k}{}^2-1)+\frac{g'}{\mu}\frac{I_1}{\sqrt{L_1}}O_{\lambda k}q_{\lambda k}\right]\right\}\chi=\epsilon\chi. \tag{21}$$

To obtain the strong coupling approximation to Eq. (13), we split the field ϕ_λ into coupled and uncoupled parts, as usual:

$$\phi_\lambda(x)=\phi_\lambda{}^0\frac{1}{I}\omega^{-2}(x)\delta(\mathbf{x}-\mathbf{z})$$
$$+\sum_{k=1}^{3}\phi_{\lambda k}{}^0\frac{1}{I_1}\omega^{-2}(x)\frac{\partial}{\partial x_k}\delta(\mathbf{x}-\mathbf{z})+\phi_\lambda{}'(x), \tag{22}$$

where $\phi_\lambda{}'$ is not coupled to the nucleon. The portion of the Hamiltonian involving just $\phi_\lambda{}^0$ and $\phi_{\lambda k}{}^0$ is

$$\sum_\lambda\left\{\frac{1}{I}(\phi_\lambda{}^0)^2+gO_\lambda\phi_\lambda{}^0+\sum_{k=1}^{3}\left[\frac{1}{I_1}(\phi_{\lambda k}{}^0)^2+\frac{g'}{\mu}O_{\lambda k}\phi_{\lambda k}{}^0\right]\right\}. \tag{23}$$

Defining $\phi_\lambda{}^0=(I/\sqrt{L})q_\lambda$ and $\phi_{\lambda k}{}^0=(I_1/\sqrt{L_1})q_{\lambda k}$ in Eq. (23), we see that this then agrees with the part of Eq. (21) that depends on the q's. Whenever the eigenvalue in the strong coupling limit depends only on the q's (and not on the canonical momenta) it is apparent that the Tomonaga method will indeed give correctly both the weak and strong coupling solutions with the choice of wave function given by Eqs. (16) and (17). With two nucleons present, a similar analysis applies.

As in strong coupling theory, we can expect to improve our approximation by including first-order effects from the remainder of the field that was neglected in the approximate Eq. (18).

To specialize Eq. (19) to particular cases, we consider first the charged scalar theory. It is convenient to introduce complex fields ϕ and ϕ^+ with respective canonical variables π and π^+. Fock variables U and V are introduced through the relations

$$\phi=(2\omega)^{-\frac{1}{2}}[U+V^+],\quad \phi^+=(2\omega)^{-\frac{1}{2}}[U^++V],$$
$$\pi=i2^{-\frac{1}{2}}\omega^{\frac{1}{2}}[U^+-V],\quad \pi^+=-i2^{-\frac{1}{2}}\omega^{\frac{1}{2}}[U-V^+]. \tag{24}$$

The total mesonic charge is

$$Q=e\int d^3x\{U^+(x)U(x)-V^+(x)V(x)\}. \tag{25}$$

Comparing this with Eq. (11), we see that U, U^+ are field variables for positive mesons while V, V^+ are those for negative mesons. The interaction term H' of Eq. (3) is now

$$H'=g[\tau_+\phi^+(z)+\tau_-\phi(z)], \tag{26}$$

where τ_+ is the operator in isotopic spin space changing a proton into a neutron and τ_- is its adjoint.

In accordance with Eq. (16) we take

$$U=a\psi_0(x),\quad V=b\psi_0(x) \tag{27}$$

and the corresponding adjoint equations.

The eigenvalue Eq. (19) becomes

$$(I/L)\{a^+a+b^+b+g2^{-\frac{1}{2}}\sqrt{L}[\tau_+(a^++b)$$
$$+\tau_-(a+b^+)]\}\chi=\epsilon\chi. \tag{28}$$

For the pseudoscalar theory with pseudovector coupling we keep the definitions (24) of the field variables U and V. The interaction, H', is now

$$H'=(g/\mu)\boldsymbol{\sigma}\cdot\nabla_z[\tau_+\phi^+(z)+\tau_-\phi(z)]. \tag{29}$$

In accordance with Eq. (17) we take

$$U(x)=\sum_{k=1}^{3}a_k\psi_k(x),\quad V(x)=\sum_{k=1}^{3}b_k\psi_k(x), \tag{30}$$

and the corresponding adjoint equations. Introducing vector notation for the a's and b's and the canonical variables

$$\mathbf{q}=2^{-\frac{1}{2}}(\mathbf{a}+\mathbf{b}^+),\quad \mathbf{p}=i2^{-\frac{1}{2}}(\mathbf{a}^+-\mathbf{b}), \tag{31}$$

we obtain the eigenvalue equation

$$\frac{I_1}{L_1}\{\mathbf{p}^+\cdot\mathbf{p}+\mathbf{q}^+\cdot\mathbf{q}-3$$
$$+(g/\mu)\sqrt{L_1}\,\boldsymbol{\sigma}\cdot[\tau_+\mathbf{q}^++\tau_-\mathbf{q}]\}\chi=\epsilon\chi. \tag{32}$$

The angular momentum [Eq. (9)] and charge [Eq. (25)] operators for the "bound" field have the respective forms:

$$\mathbf{L}=\mathbf{q}\times\mathbf{p}+\mathbf{q}^+\times\mathbf{p}^+,\quad Q=ie[\mathbf{q}^+\cdot\mathbf{p}^+-\mathbf{q}\cdot\mathbf{p}]. \tag{33}$$

III. NUCLEAR FORCES IN THE CHARGED SCALAR THEORY

We shall suppose the dynamical system to contain two nucleons with respective coordinates z_1, and z_2. The eigenvalue problem is of the form of Eq. (13) with

$$H'=g[\tau_+^{(1)}\phi^+(z_1)+\tau_-^{(1)}\phi(z_1)+\tau_+^{(2)}\phi^+(z_2)+\tau_-^{(2)}\phi(z_2)]. \quad (34)$$

Introducing the Fock variables of Eq. (24) and following the analysis leading to Eq. (15), we find that the ground state for the mesons is doubly degenerate with wave functions of the form

$$\chi_1=\omega^{-\frac{1}{2}}(x)\delta(\mathbf{x}-\mathbf{z}_1), \quad \chi_2=\omega^{-\frac{1}{2}}(x)\delta(\mathbf{x}-\mathbf{z}_2),$$

corresponding to mesons bound to either nucleon. From these we construct two orthogonal wave functions.

$$\psi_1=N[\chi_1+b\chi_2], \quad \psi_2=N[b\chi_1+\chi_2], \quad (35)$$

where

$$N^{-2}=L+b^2L+2bJ, \quad b=-J/[L+(L^2-J^2)^{\frac{1}{2}}], \quad (36)$$

$$J=\int \chi_1\chi_2 d^3x=\omega^{-3}(z_1)\delta(\mathbf{z}_1-\mathbf{z}_2). \quad (36)$$

and L is defined in connection with Eq. (16). We note that if P is the permutation operator interchanging the two nucleons, then

$$P\psi_1=\psi_2, \quad P\psi_2=\psi_1. \quad (37)$$

The Tomonaga approximation implies that we write the Fock variables of Eq. (24) as

$$U=\alpha_+\psi_1+\beta_+\psi_2, \quad V=\alpha_-\psi_1+\beta_-\psi_2, \quad (38)$$

and similar equations for the adjoint operators U^+, V^+. Substituting these definitions into H' of Eq. (34) and into H_μ of Eq. (7) gives the Tomonaga approximation to Eq. (13). To write this as a differential equation it is convenient to introduce four pairs of canonical variables, (q_1, p_1), (q_2, p_2), and the corresponding adjoint quantities by the relations

$$\begin{aligned}\alpha_+&=\tfrac{1}{2}[q_1+q_2+i(p_1^++p_2^+)],\\ \alpha_-&=\tfrac{1}{2}[q_1^++q_2^++i(p_1+p_2)],\\ \beta_+&=\tfrac{1}{2}[q_1-q_2+i(p_1^+-p_2^+)],\\ \beta_-&=\tfrac{1}{2}[q_1^+-q_2^++i(p_1-p_2)],\end{aligned} \quad (39)$$

and the corresponding adjoint equations. Denoting the q-variables by a single symbol, q, the eigenfunctions for our approximation to Eq. (13) corresponding to an eigenvalue ϵ_r will be of the form $\chi_r(q)$. Identifying $\chi_r(q)$ with S^{-1} of Eq. (10), we see that the solution, Ω, of Eq. (2) will have the form

$$\Omega=\sum_r \chi_r(q)\Omega_r'[S_1, S_2, z_1, z_2], \quad (40)$$

where S_1 and S_2 are the spin variables of the nucleons. With the assumption of small nucleon recoil effects [use of Eq. (2'')], we can keep only the term in Eq. (40) with $r=0$; i.e.,

$$\Omega=\chi_0(q)\Omega_0'[S_1, S_2, z_1, z_2]. \quad (40')$$

Denoting the triplet and singlet isotopic spin states by Σ_1^μ ($\mu=1, 0, -1$) and Σ_0 respectively, $\chi_0(q)$ will have the structure

$$\chi_0(q)=\Sigma_1^1R_1(q)+\Sigma_1^0R_2(q)+\Sigma_0R_3(q)+\Sigma_1^{-1}R_r(q). \quad (41)$$

We are now able to establish certain symmetry conditions on the R's of Eq. (41), since the permutation operator interchanging the two nucleons must change the sign of Ω by the Pauli principle. Since P commutes with the Hamiltonian in Eq. (2''), we may take Ω_0' to be an eigenfunction of P; i.e.,

$$P\Omega_0'=e\Omega_0'. \quad (42)$$

Here $e=\pm 1$ depending upon whether Ω_0' is symmetric or antisymmetric in the spins and coordinates of the two nucleons. According to Eqs. (37), (38) and (39) the interchange of the two nucleons is equivalent to leaving q_1, q_1^+ unchanged and replacing q_2, q_2^+ by $-q_2$, $-q_2^+$.

Further symmetry relations are

$$P\Sigma_1^\mu=\Sigma_1^\mu, \quad P\Sigma_0=-\Sigma_0.$$

Applying the operator P to Eq. (40') and using Eqs. (41) and (42), we have

$$\begin{aligned}&R_i(q_1, q_1^+, q_2, q_2^+)=-eR_i(q_1, q_1^+, -q_2, -q_2^+), \quad (i=1, 2, 4)\\ &R_3(q_1, q_1^+, q_2, q_2^+)=eR_3(q_1, q_1^+, -q_2, -q_2^+).\end{aligned} \quad (43)$$

Denoting by R the matrix $\{R_1, R_2, R_3, R_4\}$, the eigenvalue problem for determining ϵ_0 is

$$[H+V]R=\epsilon R, \quad (44)$$

where

$$H=\{Y^+[p_1^+p_1+q_1^+q_1-1]+Y^-[p_2^+p_2+q_2^+q_2-1]\}u \quad (45)$$

(u is the unit 4×4 matrix) and

$$V=g\begin{vmatrix} 0 & T^+q_1^+ & -T^-q_2^+ & 0\\ T^+q_1 & 0 & 0 & T^+q_1^+\\ -T^-q_2 & 0 & 0 & T^-q_2^+\\ 0 & T^+q_1 & T^-q_2 & 0\end{vmatrix} \quad (46)$$

with

$$\begin{aligned}&Y^+=(I+K)/(L+J), \quad Y^-=(I-K)/(L-J),\\ &T^+=(I+K)/(L+J)^{\frac{1}{2}}, \quad T^-=(I-K)/(L-J)^{\frac{1}{2}},\\ &K=\omega^{-2}(z_1)\delta(\mathbf{z}_1-\mathbf{z}_2)\\ &\quad=(4\pi)^{-1}\exp[-\mu|\mathbf{z}_1-\mathbf{z}_2|]/(|\mathbf{z}_1-\mathbf{z}_2|).\end{aligned} \quad (47)$$

(I, L and J have their previous definitions.)

Introducing polar coordinates[5] and writing Eq. (44) as a differential equation, the solution can be found easily in the limits of weak and strong coupling. For weak coupling this is the usual perturbation solution

$$\epsilon_0=-g^2[I-P'K] \quad (48)$$

[5] R. Serber and S. Dancoff, Phys. Rev. 63, 143 (1942).

where P' is the operator permuting coordinate and spin variables of the nucleons.

In the strong coupling limit the results of Serber and Dancoff[5] are obtained:

$$\epsilon_0 = -\tfrac{1}{2}g^2[I+K] \tag{49}$$

for $\frac{1}{2}g^2K$ large compared to the separation of isobaric states of the individual nucleons. When $\frac{1}{2}g^2K$ is small compared with the separation of isobaric states,

$$\epsilon_0 = -\tfrac{1}{2}g^2[I-\tfrac{1}{2}P'K]. \tag{50}$$

The solution to Eq. (44) for the neutron-proton system was further studied to obtain an estimate of ϵ_0 in the intermediate coupling range. Equation (44) was solved by perturbation methods to (and including) terms of order g^6. (For any finite order perturbation calculation in the Tomonaga method there is only a finite number of intermediate states, making perturbation theory relatively easy to apply.) The fourth-order ordinary potential was repulsive, while the sixth-order ordinary potential was attractive. For $g^2/4\pi=1$, the leading term was still the lowest order (of order g^2) exchange Yukawa potential. For large $g^2/4\pi$ a variational calculation was made using an expansion in terms of harmonic oscillator functions with a displaced origin. The results of these calculations are given in Fig. 1 as the ratio of ordinary to exchange force as a function of $g/(4\pi)^{\frac{1}{2}}$. The perturbation result was joined to that calculated by the variational method at $g/(4\pi)^{\frac{1}{2}}=1$. The two curves joined quite smoothly at this point. (The cut-off radius, a, was chosen so that $a\mu=\frac{1}{6}$.)

More precisely, the quantity plotted in Fig. 1 is

$$R=\int_0^\infty rV_0(r)dr \Big/ \int_0^\infty rV_e(r)dr, \tag{51}$$

where V_0 is the ordinary and V_e the exchange force.

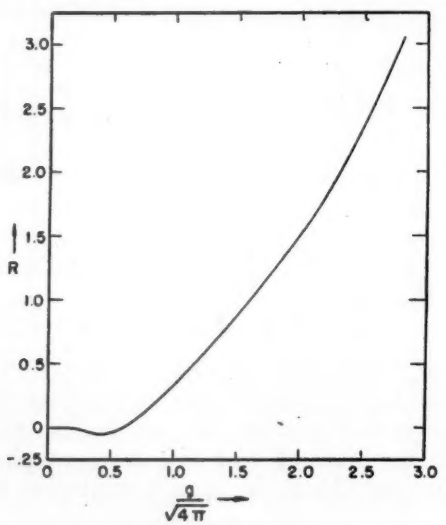

FIG. 1. The ratio, R, of ordinary to exchange force as a function of the coupling constant for the charged scalar theory. The ordinate, R, is defined in Eq. (51).

R changes sign because the ordinary force is repulsive for small g and attractive for large g. The exchange force for all values of g is attractive for states antisymmetric in the nucleon coordinates and repulsive for symmetric states. The ordinary force has a very short range[6] for small values of g, going over into the usual Yukawa potential for large g.

IV. PHOTO-MESON PRODUCTION IN THE CHARGED SCALAR THEORY

The calculation of the self-field of a nucleon in the charged scalar theory permits an immediate calculation of the production of mesons by photons. The calculation is made treating the electromagnetic charge of the meson, e, as being small in magnitude. Then the term in the Hamiltonian for the system which is most important for photo-meson production is

$$H''=-\int d^3x\mathbf{A}\cdot\mathbf{j}, \tag{52}$$

where $\mathbf{A}$ is the vector potential for the electromagnetic field and

$$\mathbf{j}=ie[\phi^+\nabla\phi-\phi\nabla\phi^+]. \tag{53}$$

We must calculate the matrix element of H'' for a transition from the state represented by a nucleon, its self-field and a photon to a state containing the nucleon, its self-field and one free meson with momentum vector $\mathbf{k}$.

The eigenfunction for the self-field of the nucleon is determined by the solution of Eq. (28). To obtain the Tomonaga Hamiltonian for the state containing a free meson, we note that according to Eq. (52) the wave function of the meson produced cannot have any partial waves of zero angular momentum, since the photon cannot be in a zero angular momentum state. This means that we can take the wave function for the outgoing meson to be a plane wave minus the partial wave of zero angular momentum. Because the meson field coupling to the nucleon is scalar, we can conclude that the meson produced by the photon will not be coupled to the nucleon.

The wave function of the meson produced with momentum $\mathbf{k}$ is then

$$\exp(i\mathbf{k}\cdot\mathbf{z})u_k(x)\equiv\mathcal{V}^{-\frac{1}{2}}\exp(i\mathbf{k}\cdot\mathbf{z}) \times\left\{\exp(i\mathbf{k}\cdot(\mathbf{x}-\mathbf{z}))-\frac{\sin k|\mathbf{x}-\mathbf{z}|}{k|\mathbf{x}-\mathbf{z}|}\right\} \tag{54}$$

normalized in a large volume $\mathcal{V}$. The Fock variables U and V of Eq. (27) are modified as

$$U=a\psi_0(x)+a_1u_k(x), \quad V=b\psi_0(x)+b_1u_k(x), \tag{55}$$

(with similar equations for U^+ and V^+) where ψ_0 is given by Eq. (16) and the phase factor $\exp(i\mathbf{k}\cdot\mathbf{z})$ is

[6] K. A. Brueckner and K. M. Watson, Phys. Rev. 78, 495 (1950).

absorbed in the operators a_1 and b_1. Also a_1, b_1 commute with a^+, b^+, etc.

The Schrödinger equation for the system now becomes

$$\{k_0[a_1^+a_1+b_1^+b]+H_T\}\chi'=\epsilon'\chi', \tag{56}$$

where $k_0=(k^2+\mu^2)^{\frac{1}{2}}$ and H_T is the Hamiltonian of Eq. (28). The desired solution to Eq. (56) is of the form

$$\epsilon'=\epsilon+k_0, \quad \chi'=v\chi,$$

where ϵ and χ are the quantities obtained from Eq. (28) and v is the eigenfunction of

$$k_0[a_1^+a_1+b_1^+b_1]v=k_0v. \tag{57}$$

The matrix element for the production of a positive meson from a proton is $(\Omega(2), H''\Omega(1))$, where according to Eqs. (2) and (2″)

$$\Omega(1)=\chi\Omega'(1), \quad \Omega(2)=\chi'\Omega'(2), \tag{58}$$

and $\Omega'(1)$ and $\Omega'(2)$ represent respectively the proton in state "1" and the neutron in state "2". The dependence of this matrix element on the meson field variables is given by

$$(\chi', H''\chi)=\frac{e(2\pi)^{\frac{1}{2}}\mathbf{k}\cdot\hat{e}_p\exp[i(\mathbf{p}-\mathbf{k})\cdot\mathbf{z}]}{p^{\frac{1}{2}}L^{\frac{1}{2}}U^{\frac{1}{2}}k_0^{\frac{1}{2}}[(\mathbf{k}-\mathbf{p})^2+\mu^2]} \times(\chi,[a+b^+]\chi) \tag{59}$$

obtained by using the definitions of U and V of Eq. (55) in the current $\mathbf{j}$ of Eq. (52). In Eq. (59), $\mathbf{p}$ is the momentum of the photon and $\hat{e}_p$ is its polarization vector. The exponential, $\exp[i(\mathbf{p}-\mathbf{k})\cdot\mathbf{z}]$, gives total momentum conservation when combined with the wave functions $\Omega'(1)$ and $\Omega'(2)$ [Eq. (58)] of the nucleons. It should be noted that our formulation of the neglect of nucleon recoil effects for virtual emission and absorption [Eq. (2″)] does not imply such a neglect for real emission and absorption processes.

As the quantity $(\chi,[a+b^+]\chi)$ is independent of the free meson momentum, we see that the angular distribution and energy dependence of the cross section will be independent of the coupling constant, g. (This conclusion is independent of the Tomonaga approximation, depending only on the fact that a meson produced by the photon is not coupled to the nucleon.)

The differential cross section for the production of a meson depends thus on the coupling only through the multiplicative factor

$$|(\chi,[a+b^+]\chi)|^2.$$

It will differ from that of perturbation theory by the deviation of this factor from its perturbation limit. As the perturbation cross section has been given by several authors,[7] we give only the ratio of the differential (and total) cross section to its perturbation limit in Fig. 2 as a function of the coupling constant (the cut-off was was chosen as $a\mu=\frac{1}{6}$). For the determination of the

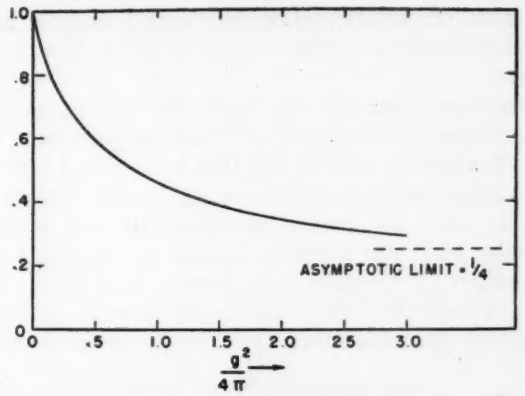

FIG. 2. The ratio of the photo-meson production cross section in the charged scalar theory to its value obtained from lowest order perturbation theory given as a function of the coupling constant. The dotted line gives the asymptotic limit of this ratio for large $g^2/4\pi$.

wave function χ, a variational method (shown to give good results by Tomonaga[1]) was used in which the trial wave functions were

$$\chi_n=\exp(-\tfrac{1}{2}D^2)\cdot(n!)^{-\frac{1}{2}}D^n \tag{60}$$

in a representation in which n represents the number of virtual mesons in the field and D is the variational parameter.

V. PHOTO-MESON PRODUCTION IN THE CHARGED PSEUDOSCALAR THEORY

The self-field of the nucleon is determined by the solution of Eq. (32). In the strong coupling limit Eq. (32) can be handled by the methods of Pauli and Dancoff.[8] We obtain then the result of these authors,

$$\epsilon_0=-(1/4\pi a^3)(g^2/4\pi\mu^2), \tag{61}$$

where a is the cut-off radius and $a\mu\ll1$.

To calculate photo-meson production, we must now evaluate the matrix element of H'' [Eq. (52)] for the transition from a state consisting of a photon and a proton to a state with a neutron and a meson. For pseudoscalar theory the meson current occurring in Eq. (52) is

$$\mathbf{j}(x)=ie[\phi^+(x)\nabla\phi(x)-\phi(x)\nabla\phi^+(x)] -(ieg/\mu)[\phi(x)\tau_--\phi^+(x)\tau_+]\delta(\mathbf{x}-\mathbf{z})\boldsymbol{\sigma}, \tag{62}$$

where $\mathbf{z}$ is again the nucleon coordinate.

In Fig. 3 is plotted the differential cross section for the production process in both the strong and weak coupling limits. The angular distribution is the same in both limits, the cross section in the strong coupling limit being just $\frac{1}{6}$ that for weak coupling. The flatness of the angular distribution has been noted by Bruckner.[7] This is due primarily to the fact that for energies not too far above threshold the second term in Eq. (62) (which is linear in the meson-field variables) is responsible for the greater part of the cross section. Indeed,

[7] K. A. Brueckner, Phys. Rev. 79, 641 (1950).

[8] W. Pauli and S. Dancoff, Phys. Rev. 62, 85 (1942).

this term causes interaction only with mesons of zero angular momentum with respect to the nucleon coordinate.

The above discussion indicates that we can calulate photo-meson production to a good approximation by including just the term in $\mathbf{j}(x)$ that is linear in ϕ and ϕ^+. This approximation makes the calculation especially simple, since the mesons produced will not interact directly with the nucleon through H' of Eq. (29). [Equation (29) couples only mesons in p-states; the linear term in Eq. (62) couples only those in s-states.]

Taking the wave function of the photo-meson to be

$$u(x)=n\sin k|\mathbf{x}-\mathbf{z}|/k|\mathbf{x}-\mathbf{z}|, \tag{63}$$

where $\mathbf{k}$ is its momentum and n normalizes u in a large volume $\mathcal{V}$, we can write the Tomonaga approximation to U and V [Eq. (30)] as

$$U(x)=\sum_{k=1}^{3} a_k\psi_k(x)+au(x),$$
$$V(x)=\sum_{k=1}^{3} b_k\psi_k(x)+bu(x), \tag{64}$$

(and similarly for U^+ and V^+).

As with the scalar theory, the Tomonaga eigenvalue problem is separable into Eq. (32) and

$$k_0[a^+a+b^+b]v=k_0'v \tag{65}$$

with wave function $\chi'=v\chi$ and eigenvalue $\epsilon'=\epsilon+k_0'$. Using Eq. (64) in Eq. (62), we obtain for the matrix element of the transition from a state consisting of proton and a photon to one consisting of a neutron and a meson:

$$(2|H''|\rho)=-ie(gn/\sqrt{2}\mu k_0^{\frac{1}{2}})(v_1, a^+v_0)\times(\chi_N, \boldsymbol{\sigma}\tau_+\chi_P)\cdot\mathbf{A}', \tag{66}$$

where v_0 and v_1 are the solutions of Eq. (65) for states represented by no free meson and one free meson, respectively; χ_P and χ_N are solutions of Eq. (32) for the self-field of a proton and neutrons, respectively; and A' is the matrix element of the electromagnetic potential for the absorption of the initial photon.

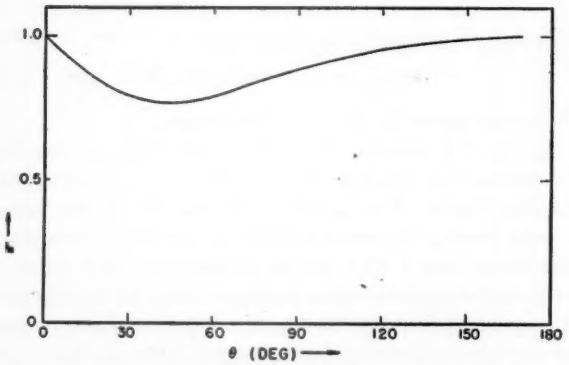

FIG. 3. The angular dependence for both strong and weak coupling cross section, σ, for the charged pseudoscalar theory with pseudovector coupling, plotted in arbitrary units in the barycentric system. Photon energy in the laboratory system is 260 Mev.

To obtain information concerning Eq. (66) in the intermediate coupling region, $(2|H''|1)$ was evaluated by perturbation methods to the seventh power of g. This gave the cross section to terms including g.[8] The result for an unpolarized photon incident on a proton of random spin orientation is given in Fig. 4. The quantity plotted is the ratio of the cross section to its value obtained by using only the lowest order perturbation formula. For $g^2/4\pi>0.2$ the power series in g apparently becomes invalid (the cross section seeming to fall off too rapidly). The asymptotic value for large g (obtained from the strong coupling solution) for the ratio is $\frac{1}{6}$. The rapid approach to the strong coupling limit is due to the strong singularities introduced by the gradient coupling in H' [Eq. (29)]. It is interesting that carrying perturbation theory to a high enough order seemed to bridge the gap between the weak and strong coupling limits (a similar expansion in powers of the coupling constant for photo-meson production in the charged scalar theory gave good agreement with the variational calculation used in obtaining the results shown in Fig. 2).

VI. CONCLUSIONS

The discussion of the validity of the Tomonaga approximation is considerably hampered by the nonexistence of a satisfactory theory to which it can be considered as an approximation. While the neglect of nucleon recoil effects is almost certainly not valid at high energies, it is not known whether there exists a range of energies for which such effects can be considered as small.

Granting the form of meson field theory in which the motion of the nucleon is nelgected, there still remains the question of the validity of the Tomonaga approximation to this theory. We have seen that the approximate method gives exact results in both the weak coupling and strong coupling limits. Extending the calculation to higher order terms will give some indication of the error incurred in the Tomonaga method. Assuming the cut-off, a, is such that $a\mu\ll1$, the fourth-order nucleon self-energy turns out to be:

Scalar Theory

$$W^{(4)}=g^4(1/2\pi)^4(1/a)\ln(1/(a\mu)^{\frac{1}{2}})$$ (Tomonaga approximation)
$$W^4=g^4(1/2\pi)^4(1/a)\ln 4$$ (rigorous)

Pseudoscalar Theory

$$W^{(4)}=(g^4/48)(1/2\pi)^4(1/a)(1/a\mu)^4$$ (Tomonaga approximation)
$$W^4=0.92(g^4/48)(1/2\pi)^4(1/a)(1/a\mu)^4$$ (rigorous).

(The factor, 0.92, comes from the evaluation of numerical factors.) The energy of separation of isobaric nucleon states is:

Scalar Theory

$$\Delta W=[2\pi^2\mu/a\mu[\ln a\mu]^2][(m^2-\tfrac{1}{4})/g^2] \quad \text{(Tomonaga approximation)}$$

$$\Delta W=8\pi\mu(m^2-\tfrac{1}{4})/g^2 \quad \text{(rigorous)}^5$$

Pseudoscalar Theory

$$\Delta W=(4\pi^2\mu^2a/g^2)[2j(j+1)-m^2-5/4] \quad \text{(Tomonaga approximation)}$$

$$\Delta W=(3\pi^2\mu^2a/g^2)[2j(j+1)-m^2-5/4] \quad \text{(rigorous)}^8$$

where m is the isobaric quantum number and j is that for the total angular momentum. In each case the Tomonaga method is incorrect by a numerical factor. The fourth-order nuclear forces in the charged scalar theory had the correct sign and very nearly the correct shape as given by the Tomonaga method, but again were multiplied by incorrect numerical factors. (It should be emphasized that by carrying the Tomonaga approximation one step farther, one could expect to obtain agreement in the above examples. One might, for instance, introduce variation parameters into the trial wave function as did Tomonaga;[1] or one might introduce formally the remainder of the meson field that is neglected in the first approximation, as is done in strong coupling theory. Also the introduction of additional trial wave functions seems capable of giving improved results. However, the equations obtained by the lowest order approximation in the Tomonaga method are sufficiently complicated that it is desirable to carry the approximation no further, when permissible.)

The source of the error in the Tomonaga method can be easily seen when higher order perturbation calculations by this method are compared with those of the rigorous theory. The same virtual emission and absorption processes occur, but the integrals occuring in the rigorous theory as replaced in the Tomonaga approximation by "average" values of the integrands, which are obtained from the corresponding lowest order perturbation values.

We can then conclude that exact numerical accuracy will certainly not be obtained by the Tomonaga approximation. However, it seems quite probable that satisfactory qualitative conclusions may often be drawn from results obtained by this method.

The rapidity with which one leaves the region of weak coupling with increasing g is indicated in Figs. 1, 2, and 4. It is highly doubtful whether the strong dependence on cut-off characteristic of the pseudoscalar theory is real. Thus one would hesitate to determine a numerical value for the coupling constant in this theory. The persisting flatness of the angular distribution for photo-meson production as the coupling increases may be significant, however, since this is in agreement with the experiments of Steinberger and Bishop.[9]

Since only the logarithm of the cut-off is important in determining the strength of the coupling in the scalar theory, somewhat more reasonable conclusions may

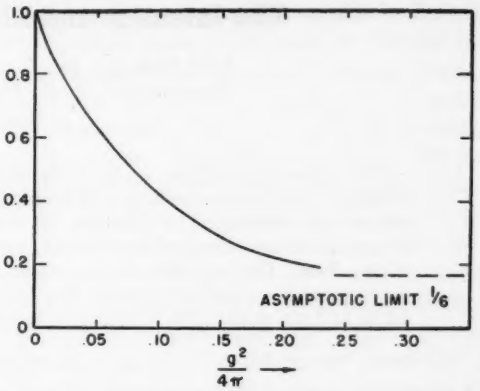

FIG. 4. The ratio of the photo-meson production cross section in the charged pseudoscalar theory to its value obtained from lowest order perturbation theory. The dotted line gives the asymptotic value for large $g^2/4\pi$.

here be drawn about coupling strength. Referring to Fig. 1, the strength of coupling to give about equal exchange and ordinary forces (as observed[10]) is $g^2/4\pi\sim 2$ which is well within the intermediate coupling region. From Fig. 2 and from Brueckner's[7] total cross section in the perturbation limit, we can fit the total cross section for photo-meson production[9] in the scalar theory with $g^2/4\pi\sim 2.5$. There is, of course, little reason to take the scalar meson theory seriously; however, the fact that one finds couplings from it that are neither weak nor strong may be meaningful.

Strong evidence against the scalar theory is the incorrect angular distribution of photo-meson (which is independent of the coupling constant) and the fact that the exchange force for the neutron-proton system has the wrong sign for all values of the coupling constant —according to the Tomonaga approximation. The evidence from photo-meson production seems to be particularly valid (in view of the results of Brueckner[7]) that nucleon recoil effects are unimportant for the lowest order perturbation calculation and first-order radiative corrections in scalar theory, and since for this theory it seems that these perturbation calculations may have some qualitative validity.

As a final conclusion, we may venture to suggest that there seems to be little justification for treating meson-nucleon couplings as weak, and that the problem of understanding intermediate couplings may be as significant and as important as the understanding of the nature of relativistic effects and divergences in meson theory.

The authors would like to express their appreciation to Professor R. Serber for his discussion of many points concerning the present problem and in particular those concerning strong coupling theory. Thanks are due Mr. K. A. Brueckner for discussions of his calculations concerning photo-meson production and to Dr. J. Steinberger for showing us his paper in advance of publication.

[9] J. Steinberger and A. S. Bishop, Phys. Rev. 78, 493, 494 (1950).

[10] R. S. Christian and E. W. Hart, Phys. Rev. 77, 441 (1950).

The Intensity and Masses of Cosmic-Ray Particles*

T. C. MERKLE, JR., E. L. GOLDWASSER, AND ROBERT B. BRODE
Department of Physics, University of California, Berkeley, California

(Received June 12, 1950)

Measurements have been made of the relative numbers of mesons and protons in the sea level cosmic radiation. The measurements include those particles that have ranges in lead between 4.0 and 13.0 cm. The masses were determined by observing the range and momentum of each particle. No evidence was found for any particles except positive protons (mass $=1893\pm50\ m_e$) and positive and negative μ-mesons (mass $=196\pm3\ m_e$). The low value of the μ-meson mass reported here may be due in part to the uncertainty of the range-energy relations in copper. As many protons as μ-mesons were observed in the range interval from 4.0 to 13.0 cm of lead. The intensity of protons decreased with increasing range.

I. INTRODUCTION

THE penetrating component of the cosmic radiation is usually interpreted as that part of the radiation which would remain when the electrons and gamma-rays have been removed. Experimentally, the penetrating and non-penetrating radiations are often separated by the assumption that 10 to 15 cm of lead will remove the electrons and gamma-rays. The use of such an absorber removes those protons and mesons which have ranges in lead less than the thickness of the absorber.

From cloud-chamber observations of the curvature of a particle's track in a magnetic field and the subsequent range of the same particle in a chamber filled with absorbing plates, it is possible to identify the penetrating character of the particle and to determine its mass. The frequency of occurrence of mesons and protons has in this way been observed for the cosmic radiation at sea level for particles with ranges between 4 and 13 cm of lead. Because the effective time of operation of the apparatus was not accurately known, an absolute flux could not be determined. The total number of penetrating particles with ranges in excess of 13 cm was, however, observed for the same time interval so that the relative number of slow mesons and protons to the penetrating radiation is known.

Previous experiments[1,2] in this laboratory have determined the masses of particles capable of penetrating 25 to 45 cm of lead. With a lead absorber of 45 cm thickness above the mass measuring equipment, an increase in the rate of collection of data was obtained. The differential range spectrum of sea level cosmic-ray mesons is known to have a maximum at about 38 cm of lead.[3] The presence of the lead above the mass measuring equipment in previous experiments eliminates the slow mesons and protons as well as any other particles with ranges less than the absorber thickness. In the present experiment, the lead absorber above the equipment has been removed so that the character of the low energy sea level radiation could be observed.

The possibility of observing particles with masses different from the more abundant mesons and protons depends on the intensity of these particles and on the resolving power of the mass spectrograph. An improvement of the resolving power over that previously used is essential in settling the question of the existence of any appreciable intensity of mesons with masses between those of the π-meson and proton. The improvements made on the apparatus in these measurements have increased the resolving power by about a factor of two.

The masses of the particles were calculated from observation of the deflection of the particles' trajectory in a magnetic field of 4700 gauss and the observation of the range of the particles in lead and copper plates. The absolute value of the magnetic field was determined to about 0.5 percent by calibrations based on the proton magnetic resonance.

II. EXPERIMENTAL PROCEDURE

The magnetic field was uniform within a few percent over the 12-inch diameter of the cloud chamber and corrections were made for the deviation from the central field. The error due to magnification and to non-uniformity of the field in the direction normal to the illuminated plane of the cloud chamber contribute together about ±1.6 percent probable error in the value of $B\rho$. Errors which might have been introduced into the curvature measurements by shrinkage or distortion of the photographic film were checked by means of straight lines etched on the inside surface of the front glass of the cloud chamber. Track distortions due to turbulence in the cloud chamber were observed by operating the equipment for several periods during each day of observation with the magnetic field off. The cloud chamber was thermally insulated from the magnet and its temperature was closely controlled by a water circulating system regulated to ±0.05°C.

A total of 315 no-field tracks indicated a turbulent curvature of $+0.0118\ M^{-1}\pm0.02\ M^{-1}$. Corrections to curvature measurements were made for the systematic portion of this distortion. The improvement in the no-field tracks in this series of observations was due to the careful temperature control and to the re-design of the cloud chamber. The expansion valves were equipped

* Assisted by the joint program of the ONR and the AEC.
[1] W. B. Fretter, Phys. Rev. 70, 695 (1946).
[2] J. G. Retallack and R. B. Brode, Phys. Rev. 75, 1716 (1949).
[3] L. S. Germain (to be published).

with pads calculated to restrict the flow velocity of the gas behind the rubber diaphragm, and thus prevent shock wave disturbance in the chamber. Each valve had an aperture of seven square inches so that although the velocity was slow, the expansion time was not long.

The ranges were observed in a second cloud chamber placed below the curvature cloud chamber. Eleven copper plates and three lead plates were used. These plates were graduated in thickness in such a way that the probable error in range was about 3.5 percent for any particle stopping in the chamber. Pictures were taken with a stereo-camera so that estimates of the track location and direction of travel could be made.

The chambers were expanded by signal from a three-tube Geiger counter telescope arranged with one tube above the curvature chamber and two tubes between the curvature and range chambers. The Geiger counter tubes were one inch in diameter and eight inches long.

The curvature and range measurements were reduced to masses by means of a chart relating these quantities, prepared by Wheeler and Ladenburg.[4] Conversion of the copper range to the equivalent lead range was calculated from range-energy relations tabulated by Aron, Williams, and Hoffman.[5]

III. RESULTS

During 1169 hours of operation, 8545 events were photographed. Each event was recorded in a set of three photographs, one of the upper chamber and two of the lower. A total of 1155 events were photographed with the magnetic field off. Single penetrating particles with ranges in excess of 13 cm of lead accounted for 5993 events. Soft particles and showers appeared in 681 pictures. There were 101 particles observed whose ranges were greater than 4 cm and less than 13 cm of lead. The masses of of these particles have been calculated and a histogram showing the distribution of masses in equal curvature intervals is shown in Fig. 1. This histogram indicates two well-defined groups of masses. In order to make an estimate of the average mass of each group, it is necessary to assign proper weights to each measurement. The masses as calculated are not the quantities which are subject to symmetrical random variation. Using range and curvature in unit magnetic field as variables, a family of curves can be drawn relating mass, range and curvature. The best mass value will be determined by that curve of constant mass that best fits the observed values of range and curvature.[6]

If an analytical expression is known for the relation between mass, range, and curvature, the graphical solution is not necessary. The values of the individual mass measurements, m_i, from each pair of range, R_i, and curvature, c_i, observations are calculated by the Wheeler-Ladenburg chart. The weight to be attached to each of these mass values can be derived from an approximate analytical function relating range, mass, and curvature. For mesons stopping in the apparatus, the relation $m=\text{const}/c^2R$ gives a good fit to the relation between the mass, curvature, and range. For protons, a suitable function is $M=\text{const}/c^3R$. A constant can be chosen for each of these equations so that the analytic expression for the mass does not differ from the value given by the Wheeler-Ladenburg charts by more than 2 percent of the mass values for particles with ranges between 4 and 13 cm of lead.

Errors in range are limited in the sense that deviations greater than one-half a plate thickness are not probable. Since the mass values vary inversely as the range, the probable error of 3.5 percent in range will introduce an error in mass of the same magnitude. The probable errors in the measurement of curvature and magnetic field are of the order of 9 percent. Because the error in range is limited in magnitude and is small in comparison to the errors in curvature, the range error has been neglected in assigning weights to the mass observations.

Since the curvature decreases as range increases, the fractional error in mass due to a constant uncertainty in curvature increases with increasing range. Minimizing the squares of the residuals in curvature in unit magnetic field, one obtains as the resulting mean mass value ($\bar{m}$) from a series of individual mass and range measurements:

$$(\bar{m})^{-1}=\frac{\Sigma_i m_i^{-1}R_i^{-1}}{\Sigma R_i^{-1}}.$$

For the proton group, the expression becomes:

$$(\bar{M})^{-1}=(\Sigma_i M_i^{-1}R_i^{-1})/\Sigma_i R_i^{-1}.$$

The 23 positive mesons and 25 negative mesons give a value $\bar{m}=196\pm3\ m_e$. The 52 protons give a value of $\bar{M}=1893\pm50\ m_e$.

During the first-half of the experiment some data were obtained which seemed to indicate the existence of particles of a mass of about 1000 m_e.

These observations now appear to be only large deviations of curvature for particles whose true mass is that of the proton. The resolving power of the apparatus is not adequate to separate a small number of 1000 m_e

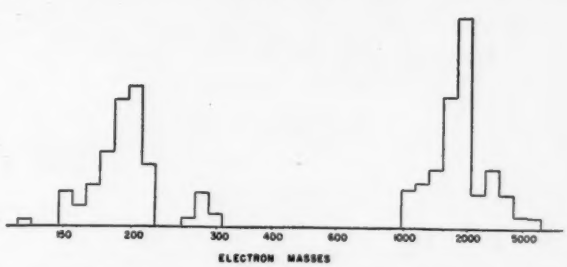

FIG. 1. Weighted mass spectrum of cosmic-ray particles at sea level with ranges between 4 and 13 cm of lead.

[4] Wheeler and Ladenburg, Phys. Rev. **60**, 754 (1941).
[5] Aron, Williams, and Hoffman, U. C. Radiation Laboratory (private communication).
[6] R. B. Brode, Phys. Rev. **75**, 904 (1949)

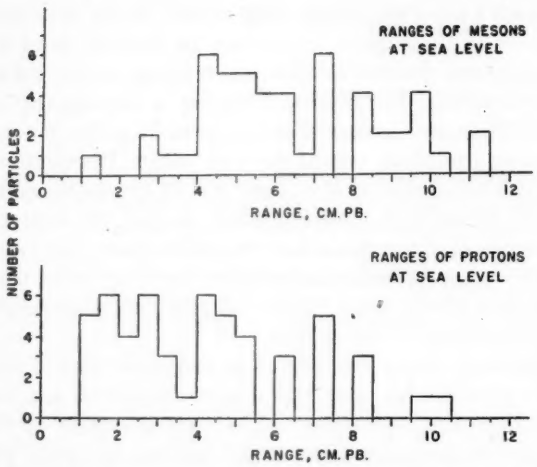

FIG. 2. Range spectrum of cosmic-ray protons and mesons at sea level. The ranges shown are the lead equivalent of the path below the curvature chamber. Material equivalent to 2 cm of lead is located above the curvature chamber.

particles from protons. None of the proton group of particles has a negative charge and none shows evidence of decay particles at the end of its range. No masses were found in the region between 300 and 1000 m_e.

The mesons which stop between 4 and 13 cm of lead constitute about one percent of the hard component. An equal number of protons stop in this same absorber. The observed range spectra of mesons and protons are shown in Fig. 2. The decrease in meson intensity above 7 cm range appears to be due in part to loss of particles from the illuminated region by scattering and insufficient illumination in the lowest section of the chamber. The number of protons with low ranges is definitely greater than the number of mesons in this same region. Since about 15 cm of wood were located above the apparatus, it is possible that at least a part of these protons may have originated in the wood. The total ranges of the particles have been calculated on the assumption that all of the particles have passed through about 15 cm of wood, the Geiger counter, and the chamber walls. Unfortunately, the wood thickness was not uniform throughout the solid angle above the chamber. Unlike the experiment of Germain,[3] no anticoincidence counters were located below the equipment so that stopping protons accompanied by fast particles were not automatically rejected. The experiment is being continued with various thicknesses of absorber above the curvature chamber to study more fully the range spectrum of protons.

The mass of the μ-meson obtained in this experiment is somewhat lower than currently reported values.[1,1] The mass calculated by the Wheeler and Ladenburg chart involves a comparison of the ranges of mesons and protons with corresponding velocities. Protons with suitable velocities would have energies of one Bev and are not readily available. The range-energy relationship has therefore been extrapolated from data at much lower energies. A small deviation in the extrapolated form of the range-energy curve could appreciably change the value of the result given here. In the mass measurements of artificially produced μ-mesons at the University of California Radiation Laboratory, protons are available with velocities comparable with the ranges of the low energy mesons and the calibration in those experiments will be much more certain.

Reaction Constants for $T^3(p,n)He^3$

G. A. JARVIS, A. HEMMENDINGER, H. V. ARGO, AND R. F. TASCHEK
Los Alamos Scientific Laboratory, Los Alamos, New Mexico*
(Received March 6, 1950)

Measurements of the differential and total cross sections for $T^3(p,n)He^3$ between the reaction threshold at 1.019 Mev and 2.49 Mev are reported. At the higher energies the neutron emission in the center-of-mass system is highly asymmetric and the energy dependence of the coefficients of a cosine expansion fit to the angular distribution is determined. Evidences for resonance effects are observed at the highest proton energies used, indicating an excited state in the continuum of the intermediate He^4 nucleus. The use of the reaction as a neutron source is discussed.

I. INTRODUCTION

A PRELIMINARY investigation of the interaction of protons with tritium[1] has shown that the neutron yield of $T^3(p,n)He^3$ is large and varies rapidly with proton energy.

The results previously reported were obtained with a small scattering chamber as the target. The design of the latter was such that rather large amounts of metal were irregularly spaced about the gas volume of the target, making it unsuitable for precise neutron yield measurements. To avoid this difficulty a thin-walled gas target has been built and used in connection with the Los Alamos electrostatic accelerator to make a detailed study of the angular distributions of the neutrons from the reaction $T^3(p,n)He^3$ from the threshold[2] at 1019 kev up to 2800-kev proton energies. The McKibben nomograph[3] for this reaction may be of help in the following discussion.

II. APPARATUS

The essential features of the tritium gas target are shown in Fig. 1. Its gas volume is about 2 cm^3. The proton beam from the electrostatic accelerator, limited by the three beam-defining diaphragms *A*, *B*, and *C*, enters the thin-walled target chamber through the thin aluminum window at *C*. The target volume is electrically insulated from the beam tube by Bakelite bushings as shown in the diagram. The Kovar filling tube has a short glass section to isolate the target electrically from the gas handling system. A barrier voltage of minus 300 volts applied to the diaphragm *B* serves to prevent electrons, coming backwards from the aluminum window, from escaping the target. Protons can strike only the window and not the diaphragm on entering the gas volume. With the retarding voltage on *B* no measurable change in current occurred when a magnetic field was applied across the gas volume, indicating that an accurate measurement of charge collected was being made. The proton current integral entering the target was measured within ± 0.2 percent with a Gittings-type current integrator.[4]

The gas handling system, Fig. 2, has been considerably simplified over the earlier arrangement.[1] The volume of the filling system is kept to a minimum by using $\frac{1}{8}''$ bore quartz tubing for the UT_3 storage tube, $\frac{1}{8}''$ bore Pyrex tubing for the mercury manometer and $\frac{1}{16}''$ bore Kovar tubing for the interconnecting leads. Likewise, the stainless steel needle valves were made to have small volumes. With this arrangement, the target can be filled to any pressure up to about an atmosphere by direct evolution from the tritium storage tube. This maximum pressure is limited by the design of the manometer and the breaking strength of the target windows, rather than by the thermal decomposition properties of UT^3.

The neutron yields were measured with two flat-response long counters.[5] One of these remained at a fixed angle and distance from the target and served primarily as a monitor for determining relative yields during the measurement of a given angular distribution at a particular energy. No provision was made for closing off the target filling tube at the target, so that it was necessary to measure the change in density of tritons in the target due to heating when the protons passed through it. Since the target gas was exposed to

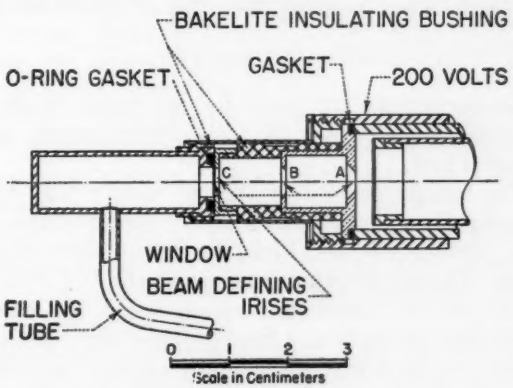

FIG. 1. Thin-walled gas target.

* This document is based on work performed at the Los Alamos Scientific Laboratory of the University of Californa.

[1] Taschek, Jarvis, Hemmendinger, Everhart, and Gittings, Phys. Rev. **75**, 1361 (1949).

[2] Taschek, Argo, Hemmendinger, and Jarvis, Phys. Rev. **76**, 325 (1949).

[3] Hanson, Taschek, and Williams, Rev. Mod. Phys. **21**, 649 (1949). For laboratory use large nomographs can be obtained from Document Sales Agency, U. S. Atomic Energy Commission, P. O. Box 62, Oak Ridge, Tennessee, as MDDC 223.

[4] H. T. Gittings, Rev. Sci. Inst. **20**, 325 (1949).

[5] A. O. Hanson and J. L. McKibben, Phys. Rev. **72**, 673 (1947).

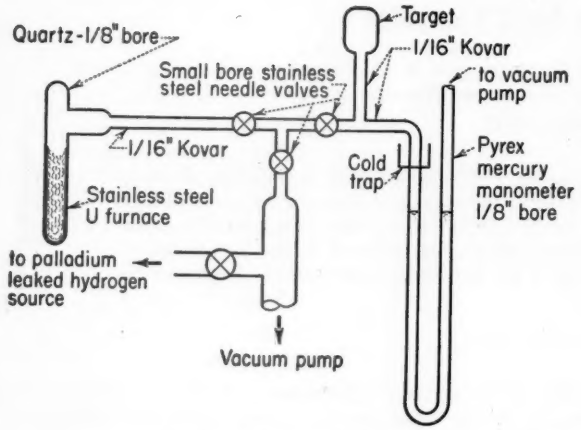

FIG. 2. Gas handling system.

the mercury manometer, heating of the target was accompanied by an actual change in the volume occupied by the tritium gas.

The second counter was mounted on a truck and pivoted to move in a circle about the center of the target. The distance from the center of the target to the counter face was 142″, corresponding to a subtended half-angle of about 4°.

Counter sensitivities were determined by placing a standard Ra—Be neutron source[6] at the target position and observing the counting rates. The calibration of the standard source is known within ±5 percent. The differential cross sections can be determined from the following considerations: $n(\theta)=\sigma(\theta)N_t l n_p$, where $n(\theta)$ =number of neutrons/steradian-microcoulomb intercepted by counter at θ; $\sigma(\theta)$=differential cross section for reaction in cm²/steradian; N_t=number of tritons/cm³; l=length of proton path through target gas in cm; n_p=number of protons/microcoulomb passing through target. Now also $n(\theta)=QC'/4\pi C$, where Q=total number of neutrons/minute from the standard Ra—Be source; C=number of counts/minute of long counter using Ra—Be source; C'=number of counts/microcoulomb of long counter using $T^3(p,n)$ reaction. Combining these two expressions we get

$$\sigma(\theta)=QC'/4\pi CN_t l n_p.$$

No corrections are made for the small change in counter sensitivity over the total neutron energy range involved here.

The tritium content of the gas sample was determined from observations on proton-proton scattering[1] just previous to installing the thin-walled neutron target. The concentration was found to be 72±2 percent of tritium. An immediate measurement of the neutron yield was then made at a fixed proton energy. After the neutron target was in place any changes in the tritium content of the gas could be determined in terms of the neutron yield at this particular proton energy, the long counter calibration being checked with the Ra—Be source.

The threshold for the $T^3(p,n)He^3$ reaction has been measured accurately and provided a convenient means of determining the energy lost by the protons in passing through the thin aluminum window containing the tritium gas in the target. One simply observes the apparent threshold for the appearance of forward neutrons from the tritium gas target. The proton energy for which this occurs will be greater than the real threshold by an amount corresponding to the mean energy lost by the protons in passing through the foil. The foil thickness for other incident proton energies can then be calculated from the range ratios of Parkinson *et al.*[7]

Actually there are several complicating factors which result in an appreciable uncertainty in the value of foil thickness which one obtains from such a measurement as that described above.

First, energy straggling of protons passing through aluminum window causes some spread in energy of protons enterging the gas volume of the target. For the nominally 0.2-mil aluminum foils[8] used, the mean spread for this type of straggling is about 10 kev, as calculated[9] and as measured by Madsen and Venkateswarlu.[10]

Second, variations in thickness of the foil material itself undoubtedly account for a large part of the energy spread which we actually observe. Figure 3 shows $T^3(p,n)He^3$ threshold curves taken using (*A*) a thick Zr+T target, and (*B*) a tritium gas target with the protons passing through an aluminum window. For this particular 0.15-mil foil it is extremely difficult to determine the average foil thickness to better than about 10 kev.

For the angular distributions taken at energies above the 90° threshold the target was filled to approximately 5.0 cm Hg tritium gas. This corresponded to a maximum proton energy loss in the gas at threshold of about 12 kev. The target pressure was measured to the nearest 0.01 cm with a traveling microscope focused on the mercury manometer.

For the data taken below the 90° threshold the target thickness was about half of the above amount.

III. PROCEDURE

Since hydrogen was introduced into the target frequently to check on the background neutrons, the following procedure for taking data was used to mini-

[6] R. L. Walker, MDDC-414 (1945).

[7] Parkinson, Herb, Bellamy, and Hudson, Phys. Rev. **52**, 75 (1937).

[8] This rather remarkably hole-free aluminum comes in about 1-inch wide continuous ribbon on a spool, the thickness varies between 0.15 mil and 0.18 mil. The foil is manufactured by Cochran Foil Company, Louisville, Kentucky.

[9] M. S. Livingston and H. A. Bethe, Rev. Mod. Phys. **9**, 282 (1937).

[10] C. B. Madsen and P. Venkateswarlu, Phys. Rev. **74**, 1782 (1948).

mize errors arising from possible further hydrogen contamination of the tritium sample.

The movable counter was placed at zero degrees and a forward yield curve taken, using very low proton currents and suitable cooling so that errors arising from gas temperature changes were negligible. The differential cross sections for the forward yield were calculated from the expression given above. All subsequent measurements were taken relative to the neutron monitor and normalized at zero degrees to the appropriate energy point on the forward yield curve.

In taking the angular distributions much larger proton currents were used (about 4 μamp.) and consequently target heating was sufficient to cause the triton density to decrease considerably during a run, but the ratio of counts for the movable counter to monitor was independent of effects due to target heating as well as hydrogen contamination.

Background runs with hydrogen in the target were made for the various proton energies used. The background neutrons were generally negligible except at the highest proton energies where they were as high as one percent of the total. The yield of the background neutrons as a function of proton energy had about the same form as those from tritium, indicating that the observed background was largely due to tritium absorbed in the target backing.

IV. RESULTS

In Fig. 4 the differential cross section for the 0° yield is plotted as a function of proton energy from the threshold up to about 2.8 Mev. The initial peak just above threshold arises primarily from geometrical effects associated with the center of mass motion, which make the neutrons come out in a cone near threshold.[11]

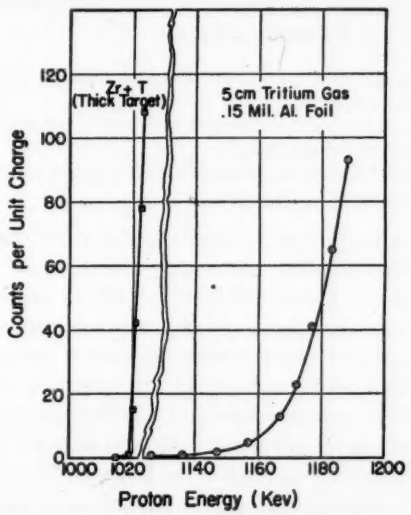

FIG. 3. Neutron yields near $T^3(p,n)He^3$ threshold taken with (a) solid target of tritium absorbed in a zirconium foil, (b) tritium gas target with beam entering target through thin aluminum window.

[11] See reference 3, p. 641.

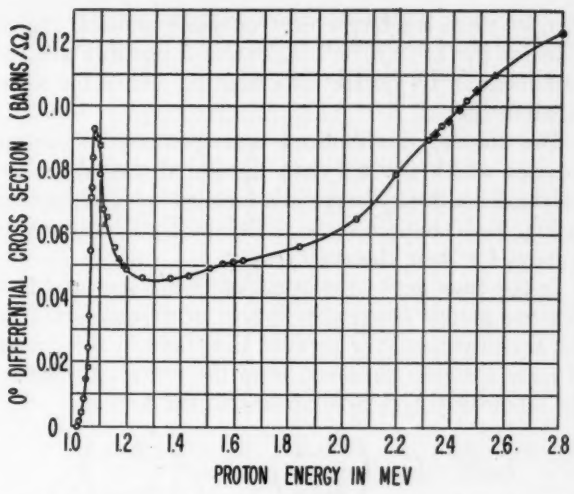

FIG. 4. Neutron yield in the forward direction plotted as a function of the incident proton energy.

It is easily shown from the relation

$$I_{\text{lab}}(\theta)d\omega_{\text{lab}}=I_{\text{c.m.}}(\phi)d\omega_{\text{c.m.}},$$

that at 0°

$$I_{\text{lab}}(0°)=2I_{\text{c.m.}}(0°)\left[1+0.1118\frac{E_p}{(E_p-E_{th})}\right],$$

where $I_{\text{lab}}(\theta)$ is the neutron intensity in the laboratory solid angle $d\omega_{\text{lab}}$ and $I_{\text{c.m.}}(\theta)$ is the intensity in the center of mass solid angle $d\omega_{\text{c.m.}}$ at angle ϕ; E_p is the proton energy and E_{th} the proton energy at the reaction theshold. Thus the solid angle transformation factor (in brackets) becomes very large as E_p approaches the threshold from above. How the laboratory yield drops to zero, rather than going to infinity, as the threshold is approached depends, of course, primarily on how $I_{\text{c.m.}}(0°)$ goes to zero, and on the secondary effects of target thickness, straggling, and counter geometry. Assuming $I_{\text{c.m.}}(0°)$ constant, the target thickness alone could account for the initial rise in the curve since the first appearance of neutrons would be from the initial negligibly thick layer of the target gas. The rise-width on this basis would be about equal to the target thickness. Actually, due to all of these effects, the observed rise-width is much greater than the target thickness.

In Fig. 5 are shown the laboratory differential cross sections for neutron production for a number of proton energies plotted as a function of the laboratory angle. For each proton energy data were recorded at 10° intervals from 0° to 120°. The number of neutron counts per datum was 5000 or more so that the statistical errors were negligible compared to the other uncertainties mentioned above.

The cross sections, measured in barns per unit solid angle, are large and make this reaction a competitor of the $Li^7(p,n)Be^7$ as a neutron source.[12] At the higher

[12] R. F. Taschek and A. Hemmendinger, Phys. Rev. 74, 373 (1948).

energies there is a larger neutron yield at back angles than for the $Li^7(p,n)Be^7$, indicating a possibly greater usefulness of $T^3(p,n)He^3$ as a neutron source for some experiments.

The angular distributions corresponding to proton energies which are less than the 90° threshold, below which all neutrons emerge in a forward cone, are shown in Fig. 6 and require some additional considerations to account for their observed shapes.

In the cone region the intensity of the slow and fast neutron groups (corresponding to neutrons ejected in the backward and the forward directions in the center of mass system) transform from the center of mass to the laboratory system according to the formula

$$I_{\text{lab}}(\theta)=I_{\text{c.m.}}{}^{f}\left(\frac{d\omega_{\text{c.m.}}}{d\omega_{\text{lab}}}\right)^{f}+I_{\text{c.m.}}{}^{s}\left(\frac{d\omega_{\text{c.m.}}}{d\omega_{\text{lab}}}\right)^{s}.$$

The superscripts s and f refer to the slow and fast neutron groups respectively, as observed at the same laboratory angle. Assuming center of mass spherical symmetry for the reaction near threshold, one finds that

$$I_{\text{lab}}(\theta)=I_{\text{c.m.}}(\phi)(d\omega_{\text{c.m.}}/d\omega_{\text{lab}})(1+E_n{}^{s}/E_n{}^{f}).$$

This function is plotted in Fig. 7 as a function of the laboratory neutron angle for two proton energies. The ratio $E_n{}^{s}/E_n{}^{f}$ always lies between unity and zero so that the factor $(1+E_n{}^{s}/E_n{}^{f})$ is not a rapidly varying function. I_{lab} is therefore dominated by the factor $d\omega_{\text{c.m.}}/d\omega_{\text{lab}}$ which has a discontinuity at the cone edge. The departures in shape of our observed angular distributions in the cone region from the type of distributions shown in Fig. 6 are believed to be due primarily to effects of the large foil straggling discussed earlier, and to a lesser extent to the target thickness and the large angle (8°) subtended by the neutron counter. Since, however, the differences between the observed and calculated angular distributions are so marked, especially at the lowest energies, it may be worth while to investigate this cone region on either this reaction, or on $Li^7(p,n)Be^7$, under more favorable conditions to assure oneself that a real effect is not being missed. If the foil difficulty can be overcome, as in solid thin Li targets, then the problem resolves itself primarily into an accurate determination of the energy dependence of the counter sensitivities. The slow group at a given angle is not too serious a problem since its intensity ratio to the fast group is the ratio of their energies.

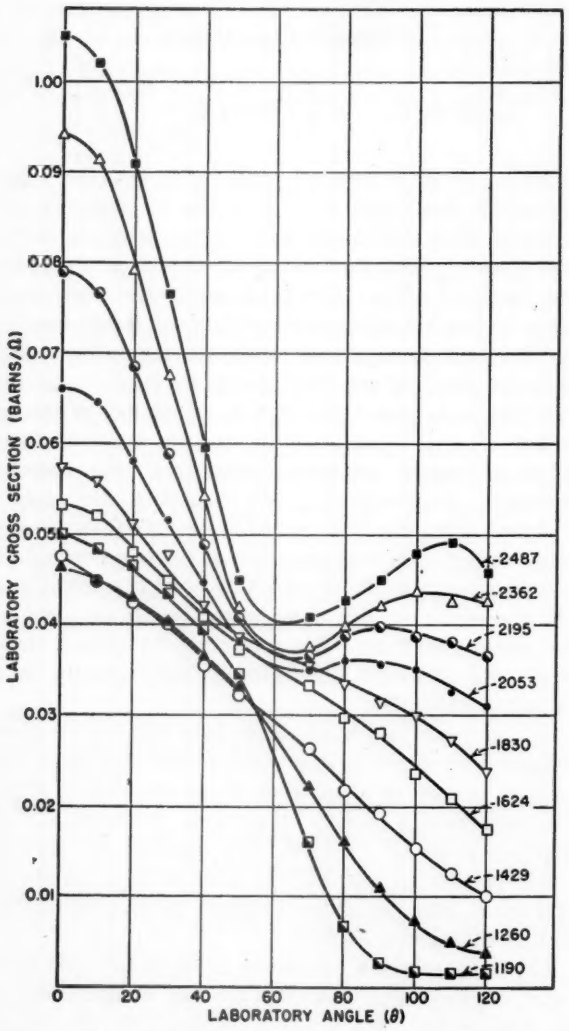

FIG. 5. $T^3(p,n)He^3$ differential cross sections in the laboratory system for proton energies above the 90° threshold. The numbers on the curves are the proton energies in kev.

The angular distributions for proton energies above the 90° threshold are not seriously affected by the foil straggling, etc., since the yields in this region have no rapid changes in intensity comparable with the cone edge discontinuities.

The maximum over-all errors in absolute differential cross sections above the threshold for neutrons at 90° laboratory angle are approximately ±10 percent and arise from the following sources:

(1) about ±5 percent in the absolute neutron yield of our Ra–Be standard source;
(2) about ±2 percent in the measurement of the concentration of the tritium in the gas sample;
(3) about ±3 percent in changes in concentration and in measuring the gas pressure in the target.

The relative errors in the angular distributions are considerably smaller than the above. For neutron energies above about 100 kev the errors are less than the 3 percent arising from uncorrected concentration changes and the measurement of target pressure. For large angles θ and low bombarding energies, i.e., below about 100-kev neutron energies, the long counter sensitivity drops in an uncertain way and here the errors in relative cross section may be as large as 10 percent.

V. CENTER OF MASS DISTRIBUTIONS

The laboratory differential cross sections for proton energies above the 90° threshold have been transformed to the center-of-mass (c.m.) system, as shown in Fig. 8, by means of the usual transformations. These curves

are calculated from *smoothed* curves through the laboratory system experimental data.

Around 1300 kev the neutron yield is seen to be approximately spherically symmetrical. However, as the proton energy is raised, an increasing fraction of the neutrons come off in the forward and backward directions, showing that higher order angular momenta strongly influence the reaction at the higher energies. The distributions are obviously not symmetrical about 90°.

VI. TOTAL CROSS SECTION

The angular distributions in the c.m. system have been fitted with a cosine series of the form

$$\sigma(\phi, E)=A(E)+B(E)\cos\phi+C(E)\cos^2\phi+D(E)\cos^3\phi.$$

Cosine cubed terms were required for a good fit of the data at the higher energies. Four fit points were used to find A, B, C, and D; the resulting expansion gave a fit that fell within the experimental errors.

The cosine series representing the c.m. angular distributions were integrated to obtain the total cross sections from

$$\sigma_{tot}(E)=2\pi\int_0^\pi \sigma(\phi)\sin\phi d\phi=4\pi[A(E)+\tfrac{1}{3}C(E)]$$

for the four terms used in the expansion. This implies an extrapolation of the c.m. yields from about 140° to 180° by means of the expansion, but the extrapolation does not produce much error in σ_{tot} since the multiplying factor $\sin\phi$ goes to zero rapidly as 180° is approached.

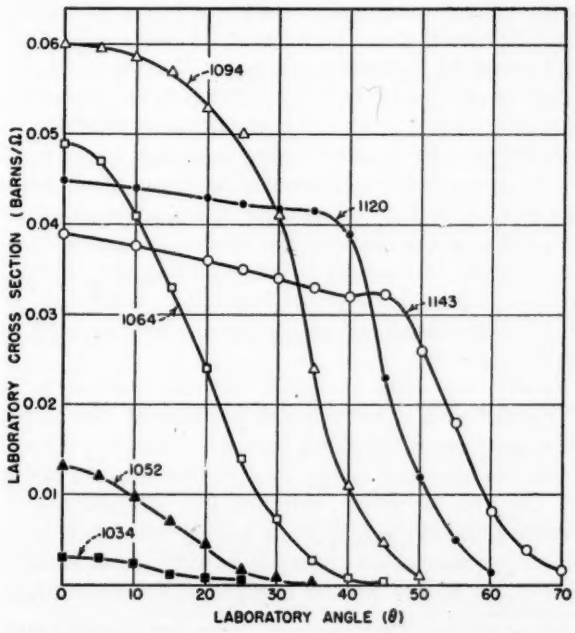

FIG. 6. $T^3(p,n)He^3$ differential cross sections in the laboratory system for proton energies below the 90° threshold. The numbers on the curves are the proton energies in kev.

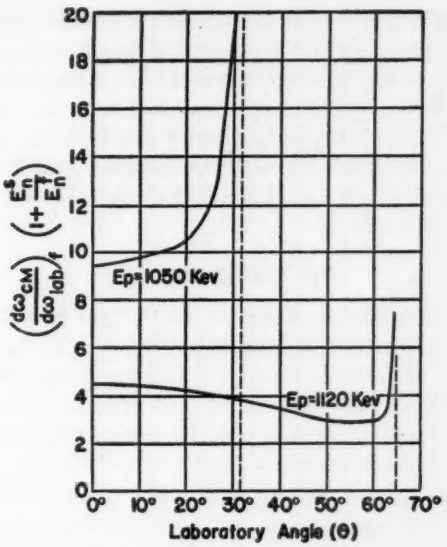

FIG. 7. Plot of the function $(d\omega_{c.m.}/d\omega_{lab})(1+E_n^2/E_n')$ *versus* laboratory angle for two proton energies in the cone region.

The laboratory distributions in the cone region were multiplied by $(\sin\theta)$ and integrated numerically to obtain the total cross sections. These, together with the total cross sections found above, are shown plotted in Fig. 9 as a function of proton energy. The total cross section is seen to rise rapidly from the threshold up to 2.3 Mev, the highest energy for which a complete angular distribution was taken.

Figure 10 shows the energy dependence of the coefficients in the cosine expansion used to fit the center-of-mass angular distributions. The predominant terms are clearly the angle independent S-wave term A, and C, the coefficient of $\cos^2\phi$, while B and D are considerably smaller. The C term, containing effects of P-wave protons, increases rapidly with proton energy. At the

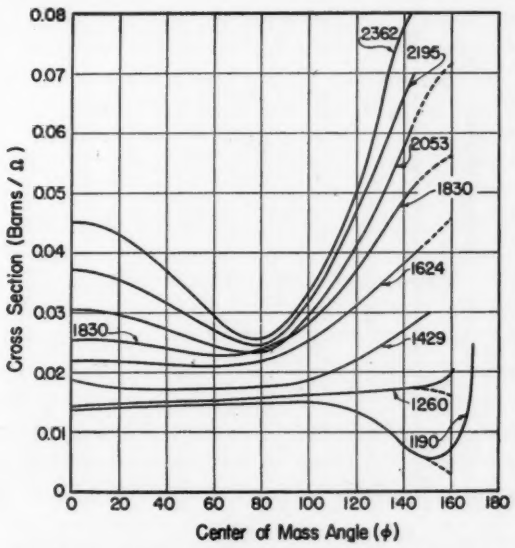

FIG. 8. $T^3(p,n)He^3$ differential cross sections in the center-of-mass system for various proton energies.

lowest energies B and D apparently change sign; this effect is probably not real, depending on the precision of the data and the functional fit. It is probable that B and D do, in fact, approach zero near the reaction threshold. No attempt has been made to fit the center-of-mass distributions with a Legendre polynomial expansion[12] since a final analysis of the data must still include spin effects.

VII. CONCLUSIONS

The data shown above on the $T^3(p,n)He^3$ reaction give some qualitative information concerning the intermediate excited nucleus He^4. The excitation energies of the He^4 lie between about 20.6 Mev and 21.6 Mev for the range of proton energies used in these experiments. This is about 1 Mev lower than the energy available to the intermediate He^4 in the $D(D,p)T^3$, but the formation of the intermediate state for $T^3(p,n)He^3$ is not hampered by the like particle selection rules of $D(D,p)T^3$.

It is immediately striking that if one considers the more reliable angular distribution data; i.e., that above the 90° threshold, only the very lowest proton energies give approximate spherical symmetry in the center-of-mass system. The asymmetry grows rapidly at 0° and 180° as the proton energy is increased, but not symmetrically around 90°. At least P-wave protons are effective in producing this asymmetry; in the $\cos\phi$ expansion fit to the center-of-mass distributions, $\cos^3\phi$ terms were found necessary, implying a finite $\cos^4\phi$ term, which, however, must have been too small to be required in the fit. In the plot of the energy dependence

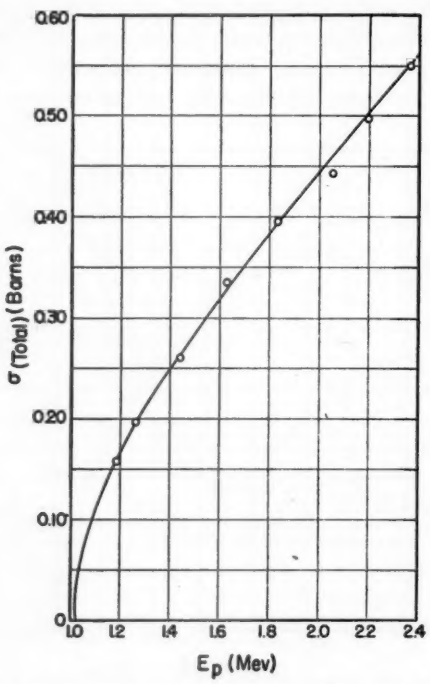

FIG. 9. Total cross sections for the reaction $T^3(p,n)He^3$ as a function of proton energy.

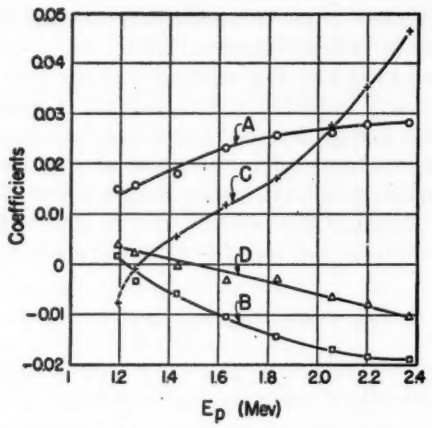

FIG. 10. Coefficients of the cosine series fits to the center-of-mass angular distributions.

of the coefficients (Fig. 10) the slope of the coefficient of $\cos^2\phi$ is increasing rapidly at the higher proton energies indicating a resonance in He^4 produced, presumably primarily by P-wave protons. Unfortunately, the maximum proton energy available was not sufficient to go over, and therefore to see such a resonance clearly. The zero degree observations show the effect rather clearly, firstly because the fraction of P wave is a maximum here, and secondly because data were obtained up to somewhat higher energies than the maximum at which a complete angular distribution was obtained. These indications of resonance effects are brought out more definitely by the observation of gamma-radiation[13] from $T^3(p,\gamma)He^4$, which places the excited state at about 2.4-Mev proton energy.

The trend of the total reaction cross section with energy (Fig. 8) does not obviously show the resonance effect discussed above because of the large admixture of S wave. If, however, one notes that even at the highest energies used here the trend of the cross section is still toward higher values, then resonance effects must be called upon to explain why leveling-off and a decrease do not appear. This argument has been made more quantitative by Dr. L. Goldstein of this laboratory who has computed the shape of the total cross section from the principle of detailed balancing using the thermal cross section[14] for $He^3(n,p)T^3$ and the assumption of its $1/v$ dependence on energy up to energies used in this experiment.

Finally, we wish to point out the usefulness of $T^3(p,n)He^3$ as a monoergic neutron source. The target techniques described above lend themselves to the use of this reaction as a rather good source down to about 150 kev, below which entrance foil straggling may become a serious limitation on energy resolution until further improvements are made in windows or in solid targets. At higher proton energies this disadvantage

[13] Argo, Gittings, Hemmendinger, Jarvis, and Taschek, Phys. Rev. 78, 691 (1950).

[14] L. D. P. King and L. Goldstein, Phys. Rev. 75, 1366 (1949). J. H. Coon and R. A. Nobles, Phys. Rev. 75, 1358 (1949).

rapidly disappears except for extremely high resolution experiments. The low threshold makes this reaction useful with accelerators for which the $Li^7(p,n)Be^7$ threshold is difficult to reach. It seems very probable that monoergic neutrons up to at least 6 Mev can be obtained with higher energy machines, since the $D(D,n)He^3$ reaction has shown no excited states in the residual He^3 nucleus to neutron energies this high; the decided advantage of $T^3(p,n)He^3$ would be, however, the low background because of proton acceleration and the large yield.

We wish to thank Messrs. H. T. Gittings and G. G. Everhart for valuable assistance in carrying out the experimental work described.

PHYSICAL REVIEW VOLUME 79, NUMBER 6 SEPTEMBER 15, 1950

Nuclear Energy Levels in Lead Isotopes*

R. E. Peterson,† R. K. Adair,** and H. H. Barschall
University of Wisconsin, Madison, Wisconsin

(Received June 1, 1950)

The total neutron cross section of radiogenic lead was studied as a function of neutron energy in the range from 15 to 750 kev, using energy resolutions of 3 to 10 kev. Several resonances were observed; these were interpreted as caused by energy levels in the compound nucleus Pb^{207}. The level spacing found in Pb^{207} was of the order of 50 kev. Maxima previously found in the cross section of ordinary lead and attributed to resonance interactions of neutrons with Pb^{208} were re-investigated with better energy resolution. No resonances were observed when earlier measurements of the cross section of Bi were extended to higher energies.

I. INTRODUCTION

In a previous measurement of the total neutron cross section of ordinary lead,[1] three distinct maxima were observed. These were attributed to the resonance interaction of neutrons with Pb^{208} to form excited states of the compound nucleus Pb^{209}. A study of these levels is of especial interest because Pb^{205} is a double closed shell nucleus consisting of 82 protons and 126 neutrons.[2] Characteristics of the compound nucleus Pb^{209} might, therefore, be compared with predictions of nuclear shell theories.

As ordinary lead consists of the isotopes Pb^{208}, Pb^{207}, Pb^{206}, and Pb^{204} in relative abundances of 52, 23, 24, and one percent, respectively, the interpretation of the resonances was complicated by the lack of knowledge of the cross sections of Pb^{206} and Pb^{207}. In the present experiment, therefore, one of the lighter lead isotopes was studied. The cross section of radiogenic lead, consisting of 88 percent Pb^{206}, nine percent Pb^{207}, and three percent Pb^{208}, was measured as a function of neutron energy from 20 to 750 kev. The experimental procedure was the same as that described earlier.[3]

II. MEASUREMENTS ON RADIO-LEAD

The variation of the cross section of radio-lead with neutron energy is shown in the upper part of Fig. 1. The different symbols represent the different energy resolutions used in the experiment, and the heights of the vertical lines through the symbols give the standard statistical errors.

Since Pb^{206} is the main constituent of the radio-lead used, the observed resonances should be due to energy levels in the compound nucleus Pb^{207}. The spacing of the levels found is of the order of 50 kev; in contrast with this, levels in Pb^{209} were previously observed to be approximately 200 kev apart.[1] Since the excitation energy in Pb^{207} in the present experiment is approximately[4,5] seven Mev and in Pb^{209}, 4.5 Mev, the variation in level density for the two lead isotopes may be explained by this difference in excitation energy.

It may be noted that several of the resonances in radio-lead appear to produce minima in the cross section. This behavior may be understood in terms of the discussion of the shape of resonances given by MacPhail.[6] His calculations show that a resonance for elastic scattering produces a minimum in the cross section when the phase shift for potential scattering approaches $-\pi/2$. On the basis of the rigid sphere model of the nucleus, the phase shift for potential scattering of s-neutrons is given by the product of the neutron wave number and the nuclear radius. Taking the nuclear radius of lead as 9×10^{-13} cm, the s-wave phase shift for 400-kev neutrons is about -1.2 radians. Since the phase shift for potential scattering of p-neutrons is small at this energy, the minima observed at 340, 380, 395, 420, and 490 kev are believed to be produced by

* This work was supported in part by the AEC and in part by the Wisconsin Alumni Research Foundation.
† Now at Los Alamos Scientific Laboratory.
** AEC Predoctoral Fellow.
[1] Barschall, Bockelman, Peterson, and Adair, Phys. Rev. **76**, 1146 (1949).
[2] M. G. Mayer, Phys. Rev. **74**, 235 (1948).
[3] Peterson, Barschall, and Bockelman, Phys. Rev. **79**, 593 (1950).
[4] Kinsey, Bartholomew, and Walker, Phys. Rev. **78**, 77 (1950).
[5] J. A. Harvey, Phys. Rev. **78**, 345 (1950).
[6] M. R. MacPhail, Phys. Rev. **57**, 669 (1940).

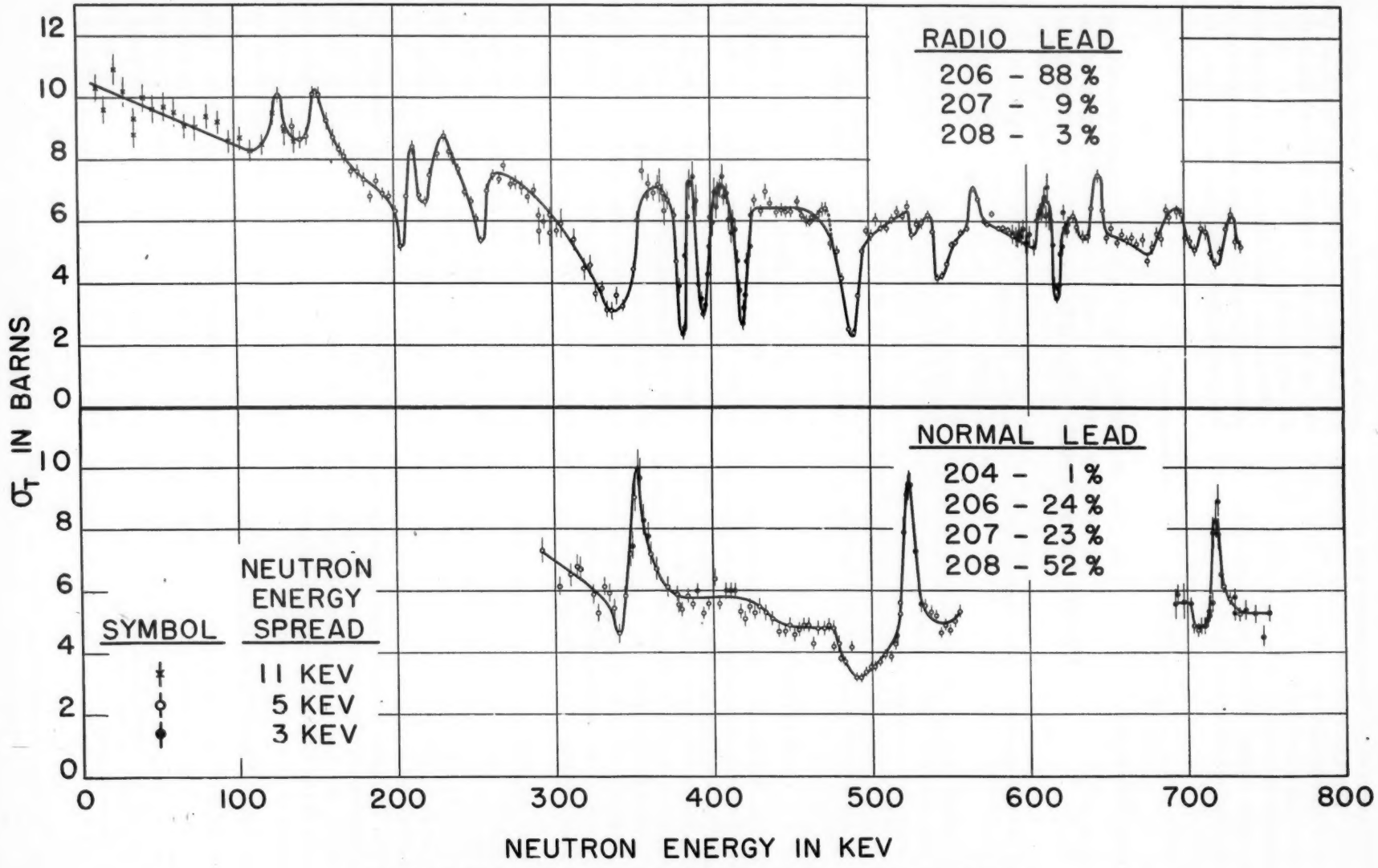

FIG. 1. Total cross sections of radiogenic and common lead as functions of neutron energy.

s-neutrons. The residual cross section of about 2.5 barns at the minima is accounted for by the cross section for p-wave scattering from Pb^{206} and by the cross sections of the less abundant isotopes.

A detailed interpretation of the level structure above 500-kev neutron energy was not attempted; however, the maxima observed at the higher energies are probably the result of resonance interactions of Pb^{206} with neutrons of one or two units of orbital angular momentum.

III. MEASUREMENTS ON COMMON LEAD

The cross section of common lead was re-measured with improved energy resolution to permit a more certain identification of the previously observed resonances. The lower part of Fig. 1 shows the results of these investigations.

If the observed maxima are to be interpreted as resonances in the cross section of Pb^{208}, allowance must be made for the effects of Pb^{206} and Pb^{207}. The cross section of Pb^{206} is known from the measurements on radiogenic lead, and may be subtracted from the common lead cross section. Assuming that the cross section of Pb^{207} varies smoothly with energy, the variation of the cross section of Pb^{208} at the resonances can be estimated. As the widths of the three resonances are greater than the energy resolution used in the experiment, the true peak heights should have been observed. These heights, measured from the minimum to the maximum of the cross section, should be equal to $2\pi k^{-2}(2J+1)$ multiplied by the relative abundance of the isotope responsible for the resonance. Here k is the neutron wave number and J is the spin of the compound state. After subtraction of the effect of Pb^{206}, the contribution of Pb^{208} to the 350 kev peak is 4 ± 0.6 barns, which agrees with the value of 3.7 barns calculated for J equal to $\frac{1}{2}$. The magnitude of the interference effects observed in the Pb^{208} cross section indicates that the resonance is caused by p-neutrons. The height of the peak observed at 525 kev is consistent with a J-value of $\frac{3}{2}$; the dip in the Pb^{208} cross section is approximately that expected if the resonance interaction at this energy were due to p-neutrons. Pb^{208} contributes 3.7 ± 0.5 barns to the height of the 720-kev maximum, which agrees with the value of 3.8 barns calculated for J equal to $\frac{3}{2}$. P-neutrons are probably responsible for this resonance also.

The natural widths of the levels which cause the resonances observed in the cross section of Pb^{208} are approximately 10 kev. The reduced width, γ^2, of a level excited by p-neutrons is given in terms of its natural width, Γ, by[3]

$$\gamma^2=(\Gamma/2k)[1+(ka)^2]/(ka)^2.$$

The reduced widths of the 350-, 525-, and 720-kev resonances are found to be about 70, 50, and 40×10^{-13} kev-cm, respectively. If the problem of the scattering of a neutron by a closed shell nucleus such as Pb^{208} could be treated as a single-particle interaction, the reduced widths of the levels would be expected to be of the order[7] of $\hbar^2/ma$, where m is the neutron mass, a is the nuclear radius. The reduced widths of the levels observed in Pb^{209} are less than one percent of $\hbar^2/ma=11\times10^{-10}$ kev-cm. In view of this it is concluded that the levels found in the present experiment are connected with the excitation of many particles and are not the single-particle levels predicted by the theory of nuclear shells.

IV. MEASUREMENTS ON BISMUTH

Since resonances in the total cross sections of both Pb^{206} and Pb^{208} were found, it was decided to re-investigate the cross section of Bi^{209}, a nucleus with a closed shell of 126 neutrons. In Bi^{209}, as in Pb^{208}, an additional neutron has a binding energy[4,5] of only about four Mev. However, in earlier studies of the Bi cross section,[1] using 10-kev resolution, no resonances were found for neutrons ranging in energy from 15 to 500 kev. An extension of the measurements on bismuth to 1100-kev neutron energy, using again 10-kev resolution, did not give any evidence for resonances in this energy range. It appears, therefore, that no levels wider than three kev occur in the energy interval from 15 to 1100 kev. Measurements of the cross section were also carried out with three-kev resolution in the range from 590- to 655-kev neutron energy. The results indicate that in this energy region there are no levels wider than one kev.

The authors wish to thank Dr. M. G. Inghram, of the Argonne National Laboratory, for making a mass spectrographic analysis of the radiogenic lead used in the experiment.

[7] E. Wigner, Am. J. Phys. **17**, 99 (1949).

Radioactivity from Enriched Isotopes of Cadmium*

J. M. Cork, W. C. Rutledge, A. E. Stoddard, C. E. Branyan, and J. M. LeBlanc
University of Michigan, Ann Arbor, Michigan

(Received May 29, 1950)

By irradiating in the pile specimens of cadmium enriched in mass 108 and in mass 114, it is possible to interpret more positively the observed radioactivities and to evaluate the gamma-rays associated with each. Cadmium 109 produced by neutron capture in cadmium 108 decays with a half-life of approximately 250 days by K-capture to silver 109 in which a strong gamma-ray of 87.5 kev is emitted. Cadmium 115 is isomeric with half-lives of 54 hours and 42.6 days, both isomers decaying to indium 115 by beta-emission. The 54-hour activity yields many gamma-rays in indium whose energies are 335.5, 343.7, 348.9, 369.3, 423.7, 451.9, 525.4, 559.1, and 713.1 kev. These gamma-energies fit well a proposed nuclear level scheme in indium 115.

I. INTRODUCTION

PREVIOUS studies of activated cadmium with its normal array of isotopes have shown the presence of certain long-lived radioactivities. The assignment of an activity to a particular isotope of cadmium has previously been based on its production by various modes of bombardment. By irradiating in the pile a cadmium isotope enriched in mass 108 and another enriched in mass 114, it is now possible to affirm the assignments more positively. The normal abundance and relative percentages of isotopes in the two enriched specimens are shown in Fig. 1. It is apparent that while enriched 108 contains about one-third the normal content of mass 114, enriched 114 has present almost no cadmium of mass 108. It is thus possible by neutron capture in the pile to produce Cd^{115}, reported[1] as being isomeric with half-lives of 2.4 and 43 days, with no accompanying activity due to either masses 107 or 109. An activity in Cd^{109} due to K-capture with a half-life somewhere between 156 and 330 days had been reported

II. RESULTS

Since the enriched Cd^{108} still retains 10.3 percent of Cd^{114}, whose capture cross section is relatively large, the early decay curves for the two specimens are quite similar as shown by the superposition of the two curves in Fig. 2. After three months, however, the Cd^{115} has a pure decay yielding half-lives of 42.6 days and 54 hours while the Cd^{109} curve begins to flatten out into its longer period. To choose between the widely divergent reported half-lives for Cd^{109}, observations must be extended over a much longer time, but indications are at present that the value is 255 days or longer.

Spectrometric photographic studies of the electron emission from the two specimens show many conversion electron lines as listed collectively in Table I, whose gamma-ray origin can be correctly assigned. One group of lines shown have K–L–M differences characteristic of silver and decay with a long half-life. They thus are associated with an 87.5 kev gamma-ray in Ag^{109} emitted following K-capture in Cd^{109}. A gamma-ray of approximately this energy emitted from a metastable state of Ag^{109} has been reported by Helmholtz.

Z	ELEMENT	MASS NUMBER 106	107	108	109	110	111	112	113	114	115	116	117
47	SILVER		51.4%		48.6%								
48	CADMIUM	1.2%	6.7 H, 23 M	0.87%	2000	12.4%	12.8%	24.1%	12.3%	28.9%	4.4 H, 43 D	7.6%	3.8 H
49	INDIUM								4.2%		95.8%		117 M, 43 M
48	ENRICHED CADMIUM 108	1.5%		24.8%		33.2%	12.0%	10.6%	4.5%	10.3%		3.6%	
48	ENRICHED CADMIUM 114	<0.1%		<0.1%		<0.3%	0.4%	2.0%	2.0%	94.2%		1.2%	

FIG. 1. The stable and radioactive isotopes of cadmium with relative abundance.

TABLE I. Electron energies from irradiated cadmium.

Electron energy (kev)	Designation $Z=47$	Designation $Z=49$	Energy sum (kev)	Electron energy (kev)	Designation $Z=47$	Designation $Z=49$	Energy sum (kev)
62.0	K^1		87.5	338.9		L^3	343.1
83.6	L_1^1		87.4	341.4		K^6	369.3
83.9	L_2^1		87.4	344.5		L^4	348.7
86.6	M^1		87.4	395.8		K^7	423.7
307.6		K^2	335.5	424.0		K^8	451.9
315.8		K^3	343.7	497.6		K^9	525.5
321.2		K^4	349.1	521.0		L^9	525.2
331.2		L^3	335.3	531.2		K^{10}	559.1
334.6		M^2 or K^5	335.4 362.5(?)	685.2		K^{11}	713.1

TABLE II. Gamma-rays from irradiated cadmium.

Arbitrary designation	Ag^{109} (~255 days)	In^{115} (54 hr.)
γ^1	87.5 kev	
γ^2		335.5 kev
γ^3		343.7
γ^4		348.9
γ^5		362.5(?)
γ^6		369.3
γ^7		423.7
γ^8		451.9
γ^9		525.4
γ^{10}		559.1
γ^{11}		713.1

* This investigation was made possible by the joint support of the AEC and the ONR.

[1] J. Cork and J. Lawson, Phys. Rev. **56**, 291 (1939); Bradt, Gugelot, Huber, Medicus, Preiswerk, Scherrer, and Steffen, Helv. Phys. Acta **18**, 256 (1945); **19**, 218 (1946); A. C. Helmholtz, Phys. Rev. **60**, 160 (1941); **70**, 982 (1946); Seren, Engelkemeir, Strum, Friedlander, and Turkel, Phys. Rev. **71**, 409 (1947).

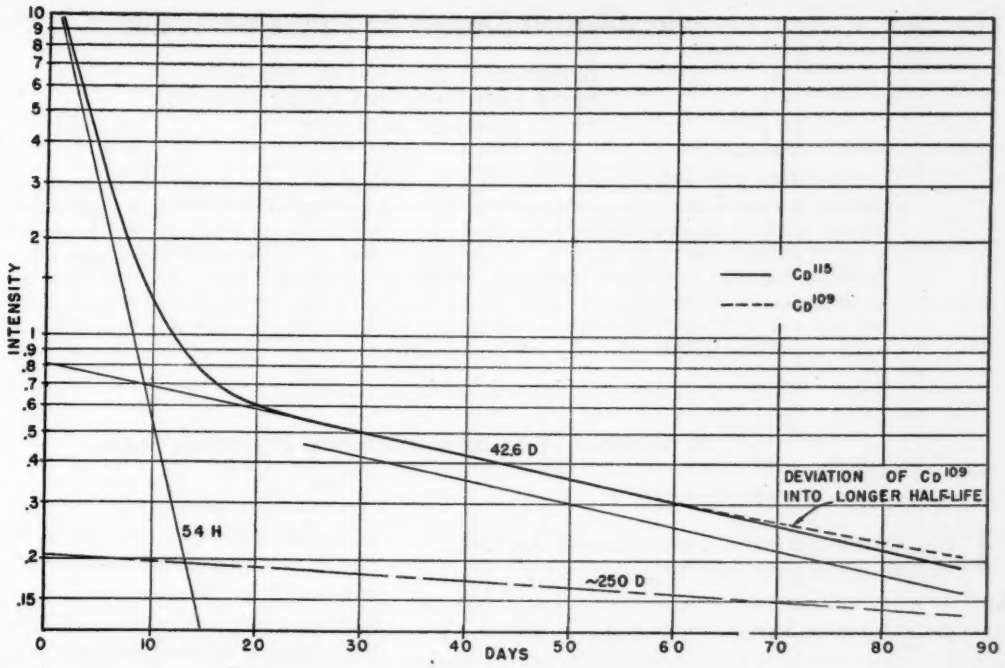

FIG. 2. Superimposed decay curves of cadmium 109 and cadmium 115.

The electron lines from Cd^{114} appear to be short-lived (54 hours) and have K–L–M differences characteristic of indium, and are thus associated with gamma-rays in In^{115} following beta-emission from Cd^{115}. These gamma-rays with arbitrarily assigned numbers are shown collectively in Table II in the order of increasing energy. No electron lines were found to be characteristic of the 42.6-day half-life, although it had at first been assumed that the gamma-ray of energy 525 kev was so related.

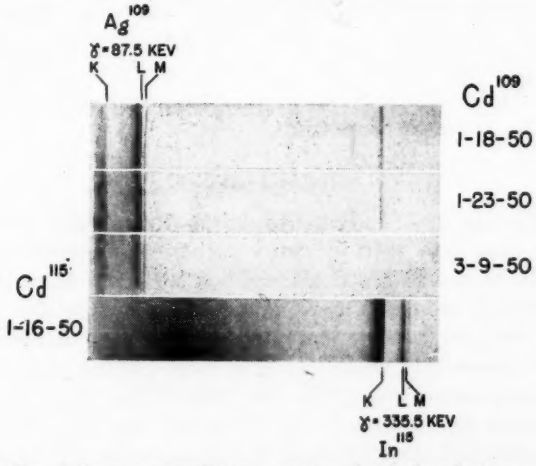

FIG. 3. Low energy electron spectra of cadmium isotopes enriched in 109 and 115.

Further evidence supporting the isomeric character of the 54-hour and the 42.6-day activity is seen in the similarity of the ratio of the initial intensities of the two activities in both enriched isotopes. This would indicate isomeric states of the same isotope rather than separate isotopic activities.

Figure 3 is a time sequence of exposures of the low energy spectrum of enriched Cd^{109}, showing the persistence of the K–L–M electron lines due to the 87.5-kev gamma-ray in Ag^{109}, together with the complete disappearance of the electron lines characteristic of the short-lived 335.5-kev gamma-ray in In^{115}, due to the existence of Cd^{115} in the enriched sample of Cd^{109}. Also shown is the same energy range of the spectrum for enriched Cd^{115}, yielding only the 335.5-kev gamma-ray. The greater intensity of the K–L–M electron lines characteristic of indium in the latter specimen is to be expected on account of the greater abundance of the parent Cd^{115} isotope.

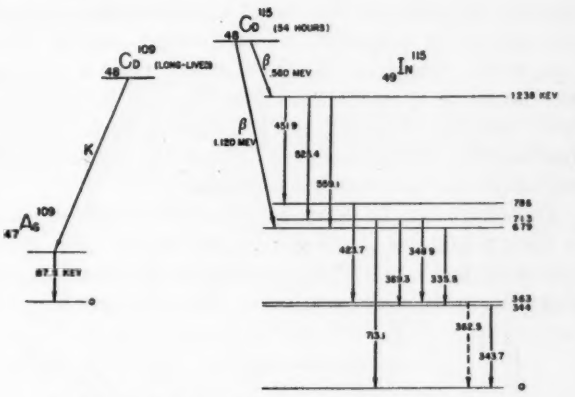

FIG. 4. Level schemes for silver 109 and indium 115.

The beta-upper limit of the 42.6-day activity in Cd^{115} appears by absorption in aluminum to be 1.46 Mev. The beta-spectrum of the 54-hour activity is complex with maximum energies at about 0.56 and 1.12 Mev.

It is possible to propose a level scheme as shown in Fig. 4 which explains quite satisfactorily the many gamma-rays associated with the In^{115} nucleus, together with the observed beta-energies. The K-capture decay in Cd^{109} is also shown.

Scintillation Studies on Potassium Iodide

B. SMALLER, J. MAY, AND M. FREEDMAN
Argonne National Laboratory, Chicago, Illinois
(Received April 5, 1950)

Scintillation studies have been conducted on the effect of thallium impurity on the fluorescence properties of potassium iodide. Coincidence techniques have demonstrated the presence of single photon emission as expected from electron trapping at impurity sites. It has been possible to distinguish between the characteristic radiation due to the impurity and the fundamental or lattice radiation from the pure potassium iodide crystal. The fluorescence efficiencies of both types of emission have been determined as a function of temperature. Measurements of the K^{40} radioactivity in the crystal result in the values $\lambda(\beta)=3.90\times10^{-10}$ per year and $\lambda(\gamma)/\lambda(\beta)\cong0.05$. Comparison of pulse height distribution with that from Cs^{137} activity gives a provisional $E_{max}(\beta)\cong1.3$ Mev.

A. Electron Trapping in Thalliated Potassium Iodide

I. INTRODUCTION

THE recent successful applications of fluorescence processes to radioactivity assaying have invited further investigation into the more detailed nature of this mechanism of energy conversion. Emission phenomena associated with ionic crystal lattices have been studied considerably by use of constant light sources and photo-cell galvanometer techniques and by spectrographic methods. These various aspects of the luminescence of solids have been treated in detail by many authors[1–5] where the distinction is made between fundamental (or lattice) emission and the characteristic radiation due to imbedded impurities.

One characteristic of impurity-activated ionic crystals is their exhibition of the glow phenomenon. The "glow curve method" developed by Urbach[6] for investigating this phenomenon is as follows. The solid is irradiated at a constant temperature, the source of radiation is then removed, and the temperature of the solid is raised; the afterglow radiation from the solid is then noted as a function of temperature and heating rate. This delayed photon emission is believed to be due to the trapping of electrons during the irradiation, followed by their release under thermal agitation.

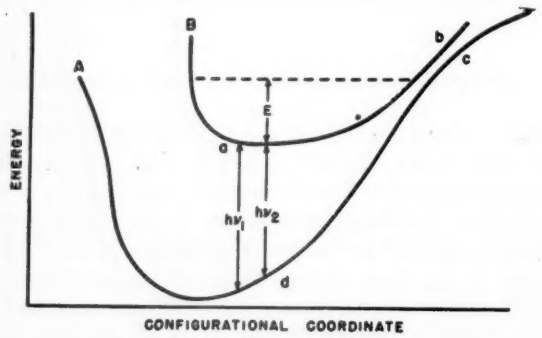

FIG. 1. Transitions between normal and excited states of a luminescent center.

The methods used to date in the investigation of these effects are essentially macroscopic in nature and do not permit a complete verification of the postulated mechanism. However, recent improvements in photo-multiplier tube design, permitting the detection of single photons with relatively high efficiency, now allow one to isolate the emission process. Thus, the phenomenon of radiation from crystal structure can be related directly to photon emission theory, and to the quantum radiation processes associated with trapped electrons. Experiments have now been carried out with these new scintillation techniques which not only verify the previous results, but also shed new light on the processes involved in the fluorescence of solids.

II. THEORY

The theory of radiation from a simple crystal lattice has been developed by many authors. The hypotheses of Gurney and Mott[7] as modified by Seitz[8] have had the most success in explaining experimental results. In its simplest aspects one can envisage the radiation process as the formation of a local excited state by photon absorption by an ion, from which state there exists a competitive action between re-emission of the photon and dissipation of the energy through lattice vibration (Fig. 1). Thus if energy $h\nu_1$ is absorbed, exciting the ions from the ground state A to the excited state B, re-emission can occur with a photon of energy $h\nu_2 \leqslant h\nu_1$ or, through an activation energy ΔE, a radiationless transition can proceed from $a\rightarrow b\rightarrow c\rightarrow d$. Hence for the two processes we have the relative fluorescence

[1] F. A. Kroger, *Some Aspects of the Luminescence of Solids* (Elsevier Publishing Company, Inc., New York, 1948).
[2] Cornell Symposium of the American Physical Society, *Preparation and Characteristics of Solid Luminescent Materials* (John Wiley and Sons, Inc., New York, 1948).
[3] N. F. Mott and R. W. Gurney, *Electronic Processes in Ionic Crystals* (Clarendon Press, Oxford, 1940).
[4] F. Seitz, *Modern Theory of Solids* (McGraw-Hill Book Company, Inc., New York, 1940).
[5] P. Pringsheim, *Fluorescence and Phosphorescences* (Interscience Publishers, Inc., New York, 1949).
[6] F. Urbach, Wien. Ber. IIa, 139, 353, 364 and 483 (1930).
[7] R. W. Gurney and N. F. Mott, Trans. Faraday Soc. 35, 69 (1939).
[8] F. Seitz, Trans. Faraday Soc. 35, 74 (1939).

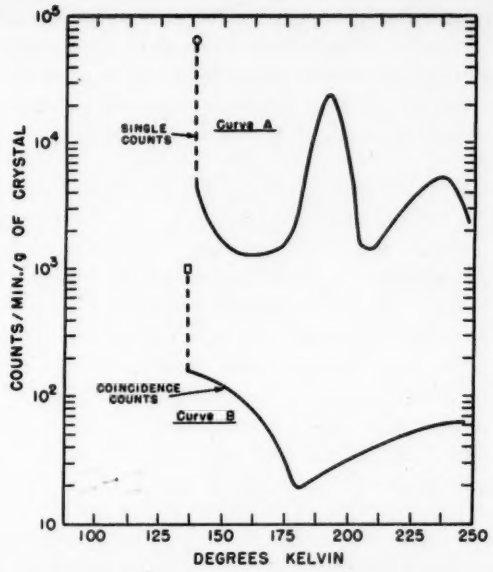

FIG. 2. Glow curve for potassium iodide (0.4 percent TlI). Exposure: 1 min., external gamma-radiation. (○ gives the single counting rate during irradiation, while □ gives the coincident counting rate during irradiation.)

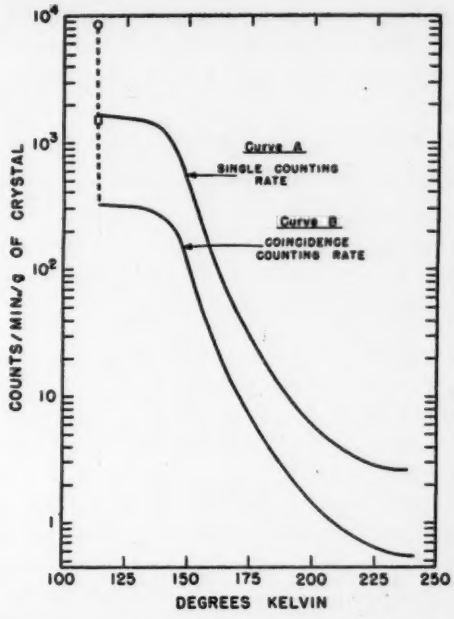

FIG. 3. Glow curve for pure potassium iodide. Exposure: 10 min., external gamma-radiation. (○ gives the single counting rate during irradiation, while □ gives the coincident counting rate during irradiation.)

efficiency η given by the equation

$$\eta = K_{\text{lum}}/(K_{\text{lum}}+K_{\text{dis}}), \tag{1}$$

where K_{lum} is the probability of return to ground state by luminescence and K_{dis} is the probability for non-radiative return. The latter probability is determined by the Boltzman probability; hence

$$K_{\text{dis}} = A\nu e^{-\Delta E/kT}, \tag{2}$$

where ν is the lattice vibrational frequency and A is the probability of transition from $b \rightarrow c$. The fluorescence efficiency, η, as a function of temperature, will thus obey the equation

$$\eta = [1+(A\nu/K_{\text{lum}})e^{-\Delta E/kT}]^{-1}, \tag{3}$$

or

$$\log[(1-\eta)/\eta] = \log(A\nu/K_{\text{lum}}) - \Delta E/kT. \tag{4}$$

The theory of impurity-activated crystals requires certain suppositions regarding the existence of luminescence centers and electron-trap centers. The study of the thermoluminescence of alkali halides was first studied intensively by Urbach,[6] and more recently by Garlick and Wilkins.[9] The theory of the electron trapping has been advanced sufficiently by Randell and Wilkins[10] and by Seitz[11] to permit quantitative verification. In the simple case of an electron-trapping center which coincides with a luminescence center, one assumes that the electron has been ejected from its ground state, by a primary ionization event, into the conduction band or quasi-conduction band, to be trapped at the impurity site. The probability of gaining an activation energy E to release the electron and re-emit the photon is expressed by

$$p = Se^{-E/kT}, \tag{5}$$

S being a constant determined by the vibrational frequency and the reflection coefficient of the potential barrier[12] ($=2.9\times10^9$ sec.$^{-1}$ for KCl). The phosphorescent decay constant τ is given by

$$\tau = 1/p = e^{E/kT}/S, \tag{6}$$

indicating a strong dependence of the decay constant on temperature. Thus if one initially exposes the crystal to radiation at a low temperature, producing a number n of trapped electrons, and then raises the temperature at a rate $dT/dt=\beta$ the number of emitted photons will be given by

$$dn/dt = -nSe^{-E/kT} \tag{7}$$

or, on integration,

$$\frac{dn}{dt} = -Sn_0 \exp\left[-\int_0^T \frac{S}{\beta}e^{-E/kT}dT\right]\cdot e^{-E/kT}. \tag{8}$$

The curve of Eq. (8) shows a maximum at a temperature T_G, the glow temperature. This temperature is related to the trap depth E by the equation

$$E = kT_G \log S + kT_G \log(kT_G^2/E\beta). \tag{9}$$

[9] G. F. J. Garlick and M. H. F. Wilkins, Proc. Roy. Soc. A184, 408 (1945).
[10] J. T. Randell and M. H. F. Wilkins, Proc. Roy. Soc. A184, 347 (1945).
[11] F. Seitz, J. Chem. Phys. 6, 150 (1938).
[12] W. Bünger, Zeits. f. Physik 66, 311 (1930); W. Bünger and W. Flechsig, Zeits. f. Physik 67, 42 (1931); 69, 637 (1932).

Since the mean time spent by an electron in a trap, i.e., the decay time τ equals $1/p$, then it follows that

$$\log\tau=[(T_G-T)/T]\log S+(T_G/T)\log(kT_G^2/E\beta). \quad (10)$$

III. EXPERIMENTAL PROCEDURE AND DISCUSSION

For the present investigations single crystals of potassium iodide with various concentrations of thallium impurity were used. The crystals used were produced by two different methods: the gradient furnace and the Kryopolis method. Using the former method the procedure was as follows. A platinum crucible was filled with a mixture of potassium iodide and one percent thallous iodide and sealed into a quartz tube; the mixture was then melted in a furnace maintained at 20° above the melting point and then slowly drawn into a furnace held at 10° below the melting point, about 24 hours being required for the crystallization. Crystals made by this method showed by spectrographic analysis 0.4±0.2 percent thallium, a relatively good penetration into the potassium iodide lattice. Unfortunately it was difficult to secure large clear crystals and hence their application was limited.

We are indebted to Dr. P. Pringsheim for crystals grown by the Kryopolis method. His procedure consisted in dipping a cooled metal rod into the potassium iodide-thallous iodide melt and then slowly withdrawing the rod while continuously rotating to insure a uniform deposition. By this method cylindrical shaped crystals weighing up to 50 g were easily obtained. However, since the thallium is free to vaporize from the melt, its penetration into the crystal is relatively inefficient. Thus, using a potassium iodide melt containing 0.1 percent thallous iodide, analysis of the crystals showed only a trace of thallium, i.e., less than 0.01 percent. The pure potassium iodide crystals were also grown by this method.

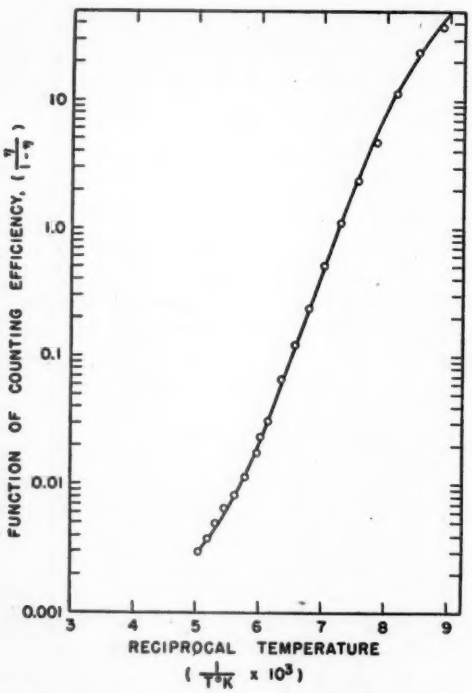

FIG. 4. Function of counting efficiency, $\eta/(1-\eta)$ (where η is the efficiency), *versus* reciprocal temperature for pure potassium iodide crystals.

The experimental arrangement used in the study of the fluorescence characteristics allowed the crystal to be mounted in a cooling chamber in a position such that it could be viewed by two 1P21 photo-multiplier tubes. One could thus differentiate between the scintillation events appearing on only a single phototube and those events recorded by both phototubes in a coincidence circuit. The latter had a resolving time of 3×10^{-7} sec. and was preceded by fast preamplifiers of decay times of 5 μsec. The phototubes were maintained at liquid nitrogen temperature to reduce thermal background while the discrimination levels of the recording circuits were set so that pulses arising from single photoelectrons emitted from the photocathode, corresponding to single incident photons, would be recorded. Considerations of light geometry and photoelectron conversion efficiency yielded an estimate of about 0.25 percent counting efficiency for single photons emitted from the crystal.

The crystal was initially cooled to about 125°K and irradiated for the desired period. The exciting radiation was gamma-rays produced by an intense ThC″ source along with the relatively low intensity radiation from the potassium 40 naturally present in the crystal. The gamma-radiation was then removed and the crystal temperature raised at a rate of about 1°/minute. The resulting single (A) and coincidence (B) counting rates for a potassium-iodide-0.4 percent thallous iodide crystal is shown in Fig. 2 and for a pure potassium iodide crystal in Fig. 3. (The circle and square indicate the single and coincidence counting rate during irradiation.) The similarity between curve 2A and similar glow curves previously obtained[1] from the gross intensity of thermoluminescence is evident. The presence of electron traps of different energy levels is indicated by the peaks in counting rate. That these are due to thallium impurity is apparent by comparison with curve 3A which shows no such peaks. The coincidence counts (B of Figs. 2 and 3) are due to fluorescence from the energetic K^{40} radiation. The temperature dependence of the two types of emission from the crystal is apparent from the data of curves 2B and 3B: (1) the characteristic radiation due to the thallium impurity (right side of curve B) shows a decrease in efficiency as the temperature is lowered and (2) the lattice radiation of pure potassium iodide (Fig. 2B and left side of Fig. 3B) shows a high negative temperature coefficient of fluorescence efficiency.

The presence of the fundamental or lattice emission allows one to verify Eqs. (3) and (4) provided the coincidence counting rate can be taken proportional to the efficiency. This assumption fails only when the counting rate approaches the maximum rate and the coin-

cidence counting rate is no longer proportional to the number of emitted photons. As is shown in Fig. 4, the linear relationship expected from Eq. (4) between $\log[(1-\eta)/\eta]$ and T^{-1} is valid in a limited region and yields an activation energy of 0.27 ev in accord with previous determinations.[1] The significance of the difference between single and coincidence counting rates of Fig. 3 is as yet unknown. Delay coincidence determinations made to ascertain whether the difference could be due to residual short-lived trapping centers showed no decay periods between 3 and 1000 μsec. as would be expected from a shallow trap. There remains the possibility that the difference is due to x-radiation resulting from the K-capture disintegration of K^{40}, but conclusive results remain difficult to obtain.

The depths of the electron traps can be determined from Fig. 2A and Eq. (9). Thus, for the peak indicated by $T_G = 190°K$, the trap depth $= 0.46$ ev, while the one indicated by $T_G = 235°K$ corresponds to a 0.57 ev depth. From the dependence of the phosphorescence decay time on temperature, Eq. (10), one can deduce the decay time at room temperature due to these traps. Thus the 0.46 ev trap corresponds to a decay time of 16 msec. at $T = 300°K$, while the 0.57 ev trap yields correspondingly a one second decay time. An inaccurate value of S or of T_G will not affect the value of E by a large amount; however, the calculated values of τ will be radically affected. Thus the calculated τ's may be in error by several factors of ten; even so, the decay times must be comparatively long.[13] These long period decay times, even at room temperature, are in sharp contrast to many organic scintillators where the decay time[8] is of the order 10^{-8} to 10^{-9} sec. There is reason to expect that

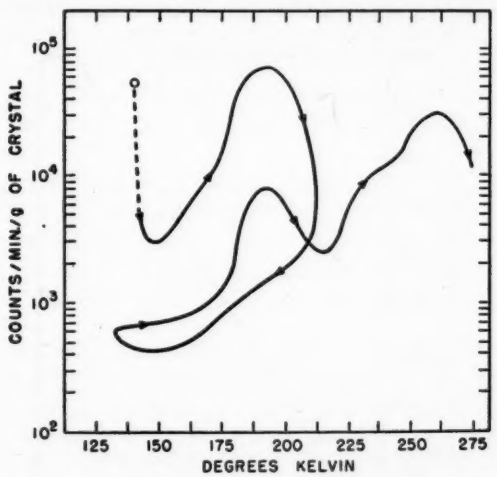

FIG. 5. Recycling of glow curve for potassium iodide (0.4 percent TlI). Exposure: 10 min., external gamma-radiation. (O gives the counting rate during irradiation.)

[13] Recent measurements by Robert Swank of the Instruments Division of this Laboratory show that the decay time at room temperature is 300 μsec. compared with our estimate of 16 msec, indicating that either the value of S used is in great error or that a shallower trap exists with a T_G below the temperature obtainable at the time of our measurements.

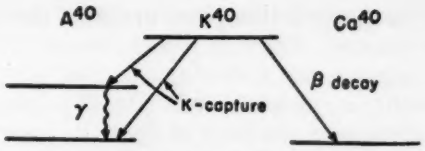

FIG. 6. Probable decay scheme of K^{40}.

the fluorescence of pure alkali halide is also of this short period. Hence it is advantageous to use this lattice type of fluorescence in scintillation circuits where fast amplifiers and coincidence circuits are required (as in the circuits used in this work).

The cumulative nature of the thermoluminescent phenomenon was shown by varying independently the duration and the intensity of the gamma-irradiation. In contrast to macroscopic radiation techniques, the total number of available traps was obviously far greater than the available free or quasi-free electrons and hence the counting rate at the glow temperature was found to be directly proportional to the product of duration and intensity of exposure. The independence of these trap levels was clearly demonstrated by a recycling process shown in Fig. 5, where the cycling path is indicated by the arrows. After a given dosage of radiation the crystal was warmed through the 190°K counting-rate maximum to 200°K and then cooled back to 130°K, held there for 30 minutes, and then re-warmed (Fig. 5). In the resulting glow curve the 190°K peak was almost completely suppressed, but the subsequent 235°K peak retained approximately the same intensity relative to the original 190°K peak as it had previously. Careful analysis of the thermoluminescence data indicates that both traps had a doublet characteristic. For simplicity this phase of the phenomenon was ignored. The presence of the suppressed 190°K peak was due to the refilling of its related traps by the internal radiation from the K^{40}. These phenomena can be explained by the strong dependence of the phosphorescence decay time on temperature.

The ability to detect single photons made it possible to determine directly the high efficiency of conversion of the primary radiation into light. A temperature of 100°K was maintained for varying periods of time during which the potassium iodide crystal was subjected to its K^{40} internal radiation. The temperature was then raised and the integrated delayed photon yield determined and compared with the total energy of excitation. The photoelectron/photon efficiency of the photo-multiplier was assumed as 5 percent,[14] and the crystal to phototube geometry determined as also 5 percent. On this basis it was found that 8×10^4 delayed photons are produced per primary beta-disintegration. This yield is considerably greater than that due to the prompt fluorescent pulse and hence it appears that

[14] This value is that published by RCA for the 1P21 photomultiplier and the variation in this value may be in error by 50 to 100 percent.

most of the energy is transposed to that of the electrons that are trapped. Assuming a mean energy of 400 kev for the beta-ray, one finds that only 5 ev are required per photon; i.e., approximately 60±30 percent of the energy appears in the form of light. In contrast, the prompt fluorescence efficiency is of the order of 2 percent. This high quantum efficiency is in agreement with that measured macroscopically by Bünger[12] for potassium chloride and also, qualitatively, by Hofstader[17] who found that the emission as measured by photographic blackening was considerably greater than expected by the size of the pulse.

B. Decay Scheme of Potassium 40

IV. DISCUSSION

The fluorescent properties of alkali halides subjected to energetic radiation have been presented in part A. The specific utilization of these properties to unravel radioactive decay schemes has proven successful where other methods have yielded ambiguous results.

The decay scheme of K^{40} has been studied extensively within the past two decades because of its important geophysical significance. A quite complete summary of this work has been presented by Weaver,[15] which work tends to confirm the following tentative decay scheme proposed by Hirzel and Wäffler[16] (Fig. 6). Thus three types of radiations, beta, gamma, and K-capture x-rays occur within the crystal lattice, each having intrinsically different scintillation properties. In order to prevent the existing electron-trapping centers from interfering in the interpretation of the scintillation events occurring due to radiation, the coincident scheme is used to separate the primary event from any subsequent phosphorescence. At 100°K, at which temperature all activity determinations were made, the fluorescence is largely of the fundamental type and independent of the presence of impurities. Since the efficiency approaches unity at this temperature, the counting rate becomes independent of temperature (Fig. 3B) and thus can be assumed to be equal to the disintegration rate.

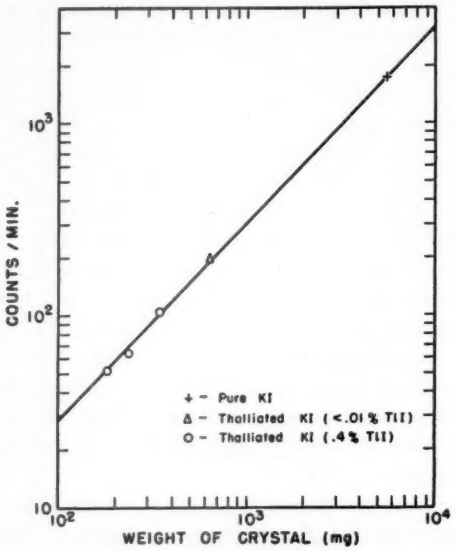

FIG. 7. Activity *versus* weight of potassium iodide crystal (coincident counting rate).

As the average number of prompt photons released per beta-disintegration is of the order of 2×10^3, the coincident counting rate is independent of crystal geometry. Thus, the usual large corrections for geometrical efficiency and for sample and external absorption which apply to Geiger tube counting (and which are so difficult to intercompare in the work of independent investigators) are eliminated. Because of the relatively short range of a beta, the counting efficiency will be unity independent of crystal size.

Internal gamma-radiation will not behave so simply. The probability of detection by photoelectric conversion or Compton recoil will be proportional to the length of path traversed, or to the cube root of the crystal volume. The resultant secondary electron can be expected to behave as a beta, in yielding a coincident pulse. The probability of detection of the K-capture radiation, an x-ray of several kev energy, is extremely low. Previous investigations with mono-energetic electrons have indicated that the fluorescence efficiency of

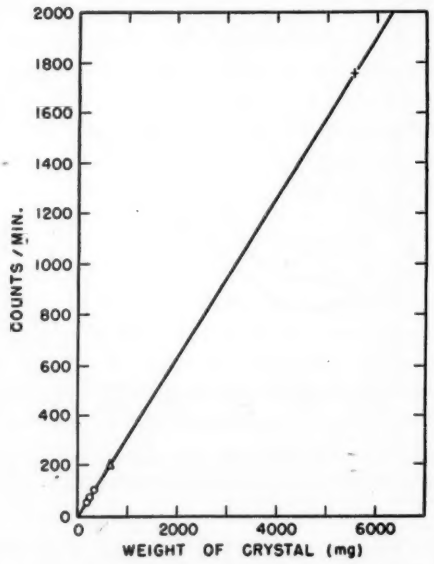

FIG. 8. Activity *versus* weight of potassium iodide crystal (coincident counting rate).

[15] B. S. Weaver, Unclassified Report No. Y-369, "The radioactivity of K^{40}," Y-12 Plant, Oak Ridge, Tennessee (November 29, 1948).

[16] O. Hirzel and H. Wäffler, Helv. Phys. Acta **19**, 216 (1946).

[17] R. Hofstader, Phys. Rev. **75**, 796 (1949).

thalliated potassium iodide crystals at room temperature declines sharply below the region of 5 kev and hence it is rather unlikely that these low energy x-rays would yield a coincidence pulse, although they could be counted in a single channel.

V. EXPERIMENTAL PROCEDURE AND RESULTS

The crystals used in the study of the K^{40} disintegration scheme were those of potassium iodide grown with and without thallium impurities by the methods presented in part **A**. The effect of crystal size on the specific activity in terms of coincidence counts is shown in Figs. 7 and 8. On the basis of the preceding assumptions, if only beta-activity were present in the crystal the total activity would be directly proportional to the weight of the crystal. Hence a log-log plot of such data would yield a straight line with unit slope. Contrariwise, for pure gamma-activity the slope would be different from unity. The actual deviation from unit slope, as can be seen by a careful inspection of Fig. 7, indicates a small percentage of gamma-radiation not in coincidence with the beta-particles, and may be presumed to be the result of *K*-capture to an excited state of A^{40}. The percentage of gamma-activity is 4 to 5 percent of the beta-activity, or $\lambda(\gamma)/\lambda(\beta)=0.05$, in agreement with previous determinations of the gamma-yield.[18] The decay constant of the beta-activity can also be determined directly from the specific activity and the known isotopic concentration of K^{40}. The slope of the linear plot of Fig. 8 reveals a specific activity of 318 ± 10 dis./min./g, this corresponds to a decay constant of

$$\lambda_\beta=3.90\times10^{-10}/\text{year},$$

if we assume an isotopic concentration[19] of 1.16×10^{-4} for K^{40}. This value for the decay constant is in good agreement with that of Borst[20] of $3.9\pm0.4\times10^{-10}$/year, who used unenriched activity, and within his limits of error for hundredfold enriched[18] K^{40} ($4.3\pm0.4\times10^{-10}$/year).

The distribution of pulse heights appearing at the output of the photo-multiplier can, with certain limitations, be related directly to the distribution in energy of the primary ionizing particles. The recent results of Jordan and Bell[21] with anthracene indicate that a direct proportionality exists. Since the fluorescence efficiency of potassium iodide is at least comparable to that of anthracene, its applicability as a scintillation spectrometer can also be expected. The relative pulse heights in the present experiments were determined by using a constant discriminator level and by varying the photo-multiplier voltage, hence the gain. The resulting integral curve for the counting rate as function of pulse height was then differentiated graphically with the result shown in Fig. 9. A direct calibration of the pulse height in terms of primary beta-energy was secured by determining the pulse height distribution of a Cs^{137} spectrum whose continuous beta-distribution has an E_{max} of 550 kev. By this means one could determine for K^{40} an $E_{max}=1.3\pm0.1$ Mev in agreement with other recent values.[22] (The suppression of appearance of the conversion line has been noted also in the anthracene scintillation spectrometer[21] and can be accounted for in part by the relatively poor resolution of the method.) Hence this method, in permitting direct determination of the K^{40} disintegration scheme, has provided greater accuracy than has heretofore been possible by removing ambiguous counting assumptions. In addition, with future use of the recently available 5819 photo-multiplier tube and more refined differential analyzer techniques, the method promises success in unraveling more complicated decay schemes.

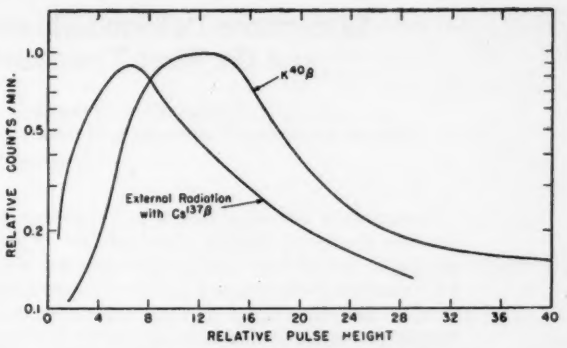

FIG. 9. Differential pulse height distribution curve.

We are greatly indebted to Dr. P. Pringsheim for the preparation of many of the crystals and, even more so for enlightening discussions during the course of the project. We also wish to express our appreciation to Dr. O. C. Simpson for his advice and suggestions during the course of the investigation and for his invaluable aid in the editing of the manuscript.

[18] J. J. Floyd and L. B. Borst, Phys. Rev. **75**, 1106 (1949).
[19] The recently determined accurate value of isotopic concentration of K^{40} of $1.19\pm0.01\times10^{-4}$ [A. O. Nier, Phys. Rev. **77**, 789 (1950)] will produce a corresponding shift in our value of λ_β.
[20] L. B. Borst and J. J. Floyd, Phys. Rev. **74**, 989 (1948).
[21] W. H. Jordan and P. R. Bell, Nucleonics **5**, 30 (1949).
[22] D. Alburger, Phys. Rev. **75**, 1442 (1949).

Microwave Determinations of Average Electron Energies and the First Townsend Coefficient in Hydrogen*

LAWRENCE J. VARNERIN, JR.† AND SANBORN C. BROWN
Research Laboratory of Electronics, Massachusetts Institute of Technology, Cambridge, Massachusetts

(Received May 26, 1950)

A microwave method of measuring the average energy of electrons in a gas in the presence of a d.c. field has been developed through a measurement of the ratio between the electron diffusion and mobility. By solving for a.c. and d.c. distribution functions it is found possible to compare quantitatively the effective a.c. ionization coefficient and the first Townsend coefficient in hydrogen. It is then possible to calculate the first Townsend coefficient from a.c. breakdown data in hydrogen and these values are compared with previously determined values. Measurements of average energy have been made and values calculated from theory compared with previous measurements of average energy. All measurements are in substantial agreement with each other and with the theoretically determined values.

I. INTRODUCTION

SOLUTIONS for the energy distribution function of electrons in a gas show a very close similarity between the distribution functions under the action of a.c. and of d.c. fields. This similarity makes it possible to compare quantitatively the first Townsend coefficient of a gas with the a.c. ionization coefficient. In addition, it makes possible an experiment for the determination of the average energy of the electrons by measuring the ratio of the diffusion coefficient of electrons, D, to the mobility coefficient, μ. The gas in a resonant cavity will break down when the losses of electrons to the walls are replenished by ionization in the body of the gas.[1] When an a.c. field is applied, the breakdown depends upon D. If a small d.c. field is applied to the gas as well, a greater number of electrons will be lost and the breakdown of the gas will depend on μ as well as on D. Breakdown measurements with and without d.c. fields applied permit a determination of the ratio D/μ.

II. THE BOLTZMANN EQUATION

The electron energy distribution function f can be determined with the aid of the Boltzmann transport equation which is the phase space continuity equation for electrons[2]

$$C=\partial f/\partial t+\mathbf{v}\cdot\nabla f+\mathbf{a}\cdot\nabla_v f, \tag{1}$$

where C is the net rate at which electrons appear in an element in phase space, $\mathbf{v}$ is the velocity, $\mathbf{a}$ the acceleration, t the time, and ∇_v the gradient operator in velocity space.

The distribution function can be expanded in spherical harmonics in the velocity

$$f=f_0+(\mathbf{v}\cdot\mathbf{f}_1)/v+\cdots. \tag{2}$$

The spherically symmetric term f_0 is much larger than the higher order terms because of the disordering effect of collisions. This expansion is rapidly convergent for the cases to be considered here.

The production term C arises from collisions and can be expanded in spherical harmonics. The electric field is given by $\mathbf{E}$, and an energy variable $u=mv^2/2e$, in electron volts, is introduced; m is the mass and e the charge of an electron. Substitution of these terms into Eq. (1) gives a scalar and a vector equation

$$C_0=\frac{\partial f_0}{\partial t}-\frac{v}{3u}\frac{\partial}{\partial u}(u\mathbf{E}\cdot\mathbf{f}_1)+\frac{v}{3}\nabla\cdot\mathbf{f}_1, \tag{3}$$

$$\mathbf{C}_1=(\partial\mathbf{f}_1/\partial t)+v\nabla f_0-v\mathbf{E}(\partial f_0/\partial u). \tag{4}$$

Elastic collisions contribute to C_0 and $\mathbf{C}_1$. By considering an elastic collision as an instantaneous process transferring an electron from one point in phase space to another, Morse, Allis, and Lamar[2] have shown that

$$C_{0,el}=(2mv/Mu)\partial(u^2f_0/l)/\partial u \tag{5}$$

and

$$\mathbf{C}_{1,el}=-v\mathbf{f}_1/l, \tag{6}$$

where l is the electronic mean free path and M is the mass of the gas molecule. The remaining contribution to the C_0 term results from inelastic collisions and is given by $-(h_x+h_i)\nu_e f_0$, where h_x and h_i are efficiencies of excitation and ionization and ν_e is used to represent v/l, the collision frequency. We assume that electrons suffering inelastic collisions have no preferred direction after collision and there is no contribution to the $\mathbf{C}_1$ term.

Equations (3) and (4) now give

$$-(h_x+h_i)\nu_e f_0=\frac{\partial f_0}{\partial t}+\frac{v}{3}\left[\nabla\cdot\mathbf{f}_1-\frac{1}{u}\frac{\partial}{\partial u}(u\mathbf{E}\cdot\mathbf{f}_1)-\frac{6m}{M}\frac{1}{u}\frac{\partial}{\partial u}\left(\frac{u^2}{l}f_0\right)\right], \tag{7}$$

$$0=\nu_e\mathbf{f}_1+\frac{\partial\mathbf{f}_1}{\partial t}+v\left[\nabla f_0-\mathbf{E}\frac{\partial f_0}{\partial u}\right]. \tag{8}$$

* This work has been supported in part by the Signal Corps, the Air Materiel Command, and ONR.

† Now at Sylvania Electric Products, Inc., Boston, Massachusetts.

[1] M. A. Herlin and S. C. Brown, Phys. Rev. 74, 291 (1948).

[2] Morse, Allis, and Lamar, Phys. Rev. 48, 412 (1935).

The electric field will be taken as

$$\mathbf{E}=\mathbf{E}_{\text{d.c.}}+\sqrt{2}\mathbf{E}_{\text{a.c.}}e^{j\omega t}, \tag{9}$$

where $\mathbf{E}_{\text{d.c.}}$ represcnts the d.c. field, $\mathbf{E}_{\text{a.c.}}$ the r.m.s. value of the a.c. field and ω its radian frequency. Each term in the distribution function can be expanded in a Fourier series in time

$$f_0=f_0^0+\sqrt{2}f_0^1e^{j\omega t}+\cdots, \tag{10}$$

$$\mathbf{f}_1=\mathbf{f}_1^0+\sqrt{2}\mathbf{f}_1^1e^{j\omega t}+\cdots, \tag{11}$$

for the steady state condition. The f_0^1 term will not be retained, as solutions will be obtained only for those cases where the mechanisms for density and energy decay are so slow that neither density nor energy fluctuations can occur in an r-f cycle. If terms of the same frequency are grouped and the second harmonic terms dropped, the product of E with f_0 and f_1 gives

$$\mathbf{E}f_0=\mathbf{E}_{\text{d.c.}}f_0^0+\sqrt{2}\mathbf{E}_{\text{a.c.}}f_0^0e^{j\omega t}+\cdots, \tag{12}$$

$$\mathbf{E}\cdot\mathbf{f}_1=\mathbf{E}_{\text{d.c.}}\cdot\mathbf{f}_1^0+\mathbf{E}_{\text{a.c.}}\cdot\mathbf{f}_1^1 +\sqrt{2}[\mathbf{E}_{\text{d.c.}}\cdot\mathbf{f}_1^1+\mathbf{E}_{\text{a.c.}}\cdot\mathbf{f}_1^0]e^{j\omega t}+\cdots. \tag{13}$$

The time independent component of Eq. (7) is now given by

$$-(h_x+h_i)\nu_e f_0^0=\frac{v}{3}\left[\nabla\cdot\mathbf{f}_1^0-\frac{1}{u}\frac{\partial}{\partial u}(u\mathbf{E}_{\text{d.c.}}\cdot\mathbf{f}_1^0) -\frac{1}{u}\frac{\partial}{\partial u}(u\mathbf{E}_{\text{a.c.}}\cdot\mathbf{f}_1^1)-\frac{6m}{M}\frac{1}{u}\frac{\partial}{\partial u}\left(\frac{u^2}{l}f_0^0\right)\right]. \tag{14}$$

The time independent and first frequency components of Eq. (8) give two equations

$$0=\nu_e\mathbf{f}_1^0+v[\nabla f_0^0-\mathbf{E}_{\text{d.c.}}\partial f_0^0/\partial u], \tag{15}$$

$$0=(\nu_e+j\omega)\mathbf{f}_1^1-v\mathbf{E}_{\text{a.c.}}\partial f_0^0/\partial u. \tag{16}$$

$\mathbf{f}_1^0$ and $\mathbf{f}_1^1$ can be obtained from Eqs. (15) and (16) and substituted into Eq. (14). If we choose coordinates so that $\mathbf{E}_{\text{d.c.}}$ is directed along the z-axis, we obtain

$$-(h_x+h_i)\nu_e f=\frac{v}{3}\left\{-l\nabla^2 f+lE_{\text{d.c.}}\frac{\partial}{\partial u}\frac{\partial f}{\partial z} +\frac{E_{\text{d.c.}}}{u}\frac{\partial}{\partial u}\left(lu\frac{\partial f}{\partial z}\right)-\frac{1}{u}\frac{\partial}{\partial u}lu\left[E_{\text{d.c.}}^2+\frac{\nu_e^2}{\nu_e^2+\omega^2}E_{\text{a.c.}}^2\right]\frac{\partial f}{\partial u} -\frac{6m}{M}\frac{1}{u}\frac{\partial}{\partial u}\left(\frac{u^2}{l}f\right)\right\}, \tag{17}$$

where f is now understood to represent f_0^0.

III. A.C. AND D.C. DISTRIBUTION FUNCTIONS

Solutions will be sought for the case in which the collision frequency ν_e can be assumed to be a constant. This holds particularly well for helium and hydrogen.[3,4]

[3] A. D. MacDonald and S. C. Brown, Phys. Rev. **75**, 411 (1949).
[4] A. D. MacDonald and S. C. Brown, Phys. Rev. **76**, 1634 (1949).

The calculations to be made will consider the particular case of hydrogen for which Brode's data[5] give $\nu_e=5.93\times10^9p$ (sec.$^{-1}$) (p in mm Hg). It is then possible to introduce an effective field defined by

$$E_e^2=E_{\text{d.c.}}^2+\frac{\nu_e^2}{\nu_e^2+\omega^2}E_{\text{a.c.}}^2, \tag{18}$$

and we shall also use the letter q to represent the quantity

$$q=m/e\cdot 3m/M\cdot\nu_e^2/E_e^2 =16.17/(E_e/p)^2 \text{ (for hydrogen)}. \tag{19}$$

We shall now consider separately the equations for the pure a.c. and pure d.c. cases in order to compare the effective distribution functions for the same fields in the two cases. We can separate the distribution functions into a space times an energy function. The difference in the spatial function comes from the factor $\exp(\alpha z)$, where α is the first Townsend coefficient, in the d.c. case because of the multiplication of the electrons in their direction of motion. This differs in the a.c. case for which a solution of the diffusion equation gives $\nabla^2 f_{\text{a.c.}}=-f_{\text{a.c.}}/\Lambda^2$, where Λ is the characteristic diffusion length of the container. Substituting

$$\eta=\alpha/E_{\text{d.c.}}.$$

Equation (17) yields for the separate cases

$$0=u\frac{d^2f_{\text{a.c.}}}{du^2}+[qu+\tfrac{3}{2}]\frac{df_{\text{a.c.}}}{du} +\left[\frac{3}{2}q-\frac{u}{E_e^2\Lambda^2}-\frac{(h_x+h_i)Mq}{2m}\right]f_{\text{a.c.}}, \tag{20}$$

$$0=u\frac{d^2f_{\text{d.c.}}}{du^2}+[(q-2\eta)u+\tfrac{3}{2}]\frac{df_{\text{d.c.}}}{du} +\left[\tfrac{3}{2}q-\tfrac{3}{2}\eta+\eta^2u-(h_x+h_i)\frac{Mq}{2m}\right]f_{\text{d.c.}}. \tag{21}$$

The substitution of

$$f_{\text{d.c.}}=\varphi_{\text{d.c.}}\exp(\eta u) \tag{22}$$

yields

$$0=u\frac{d^2\varphi_{\text{d.c.}}}{du^2}+[qu+\tfrac{3}{2}]\frac{d\varphi_{\text{d.c.}}}{du} +\left[\tfrac{3}{2}q+q\eta u-(h_x+h_i)\frac{Mq}{2m}\right]\varphi_{\text{d.c.}}. \tag{23}$$

If a differential operator L is defined as

$$L=u\frac{d^2}{du^2}+[qu+\tfrac{3}{2}]\frac{d}{du}+\tfrac{3}{2}q-(h_x+h_i)\frac{Mq}{2m}, \tag{24}$$

[5] R. B. Brode, Rev. Mod. Phys. **5**, 257 (1933).

Eqs. (20) and (23) become

$$0=[L-u/E_e\Lambda^2]f_{a.c.}, \tag{25}$$

$$0=[L+\eta qu]\varphi_{d.c.}. \tag{26}$$

The term ηqu is of the order of magnitude of $10^{-5}u$. Since this is much smaller than other terms in L, it can be dropped.

$$0=L\varphi_{d.c.}. \tag{27}$$

Equations (25) and (27) demonstrate that $f_{a.c.}=\varphi_{d.c.}$ when $E_e\Lambda$ is very large. This corresponds to a range of small E_e/p. In this range, however, η is very small as well. From Eq. (22), we deduce that

$$f_{d.c.}=f_{a.c.}, \tag{28}$$

and the quantities D, μ, and ν become identical for the a.c. and d.c. cases.

When E_e/p is large a comparison of $f_{d.c.}$ with $f_{a.c.}$ requires solutions for the distribution functions. Solutions have already been obtained for the a.c. case[4] and what is now required are solutions for the d.c. case. We shall treat separately from the higher energy part of the function that part of the distribution function below 8.9 volts where $h_x+h_i=0$.

When $u<8.9$ volts, MacDonald and Brown[4] found the solution for the a.c. case in terms of confluent hypergeometric functions. The d.c. equation can be solved by substituting

$$\varphi_{d.c.}=\psi_{d.c.}\exp(-\tfrac{1}{2}qu) \tag{29}$$

into Eq. (27) to give

$$\frac{d^2\psi_{d.c.}}{du^2}+\frac{\frac{3}{2}}{u}\frac{d\psi_{d.c.}}{du}+\left[\frac{\frac{3}{4}}{u}q-\frac{q^2}{4}\right]\psi_{d.c.}=0. \tag{30}$$

Since q^2 is extremely small for E_e/p large, the term in q^2 may be dropped to give

$$\frac{d^2\psi_{d.c.}}{du^2}+\frac{\frac{3}{2}}{u}\frac{d\psi_{d.c.}}{du}+\frac{\frac{3}{4}}{u}q\psi_{d.c.}=0. \tag{31}$$

The solutions of Eq. (31) are given by

$$\psi_{d.c.}=u^{-\frac{1}{4}}[\sin(3qu)^{\frac{1}{2}}+H\cos(3qu)^{\frac{1}{2}}] \tag{32}$$

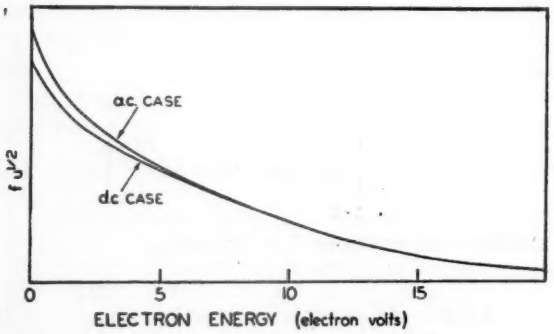

FIG. 1. Comparison of a.c. and d.c. energy distribution functions at $E_e/p=100$ for hydrogen.

giving

$$f_{d.c.}=u^{-\frac{1}{4}}[\sin(3qu)^{\frac{1}{2}}+H\cos(3qu)^{\frac{1}{2}}]\exp(\eta-\tfrac{1}{2}q)u. \tag{33}$$

When $u>8.9$ volts, the excitation terms become very important. MacDonald and Brown[4] have shown for the a.c. case that an asymptotic expansion

$$f_{a.c.}=Du^T\exp(-su)[1+d/u+\cdots] \tag{34}$$

can be used for this part of the function, where

$$\begin{aligned}T&=(B/2A)-\tfrac{3}{4},\\ s&=(A+1/2b)qb,\\ d&=(B/qb4A^2)(1-B/2A),\\ b&=[1+(2/qE_e\Lambda)^2]^{\frac{1}{2}},\\ A&=[(Mh_1/2mqb^2)+\tfrac{1}{4}]^{\frac{1}{2}},\\ B&=[(Mh_1u_x/2m)+\tfrac{3}{4}]/b,\end{aligned}$$

and the excitation-plus-ionization function has been approximated by

$$\begin{aligned}h_x+h_i&=h_1(u-u_x)\\ &=9.0\times10^{-3}(u-8.9)\text{ (for hydrogen)},\end{aligned}$$

where u_x is the excitation potential.

Since the excitation term completely dominates the equation for $f_{a.c.}$, Eq. (34) serves equally well for $f_{d.c.}$ for the same E_e/p. That this is correct was checked in the following manner. From Eqs. (25) and (27), we see that $\varphi_{d.c.}$ and $f_{a.c.}$ are identical if $\Lambda\to\infty$. $\varphi_{d.c.}$ determined in this manner determines $f_{d.c.}$ with the aid of Eq. (22). The distribution function $f_{d.c.}$ so obtained agrees with Eq. (34) within 0.5 percent at $E_e/p=70$ and within 1 percent at $E_e/p=100$ for energies up to 20 volts. This is sufficiently accurate for our purposes. There are so few electrons at higher energies that they have little bearing on integrals over the distribution function.

The constants D and H are adjusted to join solution (34) smoothly with solution (33) at the patching point[4] $u_p=9.5$ volts.

$$H=\frac{1-2(u_p/3q)^{\frac{1}{2}}\left[\dfrac{qb}{\Phi}+\dfrac{1}{2u_p}+\dfrac{q}{2}-\eta\right]\tan(3qu_p)^{\frac{1}{2}}}{2(u_p/3q)^{\frac{1}{2}}\left[\dfrac{qb}{\Phi}+\dfrac{1}{2u_p}+\dfrac{q}{2}-\eta\right]+\tan(3qu_p)^{\frac{1}{2}}},$$

$$D=\frac{u_p^{-\frac{1}{4}}[\sin(3qu_p)^{\frac{1}{2}}+H\cos(3qu_p)^{\frac{1}{2}}]\exp(\eta-\frac{1}{2}q)u_p}{u_p^T\exp(-su_p)(1+d/u_p+\cdots)},$$

where

$$qb/\Phi=[df/fdu]_{u=u_p}.$$

IV. IONIZATION COEFFICIENTS

We are now able to determine ζ_e and η from the distribution functions. The effective a.c. ionization coefficient ζ_e is defined by

$$\zeta_e=\nu_{a.c.}/D_{a.c.}E_e^2,$$

where the subscripts a.c. refer to the fact that such quantities are to be calculated from $f_{a.c.}$. This quantity is equal to $1/\Lambda^2E_e^2$ for breakdown in the a.c. case. Experimental values of $1/\Lambda^2E_e^2$ determine ζ_e.

The first Townsend coefficient η can be calculated as well. The number of ionizations per centimeter of electron drift α is $\nu_{d.c.}/\mu_{d.c.}E_{d.c.}$ since $\mu_{d.c.}E_{d.c.}$ is the drift velocity. Thus,

$$\eta=\nu_{d.c.}/\mu_{d.c.}E_{d.c.}^2,$$

where the subscripts d.c. refer to the fact that such quantities are to be calculated from $f_{d.c.}$. If we divide η by ζ_e, for the same value of E_e ($E_{d.c.}$ is the effective field for the d.c. case) in both cases, we obtain

$$\eta/\zeta_e=\nu_{d.c.}D_{a.c.}/\nu_{a.c.}\mu_{d.c.}. \tag{35}$$

The ionization rate $n\nu$ can be calculated[6] from the formula

$$n\nu=-8\pi(e/m)^2\int_{u_i}^{\infty}(u/v)\nu_c h_i f du,$$

where u_i is the lowest ionization potential. Since $f_{a.c.}=f_{d.c.}$ for the complete range of integration, it follows that

$$n_{a.c.}\nu_{a.c.}=n_{d.c.}\nu_{d.c.}. \tag{36}$$

The coefficient of mobility of electrons μ is given by

$$\mu=-\frac{1}{n}\int_0^{\infty}\frac{lv}{3}4\pi v^2\frac{\partial f}{\partial u}dv. \tag{37}$$

This equation can be integrated by parts to give

$$\mu=\frac{1}{n}\frac{e}{m}\int_0^{\infty}\frac{1}{\nu_c}4\pi v^2 f dv. \tag{38}$$

Since

$$n=\int_0^{\infty}4\pi v^2 f dv=2\pi(2e/m)^{\frac{1}{2}}\int_0^{\infty}u^{\frac{1}{2}}f du \tag{39}$$

and ν_c is a constant, Eq. (38) becomes

$$\mu=e/m\nu_c$$

whether we use $f_{a.c.}$ or $f_{d.c.}$. Thus μ without subscript serves both a.c. and d.c. cases.

When ζ_e and η are small, as was discussed previously for low E_e/p, $f_{a.c.}$ and $f_{d.c.}$ become identical so that $\nu_{d.c.}=\nu_{a.c.}$, in which case

$$\eta/\zeta_e=D/\mu. \tag{40}$$

For larger E_e/p, we now can determine the ratio $\nu_{d.c.}/\nu_{a.c.}$.

From Eq. (39), we see that the contribution to n in any energy interval is $u^{\frac{1}{2}}f$. This quantity (unnormalized) is plotted in Fig. 1 for $E_e/p=100$ volts/cm-mm Hg for both the a.c. and d.c. functions. There are about 5 percent fewer electrons in the low energy range for the d.c. than for the a.c. case. From Eq. (36), we see that this implies that $\nu_{d.c.}\cong 1.05\nu_{a.c.}$. This fact has a physical interpretation. In the d.c. case the density varies as $\exp(\alpha z)$. This dependence makes for large density gradients which allow fast electrons to diffuse back into the gas against the d.c. field, while those which are swept out by the field are drawn equally from all energy levels. The larger number of higher energy electrons contributes to the increased ν.

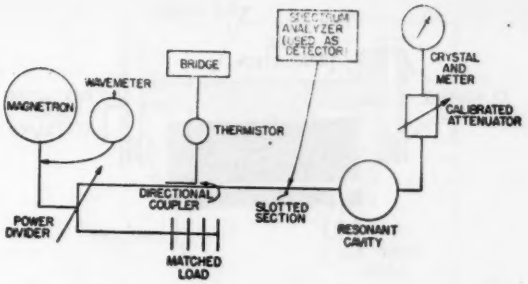

FIG. 2. Block diagram of the experimental apparatus.

In a similar way it can be shown that the diffusion coefficient calculated from $f_{d.c.}$ varies less than 5 percent from that calculated from $f_{a.c.}$. Since experimental errors in determinations of η and ζ_e are frequently larger than 10 percent, Eq. (40) can be taken to be sufficiently accurate for $E_e/p<100$ volts/cm-mm Hg.

From the integrals for D and the average energy $\bar{u}$

$$D=\frac{1}{n}\int_0^{\infty}\frac{lv}{3}4\pi v^2 f dv,\quad \bar{u}=\frac{1}{n}\int_0^{\infty}\frac{mv^2}{2e}4\pi v^2 f dv.$$

A comparison with Eq. (38) shows

$$D/\mu=\tfrac{2}{3}\bar{u}, \tag{41}$$

when ν_c is a constant. Hence D/μ is a direct measure of the average energy of the electrons. Even when ν_c is not a constant, Eq. (41) holds reasonably well. For a Druyvesteyn[7] distribution, $D/\mu=0.763\bar{u}$, while for a Maxwellian distribution we have again, $D/\mu=\frac{2}{3}\bar{u}$, whatever the dependence of ν_c on energy.

V. THE A.C.-D.C. BREAKDOWN CONDITION

The gas in a cavity will break down when the losses of electrons to the walls of the cavity are replaced by ionization in the body of the gas. When an a.c. field alone is applied, electrons are lost by diffusion. When a small d.c. sweeping field is applied, electrons are lost both by diffusion and mobility. The breakdown condition can be formulated mathematically by a consideration of these processes.

The flow of electrons Γ is given by

$$\Gamma=-n\mu\mathbf{E}_{d.c.}-D\nabla n. \tag{42}$$

When the electrons that are lost are replaced by new

[6] Formula (16), reference 4.

[7] M. J. Druyvesteyn, Physica **10**, 69 (1930).

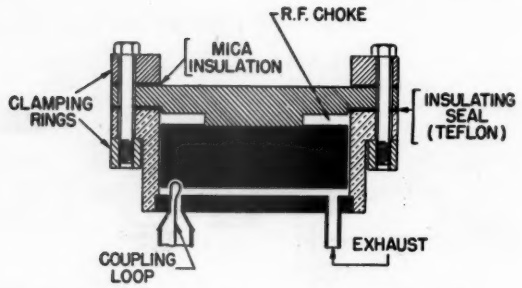

FIG. 3. Schematic diagram of the resonant cavity.

ones resulting from ionization,

$$\nabla\cdot\Gamma=\nu n. \tag{43}$$

If the divergence of Eq. (42) is equated to νn, and $\mathbf{E}_{d.c.}$ is directed along the z axis, we obtain

$$\nabla^2 n+\frac{E_{d.c.}}{D/\mu}\frac{\partial n}{\partial z}+\nu n=0. \tag{44}$$

Equation (44) can be solved readily for the case of a cylinder of axial height L and axial coordinate z, radius R and radial coordinate r. Rigorous boundary conditions require the concentration to be small at a boundary and to extrapolate to zero outside the boundary at a distance of the order of a mean free path. In the range of pressures to be considered, the mean free path is very small compared to cavity dimensions and the condition of zero concentration on the cylinder walls is imposed.

By separation of variables,

$$n=M(r)N(z),$$

we obtain two equations

$$\nabla_r^2 M+k_1^2 M=0,$$

$$\frac{d^2N}{dz^2}+\frac{E_{d.c.}}{D/\mu}\frac{dN}{dz}+\left(\frac{\nu}{D}-k_1^2\right)N=0, \tag{45}$$

where k_1^2 is the separation constant and ∇_r^2 the two-dimensional Laplacian in the plane perpendicular to z. The solutions are

$$M=\text{const. } J_0(k_1 r), \tag{46}$$

$$N=\text{const. } \sin(\pi/L)z\cdot\exp(-\mu E_{d.c.}z/2D), \tag{47}$$

where $k_1=2.404/R$ and J_0 is the zero-order Bessel function. The exponential represents the deformation of the sine caused by the sweeping of electrons. This solution is subject to the condition

$$\nu/D=1/\Lambda_{d.c.}^2, \tag{48}$$

where $\Lambda_{d.c.}$ defines a modified diffusion length given by the relation

$$1/\Lambda_{d.c.}^2=1/\Lambda^2+[E_{d.c.}/(2D/\mu)]^2. \tag{49}$$

For this case, the characteristic diffusion length is given by

$$1/\Lambda^2=(\pi/L)^2+(2.404/R)^2. \tag{50}$$

The only difference between the breakdown condition (48) in the a.c.–d.c. case and the pure a.c. case is the substitution of a modified diffusion length $\Lambda_{d.c.}$ for the characteristic diffusion length Λ. It will be noted that the modified diffusion length of a cavity is smaller than the characteristic diffusion length. A cavity whose electron losses are increased by a d.c. sweeping field is equivalent to a smaller cavity without a sweeping field.

VI. USE OF BREAKDOWN CONDITION IN DETERMINING D/μ

If we divide Eq. (48) by E_e^2, we obtain

$$\nu/DE_e^2=1/\Lambda_{d.c.}^2E_e^2. \tag{51}$$

When an a.c. field alone is applied, this quantity defines the effective a.c. ionization coefficient ζ_e previously considered. A curve of ζ_e is obtained from a.c. breakdown measurements alone by plotting $1/\Lambda^2E_e^2$ *versus* E_e/p. Equation (51) shows that this plot is the same as for $1/\Lambda_{d.c.}^2E_e^2$. If an a.c.–d.c. breakdown is observed at a given E_e/p, it is then possible to obtain the appropriate ζ_e from data taken with pure a.c. breakdown. The ζ_e so obtained is equated to $1/\Lambda_{d.c.}^2E_e^2$ and $\Lambda_{d.c.}$ is obtained. From the definition of $\Lambda_{d.c.}$, Eq. (49), D/μ is obtained. The implicit assumption that the distribution function of electrons is the same for the a.c.–d.c. case as for the a.c. case alone is best understood from the similarity of the extreme cases of d.c. field and a.c. field alone.

VII. EXPERIMENTAL PROCEDURE

A block diagram of the experimental apparatus for observing a.c.–d.c breakdown is shown in Fig. 2. A continous-wave tunable magnetron in the range of

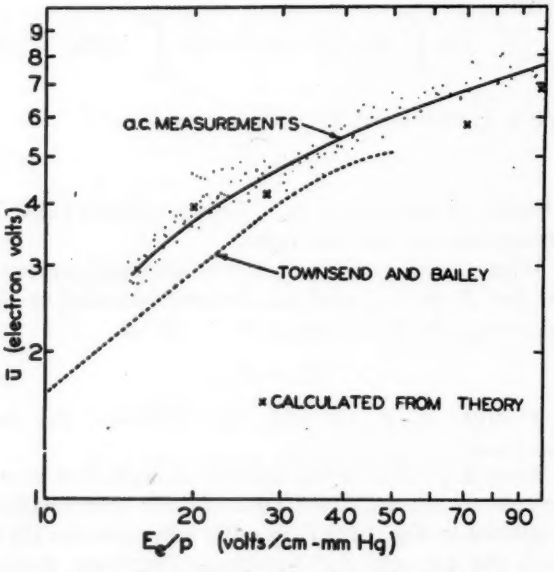

FIG. 4. Comparison of theory and experiments for the average electron energy.

10-cm wave-length supplies power to a coaxial line. For wave-length determinations, a probe in the coaxial line is connected to a cavity wave meter. A power divider provides a continuously variable control over the fraction of the power incident on the cavity, unused power being dissipated in a matched load. A known fraction of the power incident on the cavity is coupled from the line by a directional coupler to a power measuring thermistor and associate measuring bridge. A probe and slotted section in the coaxial line permit measurements of the standing wave pattern in the line immediately ahead of the cavity. Measurement of the standing wave ratio and voltage minimum as a function of frequency permits calculation of the cavity Q as well as the fraction of the incident power that is actually absorbed by the cavity. For convenience the power transmitted through the cavity is calibrated in terms of the incident power.

Figure 3 shows an oxygen-free-copper resonant cavity which can be outgassed and which permits the application of a d.c. field to the discharge region. The r-f field configuration is identical with a cylindrical TM_{010}-mode cavity of $\frac{1}{16}$ in. separation with the exception that there is a d.c. break around the diameter backed up by an r-f choke. The output loop is not shown. An insulating gasket made of sheet Teflon served to position the inner cavity assembly and to make the vacuum seal. The flanges were clamped together on the gasket with clamping rings and bolts made of No. 303 stainless steel to match the expansion of the copper. This arrangement permitted baking the cavity at 290°C.

The field within the cavity was determined by constructing an identical cavity structure provided with a small axial plug which could be inserted into the cavity. By observing the change in resonant frequency with plug insertion, after the method of Slater,[8] the relationship between the stored energy in the cavity and the square of the electric field at the point of insertion of the plug was determined. From the cavity Q and the power absorbed by the cavity, the field could be calculated. The field determinations were accurate to about 8 percent.

Measurements of D/μ converted to average energy of electrons have been carried out for hydrogen. The cavity was outgassed for a week at 290°C. Two liquid air traps were employed. With the vacuum system isolated from the oil diffusion pump by a stopcock, the system held at a pressure of the order of 3×10^{-7} mm Hg for over an hour as measured by an ionization gauge. Spectroscopically pure hydrogen was used. Figure 4 gives values of average energy as a function of E_e/p. The experimental error is approximately 8 percent. The broken curve was obtained by Townsend and Bailey[9] by observing the lateral diffusion of an electron beam moving in a uniform d.c. field. Theoretical values of average energy were calculated here from the distribution functions. The measurements were taken for only those pressures where the mean free path was much smaller than the cavity size.

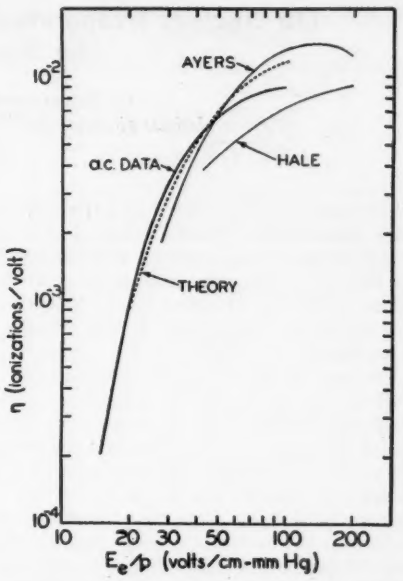

FIG. 5. Comparison of theory and experiments for the first Townsend ionization coefficients in hydrogen.

From the observed value of D/μ and ζ_e, the first Townsend coefficient η is calculated and plotted in Fig. 5 (it is shown as a smooth curve, since it was determined from two smooth curves); the maximum experimental error in this curve is about 20 percent. Theoretical values of η determined from those points for which the average energy was calculated are shown. It is seen that the present data are in substantial agreement with previous data of Ayers[10] and Hale.[11]

The authors wish to acknowledge the many valuable ideas contributed by Professor W. P. Allis in numerous discussions of the problems involved in this paper.

[8] J. C. Slater, Rev. Mod. Phys. 18, 441 (1946), Eq. (III.89).

[9] J. S. Townsend and V. A. Bailey, Phil. Mag. 42, 873 (1921).

[10] T. L. R. Ayers, Phil. Mag. 6, 23, 353 (1923).

[11] D. H. Hale, Phys. Rev. 55, 815 (1939); values of α/p *versus* E/p are given by L. B. Loeb, *Fundamental Processes of Electrical Discharges in Gases* (John Wiley and Sons, Inc., New York, 1939), p. 356.

On Nuclear Evaporation in Cosmic Rays and the Absorption of the Nucleonic Component. II.*

G. BERNARDINI,** G. CORTINI, AND A. MANFREDINI
Istituto di Fisica dell'Università, Centro di Fisica Nucleare, Roma, Italy
(Received May 29, 1950)

The nuclear evaporations produced by cosmic rays at 3500 m altitude were studied using Ilford C2 and Kodak NT4 plates. The results are discussed in comparison with the results obtained in Berkeley for stars produced by nucleons of controlled energies and with some of the data furnished by the Bristol and Brussels groups. The results are as follows. (1) The frequency of stars *versus* the number of prongs does not change very much in the transition between air and condensed materials. (2) The small transition effect observed in lead is concentrated in the first few cm of the lead and is restricted to the small stars. (3) For greater thicknesses (of the order of the nucleon-nuclei geometrical range) the differences between paraffin and lead seem to be negligible. (4) The differences between the Berkeley and the cosmic ray stars are concentrated in the large stars (more than six prongs), in agreement with the fact that a large fraction of cosmic ray stars (about 80 percent) are produced by secondary nucleons having energies not exceeding some hundreds of Mev. (5) The prongs of the small stars (less than six prongs) produced by cosmic rays show an angular distribution around the vertical which is, at least qualitatively, that which must be expected from the Berkeley results. (6) The large stars show an isotropic distribution in the heavy prongs but not in the "grey" ones, and a correlation between the number of grey and the number of black prongs seems to be evident. On the average, every grey prong is accompanied by about 3.5 black prongs. (7) The energy spectrum of the black proton- and alpha-prongs is given with a statistic based on about 4000 stars. The average excitation energy associated with every black prong is about 35 Mev; the average nuclear excitation corresponding to the black prongs emission is about 150 Mev. (8) A comparison of the experimental proton spectrum with the Weisskopf-Bagge theory seems to show satisfactory agreement, assuming a value for the Gamow barrier of about five Mev. (9) Similarly, the alpha-spectrum is in fairly good agreement with the evaluations of Le Couteur. (10) Some conclusions concerning the nuclear evaporations and the nucleonic cascade are discussed.

I. INTRODUCTION

In a previous issue[1] (Part I) some features of the behavior of the nucleonic component were examined in connection with quantitative results obtained by studying the stars produced by cosmic rays in sensitive emulsions. It was pointed out that these features seemed to indicate the existence of a fairly close correlation between the star population and the locally-produced penetrating showers. Perhaps today this correlation does not appear to be so close because Cocconi's data in lead were originally uncorrected,[2] but nevertheless it remains, and its origin in the *nucleonic cascade* becomes more and more obvious. From this correlation and from the general information collected so far on the behavior of the nucleonic component,[3] it is evident that in the intermediate atmosphere or in sufficiently thick layers of certain materials, the fast nucleons are accompanied by a large retinue of slow ones, which they have produced through a series of processes occurring as they move along. The *intermediate* stage of this nucleonic cascade (which is initiated in the high atmosphere by primary protons and heavy particles, and terminated by slow neutrons distributed in the atmosphere) is characterized by the production of these rather slow nucleons which are no longer efficient in the production of fast mesons and which lose their energy mainly through induced nuclear evaporations and ionization.

As we mentioned in Part I, there is some direct evidence of the existence of this large retinue of rather slow nucleons, particularly in the work of Adams *et al.*[4] Recently other direct information about this point was given by Conversi.[5] Conversi's data, in agreement with the figures given by Adams *et al.*, indicate the presence in the atmosphere of a large proportion of protons having energies $\sim$0.5 Bev. The decrease in the intensity of such a proton component in the atmosphere is given by an absorption thickness between 140 and 150 g/cm^2, in agreement with the behavior of the stars observed in plates or in ionization chambers. Further, these slow protons observed by Conversi show the same latitude effect as the burst intensity[6] and as the intensity of the *slow neutron component*.[7]

As we also indicated in Part I, the number of these rather slow nucleons must be somewhat high in comparison with that of the residual nucleons which have energies $\geqslant 1$ Bev and which are very efficient in the production of the penetrating showers usually observed. Because it is practically certain (see below) that an extremely large fraction of bursts are due to the nuclear stars, and that the stars are the sources of the slow neutrons and (at least under 200 g/cm^2) are in equilibrium with them, it is quite reasonable to associate the stars themselves with slow nucleons like those observed by Conversi. At the same time, the shape of

* A previous account of this paper was given at the Como conference, September 1949, to be published in Nuovo Cimento.
** Now Visiting Professor of Physics, Columbia University, New York.
[1] Bernardini, Cortini, and Manfredini, Phys. Rev. **76**, 1792 (1949).
[2] G. Cocconi, Phys. Rev. **75**, 1074 (1949).
[3] W. B. Fretter, Phys. Rev. **76**, 511 (1949); Lovati, Mura, Salvini, and Tagliaferri, Nuovo Cimento **6**, 207 (1949); B. Gregory and J. Tinlot, kindly communicated by the authors.
[4] Adams, Anderson, Lloyd, Rau, and Saxena, Rev. Mod. Phys. **20**, 334 (1939).
[5] M. Conversi, Phys. Rev. **79**, 749 (1950).
[6] White and Coor, kindly communicated by Prof. Reynolds.
[7] Simpson, Phys. Rev. **73**, 1389 (1948); L. Yuan, Phys. Rev. **74**, 504 (1948).

TABLE I. Transition effects for cosmic ray stars under a lead absorber.

No. of prongs	Stars/cm³/day Without absorber	Under two cm of lead	Number expected under two cm of lead
3	5.04±0.28	6.80±0.39	4.70
4	4.11±0.25	4.60±0.32	3.84
5	1.91±0.17	1.89±0.20	1.78
⩾6	3.07±0.22	2.80±0.25	2.85
Total	14.22±0.48	16.10±0.60	13.30

the energy spectrum of these slow nucleons is suggested by the proton spectrum at 30,000 feet (energy range ~100 to 1000 Mev) given by Adams *et al.*[4] It is characterized by a very peaked maximum around 200 Mev, and shows that these nucleons between 100 and 1000 Mev have an average energy of about 300 Mev.

Consequently, we should be lead to consider a large fraction of the nuclear evaporations produced by cosmic rays as the close relatives of those observed in the Berkeley experiments.[8] In the next paragraphs we shall examine in some detail the features of the cosmic ray stars, with the intention of analyzing their origin and properties and their peculiar differences from the stars of the Berkeley experiment.

II. THE NUMBER OF STARS *VERSUS* PRONGS DISTRIBUTION

A

A first rough classification of the stars is usually made on the basis of the frequency of stars *versus* the number of prongs. In our experiments we exposed the plates either in the open air (supported by materials of different atomic number) or under layers of different materials like Pb, Al, C, paraffin. Concerning the lead, our results are in very close agreement with our own previous results[9] and with those of George and Jason.[10]

The results indicate that at 3500 m altitude no large transition effects are observable concerning the frequency of the stars *versus* multiplicity of prongs. However, in lead a transition effect is evident. It is due to the stars of small size (3 to 4 prongs)[11] and is evident just within the first absorption thickness. For thicknesses greater than five cm the star population seems to decrease regularly following an exponential law.[1] The transition effect is clearly shown in Table I, where in the last column are given the values which must be expected with an exponential absorption[1] (absorption thickness $L=300$ g/cm²). For many reasons, which will be discussed in Part III, its origin is not completely clear (see note added in proof). Perhaps a small transition effect is present also in the plates exposed under paraffin, but if so it shows quite a different behavior. Table II shows the values for the paraffin absorber. The expected values, estimated assuming an exponential absorption with[12] $L=200$ g/cm², are given in parentheses.

TABLE II. Effect of a paraffin absorber on the production of cosmic ray stars.

Paraffin thicknesses (in cm) / Number of heavy prongs	Stars/cm³/day 0	~25	~45	~58
3	6.7 ±0.4	6.9 ±0.5 (6.0)	7.2±0.4 (5.5)	6.3±0.3 (5.3)
4	5.1 ±0.3	4.5 ±0.4 (4.6)	5.0±0.3 (4.2)	4.3±0.3 (4.1)
All stars	1.81±0.65	17.35±0.65 (16.3)	18.6±0.65 (15.0)	16.1±0.64 (14.5)

At the moment we would like to observe that at an altitude of 3500 m *the transition effects are quite small*[13] (Fig. 1). As is shown by Fig. 2, the stars *vs.* prongs distributions appear to be practically the same in different materials at thicknesses of the order of the geometrical absorption thicknesses, and not much different from the distributions observed in the plates

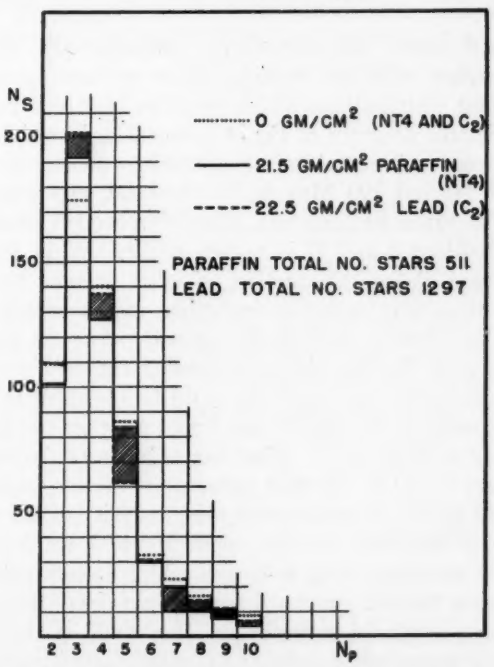

FIG. 1. Transition effects with lead and paraffin absorbers in the distributions of the number of stars N_s having N_p prongs. The histograms are all normalized to the same area (600 stars). The cross-hatched blocks indicate the differences between the lead and paraffin absorbers. The number of small stars (three to four prongs) is possibly relatively larger with lead than with paraffin, and this may be connected with the transition effect.

[8] E. Gardner and V. Peterson, Phys. Rev. **75**, 364 (1949); E. Gardner, Phys. Rev. **75**, 379 (1949).
[9] Bristol's cosmic rays symposium, 1948; Como conference, 1949.
[10] George and Jason, Proc. Phys. Soc. London **62**, 243 (1949).
[11] G. Cortini and A. Manfredini, Nature **163**, 991 (1949).
[12] This value is given for ice by Harding *et al.* (see Part I).
[13] This is not true at high altitudes, near the top of the atmosphere (see below).

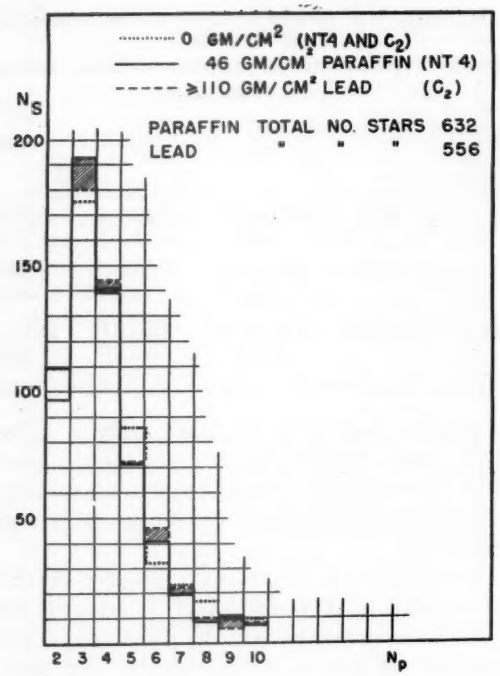

FIG. 2. The distributions of the number of stars N_s having N_p prongs, for larger thicknesses of lead and paraffin absorbers (see Fig. 1). The histograms are normalized to the same area (600 stars).

exposed above the absorbers. Consequently, for a comparison with the Berkeley stars, we first total the different distributions which we have observed in the logarithmic diagram of Fig. 3 (curve II), in which the data concerning the stars produced by deuterons between 90 and 190 Mev in the Berkeley experiments[8] are also reported (curve I). The difference between the distributions I and II is rather marked. While in the Berkeley plates the number of stars present having *more* than five prongs is negligible, in the cosmic ray stars at 3500 m altitude *it represents about 20 percent of the total.* At first sight, comparing curves I and II, one can guess that curve II could be obtained by the superposition of a curve like I and another composed mainly of large stars. After the arguments developed in Part I and in the first paragraphs of this paper, it should be easy to understand this analysis[14] of curve II. Most of the small stars are connected with the fraction of the star-producing radiation which is composed of nucleons (mainly neutrons) having energies of the order of those produced in Berkeley. The "tail" of the large stars is essentially produced by cosmic ray nucleons of higher energies. This perhaps obvious conclusion is emphasized by some recent results obtained at Berkeley with protons of different energies.[15] From these results it is clear that the distributions of the number of stars *versus* the number of prongs are not very sensitive to the value of the energy of the incident protons, at least between about 200 and 350 Mev.

This conclusion is in agreement with the theoretical expectations.[16] On the contrary, the quite large fraction of stars having more than five prongs has no obvious explanation, because the *average* value of the energy released by a *single nucleon* crossing a heavy nucleus without originating any radiative process (emission of mesons) is of the order of 100 Mev, and depends essentially on the range of nuclear forces, and for energies $\gg$100 Mev, very little on the energy of the incident nucleons.[17] However, as Wouthuysen suggests,[18] the difference can be explained at least partially by

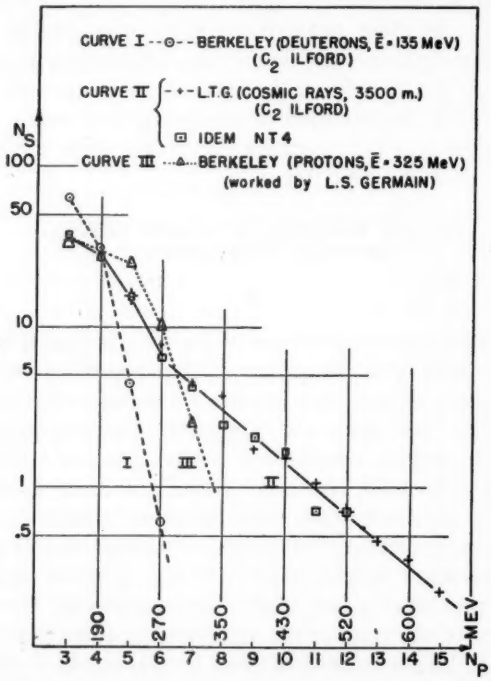

FIG. 3. Comparison between the cosmic ray star distributions and those obtained in the Berkeley experiments. Curve I was obtained from the data of Gardner and Peterson (reference 8) which correspond to 781 stars, and Curve III from the data of L. S. Germain with a total of 290 stars. Curve II corresponds to 5270 stars obtained in C2 plates and to 1870 stars in NT4 plates. The figures given above the axis of the abscissae are the values of the excitation energies as estimated by Le Couteur as a function of the total number of observable prongs (see Sec. IIIE).

[14] We should like to add that in a paper by A. Page, which is not yet published (see reference 22) the division of curve II in Fig. 3 (Page's distribution is in excellent agreement with ours) into two branches is interpreted in a rather different way. That is, by considering that it is due essentially to the contribution of stars produced in light nuclei. In our opinion this is only partly true, because the Berkeley stars are produced in heavy as well as light nuclei and show a different behavior. Furthermore, the curves obtained in the same type of plates for stars observed at very high altitudes (Minneapolis group, Rochester group, Lord and Schein) do not show the two branches appreciably.

[15] The measurements were taken by Dr. L. S. Germain, and were kindly communicated to us by Dr. E. Gardner and Dr. F. Adelman.

[16] W. Horning and L. Baumhoff, Phys. Rev. **75**, 370 (1949).

[17] Above 200 Mev, for a nucleon crossing a nucleus ($A \simeq 100$) and undergoing only elastic or quasi-elastic collisions, the energy release should decrease with increasing energy and should approach a limit that is certainly no larger than about 100 Mev. (Bagge, Ann. d. Physik (V) **39**, 512 (1941); **39**, 535 (1941); Zwanikken, Physica **14**, 530 (1948).)

[18] S. A. Wouthuysen, Phys. Rev. **75**, 1329(A) (1949).

TABLE III. Numbers of stars, $N(s, l)$, having a total of s prongs, with l proton prongs in the approximate energy range 80 to 300 Mev.

No. of prongs	$N_S=\Sigma N(s,l)$ $l=0,1,2\cdots$	$N(s,1)$	$N(s,2)$	$N(s,3)$	$N(s,\geqslant 4)$	$\frac{N(s,1)}{N_S}$	$\frac{N(s,\geqslant 2)}{N_S}$	$\frac{N(s,>1)}{N_S}$
3	369	37	2	—	—	0.10	0.005	0.10
4	319	56	12	—	—	0.17	0.04	0.21
5	179	48	18	2	1	0.27	0.12	0.38
6–7	155	37	14	4	1	0.31	0.11	0.42
8–9	44	12	7	3	2	0.3	0.3	0.6
10	74	27	20	8	5	0.35	0.45	0.80

considering, on the basis of the recent nucleon-nucleon scattering experiments,[19] the probability of *knock-on* nucleon-nucleon collisions with a rather high momentum transfer, and the production of recoil nucleons in the inelastic nucleon-nucleon collisions. As a matter of fact, in this way the expected relative yield of differently-pronged, large stars can be deduced from the probability that one or more nucleons (let us say either nuclear δ-rays or recoil nucleons) of energies appreciably greater than 20 Mev ($\sim$Fermi's limit) can be produced inside a nucleus crossed by a fast nucleon. The evaluations made by Wouthuysen (taking into account the energy spectrum of primaries) and, similarly, those made using the Monte Carlo method by Goldberger[20], for energies around[21] 100 Mev, predict a rather high number of primary knock-on and inelastic collisions *inside* the Ag and Br nuclei. According to Wouthuysen, of 100 fast nucleons (energy spectrum $f(E)=E^{\gamma}$ with $2.5\lesssim\gamma\lesssim 3$, magnetic cut-off at $E_0\simeq 3.5$ Bev) crossing a nucleus approximately 20 percent do not give rise to any process, 15 percent give rise to a secondary process, 30 percent to two secondaries, and 35 percent to three or more. These figures, on account of the rather arbitrary hypothesis introduced on the nature of collisions[22] in the spectrum of the primaries, etc., could give us, of course, only an order of magnitude of the expected number of processes, and essentially they must be used to indicate the manner in which a part of the large stars could be explained.

The fast secondary nucleons produced after the bombardment of the nucleus escape immediately from the nucleus itself, but as their number increases the average energy excitation of the residual nucleus also increases, because colliding with other nucleons before escaping they contribute to the excitation itself. In this way it is possible to explain qualitatively the *average* excitation energies larger than about 200 Mev.

As has been mentioned already, in addition to the knock-on nucleons (δ-nucleons), the recoil nucleons produced in a radiative nucleon-nucleon collision are able to produce stars of large size. In this case the evaporation process follows the emission of mesons. Thus, neglecting for the moment the probable local interactions of the mesons themselves, the meson emission from nuclei of rather high atomic number *should* be accompanied by stars having, on the average, a size larger than those produced by nuclei crossed by a single nucleon.

The data reported by the Bristol[23] and Brussels[24] groups indicate that no more than about 25 percent of the stars having *more* than five prongs show meson emission (it may be better to say they emit relativistic particles)[25] at 3500 m. For instance, the Bristol authors

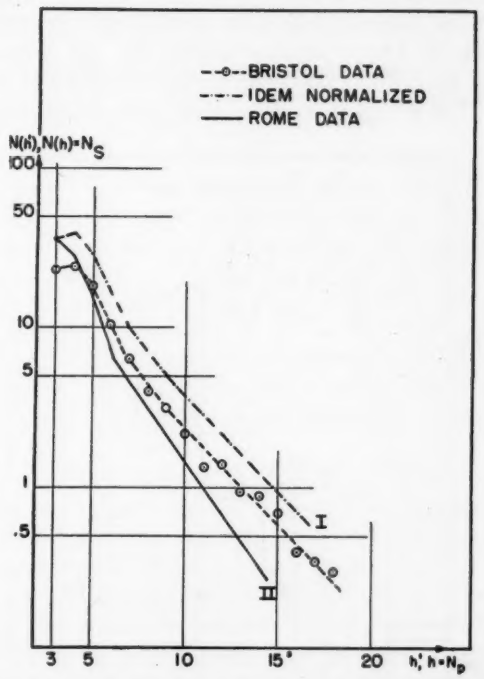

FIG. 4. Comparison between the star distributions as obtained by the Bristol and Rome groups. Curve I shows the data of the Bristol group for the number of stars *vs.* the number of heavy plus grey prongs, while Curve II shows the data of the Rome group for the number of stars *vs.* the number of heavy prongs, for stars produced by cosmic rays at 3500 meters. The Bristol data are also shown normalized to the Rome data at the points corresponding to stars of three prongs.

[19] Hadley, Kelly, Leith, Segrè, Wiegand, and York, Phys. Rev. 75, 351 (1949).
[20] M. L. Goldberger, Phys. Rev. 74, 1269 (1948).
[21] In order to obtain the order of magnitude of the probabilities for one or more elastic nucleon-nucleon collisions, Goldberger's results should be extrapolated to higher energies. This involves some difficulties which will be discussed later.
[22] Wouthuysen distinguishes in a very crude way the elastic from the inelastic collisions.
[23] Brown, Camerini, Fowler, Heitler, King, and Powell, Phil. Mag. (VII) 40, 862 (1949).
[24] Cosyns and Occhialini, Como conference, September 1949. To be published in the Nuovo Cimento.
[25] Dr. Powell, in a private communication, kindly informs us that there is evidence that the relativistic prongs for momenta between 300 and 700 Mev/c are, in a very large fraction ($\sim$90

TABLE IV. Angular distribution of the tracks of fast recoil protons from stars.

ϑ(deg)	0–30	30–60	60–90	90–120	120–150	150–180
n	59	63	58	60	112	139

observe for $Nh \geqslant 6$ stars, 419 stars of the type $\geqslant 1_p{}^n$ and 1226 of $0_p{}^n$, and most of the $1_p{}^n$ stars are *not* connected with the emission of mesons.

According to our statistics (Fig. 3), the stars at 3500 m altitude having more than five prongs comprise about 20 percent of the total star population. Consequently, *more than ten percent of the total star population is composed of stars having more than five prongs and not connected with the visible production of relativistic particles.*[26] They must be associated with knock-on collisions or with other not quite evident processes caused by rather energetic particles but not associated with the nuclear emission of mesons.

B

To check this conclusion, and to obtain in this way a clearer view of the star structure, we had to try to detect, in plates exposed to cosmic rays at 3500 m altitude (L.T.G.), protons emitted by the stars and having energies in the approximate range 80 to ~300 Mev. The β-sensitive plates were not completely developed. To calibrate their sensitivity, some very long μ-meson tracks ending in the emulsions were considered and their lengths and granulation measured. The lengths of the tracks considered were, on the average, about 3000 to 4000 microns and correspond to an initial value of $\beta^2=(v/c)^2\sim 0.2$. By comparison of the grain-densities of these μ-meson tracks with those of the singly charged prongs emitted by the stars, the energy of these prongs was estimated.[27] The first data collected just to obtain a general view of the proton prongs having energies between ~80 to 300 Mev, are summarized in Table III, where $N(s, l)$ is the number of observed stars having a total number s of prongs and l of proton prongs with energies in the above-mentioned range.

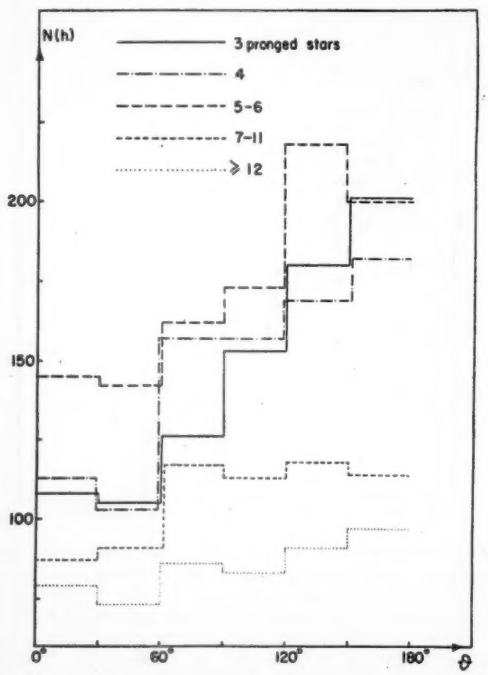

FIG. 5. Angular distribution of the prongs of the cosmic ray stars at 3500 meters around the upward vertical direction.

Together with these protons we must consider the partner neutrons which escape detection. With the probabilities given by Wouthuysen and assuming that a recoil nucleon could be, with equal chance, a proton or a neutron, we find that *on the average* at least 70 percent of the stars having more than five prongs are associated either with some δ or recoil nucleons. An examination of the directions of these fast proton trajectories has shown that most of them are directed *downward* with respect to the vertical. This fact (in agreement with the results communicated by Professor M. Cosyns at the Como conference) is indicated by Table IV, where the number n of the above-mentioned fast protons is given for different angular intervals ϑ. The angles are measured starting from the vertical in the upward direction. At the same time, contrary to what occurs for the fast proton prongs, the heavy prongs of the *large* stars (see below and also Brown *et al.*[23]) are quite isotropically distributed. *This fact seems to exclude the possibility that a large majority of these fast protons could be due to the statistical fluctuations in the nuclear evaporations, and at the same time it strengthens the argument of the secondary origin of these protons.*

By comparison of the data of the Bristol group with ours, it is also possible to obtain an idea of the correlation between the numbers of these δ and *recoil* nucleons (if they are protons most of them can be identified with the "grey" prongs of the Bristol group) and the corresponding stars. In Fig. 4 are plotted, (a) the frequency of stars *versus* prongs (grey and black) for the star-population at 3500 m altitude (curve I); and, (b) our stars-*versus*-heavy prongs distributions (curve II—the same as curve II of Fig. 3).[28] The two curves are normalized at the points corresponding to the three-pronged stars. As is shown by Table III, only about ten percent of these stars are accompanied by a fast proton. On the other hand, the total star population

percent), π-mesons. On the other hand, Dr. Cosyns has recently written to us, confirming the much lower percentage of π-mesons previously reported in his paper at the Como conference.

[26] The Bristol data give a fraction of about 20 percent, but probably some stars having three prongs were lost. However, it is correct to consider this 10 percent as a lower limit.

[27] The error in this energy estimate might be 100 percent.

[28] From the Bristol data concerning the grey prongs it is possible to guess that the stars-*versus*-black prongs distribution is in good agreement with our results. The same can be said about the results of the Brussels group, as communicated by Prof. Cosyns at the Como conference, September 1949.

TABLE V. Number of proton tracks having the projected lengths indicated in the first column and belonging to the star-type indicated in the second and third columns.

Interval (micron)	Stars 3–5 prongs	Stars 6 or more prongs	Total	Calculated total
14.5– 40	138	50	188	
40 – 75	228	87	315	
75 – 120	297	102	399	
120 – 173	224	96	320	
173 – 234	172	87	259	
234 – 306	160	83	243	
306 – 426	141	74	215	227
426 – 666	120	57	177	160
666 –3760	68	61	129	130
⩾3760	1	2	3	5
Totals	1549	699	2248	

TABLE VI. Number of alpha-particle tracks having the projected lengths indicated in the first column and belonging to the star-type indicated in the second and third columns.

Interval (micron)	Stars 3–5 prongs	Stars 6 or more prongs	Total
15.0– 23.4	228	62	290
23.4– 33.6	189	103	292
33.6– 45.4	173	93	266
45.4– 58.0	160	114	274
58.0– 72.7	206	84	290
72.7– 89	205	98	303
89 –112	132	68	200
112 –135	81	49	130
135 –158	52	30	82
158 –185	30	20	50
185 –267	40	25	65
⩾267	17	13	30
Totals	1513	759	2272

given by the Bristol group is rather low (~11 stars/cm³/day), so probably some small stars were lost in the scanning. Consequently, by normalizing the two curves at the points corresponding to the three-pronged stars, a reasonable comparison can be made between the Bristol and Rome results.

In Fig. 4 the $N(h')$ stars of curve I, having h' "black" plus "grey" prongs, correspond to the $N(h)$ stars of curve II which have h black prongs ($h'-h$ being the *average* number of grey prongs). Roughly speaking, a line in Fig. 4 drawn parallel to the abscissae connects the corresponding stars in the two distributions. It is thus possible to recognize that with stars of more than five prongs, *on the average*, for every grey prong we find rather regularly about 3.5 black prongs; or, considering the partner neutrons of the grey prongs, about two black prongs for every nucleon emitted with energy between about 80 to 300 Mev.[29] Probably, as was indicated by Cosyns at the Como conference,[30] there are some cases in which this correlation between the numbers of grey and black prongs is not so clear. However, considering the statistical fluctuations, it appears that in the large stars, *until the number of grey prongs becomes too high*, these nucleons (grey prongs), immediately-produced and emerging from the struck heavy nuclei, have contributed regularly to the subsequent evaporation of the same nuclei.[31]

The work of Goldberger indicates that also incident nucleons of rather low energies (~100 Mev) can originate particles which emerge immediately after the bombardment of a heavy nucleus, but at low energies a distinction between the immediately-projected and the evaporated black prongs is practically impossible.[32]

C

Another point can be examined to decide what limits we must place on the analogy between the cosmic ray stars and the Berkeley stars.

The Berkeley stars indicate, on the average, a strong projection of prongs in the forward direction with respect to the incident particle.[8] This is not evident in the cosmic ray stars, in which only a very small asymmetry around the vertical was observed.[33] To make this point more precise, the angular distribution around the vertical was examined in Kodak NT4 plates placed alternately in a vertical and horizontal position, over and under 2.5 cm of lead. Some results obtained by scanning the vertically-placed plates are represented in Fig. 5.[34]

The histograms show an evident projection of the prongs in the downward direction. This asymmetry is the more definite for small-size stars and in this case can be represented quite well by the law $f(\vartheta)=(1-k\cos\vartheta)$, where ϑ is the angle with the upward vertical direction and k is a constant of value around $\frac{1}{3}$. For stars having more than six prongs only a very slight asymmetry between backward and forward directions was found.

[29] We would like to observe here that the number of black prongs for every grey one is about the same as the average number of *visible* prongs observed in the Berkeley stars (~3.5). These stars are produced by deuterons (that is, by two nucleons) with energy between 80 and 300 Mev, just in the range of the grey prongs. On the other hand, the Bristol figures on the frequencies of 1_n, 1_p, and 2_p stars support the idea that a knock-on secondary nucleon can be, in about the same percentage, a neutron or a proton.

[30] We are very much indebted to Prof. Cosyns for some very interesting remarks on this point.

[31] From the Bristol data it is possible to see that the stars of the type $\geqslant 2_p{}^n$ have, on the average, about 7.5 black prongs. This is an indication that the nucleons produced in the *inelastic* collisions contribute, of course, to the subsequent evaporation of the residual nucleus (at least if the π-mesons do not contribute directly to the nuclear excitation). At the same time, the stars of the type $1_p{}^n$ have, on the average, about six black prongs. A large majority of these stars must be attributed to an incoming nucleon which suffers at least one elastic collision inside the struck nucleus. As a matter of fact, this is obvious in the case of 1_n stars. For the 1_p that can be guessed from the rather large scattering suffered by the relativistic particle (Fig. 6 of the Bristol paper) and from the fact that most of the events were observed in plates exposed without absorbers. Thus also the $1_p{}^n$ stars might, on the average, indicate the contribution of *one* knock-on nucleon.

[32] The difference is essentially in the angular distribution, which is isotropic for the evaporation prongs but not for the immediately-projected prongs.

[33] Perkins, Nature, **161**, 486 (1948); Harding, Phil. Mag. VII, **40**, 530 (1949).

[34] A more complete study of the angular distribution of prongs in cosmic ray stars will be given by A. Manfredini in the Nuovo Cimento.

TABLE VII. Distributions of the lengths of proton tracks. The first column gives the middle points of the intervals.

Middle point (micron)	Stars 3–5 prongs	Stars 6 or more prongs	Total
27	7.85 ±0.67	6.30 ±0.89	7.37 ±0.54
57	9.46 ±0.62	8.01 ±0.86	9.01 ±0.50
97	9.58 ±0.56	7.30 ±0.73	8.87 ±0.44
146	6.14 ±0.41	5.82 ±0.59	6.04 ±0.34
203	4.09 ±0.31	4.60 ±0.49	4.25 ±0.26
270	3.22 ±0.25	3.70 ±0.41	3.37 ±0.21
366	1.71 ±0.14	1.96 ±0.23	1.79 ±0.12
546	0.73 ±0.06	0.77 ±0.10	0.74 ±0.06
2200	0.032±0.004	0.064±0.008	0.042±0.005

This asymmetry, as we have already mentioned, is due essentially to the light ionizing particles; i.e., as is shown by Fig. 5, *it practically disappears if we consider particles having energies up to ~80 Mev.* We consider these results to be again in agreement with the idea that the small stars in cosmic rays are produced mainly by nucleons having energies of the same order of magnitude as those of the Berkeley experiments.

Actually, these small stars show a downward projection of the prongs which seems to be more or less of the expected order of magnitude if we consider the angular distribution of the prongs in the Berkely stars and the average angular spread of the nucleonic cascade.[3] In the small stars, observed either in the Berkeley experiments or in cosmic ray plates, the prongs have a forward projection with respect to the direction of the bombarding particle because part of the observed *heavy prongs* are produced in the primary collisions preceding the true nuclear evaporation. This is clearly indicated in the work of Goldberger[20] (see particularly[35] Table I, page 1276, and Fig. 6) and is due to the fact that the colliding particles do not have a very high momentum. On the contrary, if the incident particle has a high energy and transfers a large fraction of its momentum to a nucleon, it will not give rise to a heavy prong but to a fast recoil nucleon of the type observed in great amounts only in the large stars. And in this case, as was observed, only this fast prong is projected in the forward direction, and the heavy prongs are isotropically distributed.

III. THE ENERGY-DISTRIBUTIONS OF THE IONIZING PARTICLES EMITTED IN THE COSMIC RAY STARS[36]

A

The energy distribution of the particles emitted in cosmic ray stars has been studied recently by Perkins.[37] The Perkins energy distribution with regard to proton tracks was obtained by measuring the *granulation* of each prong of a limited number of stars which had at least one "long" prong terminating in the emulsion. From the granulation of the prong terminating in the emulsion (which gave him the energy of this prong) the author obtained a reference for the evaluation of the energies of the other prongs on the basis of their granulations.

From the experimental relations which have been determined regarding the relationship between energy and granulation[38] it is possible to deduce that, in spite of the care taken by the author, the *relative error* in the energy is more than twice the error made in the measurement of the granulation. Now the statistical error in granulation is particularly large for large energies because of the isotropic distribution of the tracks. Consequently, we believe that notwithstanding the high level of the technique achieved by Perkins, any energy measurements based on granulation will be affected by large errors, at least for tracks of small granulation-density making large angles with the plane of the emulsion.[39]

Another and perhaps quite reliable method for obtaining an evaluation of the prong-energies is the following: consider *only* the prongs totally included in the emulsion (that is, only those ending in the emulsion) and then measure the ranges of their projections. From these, reascend to the actual ranges and energies by means of some geometrical considerations and by using energy-range relations. Our data have been obtained from 4007 stars found in Ilford C2 plates 100μ thick; the plates were exposed at the Testa Grigia Laboratory. Some of them were exposed under different layers of lead. But in conjunction with the small differences observed in the number of stars *versus* number of prongs distributions, the differences between the spectrum of

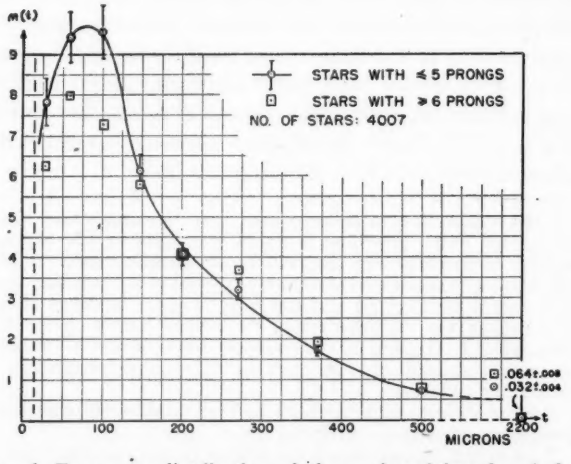

FIG. 6. Frequency distribution of the projected lengths of the proton tracks (number of tracks per unit length).

[35] We believe the opinion to be incorrect that the forward projection of the prongs (reference 16) in the Berkeley stars is due to the recoil velocity of the struck nucleus. For cosmic ray stars this point was directly checked by Harding, Phil. Mag. (VII) **11**, 530 (1949).

[36] For more detailed information about the arguments discussed in this section, see G. Cortini, Nuovo Cimento **6**, 470 (1949).

[37] Perkins, Nature **160**, 299 (1947).

[38] Lattes, Occhialini, and Powell, Nature **160**, 453, 486 (1947).

[39] It can also be observed that granulation measurements are very time-consuming and practically exclude the collection of a large amount of data; as a matter of fact, Perkins' data are based on 15 stars and 80 proton tracks.

track-projections at different thicknesses, if they exist, are completely within the limits of errors and can be neglected.

The length of the projection on the plane of the plate of the tracks terminating in the emulsion was measured and the tracks were classified as those of protons and of alpha-particles. Actually the distinction is between particles with an electronic charge (deuterons and tritons included) and particles with a larger charge; it is possible to state, however, that except for recoil nuclei the only substantial contributions to these two classes of particles come from protons and alpha-particles. In order to exclude the recoil nuclei, tracks with less than 14μ of *projection* have been excluded from the statistics; this also makes it easier to distinguish between particles of different charge, as mentioned above.

Measurements of length were made with ocular micrometers by examination of the plates with an immersion objective and the use of a high degree of enlargement. The ocular micrometers were calibrated by means of an objective micrometer. After the data were gathered, satisfactory checks were made on the consistency and accuracy of the measurements made with different microscopes and on the consistency of the measurements made with different groups of plates.

B

The results obtained are collected in Tables V and VI for protons and alpha-particles respectively. The second, third and fourth columns of Table V give the number of tracks of length specified in the first column for "small" stars (five prongs or less), "large" stars (six prongs or more), and all of the stars. Similar data are given for alpha-particles in Table VI. The last column of Table V will be explained later.

The reason for singling out the results for "large" stars lays not only in the arguments discussed in the previous paragraphs, but also in the fact that the choice of six prongs as a lower limit was considered to be sufficient to exclude practically all of the stars emitted by the light nuclei of the emulsion.[40] But because the heavy nuclei also contribute quite strongly to the number of small-size stars, in the following paragraphs evaluations for the energy spectrum have been made for all the stars in bulk.

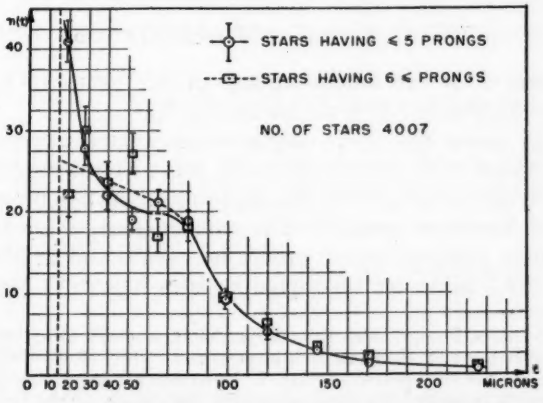

FIG. 7. Frequency distribution of the projected lengths of the alpha-particle tracks (number of tracks per unit length).

TABLE VIII. Distributions of track lengths for alpha-particles. The first column gives the middle points of the intervals.

Middle point (micron)	Stars 3–5 prongs	Stars 6 or more prongs	Total
19.2	41.0 ±2.7	22.2±2.8	34.5 ±2.0
28.5	27.9 ±2.0	30.3±3.0	28.6 ±1.7
39.5	22.1 ±1.7	23.6±2.5	22.5 ±1.4
51.7	19.1 ±1.5	27.1±2.5	21.7 ±1.3
65.3	21.2 ±1.5	17.1±1.9	19.7 ±1.1
80.8	19.0 ±1.3	18.0±1.8	18.6 ±1.1
99.5	9.6 ±0.8	9.7±1.2	9.5 ±0.7
121	5.3 ±0.6	6.4±0.9	5.7 ±0.5
145	3.1 ±0.4	3.6±0.6	3.3 ±0.4
171	1.7 ±0.3	2.2±0.5	1.8 ±0.3
226	0.72±0.1	0.9±0.2	0.78±0.1

From the experimental values given in Tables V and VI the distributions of projections were obtained by dividing the number of tracks by the corresponding interval. They are reported in Tables VII and VIII and are shown in Figs. 6 and 7, where the abscissa indicates the mean values of the considered projection intervals.

C

The data reported above give us the distributions of the track projections, but we are interested in knowing the distributions of the actual lengths of the tracks themselves. This is the source of the larger errors of our method, because we have obtained this distribution by a rough calculation and, further, by introducing some hypotheses on the angular distribution of the tracks.

It was assumed that the spatial angular distribution of the tracks is isotropic, or more specifically, that the angular-distribution function $f(\vartheta)$ is of the type

$$f(\vartheta)+f(\pi-\vartheta)=\text{const.}$$

From the results of Sec. IIIB we can consider that this assumption is quite correct. With this hypothesis, the calculation for obtaining the length distribution was performed in the following manner.

Let x be the actual length of a track, t its horizontal projection, d the thickness of the emulsion. We indicate by $f_p(x)dx$ and $f_\alpha(x)dx$ the number of either proton or alpha-particle tracks having an actual length between x and $x+dx$ per unit solid angle. The number of all the tracks is, consequently,

$$N=4\pi\int_0^\infty f(x)dx. \qquad (1)$$

[40] Either from the results of Perkins (Phil. Mag. **40**, 601 (1949)) or from finding for the production of stars a cross section proportional to the geometric one, it is reasonable to attribute to the light nuclei of the emulsion about 30 percent of the *total* number of stars.

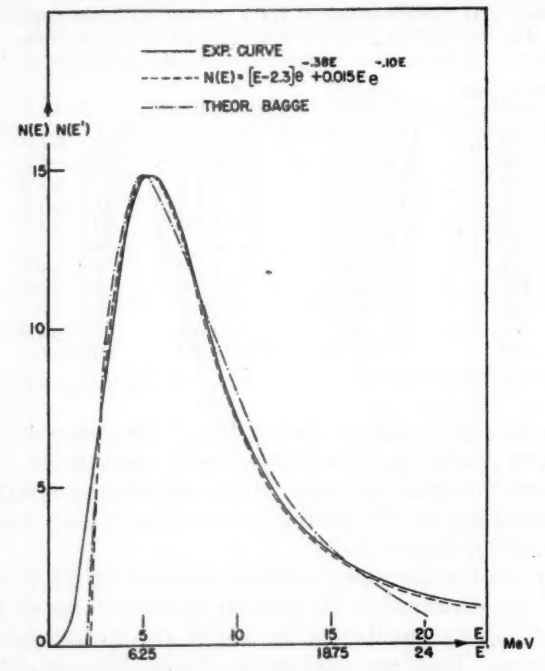

FIG. 8. Energy distribution of the protons from cosmic ray stars. The theoretical curve (Bagge) was obtained from Eq. (6) of the text, with $V'=2$ Mev. The ordinates are in arbitrary units.

The number of tracks ending in the emulsion and having a co-latitude between ϑ and $\vartheta+d\vartheta$ and a range between x and $x+dx$ is $2\pi f(x)\sin\vartheta[(d-x\cos\vartheta)/d]dxd\vartheta$. Introducing the variable t, it is easy to find that the distribution $F(t)$ of the projections is given by

$$F(t)=4\pi\frac{t}{d}\int_t^{(t^2+d^2)^{\frac{1}{2}}}\frac{f(x)}{x}\left[\frac{d}{(x^2-t^2)^{\frac{1}{2}}}-1\right]dx. \qquad (2)$$

Obviously, for $t\gg d$

$$F(t)\simeq 2\pi(d/t)f(t) \qquad (3)$$

and (3) was directly used to obtain the tail of the spectrum toward the high energies. The integral equation (2) was solved by developing the experimental distributions of the projections in functions of the type

$$\psi_i(x/a)=(x/a)^i\exp[-(x/a)^2], \qquad (4)$$

where i is an *even* number and a is some proper parameters selected to fit the experimental curves well. As is indicated by Tables V and VI, *the distributions of both protons and alpha-particles for the small stars seem to differ from those for the large stars*. The differences indicate, as is expected, a larger percentage of higher energies in the large stars. However, for the protons the difference does not exceed the limits of the statistical errors, and it was considered useless to make separate calculations for the small and large stars. For the alpha-particles the situation is a little different for the lower values of the projection lengths, and indicates clearly that for the large stars the maximum is displaced toward the higher energies. Thus we have solved Eq. (2) for the alpha-particles, distinguishing the large from the small stars. From the distribution functions $f_p(x)$ and $f_\alpha(x)$ we have obtained the energy distributions, using the well-known range-energy relations.[41] They are indicated in Figs. 8 and 9, for protons and alpha-particles respectively.

D

The method used in the solution of Eq. (2) is certainly very rough, but the evaluated distribution functions $f_p(x)$ and $f_\alpha(x)$, integrated [Eq. (1)] for all the x-values, give for the *total* number of prongs for all the observed stars a value which is in fairly good agreement with the observed one, i.e., about 15,000 after subtraction of the short prongs. Actually this number is about ten percent smaller than that calculated from f_p and f_α, but we can surmise that this deviation is essentially due to the estimate of the number of proton tracks having energies larger than 30 Mev. In the evaluated distributions there are about 1200 of these tracks, and a large fraction of them, because of their low grain-density and long range, certainly escaped observation in the C2 plates when they were appreciably inclined to the plane of the emulsion.

On the other hand, the observations made with NT4 plates (referred to in Sec. II) indicate that the proton prongs corresponding to energies larger than 30 Mev are just about ten percent of the *total* number of heavy ionizing prongs (and are clearly observable in C2 plates). In any case the figures of the last column in Table V, which were deduced from f_p, demonstrate that the calculations were quite reliable also in the upper part of the spectrum. Only the extreme tail of the spectrum itself was obviously wrong. Consequently, in spite of the crudeness of the method used to solve Eq. (2), we trust that the two deduced energy distributions represent rather closely the actual energy spectra of the singly and doubly charged prongs emitted by cosmic ray stars.

The distribution of the single-charged prongs is rather well represented by the empirical formula[42]

$$f(T)=A\{(T-2.3)e^{-0.38T}+0.015Te^{-0.10T}\} \qquad (5)$$

where T is the kinetic energy of the protons. The curve given by (5) is plotted in Fig. 8.

Of course Eq. (5) is only a simple analytical representation of the empirical results, but its form suggests a division of the prongs into nuclear evaporation prongs and knock-on prongs.[43] The average energy for the proton (single-charged) prongs between 0 and 25 Mev is $\simeq$8.2 Mev; for the alpha-particles it is $\simeq$11 Mev.

[41] Lattes, Fowler, Cuer, Proc. Phys. Soc. London **59**, 883 (1947), and reference 38. Edmont, J. de phys. et rad. (VIII) **10**, 22 (1949).

[42] We are very grateful to Mr. L. Lederman for suggesting this formula to us and for some interesting discussions on the topics of this paper.

[43] See Bagge, reference 17.

As was mentioned earlier, *there is not very much difference between the distributions of large and small stars.*[44] Consequently, these figures can be used for both. Considering our experimental data, the ratio between alpha and proton prongs is $\simeq 0.35$. This is in agreement with the results previously obtained by other authors.[45] The number of neutrons, in comparison with the charged prongs, can be estimated to be $\simeq 1.2$ (see below). Thus the average energy associated with the emission of one black prong is $\simeq 35$ Mev (the usual nuclear physics figures for the binding energies—$A = 100$—were used) and the *average* energy released per nucleus through the black prongs is $\simeq 150$ Mev (the average number of heavy prongs observed by us was $\simeq 4.7$).

E

The experimental data obtained on the structure of the stars can be more thoroughly discussed using the theoretical considerations suggested by Bagge (reference 17) and more recently by Fujimoto and Yamaguchi,[46] and particularly the very deep and extensive analysis made by Le Couteur.[47] From Le Couteur's discussion we can believe that when Bagge's dilatation of the Gamow barrier is considered, for heavy nuclei like Ag and Br the statistical considerations can be applied also for very high excitation energies. It is required only that the excitation energy be much less than the total binding energy. For Ag and Br nuclei that means less than ~ 500 Mev.

We believe it to be correct to consider as thermodynamic processes only those connected with the rather slow (heavy) prongs; certainly we cannot include among the true "evaporated" prongs most of the grey prongs, which are observed in large stars, and which have energies much larger than Fermi's limit (~ 20 Mev). For instance, the evaluations of Goldberger[20] show clearly the distinction between the immediately-projected prongs and the subsequent thermodynamic excitation, even for incident nucleons of only about 100 Mev. The angular distribution of prongs in small stars is, as we have said, an indication of the correctness of this argument. Similarly, in large stars the fastest nucleons directly produced by the incident particle

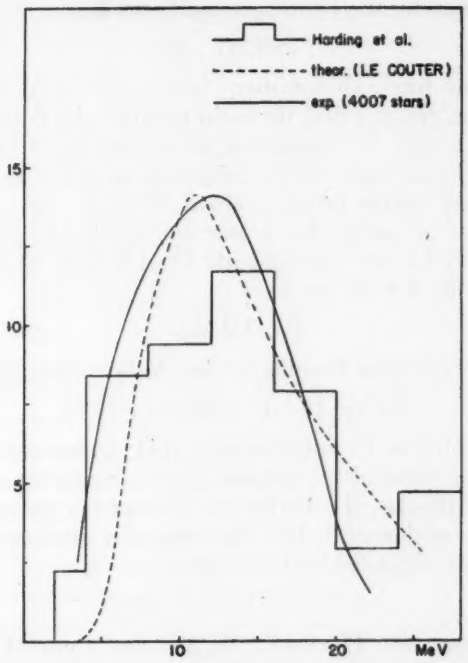

FIG. 9. Energy distribution of the alpha-particles from cosmic ray stars having more than 5 proofs. The ordinates are in arbitrary units.

(most of the grey prongs and their neutron partners) are not to be included.

Thus the application of the nuclear-thermodynamic considerations to the rather large stars produced by cosmic rays can be justified provided that: (1) only the heavy prongs (energies ~ 20 Mev) are considered; (2) in considering the total energy lost by the incident particle a distinction is made between the energy developed through the "true" evaporation and the energy belonging (after the emission from the struck nucleus) to the fastest knock-on nucleons. This distinction is necessary also because the number and energy associated with the *neutral* particles which are emitted together with the charged ones is, of course, different in the two stages of the process.

According to Bagge, taking into account the dilatation of the Gamow barrier, the energy spectrum of the protons should be given by

$$f(E)dE = \left(\frac{E-V'}{E}\right) \times \frac{E}{E+E_0} e^{-E/T_0} dE = \frac{E-V'}{E+E_0} e^{-E/T_0} dE \quad (6)$$

where E_0 is practically the binding energy of the neutrons ($\simeq 8$ Mev) and T_0 is the temperature[48] $1/T_0 = dS_0/dU$ of the initial nucleus excited to energy U. Using for S the approximate expression $S \simeq 0.63(AU)^{\frac{1}{2}}$

[44] The absence of large differences between the two distributions is due to the following facts: (1) The heavy as well as the light nuclei contribute strongly to the small stars; (2) but in the case of the light nuclei, a larger fraction of the prongs is made up of alpha-particles (Perkins, Phil. Mag. 7 series 40, 601 (1949)); (3) thus the difference is essentially concentrated in the alpha-particles and not in proton prongs. (4) As we will see later, the shape of the energy-spectrum of evaporating protons is not very sensitive to the energy excitation.

[45] Perkins, see reference 40; Addario and Tamburino, Como conference, 1949; A. Page, Proc. Phys. Soc. London (to be published) (we are very much indebted to Dr. G. Rochester and Dr. A. Page for sending us the manuscript).

[46] These authors kindly forwarded to us the manuscript of their work.

[47] We are very grateful to Dr. G. Rochester, who kindly gave us the opportunity of reading the interesting manuscript of Dr. K. J. Le Couteur.

[48] V. Weisskopf, Phys. Rev. 52, 295 (1937).

suggested by the Fermi gas model, we find

$$T_0 \simeq 3.2(U/A)^{\frac{1}{2}}. \quad (7)$$

As was mentioned earlier, taking into account the binding energies and the ratio between the number of protons and the number of alpha-particles,[49] we find that the average energy connected with the *emission* of every visible prong is about 35 Mev, the average number of prongs for a star (including two-pronged stars) is 4.7, and consequently $\bar{U} \simeq 150$ Mev. From (7), assuming $A = 100$, we have

$$T_0 \simeq 3.9 \text{ Mev}. \quad (8)$$

This means that formula (6) should be written as

$$f(E) \simeq [(E-V')/(E+8)]e^{-0.256E}. \quad (9)$$

The value of V' must be estimated. It represents the average value of the Gamow barrier during the evaporation process, the Bethe and Konopinski penetration being considered.[50] The following is a semi-empirical formula suggested by Le Couteur:

$$V' \simeq 0.7V/[1+(U/200)]. \quad (10)$$

In our case $V' \simeq 0.4V$. We find that the best value for V', which must be selected to obtain a good theoretical representation of the experimental spectrum, is $V' \simeq 2$ Mev. Thus $V \simeq 5$ Mev, which is very reasonable. In Fig. 8 the theoretical curve evaluated for $V' = 2$ Mev is plotted. The agreement is so good that an overestimate of the reliability of the thermodynamic treatment might be possible, but we believe that this agreement is partially a happy case. For instance, following the brilliant explanation of the emission of protons of very low energies ($\simeq 2$ Mev) given by Fujimoto and Yamaguchi,[51] and then Le Couteur, the percentage of these slow protons, which are due essentially to the "governor" imposed by the ratio Z/A, should be larger than that which can be estimated by our analysis of the proton spectrum. Of course, this depends on the value selected for V', for the shape of the proton spectrum is very sensitive to this value, and we are inclined to believe that our V' value is actually too low. However, it is certain that the thermodynamic treatment based on the Fermi gas model represents quite closely the general behavior of the nuclear evaporations induced by cosmic rays. For example, the ratio between alpha- and proton prongs turns out to be approximately 0.35, in excellent agreement with Le Couteur's evaluations and with the results of other authors.[45] Further, the alpha-spectrum evaluated by Le Couteur, who was considering only the large stars,[52] represents fairly well the spectrum observed by us. That is shown in Fig. 9, where the spectrum evaluated for the alpha-particles emitted with excitation energies of 400 Mev ($A \simeq 100$) is represented together with Perkins' data on 150 stars, and with our data.[53]

Finally, we would like to remark that because our experimental value for the average energy connected with every visible black prong ($\simeq 35$ Mev) is smaller than the average energy for prongs estimated starting from Le Couteur's evaluations by a factor of about 0.85, in Fig. 3 the excitation energies given on the abscissae should be reduced by the same factor.[54]

The quite definite and quantitative results obtained in this paper on cosmic ray stars will be very useful in the discussion of the nucleonic cascade which will be presented in Part III of this work.

IV. DISCUSSION AND CONCLUDING REMARKS

Even postponing any discussion of the nucleonic cascade to a following paper, some conclusions which arise immediately from the figures reported can be examined conveniently at this time.

It seems to have been proven that most of the stars produced by cosmic rays can be interpreted in a quite direct manner, taking as a model the nucleon-nuclei collision studied by Goldberger[20] and others.[16] For the arguments indicated in this paper and in Part I, the stars are usually generated by nucleons having moderate energies, i.e., some hundreds in Mev. In this energy range, and in fair agreement with theoretical expectations, the characteristics of the stars (frequency *versus* number of prongs, energy of prongs, etc.) depend very slightly on the velocity of the incident nucleons. Thus the stars of the first branch of curve II in Fig. 3 are mostly caused by nucleons distributed in a quite large energy range, say between about 100 and 500 Mev, and show correctly the same characteristics as do the stars produced in the Berkeley experiments with deuterons and protons. Strictly speaking, as has been shown by Goldberger, considering the prongs of a star as a whole they are due not only to an evaporation process, and the agreement with the Bagge theory is partially only a happy accident. Some of the prongs are directly emitted after the collision with the incident nucleons, and demonstrate this origin in their forward projection, but their energies are largely included in the common energy ranges of the nuclear evaporations. A distinction between the two types of prongs (evaporation and knock-on prongs) which is based only on the energy is thus not possible, as has been already pointed out,[55] and probably would be quite meaningless.[56]

[49] In this estimate the difference between tritons and protons, etc., can be neglected.

[50] Bethe and Konopinski, Phys. Rev. **54**, 130 (1938).

[51] Fujimoto and Yamaguchi, Prog. Theor. Phys. **3**, 4621 (1948).

[52] In this case the distinction is necessary because of the appreciable contribution of the light nuclei.

[53] The curve is that corresponding to the large stars. This distinction was not made for the protons, as was mentioned before, on account of the slight difference in the proton spectra of large and small stars.

[54] Also, concerning the behavior of the proton spectrum, the difference between Le Couteur's evaluations and our results is a factor of about 0.85 in the abscissae. If the abscissae of Fig. 8 were to be increased by this factor, the agreement between Le Couteur's spectrum and the experimental one would be excellent.

[55] We want to thank Dr. M. Cosyns for some very useful remarks concerning this argument.

[56] As we said before, a differentiation between immediately projected and evaporated prongs could be made using Fermi's

The situation is slightly different for the large-size stars, that is for the stars of the second branch of curve II in Fig. 3, showing six or more prongs. They are mostly due to the explosion of heavy nuclei strongly excited by the *simultaneous* action of the incident nucleon and some fast secondary nucleons produced inside the struck nucleus itself. In this case the distinction between the different kinds of prongs, which is based on their energies,[57] is clearer and is supported by the more evident differences in the angular distribution. But this distinction remains obviously a quite rigid scheme. However, because the *average* energy losses suffered by a fast nucleon depend, as we have already seen, very little upon its own energy, all the secondaries produced by a primary nucleon and emerging with energy above approximately 50 Mev, must contribute to the same extent to the emission of slower prongs. This must be true independently of any subtle differentiation between projected and evaporated heavy prongs, and is in agreement with the correlation found between the *average* numbers of "heavy" and "grey" prongs. From the energy spectra of the heavy prongs it is to be believed that the excitation energy (in Mev) of an evaporating nucleus emitting N_h visible "heavy" prongs is about $35N_h$. Since some energy is directly transferred to the emerging "grey" prongs, this value does not represent *all* of the energy released to the struck nucleus by the incident nucleon. Roughly, for the correlation existing between "grey" and "black" prongs, attaching to any visible "grey" prong an *initial* average energy of about 100 Mev or more,[58] we can estimate that the total energy released in the production of a large star (six heavy prongs or more, and at least one "grey" prong) is about $70N_h$ Mev or more. The Berkeley nucleons are thus generally unable to produce stars having more than six black prongs, as has been actually observed.

On the contrary, cosmic ray nucleons quite frequently have sufficient energy to produce a large star.

If the preceding interpretation of star production is correct, usually a large size star must be considered essentially as the result of the development of a nucleonic cascade inside a nucleus.[59] This point of view could be invoked to explain the *exponential* behavior of the frequency of stars *versus* number of prongs for the large stars (more than five prongs), but the uncertainties concerning the energy spectrum of the star-producing nucleons, the corresponding cross sections, and so on, would make any speculation in this direction almost meaningless.[60] However, some general remarks can be made on this point. As was mentioned in Sec. II, only about 25 percent of the large stars (more than five prongs) observed at 3500 m show relativistic prongs. We can add now that about the same proportion is indicated in the data collected by Lord and Schein.[61] Even assuming that all the observed minimum ionization prongs are mesons, we must conclude that about 75 percent of the large stars are not connected in any evident or direct manner with the inelastic nucleon-nucleon collisions.

Consequently, it would seem that these large stars must be produced by knock-on collisions. But whether we extrapolate the Goldberger results (with a $1/E$ law), or use the evaluations made by Zwanniken,[62] it is clear that the number of large stars is extremely high in comparison with that which should be expected taking into account the probabilities for the knock-on collisions. This point is strengthened if we consider that the large stars are produced by nucleons of high energy representing only a small fraction of the star-producing radiation.[63] We are thus inclined to believe that while the large stars show, in the black prongs, the normal characteristics of highly-excited nuclear evaporations, the process by which the grey prongs are created with such high frequency is quite obscure.

---

energy limit as a dividing point. It would be better to consider as projected prongs those emitted during a period of time which is less than the nuclear period, but of course this is beyond the possibilities of the nuclear emulsion technique.

[57] A strongly excited nucleus has to emit evaporation prongs having an average energy which is larger than that resulting from a weak excitation (see Figs. 6 and 7), but the number of evaporation prongs having energies around 100 Mev, like the "grey" prongs, is always very small *up to* excitation energies for which the thermodynamic model has no further meaning (reference 47).

[58] Every visible "grey" prong represents, on the average, two nucleons escaping with an energy of ~50 Mev.

[59] L. Jánossy, Phys. Rev. **64**, 345 (1943).

[60] See Part III.

[61] T. Lord and M. Schein, Phys. Rev. **77**, 19 (1950).

[62] See Zwanniken, reference 17. The evaluations of this author are made assuming a Yukawa potential, which favors the high momentum transfers.

[63] Incidentally, this means that also in the nucleonic cascade the collisions accompanied only by the projection of fast nucleons are more frequent than those in which π-mesons are produced. The observations on the penetrating showers made with the cloud chamber method (Butler and Rochester, communicated by Blackett at the Como conference) seem to support this conclusion.

Note added in proof: In a recent issue of the Nuovo Cimento **7**, 99 (1950), Dalla Porta, Merlin, and Puppi gave a brilliant interpretation of the transition effect in the star population observed in lead.

Photoelectric Emission from *F*-Centers in KI

L. APKER AND E. TAFT
General Electric Research Laboratory, Schenectady, New York
(Received May 16, 1950)

F-centers were produced in thin evaporated layers of KI by ultraviolet irradiation or by electron bombardment. Photoelectric emission became measurable for $h\nu = 2.5$ ev and increased to a plateau value near 10^{-4} electron/quantum at 4 ev. Yields rose further to a sharply peaked value about 20 times higher at 5.66 ev. This point is practically coincident with the first optical absorption maximum for pure KI as measured by Fesefeldt. The peak shifted with temperature in the same way as the optical absorption. The yield was roughly proportional to the absorption constant. Below 5 ev, the emission was attributed to direct ionization of *F*-centers. The enhanced yields at the peak were tentatively ascribed to ionization of centers by excitons produced in the optical absorption.

I. INTRODUCTION

IT has been known for many years that alkali halides containing *F*-centers show an external photoelectric effect.[1] The process, however, has not been very well understood. Several theories have been proposed.[2]

This paper presents new data taken on KI over an extended frequency range. The results suggest that two kinds of emission are possible. First, for photon energies $h\nu$ less than about 5 ev, *F*-centers are ionized directly; some of the electrons escape through the crystal surface. Second, a new phenomenon overshadows this direct ionization near $h\nu = 5.63$ ev, the peak in the first absorption band[3] of pure KI. Theoretical interpretation of this band indicates that the incident photons create excitons.[4] In the experiments described here, these apparently ionize *F*-centers in a secondary process; again, some electrons escape from the crystal.

Topics will be discussed as follows: Section II, pertinent experimental procedures not described elsewhere; Section III, production of *F*-centers in the samples; Section IV, frequency variation of the photoelectric yields, and the onset of enhanced emission.

II. EXPERIMENTAL DETAILS

Figure 1 shows the type of photo-tube used, an improved version of those previously described.[5] It was used in the same way as its predecessors, except that data could be taken as a function of emitter temperature. Reproducibility was established for 10 surfaces in four tubes.

The KI was evaporated from platinum boats onto bucket-shaped Ni or Ta emitters held near 300°K. Film thicknesses on the buckets were computed from interference patterns on the tube walls and ranged from less than 10^{-4} to 10^{-3} cm. Emitter temperatures were estimated from thermocouple measurements on dummy tubes and from the decrease in permeability of Ni buckets at the Curie point.

Precautions were taken to insure that the photoelectric currents were not limited by the electrical conductivity of the samples. The emission saturated at an applied field below 1 v/cm. From this point up to 1000 v/cm, it rose at a rate several times larger than that corresponding to a normal Schottky effect for a metal. Currents were proportional to the intensity of the incident radiation over a range of at least one decade. Except for negligible changes due to the decline in *F*-center concentration, they were constant in time when the radiation was applied to the surface. (Variations occurring within 2 seconds after the radiation struck the surface would have escaped notice, however, since this was the limit imposed by the response time of the current detector.) The results were not dependent on sample thickness. Metal films deposited on the KI showed no evidence of spurious current limitation. Thus, although the KI surfaces showed evidence of patch structures, the emission had the characteristics expected for a normal external photoelectric effect.

III. PRODUCTION OF *F*-CENTERS IN THE EMITTERS

Before irradiation in the general region of the first absorption peak at $h\nu = 5.63$ ev, samples showed no photoelectric emission. Yields varying from 3×10^{-9} electron/quantum at $h\nu = 2$ ev to 3×10^{-6} at 6 ev could have been detected.

At room temperature, 2×10^{11} quanta sec.$^{-1}$ cm^{-2} at $h\nu = 5.66$ ev were then allowed to strike the KI. Photoelectric emission became measurable in a few seconds. It rose as shown in Fig. 2. The first part of this characteristic has very roughly the form expected for a first-order reaction. In drastically oversimplified terms, it may be useful to describe it at this point as follows. A fixed number of vacant iodine ion sites capture electrons

[1] R. Fleischmann, Zeits. f. Physik **84**, 717 (1933).
[2] G. Maurer, Zeits. f. Physik **118**, 104 (1941); E. Asmus, Ann. d. Physik **26**, 723 (1936); T. Muto, J. Phys. Soc. Japan **2**, 193 (1947).
[3] H. Fesefeldt, Zeits. f. Physik **64**, 623 (1930).
[4] For discussion and references, see F. Seitz, Rev. Mod. Phys. **18**, 384 (1946) and NDRC reports on which this paper was based; *Modern Theory of Solids* (McGraw-Hill Book Company, Inc., New York, 1940); N. F. Mott and R. W. Gurney, *Electronic Processes in Ionic Crystals* (Clarendon Press, Oxford, England, 1940). See also reference 6.
[5] For many features of this design, we are greatly indebted to Miss Jean Dickey, who has used them in work on BaO. For a review, see J. A. Becker, Elec. Eng. **68**, 937 (1950). For other details, see Apker, Taft, and Dickey, Phys. Rev. **76**, 270 (1949); **75**, 1181 (1949); **74**, 1462 (1948); **73**, 46 (1948); Ind. Eng. Chem. **40**, 846 (1948).

from a constant density of excitons produced by the incident radiation. (The delayed approach to saturation may be due to other important and more complex processes discussed by Seitz in the references of footnote 4.) F-centers produced in this way give rise to an external photo-current proportional to their density.

When the irradiation was stopped (except for the negligible periods required to measure yields), the photo-current decreased with time. At 300°K, it decayed to 25 percent of its original value in about 60 hr. At 400°K, the same effect took place in 8 min., as shown in Fig. 2. The decay has the form expected for a second-order process. Assuming that the temperature dependence is fixed by the usual exponential Boltzmann factor, one concludes that an activation energy of the order of 0.7 ev is involved. This is in reasonable agreement with the thermal ionization energy,[6] 0.8 ev, of F-centers in KI. We take this as an indication that we are dealing with the well-known kind of F-center rather than with an unusual variety conceivably existing, for example, at surfaces. This point will be mentioned again.

The emitter in some cases was bombarded with 3 ma of electron current at 200 v for 2 sec. The electrons struck the total area 0.64 cm² of the end of the bucket. This type of treatment is believed to produce an F-center density of the order of magnitude 10^{19} cm^{-3} in evaporated layers of KCl.[7] Now the photoelectric yield measured directly afterward on the KI emitters was only about twice as high as when the centers were formed by ultraviolet irradiation. If most of the incident 5.66-ev photons in the latter case were absorbed[6] in a distance 2×10^{-6} cm, then 6×10^{18} quanta/cm² were absorbed per minute of irradiation. Let us say, for the moment, that each exciton produced one F-center during the initial stages of the process. Then the data in Fig. 2 indicate a final F-center density of the order 10^{19} cm^{-3} in agreement with the number mentioned above for KCl.

We wish to emphasize an alternative possibility at this point. It is conceivable that the 10^{18} quanta cm^{-2} min.$^{-1}$ incident on the surface during irradiation could go entirely into producing roughly 3×10^{18} centers localized at the KI surface. This is still only about three percent of the number of surface atoms. However, it is difficult to see how the activation energy mentioned above could be so close to that for the usual F-center if this were the case.

IV. SPECTRAL DISTRIBUTION OF THE PHOTOELECTRIC YIELD

Figure 3 shows the spectral distribution of the photoelectric yield for a concentration of F-centers near the limiting value. We attribute the emission below $h\nu=5$ ev to direct ionization of the centers. Some of the excited

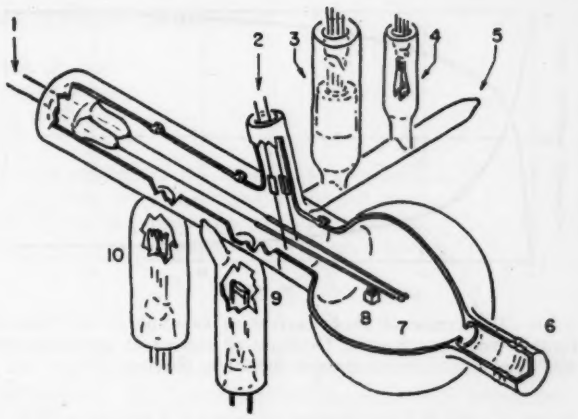

FIG. 1. Cutaway sketch of photo-tube. 1. Lead-in wires to central conductor of hairpin assembly; these two leads are connected by the bucket support 7; inside the collecting sphere they are sheathed by metal tubing supported on insulators. 2. Lead-in wires with spring contacts actuated by armatures; these wires supply current to the sheaths and through them to a small heater filament inside the bucket support 7. 3. Ionization gauge. 4. Getter. 5. Seal-off tip. 6. Quartz window. 8. Typical bucket-shaped emitter; there were eight to ten in each tube. 9. KI evaporator. 10. Evaporator for Ag or Pb [see E. A. Taft and J. E. Dickey, Phys. Rev. 78, 625 (1950)].

electrons escape through the crystal surface. One notes that the yield rises more slowly near the threshold than in the case of a metal, for example. (This must be interpreted with care, however, because surface patch structures may be pronounced for materials of such low conductivity.)[8] Near $h\nu=4$ ev, the yield reaches a plateau (of $\sim10^{-4}$ electron/quantum) presumably set by the maximum efficiency of ionization and escape from the surface.

It is interesting, therefore, to estimate an order of magnitude for the probability that an F-center will absorb a photon of energy near 5 ev. We assume an oscillator strength $f=0.1$ for a transition to a continuum of effective width $h\Delta\nu=3$ ev, keeping in mind that most of the oscillator strength for an F-center is concentrated near $h\nu=2$ ev in the F absorption band.[4] The cross section for absorption[9] is then $\sigma=(\pi h/mc)(e^2/h\Delta\nu)f=3\times10^{-18}$ cm². For an F-center concentration of 2×10^{13} per cm² of surface area in the thin KI film, the absorption amounts to 6×10^{-5}. If we assume that half of the electrons escape, the photoelectric yield becomes 3×10^{-5}. This is to be compared with the measured value of 10^{-4} above. The escape probability taken here is very high, but the final result is still too low. The agreement is probably as good, however, as can be expected in such a rough estimate.

As $h\nu$ increases above 5 ev, the optical absorption

[6] R. W. Pohl, Proc. Phys. Soc. 49 (extra part) 3 (1937); J. de Boer, *Electron Emission and Adsorption Phenomena* (Cambridge University Press, London, 1935).

[7] F. Seitz, reference 4 and work cited there.

[8] C. Herring and M. H. Nichols, Rev. Mod. Phys. 21, 185 (1949); G. Wannier, Phys. Rev. 76, 438 (1949); H. M. James, Science 110, 254 (1949). It must be remembered that the KI emitters under consideration here are not in true equilibrium. The centers are only metastable. Internal currents may be carried by both ions and electrons.

[9] H. Bethe, *Handbuch der Physik*, Vol. 24/1, p. 429; H. Fröhlich and R. A. Sack, Proc. Phys. Soc. London 59, 30 (1946).

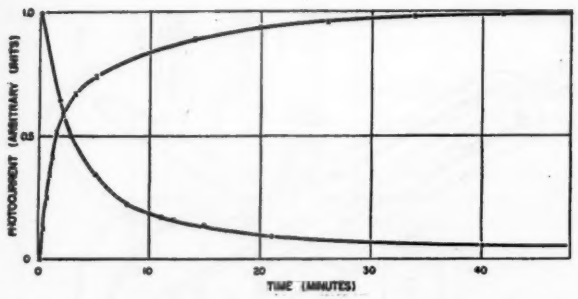

FIG. 2. Increase of photo-current at $h\nu = 5.66$ ev as F-centers form in emitter (crosses). Decrease of current at approximately 400°K as centers are destroyed thermally (circles).

increases to its maximum value at 5.63 ev. This is shown by Fesefeldt's data[3] plotted on a logarithmic scale in Fig. 3. The photoelectric yield rises to a pronounced peak at 5.66 ev. The small difference is probably within the experimental error. The yield is roughly proportional to Fesefeldt's optical absorption coefficient and reaches a value 20 times higher than that on the plateau. (This factor varied from 8 to 50 for various samples.) At a temperature of 400°K, the photoelectric peak was broadened and displaced to $h\nu = 5.55$ ev, in agreement again with Fesefeldt's data. The lower yield at the higher temperature was due to the partial destruction of the F-centers before the measurements were made.

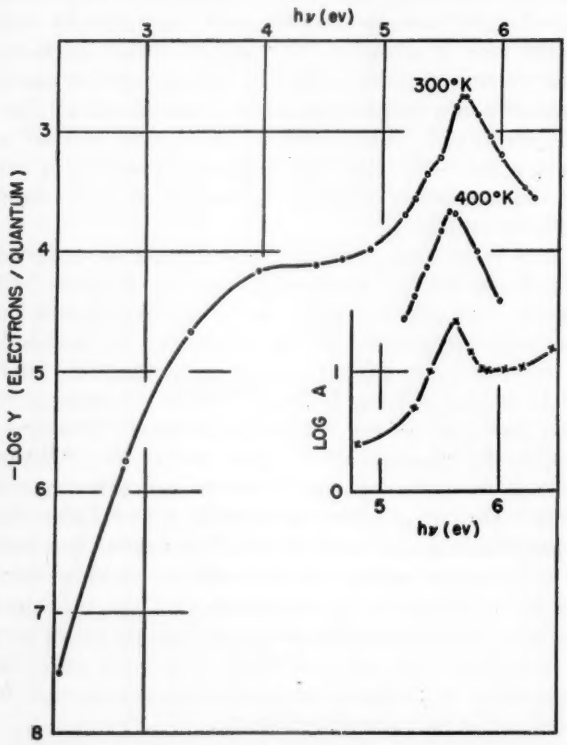

FIG. 3. Spectral distribution of the photoelectric yield Y in electrons/quantum for KI with F-centers. The small inflection just to the left of the peak on the curve for 300°K is reproducible and apparently real. Fesefeldt's values of the optical absorption constant A (in arbitrary units) for KI at 293°K are given on a logarithmic scale below the photoelectric data.

Suppose we tentatively assume that the electrons escaping from the crystal originate in a layer of thickness 10^{-6} cm or less next to the surface. This is less than the photon mean free path at 5.63 ev, where the absorption has its maximum. In accordance with previous interpretations of this absorption, we attribute it entirely to exciton production.[4] Then the number of excitons produced in the thin layer is proportional to the absorption constant at the value of $h\nu$ under consideration. Thus the results described in the paragraph above are to be expected if the photoelectric yield is proportional to the product of the densities of F-centers and excitons in the layer.

When the density of F-centers was lowered, the photoelectric yield decreased in approximately the same ratio at all values of $h\nu$. Thus, the yield due to direct ionization was proportional to the enhanced emission. If we assume that the first type of emission was proportional to the F-center density, we conclude that the second was also. This agrees with the hypothesis above and with the linearity shown by the initial portion of the activation curve in Fig. 2. Since the photoelectric yield in the peak is only 2×10^{-3} electron/quantum, we must conclude that only a small fraction of the exciton is effective in producing external emission.

V. CONCLUDING REMARKS

The main point suggested here is that excitons can increase the efficiency of photoelectric emission from F-centers by more than an order of magnitude. If accepted, it constitutes evidence for exciton mobility. The conclusion rests almost entirely on the surprisingly close similarities between Fesefeldt's optical absorption data and the photoelectric measurements given here. It indicates the possibility of photo-conductivity with an analogous origin. The simple models used in this paper seem capable of describing the gross features of the effect. However, they are presented for acceptance with caution, since the phenomena are doubtless more complex in their details than such models imply. Measurements of photo-electron energy distributions, to be submitted later, are capable of giving greater insight into the processes involved.

We wish to thank Katherine B. Blodgett for the interference step gauge used in making thickness measurements on the thin films. Jean Dickey has given us the benefit of her assistance on frequent occasions. We are grateful to Malcolm Hebb, Harvey Brooks, and Frederick Seitz for their generous interest in this work and for many valuable conversations.

Electromagnetic Forces on a Superconductor

W. V. HOUSTON AND N. MUENCH
The Rice Institute, Houston, Texas
(Received June 5, 1950)

Measurements of the eddy current damping of the rotational oscillations of a tin sphere suspended in a magnetic field from a torsion fiber give the expected results as a function of the magnetic field and the conductivity as long as the tin is a normal conductor. Below the transition temperature, however, the damping torque becomes less than 10^{-5} times its value in the normal state and no changes in period are observed except those attributable to residual frozen-in moments.

I. INTRODUCTION

THE ordinary formulation of the force exerted by an electromagnetic field on matter is divided into two parts. There is the force on charges, $\rho\mathbf{E}$, and the force on currents, $\mathbf{i}\times\mathbf{B}$. In case the matter is a conductor, the charges are located at the surface and the force is transmitted to the body by way of other forces that hold the metal together and prevent the electrons from leaving it. The force associated with a current, however, does not require the intervention of a surface, as is shown by Barlow's wheel. The force is transmitted by means of the interaction between the electrons and the crystal lattice.

The force to be expected on a superconductor has been formulated by London[1] and by von Laue.[2] The charge density is divided into a normal charge density, ρ_0, and a super charge density ρ_s. From the field equations one can show that the total charge density $\rho=\rho_0+\rho_s=0$. Since ρ_s is presumably due to electrons and is therefore negative, ρ_0 must be dominated by the positive ions. Although an electric field will not exist in a superconductor in a steady state, such a field may be present as a transient. During its transient existence it will act on the positive ρ_0 but not on ρ_s. The force on ρ_s is not transmitted to the crystal lattice, and its effect in producing a supercurrent may be described entirely in terms of the magnetic field. An experiment reported by Kikoin and Gubar[3,4] in 1940 on the gyromagnetic ratio of a superconductor can be completely described from this point of view.

Similarly, the current in a superconductor may be divided into an ordinary current, $\mathbf{i}_0$, and a supercurrent, $\mathbf{i}_s$. The normal current transmits a force to the crystal lattice in the usual way, but the supercurrent transmits force only to the surface. When no current is entering or leaving a superconductor, the supercurrent exerts an inward tension on the surface amounting to $\frac{1}{2}\lambda\mathbf{i}_s^2$. However, it transmits no force tangent to the surface.

To examine further the adequacy of this recent formulation, the torsional oscillations of a superconducting sphere in a magnetic field have been studied, and any electromagnetic forces tangent to the surface have been found to be below the limits of observation.

II. APPARATUS

The apparatus is shown schematically in Fig. 1. The sphere was cast in vacuum from spectroscopically pure tin and carefully machined to an inch in diameter. The departure from a true sphere was found to be less than 0.0004 inch. The sphere was attached by a Lucite holder to a glass rod some 80 cm long, at the top of which was a mirror. This assembly was supported by a 3-mil tungsten wire about 60 cm long which served as a torsion fiber, and gave a period of torsional oscillation in the neighborhood of 16.3 sec.

The sphere was cooled by immersion in liquid helium, which was itself surrounded by liquid air. The temperature was controlled by pumping off the helium vapor and was measured in terms of the vapor pressure. To avoid mechanical disturbances from the boiling helium, the sphere was surrounded by a glass tube open at the top to the vapor. By this means good thermal contact was maintained but mechanical contact with the liquid was avoided.

The magnetic field was provided by a pair of Helmholtz coils giving a field of 11.1×10^{-4} weber per sq. meter per ampere, uniform to better than 0.1 percent over the volume of the sphere. These coils were also used to compensate the horizontal component of the earth's field when cooling the sphere through the transition temperature. By means of such compensation any frozen-in moment was practically confined to the vertical direction. Without compensation of the earth's field, or with an additional horizontal field present while cooling the sphere, only an incomplete Meissner effect was observed, and some permanent moment was frozen-in. This moment led to a change in period in a magnetic field. It was not possible, however, to establish a relationship between the magnitude of the frozen-in moment and that of the external field in which the sphere was cooled.

[1] F. London, *Une Conception Nouvelle de la Supra-Conductibilité* (Hermann & Cie, Paris, 1937).
[2] M. von Laue, *Theorie der Supraleitung* (Springer-Verlag, Berlin, 1949).
[3] I. K. Kikoin and S. W. Gubar, J. Phys. U.S.S.R. **III**, 333 (1940).
[4] W. Meissner, Sitz. Bayerische Akademie der Wissenschaften (1948), p. 321.

III. RESULTS

The torsional oscillations were observed by means of a lamp and scale at about a meter. The damping was measured to an accuracy of about 1 percent by recording a series of maximum excursions to each side. The period was obtained to about one part in 1500 by means of a stop watch.

Figure 2 shows the damping coefficient as a function of the square of the magnetic field at a temperature of 4.2°K, and shows the expected linear relationship. The principal source of error is the change in the torsion fiber with time under the weight of the sphere. After the sphere was first suspended the damping due to the fiber steadily decreased, but it was not possible to wait long enough for it to reach a steady value. A relaxation of the stress caused the damping to increase again.

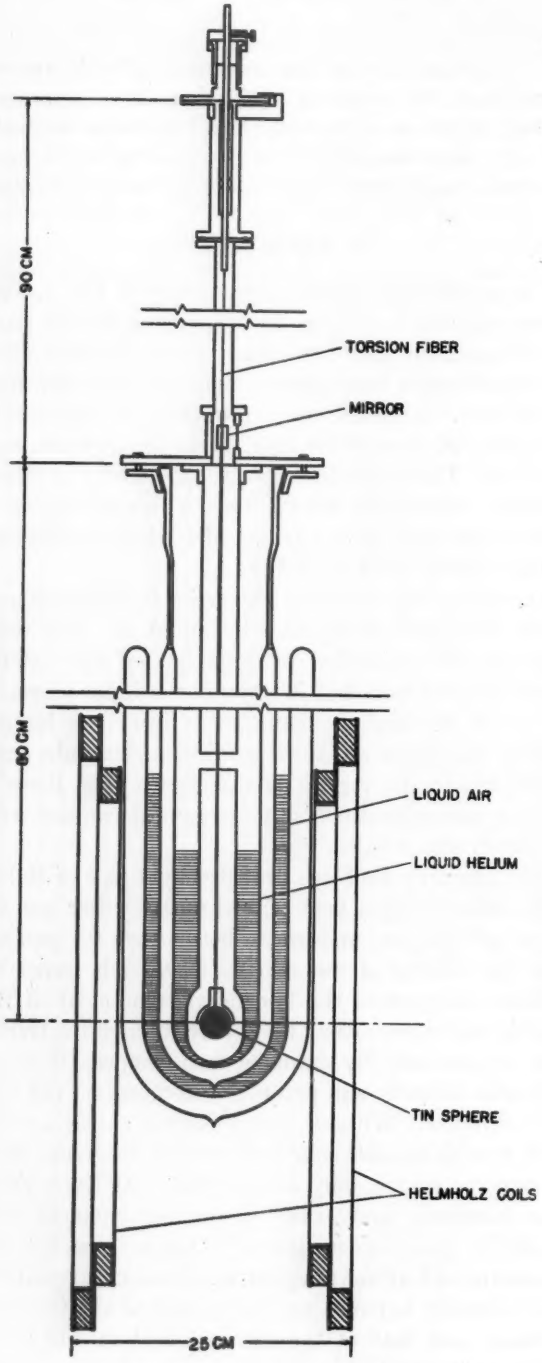

FIG. 1. Scheme of apparatus.

Figure 3 shows the damping coefficient at a temperature of 2.9°K. The observations were made in two series. The best least squares straight lines for the two series separately are designated as 1 and 2. Between series 1 and series 2 the suspension was relieved long enough to check the compensation of the magnetic field. The first reading after the sphere was again suspended led to the point marked A. This point was omitted in computing the lines, since it is obviously associated with changes in the suspension. The heavy line represents both series with a total of 24 observations. Its slope is less than 10^{-5} times the slope in Fig. 2.

Figure 4 shows the square of the period as a function of the square of the magnetic field at 4.2°K. The departures of the points from the least squares straight line represent about 0.01 sec. in period. In the superconducting state no such dependence of period on field strength was observed. The effect of the magnetic field on the period, below the transition temperature, could be associated with a small frozen-in moment.

IV. ANALYSIS AND CONCLUSIONS

One can immediately draw from these results the qualitative conclusion that the London currents in the superconductor appear to slide through the metal without any hindrance. To examine the question quantitatively, however, one must examine the currents to be expected, and the corresponding forces, in both the normal and the superconducting states.

Since the sphere oscillates through only a small angle, the field as seen from the sphere can be approximated closely by a constant field and a small alternating field at right angles to the first. The eddy current produced by the alternating field can be computed in the usual manner, and the force due to its interaction with the constant field gives the desired torque. The alternating field, and hence the torque, can be expressed in terms of the angle of rotation of the sphere. The computed torque is

$$L=-\frac{2\pi B_0^2R^3}{\mu_0}\left\{1-\frac{3\sinh x-\sin x}{x\cosh x-\cos x}\right\}\theta$$

$$-\frac{2\pi B_0^2R^3}{\mu_0\omega}\left\{\frac{3\sinh x+\sin x}{x\cosh x-\cos x}-\frac{6}{x^2}\right\}\dot{\theta}, \quad (1)$$

where $x=(2\omega\mu_0R^2/\tau)^{\frac{1}{2}}$, R is the radius of the sphere, τ is its specific resistivity, ω is the angular frequency and μ_0 is necessary because of the use of rationalized MKS units.

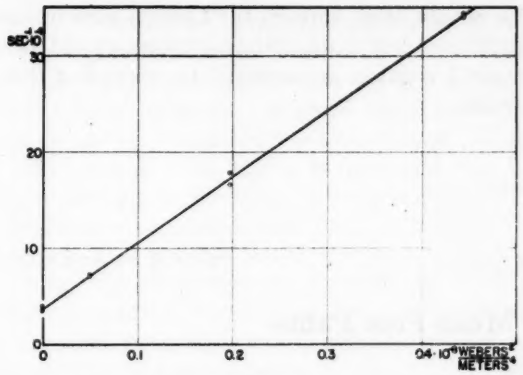

FIG. 2. Damping constant as a function of the magnetic induction with the tin sphere in the normal state at 4.2°K.

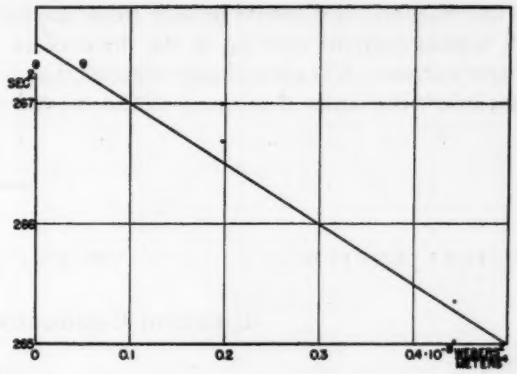

FIG. 4. Square of the period against square of the magnetic induction with the tin sphere in the normal state at 4.2°K.

The second term in Eq. (1), because of its proportionality to $\dot{\theta}$, represents a damping torque. The proportionality to B_0^2 is in accordance with the results plotted in Fig. 2. The magnitude of τ necessary to give the observed slope in Fig. 2 is a reasonable value for tin at 4.2°K.

The first term in Eq. (1) represents a restoring force which is very small until τ becomes small. However, with the τ for tin at 4.2°, x is about 2.6, so that an observable restoring force is to be expected. This is the interpretation of the period dependence on the magnetic field shown in Fig. 4.

The behavior of the sphere in the normal state is completely described by the ordinary eddy current theory in the range of conductivity for which it can be tested. One is then tempted to try to explain the results for the superconducting state along the same lines, by assuming a very small resistivity. As is shown in Fig. 5 the theoretical damping torque reaches a maximum at resistivities only a few times smaller than that of tin at 4.2°. The observed drop of the damping torque could then be explained as due to an increase in x by a factor somewhat over 10^5, corresponding to a decrease in τ by a factor of some 10^{10}. Such a change of resistance was, of course, the original interpretation of superconductivity. But Fig. 5 and Eq. (1) show that such a decrease in conductivity would also lead to a large restoring force and a decrease in period such as is not observed.

One might, however, question whether the restoring force is properly computed, since it is based on the interaction between the eddy currents and the constant field which is assumed to penetrate the sphere. If the conductivity of the sphere is really as high as must be assumed to account for the absence of damping, will the field penetrate the sphere in the time of the experiment or will it be excluded by the eddy currents?

Experimentally the dependence of the period on the magnetic field has been shown to increase with the increase in conductivity as far as its value at 4.2°K.

Theoretically if one considers the penetration of the field as a skin effect at a very low frequency but a very high conductivity, the skin depth for the small transverse field will be much less, in any case, than the penetration of the constant field which is maintained for over an hour at a time. Hence, while the calculated value of the restoring torque may not be quantitatively correct, there should at least be a significant decrease in period such as was not observed.

If the London theory is applied to the problem the damping torque and the restoring torque associated

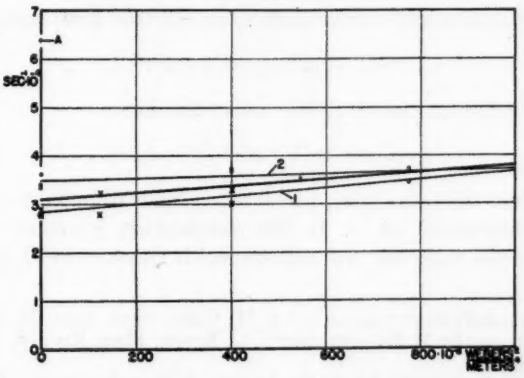

FIG. 3. Damping constant as a function of the magnetic induction with the tin sphere in the superconducting state at 2.9°K.

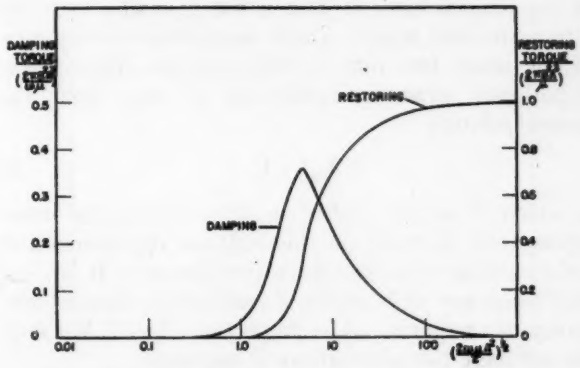

FIG. 5. Damping and restoring torques as a function of the specific resistivity as computed by ordinary methods for quasi stationary eddy currents.

with the magnetic field should be only those due to the small normal currents existing in the presence of the Meissner currents. A crude estimate suggests that these are far below the limits of accuracy of this experiment.

The results, then, support the London view of superconductivity, but a quantitative measurement of the constant λ requires an accuracy far exceeding that of this work.

PHYSICAL REVIEW VOLUME 79, NUMBER 6 SEPTEMBER 15, 1950

Electron Conductivity and Mean Free Paths

FRED P. ADLER
California Institute of Technology, Pasadena, California

AND

HENRY MARGENAU
Yale University, New Haven, Connecticut

(Received May 29, 1950)

Mean free path and electron density are calculated from measurements on the complex conductivity of a discharge. Formulas based on two alternative assumptions are tested against experimental facts; one is constancy of mean free path (independence of electron velocity), the other is constancy of mean free time.

IN a recent paper,[1] devoted to the measurement of complex electron conductivities in a positive column of a glow discharge, attention has been called to the opportunities which such experiments hold for gaining information about kinetic processes taking place in the conducting gas. It was shown that electron densities can be computed from the imaginary as well as the real part of the conductivity when the mean free path is given independently, and that the densities agree tolerably well. The purpose of the present note is to indicate how the mean free path itself can be determined from such measurements, and what light this sheds on other questions of interest in the kinetic theory of discharges.

The formula[2] used in the analysis of the experiments under discussion was based on the assumption of a constant mean free path of the electrons: λ is not a function of electron velocities v and hence is independent of the temperature, T. This is not generally true. An alternative and equally simple supposition is constancy of the mean free *time* τ, which is λ/v. What these hypotheses mean fundamentally is seen from the general relation

$$Nq\lambda=1, \tag{1}$$

in which N is the number density of molecules intercepting the electrons (in this instance Hg atoms) and q the collision cross section, a function of v. It is clear that constancy of λ implies a constant q, whereas constancy of τ requires q to be proportional to v^{-1}. We shall discuss these two alternatives in sequence.

If $\lambda=$ const., the complex conductivity is given by

$$\sigma=\frac{4}{3}\frac{e^2\lambda n}{(2\pi mkT)^{\frac{1}{2}}}[K_2(x_1)-ix_1^{\frac{1}{2}}K_{\frac{1}{2}}(x_1)]\equiv\sigma_r-i\sigma_i, \tag{2}$$

as was shown in reference 2. Here $x_1=(m\omega^2\lambda^2/2kT)$, and ω is the radian frequency of the microwaves. This formula is exact provided the distribution function for the electrons is Maxwellian, and T is the electron temperature. In reference 1, T was measured by probe methods. The ratio σ_i/σ_r is a function of x_1 alone, and it is plotted in reference 2. The experimental ratio leads therefore at once to knowledge of x_1 and, if T is known, to λ. Furthermore if the premise, $\lambda=$ const., is true, the values thus determined should not vary with T.

The situation is somewhat different if $\tau=$ const., and the analysis of reference 2 must be modified. Indeed the conductivity formula is then much simpler.[3] The equations lead to a distribution function which is strictly Maxwellian and corresponds to an electron temperature

$$T''=T+[M\gamma\tau^2/6k(1+\omega^2\tau^2)].$$

The complex conductivity[4] takes the form

$$\sigma=[ne^2\tau/m(1+\omega^2\tau^2)](1-i\omega\tau). \tag{3}$$

Here the ratio σ_i/σ_r, which is $\omega\tau$, leads directly to the determination of τ. If the assumption $\tau=$ const. is true, the ratio test will thus reveal it. Both τ and λ are,

[1] F. P. Adler, J. App. Phys. 20, 1125 (1949).
[2] H. Margenau, Phys. Rev. 69, 508 (1946).
[3] Its derivation is given by J. H. Cahn, Phys. Rev. 75, 838 (1949) and by E. Everhart and S. C. Brown, Phys. Rev. 76, 839 (1949).
[4] This is very similar to the Lorentz formula for the conductivity of electrons. It results if the friction constant, g, in the equation of motion is equated to m/τ.

of course, inversely proportional to the pressure of the gas carrying the discharge, as is evident from Eq. (1).

In Fig. 1 the experimental data are plotted against the electron temperature, the upper curve representing $p\tau$, the lower $p\lambda$. The $p\tau$-values were obtained by using the relation $\sigma_i/\sigma_r=\omega\tau$, and it is seen that the upper curve belies its premise, the constancy of $p\tau$. However, $p\lambda$, which was computed from Eq. (2), is scattered in random fashion about a constant value.

Having thus established the approximate validity of our first alternative, we may use the data to determine the electronic mean free path in Hg. It turns out to be 9.5×10^{-3} cm at 1 mm pressure.

This procedure does not prove that λ is truly independent of velocities, a result which would be very surprising in view of other facts. What it means is that at low electron velocities such as those to which our temperatures correspond, the average of λ over the range of velocities comprised in the Maxwell distribution is constant. Brode[5] has measured collision probabilities of electrons in Hg for energies somewhat higher than ours. His values show a rapid drop between energies of 1 and 2 volts; they correspond to an average λ between $\frac{1}{3}$ and $\frac{1}{2}$ of the value here obtained. If these inferences are to be in harmony, the collision probability must have a maximum in the region where Brode's measurements begin and drop to low values at smaller energies, suggesting a Ramsauer effect. Among the data published by other workers one can easily find values for λ that agree with ours (see Fig. 4 of reference 5), but it is perhaps unwarranted to look for exact numerical agreement because the present conductivity measurements were made at much higher pressures than the other observations.

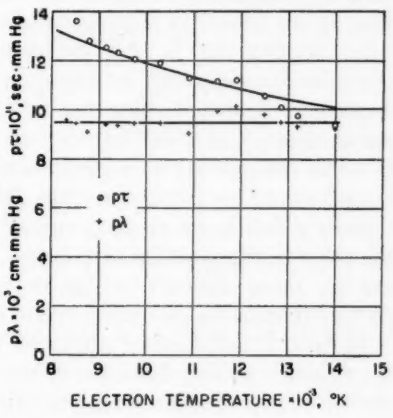

FIG. 1. Experimental data on the dependence of $p\lambda$ and $p\tau$ on electron temperature.

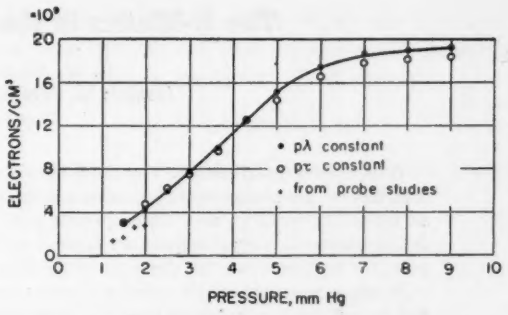

FIG. 2. Electron density as a function of pressure.

There is some internal consistency in the two curves of Fig. 1. To be sure, the upper one is not to be trusted in detail since the theory yielding it is not correct. But the trend is proper: if λ is constant, τ must decrease with v. The curve fitted through the circles corresponds in fact to $p\tau\propto(1/v)\propto T^{-\frac{1}{2}}$; i.e., to $p\lambda=$const.

When the mean free path is determined from the ratio σ_i/σ_r, the density of electrons follows uniquely from the measurements, and the ambiguity inherent in Fig. 8 of reference 1 is eliminated. Figure 2 shows the results (black dots). If the simpler formula (3) were chosen in analyzing the data, the circles would result. Thus it is seen that the electron density is not very sensitive to the kinetic assumptions from which it is derived.

[5] R. B. Brode, Proc. Roy. Soc. **A125**, 134 (1929).

PHYSICAL REVIEW VOLUME 79, NUMBER 6 SEPTEMBER 15, 1950

The S-Matrix in the Heisenberg Representation

C. N. YANG AND DAVID FELDMAN*
Institute for Advanced Study, Princeton, New Jersey
(Received May 17, 1950)

A method is described whereby the S-matrix can be formulated directly in the Heisenberg representation. This has the advantage over the customary formulation in the interaction representation in that the concepts of space-like surfaces and their normals need never be introduced. Quantum electrodynamics and the β formalism of charged mesons are treated as illustrative examples; in particular, it is shown that general rules for writing down the elements of the S-matrix for the latter case may be immediately inferred.

In the second part of this paper, a covariant procedure, independent of the canonical formalism, is carried out for making the transition from the Heisenberg to the interaction representation and is applied to several typical cases; in this way, the S-matrix of the Heisenberg picture is identified with that of other authors.

INTRODUCTION

IN the recent work of Tomonaga[1] and Schwinger,[2] these authors, in their successful attempts to cast quantum electrodynamics (and, in actual fact, all meson theory) into a completely covariant and practical form, found it necessary to introduce the concept of the interaction representation. The essential virtue of this representation is that it leads to an equation of motion for the state vector of the system which is covariant in all its aspects (unlike the Schrödinger representation) while, at the same time, the field variables obey free-field equations of motion and commutation relations (in marked contrast with the corresponding situation in the Heisenberg representation). Upon using this form of the theory, it becomes a simple matter to derive the S-matrix and, indeed, Dyson[3] has shown that the quantum electrodynamics of Tomonaga and Schwinger leads to the well-known rules of Feynman,[4] which enable one to calculate immediately the elements of the S-matrix.

The object of this note is to describe a method where the S-matrix may be formulated directly in the Heisenberg representation. Heretofore, the complexity of the commutation relations of the field quantities in this representation has been regarded as a principal deterrent to the development of a practical field theory in the Heisenberg picture. However, if one makes the basic assumption that it is valid to employ a weak-coupling approximation (which actually is already characteristic of all current relativistic field theories), then a knowledge of the complete commutation relations in the Heisenberg representation is not needed provided one can effect a separation of the motion of the system into that of a free-field part plus that of an interacting part. Tomonaga and Schwinger have done this by going over to the interaction representation. A completely equivalent procedure which we follow in this paper is simply to express each Heisenberg variable as the sum of two parts, the one being a solution of the homogeneous free-field equation (and, indeed, also satisfying the free-field commutation relations), the other being a solution of the inhomogeneous equation.

That the two methods must inevitably lead to the same final results is of course clear. Yet there are distinct advantages to the formulation in the Heisenberg representation which become readily apparent as soon as one considers a situation where one has derivative coupling (as in the pseudoscalar theory with pseudovector coupling) or where one has dynamically dependent field variables (as in the neutral vector meson theory). It is well known that for these cases one is led in the interaction representation to considerable complications involving space-like surfaces and normals thereto which however drop out at the very end;[5] on the other hand, as will be seen below, all meson theories are no more difficult to handle in the Heisenberg picture than is the case of quantum electrodynamics.

In fact, it will become apparent that one can infer the rules for writing down the elements of the S-matrix for all meson theories from the rules which Feynman has established for quantum electrodynamics.

The discussion which follows has been divided into two distinct sections. In the first, the S-matrix is defined in the Heisenberg representation for the case of quantum electrodynamics and then, as an illustration of a more complicated situation, for the case of charged scalar and vector mesons interacting with the electromagnetic field (for the sake of compactness, the β formalism is used). In the second section, it is shown by working through several typical examples that the S-matrix of the Heisenberg picture may be identified with the results of the interaction-representation formulation; here, the method of passing from the Heisenberg to the interaction representation is of especial interest since it is effected in a covariant manner without having to use the canonical formalism.[6]

* Now at the Department of Physics, University of Rochester, Rochester, New York.

[1] S. Tomonaga, Prog. Theor. Phys. **1**, 27 (1946) and later papers; Phys. Rev. **74**, 224 (1948).

[2] J. Schwinger, Phys. Rev. **74**, 1439 (1948); **75**, 651 (1949); **76**, 790 (1949).

[3] F. J. Dyson, Phys. Rev. **75**, 486, 1736 (1949).

[4] R. P. Feynman, Phys. Rev. **76**, 749, 769 (1949).

[5] S. Kanesawa and S. Tomonaga, Prog. Theor. Phys. **3**, 1, 101 (1948); A. Pais and G. E. Uhlenbeck, Phys. Rev. **75**, 1321 (1949).

[6] Cf. N. M. Kroll, Phys. Rev. **75**, 1321 (1949); P. T. Matthews, Phys. Rev. **76**, 1657 (1949); J. S. de Wet, Proc. Roy. Soc. **A201**, 284 (1950).

In fact, the so-called interaction-representation Hamiltonian will appear, in a certain sense, as the density of the S-matrix, so that all conditions of integrability are automatically satisfied.

I. DEFINITION OF THE S-MATRIX

A. Quantum Electrodynamics

We now proceed to show how to formulate the S-matrix directly in the Heisenberg representation without having to make any mention of spacelike surfaces or their normals. We consider first the case of quantum electrodynamics.

The field equations for the Heisenberg variables A_ν and ψ are[7]

$$(\gamma_\nu\partial/\partial x_\nu+m)\psi=ie\gamma_\nu A_\nu\psi, \tag{1}$$

$$(\partial\bar{\psi}/\partial x_\nu)\gamma_\nu-m\bar{\psi}=-ie\bar{\psi}\gamma_\nu A_\nu, \tag{1'}$$

$$\partial^2 A_\nu/\partial x_\lambda{}^2=-j_\nu; \tag{2}$$

where

$$j_\nu=\tfrac{1}{2}ie(\bar{\psi}\gamma_\nu\psi-\psi^T\gamma_\nu{}^T\bar{\psi}^T); \tag{2'}$$

in addition, one has the supplementary condition

$$(\partial A_\nu/\partial x_\nu)\Phi=0, \tag{3}$$

where Φ is the state vector of the system.

Equation (2) can be integrated in the usual manner of classical electrodynamics where A_ν is expressed as the sum of a freely oscillating incoming field $A_\nu{}^{\text{in}}$ and a retarded potential, *viz.*,

$$A_\nu(x)=A_\nu{}^{\text{in}}(x)+\int D^{\text{ret}}(x-x')d^4x'j_\nu(x'). \tag{4}$$

The $D^{\text{ret}}(x-x')$ function is defined, in terms of Schwinger's notation,[2] as

$$D^{\text{ret}}(x-x')=\bar{D}(x-x')-\tfrac{1}{2}D(x-x'). \tag{5}$$

The corresponding function which leads to advanced potentials is

$$D^{\text{adv}}(x-x')=\bar{D}(x-x')+\tfrac{1}{2}D(x-x'). \tag{5'}$$

Upon defining $S^{\text{ret}}(x-x')$ and $S^{\text{adv}}(x-x')$ in a similar manner, it is clear that (1) and (1') may be integrated to give

$$\psi(x)=\psi^{\text{in}}(x)-ie\int S^{\text{ret}}(x-x')d^4x'\gamma_\nu A_\nu(x')\psi(x') \tag{6}$$

and

$$\bar{\psi}(x)=\bar{\psi}^{\text{in}}(x)-ie\int\bar{\psi}(x')\gamma_\nu A_\nu(x')d^4x'S^{\text{adv}}(x'-x). \tag{6'}$$

Equations (6), (6'), and (4) should be regarded as defining the incoming fields ψ^{in}, $\bar{\psi}^{\text{in}}$ and $A_\nu{}^{\text{in}}$.[8] It is already clear that these fields satisfy the homogeneous free-field equations and that, in terms of these variables, the supplementary condition (3) is simply

$$(\partial A_\nu{}^{\text{in}}/\partial x_\nu)\Phi=0. \tag{3'}$$

It is especially important that the incoming fields also satisfy the free-field commutation relations:

$$\left.\begin{aligned}&[\psi_\alpha{}^{\text{in}}(x),\bar{\psi}_\beta{}^{\text{in}}(x')]_+=-iS_{\alpha\beta}(x-x')\\&[A_\nu{}^{\text{in}}(x),A_\lambda{}^{\text{in}}(x')]=i\delta_{\nu\lambda}D(x-x')\\&[A_\nu{}^{\text{in}}(x),\psi_\alpha{}^{\text{in}}(x')]=0\end{aligned}\right\}. \tag{7}$$

To see that Eqs. (7) hold, we notice that at $t=-\infty$ the fields ψ^{in}, $\bar{\psi}^{\text{in}}$, and $A_\nu{}^{\text{in}}$ (and their derivatives) are identical with the true fields ψ, $\bar{\psi}$, and A_ν (and their derivatives) which in turn satisfy the free-field commutation relations at $t=-\infty$. Moreover, ψ^{in}, $\bar{\psi}^{\text{in}}$, and $A_\nu{}^{\text{in}}$ develop with time according to the free-field equations so that Eqs. (7) follow as immediate consequences.

It is evident that, besides Eqs. (6), (6'), and (4), one can write down another set of solutions of the Heisenberg field equations which are expressed in terms of freely oscillating outgoing fields and advanced potentials, i.e.,

$$\left.\begin{aligned}&\psi(x)=\psi^{\text{out}}(x)-ie\int S^{\text{adv}}(x-x')d^4x'\gamma_\nu A_\nu(x')\psi(x')\\&\bar{\psi}(x)=\bar{\psi}^{\text{out}}(x)-ie\int\bar{\psi}(x')\gamma_\nu A_\nu(x')d^4x'S^{\text{ret}}(x'-x)\\&A_\nu(x)=A_\nu{}^{\text{out}}(x)+\int D^{\text{adv}}(x-x')d^4x'j_\nu(x')\end{aligned}\right\}. \tag{8}$$

Once again, the outgoing fields ψ^{out}, $\bar{\psi}^{\text{out}}$, and $A_\nu{}^{\text{out}}$ obey the interaction-free equations and the simple commutation relations

$$\left.\begin{aligned}&[\psi_\alpha{}^{\text{out}}(x),\bar{\psi}_\beta{}^{\text{out}}(x')]_+=-iS_{\alpha\beta}(x-x')\\&[A_\nu{}^{\text{out}}(x),A_\lambda{}^{\text{out}}(x')]=i\delta_{\nu\lambda}D(x-x')\\&[A_\nu{}^{\text{out}}(x),\psi_\alpha{}^{\text{out}}(x')]=0\end{aligned}\right\}. \tag{9}$$

Physically, the meaning of the incoming fields is clear. They coincide at $t=-\infty$ with the Heisenberg fields and would represent the development of the Heisenberg fields with time if the interaction were absent. A similar meaning holds for the outgoing fields except that they reduce to the true Heisenberg variables at $t=+\infty$. Since both the incoming and outgoing fields satisfy the identical commutation relations (7) and (9), we conclude that they are related by a unitary transformation in the following way:

$$\left.\begin{aligned}&\psi^{\text{out}}(x)=\mathbf{S}^{-1}\psi^{\text{in}}(x)\mathbf{S}\\&\bar{\psi}^{\text{out}}(x)=\mathbf{S}^{-1}\bar{\psi}^{\text{in}}(x)\mathbf{S}\\&A_\nu{}^{\text{out}}(x)=\mathbf{S}^{-1}A_\nu{}^{\text{in}}(x)\mathbf{S}\end{aligned}\right\}. \tag{10}$$

[7] We use natural units throughout with $\hbar=c=1$. The notation A^T denotes the transpose of the matrix A.

[8] These equations have also been obtained by G. Källén. The authors wish to thank Dr. Källén for sending them his manuscript before publication.

The unitary matrix S is the S-matrix of Heisenberg. It is uniquely determined by Eqs. (10) except for an arbitrary multiplicative phase factor. We shall defer until Section II the proof that the S-matrix thus defined is indeed identical with the S-matrix which is dealt with in the more customary interaction-representation formulation.

In order to write down explicitly the matrix elements of S, it is possible to proceed by solving Eqs. (6), (6′), and (4) by successive approximations in powers of e and then using Eqs. (8) and (10). In this way, general rules can be formulated for writing down the various terms to any order in e but, for practical computations, they are usually more complicated than Feynman's rules.

B. The Electromagnetic Properties of Charged Mesons in the β-Formalism

The S-matrix formalism may be readily extended to this case in the following way. The equations of motion in the Heisenberg representation now read

$$\left.\begin{aligned}[\beta_\nu(\partial/\partial x_\nu)+\mu]u&=ie\beta_\nu A_\nu u\\ (\partial u^\dagger/\partial x_\nu)\beta_\nu-\mu u^\dagger&=-ieu^\dagger\beta_\nu A_\nu\\ \partial^2 A_\nu/\partial x_\lambda{}^2&=-j_\nu\end{aligned}\right\},\quad(11)$$

where

$$j_\nu=\tfrac{1}{2}ie(u^\dagger\beta_\nu u+u^T\beta_\nu{}^T u^{\dagger T});\qquad(11')$$

we follow here the notation used by Pauli.[9] Besides Eqs. (11), there is also the usual supplementary condition given by Eq. (3). As before, one may replace the differential equations (11) by corresponding integral equations with the aid of appropriate Green's functions. To determine these, we observe that

$$\left(\beta_\nu\frac{\partial}{\partial x_\nu}+\mu\right)\left[\beta_\lambda\frac{\partial}{\partial x_\lambda}-\frac{1}{\mu}\left(\beta_\lambda\frac{\partial}{\partial x_\lambda}\right)^2-\frac{1}{\mu}\left(\mu^2-\frac{\partial^2}{\partial x_\lambda{}^2}\right)\right]=\left(\frac{\partial^2}{\partial x_\nu{}^2}-\mu^2\right),\quad(12)$$

whence, defining $T^{\rm ret}(x-x')$ by

$$T^{\rm ret}(x-x')=\left[\beta_\nu\frac{\partial}{\partial x_\nu}-\frac{1}{\mu}\left(\beta_\nu\frac{\partial}{\partial x_\nu}\right)^2-\frac{1}{\mu}\left(\mu^2-\frac{\partial^2}{\partial x_\nu{}^2}\right)\right]\Delta^{\rm ret}(x-x'),\quad(13)$$

it follows that

$$[\beta_\nu(\partial/\partial x_\nu)+\mu]T^{\rm ret}(x-x')=-\delta(x-x').\quad(14)$$

It should be noticed that, in virtue of the properties of the $\Delta^{\rm ret}$-function, $T^{\rm ret}(x-x')$ vanishes if x lies outside the future light cone of x'. One may also define the $T^{\rm adv}$ and T_F functions by replacing $\Delta^{\rm ret}$ in (13) by $\Delta^{\rm adv}$ and Δ_F, respectively.[10]

The solutions of (11) may now be written in the following integral form:

$$\left.\begin{aligned}u(x)&=u^{\rm in}(x)-ie\int T^{\rm ret}(x-x')d^4x'\beta_\nu A_\nu(x')u(x')\\ u^\dagger(x)&=u^{\dagger\rm in}(x)-ie\int u^\dagger(x')\beta_\nu\times A_\nu(x')d^4x'T^{\rm adv}(x'-x)\\ A_\nu(x)&=A_\nu{}^{\rm in}(x)+\int D^{\rm ret}(x-x')d^4x'j_\nu(x')\end{aligned}\right\}.\quad(15)$$

It is once again essential to note that the incoming fields $u^{\rm in}$, $u^{\dagger\rm in}$ and $A_\nu{}^{\rm in}$ are to be regarded as defined by Eqs. (15). They not only satisfy the free-field equations but also, by an argument similar to that used in our earlier discussion of quantum electrodynamics, the free-field commutation relations, *viz.*,

$$\left.\begin{aligned}[u_\alpha{}^{\rm in}(x),\,u_\beta{}^\dagger(x')]&=-i\left[\beta_\nu\frac{\partial}{\partial x_\nu}-\frac{1}{\mu}\left(\beta_\nu\frac{\partial}{\partial x_\nu}\right)^2\right]_{\alpha\beta}\Delta(x-x')\\ [A_\nu{}^{\rm in}(x),\,A_\lambda{}^{\rm in}(x')]&=i\delta_{\nu\lambda}D(x-x')\\ [A_\nu{}^{\rm in}(x),\,u_\alpha{}^{\rm in}(x')]&=0\end{aligned}\right\};\quad(16)$$

the supplementary condition reduces as before to Eq. (3′).

One can write down, besides Eqs. (15), another set of integral solutions of (11):

$$\left.\begin{aligned}u(x)&=u^{\rm out}(x)-ie\int T^{\rm adv}(x-x')d^4x'\beta_\nu A_\nu(x')u(x')\\ u^\dagger(x)&=u^{\dagger\rm out}(x)-ie\int u^\dagger(x')\beta_\nu\times A_\nu(x')d^4x'T^{\rm ret}(x'-x)\\ A_\nu(x)&=A_\nu{}^{\rm out}(x)+\int D^{\rm adv}(x-x')d^4x'j_\nu(x')\end{aligned}\right\}.\quad(17)$$

The outgoing fields $u^{\rm out}$, $u^{\dagger\rm out}$, and $A_\nu{}^{\rm out}$ obey the free-field equations and commutation relations. It therefore follows that there exists a unitary transformation con-

[9] W. Pauli, Rev. Mod. Phys. 13, 203 (1941).

[10] The Δ_F-function which we use is identical with Dyson's. We shall later also use the S_F function which is defined by

$$S_F(x-x')=[\gamma_\lambda(\partial/\partial x_\lambda)-m]\Delta_F(x-x').$$

necting the incoming and outgoing quantities, *viz.*,

$$\left.\begin{aligned} u^{\text{out}}(x)&=\mathbf{S}^{-1}u^{\text{in}}(x)\mathbf{S}\\ u^{\dagger\text{out}}(x)&=\mathbf{S}^{-1}u^{\dagger\text{in}}(x)\mathbf{S}\\ A_\nu^{\text{out}}(x)&=\mathbf{S}^{-1}A_\nu^{\text{in}}(x)\mathbf{S}\end{aligned}\right\},\quad(18)$$

where $\mathbf{S}$ is once again the S-matrix of Heisenberg.

One can calculate the elements of the S-matrix from Eqs. (15) to (18) following a procedure which is identical with that described for the case of quantum electrodynamics. It is therefore clear that at no point in the evaluation of $\mathbf{S}$ is it necessary to resort to the concept of space-like surfaces and their normals. It is an essential advantage of the formulation of the S-matrix in the Heisenberg representation that the extraneous complications associated with space-like surfaces do not enter.[11]

A further advantage of this procedure is that it becomes possible to formulate rules for writing down the elements of the S-matrix which are the exact analogues of the Feynman-Dyson rules of electrodynamics. In fact, it is only necessary to replace the S_F function[10] of electrodynamics by the T_F function, and the γ_ν-matrices by β_ν-matrices; the sign of the term corresponding to any Feynman diagram differs in the β-formalism from quantum electrodynamics by a factor $(-1)^l$ where l is the number of closed meson loops.[12]

The proof is based upon the fact that, while the Tomonaga-Schwinger equations for the various cases which are encountered in meson theory assume a more or less complicated form according to whether one does or does not have derivative coupling or dynamically dependent field components, the equations defining the S-matrix in the Heisenberg representation are of a comparatively simple nature and, in fact, are very similar to one another in form. This last fact enables one to infer immediately the above-mentioned rules for the case of the β-formalism from the corresponding Feynman-Dyson rules for electrodynamics. The factor $(-1)^l$ is a complication which arises due to the fact that the particles with which we are dealing obey Bose statistics.[13]

We wish finally to remark that all of these considerations (*viz.*, the definition of the S-matrix in the Heisenberg representation and its subsequent characterization by a set of Feynman-like rules for writing down the various matrix elements) may be directly extended to the various cases of meson-nucleon couplings.

[11] For a discussion of charged meson theories in the interaction representation with the β-formalism see M. Neuman and W. H. Furry, Phys. Rev. **76**, 1677 (1949); R. G. Moorhouse, Phys. Rev. **76**, 1691 (1949); D. C. Peaslee, Phys. Rev. (to be published); and T. Kinoshita, Prog. Theor. Phys. (to be published).

[12] Similar results have been noted by R. P. Feynman using his method of space-time approach to field theory. Cf. footnote 24, Phys. Rev. **76**, 769 (1949).

[13] The easiest way to see this is to derive first the rules for the case of two scalar fields φ_1 and φ_2 coupled by the term $\varphi_1^*\varphi_1\varphi_2$. This can be done by Dyson's method just as easily as in quantum electrodynamics, since there are no complications due to surfaces and their normals. One has then only to compare the equations defining the S-matrix in this case with Eqs. (15) to (18) to arrive at the rules for the β formalism.

II. IDENTIFICATION OF THE S-MATRIX

A. Quantum Electrodynamics

It remains to verify that the S-matrix as defined in the Heisenberg representation is indeed the same as that which emerges from the Tomonaga-Schwinger theory. We shall see that, by generalizing suitably the concepts of incoming and outgoing fields which were introduced earlier, we are led directly to a product representation for the S-matrix which is, in fact, Dyson's representation.

In order to go to over to the interaction representation, let us introduce a set of space-like surfaces $\sigma(x)$ and denote their normals by $n_\nu(x)$. Define the function $D^\sigma(x, x')$, where x and x' are not necessarily on the surface σ, in the following way:

$$D^\sigma(x, x')=D^{\text{ret}}(x-x') \quad \text{if } x' \text{ is later than } \sigma,$$

$$D^\sigma(x, x')=D^{\text{adv}}(x-x') \quad \text{if } x' \text{ is earlier than } \sigma,$$

that is,

$$D^\sigma(x, x')=\frac{1-\epsilon(\sigma, x')}{2}D^{\text{ret}}(x-x')+\frac{1+\epsilon(\sigma, x')}{2}D^{\text{adv}}(x-x'),\quad(19)$$

where

$$\epsilon(\sigma, x')=+1 \quad \text{if } \sigma \text{ is later than } x',$$
$$\epsilon(\sigma, x')=-1 \quad \text{if } \sigma \text{ is earlier than } x'.$$

It is clear that an equivalent representation of $D^\sigma(x, x')$ is given by

$$D^\sigma(x, x')=-\tfrac{1}{2}[\epsilon(x-x')-\epsilon(\sigma, x')]D(x-x'),\quad(19')$$

where $\epsilon(x-x')$ equals $+1$ or -1 according as x is later or earlier than x'.

Let us also define

$$S^\sigma(x, x')=[\gamma_\nu(\partial/\partial x_\nu)-m]\Delta^\sigma(x, x').\quad(19'')$$

Then, with aid of the generalized Green's functions $D^\sigma(x, x')$ and $S^\sigma(x, x')$, Eqs. (1) and (2) may be integrated to give the following:

$$\left.\begin{aligned}\psi(x)&=\psi(x, \sigma)-ie\int S^\sigma(x, x')d^4x'\gamma_\nu A_\nu(x')\psi(x')\\ A_\nu(x)&=A_\nu(x, \sigma)+\int D^\sigma(x, x')d^4x'j_\nu(x')\end{aligned}\right\}.\quad(20)$$

The quantities $\psi(x, \sigma)$ and $A_\nu(x, \sigma)$ are to be regarded as defined by Eqs. (20). For fixed σ, they satisfy the free-field equations and, when x is on σ, they reduce to the Heisenberg fields $\psi(x)$ and $A_\nu(x)$; this reduction holds also for $\partial A_\nu(x, \sigma)/\partial x_\lambda$.

It will be convenient for what follows to introduce the symbols $\psi(x/\sigma)$ and $\partial\psi(x/\sigma)/\partial x_\nu$ by

$$\psi(x/\sigma)=[\psi(x,\sigma)]_{x \text{ on } \sigma},$$
$$\partial\psi(x/\sigma)/\partial x_\nu=[\partial\psi(x,\sigma)/\partial x_\nu]_{x \text{ on } \sigma}.$$

With this notation, one then has

$$\psi(x/\sigma)=\psi(x),\quad A_\nu(x/\sigma)=A_\nu(x),$$
$$\partial A_\nu(x/\sigma)/\partial x_\lambda=\partial A_\nu(x)/\partial x_\lambda.$$

Note that, as $\sigma\to-\infty$, $D^\sigma(x,x')\to D^{\text{ret}}(x-x')$ so that $A_\nu(x,\sigma)$ goes over into the incoming field $A_\nu^{\text{in}}(x)$. Correspondingly, as $\sigma\to+\infty$, $D^\sigma(x,x')\to D^{\text{adv}}(x-x')$ so that $A_\nu(x,\sigma)$ goes over into the outgoing field $A_\nu^{\text{out}}(x)$.[14]

In contrast to Eq. (3′), the supplementary condition becomes in terms of $A_\nu(x,\sigma)$

$$\left[\frac{\partial A_\nu(x,\sigma)}{\partial x_\nu}-\int_\sigma D(x-x')j_\nu(x')d\sigma_\nu'\right]\Phi=0. \tag{21}$$

The commutation relations of the $\psi(x,\sigma)$ and $A_\nu(x,\sigma)$ are the usual free-field expressions:

$$\left.\begin{aligned}&[\psi_\alpha(x,\sigma),\bar\psi_\beta(x',\sigma)]_+=-iS_{\alpha\beta}(x-x')\\&[A_\nu(x,\sigma),A_\lambda(x',\sigma)]=i\delta_{\nu\lambda}D(x-x')\\&[A_\nu(x,\sigma),\psi_\alpha(x',\sigma)]=0\end{aligned}\right\}. \tag{22}$$

These are obviously correct for x and x' on σ and, since $\psi(x,\sigma)$ and $A_\nu(x,\sigma)$ satisfy free-field equations, they are true in general.

Now, a set of Eqs. (22) holds for every surface σ whence it follows that there exists a unitary transformation $U(\sigma,\sigma')$, such that

$$\left.\begin{aligned}&\psi(x,\sigma)=U^{-1}(\sigma,\sigma')\psi(x,\sigma')U(\sigma,\sigma')\\&A_\nu(x,\sigma)=U^{-1}(\sigma,\sigma')A_\nu(x,\sigma')U(\sigma,\sigma')\end{aligned}\right\}. \tag{23}$$

It is clear that $U(\infty,-\infty)$ is the **S**-matrix which we have defined earlier.

We proceed next to obtain an explicit representation for the **S**-matrix. To do this, we note that the following relation is valid:

$$U(\sigma,\sigma')=U(\sigma'',\sigma')U(\sigma,\sigma''). \tag{24}$$

It is therefore natural to write

$$\begin{aligned}\mathbf{S}&=U(\infty,-\infty)\\&=\cdots U(\sigma_0,\sigma_{-1})U(\sigma_1,\sigma_0)U(\sigma_2,\sigma_1)\cdots,\end{aligned} \tag{25}$$

where $\cdots\sigma_1,\ \sigma_0,\ \sigma_{-1},\ \cdots$ denote an infinite sequence of space-like surfaces which proceed steadily into the past. To obtain an explicit expression for **S**, we let the surfaces approach one another so that (25) expresses **S** as the product of infinitesimal unitary transformations. It is therefore sufficient to obtain $U(\sigma,\sigma')$ to the first order as $\sigma\to\sigma'$. We accordingly write

$$U(\sigma,\sigma')=1-i\int_{\sigma'}^{\sigma}H(x'/\sigma)d^4x'+\cdots, \tag{26}$$

where

$$H(x'/\sigma)=i[\delta U(\sigma,\sigma')/\delta\sigma(x')]_{\sigma=\sigma'}. \tag{26′}$$

Strictly speaking, we should have used the notation $H(x',\sigma)$ in place of $H(x'/\sigma)$ in Eq. (26); however, the procedure which we have followed is not inconsistent since, in the end, σ is made to approach σ'.

Substituting (26) into (25), we get

$$\begin{aligned}\mathbf{S}=\cdots&\left[1-i\int_{\sigma_{-1}}^{\sigma_0}H(x/\sigma)d^4x\right]\\&\times\left[1-i\int_{\sigma_0}^{\sigma_1}H(x/\sigma)d^4x\right]\cdots.\end{aligned} \tag{25′}$$

To find $H(x/\sigma)$, we differentiate (23) with respect to σ and set $\sigma=\sigma'$; then,

$$\left.\begin{aligned}&i\frac{\delta\psi(x,\sigma)}{\delta\sigma(x')}=[\psi(x,\sigma),H(x'/\sigma)]\\&i\frac{\delta A_\nu(x,\sigma)}{\delta\sigma(x')}=[A_\nu(x,\sigma),H(x'/\sigma)]\end{aligned}\right\}. \tag{27}$$

Now, from (20), we have

$$\begin{aligned}\psi(x,\sigma)-\psi(x,\sigma')&=ie\int[S^\sigma(x,x')-S^{\sigma'}(x,x')]\\&\qquad\times d^4x'\gamma_\nu A_\nu(x')\psi(x')\\&=ie\int_{\sigma'}^{\sigma}S(x-x')d^4x'\gamma_\nu A_\nu(x')\psi(x'),\end{aligned} \tag{28}$$

$$A_\nu(x,\sigma)-A_\nu(x,\sigma')=-\int_{\sigma'}^{\sigma}D(x-x')d^4x'j_\nu(x'). \tag{28′}$$

But, $\delta\psi(x,\sigma)/\delta\sigma(x')$ and $\delta A_\nu(x,\sigma)/\delta\sigma(x')$ can be determined directly from (28) and (28′) whence

$$\left.\begin{aligned}&[\psi(x,\sigma),H(x'/\sigma)]=-eS(x-x')\gamma_\nu\\&\qquad\times A_\nu(x'/\sigma)\psi(x'/\sigma)\\&[A_\nu(x,\sigma),H(x'/\sigma)]=-iD(x-x')j_\nu(x'/\sigma)\end{aligned}\right\}. \tag{29}$$

It is at once clear from (29) and (22) that

$$H(x'/\sigma)=-j_\nu(x'/\sigma)A_\nu(x'/\sigma), \tag{30}$$

so that the **S**-matrix assumes the form

$$\begin{aligned}\mathbf{S}=\cdots&\left(1+i\int_{\sigma_{-1}}^{\sigma_0}j_\nu(x/\sigma)A_\nu(x/\sigma)d^4x\right)\\&\times\left(1+i\int_{\sigma_0}^{\sigma_1}j_\nu(x/\sigma)A_\nu(x/\sigma)d^4x\right)\cdots.\end{aligned} \tag{31}$$

[14] We are indebted to Dr. R. J. Glauber for pointing out this generalization of the incoming and outgoing fields and their relation to the Hamiltonian in the interaction representation. Cf. also M. Neuman and W. H. Furry, reference 11; K. V. Roberts, Phys. Rev. 77, 146 (1950); J. S. de Wet, reference 6.

To complete the identification with Dyson's result, we note that Eqs. (23) imply

$$\left.\begin{aligned}\psi(x/\sigma)&=U^{-1}(\sigma,-\infty)\psi^{\text{in}}(x)U(\sigma,-\infty)\\ A_\nu(x/\sigma)&=U^{-1}(\sigma,-\infty)A_\nu^{\text{in}}(x)U(\sigma,-\infty)\end{aligned}\right\} \quad (32)$$

or

$$\left.\begin{aligned}U(\sigma,-\infty)\psi(x/\sigma)&=\psi^{\text{in}}(x)U(\sigma,-\infty)\\ U(\sigma,-\infty)A_\nu(x/\sigma)&=A_\nu^{\text{in}}(x)U(\sigma,-\infty)\end{aligned}\right\}. \quad (32')$$

It is clear from (32′) that pulling a factor $\psi(x/\sigma)$ [or $A_\nu(x/\sigma)$] through from the right to the left of $U(\sigma,-\infty)$ converts it into a $\psi^{\text{in}}(x)$ [or $A_\nu^{\text{in}}(x)$]. By applying this procedure successively to all the factors of Eq. (31) taken in the order of decreasing time, we find

$$S=\cdots\left(1+i\int_{\sigma_0}^{\sigma_1} j_\nu^{\text{in}}(x)A_\nu^{\text{in}}(x)d^4x\right)\times\left(1+i\int_{\sigma_{-1}}^{\sigma_0} j_\nu^{\text{in}}(x)A_\nu^{\text{in}}(x)\right)\cdots, \quad (33)$$

which is identical with Dyson's expression if we take the field quantities in the interaction representation to be the incoming fields.

B. Neutral Vector Mesons with Vector Coupling

In the remainder of this paper, we shall consider briefly those complications which arise on making the transition to the interaction representation when the field components are not all dynamically independent or when one has derivative coupling. The case of neutral vector mesons interacting with nucleons through vector coupling will serve as an illustration of the former situation. The equations of motion of the field variables in the Heisenberg representation are

$$\left.\begin{aligned}[\gamma_\nu(\partial/\partial x_\nu)+M]\psi&=\tfrac{1}{2}if\gamma_\nu(A_\nu\psi+\psi A_\nu)\\ \partial A_\nu/\partial x_\nu&=0\\ (\partial^2/\partial x_\lambda^2-\mu^2)A_\nu&=-j_\nu\end{aligned}\right\}, \quad (34)$$

where

$$j_\nu=\tfrac{1}{2}if(\bar\psi\gamma_\nu\psi-\psi^T\gamma_\nu{}^T\bar\psi^T). \quad (34')$$

Note that these equations have been put into a form which is invariant with respect to charge conjugation.

The solutions of (34) are

$$\left.\begin{aligned}\psi(x)=\psi(x,\sigma)&-\tfrac{1}{2}if\int S^\sigma(x,x')d^4x'\gamma_\nu\times[A_\nu(x')\psi(x')+\psi(x')A_\nu(x')]\\ A_\nu(x)=A_\nu(x,\sigma)&+\int\left(\delta_{\nu\lambda}-\frac{1}{\mu^2}\frac{\partial^2}{\partial x_\nu\partial x_\lambda}\right)\times\Delta^\sigma(x,x')d^4x'j_\lambda(x')\end{aligned}\right\}. \quad (35)$$

It is here necessary to include the term involving second derivatives in the Green's function in order to guarantee that

$$\partial A_\nu(x,\sigma)/\partial x_\nu=0. \quad (36)$$

It is important to note that, when x is on σ, $A_\nu(x,\sigma)$ and its derivatives do *not* reduce to $A_\nu(x)$ and its derivatives; in fact,

$$A_\nu(x/\sigma)=A_\nu(x)-(1/\mu^2)n_\nu n_\lambda j_\lambda(x). \quad (37)$$

On the other hand, it is the $A_\nu(x/\sigma)$ and not the $A_\nu(x)$ which obey the free-particle commutation relations; as a consequence, the following equations are valid:

$$\left.\begin{aligned}[\psi_\alpha(x,\sigma),\bar\psi_\beta(x',\sigma)]_+&=-iS_{\alpha\beta}(x-x')\\ [A_\nu(x,\sigma),A_\lambda(x',\sigma)]&=i\left(\delta_{\nu\lambda}-\frac{1}{\mu^2}\frac{\partial^2}{\partial x_\nu\partial x_\lambda}\right)\times\Delta(x-x')\\ [A_\nu(x,\sigma),\psi_\alpha(x',\sigma)]&=0\end{aligned}\right\}. \quad (38)$$

It is therefore evident from (36) and (38) that, for any two surfaces σ and σ', there exists a unitary transformation $U(\sigma,\sigma')$ such that

$$\left.\begin{aligned}\psi(x,\sigma)&=U^{-1}(\sigma,\sigma')\psi(x,\sigma')U(\sigma,\sigma')\\ A_\nu(x,\sigma)&=U^{-1}(\sigma,\sigma')A_\nu(x,\sigma')U(\sigma,\sigma')\end{aligned}\right\}. \quad (39)$$

We now take over Eqs. (26), (26′), and (25′) from the preceding case and proceed to calculate $H(x'/\sigma)$. The method is exactly the same as before; in place of Eqs. (28) and (28′), however, we have

$$\psi(x,\sigma)-\psi(x,\sigma')=\tfrac{1}{2}if\int_{\sigma'}^{\sigma}S(x-x')d^4x'\gamma_\nu\times[A_\nu(x')\psi(x')+\psi(x')A_\nu(x')], \quad (40)$$

$$A_\nu(x,\sigma)-A_\nu(x,\sigma')=-\left(\delta_{\nu\lambda}-\frac{1}{\mu^2}\frac{\partial^2}{\partial x_\nu\partial x_\lambda}\right)\times\int_{\sigma'}^{\sigma}\Delta(x-x')d^4x'j_\lambda(x'). \quad (40')$$

One finds ultimately that

$$[\psi(x,\sigma),H(x'/\sigma)]=-\tfrac{1}{2}fS(x-x')\gamma_\nu\times[A_\nu(x')\psi(x')+\psi(x')A_\nu(x')], \quad (41)$$

$$[A_\nu(x,\sigma),H(x'/\sigma)]=-i\left(\delta_{\nu\lambda}-\frac{1}{\mu^2}\frac{\partial^2}{\partial x_\nu\partial x_\lambda}\right)\times\Delta(x-x')j_\lambda(x'). \quad (41')$$

Equation (41) may be rewritten in the following form with aid of (37):

$$\begin{aligned}[\psi(x,\sigma),H(x'/\sigma)]&=-fS(x-x')\gamma_\nu A_\nu(x'/\sigma)\psi(x'/\sigma)\\ &\quad-(f/2\mu)n_\nu(x')n_\lambda(x')S(x-x')\gamma_\nu\\ &\quad\times[j_\lambda(x'/\sigma)\psi(x'/\sigma)+\psi(x'/\sigma)j_\lambda(x'/\sigma)].\end{aligned} \quad (41'')$$

One must therefore have

$$H(x'/\sigma)=-j_\nu(x'/\sigma)A_\nu(x'/\sigma) -(1/2\mu^2)[n_\nu(x')j_\nu(x'/\sigma)]^2. \quad (42)$$

It is evident from the discussions of the previous case that the S-matrix is finally given by

$$\mathbf{S}=\cdots\left[1-i\int_{\sigma_0}^{\sigma_1}H^{\text{in}}(x/\sigma)d^4x\right] \times\left[1-i\int_{\sigma_{-1}}^{\sigma_0}H^{\text{in}}(x/\sigma)d^4x\right]\cdots, \quad (43)$$

where[15]

$$H^{\text{in}}(x/\sigma)=-j_\nu^{\text{in}}(x)A_\nu^{\text{in}}(x) -(1/2\mu^2)[n_\nu(x)j_\nu^{\text{in}}(x)]^2. \quad (44)$$

C. Pseudoscalar Mesons with Pseudovector Coupling

As a last example, let us consider a situation where we have derivative coupling, *viz.*, the case of pseudoscalar mesons interacting with nucleons through pseudovector coupling. The equations of motion have the form

$$\left.\begin{aligned}\left(\gamma_\nu\frac{\partial}{\partial x_\nu}+M\right)\psi&=\tfrac{1}{2}ig\gamma_5\gamma_\nu\left(\psi\frac{\partial\varphi}{\partial x_\nu}+\frac{\partial\varphi}{\partial x_\nu}\psi\right)\\ \left(\frac{\partial^2}{\partial x_\nu^2}-\mu^2\right)\varphi&=\frac{\partial j_\nu}{\partial x_\nu}\end{aligned}\right\}, \quad (45)$$

where

$$j_\nu=\tfrac{1}{2}ig(\bar\psi\gamma_5\gamma_\nu\psi-\psi^T\gamma_\nu{}^T\gamma_5{}^T\bar\psi^T). \quad (45')$$

The solutions of (45) are

$$\psi(x)=\psi(x,\sigma)-\tfrac{1}{2}ig\int S^\sigma(x,x')d^4x'\gamma_5\gamma_\nu \times\left[\psi(x')\frac{\partial\varphi(x')}{\partial x_\nu'}+\frac{\partial\varphi(x')}{\partial x_\nu'}\psi(x')\right], \quad (46)$$

$$\varphi(x)=\varphi'(x,\sigma)-\int\Delta^\sigma(x,x')d^4x'\frac{\partial j_\nu(x')}{\partial x_\nu'}. \quad (46')$$

Actually, it is more appropriate to modify the Green's function in (46′) so as to give

$$\varphi(x)=\varphi(x,\sigma)-\int\frac{\partial\Delta^\sigma(x,x')}{\partial x_\nu}d^4x'j_\nu(x'). \quad (46'')$$

By choosing the Green's function in this way, we have arranged for $\varphi(x,\sigma)$ to satisfy the following boundary conditions:

$$\left.\begin{aligned}\varphi(x/\sigma)&=\varphi(x)\\ \partial\varphi(x/\sigma)/\partial x_\nu&=\partial\varphi(x)/\partial x_\nu+n_\nu n_\lambda j_\lambda(x)\end{aligned}\right\}. \quad (47)$$

The term involving the normals is precisely what is needed in order that the commutation relations of the $\psi(x,\sigma)$ and $\varphi(x,\sigma)$ shall reduce to those of the free-field quantities, i.e.,

$$\left.\begin{aligned}[\psi_\alpha(x,\sigma),\bar\psi_\beta(x',\sigma)]_+&=-iS_{\alpha\beta}(x-x')\\ [\varphi(x,\sigma),\varphi(x',\sigma)]&=i\Delta(x-x')\\ [\varphi(x,\sigma),\psi_\alpha(x',\sigma)]&=0\end{aligned}\right\}. \quad (48)$$

From this point on, things go exactly as before. One is led to

$$[\psi(x,\sigma),H(x'/\sigma)]=-\tfrac{1}{2}gS(x-x')\gamma_5\gamma_\nu \times\left[\psi(x')\frac{\partial\varphi(x')}{\partial x_\nu'}+\frac{\partial\varphi(x')}{\partial x_\nu'}\psi(x')\right], \quad (49)$$

$$[\varphi(x,\sigma),H(x'/\sigma)]=i\frac{\partial\Delta(x-x')}{\partial x_\nu}j_\nu(x'). \quad (49')$$

We rewrite Eq. (49) using (47):

$$\begin{aligned}&[\psi(x,\sigma),H(x'/\sigma)]\\ &\quad=-gS(x-x')\gamma_5\gamma_\nu\psi(x'/\sigma)[\partial\varphi(x'/\sigma)/\partial x_\nu']\\ &\qquad+\tfrac{1}{2}gn_\nu(x')n_\lambda(x')S(x-x')\gamma_5\gamma_\nu\\ &\qquad\times[\psi(x'/\sigma)j_\lambda(x'/\sigma)+j_\lambda(x'/\sigma)\psi(x'/\sigma)].\end{aligned} \quad (49'')$$

One has therefore

$$H(x'/\sigma)=-j_\nu(x'/\sigma)\frac{\partial\varphi(x'/\sigma)}{\partial x_\nu'}+\tfrac{1}{2}[n_\nu(x')j_\nu(x'/\sigma)]^2. \quad (50)$$

Evidently Eq. (43) can be taken over for the present case with

$$H^{\text{in}}(x/\sigma)=-j_\nu^{\text{in}}[\partial\varphi^{\text{in}}(x')/\partial x_\nu'] +\tfrac{1}{2}[n_\nu(x')j_\nu^{\text{in}}(x')]^2. \quad (50')$$

We wish to thank Professors J. R. Oppenheimer and W. Pauli for helpful discussions.

[15] Cf. Y. Miyamoto, Prog. Theor. Phys. 3, 124 (1948).

Effect of Inclusions on Coercive Force of Iron

L. J. DIJKSTRA AND C. WERT
Institute for the Study of Metals, University of Chicago, Chicago, Illinois
(Received May 19, 1950)

A theory is developed for the contribution to the coercive force of iron of randomly distributed non-magnetic inclusions. Two contributing effects are examined: (1) the surface tension effect, and (2) the effect of internal magnetic poles. It is found that the coercive force depends both on the total volume fraction of inclusions and the state of dispersion. For a given composition of alloy, for particles both much larger and much smaller than the thickness of the domain wall, δ, the net contribution to the coercive force is small. The largest effect occurs for particles whose diameter is about equal to δ. Measurements have been made using a dispersion in iron of Fe_3C in the shape of spheres, the diameters of which could be varied over the desired range. The maximum effect on coercive force is found to occur for particles of size about 1200 angstroms, indicating a value for δ of about this magnitude. For this value of d the measured value of the coercive force is found to agree well with the calculated value.

I. INTRODUCTION

IN recent years considerable progress has been made in understanding the origin of the coercive force in ferromagnetic materials. The effect on coercive force of non-magnetic inclusions was first clearly recognized by Kersten.[1] He proposed that the increase in coercive force caused by the presence of inclusions was a simple surface tension effect; the domain wall has a definite surface tension and therefore a strong tendency to stick to the inclusions in order to reduce the total wall energy (Fig. 1a and 1b).

Kersten's work was criticized by Néel,[2] who expressed the idea that the main effect was caused by the presence of internal poles at the interface between inclusions and matrix. In passing an inclusion the domain wall causes a redistribution of these magnetic poles. This results in a lowering of magnetostatic energy (Fig. 1c and 1d) and hence a tendency of the wall to stick to the inclusions.

The experimental work described in this paper deals with the effect of inclusions in iron. The paper itself has two aims: (1) to re-examine the various contributions to the coercive force which non-magnetic inclusions can make, and (2) to interpret the results of the experimental work in the light of this analysis.

II. EFFECT OF INCLUSIONS

In examining the effect of inclusions we shall follow a different procedure from that used by Néel.[2] He used a three-dimensional Fourier series method to represent the lattice inhomogeneities, both inclusions and lattice strains. In this paper we use a less elaborate mathematical treatment, but shall keep closely from the very outset to the physical picture of inclusions which we set up. Lattice strains we neglect entirely, even those strains set up by the inclusions themselves.

The assumptions and conventions used are the following. The ferromagnetic matrix in the demagnetized state is divided into a larger number of domains, which for simplicity are assumed to have the shape of cubes with edges of length L. The coordinate system x, y, z has its axes along the cube edges. The x direction is a preferred direction of magnetization.[3] The 180° domain wall, which we consider as moving through a particular domain, is parallel (except for a possible slight curvature) to the xy-plane. On the $-z$ side of the wall the magnetization I_s is in the $-x$ direction; on the $+z$ side, in the $+x$ direction. Under the action of an applied field H in the $+x$ direction the domain wall thus has a tendency to shift in the $+z$ direction. Each domain contains n non-magnetic inclusions distributed at random in the matrix. The exact shape of these particles is immaterial so long as their dimensions in all directions are about the same. In carrying out the calculations we shall assume that the particles are spherical with diameter d.

III. GENERAL ANALYSIS

First we consider the domain wall as being rigid and plane. The wall, to which we attribute the thickness δ,

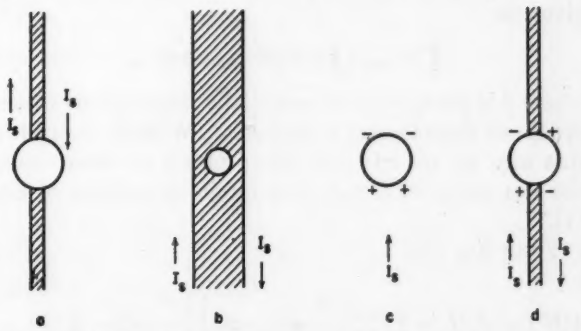

FIG. 1. (a) and (b) show how the total wall energy is reduced by non-magnetic inclusions. In Fig. 1a the diameter of the inclusion is larger, in Fig. 1b smaller than the wall thickness δ. (c) and (d) demonstrate the re-distribution of internal poles which occurs when a domain wall passes the inclusion. The magnetostatic energy in Fig. 1(d) is lower than in Fig. 1(c). I_s is the intensity of magnetization.

[1] M. Kersten, *Ferromagnetische Hysterese u. Koerzitionkraft* (S. Hirzel, Leipzig, 1943).
[2] L. Néel, Ann. Univ. Grenoble 22, 299 (1945–1946).
[3] For a general picture of the present view of domain theory the reader is referred to C. Kittel. Rev. Mod. Phys. 21, 541 (1949).

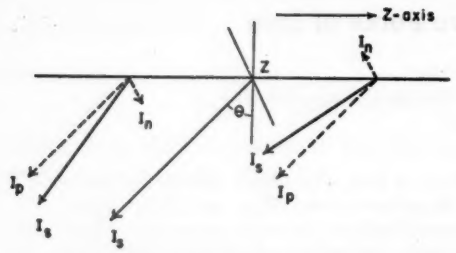

FIG. 2. Model for the calculation of the magnetostatic energy for an inclusion inside the domain wall.

is located at z_0. The average number of particles cut or absorbed (partially or completely) by the domain wall and which have their centers on either the $+z$ or $-z$ side of the wall is $n(d+\delta)/2L$. The mean deviation of this number [which is of order $(n(d+\delta)/2L)^{\frac{1}{2}}$] gives rise to the coercive force H_c. We introduce the function $\phi(z-z_0)$ as being the reduction in energy of the system due to the interaction between the domain wall and an inclusion centered at (x, y, z); $\phi(z-z_0)$ will be specified later. If we distinguish among the various inclusions by the index i, then the equilibrium value of H necessary to hold the wall at z_0 is given by

$$2H(z_0)I_s L^2=\sum_i \partial[\phi(z_i-z_0)]/\partial z_0. \tag{1}$$

In this expression I_s is the intensity of magnetization and the $\sum_i$ is to be taken over all particles in the domain for which $\phi\neq 0$.

Since the equilibrium value of $H(z_0)$ determined by Eq. (1) depends on z_0, there is for each domain a particular value of z_0 for which $H^2(z_0)$ is a maximum; this maximum we denote as $H_{\max}^2$. We will then define the coercive force for the specimen as a whole to be $H_c=[\![\langle H_{\max}^2\rangle]\!]^{\frac{1}{2}}$; the double brackets indicating the average over the domains. If $\langle H^2(z_0)\rangle$ is the mean value of $H^2(z_0)$ over z_0, then the relation between $[\![\langle H_{\max}^2\rangle]\!]$ and $\langle H^2(z_0)\rangle$ is, according to Néel,[2] most conveniently given as

$$[\![\langle H_{\max}^2\rangle]\!]\approx 2\langle H^2(z_0)\rangle \ln p, \tag{2}$$

where p is the number of essentially independent values $H(z_0)$ can assume over a distance L. With H_c defined in this way we are left with the problem of determining the *rms* values of $H(z_0)$. This we do by analysis of Eq. (1).

From Eq. (1)

$$4\langle H^2(z_0)\rangle I_s^2 L^4=\sum_i\sum_j\left\{\frac{\partial}{\partial z_0}\phi(z_i-z_0)\right\}\left\{\frac{\partial}{\partial z_0}\phi(z_j-z_0)\right\}$$

$$=n\left\langle\left\{\frac{\partial}{\partial z}\phi(z-z_0)\right\}^2\right\rangle, \tag{3}$$

since $\partial\phi(z_i-z_0)/\partial z_0$ and $\partial\phi(z_j-z_0)/\partial z_0$ are independent if $i\neq j$, and $\partial\phi(z_i-z_0)/\partial z_0=0$. The probability that the center of a particle lies between z and $z+dz$ is dz/L, so from Eq. (2) we obtain

$$4\langle H^2(z_0)\rangle I_s^2 L^4=n\int_{z_0-\frac{1}{2}(d+\delta)}^{z_0+\frac{1}{2}(d+\delta)}\left\{\frac{\partial}{\partial z}\phi(z-z_0)\right\}^2\frac{dz}{L}. \tag{3a}$$

The factor p in Eq. (2) must yet be determined in terms of the geometry of our picture. Clearly, for values of z_0 for which $|\Delta z_0|$ is at least of order $\frac{1}{2}(d+\delta)$, the distribution of particles will show no correlation. This means that p is of the order $2L/(d+\delta)$. Hence from Eqs. (2) and (3a)

$$H_c=\left[2n\ln\left(\frac{2L}{d+\delta}\right)\right.$$

$$\left.\times\int_{z_0-\frac{1}{2}(d+\delta)}^{z_0+\frac{1}{2}(d+\delta)}\left\{\frac{\partial}{\partial z}\phi(z-z_0)\right\}^2 dz\right]^{1/2}\Big/ 2I_s L^{5/2}. \tag{4}$$

With this expression the problem of computing the value of H_c is reduced to that of finding the function $\phi(z-z_0)$. The remainder of this section will be devoted to an evaluation of this quantity for the "surface tension" effect as well as for the "internal magnetic poles" effect.

The Surface Tension Effect

The reduction in energy of the system in this case is considered to be caused simply by the lowering of the net wall "volume" when the wall contains an inclusion.[1] It is assumed that the presence of the inclusion in no way affects the direction of I_s in the matrix or in the wall. For calculation of this effect it is convenient to consider the two extreme cases: (1) for $d\gg\delta$ and (2) for $d\ll\delta$.

For the first case

$$\phi(z-z_0)=\pi\gamma_{180^\circ}[\tfrac{1}{4}d^2-(z-z_0)^2] \text{ for } |z-z_0|<\tfrac{1}{2}d, \tag{5}$$

where γ_{180° is the wall energy per unit area for a 180° wall. Direct substitution of this expression into Eq. (4) gives for the coercive force for this case

$$H_c\approx 1.75(\gamma_{180^\circ}/I_s L)\alpha^{\frac{1}{2}}(\ln 2L/d)^{\frac{1}{2}} \text{ for } d\gg\delta, \tag{6}$$

where n has been eliminated by means of the expression $n\pi d^3/6L^3=\alpha$, the volume fraction of inclusions. Equation (6) is identical with the result of Néel,[2] if one takes his "distance de correlation" η to be of the order of d.

For $d\ll\delta$

$$\phi(z-z_0)=\tfrac{1}{6}\pi d^3 E(z-z_0) \text{ for } |z-z_0|<\tfrac{1}{2}\delta. \tag{7}$$

Here $E(z-z_0)$ is the energy per unit volume of the wall at a point z inside the wall. $E(z-z_0)$ can be calculated exactly but since we are interested only in $\langle(\partial\phi/\partial z)^2\rangle$ (see Eq. (3)), the approximation $\partial E/\partial z=$ const. must lead to a reasonably accurate result for H_c. By this procedure H_c is underestimated somewhat. Since

$$\int_{z_0-\frac{1}{2}\delta}^{z_0+\frac{1}{2}\delta} E dz=\gamma_{180^\circ},$$

we approximate E by

$$E=(2\gamma_{180°}/\delta)[1\pm 2(z-z_0)/\delta] \text{ for } z<z_0 \text{ or } z>z_0. \quad (7a)$$

It is a simple calculation to show that

$$H_c\approx 2.8(\gamma_{180°}/I_sL)(d/\delta)^{\frac{1}{2}}\alpha^{\frac{1}{2}}(\ln 2L/\delta)^{\frac{1}{2}} \text{ for } d\ll\delta. \quad (8)$$

Analogous calculations can be made for any value of d/δ. For the limiting case $d\approx\delta$, (6) and (8) give the same value apart from a small numerical factor. A more exact calculation gives

$$H_c\approx\frac{7}{8}\frac{\gamma_{180°}}{I_sL}\alpha^{\frac{1}{2}}\left(\ln\frac{L}{\delta}\right)^{\frac{1}{2}} \text{ for } d\approx\delta. \quad (9)$$

Curve a in Fig. 4 gives a plot of H_c *vs.* d for constant α according to Eqs. (4) to (9). For this purpose we have used the values $\alpha=3\times10^{-3}$, $\gamma_{180°}=2$ ergs/cm², $I_s=1700$ gauss, $L=10^{-3}$ cm,[4] and $\delta=10^{-5}$ cm. For $d\approx5\delta$, H_c passes through a faint maximum of about 0.2 oersted.

"Internal Magnetic Poles" Effect

A spherical non-magnetic inclusion present in the matrix corresponds to a magnetic dipole of self-energy

$$E_{\text{dip}}=\tfrac{1}{2}(4\pi/3)I_s^2V, \quad (10)$$

where V is the volume of the particle (Fig. 1c). As soon as a particle is partially or completely enclosed by a domain wall a redistribution of the internal magnetic poles takes place. This results in a lowering of the magnetostatic energy. In principle this effect can be understood from the symmetrical situation shown in Fig. 1d. A 180° wall passing through the center of an inclusion gives rise to a magnetic quadrupole of self-energy[5]

$$E_{\text{quad}}\approx\tfrac{1}{2}E_{\text{dip}}=\pi I_s^2V/3. \quad (10a)$$

In treating the effect of internal poles it is in general not correct to assume that I_s remains unchanged in the vicinity of these inclusions. The magnetic field originating from the internal magnetic poles tends to rotate I_s in the vicinity of an inclusion out of the original direction in such a way that the magnetostatic energy is partially released. In neglecting this interaction one would obtain for particles for which $d\gtrsim\delta$ a value for the coercive force which is much too high.

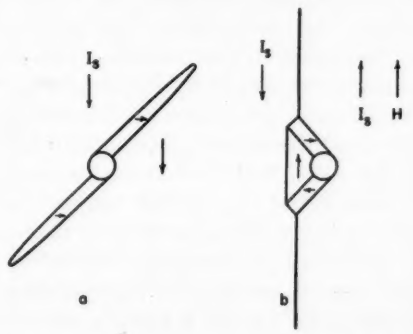

FIG. 3. (a) Observed domain pattern around a non-magnetic inclusion. (b) Structure after a 180° wall has passed the inclusion. The lowest energy state in the absence of a magnetic field is obtained for the wall passing through the center of the inclusion.

[4] Bozorth and Dillinger, Phys. Rev. **41**, 345 (1932).
[5] L. Néel, Cahiers phys. **25**, 21 (1944).

TABLE I. Dependence of E_{dip} on particle size.

d	10^{-3} cm ($\sim100\delta$)	10^{-4} cm ($\sim10\delta$)
k	30	5
$E_{\gamma_{90°}}$	0.8×10^{-4} ergs	1.2×10^{-7} ergs
E_d	1×10^{-4} ergs	2.5×10^{-7} ergs
E_{dip}	30×10^{-4} ergs	30×10^{-7} ergs

For the case in which $d\ll\delta$, however, the interaction between I_s and the internal magnetic poles can be safely neglected since the exchange forces oppose a rotation of I_s on such a local scale. The main term of $\phi(z-z_0)$ in this case is obtained in the following way. For any point z inside the wall the vector I_s makes a certain angle θ with the preferred direction. In a small region about z we split I_s up into the two components I_n and I_p, respectively, normal and parallel to I_s at z. (Fig. 2.) For a region in which the total change of direction of I_s, $\Delta\theta$, is small we can write

$$I_p=I_s[1-\tfrac{1}{2}(\Delta z d\theta/dz)^2]; \quad I_n=I_s\Delta z d\theta/dz.$$

It is easy to see that for a particle with center located at z the component I_p gives rise to a dipole, I_m to a quadrupole. Because of the symmetry, there is no mutual interaction. Taking average values for I_p and I_n over Δz, we find for the corresponding energy terms

$$E_{\text{dip}}'=\frac{2\pi}{3}I_s^2V\left[1-\frac{1}{12}\left(\frac{d\theta}{dz}\right)d^2\right],$$

$$E_{\text{quad}}'=\frac{\pi}{48}I_s^2V\left(\frac{d\theta}{dz}\right)^2d^2.$$

Hence

$$\phi(z-z_0)=E_{\text{dip}}-(E_{\text{dip}}'+E_{\text{quad}}')$$
$$=\pi V\left(\frac{1}{18}-\frac{1}{48}\right)I_s^2\left(\frac{d\theta}{dz}\right)^2d^2. \quad (11)$$

The function $\theta(z)$ can be calculated.[2] However, to simplify the calculation we shall follow the same procedure as we used previously; namely, since in Eq. (2) $\langle(\partial\theta/\partial z)^2\rangle$ occurs, we take

$$(d\theta/dz)^2=(2\pi^2/\delta^2)[1\pm(2/\delta)(z-z_0)] \text{ for } z<z_0 \text{ or } z>z_0. \quad (11a)$$

By carrying through the remainder of the calculation indicated by Eq. (4), one readily finds that

$$H_c\approx 2.8(I_sd^{7/2}/L\delta^{5/2})\alpha^{\frac{1}{2}}(\ln 2L/\delta)^{\frac{1}{2}} \text{ for } d\ll\delta. \quad (11b)$$

It is instructive to make a comparison here. By comparison of Eqs. (8) and (11b) it is seen that for

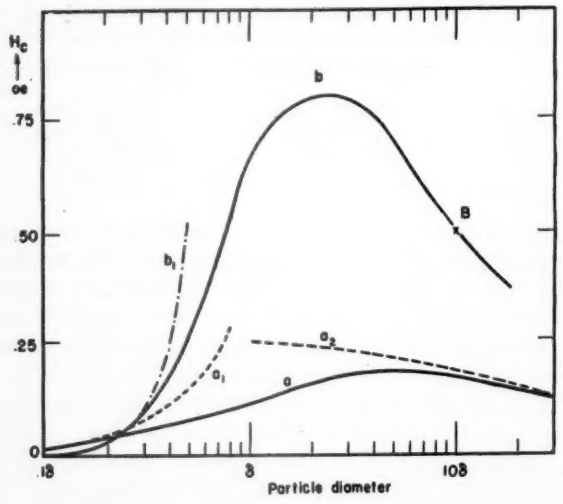

FIG. 4. Expected behavior of the coercive force H_c in iron caused by a volume fraction of a random distribution of non-magnetic inclusion equal 3×10^{-3} as a function of the particle diameter d. Curve (a) is for the surface tension effect, curve (b) for the "internal poles" effect; (a_1), (a_2), and (b_1) are the extrapolated curves according to Eqs. (8), (6), and (11b), respectively. Point B is calculated from Eq. (13). The curves give only orders of magnitude.

small particles ($d\ll\delta$) the effect of "internal magnetic poles" is $I_s^2d^2/\gamma_{180°}\delta$ times as large as the "surface tension" effect. For extremely small particles the surface tension effect, though itself small, is the larger of the two. For particles of the order $\frac{1}{4}\delta$ the two effects are about equal; for particles larger than this the magnetic pole effect starts to predominate.

For $d\geqq\delta$ the interaction between the internal poles and the vector I_s can no longer be neglected. For $d\gg\delta$ almost complete release of magnetic energy takes place with the appearance of a secondary domain structure as drawn in Fig. 3a.[5,6] The relation between d and the equilibrium value of l (2× the length of a secondary domain) follows essentially from an early study by Döring.[7] The usual approach is to assume that the domains have the shape of an ellipsoid of revolution with short axis d and long axis l. Then the total wall energy

$$E_{\gamma_{90°}}=\gamma_{90°}\times\text{surface area}=\tfrac{1}{4}\pi^2\gamma_{90°}ld.$$

The magnetostatic energy, E_d, stored in the demagnetizing field is given by

$$E_d=aNI_s^2\times\text{vol}=\tfrac{1}{6}\pi aNI_s^2ld.$$

The demagnetizing factor $N=(4\pi^2/k^2)(\ln2k-1)$ if $k=l/d\gg1$. The factor a has been introduced by Williams, Bozorth, and Shockley[6] to take into account the permeability of the matrix. For pure iron $a=\frac{1}{16}$. Finally the energy term due to the applied field H,

$$E_H=HI_s\times\text{vol}=\tfrac{1}{6}\pi HI_sld^2.$$

Minimizing $E=E_{\gamma_{90°}}+E_d+E_H$ with respect to l one easily finds

$$k^2=\frac{8\pi aI_s^2d(\ln2k-2)}{3\pi\gamma_{90°}-2HI_sd}. \tag{12}$$

Taking $H=1$ oersted, $\gamma_{90°}=1$ erg/cm², one can calculate k for values of d up to 3×10^{-5} cm when the denominator goes to zero, which means that the secondary domains grow until they join the domain walls. To show that by this secondary domain structure an almost complete release of magnetostatic energy E_{dip} does take place Table I shows values calculated neglecting the term $2HI_sd$ in Eq. (7). We see from Table I that for very large particles the release of energy is almost complete, but that less is released as the size of the particle decreases. As d approaches δ a yet smaller fraction of the dipole energy is released, especially when the inclusion becomes too small for the formation of well-developed secondary domains.

It is not difficult to show that when well-developed secondary domains are formed the average equilibrium field is given by

$$2(\langle H^2\rangle)^{\frac{1}{2}}I_sL^2=(l/L)n\pi d\gamma_{180°}.$$

Since $l=kd$

$$H_c\approx(\langle H^2\rangle)^{\frac{1}{2}}\approx(3\gamma_{180°}k/I_sd)\alpha\text{ for }d\gg\delta. \tag{13}$$

According to Eqs. (12) and (13) H_c will decrease rather slowly with increasing d. In case $L\gg kd$ the right member of Eq. (13) must be multiplied by $(2\ln2L/kd)^{\frac{1}{2}}$ to account for the difference between $\langle H^2(z_0)\rangle$ and $[\langle H_{\max}{}^2\rangle]$. The application of Eq. (13) to practical cases is rather limited, since, in general, for a well-developed domain structure kd is of the same order as L. For $\alpha=3\times10^{-3}$, formal substitution of $d=10^{-4}$ cm yields $H_c\sim0.4$ oersted.

For $d\approx\delta$, the secondary domains have shrunk to a disturbed region of dimension δ around the inclusion. A calculation of the energy terms involved in this case is rather difficult, and we shall only make a rather crude estimate by interpolating the results for $d\gg\delta$ and $d\ll\delta$. According to the preceding paragraphs, the release in magnetostatic energy E_{dip} as given by Eq. (1) due to the interaction between the internal charges at the interface and the vector I_s is complete for $d\gg\delta$ and negligible for $d\ll\delta$. For $d\sim\delta$ it seems reasonable to assume a reduction of E_{dip} by this interaction of about $\frac{1}{2}$. To find the magnitude of ϕ we must make a further estimate; neglecting the foregoing interaction between dipole and matrix we find by interpolation of Eqs. (10a) through (11) that for a particle, for which $d\approx\delta$, located symmetrically in the domain wall E_{dip} is reduced by a factor of about $\frac{1}{4}$. Hence the magnitude of ϕ is about $E_{\text{dip}}/8$. We compare this to the surface tension effect, where the corresponding value of ϕ is of the order $\gamma_{180°}V/\delta$. Hence the "magnetic pole effect" will be of the order of $\frac{1}{8}E_{\text{dip}}/(\gamma_{180°}V/\delta)\sim4$ times as large

[6] Williams, Bozorth, and Shockley, Phys. Rev. **75**, 155 (1949).
[7] Becker and Döring, *Ferromagnetismus* (Verlag Julius Springer, Berlin, 1938), p. 192.

as that due to the surface tension effect. (It is clear that this may be in error by a factor of 2 or more.) The expected behavior of H_c is shown in Fig. 4 by the curve b taking $\alpha=3\times10^{-8}$. After a rapid increase for $d<\delta$, H_c tends for $d>\delta$ to approach a behavior as expressed by Eq. (13). For $d\sim\delta$, H_c passes through a maximum of the order of one oersted.

IV. EXPERIMENT

It is apparent from the foregoing analysis that one might expect inclusions to have a pronounced effect on the coercive force; for a given value of α the most striking effects might be observed for particles of the same order of size as the thickness of the Bloch wall. We have examined experimentally this possibility in iron using the compound Fe_3C in finely dispersed form. Since for iron the 180° Bloch wall has a theoretical thickness of about 1000A, it was necessary to have particles of controllable dimensions of about this size. By the metallurgical treatment described below it was possible for us to prepare samples of iron containing inclusions of Fe_3C in the form of randomly distributed spheres, the diameters of which were varied between 400 and 3000A. With these samples we were able (1) to find the "critical size" for maximum effect for given α on the coercive force, and (2) to determine the magnitude of H_c for a given volume fraction of inclusions of this critical size.

The samples were prepared and the measurements were made in the following manner. The specimens were Puron iron wires drawn to a size of 0.03 in. diameter by one foot long. Highly super-saturated solid solutions of C in α-Fe were prepared by quenching to room temperature from 720°C an alloy of 0.02 percent in α-Fe. These specimens were then tempered at selected temperatures in the range 125°C to 350°C, which tempering resulted in the gradual disappearance of C from solid solution into a second phase, Fe_3C, in α-Fe. This phase change was traced by means of the internal friction found in this alloy. During the phase change the coercive force was also measured at intervals at 20°C.

The detailed analysis of the results depends entirely upon certain facts which we believe applies to this phase change. These facts are the following: (1) the Fe_3C precipitates in the form of spheres, and (2) the number of these spheres per unit volume remains constant during the major part of the precipitation at a given temperature. Originally these proposals were supported only by some rather indirect analyses of earlier experimental work.[8] More recently, however, these proposals have been given additional support by examination of specimens using an electron microscope.[9]

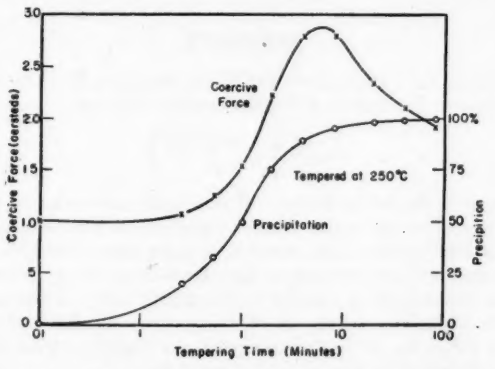

FIG. 5. Coercive force and precipitation as a function of time for an alloy of 0.02 percent of carbon in iron which was tempered at 250°C.

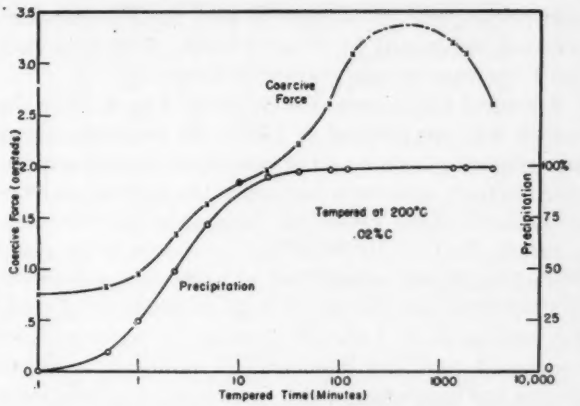

FIG. 6. Coercive force and precipitation for an alloy tempered at 200°C.

Since we wish to know the manner in which the coercive force varies with the particle size, we must have some way of computing the particle diameter. Clearly this is given by the expression

$$\alpha=\tfrac{1}{6}\pi d^3N', \tag{14}$$

where N' is the number of particles per unit volume. This expression, of course, is valid if the particles are all the same size; a condition which is a consequence of the two proposals made above. Since α can be calculated readily, d can be computed once N' is known. N' itself may be calculated from the expression,[10]

$$N'=(3/4\pi)(2D\tau)^{-\frac{3}{2}}[(n_0-n_1)/(n_\infty(0)-n_1)]^{\frac{3}{2}}. \tag{15}$$

In this expression n_0, n_1 and $n_\infty(0)$ are carbon concentrations referring to (1) concentration of C in Fe_3C, (2) equilibrium solid solubility at the temperature of tempering and (3) initial concentration in solid solution, respectively. D is the diffusion coefficient of C in α-Fe, which has been determined accurately as a function of temperature by one of the authors.[11] τ is an empirically measured time constant, it is the time required for the phase transformation to become 60

[8] C. Wert, J. App. Phys. **20**, 943 (1949); C. Zener, J. App. Phys. **20**, 950 (1949).

[9] Unpublished results of an investigation made by J. Radavich, Purdue University.

[10] C. Wert and C. Zener, J. App. Phys. **21**, 5 (1950). This expression was given incorrectly in this reference. All calculations in this paper and in reference 10 were made with the correct expression, Eq. (15).

[11] C. Wert (to be published).

percent complete. N' is found to vary rapidly with temperature, decreasing by about a factor of 10 with each 100°C increase in temperature of tempering.

A typical measurement is shown in Fig. 5. Here the carbon was precipitated at 250°C. At intervals during the tempering the amount of precipitate formed and the coercive force were both measured; the time dependence of both of these quantities is shown. At this temperature $D=1.3\times10^{-10}$ cm²/sec., τ is seen to be about 70 sec., $n_\infty(0)$ was about 0.02 wt percent, $n_1\approx0$ and n_0 is about 6 wt percent, hence $N_{250°}'$ was calculated using Eq. (15) as about 1.8×10^{12} particles/cc. Since we have concluded that this number, N', is about constant during the tempering, d can be computed at any stage of the phase change by means of Eq. (14). For example, at the 95 percent precipitation point $\alpha\approx0.003$, hence at this point $d\sim1400$A. The increase in coercive force due to this volume fraction of precipitate in this state of dispersion is about 1.9 oersteds. (The initial value of about one oersted is apparently caused by other inclusions (perhaps oxides), internal stress or grain boundaries.)

There is one aspect of the curves in Fig. 6 which must yet be explained; this is the decrease in the coercive force when the precipitation is slowly drawing to a close. We can offer at present only a qualitative explanation of this phenomenon; we believe it to be due to the coalescence of precipitate particles, which coalescence takes place only after the precipitation is essentially complete. It results in a decrease in N' and an increase in d; as we shall show shortly, particles of diameter 1400A are already "oversize;" a further increase in d can only lessen the coercive force. Hence in this case H_c drops upon coalescence. It must not be supposed, however, that this coalescence after precipitation always results in a decrease in coercive force; Fig. 6 shows this not to be the case. At 200°C for 95 percent precipitation $d\sim1000$A; this, as it turns out, is "undersize" for maximum effect. Hence coalescence will at first increase the coercive force until the particles reach an optimum size, after which further coalescence causes a decrease as the particles become now "oversize." Since we have no way even of estimating the rate of coalescence, we can offer at present no quantitative arguments to support our view.

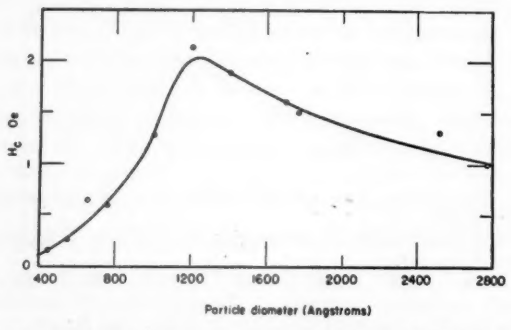

FIG. 7. Coercive force as a function of particle size for $\alpha\approx0.003$.

Data and calculations pertinent to the theory developed in Sec. II taken from data shown in Figs. 6 and 7 and from numerous other measurements not shown in detail are presented in Fig. 7. Here is plotted the coercive force as a function of partizle size for a given value of α, namely, 0.003 (which we have seen occurs at the 95 percent transformation point). The curve in Fig. 8 shows that the critical size for maximum effect on coercive force is about 1200A. Since the theory developed earlier indicates a maximum effect for $d\sim\delta$, this means that δ for α-Fe must be about 1200A also. The magnitude of H_c at the maximum, two oersteds is also in reasonable agreement with the order of magnitude of one oersted predicted in Sec. II.

Unfortunately, Fe_3C is ferromagnetic itself with a saturation magnetization of about 1200 gauss and a Curie point of 200°C. If the magnetic anisotropy of Fe_3C would be very small compared with Fe, the internal poles effect would be smaller by a factor $I_2^2(\text{Fe})/I_s^2(\text{Fe}_3\text{C})\approx10$ below the Curie point of Fe_3C. At the Curie point a rise in H_c could then be expected. On the other hand, for a very large anisotropy particles of this small size will approximately give the same contribution as if they were non-magnetic.

It is not clear then how to take into account the ferromagnetic properties of Fe_3C in consideration of either the "surface tension" or "magnetic poles" effect. To try to throw a little light on this problem we have made one further measurement. A specimen of iron containing carbon in solid solution was tempered at 210°C to give nearly complete precipitation. The Fe_3C in this state was dispersed in spheres of diameter 3200A. The coercive force of this sample was measured as a function of temperature up to 300°C. That part of the coercive force due to the inclusions is shown plotted as a function of temperature in Fig. 8. It is to be observed that no sudden change in the coercive force occurs at 200°C, the Curie point of Fe_3C. The simplest way to account for this effect is to consider the small Fe_3C particles to behave as non-magnetic inclusions.

APPENDIX

To allow for a small curvature of the domain wall we represent the plane of the wall by a Fourier series as follows:

$$z=z_0+\sum_q z_q \begin{matrix}\sin\\ \cos\end{matrix}\left(\frac{2\pi qy}{L}\right). \tag{A1}$$

where z_0 is the mean distance of the plane above the xy plane. The x-components in the Fourier development can be neglected for, as Néel[2] pointed out, since I_s is along the x-direction these components would give rise to very large extra energy terms due to the appearance of internal free magnetic poles at the surface of the wall. The energy E of the system can be written as $E=E_1+E_2+E_3$. E_1 is the energy of the slightly curved wall if no inclusions were present and is equal to

$$E_1=I^2\gamma_{180°}+\tfrac{1}{2}\pi^2\gamma_{180°}\sum_q q^2z_q^2.$$

E_2 is the decrease in E by the inclusions and is given by

$$E_2=-\sum_i \phi[z_i-z(x_i, y_i)].$$

E_3 is the magnetic energy terms, hence

$$E_3=-2HI_sL^2z_0.$$

For equilibrium of the wall at z_0, H, and z_q have to satisfy $\partial E/\partial z_0=0$ and $\partial E/\partial z_q=0$. The first condition gives

$$2HI_sL^2=-\sum_i \frac{\partial}{\partial z}[z_i-z(x_i, y_i)]. \tag{A2}$$

The second condition gives

$$\pi^2\gamma_{180°}q^2z_q=-\sum_i\left\{\frac{\partial}{\partial z}\phi[z_i-z(x_i, y_i)]\sin(\cos)\frac{2\pi qy_i}{L}\right\}. \tag{A3}$$

Equations (A2) and (A3) determine one or perhaps more solutions for H and z_q. Since these equations are difficult to solve we shall approximate $\phi(z_i-z)$ by the following linear expression

$$\phi(z-z_i)=\phi(0)\left[1\pm\frac{2}{d+\delta}(z_i-z)\right];\quad \pm \text{ for } z_i\lesseqgtr z. \tag{A4}$$

From (A3) and (A4) we find

$$\pi^2\gamma_{180°}q^2z_q=\Sigma\mp\frac{2\phi(0)}{d+\delta}\sin(\cos)\frac{2\pi qy_i}{L}. \tag{A5}$$

As we see the main contribution in (A5) comes from the two terms with $q=1$. Substitution of z_q given by (A5) in (A1) gives

$$z-z_0=\frac{2\phi(0)}{\pi^2\gamma_{180°}(d+\delta)}\left[\sum_q\frac{1}{q^2}\sum_i\mp\cos\frac{2\pi q}{L}(y_i-y)\right]$$

and the "mean" value

$$\{\langle(-z_0)^2\rangle\}^{\frac{1}{2}}=\frac{\phi(0)}{6\gamma_{180°}(d+\delta)}\left(\sum_i i^0\right)^{\frac{1}{2}}. \tag{A6}$$

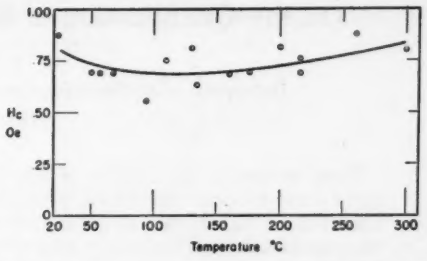

FIG. 8. H_c *vs.* temp. for a stable alloy consisting of 0.003 volume fraction inclusions dispersed in particles about 3200A in diameter.

Consider, for example, the surface tension effect.

In the case that $d\gg\delta$ the factor $\phi(0)=\frac{1}{4}\pi d^2\gamma_{180°}$ and for a slightly curved wall $\Sigma_i i^0\approx nd/L$. This gives $\{\langle(z-z_0)^2\rangle\}^{\frac{1}{2}}=0.17\alpha^{\frac{1}{2}}L$. In the experimental work the volume fraction of inclusions $\alpha=3\times10^{-2}$. For this value

$$\{\langle(z-z_0)^2\rangle\}^{\frac{1}{2}}\approx10^{-5}\text{ cm}\approx\delta.$$

For $d\ll\delta$ the value of $\phi(0)=\pi d^3/24\delta$ and $\Sigma_i i^0=n\delta/L$. From these values and Eq. (6) we find

$$\{\langle(z-z_0)^2\rangle\}^{\frac{1}{2}}=0.23(d/8)^{\frac{1}{2}}\alpha^{\frac{1}{2}}L\approx\delta(d/\delta)^{\frac{1}{2}}.$$

These results justify the calculations for the given value of α.

From Eqs. (A2) and (A4) we see that in this approximation the coercive force H_c is the same as for a rigid, plane boundary. One remark must be made. For the usual particle shape quadratic terms enter in the expression for $\phi(z-z_0)$. Because of these terms value of $\langle H^2(z_0)\rangle$ and of H_c when the domain wall adjusts itself to the particle distribution is somewhat smaller than in case of a rigid, plane wall.

On the Quantization of Einstein's Gravitational Field Equations

F. A. E. PIRANI AND A. SCHILD
Department of Mathematics, Carnegie Institute of Technology, Pittsburgh, Pennsylvania
(Received February 14, 1950)

Weiss' method of quantization of field theories characterized by first-order Lagrangians can be carried out in a non-metrical "amorphous" space, as was first stated by Bergmann and Brunings. The gravitational equations can be regarded as differential equations for the field variables $g_{\mu\nu}$ in an amorphous space and the quantization procedure can be applied to them. The gravitational field equations are written in canonical form, the Hamiltonian being a function of generalized coordinates, momenta, and velocities. This Hamiltonian is obtained using a method developed by Dirac for Lorentz invariant theories.

I. INTRODUCTION

THE quantization of a Lorentz-invariant field theory characterized by a Lagrangian has been carried out by Heisenberg and Pauli[1] by consideration of the analogy with non-relativistic quantum mechanics of systems with a finite number of degrees of freedom. Relativistic invariance was proved by direct computation of the transformation properties after the theory had been set up. This quantization was first put into an obviously Lorentz-invariant form by Weiss,[2] and was subsequently improved by Dirac.[3] The quantization of Lorentz-invariant field theories has been applied mainly to quantum electrodynamics and to meson theories.

It is of interest to apply the quantization procedure to the remaining field theory of modern physics, namely Einstein's theory of gravitation. The essential idea is to regard the components $g_{\mu\nu}$ of the metric tensor as field variables without any intrinsic geometrical significance, at least as far as the formal procedure of quantization is concerned.[4]

In this connection, one point in particular deserves special attention. In a Lorentz-invariant theory, the field variables (e.g., the $F_{\mu\nu}$ in quantum electrodynamics) are treated as c-numbers in the classical theory, and as non-commuting q-numbers in the quantum theory. Quite apart from these field variables, there occurs the Minkowski metric tensor $\eta_{\mu\nu}$, which is treated as a c-number in both the classical and quantum theories. Thus, in the theories of both Weiss and Dirac there occur constructs involving the $\eta_{\mu\nu}$, such as the unit normal to a surface. However, when the $g_{\mu\nu}$ are regarded as field variables, there is no such auxiliary tensor which remains a c-number under the quantization. It is therefore important to realize that the formalism developed by Weiss can actually be carried out in an amorphous space, i.e., one without any metrical structure. This forms the basis for an interesting paper by Bergmann and Brunings.[5] We shall now show heuristically how Weiss' procedure can be carried out in an amorphous space. Let a field theory in four-dimensional space-time be characterized by a Lagrangian density L, a function of the field variables y_A and their derivatives $y_{A,\sigma}$.[6] Weiss considers three-dimensional surfaces and on these regards the y_A as analogs of classical coordinates, and expressions

$$\pi^A=(\partial L/\partial y_{A,\sigma})l_\sigma \tag{1}$$

as their canonically conjugate momenta. Here the l_σ denote the components of the normal to the surface. The quantization procedure consists essentially in writing down commutation relations of the form

$$[y_A(P), \pi^B(P')]=\delta_A{}^B\delta(P, P'), \tag{2}$$

where the left-hand side is the usual quantum-mechanical commutator and $\delta(P, P')$ is some Dirac δ-function of a pair P, P' of points on the surface. In (1) it is only the *covariant* components of the normal to the surface which appear. These can always be defined in an amorphous space by the relations

$$l_\sigma\delta x^\sigma=0 \tag{3}$$

for all infinitesimal displacements δx^σ in the surface. We do not discuss here the normalization of the l_σ, which can be performed without difficulty.

The familiar Lagrangian $(-g)^{\frac{1}{2}}R$ of gravitational theory contains second derivatives of the $g_{\mu\nu}$. By splitting off a divergence term, it can be replaced by the first-order differential expression[7]

$$L\equiv(-g)^{\frac{1}{2}}g^{\mu\nu}\left[\begin{Bmatrix}\sigma\\ \rho\sigma\end{Bmatrix}\begin{Bmatrix}\rho\\ \mu\nu\end{Bmatrix}-\begin{Bmatrix}\rho\\ \mu\sigma\end{Bmatrix}\begin{Bmatrix}\sigma\\ \nu\rho\end{Bmatrix}\right]. \tag{4}$$

However, $(-g)^{\frac{1}{2}}R$ is a relative invariant, but the Lagrangian defined by (4) is not.

[1] W. Heisenberg and W. Pauli, Zeits. f. Physik **56**, 1 (1929).
[2] P. Weiss, Proc. Roy. Soc. **A169**, 102, 119 (1938).
[3] P. A. M. Dirac, Phys. Rev. **73**, 1092 (1948); Mimeographed Notes, Canadian Mathematical Congress, Second Summer Session Seminar (1949): this paper will be referred to as [*D*]. *Added in proof:* Part of [*D*] has now appeared in Can. J. Math. **2**, 129 (1950).
[4] After the quantization has been accomplished, there is no reason why the geometrical character of the metric tensor should not be restored.
[5] P. G. Bergmann and J. H. M. Brunings, Rev. Mod. Phys. **21**, 480 (1949); this paper will be referred to as [*B*].
[6] See reference 8.
[7] H. Weyl, *Space—Time—Matter* (Methuen and Company, Ltd., London, 1922), p. 240. Weyl's notation differs from ours in the sign of the Ricci tensor.

It can be shown that if L is a relative invariant, then the π^A defined by (1) transform tensorially; π^A transforms essentially contragrediently to y_A; i.e., if z_A transforms cogrediently to y_A then $\pi^A z_A$ is a relative invariant. It follows that the commutation relations (2) are covariant. Since the Lagrangian (4) is not a relative invariant, the covariance of the commutation relations, using this Lagrangian, requires discussion. Again we present a heuristic argument. In the gravitational case the momenta (1) are homogeneous linear combinations of the $g_{\mu\nu,\rho}$. Under a transformation of space-time coordinates we have

$$g'_{\mu\nu,\sigma}=g_{\alpha\beta,\rho}\frac{\partial x^\alpha}{\partial x'^\mu}\frac{\partial x^\beta}{\partial x'^\nu}\frac{\partial x^\rho}{\partial x'^\sigma}+\cdots, \tag{5}$$

where the terms indicated by dots spoil the tensor character of the transformation. However, these terms are independent of the $g_{\mu\nu,\rho}$ and will therefore commute with the $g_{\mu\nu}$. Thus, although the momenta in the present theory will not be tensors, the commutators (2) will have tensor character.

In order that they may be taken over readily into quantum theory, it is necessary that the classical equations of motion be in Hamiltonian form. Here we follow Dirac's procedure [D], which differs from that of Bergmann [B]. Dirac's procedure yields an explicit expression for the Hamiltonian which contains velocities as well as coordinates and momenta. With this Hamiltonian the equations of motion reduce to the field equations in a general form. On the other hand, any explicit form of Bergmann's Hamiltonian corresponds to a special choice of the space-time coordinates.[7a]

II. GENERAL THEORY

(A) Canonical Variables

We consider a field theory characterized by a Lagrangian density L, which is a function of field variables y_A and of their first partial derivatives:

$$L\equiv L(y_A, y_{A,\sigma}). \tag{6}$$

The corresponding action integral is

$$S\equiv\int L d^4x, \tag{7}$$

and the variational principle $\delta S=0$ yields the field equations. The field variables and the Lagrangian density are assumed to transform as in [B, Section 1].

We now introduce a family of three-dimensional surfaces in space-time. The points in each surface are described by three parameters u^s ($s=1, 2, 3$). The individual surfaces of the family are labeled by values of a fourth parameter t. The action integral (7) can now be written as

$$S\equiv\int JL du dt, \tag{8}$$

where J is the Jacobian

$$J\equiv|\partial x^\sigma/\partial(u^s, t)|. \tag{9}$$

The Lagrangian JL is regarded throughout as a function of the variables[8] $x^\rho{}_{|s}$, y_A, $y_{A|s}$, $\dot{x}^\rho$, $\dot{y}_A$.

Momentum densities, canonically conjugate to x^ρ and y_A are introduced by the definitions[9]

$$\begin{aligned}\pi^A&=\partial(JL)/\partial\dot{y}_A\equiv Jt_{,\sigma}(\partial L/\partial y_{A,\sigma}),\\ \lambda_\rho&=\partial(JL)/\partial\dot{x}^\rho\equiv Jt_{,\sigma}[L\delta_\rho{}^\sigma-y_{A,\rho}(\partial L/\partial y_{A,\sigma})].\end{aligned} \tag{10}$$

In analogy with systems with a finite number of degrees of freedom, we shall refer to x^ρ, $x^\rho{}_{|s}$, y_A, $y_{A|s}$ as *coordinates*, to $\dot{x}^\rho$, $\dot{y}_A$, as *velocities*, and to λ_ρ, π^A as *momenta*.

Following Dirac, [D], two standards of equality are distinguished. An equation is called a *strong* equation if it remains valid after an infinitesimal variation is performed, coordinates, velocities, and momenta being varied *independently*—in particular, independently of (10). *Weak* equations are those which, in general, do not remain valid after such a variation. Strong equations are written with the sign $\equiv$, weak equations with the sign $=$. Clearly (10) are weak equations, since they do not remain valid when λ_ρ and π^A are varied independently of the coordinates and velocities which compose the right-hand sides. All other defining equations, such as (7), are strong equations. Further strong equations can be obtained by multiplying together two weak equations: If $A=0$, $B=0$, then $AB\equiv 0$, since $\delta(AB)\equiv\delta A\cdot B+A\delta\cdot B=0$. For example, from (10) we can form the strong equations

$$(\pi^A-\partial(JL)/\partial\dot{y}_A)(\pi^B-\partial(JL)/\partial\dot{y}_B)\equiv 0. \tag{11}$$

By writing them out explicitly, or by using Euler's relations, the following expressions can be shown to be homogeneous in the velocities $\dot{x}^\rho$, $\dot{y}_A$: The Jacobian J is of degree 1; the $y_{A,\sigma}$ are of degree 0; it follows that L is of degree zero and JL of degree 1. Thus the right-hand sides of (10) are homogeneous of degree 0 in the velocities. Hence, in (10), the $N+4$ momenta are expressed as functions of the coordinates and of $N+3$ *ratios* of the velocities. If the velocities are eliminated

[7a] After completing the work presented in this paper, we learned that Bergmann and his co-workers had independently obtained a Hamiltonian for the gravitational field, using methods quite different from ours. Their work will be published shortly.

[8] The notation is, thus far, the same as in [B]: Greek suffixes range over 1, 2, 3, 4 and refer to the space-time coordinates. A comma followed by a Greek suffix denotes partial differentiation with respect to a space-time coordinate: $y_{A,\sigma}\equiv\partial y_A/\partial x^\sigma$. Capital Latin suffixes range over 1, 2, $\cdots$, N and refer to the field variables y_A. Lower case Latin suffixes range over 1, 2, 3, and refer to the parameters u^s. A stroke followed by a lower case Latin suffix denotes partial differentiation with respect to a parameter u^s: $y_{A|s}\equiv\partial y_A/\partial u^s$. A dot denotes partial differentiation with respect to the parameter t: $\dot{y}_A\equiv\partial y_A/\partial t$.

[9] Since $t_{,\sigma}x^\sigma{}_{|s}\equiv\partial t/\partial u^s\equiv 0$, $Jt_{,\sigma}$ is a normal to the surface $t=$constant. This gives the connection between (10) and the expression (1).

from these equations, there must result at least one relation involving coordinates and momenta only. In general there will be several such independent relations:

$$\phi_a(x^\rho{}_{|s}, y_A, y_{A|s}; \lambda_\rho, \pi^A)=0, \quad a=1, 2, \cdots, M. \quad (12)$$

These relations hold only in the weak sense. The argument above shows that $M \geqslant 1$. However, for a completely covariant theory of the type considered here, M is at least 8. As will be seen later, this is because the four parameters and the four coordinates can be chosen in a completely arbitrary way, so that any set of covariant field equations must have an eightfold infinity of solutions. Any further invariance property of the field theory (e.g., gauge-invariance) gives rise to additional relations $\phi_a=0$ (see Section IIIC). In [B], seven of the ϕ_a are obtained explicitly for a general Lagrangian JL. One of the principal objects here is to find the eighth ϕ_a for the case of the gravitational field.

(B) Hamiltonian

The Hamiltonian density is defined in the usual manner:

$$H \equiv \lambda_\rho \dot{x}^\rho + \pi^A \dot{y}_A - JL. \quad (13)$$

Using (10), this becomes

$$H=(\partial(JL)/\partial\dot{x}^\rho)\dot{x}^\rho+(\partial(JL)/\partial\dot{y}_A)\dot{y}_A-JL.$$

This expression vanishes because JL is homogeneous of degree 1 in the velocities $\dot{x}^\rho, \dot{y}_A$. Thus H vanishes in the weak sense:

$$H=0. \quad (14)$$

In [D] it is shown that H can be expressed in the strong sense as a linear combination of the ϕ_a:

$$H \equiv \beta_a \phi_a, \quad (15)$$

where the β_a are functions of the coordinates, velocities, and momenta. Since this result is of importance here, we now give a short sketch of Dirac's proof.

Varying (13), we find that the terms in δH which involve $\delta\dot{x}^\rho$ and $\delta\dot{y}_A$ are

$$\lambda_\rho \delta\dot{x}^\rho+\pi^A\delta\dot{y}_A-(\partial(JL)/\partial\dot{x}^\rho)\delta\dot{x}^\rho-(\partial(JL)/\partial\dot{y}_A)\delta\dot{y}_A.$$

These vanish by virtue of (10). Thus δH is independent of the variations of the velocities. It follows from (14) that

$$\delta H=0 \quad (16)$$

if the coordinates and momenta are varied in such a way that (10) can be satisfied both before and after the variation. The only restriction that this imposes on the variations of the coordinates and momenta is that they comply with the relations (12):

$$\delta\phi_a=0. \quad (17)$$

More concisely, (16) holds, provided that $\delta x^\rho{}_{|s}$, δy_A, $\delta y_{A|s}$, $\delta\lambda_\rho$, $\delta\pi^A$ satisfy the linear Eqs. (17). This shows that δH must be a linear function of the $\delta\phi_a$ for arbitrary variations of coordinates, momenta, and velocities:

$$\delta H=\beta_a\delta\phi_a=\beta_a\delta\phi_a+\phi_a\delta\beta_a=\delta(\beta_a\phi_a),$$

by (12). Integrating, we now obtain (15) except for a possible constant of integration. However, such a constant must be zero, by (12) and (14). This establishes (15).

The result (15) is important. Besides giving a Hamiltonian which can be used to write down the equations of motion, it gives also a method for the discovery of the explicit forms of the ϕ_a. Note that the transition from (13) to (15) must be made using only strong equations.

(C) Poisson Brackets

We introduce Poisson brackets in an abstract manner by listing their properties. The reason for this is twofold. The identities satisfied by classical Poisson brackets are also satisfied by the commutators which are their quantum analogs.[10] Also, we shall have to consider Poisson brackets of functions of velocities; these can be written down formally but they cannot be equated to ordinary functions (i.e., they cannot be evaluated). However, such Poisson brackets will always be multiplied by zero in the final equations and will thus appear only in intermediate stages of the theory.

We consider only the Poisson brackets of functions and functionals of coordinates, velocities, and momenta, assigned over the same space-like surface $t=$constant. Such Poisson brackets are assumed to satisfy the usual algebraic relations of skew-symmetry and linearity, and the Jacobi identities. If F is any function of B_1, B_2, $\cdots$, then

$$[A, F] \equiv (\partial F/\partial B_1)[A, B_1] + (\partial F/\partial B_2)[A, B_2]+\cdots. \quad (18)$$

If $A \equiv$ a constant, then for all B,

$$[A, B]=0. \quad (19)$$

This is not in general true if A is constant in the weak sense only.

In addition to the general properties postulated above we define some particular Poisson brackets: If $\mathbf{u}$ refers to a point (u^1, u^2, u^3) of a 3-surface $t=$constant, and $\mathbf{u}'$ to another point of the same surface, then

$$[y_A(\mathbf{u}), \pi^B(\mathbf{u}')] \equiv \delta_A{}^B\delta(\mathbf{u}-\mathbf{u}'), \quad (20)$$

$$[x^\rho(\mathbf{u}), \lambda_\sigma(\mathbf{u}')] \equiv \delta_\sigma{}^\rho\delta(\mathbf{u}-\mathbf{u}'), \quad (21)$$

and all other Poisson brackets formed from pairs of the variables x^ρ, λ_ρ, y_A, π^A vanish. Here $\delta(\mathbf{u}-\mathbf{u}')$ is the usual three-dimensional Dirac δ-function.

We assume finally that the process of forming Poisson brackets commutes with ordinary limiting operations. Then the differentiation and integration of Poisson

[10] P. A. M. Dirac, *Principles of Quantum Mechanics* (Clarendon Press, Oxford, 1935), second edition, Section 25.

brackets follows at once from the linearity properties. Poisson brackets involving the $x^\rho{}_{|s}$ or the $y_{A|s}$ can be deduced from (20) and (21) by differentiation. It is then possible to obtain the Poisson bracket of any two functions or functionals which involve the coordinate or momentum variables only.[11]

(D) Equations of Motion

In order to derive canonical equations of motion, the expression (13) for the Hamiltonian is used. If $[y_A(\mathbf{u}), H(\mathbf{u}')]$ is formed, some terms are obtained with Poisson brackets which involve velocities. These are

$$\lambda_\rho(\mathbf{u}')[y_A(\mathbf{u}), \dot{x}^\rho(\mathbf{u}')]+\pi^B(\mathbf{u}')[y_A(\mathbf{u}), \dot{y}_B(\mathbf{u}')] -(\partial(JL)/\partial\dot{x}^\rho)|_{\mathbf{u}'}[y_A(\mathbf{u}), \dot{x}^\rho(\mathbf{u}')] -(\partial(JL)/\partial\dot{y}_B)|_{\mathbf{u}'}[y_A(\mathbf{u}), \dot{y}_B(\mathbf{u}')].$$

This expression vanishes in the weak sense by (10). The remaining terms can be computed from the postulates of Section IIC. We find

$$[y_A(\mathbf{u}), H(\mathbf{u}')]=\dot{y}_A(\mathbf{u})\delta(\mathbf{u}-\mathbf{u}'). \tag{22}$$

Similarly

$$[x^\rho(\mathbf{u}), H(\mathbf{u}')]=\dot{x}^\rho(\mathbf{u})\delta(\mathbf{u}-\mathbf{u}'). \tag{23}$$

We now introduce the field equations obtained from the variational principle $\delta S=0$, where S is given by (8). The field equations are

$$\frac{\delta(JL)}{\delta y_A}-\frac{\partial}{\partial t}\left(\frac{\partial(JL)}{\partial\dot{y}_A}\right)=0,$$

$$\frac{\delta(JL)}{\delta y_A}\equiv\frac{\partial(JL)}{\partial y_A}-\left(\frac{\partial(JL)}{\partial y_{A|s}}\right)_{|s}, \tag{24}$$

$$\frac{\delta(JL)}{\delta x^\rho}-\frac{\partial}{\partial t}\left(\frac{\partial(JL)}{\partial\dot{x}^\rho}\right)=0, \quad \frac{\delta(JL)}{\delta x^\rho}\equiv-\left(\frac{\partial(JL)}{\partial x^\rho{}_{|s}}\right)_{|s}, \tag{25}$$

By (10), we can write these equations

$$\delta(JL)/\delta y_A-\dot{\pi}^A=0, \tag{26}$$

$$\delta(JL)/\delta x^\rho-\dot{\lambda}_\rho=0. \tag{27}$$

From (13), (26), and (27), a straightforward computation yields

$$[\pi^A(\mathbf{u}), H(\mathbf{u}')]=\dot{\pi}^A(\mathbf{u}')\delta(\mathbf{u}-\mathbf{u}') +\partial(JL)/\partial y_{A|s}|_{\mathbf{u}}(\partial/\partial u'^s)\delta(\mathbf{u}-\mathbf{u}'), \tag{28}$$

$$[\lambda_\rho(\mathbf{u}), H(\mathbf{u}')]=\dot{\lambda}_\rho(\mathbf{u}')\delta(\mathbf{u}-\mathbf{u}') +\partial(JL)/\partial x^\rho{}_{|s}|_{\mathbf{u}}(\partial/\partial u'^s)\delta(\mathbf{u}-\mathbf{u}'). \tag{29}$$

Integrating with respect to the variables $\mathbf{u}'$, the equations of motion take the more familiar form

$$\begin{aligned}\dot{y}_A&=[y_A, \mathfrak{H}], \quad \dot{x}^\rho=[x^\rho, \mathfrak{H}],\\ \dot{\pi}^A&=[\pi^A, \mathfrak{H}], \quad \dot{\lambda}_\rho=[\lambda_\rho, \mathfrak{H}],\end{aligned} \tag{30}$$

where $\mathfrak{H}$ is the Hamiltonian functional

$$\mathfrak{H}\equiv\int H(\mathbf{u})d\mathbf{u}. \tag{31}$$

Using the general properties of Poisson brackets, it follows from (30) that

$$[F, \mathfrak{H}]=\dot{F}, \tag{32}$$

where F is any function or functional of coordinates and momenta only.

In order to derive the equations of motion (30), the form (13) of the Hamiltonian density was used. However, in order to write down the canonical field equations we must use (15). The Poisson brackets which contain the β_a, and thus involve velocities, do not enter the final equations because they are multiplied by the ϕ_a, which vanish:

$$\begin{aligned}&[F(\mathbf{u}), H(\mathbf{u}')]\\ &\quad=\beta_a(\mathbf{u}')[F(\mathbf{u}), \phi_a(\mathbf{u}')]+[F(\mathbf{u}), \beta_a(\mathbf{u}')]\phi_a(\mathbf{u}')\\ &\quad=\beta_a(\mathbf{u}')[F(\mathbf{u}), \phi_a(\mathbf{u}')].\end{aligned} \tag{33}$$

By integration with respect to $\mathbf{u}'$ we obtain the left-hand side of (32).

The equations of motion do not determine the functional dependence of the β_a on the parameters u^s and t. For example, in the case of the gravitational field [see Eq. (50)], four of the β_a are $\dot{x}^\rho$, and the equations $[x^\rho, \mathfrak{H}]=\dot{x}^\rho$ reduce to the empty statements $\dot{x}^\rho=\dot{x}^\rho$. In general, the β_a are arbitrary functions of u^s, t. As was indicated in Section IIA, this arbitrariness reflects the eightfold freedom inherent in the choice of space-time coordinates and parameters.

Since $\phi_a=0$ must hold on all surfaces $t=$constant, we must have

$$\dot{\phi}_a(\mathbf{u})=[\phi_a(\mathbf{u}), \mathfrak{H}]=\int\beta_b(\mathbf{u}')[\phi_a(\mathbf{u}), \phi_b(\mathbf{u}')]d\mathbf{u}'=0. \tag{34}$$

In the general case discussed in [D], Eqs. (34) impose further constraints on the dynamical system. Here we restrict ourselves to the case in which[12]

$$[\phi_a(\mathbf{u}), \phi_b(\mathbf{u}')]=0 \tag{35}$$

by virtue of the relations $\phi_a=0$, so that Eqs. (34) are satisfied automatically, and there are no additional constraints. This special case includes the gravitational and electromagnetic fields.

(E) Quantization

Once a field theory is expressed in canonical form, the transition to quantum mechanics proceeds in the usual manner; coordinates and momenta become noncommuting Hermitian operators and Poisson brackets are replaced by commutators according to the scheme

$$[F_1, F_2]=-i\hbar^{-1}(F_1F_2-F_2F_1). \tag{36}$$

[11] Bergmann's definition of Poisson brackets [B. 3.23] can be deduced by integration.

[12] In the language of [D], all the ϕ_a are first class, and there are no χ equations.

The non-commuting terms in the Hamiltonian must be arranged so that H is Hermitian. It will be seen that all terms in the Hamiltonian of the gravitational field are products of momenta and functions of the coordinates, so that H can readily be made Hermitian by symmetrization.

III. GRAVITATIONAL THEORY

(A) Canonical Variables

The usual Lagrangian of gravitational theory is $(-g)^{\frac{1}{2}}R$ where R is the curvature scalar. By splitting off a divergence term, $(-g)^{\frac{1}{2}}R$ can be replaced by an alternative Lagrangian which contains only first derivatives of the field variables $g_{\mu\nu}$:

$$L\equiv(-g)^{\frac{1}{2}}g^{\alpha\beta}\left[\left\{\begin{matrix}\rho\\ \alpha\beta\end{matrix}\right\}\left\{\begin{matrix}\sigma\\ \rho\sigma\end{matrix}\right\}-\left\{\begin{matrix}\rho\\ \alpha\sigma\end{matrix}\right\}\left\{\begin{matrix}\sigma\\ \beta\rho\end{matrix}\right\}\right]$$

$$\equiv\tfrac{1}{4}(-g)^{\frac{1}{2}}\{2g^{\alpha\sigma}g^{\beta\rho}g^{\mu\nu}-g^{\alpha\beta}g^{\rho\sigma}g^{\mu\nu}-2g^{\alpha\mu}g^{\nu\sigma}g^{\beta\rho}$$
$$+g^{\alpha\mu}g^{\beta\nu}g^{\rho\sigma}\}g_{\alpha\beta,\sigma}g_{\mu\nu,\rho}. \quad (37)$$

The canonical variables are defined as in (10), with a slight change to preserve symmetry:

$$\lambda_\rho=\partial(JL)/\partial\dot{x}^\rho$$

$$\pi^{\mu\nu}=\tfrac{1}{2}\left(\frac{\partial(JL)}{\partial\dot{g}_{\mu\nu}}+\frac{\partial(JL)}{\partial\dot{g}_{\nu\mu}}\right)$$

$$=\tfrac{1}{4}(-g)^{\frac{1}{2}}\{2g^{\alpha\sigma}g^{\beta\rho}g^{\mu\nu}+g^{\mu\rho}g^{\nu\sigma}g^{\alpha\beta}+g^{\nu\rho}g^{\mu\sigma}g^{\alpha\beta}$$
$$-2g^{\alpha\beta}g^{\mu\nu}g^{\rho\sigma}-2g^{\alpha\mu}g^{\nu\sigma}g^{\beta\rho}-2g^{\alpha\nu}g^{\mu\sigma}g^{\beta\rho}$$
$$+2g^{\alpha\mu}g^{\beta\nu}g^{\rho\sigma}\}g_{\alpha\beta,\sigma}l_\rho, \quad (38)$$

where

$$l_\rho\equiv Jt_{,\rho} \quad (39)$$

is a normal to the surface $t=$ constant.

Before proceeding to the computation of the functions ϕ_a and of the Hamiltonian density, we require two simple lemmas:

(a) The expressions l_ρ of (39) are the minors of $\dot{x}^\rho$ in the Jacobian determinant

$$J\equiv|x^\sigma{}_{|s},\dot{x}^\sigma|.$$

Thus l_ρ is a function of the coordinates $(x^\sigma{}_{|s})$ only and does not involve the velocities $(\dot{x}^\sigma)$.

(b) If A is any function of the coordinates only, then

$$A_{,\rho}l_\sigma-A_{,\sigma}l_\rho\equiv A_{|s}(u^s{}_{,\rho}l_\sigma-u^s{}_{,\sigma}l_\rho), \quad (40)$$

the terms in $\dot{A}$ canceling. It can be shown also, by writing them out explicitly or by differentiation, that the expressions $(u^s{}_{,\rho}l_\sigma-u^s{}_{,\sigma}l_\rho)$ do not involve the velocities $\dot{x}^\sigma$. Thus any expression of the form of the left-hand side of (40) is a function of coordinates only. In particular

$$T_{\alpha\beta\rho\sigma}\equiv g_{\alpha\beta,\rho}l_\sigma-g_{\alpha\beta,\sigma}l_\rho \quad (41)$$

is a function of the coordinates only.

(B) Hamiltonian

Multiplying (38) by l_ν, we obtain

$$\pi^{\mu\nu}l_\nu=\tfrac{1}{4}(-g)^{\frac{1}{2}}g^{\mu\tau}(2g^{\alpha\sigma}g^{\beta\rho}-g^{\alpha\beta}g^{\rho\sigma})T_{\alpha\beta\sigma\tau}l_\rho.$$

Noting that the right-hand side is a function of the coordinates only, this gives us four of the functions ϕ_a:

$$\phi^\sigma\equiv\pi^{\sigma\nu}l_\nu-\tfrac{1}{4}(-g)^{\frac{1}{2}}g^{\sigma\tau}(2g^{\alpha\delta}g^{\beta\rho}-g^{\alpha\beta}g^{\rho\delta})T_{\alpha\beta\delta\tau}l_\rho=0. \quad (42)$$

These are essentially four of the ϕ_a obtained in [$B(3.6)$] for a general Lagrangian.

The Hamiltonian density (13) is now

$$H\equiv\lambda_\rho\dot{x}^\rho+\pi^{\alpha\beta}\dot{g}_{\alpha\beta}-JL\equiv\dot{x}^\gamma H_\gamma, \quad (43)$$

where

$$H_\gamma\equiv\lambda_\gamma+\pi^{\alpha\beta}g_{\alpha\beta,\gamma}-Ll_\gamma. \quad (44)$$

We know from the general theory that it is possible to write H in the form (15). Because of the arbitrariness of the space-time coordinates, the $\dot{x}^\gamma$ cannot be determined by the equations of motion and must remain general functions of the parameters u^s, t; we can therefore assume that the $\dot{x}^\gamma$ are identical with four of the β_a. It follows that it must be possible to write H_γ in the form

$$H_\gamma\equiv\varphi_\gamma+c_{\gamma\sigma}\phi^\sigma, \quad (45)$$

where φ_γ are four functions of coordinates and momenta only, ϕ^σ are as in (42), and $c_{\gamma\sigma}$ are functions of coordinates, momenta, and velocities. Then

$$H\equiv\dot{x}^\gamma\varphi_\gamma+\dot{x}^\gamma c_{\gamma\sigma}\phi^\sigma. \quad (46)$$

Since $H=0$ and $\phi^\sigma=0$, it follows that $\dot{x}^\gamma\varphi_\gamma=0$, and since the $\dot{x}^\gamma$ are independent, that

$$\varphi_\gamma=0. \quad (47)$$

Thus φ_γ, ϕ^σ are the eight functions ϕ_a of (15), and $\dot{x}^\gamma$, $\dot{x}^\gamma c_{\gamma\sigma}$ are the eight coefficients β_a.

The main problem now is to express (44) in the form (45), using (42) and strong equations obtained by forming products of the weak Eqs. (38). This means that, with the exception of terms proportional to ϕ^σ, we must eliminate all velocities from (44).

In (44), $\pi^{\alpha\beta}g_{\alpha\beta,\gamma}$ contains momenta as well as velocities, Ll_γ contains velocities and coordinates but no momenta. We now proceed as follows: We ignore all terms containing velocities but no momenta and all terms containing no velocities. The remaining terms containing velocities and momenta are of a simple structure, and it is easy to eliminate the velocities from these terms. When this is done all other terms must automatically be free of velocities, so that our objective is achieved. If this were not so, then there would have to be some strong equations involving velocities but no momenta for the elimination of such terms from H_γ, since we know from the general theory that it is possible to reduce H_γ to the form (45). However, the only strong equations which can be used to eliminate

velocities are obtained from (38) and therefore contain momenta. This contradiction proves the assertion above.

Let us rewrite (38) in the form

$$C^{\mu\nu}\equiv\pi^{\mu\nu}-\tfrac{1}{2}(\partial(JL)/\partial\dot{g}_{\mu\nu})+\partial(JL)/\partial\dot{g}_{\nu\mu})=0. \quad (48)$$

From these weak equations we can form the strong equations

$$C^{\mu\nu}C_{\mu\nu}\equiv 0, \quad C^2\equiv 0, \quad (49)$$

where $C_{\mu\nu}\equiv g_{\mu\alpha}g_{\nu\beta}C^{\alpha\beta}$, $C\equiv g_{\alpha\beta}C^{\alpha\beta}$. Using the technique outlined above, it is easy to see that we must add $l_\gamma(C^{\mu\nu}C_{\mu\nu}-\frac{1}{2}C^2)/(-g)^{\frac{1}{2}}g^{\alpha\beta}l_\alpha l_\beta$ to (44) in order to reduce H_γ to the form (45). After a straightforward computation we obtain the following expression for the Hamiltonian density:

$$H\equiv\dot{x}^\gamma\varphi_\gamma+2Jl^{-2}g^{\alpha\beta}[\alpha\beta,\sigma]\phi^\sigma, \quad (50)$$

where $[\alpha\beta,\sigma]$ is a Christoffel symbol of the first kind, where

$$\varphi_\gamma\equiv\lambda_\gamma+l^{-2}\pi^{\alpha\beta}T_{\alpha\beta\gamma\rho}l^\rho+l^{-2}l_\gamma[2g^{\rho\beta}\pi^{\alpha\sigma}T_{\alpha\beta\sigma\rho}$$
$$+\tfrac{1}{2}(-g)^{-\frac{1}{2}}(2g_{\alpha\mu}g_{\beta\nu}-g_{\alpha\beta}g_{\mu\nu})\pi^{\alpha\beta}\pi^{\mu\nu}$$
$$+G^{\alpha\beta\sigma\rho\epsilon\iota\lambda\kappa}T_{\alpha\beta\sigma\rho}T_{\epsilon\iota\lambda\kappa}]=0, \quad (51)$$

$$G^{\alpha\beta\sigma\rho\epsilon\iota\lambda\kappa}\equiv\tfrac{1}{16}(-g)^{\frac{1}{2}}\{g^{\alpha\beta}g^{\epsilon\iota}-2g^{\alpha\epsilon}g^{\beta\iota})g^{\rho\kappa}g^{\sigma\lambda}$$
$$-8(g^{\alpha\rho}g^{\beta\kappa}g^{\epsilon\sigma}g^{\iota\lambda}-g^{\epsilon\beta}g^{\iota\rho}g^{\alpha\kappa}g^{\sigma\lambda})\}, \quad (52)$$

$$l^\rho=g^{\rho\sigma}l_\sigma, \quad l^2=l_\rho l^\rho, \quad (53)$$

and where ϕ^σ, $T_{\alpha\beta\rho\sigma}$ are given by (42), (41) respectively.

The Hamiltonian formulation of the gravitational equations consists of the equations

$$\phi^\sigma=0, \quad \varphi_\gamma=0, \quad (54)$$

the Poisson bracket relations

$$[x^\rho(\mathbf{u}),\lambda_\sigma(\mathbf{u}')]\equiv\delta_\sigma{}^\rho\delta(\mathbf{u}-\mathbf{u}'),$$
$$[g_{\alpha\beta}(\mathbf{u}),\pi^{\mu\nu}(\mathbf{u}')]\equiv\tfrac{1}{2}(\delta_\alpha{}^\mu\delta_\beta{}^\nu+\delta_\alpha{}^\nu\delta_\beta{}^\mu)\delta(\mathbf{u}-\mathbf{u}'), \quad (55)$$

all other Poisson brackets between pairs of the variables x^ρ, $g_{\mu\nu}$, λ_ρ, $\pi^{\mu\nu}$ being zero, and the equations of motion

$$\dot{F}=[F,\mathfrak{H}] \quad (56)$$

where $\mathfrak{H}$ is given by (31) and (50), and F is any function or functional of coordinates and momenta only. The β_α variables $\dot{x}^\gamma$ and $2Jl^{-2}g^{\alpha\beta}[\alpha\beta,\sigma]$ are arbitrary functions of the parameters u^s, t. The formal quantization of the gravitational field can now proceed as in Section IIE.

(C) Combined Gravitational and Electromagnetic Fields

The addition of an electromagnetic field to the gravitational field introduces no new difficulties. The electromagnetic field variables are the potentials A_μ and the Lagrangian is now

$$L\equiv L_1-\kappa(-g)^{\frac{1}{2}}F_{\mu\nu}F^{\mu\nu}, \quad (57)$$

where

$$F_{\mu\nu}\equiv A_{\mu,\nu}-A_{\nu,\mu}, \quad F^{\mu\nu}\equiv g^{\mu\alpha}g^{\nu\beta}F_{\alpha\beta}, \quad (58)$$

where κ is the gravitational constant, and where L_1 is the Lagrangian (37) of the gravitational field.

The momentum variables $\pi^{\mu\nu}$ conjugate to the $g_{\mu\nu}$ remain unchanged and are given by (38). The new momentum variables conjugate to the A_μ are

$$\pi^\mu=-4\kappa(-g)^{\frac{1}{2}}F^{\mu\nu}l_\nu. \quad (59)$$

The λ_ρ are no longer those of the purely gravitational field; they are still given by (10), but their explicit form is of no interest here.

From (59) we derive immediately the new identity

$$\phi\equiv\pi^\mu l_\mu=0. \quad (60)$$

The expressions (42) for the ϕ^σ are the same as before.

Using the method and results of Section IIIB a short computation yields the Hamiltonian density:

$$H\equiv\dot{x}^\gamma\varphi_\gamma+2Jl^{-2}g^{\alpha\beta}[\alpha\beta,\sigma]\phi^\sigma+l^\alpha l^{-2}\dot{A}_\alpha\phi. \quad (61)$$

Here the new φ_γ are given by the expression (51) with the added terms

$$l^{-2}T_{\alpha\beta\gamma}(l^\alpha\pi^\beta-l^\beta\pi^\alpha)-l_\gamma l^{-2}[(8\kappa)^{-1}(-g)^{-\frac{1}{2}}g_{\alpha\beta}\pi^\alpha\pi^\beta$$
$$+\kappa(-g)^{\frac{1}{2}}g^{\rho\sigma}(2g^{\alpha\nu}g^{\beta\mu}-g^{\alpha\mu}g^{\beta\nu})T_{\alpha\beta\rho}T_{\mu\nu\sigma}, \quad (62)$$

where

$$T_{\alpha\beta\rho}\equiv A_{\alpha,\beta}l_\rho-A_{\alpha,\rho}l_\beta. \quad (63)$$

In (61), the ninth β_α variable $l^\alpha l^{-2}\dot{A}_\alpha$ corresponds to the freedom in the choice of gauge.

Effects of Plasma Boundaries in Plasma Oscillations

D. BOHM AND E. P. GROSS*
Department of Physics, Princeton University, Princeton, New Jersey
(Received March 28, 1950)

The discussion of electron plasma oscillations is extended to include some of the effects of boundaries. It is first shown that an electron taking part in a traveling plasma oscillation will be reflected at a sheath of infinitesimal thickness with velocity appropriate to the oscillation traveling in the reverse direction. This means that standing waves may be built up without loss at the sheaths. This approach is extended to sheaths where a finite time of penetration is necessary before reflection occurs and also to the case of reflection at metallic electrodes. In both cases expressions for the damping are derived and it is concluded that for low pressure discharges damping resulting from imperfect reflection from electrode sheaths may be comparable with collision damping but that damping arising from conducting electrodes is unimportant.

The excitation of the plasma by sharp beams is considered briefly and expressions are derived for the energy transfer of a beam to growing and of stationary amplitudes. It is pointed out that beams should excite oscillations only when a regular geometry exists. With irregular geometry bunching pulses are to be expected, of the type observed by Merrill and Webb. A detailed analysis is given of the bunching and of the Merrill and Webb experiments. Good agreement is obtained if one assumes that the pulses are maintained because high harmonic waves in the pulse cannot be shielded out by the plasma. These feed back energy towards the cathode and continuously modulate the beam.

I. INTRODUCTION

IN two previous papers[1,2] we have developed a theory of oscillations of an unbounded plasma describing the origin of medium-like behavior, and some of the conditions under which plasma oscillations become unstable. In this paper, we extend these results to include the effects of boundary walls, which are especially important in discharge tubes.

II. REFLECTION OF PLASMA WAVES AT A PLASMA BOUNDARY

In a discharge tube a plasma is usually bounded by a positive ion sheath, the thickness of which depends on the ion density and on the electrode potential, but which is usually of the order of 0.1 mm thick. This sheath surrounds the boundary electrode and shields it from the rest of the plasma. Within the sheath all those positive ions which strike the sheath edge as a result of thermal motions are accelerated, while all but a very few of the most energetic electrons are repelled. Since the sheath potential drop is usually of the order of several times the mean kinetic energy of the plasma electrons, one can as a first approximation neglect the few electrons which are not reflected, and assume that the process of reflection of electrons is elastic. The electrons do, however, penetrate part of the sheath, with the result that the time taken for an electron to be reflected is of the order of 10^{-10} second, which is also of the order of a period of a plasma oscillation. Furthermore, the time required for reflection is not the same for all reflections, since the faster electrons penetrate further into the sheath than do the slower ones.

We must now investigate the effect of these processes on the reflection of a plasma wave. When a plasma wave is present, each particle experiences a small periodic shift in velocity and in its contribution to the net charge density, which depends on the amplitude and wavelength, according to reference 1, Eqs. (12) and (4). The important question here is whether the electrons which rebound from the sheath come off with velocity perturbations which have a phase and amplitude appropriate to a reflected wave. One can see that because each electron experiences a phase lag in the process of reflection, it may turn out that all of the energy of the incident wave does not appear as a single reflected wave.

Let us first consider the idealized case of a sheath of infinitesimal thickness, so that there is no phase lag on reflection. We take the reflecting plane to be $z=0$, and consider a wave of propagation vector with components (o, o, k). The analysis is easily generalized for waves with x and y components of the propagation vector.

In this section we shall show that the bounded plasma permits the existence of standing plasma waves in which the reflection of particles at the boundary does not give rise to energy losses. Let us consider the standing wave

$$\begin{aligned}\varphi&=\varphi_0\left[e^{i(kz-\omega t)}+e^{-i(kz+\omega t)}\right],\\ \partial\varphi/\partial z&=ik\varphi_0\left[e^{i(kz-\omega t)}-e^{-i(kz+\omega t)}\right].\end{aligned}\tag{1}$$

The potential has an antinode at the boundary, the field has a node, as is easily seen by taking the real parts of the potential and field.

A particle of velocity V_0, according to reference 1, Eq. (12), has a velocity perturbation

$$\delta V_{1z}=\frac{\epsilon k\varphi_0}{m}\frac{e^{i(kz-\omega t)}}{\omega-kV_{0z}}-\frac{\epsilon k\varphi_0}{m}\frac{e^{-i(kz+\omega t)}}{\omega+kV_{0z}}.\tag{2}$$

Immediately after such an electron rebounds from the plane, the z component of its total velocity, per-

* Now at the Laboratory for Insulation Research, Massachusetts Institute of Technology, Cambridge, Massachusetts.

[1] D. Bohm and E. P. Gross, Phys. Rev. **75**, 1851 (1949).

[2] D. Bohm and E. P. Gross, Phys. Rev. **75**, 1864 (1949).

turbed plus unperturbed, is reversed, while the other components are left unaltered. Thus the electron becomes a particle with unperturbed velocity $\mathbf{U}_0$ which is the negative of its previous unperturbed velocity, and which has at the plane $z=0$ a perturbed velocity which is the negative of its previous value. The key question in studying the energy loss at boundaries is whether the perturbation in velocity after collision is appropriate to a particle taking part in the organized oscillation. In the present case dealing with an idealized boundary we shall verify that the correct perturbation for a particle of velocity $\mathbf{U}_0=-\mathbf{V}_0$, at the boundary, is indeed the negative of Eq. (2), but this will not be the case when the finite time necessary for reflection is taken into account.

To verify the above statment we note that the perturbation of a particle of velocity $\mathbf{U}_0=-\mathbf{V}_0$ at the boundary is according to Eq. (2)

$$\delta V_{2z}(\mathbf{U}_0)=\frac{\epsilon k\varphi_0}{m}\frac{e^{-i\omega t}}{\omega+kV_{0z}}-\frac{\epsilon k\varphi_0}{m}\frac{e^{-i\omega t}}{\omega-kV_{0z}}. \tag{3}$$

Comparison of Eqs. (3) and (2) shows that

$$\delta V_{2z}(\mathbf{U}_0)=-\delta V_{1z}(\mathbf{V}_0)$$

at the boundary, as required.

For small $\mathbf{k}\cdot\mathbf{V}_0/\omega$ the z component of $\delta\mathbf{V}$ reduces to

$$\delta V_z(\mathbf{V}_0)\cong(2\epsilon/m\omega^2)k^2V_{0z}\varphi_0e^{-i\omega t}. \tag{4}$$

This means that, in general, a particle arrives at $z=0$ with some perturbation in its velocity, produced by the action of the wave. As the wave-length approaches infinity, however, this perturbation approaches zero.

III. REFLECTION FROM A SHEATH

Let us now consider the effects of finite sheath thickness. Since the time taken to penetrate the sheath is usually comparable with the period of a plasma oscillation or greater, and since this time varies strongly with the velocity of the particle, any perturbation in velocity with which the particle strikes the sheath will lose its coherence with the wave, by the time the particle gets back out. In order to form a reflected wave, however, the perturbation in velocity of the reflected particles must match that demanded by Eq. (3). Since such a match is impossible after particles have penetrated the sheath, the variation in perturbation in velocity which exists when the particles strike the sheath will not give rise to an organized reflected wave. Instead, this part of the ordered wave energy is dissipated in the form of random thermal motion.

One can describe this process in terms of the results of reference 1, Sec. VI, where it was shown that for each k, an arbitrary angular frequency, ω, is possible, but that only the value of ω corresponding to the dispersion relation Eq. (9) leads to organized motion of all the particles, for which the potential persists indefinitely. Other values of w correspond to waves in which most of the potential is due to density fluctuations of small groups of particles of some definite velocity. Such motion is disorganized, in the sense that contributions of different groups of particles to the potential soon get out of phase with each other, so that the macroscopic average of the potential is very small.

In our problem, we use the result to note for each ω, waves of arbitrary k are possible, but only those waves for which k is given by the dispersion relation can produce a macroscopically observable potential at an appreciable distance from the sheath. Hence, the disorganized motions involved in waves which do not satisfy the dispersion relation are just another way of describing random thermal motions.

In general, if the phase of $\delta\mathbf{V}$ for the reflected particles is not equal to that demanded by an organized reflected wave for which k satisfies the dispersion relation, it will still be equal to that demanded by a wave with some other value of k, not satisfying the dispersion relation. This means that the ordered component of velocity perturbation $\delta\mathbf{V}$, with which a particle strikes the sheath will give rise on reflection to waves which lead only to disorganized motion. The result of this energy dissipation will be, of course, to cause the reflected wave to have a smaller intensity than the incident wave has.

In order to estimate the energy dissipated in this way, we note that the time average of the ordered component of the energy of particles of velocity $\mathbf{V}_0$ striking the sheath is

$$\langle\Delta E\rangle_{Av}=\tfrac{1}{2}m\langle(\mathbf{V}_0+\delta\mathbf{V})^2-V_0^2\rangle_{Av}$$
$$=m\langle\mathbf{V}_0\cdot\delta\mathbf{V}+\tfrac{1}{2}\delta V^2\rangle_{Av}=\tfrac{1}{2}m\langle(\delta V)^2\rangle_{Av}, \tag{5}$$

since $\langle\delta V\rangle_{Av}$ vanishes.[3] For small k, we obtain $\delta\mathbf{V}$ from Eq. (4). The result, averaged over velocities is

$$[\langle\Delta E\rangle_{Av}]=(\epsilon^2k^4\varphi_0^2/m\omega^4)\langle V_{0z}^2\rangle_{Av}\cong\kappa T\epsilon^2\varphi_0^2k^4/m\omega^4. \tag{6}$$

To obtain the mean rate of energy dissipation per unit per unit time, we multiply by three times[4] the mean current of particles striking the sheath, which is

$$j=n_0(\kappa T/2\pi m)^{\frac{1}{2}}$$

---

[3] For a damped wave ω is complex and $\langle\delta V\rangle_{Av}$ doesn't vanish. However, we shall be concerned mainly with plasmas in which an exciting source of energy is present so that a steady state is reached. This term then gives no contribution to the energy loss.

[4] The factor 3 enters because we are looking for the energy striking unit surface of electrode per second. This is

$$\int_{V_{0z}>0}\langle nV_z\Delta E\rangle_{Av}d\mathbf{V}_0.$$

This may be written

$$\tfrac{1}{2}m\int_{V_{0z}>0}\langle(n_0V_{0z}+V_{0z}\delta n+n_0\delta V_z)\Delta E\rangle_{Av}d\mathbf{V}_0$$
$$=\tfrac{3}{2}m\int_{V_{0z}>0}\langle n_0V_{0z}\delta V^2\rangle_{Av}d\mathbf{V}_0.$$

The second term has been neglected since k is assumed small.

obtaining

$$dW_1/dt=(\kappa T/m)^{\frac{1}{2}}[3\epsilon^2\varphi_0^2/(2\pi)^{\frac{1}{2}}m](k^4/\omega^4)n_0. \quad (7)$$

This result shows that for long wave-lengths, the energy dissipated in this manner becomes very small. The reason is that, according to Eq. (4), the sheath is very nearly a node of velocity, so that there is only a small component of the ordered oscillatory velocity present here.

IV. REFLECTION FROM A GROUNDED ELECTRODE

In order to obtain a reflected plasma wave, one must, according to Eq. (1), have an antinode in the potential. This is possible at an insulating electrode. The reflection of a plasma wave from a metallic electrode presents problems beyond those due to penetration of the sheath. We shall first indicate how this problem is solved for the special case of a one-dimensional plasma, contained between two metallic electrodes at $Z=0$ and $Z=a$, which are kept at zero potential.[5] If the electrodes were not conducting, each incident wave would have a reflected wave with a potential antinode at $Z=0$ and $Z=a$. The potential would be

$$\varphi=2\varphi_0 e^{-i\omega t}\cos(n\pi Z/a), \quad (8)$$

where n is an integer.

Let us now recall that, as was shown in reference 1, Eq. (8), an arbitrary solution of Laplace's equation is always a solution of the plasma equations. For the one-dimensional problem the most general such solution is $\varphi=AZ+B$. One can then choose A and B such that the potential is zero at the electrodes. When n is even, one chooses $A=0$ and $B=-2\varphi_0 e^{-i\omega t}$, obtaining

$$\varphi=2\varphi_0 e^{-i\omega t}[\cos(n\pi Z/a)-1]. \quad (9)$$

For n odd, we choose $A=(4\varphi_0/a)e^{-i\omega t}$ and $B=-2\varphi_0 e^{-i\omega t}$ obtaining

$$\varphi=2\varphi_0 e^{-i\omega t}[\cos(n\pi z/a)+(2z-a)/a]. \quad (10)$$

It is now necessary to investigate whether particles rebound from the sheath with a velocity appropriate to that of the reflected wave. We shall in this work assume that the sheath is of negligible thickness since for small k the finite sheath thickness causes only a very small energy dissipation.[6]

For a particle moving toward the electrode at $Z=0$ with a velocity $\mathbf{V}_0$, Newton's equation of motion, reference 1, Eq. (19), shows that because of the additional component of electric field in Eq. (12), Eq. (2) for δV must be replaced by (at $Z=0$)

$$\delta V_{1z}=i\frac{4\pi\epsilon\varphi_0}{m\omega a}e^{-i\omega t}+\frac{\epsilon k\varphi_0}{m}e^{-i\omega t}\left[\frac{1}{\omega-kV_{0z}}-\frac{1}{\omega+kV_{0z}}\right]. \quad (11)$$

The process of reflection changes $\mathbf{V}_0$ to $-\mathbf{V}_0$, $\delta\mathbf{V}$ to $-\delta\mathbf{V}$. Immediately after reflection, one has therefore

$$\delta V_{2z}=-i\frac{4\pi\epsilon\varphi_0}{m\omega a}e^{-i\omega t}-\frac{\epsilon k\varphi_0}{m}e^{-i\omega t}\left[\frac{1}{\omega-kV_{0z}}-\frac{1}{\omega+kV_{0z}}\right] \quad (12)$$

where $\mathbf{U}_0=-\mathbf{V}_0$ is the unperturbed velocity of the particle after reflection. We see, that as was to be expected, the second term on the right yields a contribution to $\delta\mathbf{V}$, which is appropriate for a particle going in the reversed direction. The first term, however, has the wrong sign, since Eq. (11) demands a positive sign for all velocities. A similar result is obtained, of course, for particles reflecting at $Z=a$.

Once again, we have a situation in which the reflected particles do not have exactly the right velocity perturbation to make up an ordered reflected wave. This part of the energy is therefore dissipated and becomes random thermal motion, as in the case of the particles reflecting from the sheath of finite thickness. The amount of energy dissipated by a single particle striking the sheath corresponds to the component of $\delta\mathbf{V}$ resulting from the solutions of Laplace's equation. From Eqs. (5) and (11), we get

$$\langle\Delta E\rangle_{Av}=16\epsilon^2\varphi_0^2/m\omega^2a^2. \quad (13)$$

To obtain the mean rate of loss of energy per square centimeter per second, we multiply by three times the mean current of particles striking the sheath,

$$j=n_0(\kappa T/2\pi m)^{\frac{1}{2}}$$

and obtain

$$dW_2/dt=48(\kappa T/2\pi m)^{\frac{1}{2}}(n_0\epsilon^2\varphi_0^2/m\omega^2a^2). \quad (14)$$

Note that for large electrode separations, the above becomes small. If one had a standing wave trapped between two conducting electrodes, it would then be damped,[7] both because of the above-mentioned energy loss, and because of the losses at the sheath. To obtain the net rate of loss of energy per cm², one adds Eq. (7) to Eq. (14) and doubles the result to take into account the two electrodes, thus finding

$$\frac{dW}{dt}=-2\left[\frac{dW_1}{dt}+\frac{dW_2}{dt}\right]=-6\left(\frac{\kappa T}{2\pi m}\right)^{\frac{1}{2}}\frac{n_0\epsilon^2\varphi_0^2}{m\omega^2}\left[\frac{16}{a^2}+\frac{\kappa T}{m}\frac{k^4}{\omega^2}\right]. \quad (15)$$

[5] This is a problem treated by J. R. Pierce for the one beam plasma. For treatments of boundary conditions for a one beam plasma see: J. R. Pierce, J. App. Phys. **15**, 721 (1944); W. O. Schumann, Zeits. f. Physik **121**, 7 (1943). More general problems involving circuit elements are treated by Schumann.

[6] For n odd we shall see that plasma waves are damped because of the presence of conducting electrodes. For n even, that is, for wave-lengths such that k is an even multiple of π/a, Eq. (9) for the potential shows that the addition of solutions of Laplace's equation introduces no additional terms in the electric field. Hence there is no additional component of δV and we obtain the result that even for conducting electrodes, undamped waves of appropriate wave-length can exist.

[7] The damping because of the conducting nature of the electrodes occurs for n odd.

To obtain the rate of damping, we must know how much energy is in the system. The potential energy is $\int \epsilon^2 d\tau/8\pi$ where ϵ is the electric field. This is equal to $k^2\varphi_0^2 a/16\pi$ per unit area of electrode. Since in a harmonic oscillator the kinetic energy is equal to the potential the total energy is

$$W = k^2\varphi_0^2 a/8\pi. \tag{16}$$

Elimination of φ_0 from Eq. (15) yields

$$\frac{dW}{dt} = -48\pi \frac{n_0\epsilon^2}{m\omega^2} \frac{1}{k^2 a}\left(\frac{\kappa T}{2\pi m}\right)^{\frac{1}{2}}\left[\frac{16}{a^2}+\frac{\kappa T}{m}\frac{k^4}{\omega^4}\right]W. \tag{17}$$

This shows that the wave is damped, and that the damping rate resulting from dissipation at the electrodes is

$$R = -\frac{3\omega_P^2}{\omega^2}\left(\frac{8\kappa T}{\pi m}\right)^{\frac{1}{2}}\left[\frac{16}{k^2a^2}+\frac{\kappa T}{m}\frac{k^2}{\omega^2}\right]. \tag{18}$$

For a typical case, $\omega \cong \omega_P \cong 10^{10}$ c.p.s., $k \cong 10$ cm^{-1}, $a \cong 10$ cm, $\kappa T \cong 1$ ev, one obtains

$$R = -(12/10\sqrt{\pi})10^8[16\times 10^{-4}+2] \cong -10^8 \text{ sec.}^{-1}.$$

This compares with $1/\tau_{\text{coll}} \cong 10^7$ sec.$^{-1}$ for damping due to collisions [reference 2, Eq. (12)]. We conclude that for rarified gases damping resulting from imperfect reflection from the electrode sheaths may be comparable with or greater than collision damping, but that in most cases imperfect reflection from the conducting electrodes is quite unimportant.

One can give a similar treatment for electrodes of arbitrary shape. First, one solves the plasma problem ignoring the conducting properties of the electrodes; then one adds suitable solutions of Laplace's equation to make the electrode potential vanish, and notes that these latter can lead to energy dissipation by particles which are reflected from the electrode. A rough estimate of the energy dissipation can be obtained by replacing φ_0/a in Eq. (16) by ϵ, where ϵ is the electric field at the electrode, which results from that solution of Laplace's equation needed to make the electrode potential vanish.

V. EXCITATION DUE TO FAST BEAMS EMITTED FROM AN ELECTRODE

In reference 2, it was shown that, in an unbounded plasma, groups of particles above the mean thermal speeds, or groups of particles of well-defined velocity, could make the plasma unstable. In this section, we wish to discuss the corresponding problem in which beams of electrons are introduced into the plasma at an electrode, which is held at a fixed potential, and emits electrons at a fixed rate. Just as in Sec. V of reference 2 the system acts like two interpenetrating plasmas, and the beam of sharply defined velocity adds another degree of freedom. The main plasma, with a smooth and Maxwellian-like velocity distribution, can then be treated approximately in terms of the organized motions, described by the dispersion relation Eq. (9) of reference 1, if we are interested in oscillations which persists for a long time.[8]

In an unbounded plasma an arbitrary disturbance can be Fourier analyzed as a sum of waves of the form $\exp(i\mathbf{k}\cdot\mathbf{x})$, but one is restricted to real values of k, since complex values imply that the potential becomes infinite in some direction. If the system is bounded, one can use complex values of k, as well as real values. In studying the stability of a bounded plasma, however, one must be careful to distinguish oscillations which grow exponentially in time because they are really forced oscillations, produced by an ever-increasing external emf, impressed on a boundary electrode. In order to illustrate the problems involved, consider the dispersion relation [reference 1, Eq. (11)],

$$\omega^2 = \omega_P^2 + (3\kappa T/m)k^2.$$

By writing $k = k_R + i\beta$, $\omega = \omega_R + i\lambda$ one can obtain waves of complex k and w. From the dispersion relation, it follows, for small k, that

$$\omega^2 \cong \omega_P^2 + (3\kappa T/m)k_R^2, \quad \lambda \cong (3\kappa T/m)\beta k_R/\omega_R. \tag{19}$$

The wave then takes the form of

$$\varphi = \varphi_0 e^{-\beta z + \lambda t} e^{i(k_R z - \omega_R t)},$$

which increases with time, but decreases with increasing z. In order that φ remain finite, it is necessary thtat the plasma be bounded on the left-hand side; for convenience, one can take the boundary at $z=0$. We see that Eq. (19) corresponds to a wave in which the electrode potential is $\varphi = \varphi_0 e^{-i\omega t}$. Since the group velocity $V_g = \partial\omega_R/\partial k_R$ is positive, one concludes that the wave energy must be coming out of the electrode; hence such a wave does not represent a genuine internal instability of the plasma. This is generally true whenever the amplitude decreases in the direction in which energy is carried; for in this case, the exponential growth is due to a transport of energy from the more intense to the less intense parts of the wave.

Let us now return to the one-dimensional problem of studying oscillations of the fast beam of electrons, entering the plasma at $Z=0$ with a fixed density, n_1 and a fixed velocity, V_1. We seek solutions of the form, $\exp[i(\mathbf{k}\cdot\mathbf{x}-\omega t)]$, where ω and k may be complex. According to reference 2, Eq. (41), the dispersion relation is

$$\omega^2 \cong \omega_P^2 + \frac{3\kappa T}{m}k^2 + \frac{\omega_1^2}{[1-(kV_1/\omega)]^2 - k^2\delta^2/\omega^2},$$

where $\omega_P^2 = (4\pi n_0\epsilon^2/m)$, and n_0 is the density of the main plasma, $\omega_1^2 = 4\pi n_1\epsilon^2/m$ and δ is the velocity spread of the beam. Let us choose $\delta = 0$. In order to

[8] Analogous problems have been discussed by Pierce, Haeff, and others in the theory of traveling wave tubes and double stream amplifiers. See J. R. Pierce, Bell Sys. Tech. J. **29**, 1 (1950).

demonstrate some of the properties of the solutions in a simple way, we shall also take a special case for which $\omega=\omega_P$, the resulting equation is

$$(3\kappa T/m)k^2[1-(kV_1/\omega_P)]^2=-\omega_1^2$$

with the solution

$$k=\frac{\omega_P}{2V_1}\left\{1\pm\left[1\pm 4iV_1\frac{\omega_1}{\omega_P}\left(\frac{m}{3\kappa T}\right)^{\frac{1}{2}}\right]^{\frac{1}{2}}\right\}. \tag{20}$$

All four roots are complex. If $(\omega_1V_1/\omega_P)(m/3\kappa T)^{\frac{1}{2}}$ is small, for example, as usually is the case, one obtains

$$k_{1,2}=(\omega_P/V_1)[1\pm i(\omega_1V_1/\omega_P)(m/3\kappa T)^{\frac{1}{2}}],$$

$$k_{3,4}=\pm i\omega_1(m/3\kappa T)^{\frac{1}{2}}.$$

The most general solution is

$$\varphi=\Sigma A_n e^{i(k_nz-\omega t)},$$

where A_n are arbitrary constants, and n runs from 1 to 4.

The boundary conditions on the fast beam particles may be taken as $\delta V_1=0$, $\delta n_1=0$ at $Z=0$. As for the particles in the main plasma, the boundary conditions are discussed in Secs. II, III, IV. According to Eq. (4), one must have $\partial\varphi/\partial z=0$ at $Z=0$ to satisfy these conditions. If the electrode potential is held fixed, then one also has $\varphi=0$ at $Z=0$. These boundary conditions can be satisfied by a proper choice of the four arbitrary constants to which, however, it will be necessary to add a suitable solution of Laplace's equation, which will introduce a small dissipation of ordered energy at the boundary (see Sec. IV). In this solution we shall obtain two waves which increase exponentially in amplitude as one leaves the electrode, and two waves which decrease. The physical significance of the exponentially increasing waves is that small perturbations which may be present near the electrode produce bunching of the fast particles which cumulatively amplifies the original perturbation as it travels along the beam. The process is very similar to that occurring in the "traveling wave tube."[8] We thus obtain a wave which grows exponentially in space, as one leaves the electrode, until the linear approximation breaks down.

Thus far we have assumed that $\omega=\omega_P$. One can readily show that similar results are obtained for ω near ω_P, even when ω is complex. To do this, one writes, for example,

$$\alpha=(\omega^2-\omega_P^2)/k^2.$$

Equation (41) of reference 2 becomes

$$\left(\frac{3\kappa T}{m}-\alpha\right)k^2\left(1-\frac{kV_1}{\omega}\right)^2=-\omega_1^2$$

and the approximate solutions for k are (with kV_1/ω small)

$$k_{1,2}\cong\frac{\omega_P}{V_1}\left\{1\pm\frac{\omega_1}{\omega_P}V_1\left[\frac{1}{(3\kappa T/m)-\alpha}\right]^{\frac{1}{2}}\right\},$$

$$k_{3,4}\cong\pm i\omega_1\left[\frac{1}{(3\kappa T/m)-\alpha}\right]^{\frac{1}{2}}. \tag{21}$$

One can readily choose α so that both ω and k are complex; thus one obtains waves which grow with time, and which increase exponentially in space. If the wave is growing with time, then the dissipation caused by imperfect reflection of the wave at the electrode will merely slightly decrease the rate of growth.

VI. THE ENERGY TRANSFER METHOD

When the charge density of the fast beam is considerably less than that of the main plasma, one can study the stability of oscillations by calculating the mean energy transfer from particles to the plasma oscillations of the rest of the ion gas. If this is positive and greater than that dissipated, the wave will be excited; otherwise, damped.[9]

In order to illustrate the method, we being by applying it to the problem already treated in the last section, in which a beam of particles enters the plasma at a fixed velocity from an electrode of fixed potential. We assume that the beam enters at an electrode at $Z=0$, and leaves by striking another electrode at $Z=a$, which is held at the same potential as the electrode at $Z=0$. Although this is a somewhat idealized problem, it does yield a fairly good indication of what is to be expected under more general conditions.

It may often happen that for a wave of fixed amplitude the mean energy transfer vanishes, while for a wave of exponentially increasing amplitude it does not. In order to maintain such a wave, however, it is necessary that the beam supply enough energy not only to balance what is dissipated, but also that needed to maintain the assumed rate of growth. If $\omega=\omega_R+i\lambda$, one can show that the energy density grows at the rate $W=W_0e^{2\lambda t}$, so that $dW/dt=2\lambda W$.

The energy dissipated is the sum of that due to collisions, and that due to reflection at electrodes. According to reference 2, Eq. (12), collisions tend to create a damping factor $e^{-t/2\tau}$, where τ is the mean time between collisions, from which one concludes that the rate of dissipation due to collisions is $(dW/dt)_c=-W/\tau$. The rate of dissipation at the electrodes is given in Eq. (20). To obtain excitation the total energy that must be supplied by the beam must then be

$$(dW/dt)_b\geqq W(2\lambda+R+1/\tau), \tag{22}$$

where R is given by Eq. (20).

Let us now compute the mean rate of transfer of

[9] This method was used in reference 2, Sec. V, to demonstrate that in an unbounded plasma particles slightly faster than the wave excited it, while particles slightly lower damped it.

energy from the beam particles to the wave. Although one actually has a standing wave, such as, for example, that given by Eq. (9) (with n an even integer) one can write it as the sum of two running waves.

$$\varphi=\varphi_0[\cos(\omega t-2\pi nz/a)+\cos(\omega t+2\pi nz/a)-2].$$

As shown in reference 2, Sec. V, the energy transfer will be large only when the beam particles are moving with very nearly the wave velocity. Hence one need consider only the effects of the wave which moves in the same direction as the particle.

The energy transferred by a given particle to the wave is

$$\Delta E=-m[V_0\delta V+\tfrac{1}{2}(\delta V)^2],$$

where δV is the change of velocity of the particle as it moves from one electrode to the other. We shall be interested in averaging this over a long time, covering many periods of oscillation. To find the mean rate per unit area at which the wave gains energy, we must average the above over all possible times, t_0, at which the particle enters the plasma, and multiply by the current, which we take to be constant and equal to n_1V_0. Thus we get

$$\langle dW/dt\rangle_{Av}=-n_1V_0m\langle V_0\delta V+\tfrac{1}{2}(\delta V)^2\rangle_{Av}. \quad (23)$$

We shall see that the first order terms in φ_0 may drop out of this average; hence it is necessary to go to the second order. Let us write δV_1 as the first order expression, and δV_2 as the second order correction to δV. Then to second order, we get (noting that $\langle\delta V_1\rangle_{Av}=0$)

$$\langle dW/dt\rangle_{Av}=-n_1V_0m[V_0\langle\delta V_2\rangle_{Av}+\langle\delta V_1{}^2/2\rangle_{Av}]. \quad (24)$$

δV_1 and δV_2 must be obtained by solving the equations of motion in the assumed potential,

$$\varphi=Re\{\varphi_0\exp[i(\mathbf{k}\cdot\mathbf{x}-\omega t)]\}.$$

For w real, one obtains from Eq. (39), of the Appendix

$$\left\langle\frac{dW}{dt}\right\rangle_{Av}=-\frac{n_1\epsilon^2\varphi_0{}^2k^2}{2m}\frac{\omega V_0}{(kV_0-\omega)^3}$$
$$\times\left[\frac{(kV_0-\omega)z}{V_0}\sin\frac{(kV_0-\omega)z}{V_0}-4\sin^2\frac{(kV_0-\omega)z}{2V_0}\right]. \quad (25)$$

It is clear that the energy transfer is largest when V_0 is close to ω/k. For small values of z of $V_0-\omega_k$, it is readily shown that the energy transfer is positive when $V_0>\omega/k$. negative when $V_0<\omega/k$, a result in agreement with that obtained in reference 2 for a plasma without boundaries. For large values of Z, however, the conditions for positive energy transfer become more complicated and by varying Z in Eq. (25) we find regions of positive and negative energy transfer.

When ω is complex, the expressions become much more cumbersome. If, however, λ is small, while $Z\lambda/V_0$ is fairly large, then the following relatively simple expression is obtained (see Eq. (46), Appendix).

$$\left\langle\frac{dW}{dt}\right\rangle_{Av}\cong-\frac{n_1\epsilon^2\varphi_0{}^2k^2e^{2\alpha t_0}}{2m(kV_0-\omega_R)^2}e^{2(\alpha z/V_0)}$$
$$\times\left[\frac{\omega_R}{kV_0-\omega_R}+\frac{1}{2}\right]V_0. \quad (26)$$

Here one obtains positive energy transfer when $V_0>\omega/k$, and also when $V_0<\omega/k$.

It is readily verified that if V_0 is close to ω/k, one can usually choose n_1 large enough so that $\langle dW/dt\rangle_{Av}$ is large enough to overcome the dissipation given in Eq. (24). Hence we verify by this method that a plasma with a beam entering at a definite place and leaving at a different place is, in general, unstable in the linear approximation.

VII. ENERGY TRANSFER METHOD IN NON-LINEAR THEORY

As was shown in reference 1, Sec. III, the effect of a very large potential will be to trap particles in the wave, so that the linear approximation fails. This will happen whenever

$$\epsilon\varphi>\tfrac{1}{2}m(V_0-\omega/k)^2.$$

As in the theory of the unbounded plasma given in reference 1, one can easily see that non-linear effects tend to reduce the energy transfer below that calculated in the linear approximation. Consider, for example, a particle which starts out faster than the wave. As the particle begins to climb out of the potential trough, it is slowed down and, if it is trapped, it eventually falls back in. At this stage, it is actually going backwards in the coordinate system in which the wave is at rest, so that it is slower than the wave. Eventually the particle begins to climb the trough in the opposite directions and gains energy at the expense of the wave. These possibilities are neglected in the linear approximation, which does not permit the correct description of such large changes in the velocity. For particles with V_0 near ω/k, the linear approximation overestimates the possible energy transfers, since it treats such particles as though they remained in phase for a long time experiencing velocity changes of the same sign.

One can obtain an upper limit on the possible amplitude of a plasma oscillation by setting the maximum rate of energy supplied equal to the rate at which it is dissipated. The rate of dissipation is $K\varphi_0{}^2$, where the constant, K, can be obtained from Eq. (15), for the special case of a one-dimensional plasma. More generally, K depends on the shape of the plasma region, and must be calculated for each specific case. The maximum energy which can be given up by a particle to a wave will be that obtained from a particle which is barely trapped. If such a particle enters the plasma at the trough of a wave and leaves at the same trough when it is traveling backward relative to the wave, its change

of velocity is $\delta V=-2(4\epsilon\varphi_0/m)^{\frac{1}{2}}$ as can be verified by going to the coordinate system in which the wave is at rest. Its transfer of energy in the laboratory system is

$$\Delta W=mV_0\cdot 2(4\epsilon\varphi_0/m)^{\frac{1}{2}}-8\epsilon\varphi_0. \tag{27}$$

The condition for a balance of energy supplied and dissipated is then

$$j_1[2mV_0(4\epsilon\varphi_0/m)^{\frac{1}{2}}-8\epsilon\varphi_0]=K\varphi_0^2, \tag{28}$$

where γ_1 is the current of beam particles entering the plasma. If φ_0 is not too large, one can neglect the second term on the left, obtaining

$$\varphi_{\max}\cong[j_1\cdot 2mV_0(4\epsilon/m)^{\frac{1}{2}}/K]^{\frac{2}{3}}. \tag{29}$$

Another limitation on the amplitude of oscillation, often more stringent, arises from the processes described in connection with the breakdown of the linear approximation, which cause the particle to gain energy if it stays in the wave too long before it strikes a collecting electrode. The calculation of the conditions under which this happens is very similar to what is done for the klystron.[10] Although the precise details are rather complex, it may be expected that as in the klystron calculations one can get a fairly good estimate of the most favorable condition for energy transfer by considering two extreme particles, one of which is emitted into the trough of the wave, and the other into the crest. We require that the particles emitted into the trough undergo the maximum possible deceleration.

This means that these particles must be returned to the trough just before they strike the anode; if they stayed in the wave any longer they would begin to be accelerated. We then require that a particle entering at the crest barely reach the next crest, just as it is collected, so that it undergoes no net energy exchange. Investigations of klystrons have shown that this operation condition provides very nearly the maximum possible energy transfer. If φ_0 is increased much beyond this point the particles entering at the crest begin to be accelerated again, and it turns out that this more than compensates for the additional deceleration experienced by particles collected near the trough.

The oscillations described above resemble those found in a resonance cavity containing electromagnetic waves. As with electromagnetic waves, strong oscillations of this kind occur only with simple geometries and small loss systems. This conclusion has been verified experimentally by Sluzkin and Maydanov,[11] who have shown that a plasma with cylindrical geometry excited by a beam of fast electrons oscillates with much greater intensity than does one with a less regular geometry.

One can see that large amplitude oscillations can have a new kind of stability not possessed by small oscillations. This consists of a tendency to remain near a definite state of oscillation, and to return to this state, when perturbed. Thus, if we have a state of stable oscillation in the previous example, and if φ_0 is increased, the losses increase, while the energy supply decreases, or increases at a smaller rate, so that the wave tends to return to its original amplitude. Similarly, if φ_0 is reduced. the losses are decreased, while the energy supply is increased. This stability may be incomplete, however, in that the excitation may be transferred from one mode to another in relaxation oscillations, because of non-linear coupling.

[10] J. Marcum, J. App. Phys. **17**, 4 (1946).
[11] A. Sluzkin and P. Maydanov, J. Phys. USSR **VI**, 7 (1942).

VIII. NON-LINEARITY IN BUNCHING—PLASMA SHOCK WAVES[12]

In the energy transfer method of treating instability, one assumes that the interaction of the fast beam particles with each other can be neglected. Because of the possibility of bunching, however, the interaction of the beam particles with each other may be surprisingly large even with very small currents.

In order to illustrate this effect, let us imagine that a homogeneous beam of velocity V_0 receives at $Z=0$ a small trigonimetric modulation in its velocity, which could be produced, for example, by a small localized electric field. The velocity of a beam particle then becomes $V_0+\delta V_0\sin\omega t_0$ where t_0 is the time at which the particle passes through $Z=0$. If the particle meets no electric fields, it just drifts with constant velocity thereafter. A particle emitted at $Z=0$, $t=t_0$, will at the time, t, reach the point $Z=(V_0+\delta V_0\sin\omega t_0)(t-t_0)$. The particle starting at $t_0+\delta t_0$, will have a velocity, $V_0+\delta V_0\sin\omega(t_0+\delta t_0)$. The separation of the two particles as a function of time is therefore

$$\delta Z=\delta t_0\{V_0+\delta V_0\sin\omega(t_0+\delta t_0)\}+(t-t_0)\delta V_0\{\sin\omega t_0-\sin\omega(t_0+\delta t_0)\}. \tag{30}$$

For small δt_0, this becomes

$$\delta z=V_0\delta t_0+\delta V_0\delta t_0\{\sin\omega t_0-\omega(t-t_0)\cos\omega t_0\}.$$

We see that for $t-t_0=(V_0+\delta V_0\sin\omega t_0)/(\omega\delta V_0\cos\omega t_0)$, δz vanishes; all particles emitted in a range, δt_0, then reach the same point at the same time (to first order in δt_0. To obtain the density, one writes

$$\rho(z)=\rho(0)\delta z_0/\delta z$$

$$=\rho(0)\frac{V_0}{V_0+\delta V_0\left\{\sin\omega\left(t_4-\frac{z}{V_0}\right)-\frac{\omega z}{V_0}\cos\omega\left(t-\frac{z}{V_0}\right)\right\}}, \tag{31}$$

[12] The following sections contain a treatment of the well-known Webster bunching theory in a form adapted to our purposes and also an analysis of the experiments of Merrill and Webb. Delays have held up the publication of this paper and in the meantime a note by Neill has appeared, describing experiments similar to those of Merrill and Webb. The explanation given is substantially the same as that of Sec. IX. Neill's experiments seem to establish conclusively that this mechanism is correct. However, only a very brief description of his results has been published and we have though it worth while to include our analysis of the Merrill and Webb experiments. See T. R. Neill, Nature **163**, 59 (1949).

where t_0 is now replaced by $t-z/V_0$, which is adequate for a first order calculation. One sees that there is an infinite density at the point

$$Z=V_0^2/\omega\delta V_0. \tag{32}$$

As one approaches this point, the variations in density become larger and larger, taking the form of waves which travel toward the point, rising very steeply in amplitude when they get near it. The rate of rise is so abrupt, in fact, that they resemble shock waves in form.

The denominator can become infinite at some time for all values of Z larger than $V_0^2/\omega\delta V_0$. But the value chosen produces a singularity when $\cos\omega(t-Z/V_0)=1$, at which times the cosine has a maximum. This means that the degree of singularity is higher than that for any other value of Z. It will be seen that this value of Z corresponds to the crossing of a whole range of orbits, i.e., it is a focus, while infinities at other values of Z correspond to the crossing of only two orbits.

To estimate the width of the pulse, one must go to higher powers of δt_0. Let us therefore expand δz as a function of δt_0, retaining only up to third order terms. Differentiation of Eq. (30) yields

$$\begin{aligned}(\partial\delta z/\partial\delta t_0)_{\delta t_0=0}&=V_0+\delta V_0\sin\omega t_0\\&\quad-\omega(t-t_0)\delta V_0\cos\omega t_0,\\(\partial^2\delta z/\partial\delta t_0^2)_{\delta t_0=0}&=2\omega\delta V_0\cos\omega t_0\\&\quad+(t-t_0)\omega^2\delta V_0\sin\omega t_0,\\(\partial^3\delta z/\partial\delta t_0^3)_{\delta t_0=0}&=-3\omega^2\delta V_0\sin\omega t_0\\&\quad+(t-t_0)\delta V_0\omega^3\cos\omega t_0.\end{aligned} \tag{33}$$

Choosing $t-t_0=(V_0+\delta V_0\sin\omega t_0)/(\omega\delta V_0\cos\omega t_0)$ and $\omega t_0\cong 2n\pi$, we get

$$\delta z=(\omega^3 z/6V_0)\delta V_0(\delta t_0)^3. \tag{34}$$

This shows that the width of the beam depends on what range of emission times, δt_0, one wishes to consider. For example, if we choose $\omega\delta t_0\cong 1$ we include about one-sixth of the total charge injected during a cycle. This charge is then focused into a region of width.

$$\delta z\cong Z\delta V_0/6V_0.$$

Hence if δV_0 is small, the width of focus will be only a small fraction of the distance from electrode to focal point. As a typical numerical example, take

$$\delta V_0/V_0=0.01,\quad V_0=3\cdot 10^8\text{ cm/sec.},\quad \omega=10^{10}\text{ r.p.s.}$$

One obtains for the focal point, $Z=3$ cm, and for the width of the pulse, $\delta z=5\cdot 10^{-3}$ cm.

If this beam of space charge is moving through a plasma, the latter tends to shield out the pulse, but since the pulse is very sharp it contains Fourier components far above the plasma frequency which cannot be shielded out in this way. Hence, while the pulse is broad, it may be partly shielded, but this will only increase the abruptness with which the potential appears when the particles focus. As a first approximation one can therefore neglect the effect of the beam space charge on itself until the actual focus appears. When the focus appears, however, the resulting potential will spread the velocities of the beam particles, because the different particles go through at different times, and the potential is changing very rapidly.

Let us estimate the maximum potential drop across the focus. To do this, we take a simplified model, in which the charge is assumed to be in a sheet of thickness, δz. If j is the current per unit area in the beam, then j/w will be the amount of charge per unit area in the pulse. The electric field (in e.s.u.) developed in this layer will be of the order of $4\pi(j/2\omega)$, and the resulting potential drop across the pulse will be

$$\delta\varphi\cong(2\pi j/\omega)\delta z. \tag{35}$$

With a typical beam current of 100 ma/cm^2, and $w=10$ r.p.s., one obtains

$$\epsilon=2\pi\gamma/\omega\cong(2\pi/10^{10})\cdot 300\cdot 10^6$$
$$\cong 0.2\text{ e.s.u.}\cong 60\text{ volts/cm.}$$

The potential drop across the pulse given in the previous example will then be 0.3 volt.

After the particles bunch, further bunching will develop, as a result of the velocity changes produced by the fields generated by the pulse. Because δV_0 will usually be larger than it was originally, the second pulse will be closer to the first than the first was to the modulated electrode. In this way a cascade of pulses will develop and will continue until the beam is so spread out in velocity that no more bunching is possible. It is not necessary to assume, as in our example, that the oscillatory field causing the original bunching is localized. Waves of arbitrary shape can produce essentially the same result. Although the precise location and width of the focus will depend somewhat on the shape of the field, the example given here will provide a general order of magnitude estimate of what can be expected.

IX. RESULTS OF MERRILL AND WEBB[13]

It has long been known that beams of electrons in a plasma are scattered much more rapidly than can be accounted for by collisions with other particles.[14] Furthermore, although the scattered particles lose energy on the average, some of them gain energy. Plasma oscillations have already been suggested as an explanation.[14] As shown in the argument in reference 2, Sec. V, it has been realized that a small oscillation potential can transfer very large quantities of energy. We have seen in this paper, and in reference 2, that the beam is generally unstable so that such oscillations are to be expected. If the geometry is simple, e.g., plane or cylindrical, one can expect to build up large oscillations of the entire system. With unsymmetrical geometry,

[13] H. J. Merrill and H. W. Webb, Phys. Rev. **55**, 1191 (1939).
[14] I. Langmuir, Proc. Nat. Acad. Sci. **14**, 627 (1928).

however, localized pulses due to bunching are more likely to be the most important type of oscillations present.

Merrill and Webb have made a more precise investigation of the space distribution of oscillation, and have found that the points of scattering of the beam are very well-defined. Briefly, they show that an electron beam of 19.5 ev energy and a current density of about 100 ma/cm² has a spread of only ±1 ev as it leaves the cathode, but that at a point about 4.3 mm from the cathode the spread increases abruptly to ±5 ev, within a space of less than ¼ mm. At about 6.1 mm an equally abrupt scattering takes place, after which the velocity distribution is practically uniform from 0 to 30 ev. Beyond this point very little scattering takes place. No appreciable plasma oscillations were observed in the region from the probe to the first scattering point, but beyond each scattering point it was found that strong oscillations were picked up in a region a few mm wide. It was believed that these were not genuine oscillations of the main plasma but variations in probe current resulting from the bunching of fast particles at the previous scattering points.

With higher current densities and pressures the scattering point moved closer to the cathode, and the beam as it emerged from the cathode had a greater spread. At very high densities only irregular oscillations close to the cathode were observed.

It seems clear that these experiments should be interpreted in terms of the plasma shock waves discussed previously. Let us defer, for the time, consideration of how the initial bunching is maintained in the region between the cathode and the first scattering point except to note that it is due to feedback of some of the oscillatory energy developed in the shocks. If the original bunching impulse had a sine wave form, then from Eq. (32) setting $Z=4.3$ mm, $V_0=3\times10^8$ cm/sec., and $\omega=10^{10}$ r.p.s. (observed value), one obtains

$$\delta V_0/V_0=V_0/\omega z=3\cdot10^8/10^{10}(0.43)\cong0.07.$$

This implies that the original velocity spread was seven percent, or the energy spread about 14 percent of 20 ev, which is about 2.8 ev. This is almost twice the observed spread, hence there seems at first sight to be a discrepancy. Let us remember, however, that the original bunching impulse is due, in part, to feedback of the bunching shock, which latter contains many high harmonics. The general effect of such harmonics is to increase the value of ω appearing in the denominator of (32), and thus to decrease the value of δV_0 needed to produce bunching at a given Z.

If we tentatively assume that the first few harmonics were the most important cause of bunching, we obtain $\delta V_0/V_0\cong0.04$, leading to $\delta E\cong1.6$ ev which agrees with that observed.

The width of the bunching shock becomes

$$\delta z\cong\tfrac{1}{6}(0.04)(0.43)\cong0.03 \text{ mm}.$$

To calculate the potential drop across the pulse, we must know the current density, which was of the order of 100 ma/cm². With $\omega\cong10^{10}$ r.p.s. one obtains $\Delta\varphi=60\delta z$ volts, which is of the right order of magnitude to explain the observed increase of velocity spread suffered by the particles as they cross the bunching point. The next bunching process will be more complicated, and the exact bunching produced by the shock is probably almost unpredictable, but a bunching distance of $6.1-4.3=1.8$ cm is certainly not inconsistent with the greater spread of velocities. After the second pulse the definition of the beam is too poor to allow further bunching.

Let us now return to the question of what produced the original bunching. Because a plasma containing a beam of fast electrons is unstable the plasma is certain to start oscillating, as a result of random fluctuations. These oscillations will start the bunching process. On the other hand the fields produced by the bunching will feed energy back into the plasma oscillation, and in this way it is maintained indefinitely. It is necessary, however, for a steady state of oscillation, that the feedback of energy from bunching be just that needed to maintain the dissipative losses in the plasma oscillations. In order to show that such an adjustment tends to occur automatically we first note that the bunching pulse consists of a wave moving with the beam velocity, V [see Eq. (31)]. Hence plasma oscillations near this velocity are the ones which are excited most effectively.

In order to see what determines the wave-length, note that the electric field of the bunching pulse is strong only for a short time, and in the neighborhood of the pulse itself. This field therefore transfers energy and mostly to the particles of the main plasma which happen to be near the pulse; whether they absorb energy from the field, however, depends on whether on the average they are moving in a direction such that the field tends to push them. If, for example, there is a node of velocity at the pulse, then only a negligible energy will be delivered to the wave. Now the plasma does not actually dissipate much energy,[15] hence it may be expected that there will be a node of velocity near the pulse in the steady state. The adjustment of the energy transfer to equal the energy dissipated requires only a slight shift in pulse position, which correspondingly shifts the distance between the pulse and the node. That this adjustment is automatic can be inferred from the fact that if too little energy is supplied, the wave amplitude drops, and causes the pulse to move out [see Eq. (32)]. If the system has been oscillating in such a way that pulse is slightly beyond the nodal point then this will move the pulse into a position such

[15] The energy dissipated is the sum of that due to collisions, plus that lost at the cathode sheath, plus that carried away by the group velocity of the electrons; it is readily shown that under the conditions of this experiment this is much less than could be supplied by the pulse if the plasma wave had an antinode at the pulse.

that the wave gains more energy. If too much energy is supplied by the pulse, the opposite adjustment takes place.

Since there is also a node of velocity at the cathode sheath, the pulses at 4.3 mm and 6.1 mm imply a wavelength of 1.8 mm. The wave velocity is

$$V_W=\omega/k=10^{10}(0.18)/2\pi\cong 3\times 10^8 \text{ cm/sec.}$$

This is very close to the velocity of the beam, a result which is in agreement with our own conclusion that the wave velocity must be close to the beam velocity for strong excitation. Hence the position of the pulses in these experiments is consistent with the explanation offered here.

At large current densities and high pressures the neglect of the beam space charge in the region between the cathode and the pulse is not valid; in fact, it is known from klystron theory that space charge decreases the bunching. This explains the fact that the peaks were much less distinct at high currents and pressures.

APPENDIX

We wish to calculate δV_1, and δV_2, which are, respectively, the first- and second-order changes of velocity resulting from the interaction between fast beam particles and wave, in order to insert this result into Eq. (24), for the mean rate of energy transfer to the wave. We begin with the equation of motion

$$dV/dt=Re\{(i\epsilon k\varphi_0/m)e^{i(kz-\omega t)}\},$$

where $\omega=\omega_0+i\lambda$. From this, we must solve for the value of V for a particle at the point z, under the assumption that it starts at $z=0$ and $t=t_0$ with the velocity V_0. Let us begin by calculating δV_2. If we introduce the abbreviations $\alpha=kV_0-\omega$ and $\tau=t-t_0$, Eq. (49) of reference 2 (Appendix) may be written[16]

$$\delta V_2=Re\left\{\frac{i\epsilon k\varphi_0}{m}e^{-i\omega t_0}\left[\frac{e^{i\alpha\tau}-1}{i\alpha}+ik\int_0^\tau e^{i\alpha\tau}\delta z_1 d\tau\right]\right\}$$

δz_1 is given in Eq. (50) of reference 2 (Appendix) as

$$\delta z_1=Re\left\{\frac{\epsilon k\varphi_0}{m\alpha}e^{-i\omega t_0}\left[\frac{e^{i\alpha\tau}-1}{i\alpha}-\tau\right]\right\}.$$

Now τ must be eliminated in terms of z since we want the energy transferred by particles going a fixed distance. In a second order term, such as the second, it is adequate to write $\tau\cong z/V_0$ but in a first order term, one must write $z=V_0\tau+\delta z_1$ or $\tau=(z/V_0)-(\delta z_1/V_0)$. We then obtain to second order

$$\delta V_2=Re\left\{\frac{\epsilon k\varphi_0}{m}e^{-i\omega t_0}\left[\frac{e^{i(\alpha z/V_0)}-1}{\alpha}\right]\right\}-Re\left\{\frac{ik\epsilon\varphi_0}{mV_0}e^{-i\omega t_0}e^{i(\alpha z/V_0)}\delta z_1\right\}$$
$$-Re\left\{\frac{\epsilon k^2\varphi_0}{m}e^{-i\omega t_0}\int_0^{z/V_0}d\tau e^{i\alpha\tau}\delta z_1\right\}. \quad (36)$$

Let us now average these terms over t_0. We shall first consider the case in which ω is real. Then the average of the first term over a cycle vanishes. To evaluate the second order terms, we use the theorem that if f and g are complex numbers proportional to $e^{-i\omega t_0}$, then

$$\langle Re(f)\cdot Re(g)\rangle_{Av}=\tfrac{1}{2}Re\langle f^*g\rangle_{Av}.$$

We get

$$\langle\sigma V_2\rangle_{Av}=-\frac{1}{2}\left(\frac{\epsilon k\varphi_0}{m}\right)^2\left[\frac{1}{V_0}\frac{\partial}{\partial\alpha}\left(\frac{1-\cos\alpha z/V_0}{\alpha}\right)\right.$$
$$\left.-k\frac{\partial}{\partial\alpha}\left(\frac{1-\cos\alpha z/V_0}{\alpha^2}\right)\right]. \quad (37)$$

To obtain the total energy transfer we must also compute $\langle\delta V_1^2/2\rangle_{Av}$. This is simple and gives

$$\langle\delta V_1^2/2\rangle_{Av}=(\epsilon k\varphi_0/m\alpha)^2\sin^2\alpha z/2V_0. \quad (38)$$

The rate of energy transfer is then

$$\left\langle\frac{dW}{dt}\right\rangle_{Av}=-\frac{n_1V_0m}{2}\left(\frac{\epsilon k\varphi_0}{m}\right)^3\frac{\omega}{\alpha^3}\left[\frac{\alpha z}{V_0}\sin\frac{\alpha z}{V_0}-4\sin^2\left(\frac{\alpha z}{2V_0}\right)\right]. \quad (39)$$

For small $\alpha z/V_0$ this expression becomes

$$\langle dW/dt\rangle_{Av}=(n_1V_0m/24)(\epsilon k\varphi_0/m)^2\omega\alpha(z/V_0)^4.$$

The energy transfer is positive for $V_0>\omega/k$. For larger values of $\alpha z/V_0$ the energy exchange is particularly large for V_0 near ω/k, and by varying z we find successively regions of positive and negative energy transfer.

The above expressions are valid for large z provided φ_0 is so small that we always satisfy $\epsilon k\varphi_0 z/mV_0\alpha\ll 1$. It is possible to derive expressions which hold for all z as long as

$$[\epsilon\varphi_0/m(V_0-\omega/k)^2]\ll 1,$$

but we shall not reproduce this calculation here.

We start the calculation for complex ω by using Eq. (36). We treat only the case where λ is small but $\lambda z/V_0\gg 1$. It is then sufficient to retain only terms proportional to $e^{2\lambda z/V_0}$. To this approximation we may write

$$\delta V_2\cong -Re\left\{\frac{ik\epsilon\varphi_0}{mV_0}e^{-i\omega t_0}e^{i\alpha z/V_0}\right\}Re\left\{\frac{\epsilon k\varphi_0}{m\alpha}\frac{e^{-i\omega t_0}e^{i\alpha z/V_0}}{i\alpha}\right\}$$
$$-Re\left\{\frac{\epsilon k^2\varphi_0}{m}e^{-i\omega t_0}\int_0^{z/V_0}d\tau e^{i\alpha\tau}\right\}$$
$$\times Re\left\{\frac{\epsilon k\varphi_0}{m\alpha}\frac{e^{-i\omega t_0}e^{i\alpha\tau}}{i\alpha}\right\}. \quad (40)$$

Evaluation of these terms gives, with $\alpha=\alpha_r-i\lambda$

$$\langle\delta V_2\rangle_{Av}=-\left(\frac{\epsilon k\varphi_0}{m}\right)^2\frac{e^{2\lambda t_0}e^{2\lambda z/V_0}}{(\alpha_r^2-\lambda^2)^2+4\lambda^2\alpha_r^2}\left[\frac{\lambda^2-\alpha_r^2}{2V_0}+\frac{k\alpha_r}{2}\right]. \quad (41)$$

For $\lambda\ll\alpha_r=kV_0-\omega$, we obtain

$$\langle\delta V_2\rangle_{Av}=-\frac{1}{2}\left(\frac{\epsilon k\varphi_0}{m}\right)^2e^{2\lambda t_0}e^{2\lambda z/V_0}\frac{\omega_0}{V_0\alpha_r^3}. \quad (42)$$

In addition we have

$$\left\langle\frac{\delta V_1^2}{2}\right\rangle_{Av}\cong\frac{1}{2}\left(\frac{\epsilon k\varphi_0}{m}\right)^2\frac{e^{2\lambda t_0}e^{2\lambda z/V_0}}{2\alpha_r^2}. \quad (43)$$

The total average energy transfer is therefore

$$\left\langle\frac{dW}{dt}\right\rangle_{Av}=-\frac{n_1V_0m}{2}\left(\frac{\epsilon k\varphi_0}{m}\right)^2\frac{e^{2\lambda t_0}e^{2\lambda z/V_0}}{\alpha_r^2}\left[\frac{\omega_0}{\alpha_r}+\frac{1}{2}\right]. \quad (44)$$

[16] Note that the condition $k\delta z_1\ll 1$ requires $\epsilon k\varphi_0 z/mV_0\alpha\ll 1$.

Letters to the Editor

PUBLICATION of brief reports of important discoveries in physics may be secured by addressing them to this department. The closing date for this department is five weeks prior to the date of issue. No proof will be sent to the authors. The Board of Editors does not hold itself responsible for the opinions expressed by the correspondents. Communications should not exceed 600 words in length.

On Spin Dependent Nuclear "Radii"

C. O. MUEHLHAUSE
Argonne National Laboratory, Chicago, Illinois
July 17, 1950

IN applying the Breit-Wigner scattering formula to low energy neutron scattering ($J=I\pm\frac{1}{2}$) the nuclear radius, R, enters as a potential scattering amplitude. At thermal energies the total scattering cross section, σ_s, is given by:

$$\sigma_s/4\pi=g_+|R+a_+|^2+g_-|R+a_-|^2$$

where the + and − refer to states having total angular momenta J_+ and J_-, respectively. The a_+ and a_- are sums of all resonance amplitudes of states having J_+ and J_-, respectively, and the g_+ and g_- are statistical weight factors corresponding to the J.

It is possible that the apparent size of the nucleus (i.e., R, the range of the infinitely repulsive potential) may depend upon the incoming neutron spin orientation. This would yield an R_+ and an R_- and require σ_s to be given by

$$\sigma_s/4\pi=g_+|R_++a_+|^2+g_-|R_-+a_-|^2.$$

Similarly, the incoherent (spin effect) thermal scattering cross section, σ_{inc}, would be given by

$$\sigma_{\text{inc}}/4\pi=g_+g_-|R_++a_+-R_--a_-|^2.$$

For isotopes in which there are no significant resonance contributions to the thermal scattering cross section, this reduces to

$$\sigma_{\text{inc}}/4\pi=g_+g_-(R_+-R_-)^2.$$

It is an observed fact that materials having no significant low energy neutron resonance scattering also have no incoherent scattering.[1] From this it immediately follows that the *off-resonance* radii, R_+ and R_-, are equal. However, such may not always be the case for materials having low energy neutron resonances. In the cases of vanadium[2] and manganese[3] it is possible to fit observed cross-section data using only a single nuclear radius. In the cases of sodium[4] and cobalt[5] a single radius fit does not seem possible. This implies that the radius appearing in the resonance formula may not, in general, be given by the $A^{\frac{1}{3}}$ rule or even be given uniquely; rather, it should be treated as a double parameter.

[1] Compilation by E. O. Wollan, unpublished. (See odd Z or odd N—e.g. Be, F, Al, Nb, Bi.)
[2] M. Hamermesh and C. O. Muehlhause, Phys. Rev. **78**, 175 (1950).
[3] Harris, Hibdon, and Muehlhause (to be published).
[4] Hibdon, Muehlhause, Selove, and Woolf, Phys. Rev. **77**, 730 (1950).
[5] Harris, Muehlhause, and Thomas, Phys. Rev. **79**, 11 (1950).

The Generation of Vacancies by Dislocations

FREDERICK SEITZ
University of Illinois, Urbana, Illinois
July 19, 1950

SEVERAL processes have been observed which require the generation of large numbers of vacancies within crystals: (1) The darkening of the alkali halides by x-rays and cathode rays.[1] Apparently somewhat over 10^{18} and probably as many as 10^{19} F-centers per cc can be generated in this way; (2) Gyulai and Stepanow have observed[2] an increase in ionic conductivity during plastic flow in NaCl that implies the generation of the order of 10^{18} vacancies per cc; (3) The Kirkendall effect[3] (relative motion of markers during diffusion experiments by a process presumably related to plastic flow) in metals implies the generation of at least 10^{20} and probably as high as 10^{22} vacancies per cc within a small volume. The Kirkendall effect has not yet been observed in single crystals, so the generation of vacancies may occur at grain boundaries; however, it seems reasonable at this stage, to assume that it is a relatively universal phenomena and will be found in diffusion within well-made single crystals. Both process (1) and (2), particularly the latter, seem to require the generation of far more vacancies than can be explained by assuming the only source is the group of vacancies frozen-in on cooling from the melting point,[4] unless the dislocations formed by these can act as catalysts for very extensive generation.

Apparently it is necessary to determine a mechanism by which a very large number of vacancies can be generated within a small volume of a crystal, for example within a volume of the order of mosaic dimensions (10^{-13} cm^3). A clue concerning such a mechanism is given by the following consideration. Suppose the crystal contains a small "patch" or disk of interstitial atoms which are arranged as part of an extra interstitial plane, perhaps five or so atoms in linear dimensions, which is in registry with its neighbors. This disk constitutes a small general dislocation ring having a finite projection on a plane normal to its Burgers vector. It can grow by taking atoms from the neighboring completed planes, between which it is sandwiched, thereby forming vacancies. Given one such disk more or less, on each plane, in the volume under consideration, an almost unlimited number of vacancies could be generated, assuming the temperature is adequate to furnish the activation energy which should be nearly the same as that required to form a vacancy near the surface. Isolated disks of this type cannot be expected to occur very generally in a crystal in which vacancies are the predominant lattice defect. Even if a relatively small number of Frenkel defects were produced at elevated temperatures, the vacancies which are formed in greater numbers would annihilate the interstitial atoms during cooling. On the other hand, a dislocation which runs through a slip plane passing across the volume apparently can provide the equivalent of a large number of disks of interstitial atoms. This dislocation may, for example, be one of the type which promote crystal growth through Frank's mechanism,[5] in which its Burgers or screw character is of importance. In general a dislocation of this type will meander through the slip plane, changing its character from Burgers to Taylor-Orowan (edge) type and back again along its path. Each segment having Taylor-Orowan type may act as a source of vacancies. The generation of vacancies will cause the dislocation line to move out of the slip plane by growth of the "extra" plane. The line will loop around the edge of this plane. In other words, each kink in the dislocation line at which it possesses a strong component of Taylor-Orowan Character has the properties of a disk of interstitial atoms. Should a very large number of vacancies be required, as during a diffusion process in which the Kirkendall effect is prominent, there seems to be no reason why a large number of kinks of this type should not occur. For example, growth of the extra planes at the kinks initially present will have the effect of producing motion of the portions of the dislocation in the slip plane in a direction parallel to the extra planes (normal to the Burgers vector). Additional kinking can occur at points where the dislocation becomes stuck. Such sticking may occur at F-centers or V-centers, when these are being generated, or at regions of inhomogeneity during the diffusion process.

It also seems possible to employ the endless screw character of a Burgers dislocation to generate an endless spiral of interstitial planes from a single small disk of interstitial atoms which form a part of an interstitial plane that is in registry with its neighbors. The first time such a disk has grown around the dislocation line, the two ends which meet in a plane passing through the axis of the screw are separated by a plane of the screw, equal in thickness to the Burgers vector of the screw. There will be a tendency for

the two ends to glide toward one another, causing, in effect, a split of the intervening plane, each edge of the extra plane joining one-half of the split. This process can occur even if the Burgers vectors associated with the extra plane and with the screw dislocation are different. However, if the extra plane involves only a few atoms, an activation energy will be required to produce the split in the intervening plane. Should this not be supplied, the two ends may continue growth past the meeting point without joining the regular lattice, in which case a three-dimensional spiral extra plane can form. This spiral resembles somewhat the spiral surfaces employed by Frank[5] in his treatment of crystal growth, although the dislocation considered here is profoundly different in the sense that the layers of the spiral are separated by the planes of the original screw during the early state of formation, when the radius of a given arm of the spiral is of the order of a few atomic dimensions. Once the spiral has grown sufficiently in the direction normal to the axis of the initial Burgers dislocation, the planes will assume the normal characteristics of dislocations and can move in the direction of the Burgers vector associated with them in such a way as to establish a more nearly equilibrium configuration. The edges of the spiral extra plane, which constitutes the dislocation line, may be expected to spiral on the surface of a double "cone" formed by abutting the bases of two cones whose apexes point in opposite directions and whose common axis lies along the axis of the original Burgers dislocation. We shall call these dislocations *spiral prismatic dislocations* since they possess a strong component of what the writer[6] has termed prismatic character. The formation of a dislocation of this type, and its growth by the borrowing of atoms from neighboring planes, evidently can yield an almost unlimited supply of vacancies. It should be added that the initial interstitial disk from which the spiral dislocation can be generated may be replaced by an edge dislocation which lies in a plane cutting the initial Burgers dislocation obliquely and which grows in such a manner as to intersect the Burgers dislocation by addition of atoms to the extra plane associated with the edge dislocation.

[1] F. Seitz, Rev. Mod. Phys. **18**, 384 (1946); Estermann, Leivo, and Stern, Phys. Rev. **75**, 627 (1949); Casler, Pringsheim, and Yuster, J. Chem. Phys. **18**, 887 (1950); H. U. Harten, Zeits. f. Physik **126**, 619 (1949).
[2] Z. Gyulai and D. Hartly, Zeits. f. Physik **51**, 378 (1928); Z. Gyulai, Zeits. f. Physik **78**, 630 (1932); A. W. Stepanow, Zeits. f. Physik **81**, 560 (1933); also a coordinating paper by the writer to appear in the Physical Review.
[3] A. D. Smigelskas and E. O. Kirkendall, Trans. A. I. M. E. **171**, 130 (1947); L. S. Darken, Trans. A. I. M. E. **175**, 184 (1948); J. Bardeen, Phys. Rev. **76**, 1403 (1949); F. Seitz, Acta Crys. **3**, 335 (1950). The experimental work has been extended in a very important way by da Silva and Mehl (as yet unpublished work) which the writer has had the privilege of reading.
[4] F. Seitz, Phys. Rev. **79**, 890 (1950).
[5] F. C. Frank, discussion of the Faraday Society, No. 5 (1949), p. 48.
[6] F. Seitz, Phys. Rev. **79**, 723 (1950).

Spiral Prismatic Dislocations and the Origin of Slip Bands

FREDERICK SEITZ
University of Illinois, Urbana, Illinois
July 19, 1950

SPIRAL prismatic dislocations, closely related to those described in the previous letter, apparently can be formed by condensation of vacancies. For example, the vacancies present in metals and salts at the melting point may condense[1] along dislocations having a strong component of Burgers character and generate prismatic dislocations of this type. It is perhaps easiest to visualize the process of formation by assuming that the vacancies first condense along a short length of the dislocation, perhaps because of a component of edge character which is mixed with the Burgers character, and then condense in the direction of planes normal to the axis of the dislocation, dissolving away neighboring planes of the spiralling lattice. It should be possible in a metal, such as copper, to generate 10^{12} precipitates of this form per unit volume, each of which possesses of the order of 10^7 vacancies. In the energetically most stable form of a precipitate-dislocation of this type the vacancies would be contained in one plane corresponding to one revolution or less of the spiral. However, the spiral may have a number of revolutions if the vacancies condense during a period of cooling which endures for a sufficiently short time that the equilibrium arrangement is not achieved. Let us assume that the dislocation spirals n times on each half of the double "cone" on which it is distributed and that the radius of the base of the cone is r. We shall assume for simplicity that the thickness of each plane of the lattice is one atomic distance a and that the height of one of the cones is $x=na$. The number of vacancies associated with the cone is then approximately

$$N_v=2\pi(r/a)^2(x/a)/3. \tag{1}$$

n is related to the spacing d between two successive revolutions of the spiral in the direction normal to the axis of the spiral by the equation

$$d/a=r/n=(r/a)/(x/a). \tag{2}$$

Substituting in (1), we obtain

$$r/a=(3N_vd/2\pi a)^{\frac{1}{3}}. \tag{3}$$

If x is small compared with r, corresponding to the most stable limit of the configuration, the energy of the dislocation[2] is, in order of magnitude,

$$\mathrm{E}=\pi r^2E_0\theta f \tag{4}$$

in which $E_0=Ga/4\pi(1-\sigma)$, where G is the shear modulus and σ is Poisson's ratio, θ is $2x/r$ for the limit of interest to us in which x is small compared with r and f is a slowly varying function of x/r, which we shall assume is of the order of unity. The energy per vacancy in the spiral dislocation is

$$\epsilon=(3/4\pi)[G/n_0(1-\sigma)](a/r)f \tag{5}$$

which, with the use of (3), may be expressed in the form

$$\epsilon=(3/4\pi)[G/n_0(1-\sigma)](2\pi a/3N_vd)^{\frac{1}{3}}f. \tag{6}$$

In these equations, n_0 is the number of atoms per unit volume, so that $G/n_0(1-\sigma)$ is an energy of the order of 10 ev for a typical material. If N_v is 10^7 and r takes its maximum value of 1.7×10^3a, corresponding to a single revolution of the spiral, (5) is of the order of 5×10^{-3} ev or about 100 cal./mole of precipitated vacancies. On the other hand, if d/a is 100, this is multiplied by about 1.8. Hence there is no radical difference in the energy per vacancy in a spiral having one revolution and one having eight revolutions. In other words, spiral prismatic dislocations, formed by precipitation of vacancies, which contain of the order of 10^7 vacancies have substantial probability of occurring in a form in which the spacing between neighboring arms in the direction normal to the axis of the cone is of the order of 200A.

Spiral dislocations of this type have the following two important characteristic properties:

(1) They may contribute to the mosaic structure of the crystal. The distortion introduced into the lattice by such a spiral is the same as if the volume of the double cone on which the spiral winds were removed from the lattice, the material were drawn together and the surface rejoined. This process would cause the portions of the crystal on either side of the cone to be rotated through an angle θ, relative to one another. θ is of the order of 10^{-2} radians if d is $100a$. Hence the contribution to the mosaic structure is by no means negligible. It may be noted that each spiral of this type has many of the characteristics required of a mosaic boundary. For example, it should be relatively stable when the crystal is annealed since the energy of instability is relatively small.

Presumably neighboring spirals will interact with one another as a result of the elastic deformation each spiral induces in the medium. The writer visualizes the spirals as forming a primitive type of lattice structure in which the distance between spirals is comparable to the linear dimension r of a given spiral.

(2) The spirals, when used in connection with Frank and Read's "static" mechanism[3] for the multiplication of dislocations,

provide an explanation of the regularity of slip bands observed in aluminum by Heidenreich and Shockley.[4] In the course of a single revolution of one arm of the spiral, the spiral becomes tangent to the potential slip plane or planes which may operate with use of the Burgers vector associated with the spiral. A given slip plane occupies this tangent position at least twice in one revolution. Regions of tangency of this type satisfy in an almost ideal manner the conditions required for multiplication. It is true that the length of the spiral which lies in the slip plane is small if the spiral is smooth. On the other hand, the spiral becomes elongated in the direction of the Burgers vector by a slip mechanism when a shearing stress which has a component in this direction is present. Opposite ends of the spiral move in opposite directions. Since vacancies become redistributed during this motion as a result of local heating and the expansion and interaction of portions which lie in the slip planes, there appears to be little to inhibit multiplication in the neighborhood of the tangent planes. There are $2n$ tangent planes spaced a distance d apart if the double spiral possesses n revolutions in total, and if the spacing between neighboring arms is d.

Multiplication need not be restricted to the tangent planes if the shearing stress field becomes sufficiently large; however, simple considerations show that there is much less interference in these planes during early stages of plastic flow so that they possess a natural preference. Considerations of this type also suggest that thermal agitation will greatly aid in the multiplication process. It would be very interesting to know if slip bands are formed as readily in metals deformed plastically at very low temperatures as in those deformed at room temperature or above. Multiplication is by no means[5] necessary for plastic flow if there are as many as 10^{12} dislocations rings in a unit volume.

[2] F. Seitz, Phys. Rev. **79**, 890 (1950).
[3] The notation employed here is essentially that of W. T. Read and W. Shockley, Phys. Rev. **78**, 275 (1950).
[3] F. C. Frank and W. T. Read, Phys. Rev. **79**, 722 (1950).
[4] R. D. Heidenreich and W. Shockley, "Report of Bristol Conference on The Strength of Solids" (Phys. Soc. London, 1948).
[5] See for example the discussion by the writer in "Report of Pittsburgh Symposium on Plastic Deformation in Crystalline Solids" (Naval Research Laboratory, 1950).

The 2.7μ-Bands of Carbon Dioxide

ROBERT JONES AND ELY E. BELL
Mendenhall Laboratory of Physics, Ohio State University, Columbus, Ohio
July 20, 1950

THE $\nu_1+\nu_3$ and $2\nu_2^0+\nu_3$ bands of carbon dioxide have not been well measured because they lie in the region of the 2.7μ-water vapor band. By the use of the vacuum grating instrument we have been able to record the carbon dioxide bands with no interference from water vapor. A cell of 28 cm length with 10.5 cm of Hg pressure was used in the measurements. A boat of phosphorus pentoxide in the cell removed any trace of water vapor left in the gas sample. The bands were well resolved with a slit width of 0.6 cm^{-1} by a 7500 lines-per-inch replica echelette grating.

The low frequency side of the $2\nu_2^0+\nu_3$ band was disturbed by what is believed to be a $C^{13}O_2^{16}$ band. The center of this isotope band has not been located.

By use of combination relations applied to the rotational lines, we have obtained the following results:

Band	ν cm^{-1}	$B''=B_{000}$ cm^{-1}	$B'-B''$ cm^{-1}
$\nu_1+\nu_3$	3715.70	0.3893	−0.0031
$2\nu_2^0+\nu_3$	3613.68	0.3896	−0.0028

The value of B_{000} is in good agreement with other measurements. The values of ν are in good agreement with the values calculated by Adel and Dennison, as adjusted by Herzberg.[1]

[1] G. Herzberg, *Infrared and Raman Spectra* (D. Van Nostrand and Company, Inc., New York, 1945), page 274.

Cross-over Transitions in Ir^{194}, Ag^{110}, Cs^{134}

RICHARD WILSON
Clarendon Laboratory, Oxford, England*
July 17, 1950

ACCORDING to the accepted decay schemes[1–3] for these isotopes, cross-over transitions might be expected. A search has been made for these transitions using the photo-disintegration of beryllium and deuterium as threshold detectors for high energy γ-radiation. The photo-neutrons were detected by a Szilard-Chalmers reaction in ethyl iodide[4] under conditions in which the detection efficiency had been measured as a function of energy.[5]

Approximate estimates of the intensities have been made, using pile activation data to give the disintegration rate of the isotope; the accuracy of these is about 50 percent. The results are shown in Table I.

TABLE I. Cross-over transition data.

Isotope	Ir^{194}		Ag^{110}		Cs^{134}
Expected energy (Mev)	1.7	>2.2	2.21 or 1.8	2.3 or 2.9	1.96
Expected intensity (photons/disintegration)	3×10^{-6} or 10^{-3}	nil	—	—	10^{-5}
Observed intensity (photons/disintegration)	1.4×10^{-3}	2×10^{-6}	3×10^{-4}	$<10^{-4}$	$<10^{-4}$

Ir^{194}—The 0.3 Mev and the 1.4 Mev γ-rays are assumed to be electric quadrupole in cascade; the expected intensities are calculated for the two alternatives of the 1.4 Mev or the 0.3 Mev γ-ray being emitted first. The assumption is made that the cross-over is 16 pole. The results suggest that the 0.3 Mev γ-ray is emitted first. The γ-ray which disintegrates deuterium does not fit the decay scheme; the intensity is 100 times too great to be attributed to bremsstrahlung from the high energy β-ray.

Cs^{134}—The upper limit to the intensity is in good agreement with the results of Fluharty,[6] which had escaped notice until the experiment had been completed.

Ag^{110}—The spectrum is very complex and the only definite conclusion is that an "intermediate" cross-over occurs with measurable intensity.

The author wishes to thank Dr. P. F. D. Shaw for his advice on the Szilard-Chalmers reaction, the Isotope Division, AERE Harwell, for the speedy supply of the isotopes, and Mr. G. R. Bishop and Dr. H. Halban for helpful discussions.

* Now at the University of Rochester, Rochester, New York.
[1] J. Mattauch and A. Flammersfeld, *Isotopenbericht* (1949).
[2] K. Siegbahn, Phys. Rev. **75**, 1277 (1949).
[3] L. G. Elliott and R. G. Bell, Phys. Rev. **72**, 979 (1947).
[4] P. F. D. Shaw and C. H. Collie, J. Chem. Soc. **264**, 1217 (1949).
[5] R. W. Parsons (private communication).
[6] R. G. Fluharty and M. Deutsch, Phys. Rev. **76**, 182 (1949).

On Time-Independent Integrals of Motion of the One-Body Problem in Dirac Theory

A. W. SÁENZ
Applied Mathematics Branch, Mechanics Division, Naval Research Laboratory, Washington, D. C.
June 28, 1950

THE purpose of this note is to point out two results concerning time-independent integrals of motion in Dirac's theory of the electron, which to the author's best knowledge have not been stated heretofore in the literature. For the proofs of the theorems given below the reader is referred to the author's thesis.[1]

In what follows, we will be concerned with dynamical operators which commute with the Hamiltonian[2]

$$H=c\alpha^k\left(p_k+\frac{e}{c}\Phi_k\right)+mc^2\alpha^4-e\Phi_0 \quad (k=1,2,3) \tag{1}$$

where the Φ_k are the components of the vector potential, Φ_0 is the scalar potential α^5 has its usual significance, and $\alpha^4=\beta$. The results are summarized below.

Theorem I.—Any integral of motion of (1), which is a polynomial in the momenta p_k, must contain at least one element of the biquaternion group[3]

$$I;\quad \alpha^4;\quad \alpha^2\alpha^3,\quad \alpha^3\alpha^1,\quad \alpha^1\alpha^2;\quad \alpha^2\alpha^3\alpha_1{}^4\alpha^3\alpha^1\alpha_1{}^4\alpha^1\alpha^2\alpha^4 \qquad (2)$$

where I is the identity of the group.

This result suggests the existence of a close relation between the sixteen-group of Dirac[3] and the structure of integrals of motion of the system defined by (1) in terms of the α^μ, and indicates the desirability of pursuing such studies more systematically.

Theorem II.—In the case when $\Phi_k=0$ and $\Phi_0=\Phi_0(r)$, no integrals of motion of first degree in p_k, which are linearly independent of those integrals of first degree already known,[4] are possible.

This theorem implies that no essentially new integrals linear in the momenta exist in the Dirac one-body problem with spherically symmetric scalar potential.

I wish to thank Professor O. Laporte for stimulating discussions during the course of this work, and in particular for pointing out to me the connection between the method used in proving Theorem II and a corresponding calculation in a problem in classical point dynamics.[5]

[1] A. W. Sáenz, thesis, University of Michigan, 1949, unpublished.
[2] Our notation is essentially that of W. Pauli, *Handbuch der Physik* (Springer, Berlin, 1933), second edition, 24, Part I.
[3] A. Sommerfeld, *Atombau und Spektrallinien* (Braunschweig, Vieweg, 1939), Chapter 4, Section 5.
[4] These are the well-known set consisting of the Hamiltonian, the three components of the total angular momentum, and the scalar integral K. See, for example, V. Rojansky, *Introductory Quantum Mechanics* (Prentice Hall, Inc., New York, 1942), chapter 14.
[5] E. T. Whittaker, *Analytical Dynamics* (Cambridge University Press, London, 1937), chapter 12, Section 152.

Superconductivity and Debye Modes*

WILLIAM BAND
Department of Physics, State College of Washington, Pullman, Washington
July 25, 1950

IT can be shown that the coherence-incoherence transition temperature T_c among the phase domains of the Debye modes of a single crystal[1] is such that

$$kT_c=\Delta E\Delta\phi/2\pi \qquad (1)$$

where ΔE is the total mean energy of misfit on the surface of a single domain, and $\Delta\phi$ is the phase tolerance, or the greatest difference in phase between two adjacent domains still counted as coherent. If ΔE is regarded as an uncertainty in the energy of a domain, $\Delta\phi$ as due to the conjugate uncertainty in time, then Eq. (1) leads to

$$kT_c=\hbar\nu_0 \qquad (2)$$

where ν_0 is the lowest frequency of one domain. If the average domain contains about 10^8 atoms, this gives the correct order of magnitude for T_c.

Two crystals with identical structure and lattice constant and the same domain size, differing only in their isotopic mass, will have transition temperatures proportional to the velocity of sound and therefore inversely proportional to the square root of their density.[2]

The specific heat hump at a coherence-incoherence transition is due to the energy of misfit between the surfaces of the domains, and matches the observed order of magnitude,[3] 4.10^4 erg/mole, if each atom in a domain surface can contribute 3.10^{-17} erg to the total. This demands an anomalous displacement due to misfit of the order 10^{-11} cm, while (1) yields a phase tolerance of 10^{-4} radian. This in turn requires an amplitude about 10^{-7} cm and therefore a zero point energy of 10^9 erg/g, agreeing with a Debye temperature near 100°K.

It is emphasized that the existence of a phase coherence transition in a crystal does not necessarily produce superconductivity but merely provides necessary conditions under which it may occur. It is conceivable that there may exist a phase tolerance for electron scattering at the domain surfaces which may be more stringent than that for absence of energy of misfit between domains. The anomalous specific heat would still appear at a transition temperature but without superconductivity; as, for example, with Na at 7°K and Be at 11°K.[4] Clearly Eq. (1) would lead to a relatively high value of T_c but the same specific heat anomaly as in superconductivity transitions.

In a recent letter Bardeen[5] has considered possible interaction between electron states and coherent groups of Debye waves, as a means of explaining the diamagnetism of closed superconductor circuits. This is not inconsistent with the present suggestions which are necessary to explain the disappearance of residual resistance in large open circuit superconductors.

* The work was supported by the ONR.
[1] W. Band, Phys. Rev. 79, 739 (1950).
[2] Serin, Reynolds, and Nesbitt, Phys. Rev. 78, 813 (1950).
[3] D. Shoenberg, *Superconductivity* (Cambridge University Press, London, 1938).
[4] G. L. Pickard and F. E. Simon, Proc. Phys. Soc. London 61, 1 (1948).
[5] J. Bardeen, Phys. Rev. 79, 167 (1950).

Erratum: Range-Energy Relations for Protons in Substances Containing C, H, O, A, and Xe

[Phys. Rev. 73, 207 (1948)]
J. O. HIRSCHFELDER* AND J. L. MAGEE**
Los Alamos Scientific Laboratory, Los Alamos, New Mexico

DR. Robert Platzman has called the authors' attention to the following errors:

In Eq. (22), for $\log_e\eta_K$ substitute $\log_e(3.63\eta_K)$.

In Eq. (25b), for the constant 22.496, substitute 23.118.

In the definition following Eq. (25c), for $\eta_L=E/0.09036$ substitute $\eta_L=E/0.08669$.

The values of B_0 in Table VI for $E\leq 1.4$ Mev should be replaced by the following:

E Mev	B_0	E Mev	B_0	E Mev	B_0	E Mev	B_0
0.005	0.0684	0.04	1.633	0.30	13.809	0.90	22.427
0.010	0.171	0.05	2.421	0.40	16.104	1.00	23.329
0.015	0.311	0.10	5.922	0.50	17.815	1.10	24.053
0.02	0.484	0.15	8.645	0.60	19.187	1.20	24.793
0.03	0.983	0.20	10.719	0.70	20.448	1.30	25.443
				0.80	21.490	1.40	26.095

The ranges in glycerol tristearate, R' of Table VI should be 0.2 percent smaller than the values listed for $E\leq 1.4$ Mev and 0.007 smaller for $E\geq 1.4$ Mev.

* Now at University of Wisconsin, Madison, Wisconsin.
** Now at University of Notre Dame, Notre Dame, Indiana.

Erratum: The Bohr Formula for the Rydberg Constant

[Phys. Rev. 79, 193 (1950)]
RAYMOND T. BIRGE
University of California, Berkeley, California

THE following corrections should be made.

(a) line 12 of column 1, p. 194, should read
". . . to an expression, Eq. (12), which is believed . . ."
(b) line 1 of column 2, p. 194, should read
"Combining Eqs. (6, 7, 8) one gets . . ."

(c) line 5 of column 2, p. 194, should read
". . . to transform Eq. (5) into . . ."
(d) line 7 of column 2, p. 194, should read
"with e'/m given by Eq. (8)."
(e) line 14 of column 2, p. 194, omit the word "hence" at the end of the line.
(f) the equation two lines below Eq. (12) is typographically ambiguous and should read

$$\frac{4c}{3}\frac{2I+1}{I}\left(\frac{m_r}{m}\right)^3\left(\frac{\mu_e}{\mu_0}\right)=(15.98053\pm0.00033)\times10^{10}\text{ cm/sec.}$$

Extensive Air Showers and Total Cosmic Radiation

G. Cocconi
Cornell University, Ithaca, New York
July 17, 1950

THE experimental evidence that in extensive air showers electrons, photons, mesons, and nucleons are present; i.e., all kinds of particles which have been found in the cosmic radiation present in the lower atmosphere, leads one to support the hypothesis that the event called "extensive air shower," is actually not a special event, but rather the *unique process* in which the cosmic radiation present in the lower atmosphere is created.[1] Such an assumption is equivalent to saying that any particle observed in the lower atmosphere is a part of an extensive shower.

This is only apparently in contradiction with the fact that the cosmic radiation observed with ordinary detectors appears to consist of incoherent particles. In fact, two cases are possible:

(a) The observed particle is the only survivor of the extensive shower, at the level where it is detected. In this case, its associated shower particles can be detected only if detectors are located at a higher level, in the direction of the axis of the shower. No experiment of this kind has been performed so far.

(b) The observed particle arrives at the level where it is detected, accompanied by other particles. In this case the other particles can be efficiently detected only if detectors are used whose area S is larger than $\sim1/\Delta$, Δ being the density of the shower in the region where the detectors are located. No apparatus has been so far designed, capable of recording efficiently showers with local densities smaller than about 2 particles per m².

We shall try to estimate what fractions of the various components of the total radiation in the lower atmosphere have been actually observed as particles coherent with other particles, i.e., belonging to extensive showers. Our estimate refers to the altitude of Echo Lake, Colorado (3260 m, average atmos. pressure 708 g/cm²).

At this altitude:

(1) The intensity of the total electronic component of the cosmic radiation coming from the upper hemisphere,[2] is 2.2×10^{-2} cm^{-2} sec.$^{-1}$. This figure includes 1.4×10^{-2} cm^{-2} sec.$^{-1}$ electrons produced by μ-meson decay and knock-on processes. The difference $e=(2.2-1.4)\times10^{-2}=8\times10^{-3}$ cm^{-2} sec.$^{-1}$ is the intensity to be compared with the figure which will be deduced from the data on extensive showers.

(2) The intensity of the μ-meson component[2] is $\mu=2.5\times10^{-2}$ cm^{-2} sec.$^{-1}$.

(3) The data available on the intensity of the N-component are crude estimates made by various authors on the basis of the observed frequencies of nuclear disintegrations. Notwithstanding the large uncertainties involved in the calculations, the results concerning stars and neutron-producing radiation[3] agree in indicating that the intensity of the N-component is about 20 percent of the total ionizing radiation, at the altitude we are considering. This gives an intensity $N=1\times10^{-2}$ cm^{-2} sec.$^{-1}$.

(4) The frequency of the showers for which the density is larger than Δ is given by

$$F(\Delta)=K\Delta^{-\gamma}$$

where K and γ vary with Δ slowly enough to be considered as constants over a rather large range of densities.[4]

The number e_S of electrons belonging to air showers falling on the surface s in the unit time is then:

$$e_S=\int_{\Delta_{\min}}^{\infty}\frac{dF}{d\Delta}(1-e^{-s\Delta})d\Delta$$

$$=\frac{sK}{\Delta_{\min}{}^{(\gamma-1)}}\left\{1+\frac{1}{\gamma-1}+\frac{(s\Delta_{\min})^{\gamma-1}}{(\gamma-1)(\gamma-2)}\Gamma(3-\gamma)\right\}. \quad (1)$$

This formula shows that the main contribution to e_S comes from showers with densities near $\Delta_{\min}$, hence it justifies the assumption that K and γ are constants, provided that they satisfy the experimental spectrum near $\Delta_{\min}$. As discussed previously, the value of $\Delta_{\min}$ depends on the surface of the apparatus used to detect the showers. In reference 4, the maximum counter surface used was 0.5 m², which corresponds to an average density of about 5 particles per m². As a contribution to this average density comes from showers whose density is about 10 times smaller, the experimental results show that a power spectrum holds down to $\Delta_{\min}=0.5$ m^{-2} with $K=1.29$ and $\gamma=1.25$ (Δ in m^{-2}, time in sec.). With $s=1$ cm$^2=10^{-4}$ m², from formula (1), one has

$$e_S=7.5\times10^{-4}\text{ cm}^{-2}\text{ sec.}^{-1}.$$

(5) Using the result[5] that in the extensive showers the ratio

$$R_\mu=\frac{\mu\text{-meson density}}{\text{electron density}}=\sim2\times10^{-2},$$

we obtain

$$\mu_S=e_S\times R_\mu=1.5\times10^{-5}\text{ cm}^{-2}\text{ sec.}^{-1}.$$

(6) Using the result that[6]

$$R_N=\frac{N\text{-component density}}{\text{electron density}}=\sim1\times10^{-2},$$

we obtain

$$N_S=e_S\times R_N=7.5\times10^{-6}\text{ cm}^{-2}\text{ sec.}^{-1}.$$

The ratios between these figures and the figures previously given for the various components of the total cosmic radiation, are

$$e_S/e=1/11,\quad \mu_S/\mu=1/1600\quad\text{and}\quad N_S/N=1/1300.$$

The ratio 1:11 found for electrons shows that our estimate accounts for about 10 percent of the electrons in the soft component (excluding the electrons due to decay and knock-on processes of μ-mesons). As pointed out before, our estimate does not include the electrons belonging to showers whose density is smaller than 0.5 cm^{-2}, which are certainly very numerous. In fact, such low electron densities must occur very frequently, since they are produced: (a) by showers of rather small energies which are almost exhausted at the level of observation; (b) by energetic showers whose core strikes very far from the surface s considered. These last events are not very frequent, but the enormous surface they cover makes their probability of being recorded very high. In fact, except for the gradual decrease of γ in the density spectrum for small values of Δ, the integral in Eq. (1) would diverge.

With these arguments in mind, we feel justified in concluding that it is not unlikely that all electrons which are not secondaries of μ-mesons present in the cosmic radiation, are accounted for by the electrons belonging to extensive air showers.

The situation is not necessarily different for μ-mesons and for the particles of the N-component, notwithstanding the fact that our estimates cover only very small fractions of the corresponding total intensities in the cosmic radiation. In fact, one must keep in mind that our estimates refer only to those particles which arrived at the surface s accompanied by ionizing particles with densities larger than 0.5 m^{-2}. Now, since in air the *absorption* lengths of the μ-mesons and of the N-component are about 2000 g/cm² and 160 g/cm², respectively, while the absorption length of low energy electrons is about 40 g/cm², one must expect the

mesons and the nucleons to survive longer than the electrons, hence to arrive in the lower atmosphere accompanied by ionizing particles with extremely low densities. On the other hand, evidence has been found[7] that an appreciable fraction of the penetrating showers do not contain any electro-magnetic radiation. If this kind of process is possible at high energies, part of the penetrating component could be created without the accompanying electrons of the extensive showers.

Support for the hypothesis that all particles observed in the lower atmosphere are generated in extensive showers, is provided by the facts that, whenever three or more coherent penetrating particles coming from the air have been recorded, an extensive shower accompanying them has been recorded too; and that the probability of recording an extensive shower accompanying the N-component increases when the energy of the N-component increases.[8]

[1] We disregard here the tail of primary radiation which may cross the atmosphere without interacting with any nucleus of the air.
[2] B. Rossi, Rev. Mod. Phys. **20**, 537 (1948).
[3] George and Jason, Proc. Phys. Soc. London **A62**, 243 (1949). V. Cocconi Tongiorgi, Phys. Rev. **76**, 517 (1949).
[4] Cocconi, Cocconi-Tongiorgi, and Greisen, Phys. Rev. **75**, 1058 (1949).
[5] Cocconi, Cocconi-Tongiorgi, and Greisen, Phys. Rev. **76**, 1020 (1949).
[6] Cocconi and Cocconi-Tongiorgi, Phys. Rev. **79**, 730 (1950).
[7] See, e.g. W. B. Fretter, Phys. Rev. **76**, 511 (1949).
[8] Greisen, Walker, and Walker, Phys. Rev. (to be published).

Disintegration Scheme of Scandium [46]

B. N. Sorensen,* B. M. Dale, and J. D. Kurbatov
Department of Physics, Ohio State University, Columbus, Ohio
July 21, 1950

THE disintegration of the ground state of Sc^{46} was described previously as a complex beta-decay followed by emission of two successive gamma-rays. The predominant disintegration was found to be beta-emission of 0.36 Mev. The relative abundance of a second beta-emission of 1.49 Mev was determined to be six percent and later this was reduced to two percent.[1] In subsequent work with a magnetic lens spectrometer and coincidence counter these results on the beta-disintegration of 1.49 Mev were not confirmed.[2-4]

In recent work the successive emission of gamma-quanta of 1.12 Mev and 0.89 Mev by excited states of Ti^{46} was designated as electric quadruples with no change in parity.[5] Consequently additional information on the 1.49-Mev beta-decay would be of value in assignment of the angular momentum of Sc^{46}.

For the present work scandium oxide was activated by neutrons at the Oak Ridge National Laboratory. This was chemically purified and first studied with G-M coincidence counters. The arrangement of the coincidence counters allowed the use of G-M tubes of different potentials with resolving time of about 10^{-7} sec.

From determinations of beta-gamma- and gamma-gamma-coincidences the following results were obtained. The end point at 110 mg cm^{-2} of Al for the emitted beta-radiation in coincidence with gamma was in agreement with the previous value known for the beta-disintegration of 0.36 Mev. The beta-gamma-coincidences per beta recorded and gamma-gamma-coincidences per gamma recorded gave 5.01×10^{-3} and 2.50×10^{-3} values respectively. These correspond to a simple beta-spectrum followed by two gamma-rays in cascade with an upper limit for a second beta-disintegration of 0.2 percent.

With the aim of improving the upper limit of the second beta-disintegration Sc^{46} was studied in a cloud chamber. The sample was placed on zapon film and mounted in the center of the chamber. Eleven thousand tracks of electrons of energies less than 0.36 Mev were obtained in a magnetic field. Only twelve tracks were found having energies higher than 0.36 Mev. Of these ten electrons were in the range between 0.65 Mev and 0.9 Mev. With the assumption that some electrons in this energy range are due to scattering and to internal conversion of the gamma-rays emitted the upper limit for the beta-decay of 1.49 Mev in Sc^{46} can be estimated as less than 0.05 percent of the 0.36-Mev beta-disintegration.

It is a pleasure to acknowledge the financial assistance for construction of instruments received from The Development Fund of Ohio State University. Aid from the Graduate School of Ohio State University is gratefully appreciated by the authors.

* Present address of Lt. Colonel B. N. Sorensen: U. S. Air Force, Washington, D. C.
[1] C. L. Peacock and R. G. Wilkinson, Phys. Rev. **72**, 251 (1947); **74**, 297 (1948).
[2] A. E. Miller and M. Deutsch, Phys. Rev. **72**, 527 (1947).
[3] I. Feister and L. S. Curtiss, J. Research Nat. Bur. Stand. **38**, 411 (1947).
[4] C. E. Mandeville and M. V. Scherb, Phys. Rev. **73**, 141 (1948).
[5] F. Metzger and M. Deutsch, Phys. Rev. **78**, 551 (1950), and E. L. Brady and M. Deutsch, Phys. Rev. **78**, 558 (1950).

The Microwave Spectrum of BrCl

D. F. Smith, M. Tidwell, D. V. P. Williams
Carbide and Carbon Chemicals Division, K-25 Plant, Oak Ridge, Tennessee*
July 24, 1950

BY mixing Br_2 and Cl_2, an equilibrium is established between these two halides and BrCl. With equal amounts of Br_2 and Cl_2 at room temperature, a mixture containing roughly 60 percent BrCl is obtained rapidly, but because of the speed of reaction this BrCl is not separated readily.[1] An unseparated mixture has been employed to observe the transitions corresponding to the $J=0\rightarrow1$ rotational spectrum of BrCl in the region of 9000 Mc/sec.

Since there are two isotopes for Br and Cl, there are four isotopic species of BrCl. All of the nuclei have spins of $\frac{3}{2}$ and exhibit appreciable quadrupole coupling. In all, some 29 lines have been observed and their frequencies measured. Two of these lines correspond to the two strongest transitions of the molecules in the first excited vibrational state.

All of these lines have been identified, and the parameters of the molecule obtained using the method of Bardeen and Townes[2] for the first-order quadrupole coupling and for the second-order quadrupole coupling due to the bromine,[3] the latter being of the form $(eqQ\mathrm{Br})^2/B$. Second-order coupling terms of the form $(eqQ\mathrm{Cl})(eqQ\mathrm{Br})/B$ and $(eqQ\mathrm{Cl})^2B$ have not been included. The precision of the measurements does not justify introducing magnetic coupling terms of the form $c(\mathbf{I}\cdot\mathbf{J})$. In Table I the calculated values of the transition frequencies using the parameters given in Table II, are compared with the observed frequencies, and the differences are given. The designations are those of the final $J=1$ state. The average deviation of 140 kc/sec. is to be compared with the average probable error of the individual measurements of 110 kc/sec. For the $F_1=\frac{1}{2}$, $F=2$ transitions, the deviations are all anomalously large, but the manner of

Table I. Frequencies of BrCl transitions in Mc/sec.

Designation F_1	F	$Br^{79}Cl^{35}$ Observed frequency	$Br^{79}Cl^{35}$ Computed frequency	Dev.	$Br^{81}Cl^{35}$ Observed frequency	$Br^{81}Cl^{35}$ Computed frequency	Dev.
3/2	2	9307.96	9307.97	0.01	9209.57	9209.51	0.06
3/2	3	9291.61	9291.50	0.11	9193.26	9193.16	0.10
5/2	1	9088.61	9088.32	0.29	9026.17	9026.21	0.04
5/2	4	9080.73	9080.71	0.02	9018.40	9018.50	0.10
5/2	2	9074.91	9074.78	0.13	9012.97	9012.83	0.14
5/2	3	9063.77	9063.91	0.14	9001.44	9001.63	0.19
1/2	2	8899.50	8899.87	0.37	8865.66	8865.26	0.40
5/2	$4_F=1$	9034.14	9034.27	0.14	8972.41	8972.50	0.09
		$Br^{79}Cl^{37}$			$Br^{81}Cl^{37}$		
3/2	2	8964.19	8964.18	0.01	—	8865.82	—
3/2	3	8951.38	8951.36	0.02	8852.93	8852.97	0.04
5/2	1	8745.17	8745.20	0.03	8683.06	8682.72	0.34
5/2	4	8738.47	8738.71	0.24	8676.37	8676.37	0
5/2	2	8733.84	8733.83	0.01	8671.87	8671.66	0.21
5/2	3	8725.49	8725.40	0.09	8663.40	8663.22	0.18
1/2	2	8559.58	8559.15	0.43	8525.53	8626.03	0.50

TABLE II. Parameters derived from the spectra.

	B_e	α
$Br^{79}Cl^{35}$	4570.92 ±0.04 Mc/sec.	23.22 ±0.03 Mc/sec.
$Br^{81}Cl^{35}$	4536.14 ±0.04	22.95 ±0.03
$Br^{79}Cl^{37}$	4499.84 ±0.04	21.94 ±0.03
$Br^{81}Cl^{37}$	4365.01 ±0.04	21.67 ±0.03
	$eqQ(Br^{79}) = +876.8 \pm 0.9$ Mc/sec.	
	$eqQ(Br^{81}) = +732.9 \pm 0.5$	
	$eqQ(Cl^{35}) = -103.6 \pm 0.1_5$	
	$eqQ(Cl^{37}) = -\ 81.1_4 \pm 0.1_5$	
	$r_e = 2.138(10)^{-8}$ cm	
	$\mu = 0.57 \pm 0.02$ Debye units	

variation from one isotopic species to another suggests that these are random experimental errors.

The value of the dipole moment has not been obtained by exact computation but has been estimated on the assumption that, neglecting quadrupole effects, the dipole moment lies between that obtained from the largest and the smallest observed Stark coefficients, and that the best value is given by the average of the observed Stark coefficients.

The values of the vibrational stretching coefficient for the Cl^{37} isotopic species have been obtained from the known variation of α with the $\frac{3}{2}$ power of the reduced mass, and used to obtain the equilibrium rotational constants. These lead to two semi-independent values for the chlorine mass ratio. The ratio $m(Cl^{35})/m(Cl^{37})$ is 0.945987±0.000008 for the $Br^{79}Cl^{35}$, $Br^{79}Cl^{37}$ pair, and 0.945986±0.000008 for the $Br^{81}Cl^{35}$, $Br^{81}Cl^{37}$ pair. This is to be compared with the value 0.945980±0.000005 obtained from[4] ICl and 0.945977_5±0.000004 obtained in[5] ClF, and as pointed out by Townes, Merritt, and Holden[4] to be contrasted with the mass spectrographic results 0.945944_8±0.000007.

The values for $m(Br^{79})/m(Br^{81})$, 0.975218±0.000028 for the $Br^{79}Cl^{35}/Br^{81}Cl^{35}$ pair and 0.975210±0.000028 for the $Br^{79}Cl^{37}$, $Br^{81}Cl^{37}$ pair are considerably lower than the mass spectrographic values[6] of 0.975316±0.000005. A recalculation of this ratio in[7] BrF yields 0.975168±0.000068.

The ratio of the chlorine quadrupole moment ratios $eqQ(Cl^{35})/eqQ(Cl^{37})$, 1.2768±0.004 is in better agreement with the ratio obtained from measurements of the moments in atomic beams $1.279 \pm 0.0026_5$ than was found[5] for ClF, 1.2704±0.004. The ratio for the bromine quadrupole coupling appears to be in excellent agreement with that obtained in other compounds. Professor B. P. Dailey, in private conversation, has pointed out that the magnitudes of the coupling coefficients for chlorines are considerably larger than expected, and that to a lesser extent the bromine coupling coefficients are also large.

* This document is based on work performed for the AEC by Carbide and Carbon Chemicals Division, Union Carbide and Carbon Corporation, at Oak Ridge, Tennessee.

[1] H. G. Vesper and G. K. Rollefson, J. Am. Chem. Soc. **56**, 620 (1934).
[2] J. Bardeen and C. H. Townes, Phys. Rev. **73**, 97 (1948).
[3] J. Bardeen and C. H. Townes, Phys. Rev. **73**, 627, 1204 (1948).
[4] Townes, Merritt, and Wright, Phys. Rev. **73**, 1334 (1948).
[5] Gilbert, Roberts, and Griswold, Phys. Rev. **76**, 1723 (1949).
[6] R. Ogata, Phys. Rev. **75**, 200 (1949).
[7] Smith, Tidwell, and Williams, Phys. Rev. **77**, 420 (1950).

Transport Rates of the Liquid He II Film over Various Surfaces

H. A. BOORSE* AND J. G. DASH†
Pupin Physics Laboratories, Columbia University,‡ New York, New York
July 26, 1950

OUR recent letter[1] describing a new method for measuring transport rates of the He II film reported that the rate over copper was significantly higher than that over glass. Owing to the fact that the transport rate was found to be strongly dependent on surface treatment, numerical values were not given, it being felt that details might await the publication of a full report. While the letter was in press, however, Mendelssohn and White[2] reported measurements of the transport rate over nickel and platinum which demonstrated a dependence on substrate and surface treatment.

It seems worth while, therefore, to point out that we have found the effect to be quite general and that both metals and dielectrics show rates different from each other and from glass. In fact, of all of the substances which we have measured, glass shows the smallest rate at any given temperature, as is apparent from Table I below. In each experiment the rate over glass was measured for comparison purposes and to be sure that there was no significant contamination arising from gases solidified on the transfer surfaces.

TABLE I. Transport rate in cm³/cm-sec. ×10⁵.

	1.3°	1.5°	1.8°	2.0°
Pyrex glass	7.6	7.5	—	—
Lucite	14.4	16.6	11.5	—
Stainless steel	10.4	9.7	6.8	3.3
Lead	33.3	31.1	26.6	16.5
Cold-rolled steel	10.5	—	—	—
Machined copper	14.8	14.8	12.4	7.9
Polished copper	23.0	19.8	14.7	7.1
Etched copper	51.2	49.0	40.0	24.8
Etched copper, oxidized	26.0	24.8	20.4	13.7

It seemed of particular interest to determine whether or not the rate over a metal in the superconducting state was different from the normal state, the temperature being constant. The experiment was tried using lead, the normal state being achieved by the application of a sufficiently strong transverse magnetic field. While there appeared to be small systematic differences at various temperatures, further investigations (now under way) will be necessary to determine whether these are real. The same remarks apply to iron, transversely magnetized and in the non-magnetized state.

* Barnard College, Columbia University.
† AEC Pre-doctoral Fellow.
‡ Assisted by ONR, Research Corporation, and The Linde Air Products Company.
[1] H. A. Boorse and J. G. Dash, Phys. Rev. **79**, 734 (1950).
[2] K. Mendelssohn and G. K. White, Nature **166**, 27 (1950).

Displacement of Oxygen in $BaTiO_3$

EDWIN T. JAYNES
Palmer Physical Laboratory, Princeton University, Princeton, New Jersey
July 19, 1950

ATTEMPTS to explain the ferroelectric character of $BaTiO_3$ in terms of ionic displacements[1–7] have usually concentrated attention on the Ti ion. Megaw[1] has pointed out that if one assumes the Goldschmidt ionic radii, the Ba ions at the corners of the unit cell are slightly too large to fit into a close-packed perovskite structure; consequently the lattice is expanded and the Ti ions, at the body centers, are free to move through small distances. In such a model each oxygen ion, at a face center, is squeezed between four Ba ions, but is free to move at right angles to the plane of Ba ions, toward the Ti ions. Devonshire[5] has estimated the forces on the Ti and O ions following Born's treatment, with the result that the Ti ion is definitely bound to its symmetrical position, but the force restoring an oxygen ion to its symmetrical position is much smaller, and of uncertain sign. It therefore appears that any theory of $BaTiO_3$ based on this model must consider displacement of the oxygen ions as being at least as effective a cause of polarization as is Ti displacement.

A model in which ionic polarization arises chiefly from the oxygen ions is capable of explaining in a very simple way the observed three phase transitions, and predicts the correct magnitude of the transverse electrostriction in the tetragonal phase. Each unit cell contains three oxygen ions, O_x, O_y, O_z, which are

free to move in the x-, y-, and z-directions respectively. Starting with cubic $BaTiO_3$ above 120°C, and cooling the crystal, the effect of the mismatch in ionic size as the lattice contracts is first to squeeze one of the oxygens, say O_z, out of its plane of Ba ions. This results in a spontaneous polarization and a deformation of the crystal, the symmetry becoming tetragonal. Contraction in the directions at right angles to the polarization occurs, since the Ba ions, which were pressing against the O_z ion, can now come together by a small amount proportional to the square of the O_z displacement z. A simple geometrical argument based on hard spheres in contact gives for the transverse contraction $-\Delta a/a = (z/a)^2$, where "a" is the lattice constant. The polarization P_{0z} due to displacement of O_z is $2eza^{-3}$, so that the transverse contraction becomes

$$-\Delta a/a = (a^4/4e^2)P_{0z}^2 = 3.8\times10^{-12}P_{0z}^2.$$

Experimentally,[8] $-\Delta a/a$ is found to be accurately proportional to the square of the total polarization, with a coefficient of 1.2×10^{-12}. Thus, if P_{0z} represents 56 percent of the total polarization, the transverse electrostriction is given correctly.

The displacement of O_z relieves the instability of the lattice to a certain extent; as we further cool the crystal, a second group of oxygens, say the O_y, get squeezed out of their symmetrical positions, and the polarization now has equal components in the z and y directions, the crystal distorting to orthorhombic symmetry. On further cooling, the O_x ions are squeezed out of place, resulting in a net polarization directed toward the diagonal of the original cube, and the symmetry becomes rhombohedral. All of these changes of phase and polarization direction are observed experimentally.[8]

Certain obvious refinements of this model would change the above numerical estimates, but it is clear that we get a qualitative understanding of two of the most puzzling features of $BaTiO_3$, namely the existence of three phase transitions with shifts of the direction of spontaneous polarization, and the very large electromechanical coupling.

I am indebted to Professor E. P. Wigner and Dr. B. T. Matthias for helpful discussions.

[1] H. D. Megaw, Trans. Faraday Soc. **42A**, 224 (1946).
[2] Rushman and Strivens, Trans. Faraday Soc. **42A**, 231 (1946).
[3] Mason and Matthias, Phys. Rev. **74**, 1622 (1948).
[4] G. H. Jonker and J. H. van Santen, Science **109**, 632 (1949).
[5] A. F. Devonshire, Phil. Mag. (Series 7) **40**, 1040 (1949).
[6] P. W. Anderson, Phys. Rev. **78**, 341 (1950).
[7] J. C. Slater, Phys. Rev. **78**, 748 (1950).
[8] W. J. Merz, Phys. Rev. **76**, 1221 (1949).

On the Hyperfine Structure of Hydrogen and Deuterium*

A. G. Prodell and P. Kusch
Columbia University, New York, New York
July 17, 1950

A NEW determination of the hyperfine structure separation of both hydrogen and deuterium in the $^2S_{\frac{1}{2}}$ state has been made by the atomic beam method. The new values are, for several reasons, of considerably greater precision than those previously reported.[1] The r-f circuit which produced the oscillating magnetic field was arranged so that no Doppler effect[2] could occur to shift or broaden the lines. The deflecting fields, which were set up by current carrying conductors, were sufficiently remote from the transition region to have a negligible effect on the field in that region. The transition field itself was extremely stable since the transitions were observed in the permanent residual laboratory field of about 0.3 gauss. The Pirani gauge detector, of a design proposed by Zacharias,[3] was extremely fast so that no very great demands were put on the stability of the frequency source, and it was possible to accumulate a large body of significant data.

In the case of hydrogen, the σ-line $(1,0)\leftrightarrow(0,0)$ and the two π-lines $(1,1)\leftrightarrow(0,0)$ and $(1,0)\leftrightarrow(1,-1)$ were observed. The σ-line gives the hyperfine structure separation, ν_H, directly after the application of a small quadratic correction of about 0.3 kc in these measurements. The difference in the frequencies of the two π-lines is identically equal to ν_H. All frequency measurements were made in terms of the 5 Mc signal from WWV. For several runs, each of which consisted of many measurements of the line centers, the following results were obtained:

Run	Method	$\nu_H\times10^{-6}$ sec.$^{-1}$
1	σ-line	1420.4056±0.0010
2	σ-line	1420.4053±0.0005
2	π-lines	1420.4051±0.0016
3	σ-line	1420.4048±0.0005
	Weighted Mean	1420.4051±0.0003

The stated uncertainty is about twice the usual probable error.

Deuterium has two nearly field independent, unresolved π-lines at weak fields, $(\frac{1}{2},\frac{1}{2})\leftrightarrow(\frac{1}{2},-\frac{1}{2})$ and $(\frac{3}{2},-\frac{1}{2})\leftrightarrow(\frac{1}{2},\frac{1}{2})$. The frequency separation of these lines is $2g_I\mu_0H/h$ which in our case is about 0.4 kc. Since the probability of each of these transitions is the same, and since atoms in the states $(\frac{3}{2},\frac{1}{2})$ and $(\frac{3}{2},-\frac{1}{2})$ have substantially identical trajectories in the apparatus as have also atoms in the states $(\frac{1}{2},\frac{1}{2})$ and $(\frac{1}{2},-\frac{1}{2})$, the center of gravity of the observed line, of about 22 kc half width, can be used to fix ν_D without ambiguity. From numerous measurements on these lines and from less precise measurements on other π-lines to determine the quadratic correction, we find:

$$\nu_D = (327.38424\pm0.00014)\times10^{-6}\ \text{sec.}^{-1}.$$

From these results, the experimental value of the ratio of ν_H ν_D is:

$$(\nu_H/\nu_D)_{\text{exp}} = 4.3386484\pm0.0000020.$$

This value may be compared to the theoretical value of the ratio which is given by the expression:

$$(\nu_H/\nu_D)_{\text{theor}} = 4/3(m_H/m_D)^3(\mu_H/\mu_D)$$

where m_H and m_D are the reduced masses of an electron in hydrogen and deuterium respectively. Using the value of μ_H/μ_D determined by Smaller, Yasaitas, and Anderson,[4] and $m_H/m_e = 1835.979\pm0.056$:[5]

$$(\nu_H/\nu_D)_{\text{theor}} = 4.3393876\pm0.0000008.$$

The discrepancy between the experimental and theoretical ratio may be written as:

$$(\nu_H/\nu_D)_{\text{exp}} = (\nu_H/\nu_D)_{\text{theor}}[1-(1.703\pm0.007)\times10^{-4}].$$

This result agrees with the less accurate result of Nafe and Nelson.[1]

From theoretical considerations of the effects of internal nuclear motion on the hyperfine structure of deuterium, Low[6] obtains:

$$(\nu_H/\nu_D) = (\nu_H/\nu_D)_{\text{theor}}[1-(1.83\pm0.22)\times10^{-4}].$$

In view of the large uncertainty in the theoretical calculation, it is not possible to draw a significant conclusion from the disagreement between the observed and calculated values. However, the accurately known discrepancy between the deserved and calculated values of the ratio of the ν's makes possible a careful investigation of the structure of the deuteron.

The fine structure constant, α, may be found[7] from the known value of ν_H and from the known value of μ_H/μ_0. The new value of ν_H does not significantly alter the previously stated value of α. However, the present precision in ν_H is greater than that of any other quantity in the theoretical relationship. It is of interest to note that a very much improved precision in the value[8] of μ_H/μ_0, new calculations for the diamagnetic fields at a nucleus in a molecule,[9] a new [10] fourth-order correction of the spin magnetic moment of the electron, and a very much improved value of the velocity of light[11] now suggest the possibility of obtaining α to a

very high degree of precision, limited by the theoretical approximations in the relationship between ν_H and μ_H.

* Supported in part by the ONR.
[1] J. E. Nafe and E. B. Nelson, Phys. Rev. **73**, 718 (1948).
[2] E. B. Nelson and J. E. Nafe, Phys. Rev. **75**, 1194 (1949).
[3] J. R. Zacharias, private communication; R. Julian, thesis, Massachusetts Institute of Technology, 1947.
[4] Smaller, Yasaitas, and Anderson, Bull. Am. Phys. Soc. **25**, No. 4, 22 (1950).
[5] Hipple, Sommer, and Thomas, Phys. Rev. **76**, 1877 (1949).
[6] F. Low, Phys. Rev. **77**, 361 (1950).
[7] H. Taub and P. Kusch, Phys. Rev. **75**, 1481 (1949).
[8] L. H. Gardner and E. M. Purcell, Phys. Rev. **76**, 1262 (1949).
[9] N. F. Ramsey, Phys. Rev. **78**, 699 (1950).
[10] R. Karplus and N. M. Kroll, Phys. Rev. **76**, 846 (1949).
[11] J. W. M. DuMond, Informal report to the N.R.C. Committee on Constants at The Bureau of Standards, April 27, 1950.

The Nuclear Magnetic Moment of Scandium[45]

NORMAN F. RAMSEY
Harvard University, Cambridge, Massachusetts
July 28, 1950

IN a recent letter with the above title in this journal, Sheriff and Williams[1] present a value of 4.7617 ± 0.0010 nuclear magnetons for the magnetic moment of Sc^{45} after having made a diamagnetic correction of 0.260 percent in accordance with Lamb's[2] formula.

It is the purpose of this note to point out that the diamagnetic correction according to Lamb's formula is 0.151 instead of 0.260 percent. When Sheriff and Williams' experimental results are recalculated with this value of the Lamb correction they give for the magnetic moment of Sc^{45}

$$\mu(Sc^{45})=4.7564\pm0.0010 \text{ nuclear magnetons.}$$

Although the result of Sheriff and Williams originally disagreed with the recent results of Proctor and Yu[3] and Hunten,[4] the above correction brings it into agreement within the experimental limit of error.

[1] R. E. Sheriff and D. Williams, Phys. Rev. **79**, 175 (1950).
[2] W. E. Lamb, Phys. Rev. **60**, 817 (1941).
[3] W. G. Proctor and F. C. Yu, Phys. Rev. **78**, 471 (1950).
[4] D. M. Hunten, Phys. Rev. **78**, 806 (1950).

Gamma-Rays of Ag^{105} and Ag^{106}

J. Y. MEI, C. M. HUDDLESTON, AND ALLAN C. G. MITCHELL
*Indiana University, Bloomington, Indiana**
July 10, 1950

THE gamma-rays of Ag^{106} (8.2*d*) and Ag^{105} (45*d*) have been measured by Enns[1] and Deutsch *et al.*[2] The results are shown in Table I.

Since the measurements were made a number of years ago when techniques had not been developed to their present state, it was decided to repeat these measurements. In addition it was hoped that the energy levels of Pd^{106} determined from K-capture in Ag^{106} could be checked against those determined from the disintegration of Rh^{106}.

In the present experiments Ag^{106} and Ag^{105} were produced by bombarding Pd with deuterons or Rh with alpha-particles in the Indiana University cyclotron. The first reaction also gave some Ag^{111} in addition to Ag^{105} and Ag^{106}. In no case were Ag^{106} and Ag^{105} produced separately since in the bombardment with alpha-particles both $Rh(\alpha, n)$ and $Rh(\alpha, 2n)$ reactions took place. Chemical separations to isolate silver were made. The assignment of the lines to the several isotopes was made by watching the decay of the source.

The lines having an 8-day period, and hence attributed to Ag^{106}, have energies of 0.515, 0.722, 1.04 and 1.54 Mev. In comparing these results with those of Peacock[3] on Rh^{106} it is to be noted that he finds lines at 0.51, 0.75 and 1.25 Mev but none at 1.04 and 1.54 Mev, while the line at 1.26 Mev is not seen in Ag^{106}.

The gamma-rays associated with the 45-day period, Ag^{105}, have energies of 0.064, 0.278, 0.340 Mev with two weak lines at 0.220 and 0.437 Mev. From energy considerations it would appear that the line at 0.340 Mev is probably in parallel with the lines at 0.278 and 0.064 Mev which are in cascade. The lines 0.220 and 0.437 Mev are probably in another branch of the K-capture process.

TABLE I. Early measurements on gamma-rays of Ag^{106}, Ag^{105}.

	Ag^{105} (Energy in Mev)	Ag^{106} (Energy in Mev)
Enns	0.29, 0.42, 0.51, 0.62	0.69, 1.06
Deutsch, Roberts, Elliott	0.282, 0.345, 0.430, 0.650	0.505, 1.06, 1.63, 0.72(?)

The source produced from the $Pd(dn)$ reaction contained Ag^{111} (7.5 days). The beta-ray spectrum was measured and a Fermi plot made of the data. The beta-ray spectrum of Ag^{111} appears to be simple with an end point at 1.06 Mev, in agreement with the work of Helmholtz, *et al.*[4] In addition, internal conversion lines for gamma-rays at 0.515 (Ag^{106}), 0.338, 0.278 and 0.064 (Ag^{106}) were obtained. An Auger line at 19 kev was observed which corresponds to the $K-L-M$ energy difference in Pd.

We are indebted to Dr. M. B. Sampson and the cyclotron crew for making the bombardments.

* This work was supported by the joint program of the ONR and AEC.
[1] T. Enns, Phys. Rev. **56**, 872 (1939).
[2] Deutsch, Roberts, and Elliott, Phys. Rev. **61**, 389 (1942).
[3] W. C. Peacock, Phys. Rev. **72**, 1049 (1947).
[4] Helmholz, Hayward, and McGinness, Phys. Rev. **75**, 1469 (1949).

Detection of Scintillations from Crystals with a Photo-Sensitive Geiger-Müller Counter*

C. E. MANDEVILLE AND H. O. ALBRECHT
Bartol Research Foundation of The Franklin Institute, Swarthmore, Pennsylvania
July 26, 1950

PHOTO-SENSITIVE Geiger-Müller counters have been the subject of long study at this laboratory. Very high quantum efficiencies, as indicated by his often-mentioned starlight experiments, were achieved by Locher[1,2] who employed a multitude of photo-cathode surfaces in making his photon counters at Bartol. Locher's account[1] of his work in photo-sensitive surfaces at the Rice Institute remains even today one of the very best available discussions of photon counting.

Glasser and Beaseley[3,4] describe interesting measurements in which long-period *phosphorescence* from gamma-rays on NaCl was observed with the use of a photo-sensitive G-M counter. This type of emission is to be differentiated from instantaneous fluorescence employed in the detection of nuclear particles by photo-multipliers.

Interest in photon counting was revived at Bartol when Scherb[5] discovered a discharge technique at liquid air temperatures which increased considerably the photo-sensitivity of the thus treated counter. The use of scintillating phosphors in conjunction with photo-multipliers again focused attention at this laboratory on the possibility of detecting fluorescent scintillations with G-M counters, and the feasibility of photon counters for scintillation detection was speculated upon in discussions at Oak Ridge.[6]

In the past several months, the writers have devoted considerable effort to reproducing many of Locher's early photon counters in an effort to attain sufficient quantum efficiency to detect scintillations from currently used crystals such as NaI. However, difficulties were encountered in matching the wave-lengths of the scintillations from the crystals with the peak of the spectral response of the cathode surfaces of the various counters. The alkali metals were usually employed, but it was found that appreciable response at wave-lengths greater than 3600A was difficult to obtain. Moreover, counters of the alkali metals seemed to have a high background arising, perhaps, from thermionic effects.

Finally it was decided to abandon the attempt to find cathode surfaces suitable for use with currently available crystals and to concentrate upon development of crystals which might fluoresce

in the deep ultraviolet when bombarded by nuclear particles. Crystals of this type would actuate ordinary G-M counters. The first step in the new procedure was to reconsider the experiments of Glasser and Beaseley. It was concluded that detection of delayed phosphorescence would at least constitute a hopeful indication of good quantum efficiency. Rather than irradiating NaCl with a strong gamma-ray source as in their case, silver-activated NaCl was irradiated with electrons of a high frequency discharge and with the hard beta-rays of $Ce^{141} \xrightarrow{\beta} Pr^{141} \xrightarrow{\beta} Nd^{141}$. In each case, a long period phosphorescence was observed, although no appreciable immediate fluorescent pulses were produced. However, when NaCl-Ag was irradiated with the alpha-particles of polonium, the crystals fluoresced vigorously in the deep ultraviolet, emitting quanta at wave-lengths for the most part less than 2600A. The quantum radiations were detected with a high efficiency in several different photon counters.[7] The counters had wire gauze cathodes, and the glass sidewalls were made of Corning 9741 glass. When a quartz jacket was coated with NaCl-Ag and slipped over the counter, an absolute efficiency of about 15 percent for the polonium alphas was observed. The counters in which this efficiency was noted were relatively insensitive, and the geometry can be improved enormously. It is certain that the absolute efficiency for alpha-particles can be increased to 100 percent. The activity of the NaCl-Ag crystals was proportional to the concentration of AgCl in the interval 0.03 percent to 1.0 percent by weight. Below this interval the activity decreased rapidly, and above it the crystals lost transmission and became cloudy, perhaps due to the fact that some silver did not remain in solution. The decay constant of NaCl-Ag was kindly measured for us by Dr. W. C. Elmore of Swarthmore College, using a 1P28 photomultiplier and a fast oscilloscope. By a comparison with gamma-rays on NaI-Tl, it was concluded that the decay constant must be less than 0.2 μsec. Accurate measurements below this value are not permitted by the resolution of his apparatus.

It has often been remarked that secondary pulses or "double" pulses are found in photo-sensitive Geiger counters. The behavior of the photon counter was observed for a period of 500 μsec. after the initiation of each discharge. This time was several times greater than that necessary for collection of the positive ion sheath. No spurious delayed counts were found.

Now that it has been demonstrated that Geiger counters do possess enough quantum efficiency in the deep ultraviolet to use them as scintillation counters, an effort is being made to find crystals which will give copious ultraviolet fluorescence when irradiated by beta-rays and gamma-rays. Counters of a more advanced and efficient design are under construction.

It is evident that great possibilities are here indicated for the development of a highly efficient gamma-ray counter. Consideration must also be given to the use of scintillation Geiger counters in the proportional region.

Note added August 10, 1950:—Using a highly sensitized scintillation Geiger counter, short-lived fluorescent pulses have been observed when NaCl-Ag is irradiated by the beta-spectrum of RaE. Using a relatively poor geometry, an efficiency of about ten percent was achieved. This value can be increased.

Note added August 31, 1950:—Scintillations from million volt gamma-rays on NaCl-Ag have been detected in a photo-sensitive Geiger counter. On surrounding the counter with crystals, the "apparent efficiency" for gamma-rays at 1 Mev was increased by a factor of two and one-half.

* Assisted by the joint program of the ONR and AEC.

[1] G. L. Locher, Phys. Rev. **42**, 525 (1932).
[2] G. L. Locher, Phys. Rev. **50**, 1099A (1936); **51**, 386A (1937); **53**, 333A (1938); **55**, 675A (1939).
[3] Glasser and Beaseley, Phys. Rev. **47**, 789A (1935).
[4] Glasser and Beaseley, Phys. Rev. **47**, 570 (1935).
[5] M. V. Scherb, Phys. Rev. **73**, 86 (1948).
[6] Mandeville, Scintillation Counter Symposium, Oak Ridge National Laboratory, June 3–4, 1949.
[7] It should perhaps be mentioned that every precaution was taken to establish the genuine nature of the effect. With 0.01 millicurie of polonium near a counter, only the cosmic-ray background was observed, since the alphas were stopped in the glass wall. Addition to the counter of the crystal-coated quartz jacket gave a counting rate of 50,000 counts per minute. Freshly-prepared untreated Bartol counters equipped with copper cathodes and thin Pyrex bubble windows gave a counting rate a hundred times greater than cosmic-ray background when an NaCl-Ag crystal and a polonium source of strength 0.10 millicurie were placed near them.

Radioactivities of Nb^{99}, Ta^{185}, and W^{185}, and the Relative (γ,n) and (γ,p) Cross Sections of Mo^{100}*†

R. B. Duffield, L. Hsiao, and E. N. Sloth
University of Illinois, Urbana, Illinois
July 14, 1950

THE irradiation of molybdenum, enriched to 93 percent in Mo^{100}, with 23-Mev betatron x-rays has been found to produce radioactive Nb^{99} by a (γ, p) reaction.[1] This hitherto unknown isotope has a half-life of 2.5 min. and decays by the emission of 3.2-Mev β^--rays. The beta-energy was determined by an aluminum absorption curve. The activity has been chemically identified as niobium.

The radioactivity of this isotope of niobium provides the means of observing the relative probabilities of neutron and proton emission from a nucleus excited by photon absorption, the nucleus being Mo^{100}. The yields of Mo^{99} and Nb^{99} were measured at betatron energies from 10 to 23 Mev by counting the induced activities. Assuming the x-ray spectrum to be that given by Schiff,[2] the relative cross section for the two reactions were calculated for discrete x-ray energies. The cross section for the (γ, n) reaction showed a maximum at approximately 17 Mev, that for the (γ, p) reaction continued to increase up to the highest energy which we could reach. The ratio of the (γ, p) to (γ, n) cross sections at all energies is approximately 100 times larger than that predicted by the statistical theory of nuclear reactions, assuming independent competition among different modes of decay of an intermediate excited state.[3] This is in agreement with the observations of Hirzel and Wäffler[4] on other photo-nuclear reactions produced by 17.3-Mev gamma-rays from the reaction $Li(p, \gamma)$, but is somewhat more direct. They did not measure the two cross sections for the same parent nucleus, but rather interpolated $\sigma(\gamma, n)$ between values for nearby isotopes.

Similar irradiations of separated W^{186} have been found to produce, in addition to the known 74-day W^{185}, a 1.85-min. isomer of W^{185} by a (γ, n) reaction and a 46-min. Ta^{185} by a (γ, p) reaction. Production of the last of these by irradiation of normal tungsten with x-rays has recently been reported by Butement.[5]

Examination of the radiation from the 1.85-min. W^{185} isomer with an anthracene scintillation proportional counter and pulse analyzer shows conversion electrons of approximately 75 kev and a very high conversion coefficient.

The Ta^{185} decays by the emission of 1.7 Mev β^--rays and also conversion electrons of the same energy as these observed from the 1.85-min. W^{185} isomer, leading to the belief that decay occurs to the metastable state of W^{185}, but no coincidence work has been done to verify this.

* Assisted by the joint program of the ONR and AEC.
† This material was originally submitted as a contributed paper to the Washington meeting of the American Physical Society, April, 1950. The abstract was lost in the mail, however, and the paper appeared on the post deadline program at the meeting.
[1] The separated isotopes used in this investigation were supplied by Carbide and Carbon Chemicals Corporation, Y-12 Plant, Oak Ridge, Tennessee, and obtained on allocation from the Isotopes Division of the AEC.
[2] L. I. Schiff, private communication. See also H. W. Koch and R. E. Carter, Phys. Rev. **77**, 165 (1950).
[3] V. F. Weisskopf and D. H. Ewing, Phys. Rev. **57**, 472 (1940).
[4] O. Hirzel and H. Wäffler, Helv. Phys. Acta **20**, 373 (1947).
[5] F. D. S. Butement, Nature **165**, 149 (1950).

Changes in the Activation Energy of Tellurium

T. S. Moss
Department of Colloid Science, Cambridge University, Cambridge, England
July 3, 1950

MEASUREMENTS have been carried out by Bridgman[1] on the variation of resistance with pressure in tellurium, the resistance falling off by a factor of several hundreds in the range of measurements. As pointed out by Bardeen[2] this effect can be

related to a change in the thermal activation energy of the semiconductor due to the applied pressure.

If the activation energy calculated for the various pressures is plotted against the dilatation, $\Delta V/V$, a straight line is obtained, provided the value of activation energy of 0.38 ev found from Hall effect measurements by Johnson[3] is used for the value at zero pressure.

From the graph it is found that

$$\Delta E/(\Delta V/V)=0.041 \text{ ev per one percent dilatation.}$$

Photo-conductive films of tellurium have been prepared by the author, and from measurements of the spectral distribution of sensitivity, a value of the optical activation energy can be obtained. It was found that for different layers the sensitivity fell to half-value at wave-lengths in the range 3.2μ to 3.5μ, corresponding to an optical activation energy of 0.35 to 0.38 ev. There is thus good agreement between the optical and thermal activation energies.

It has also been observed that the "threshold" wave-length of sensitivity is temperature dependent, moving to longer wavelengths on cooling, and the extent of the shift has now been measured. Unfortunately the sensitivity of tellurium cells falls rapidly with increasing temperature, and in general spectral sensitivity measurements cannot be carried out much above 150°K. However, fairly good results were obtained on two cells from 77°K to 161°K and 77°K to 195°K respectively. The observed shifts of 0.16μ and 0.20μ, give an energy change:—

$$\Delta E/\Delta T=2.1\times10^{-4} \text{ and } 1.9\times10^{-4} \text{ ev/°C.}$$

As a result of the restricted temperature range, the accuracy is not high, but a mean value of $\Delta E/\Delta T=2\times10^{-4}$ ev/°C may be taken. Since the thermal expansion coefficient, $\Delta V/V\cdot\Delta T=51\times10^{-6}$/°C, we obtain from the optical measurements, $\Delta E(\Delta V/V)=0.04$ ev per one percent dilatation.

This figure is almost identical with that calculated from the pressure measurements. Such close agreement is fortuitous, but we may conclude that within the accuracy of the measurements the values of the energy change with dilatation are the same in the two cases. The energy gap is thus determined primarily by the volume, the forbidden zone decreasing in width as the atoms move closer together. Bardeen has suggested that the opposite effect occurs in germanium.

An interesting conclusion to be drawn from the above results is that a film of tellurium operated at 20,000 kg/cm² and suitable low temperature, should be photo-conductive at wave-lengths $\sim12\mu$.

Acknowledgment is due to the Chief Scientist, British Ministry of Supply, for permission to publish this letter.

[1] P. W. Bridgman, Proc. Am. Acad. 72, 159 (1938).
[2] J. Bardeen, Phys. Rev. 75, 1777 (1949).
[3] V. A. Johnson, Phys. Rev. 74, 1255 (1948).

Boride Cathodes

J. M. Lafferty
General Electric Research Laboratory, Schenectady, New York
July 20, 1950

THE thermionic emission properties of the borides of the alkaline-earth and rare-earth metals and thorium have been investigated. These compounds all have the same formula MB_6 and the same crystal structure consisting of a three-dimensional boron framework in whose interlattice spaces the metal atoms are embedded. The valence electrons of the metal atoms are not accepted by the B_6 complex, thus giving rise to the presence of free electrons which impart a metallic character to these compounds.

This is evident from their high electrical conductivity. Lanthanum boride, for example, has a specific resistance of 27 μohm-cm at room temperature and a positive resistance-temperature coefficient of 0.071 μohm/°C. Hall effect measurements on sintered lanthanum boride show approximately one free electron per lanthanum atom. The strong binding forces between the boron atoms lead to a series of compounds which are very refractory, with melting points above 2100°C. The hexaborides are also very stable chemically; moisture, oxygen and even hydrochloric acid do not react with them.

When this structure is heated to a sufficiently high temperature, the metal atoms at the surface evaporate away. They are, however, immediately replaced by diffusion of metal atoms from the underlying cells. The boron framework does not evaporate but remains intact. This process gives a mechanism for constantly maintaining an active cathode surface. This feature, together with the high electrical conductivity and high thermal and chemical stability, gives ideal properties for a cathode material.

Thermionic emission measurements show the rare-earth metal borides to be superior to the others. The emission constants obtained from Richardson plots for the hexaborides are shown in Table I. Lanthanum boride gave the highest emission and was found to have a relatively low evaporation rate corresponding to a latent heat of evaporation of 169 kcal./mole.

TABLE I. Hexaboride electron emission constants determined for Dushman's equation.

Boride	A	ϕ
CaB_6	2.6 amp./cm²/deg. K²	2.86 volts
SrB_6	0.14	2.67
BaB_6	16	3.45
LaB_6	29	2.66
CeB_6	3.6	2.59
ThB_6	0.53	2.92

Boride cathodes require no special activation. When they are heated for a few minutes at 1400°C to 1600°C for outgassing, they are found to be completely active. When lanthanum boride is bombarded with mercury ions which exceed energies of approximately 20 ev lanthanum atoms are readily sputtered off the surface making the cathode inactive. However, at 1400°C, the lanthanum atoms diffuse rapidly to the surface, making the cathode active again.

The pulsed emission is the same as the d.c. emission for the boride cathodes.

If these cathode materials are operated in contact with the refractory metals, the boron atoms diffuse into their metal lattices forming interstitial boron alloys with them. When this occurs, the boron framework which holds the alkaline-earth or rare-earth metal atoms collapses, permitting them to evaporate. The hexaborides may be operated in contact with tantalum carbide or carbon.

On the Spins of Li^6 and B^{10}

G. Racah and N. Zeldes
Department of Physics, Hebrew University, Jerusalem, Israel
July 5, 1950

IT was pointed out by Feenberg[1] that according to the p^n shell model, the spins of Li^6 and B^{10} are one in LS coupling, but three in jj coupling; it was therefore natural to ask if the different spins of these two nuclei can be explained by intermediate coupling. Calculations are in progress on this subject, and the first results are very satisfactory.[2]

In the meantime it has been suggested by Inglis, Mayer, and Kurath[3] that the coupling should be extreme jj and the mixture of exchange forces should be such as to give the correct spins for Li^6 and B^{10}. We wish to discuss now some consequences of this hypothesis.

Since the configuration $p_{\frac{1}{2}}^6$ is the almost closed shell corresponding to $p_{\frac{1}{2}}^2$, the relative positions of the levels will be the same in the first approximation, and an inversion can take place only if there is degeneracy in the first approximation.

If we assume for the nuclear interaction the expression

$$-[(1-m-b-h)+mP_x+bP_\sigma+hP_xP_\sigma]J(r), \quad (1)$$

the energy difference between the levels with $I=1$ and $I=3$ has the same sign as $m+b$, and the condition for the degeneracy in the first approximation is

$$m+b=0. \quad (2)$$

In order to obtain the difference E_1-E_3 in the second approximation, we calculated the transformation matrix from LS to jj coupling by diagonalizing the matrix of spin-orbit interaction,[2] and then transformed the matrix of nuclear interaction[4] to the jj scheme and calculated the second approximation by the ordinary formulas.

The result is

$$E_1-E_3=-15F_2^2/\alpha \quad \text{for } p_{\frac{1}{2}}^2, \quad (3)$$

and

$$E_1-E_3=-15(F_2^2/\alpha)+(40/9\alpha)[m(F_0-5F_2)-3(h-m)F_2]^2 \quad \text{for } p_{\frac{1}{2}}^6, \quad (4)$$

where $\alpha=-\frac{1}{2}\zeta$ is the (positive) parameter of spin-orbit coupling, and F_0 and F_2 are the (generalized) parameters of Slater.

We see therefore that (2) is sufficient to give the correct spin for Li^6 in extreme jj coupling, but the correct spin of B^{10} can be obtained only by an appropriate choice of m and h.

If we remember that[5]

$$q=1-2b-2h\approx 0.6, \quad (5)$$

we obtain from (2) that

$$h-m\approx 0.2. \quad (6)$$

Introducing this value into (4) we see that the correct spin of B^{10} cannot be obtained on the hypothesis of Inglis[3] that $m=b=0$, nor on the hypothesis of Mayer[6] that $J(r)=\delta(r)$, from which it follows that $F_0=5F_2$.

Only an interaction of finite range, with a strong Majorana component opposed by an equally strong Bartlett component, and also accompanied by a stronger Heisenberg component, can explain the spins of Li^6 and B^{10} in extreme jj coupling. It is rather doubtful whether such an interaction corresponds to reality.

[1] E. Feenberg, Phys. Rev. **76**, 1275 (1949).
[2] N. Zeldes, in preparation.
[3] D. R. Inglis, Phys. Rev. **77**, 724 (1950).
[4] G. Racah, Helv. Phys. Acta, Suppl. III, 229 (1950).
[5] L. Rosenfeld, *Nuclear Forces* (Interscience Publishers, New York, 1948), p. 161.
[6] M. G. Mayer, Phys. Rev. **78**, 22 (1950).

Neutral Impurity Scattering in Semiconductors

CAVID ERGINSOY
High Voltage Laboratory, Queen Mary College, London, England
May 29, 1950

A THEORY of the scattering of conduction electrons in a semiconductor by ionized impurity centers was recently proposed by Conwell and Weisskopf.[1] Another important source of resistivity at low temperatures is the scattering due to neutral impurity atoms which must be considered particularly in the case of semiconductors showing a small degree of ionization. Pearson and Bardeen[2] have pointed out that the theoretical treatment of the problem should be similar to the scattering of slow electrons by hydrogen atoms, and have shown by approximate calculations that the effective scattering cross sections of ionized and neutral impurities are comparable at temperatures of the order of 100°K. In this letter we suggest a more exact solution of the problem, using the results of Massey and Moiseiwitsch's recent work[3] on the slow collisions of electrons and hydrogen atoms.

For small incident velocities the scattering is spherically symmetrical and only the zero-order phase angle[4] need be considered. Thus the differential cross section of scattering is reduced to

$$I_0(\theta)=(1/k^2)\sin^2\eta_0 \quad (1)$$

where η_0 is the zero-order phase angle, θ is the angle of scattering, k is $2\pi mv/h$, and v is the velocity of the incident electron. In a semiconductor the orbit of the bound electron or hole about the corresponding ion (i.e., the equivalent of the Bohr radius in an hydrogen atom) is given by

$$a_0=\kappa h^2/4\pi^2me^2 \quad (2)$$

where κ is the effective dielectric constant.

η_0 has been calculated by McDougall[5] by numerical integration for different values of ka_0, using the static field of the hydrogen atom. The complete solution, however, must include the electron exchange effects (which are particularly important for slow electrons), and also the effect of the polarization of the atom by the incident electron.

In their recent work Massey and Moiseiwitsch,[3] using Hulthén's variational method have included both these effects. It may be seen from their Fig. 1(d) that the dimensionless quantity

$$k^2Q_0=2\pi k^2\int_0^\pi I_0(\theta)\sin\theta d\theta=4\pi\sin^2\eta_0 \quad (3)$$

is proportional to ka_0 for a wide range of incident velocities. Q_0 is the zero-order partial cross section. Up to $ka_0=0.5$ (i.e., incident energies of up to 25 percent of the ionization energy) an analytical expression of the form

$$k^2Q_0=20ka_0 \quad (4)$$

may be used as a good approximation.

In determining the resistivity it is useful to introduce τ, the relaxation (or collision) time; $1/\tau$ may be considered as the total scattering probability. It is related to the differential cross section by the expression

$$1/\tau=N_nv\int_0^\pi 2\pi I_0(\theta)\sin\theta(1-\cos\theta)d\theta \quad (5)$$

where N_n is the concentration (per cm³) of neutral impurities.

With substitution for $I_0(\theta)$ from Eq. (1) this integral gives

$$1/\tau=N_nv(4\pi/k^2)\sin^2\eta_0=N_nvQ_0. \quad (6)$$

Combining with the Eq. (4) and using $a_0=\kappa h^2/4\pi^2me^2$ and $k=2\pi mv/h$ we obtain

$$1/\tau=20\kappa N_nh^3/8\pi^3m^2e^2. \quad (7)$$

The significance of this result is that τ is independent of the velocity of the electrons. In Conwell and Weisskopf's case τ is seen to vary as v^3.

The expression for the resistivity is easily obtained from Eq. (7)

$$\rho_n=m/ne^2\tau=20\kappa N_nh^3/8\pi^3nme^4 \quad (8)$$

where n, e and m are the concentration, charge and effective mass of the conduction electrons (or holes) respectively.

Expressing ρ_n in ohm-cm and substituting for the constants we obtain

$$\rho_n=4.35\times10^{-4}\kappa N_n/n \text{ ohm-cm}. \quad (9)$$

TABLE I. Comparison of ρ_n and ρ_i calculated for Pearson and Bardeen's silicon samples 2 and B (reference 2). $N_{\text{total}}=N_n+N_i$ (cm^{-3}); ρ_n and ρ_i in ohm-cm.

$1/T$ (°K)$^{-1}$	Sample 2 ($N_{\text{total}}=6\times10^{17}$) $n(=N_i)$	ρ_n	ρ_i	Sample B ($N_{\text{total}}=1.25\times10^{18}$) $n(=N_i)$	ρ_n	ρ_i
12×10^{-3}	3.7×10^{16}	0.0866	0.0526	5.3×10^{17}	0.0077	0.0283
12×10^{-3}	7.4×10^{16}	0.0402	0.0390	5.3×10^{17}	0.0077	0.0250
6×10^{-3}	2.37×10^{17}	0.0086	0.0194	7.4×10^{17}	0.0031	0.0155
5×10^{-3}	3.3×10^{17}	0.0046	0.0153	8.25×10^{17}	0.0029	0.0129

Similarly, Conwell and Weisskopf's Eq. (19) giving ρ_i, the resistivity due to scattering by ionized impurities may be written as

$$\rho_i = 1.9\times10^{3}\kappa^{-2}T^{-\frac{1}{2}}\log\{1+3.22\times10^{6}\kappa^{2}T^{2}N_i^{-\frac{1}{3}}\}\ \text{ohm-cm}. \quad (10)$$

As an example for comparison of the two resistivities we have calculated ρ_n and ρ_i from Eqs. (9) and (10) for two non-degenerate silicon samples ($\kappa=13$) investigated by Pearson and Bardeen.[2] Table I shows that at temperatures below 100°K, ρ_n is larger than ρ_i for their sample 2 which has a relatively small degree of ionization. In the case of their sample B, however, ρ_i is in the whole range larger than ρ_n owing to very strong ionization of impurities obtaining already at low temperatures.

[1] E. Conwell and V. F. Weisskopf, Phys. Rev. **77**, 388 (1950).
[2] G. L. Pearson and J. Bardeen, Phys. Rev. **75**, 865 (1949).
[3] H. S. W. Massey and B. L. Moiseiwitsch, Phys. Rev. **78**, 180 (1950).
[4] N. F. Mott and H. S. W. Massey, *The Theory of Atomic Collisions* (Clarendon Press, Oxford, 1949), second edition, Chapter X.2.
[5] J. McDougall, Proc. Roy. Soc. A139, 549 (1932).

Electron Capture/Beta-Decay Ratio in K^{40}

T. GRÁF
L. Meitner Laboratory, Royal Institute of Technology, Stockholm, Sweden
July 27, 1950

WHILE some of the hitherto published results[1-3] on the capture/beta-branching ratio of K^{40} indicate a value of the order of 2, others, deduced from determinations of the argon content in old potassium minerals, seem to yield a value[4-6] smaller than 0.10.

In view of the geophysical significance of this branching ratio,[7,8] it seemed to be of interest to obtain further evidence on its magnitude. The aim of the present letter is to report the preliminary result of experiments started here to that purpose about a year ago.

The intensity of the x-rays accompanying electron capture was measured by using a method of selective detection. An internal-source G-M counter was filled alternately with two gases, one possessing low, the other high efficiency for the K_α x-rays of argon (4.18A). If the counter response to particles and to gamma-rays be assumed to be the same for the two fillings, the difference of the counting rates obtained with them should be proportional to the intensity of the x-rays emitted by the source. The proportionality factor could be calculated fairly accurately by numerical integration over the entire counting volume. As filling gases argon and krypton were used at a total pressure of 20 cm of Hg each, together with ethyl alcohol at 1.5 cm. The absorption coefficient of krypton for x-rays of 4.18A, computed with the help of the tables of Jönsson,[9] turned out to be even higher than that of xenon. Repeated measurements made with the internal source covered with a 2.3-mg/cm² Al foil (to absorb the x-rays), and with external pure beta-sources, showed that for the same overvoltage the counting rates were identical within less than 0.2 percent. The computed mean values of the x-ray efficiency were 8 and 69 percent, respectively (counter diameter 1.34 cm, wire length 7.4 cm).

A layer of KF of about optimum thickness (3.44 mg/cm²) was obtained by evaporation in vacuum.[10] KF being hygroscopic precautions had to be taken to keep the layer dry. The active surface was of 5.92×0.49 cm² on each of the six Al holders which, placed side by side, formed the greatest part of the counter wall. This inside source was covered with a graphite layer of 0.5 mg/cm², which absorbed about eight percent of the x-rays, but appeared at the same time to improve greatly the stability of the counter operation.

Computation yielded a difference of 0.87 count/min., when assuming a branching ratio equal to one. This represents about two percent of the counting rate with argon filling (47 counts/min.). Actually, in three long runs, differences of 0.66 ± 0.16, 0.73 ± 0.13, and 0.43 ± 0.11 count/min. were obtained, with the indicated standard deviations. Their mean value corresponds to a branching ratio of 0.67 ± 0.20, which figure also accounts for electron capture from the L_I shell.[10]

The limits given include no systematic errors. Owing to the higher counter voltage with krypton, small spurious effects, if present, would tend to increase the observed rate difference. Therefore, the value of 0.67 should rather be considered as an upper limit of the branching ratio.

In the computation, 0.12 ± 0.02 was assumed for the fluorescence yield in argon.[11] The branching ratio is given in terms of a specific activity of 26.8 ± 1.2 beta-rays per second per gram of potassium.[12] The latter value, together with the recent result of 0.0119 ± 0.0001 percent[13] for the isotropic abundance of K^{40}, yields $(1.50\pm0.07)\times10^{9}$ yr. for the half-life of the beta-decay, and, combined with the above value of the branching ratio, a lower limit of 0.9×10^{9} yr. for the total half-life.

The present result indicates that the values of the branching ratio of references 1 to 3 are much too high. On the other hand, the values deduced from argon determinations[4-6] are smaller than the lower limit of the branching ratio. This limit is given by the gamma/beta-ratio, and its value, 0.127 ± 0.012, seems to be fairly well established.[13]

A more detailed account will be given in a paper on the radioactivity of K^{40}, to be published in *Arkiv f. Fysik*.

The author wishes to thank Professor L. Meitner for her continued interest in this work.

[1] F. C. Thompson and S. Rowlands, Nature **152**, 103 (1943).
[2] E. Bleuler and M. Gabriel, Helv. Phys. Acta **20**, 67 (1947). For corrected results see reference 12.
[3] L. H. Ahrens and R. D. Evans, Phys. Rev. **74**, 279 (1948).
[4] P. Harteck and H. Suess, Naturwiss. **34**, 214 (1947).
[5] H. E. Suess, Phys. Rev. **73**, 1209 (1948).
[6] L. T. Aldrich and A. O. Nier, Phys. Rev. **74**, 876 (1948).
[7] E. Gleditsch and T. Gráf, Phys. Rev. **72**, 641 (1947).
[8] T. Gráf, Phys. Rev. **74**, 831 (1948).
[9] E. Jönsson, Inaugural dissertation, Uppsala (1928). Also in M. Siegbahn, *Spektroskopie der Röntgenstrahlen* (Berlin, 1931), p. 470.
[10] The author is indebted to Mr. J. E. Flinta for help with the evaporation.
[11] M. E. Rose and J. L. Jackson, Phys. Rev. **76**, 1540 (1949).
[12] See, for example, A. H. Compton and S. K. Allison, *X-Rays in Theory and Experiment* (London, 1935), second edition, p. 477.
[13] T. Gráf, Phys. Rev. **74**, 831 (1948).
[14] A. O. Nier, Phys. Rev. **77**, 789 (1950).

A Note on 11.5-Day Tl^{202}

GEOFFREY WILKINSON
Radiation Laboratory, Chemistry Department, University of California Berkeley, California*
July 21, 1950

THIS well-known[1] isotope has been re-examined to check on the possibility of negative beta-particle decay. The activity was produced by deuteron bombardment of mercury. The target consisted of dental amalgam (five parts commercial alloy to nine parts of mercury by weight) pounded into a channel in a water-cooled copper plate; no loss was apparent during several hours bombardment with a 10 μamp. deuteron beam. After dissolving the target in nitric acid, the solution was made $>6N$ in hydrochloric acid and the thallium extracted by ether. The ether was evaporated, holdback carriers added and the thallium re-extracted. No carrier was added. After four extraction cycles additional chemistry on a portion of the sample showed this to be pure thallium.

The aluminum and lead absorption curves taken on carrierless samples mounted on very thin backing showed electrons range 100 mg/cm² aluminum (0.35 Mev), L and K x-radiation and a gamma-ray of half-thickness 3.7 g/cm² lead (0.43 Mev). The ratios of the radiations corrected for absorption in counter windows, fluorescence yield, counting efficiency, etc. were 0.35 Mev ϵ^-:L x-ray:K x-ray:0.43 Mev $\gamma=\sim0.1:\sim1.7:1:0.6$. Assuming that both L and K x-radiations are produced from conversion, then ~0.9 of the measured K x-radiation represents one

disintegration by K-electron capture. Since only 0.7 L rays are to be expected for each K shell electron removed it appears that the isotope decays almost equally by L and K orbital electron capture.

From a study on a 257° mirror focusing spectrometer, the γ-ray energy was determined as 0.427 Mev. No evidence for a continuous beta-spectrum could be determined either in absorptions or on the spectrometer, and decay by beta-emission is less than 1/200 that by orbital electron capture.

The decay of electrons and electromagnetic radiations followed separately through over eight periods gave a value of 11.50±0.05 days for the half-life after subtraction of background due to the 2.7-year Tl^{204}.

Note added in proof:—The limits in the value of the energy of the gamma-ray should read 0.435±0.005 Mev.

* This work was performed under the auspices of the AEC.

[1] G. T. Seaborg and I. Perlman, Rev. Mod. Phys. 20, 585 (1948).

Induced Absorption Bands in MgO Crystals

J. P. Molnar and C. D. Hartman
Bell Telephone Laboratories, Murray Hill, New Jersey

July 10, 1950

ABSORPTION bands induced in single crystals of MgO by pile radiation and by high voltage electrons have been reported by Boyd, Rich, and Avery.[1] In this note we wish to report, without attempt at interpretation, measurements we have made of the optical absorption bands induced by 40-kv x-rays. We have found three distinct induced bands as shown in Fig. 1,

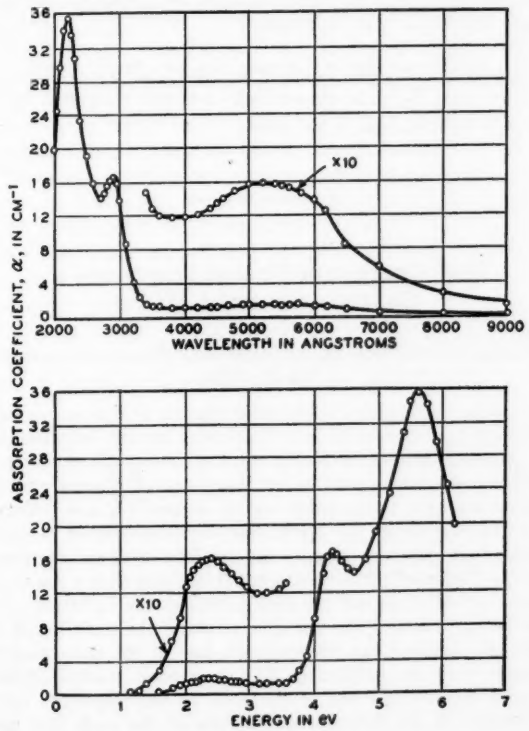

FIG. 1. Absorption bands induced in MgO crystals by 40-kv x-rays.

two in the ultraviolet with peak absorption at 2200A and 2850A and a weaker broad band at 5250A. The visible band gives the exposed crystal a weak purplish tinge. This coloration, produced by exposure to ultraviolet light, has been reported by Hibben.[2] The two ultraviolet bands maintain a constant ratio of intensity which is equal to 2.1 at the wave-lengths given above for the peak absorption. There appears to be no fixed ratio between the intensity of 5250A band and the ultraviolet bands.

The build-up of absorption with time of x-ray exposure is shown in Fig. 2. We were able to fit the data for the 5250A band to an

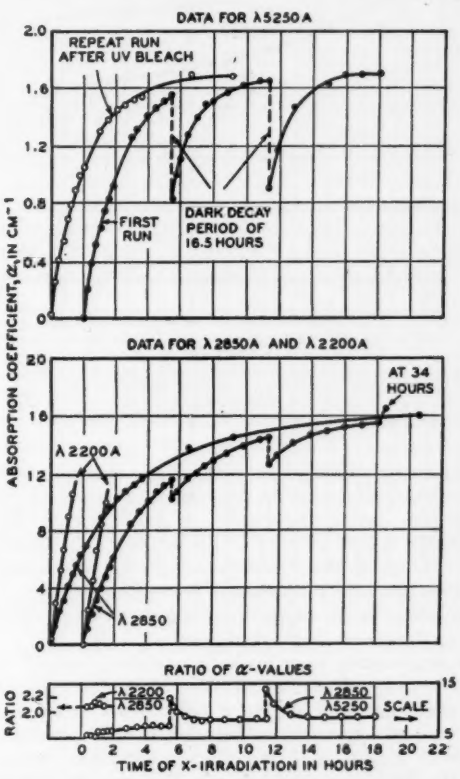

FIG. 2. The upper two plots give the induced absorption at the wave-lengths indicated as a function of the time of exposure of the crystal to x-rays. The lowest plot gives the ratio of the absorption coefficients for the wave-lengths indicated.

exponential formula of the type $\alpha=\alpha_0(1-e^{-kt})$, but the build-up of the ultraviolet bands proceeds slowly even after long exposure to x-rays, so no fit could be made to such a formula. The curves in Fig. 2 show also the decay in absorption which occurs when the crystals are kept at room temperature in the dark.

Light of wave-length anywhere in the range of the induced absorption bands will cause *all* bands to decrease in intensity. This experiment can be carried out most unambiguously when light in the wave-length range above 6900A is used. The data obtained in such an experiment are shown in Fig. 3. The absorption at 2850A and 5250A are seen to decrease with time of exposure, with, however, the absorption at 5250A decreasing more rapidly. The amount of decrease in the absorption coefficient, $\Delta\alpha$, at the two wave-lengths was found to be in constant ratio, thus suggesting that for each center giving rise to the 5250A absorption which is destroyed in the bleaching process, a constant number of centers giving rise to the 2850A absorption are destroyed. During the bleaching process the ratio of the intensities of the two ultraviolet bands remained constant.

When the induced absorption bands were measured on a crystal reduced in temperature to that of liquid nitrogen, only a very slight sharpening of the bands was found. The bleaching effects were qualitatively the same as at room temperature.

The x-rayed crystals were weakly luminescent. The light emitted could be detected by laying the crystal on a photographic film in the dark. The rate of decay of light emission seemed roughly comparable to the rate of change of the 5250A absorption band in the dark. The wave-length of emitted light was found, by interposing filters, to be in the range from 5000 to 6000A.

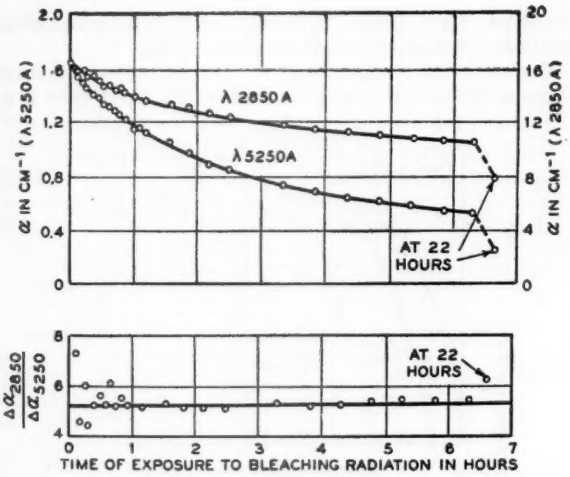

FIG. 3. The upper plot shows the effect of exposure to radiation from a tungsten lamp at wave-lengths greater than 6900A on the induced absorption at two wave-lengths. The lower plot gives the ratio of the *change* in absorption at these wave-lengths.

Attempts to make photo-conductivity measurements were confused and confounded by the presence of dark current which was variable during the course of measurement, and which undoubtedly contributed to a space-charge distortion of the electric field within the crystal. About all that can be stated with certainty is that after a crystal had been exposed to x-rays, visible light anywhere in the region of optical absorption gave rise to a change in the current through the crystal.

All measurements were made on samples obtained from the Norton Company, Niagara Falls, New York. Many of these were crystal clear, but some showed a slight yellow or greenish tinge. Others showed appreciable absorption in the ultraviolet before exposure to x-rays, as if they already contained centers giving rise to the 2850A and 2200A bands. The measurements we have here reported were made only on clear samples that exhibited a monotonically rising absorption in ultraviolet below 2500A. Spectrographic analysis revealed no impurities other than calcium ($\approx$0.1 percent).

The authors wish to express their appreciation to Miss Dorothy M. Dodd of these Laboratories for operating the spectrophotometer used in the experiments reported here.

[1] Boyd, Rich, and Avery, AEC Report No. MDDC-1508 (1947) (unpublished).
[2] J. H. Hibben, Phys. Rev. **51**, 530 (1937).

Further Studies of Infra-Red Absorption by Homopolar Diatomic Molecules

ROBERT VAN ASSELT AND DUDLEY WILLIAMS
Mendenhall Laboratory of Physics, Ohio State University, Columbus, Ohio
July 20, 1950

IN an earlier note[1] a report of studies of the infra-red absorption spectra of liquid nitrogen and liquid oxygen was given. These studies revealed the presence of a strong absorption band with center near 6.4μ in the spectrum of liquid oxygen and a strong band near 4.3μ in the spectrum of liquid nitrogen. These bands appear at positions where absorption would be expected if the fundamental vibrations of O_2 and N_2 were infra-red active. Several possible absorption mechanisms were suggested. After the presentation of, but prior to the publication of the earlier report, the note by Crawford *et al.*,[2] appeared; these authors gave an account of their work on O_2 and N_2 at high pressures and in the liquid state. They presented evidence that the bands at 4.3μ and 6.3μ are due to absorption by collision-induced dipoles.

Since the publication of our first note further studies of the spectra of liquid N_2 and O_2 have been made by another group at this university,[3] and we have studied the absorption of dry O_2 and CO_2-free N_2 in a vacuum prism-grating spectrograph. These gases were studied at a pressure of approximately one atmosphere. Although the early prism studies of Snow[4] indicated the presence of weak absorption bands in gaseous O_2 and N_2, we failed to observe any absorption that could be attributed to oxygen or nitrogen molecules. Careful studies with 7500 line/in. and 3600 line/in. gratings revealed no rotational lines for either gas when a path length of 5 meters of gas at a pressure of one atmosphere was employed. The only changes observed when O_2 and N_2 were introduced to the spectrograph was an enhancement of the residual H_2O and CO_2 lines still observed when the spectrograph was evacuated as thoroughly as possible. On the basis of a rough determination of molecular absorption coefficients from measurements of absorption by liquids, a strong absorption was expected for a path length of 5 m in the gases. The absence of *any* observable absorption by the gases indicates that the close proximity of neighboring molecules is a necessary condition for the absorption process. Hence, this result supports rough theoretical calculations which indicate that processes involving magnetic-dipole and electric-quadrupole radiation do not contribute appreciably to the absorption observed for the liquids. Positive elimination of these two possibilities leaves us with only absorption mechanisms involving polymers and collision-induced dipoles as possible absorption mechanisms. Although we have obtained no evidence which would entirely eliminate the possibility of polymer formation in the liquid state, the results of the Canadian group[2] indicate that the collision-induced dipoles are chiefly responsible for the observed effects and we have obtained no evidence that is in disagreement with this hypothesis.

[1] M. L. Oxholm and Dudley Williams, Phys. Rev. **76**, 151 (1949).
[2] Crawford, Welsh, and Locke, Phys. Rev. **75**, 1607 (1949).
[3] A. L. Smith, W. E. Keller, and H. L. Johnston, Phys. Rev. **79**, 728 (1950).
[4] C. P. Snow, Phil. Mag. **8**, 369 (1929).

Total Charges of Fission Fragments in Gaseous and Solid Media

N. O. LASSEN
Institute for Theoretical Physics, University of Copenhagen, Denmark
July 17, 1950

IN earlier experiments[1,2] the total charges of fission fragments emerging into vacuum from a uranium layer were determined by a measurement of the curvature of the paths described by the fragments in the magnetic field of the cyclotron. Recently further experiments have been carried out by means of a new deflection apparatus similar to the earlier one, but constructed in such a manner that the space between the uranium layer and the ionization chamber used for detection could be filled with a gas to any desired pressure. At not too high pressures the variation of the mean charge, e, and the velocity, v, along the path inside this deflection chamber can be neglected, and at the same time the pressure may be sufficiently high to ensure that equilibrium between capture and loss of electrons by the fragments will be established in the first few millimeters of the path, the entire length of which inside the deflection chamber is 200 mm. In this case the deflection will be proportional to the mean charge of the fragments in the gas considered. If the deflection chamber is evacuated, the deflections will be proportional to the charges of the fragments in the uranium layer, when the latter is uncovered. By covering it with a thin layer of another metal one obtains the charges in this metal. In the same way as earlier,[2] the charges were determined for each of the two groups separately.

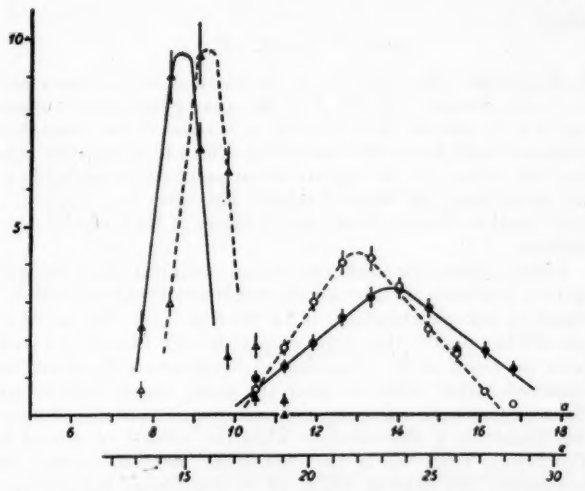

FIG. 1. Distribution of deflection of fission fragments. Abscissa: Deflection $a = \text{const.} \times e/mv$. Approximate scale of e below. Circles refer to fragments having traversed a thin Be layer and emerging into vacuum. Triangles refer to fragments emerging into argon at a pressure of 0.9 mm. White and black points correspond to the light and heavy fragments, respectively.

As an example Fig. 1 shows the result of two measurements, one giving the charges in beryllium, the other giving the charges in argon. Only small differences were found between the charges in various solid stopping media or between the charges in various gases, but, as is seen, the charges are much lower in gases than in solids. In gases the light fragment has the higher charge, opposite to what is the case in solids. This order of the charges is in agreement with previous determinations of the effective charges from ionization measurements.[3,4] The latter charges were somewhat higher than the values now obtained, but at least part of the difference may be accounted for as due to a dependence of the charge on pressure, see below. The difference between the widths of the distribution curves in gases and in solids gives an nteresting illustration of the fluctuation of the charges. With a gas at a sufficiently high pressure in the chamber many interchanges of charge occur along the path, and the deflection is determined merely by the mean value taken over the part of the range considered.

Figure 2 gives the most frequent deflections obtained for various pressures of argon in the chamber. As mentioned, the initial values of the deflections correspond to the most frequent charges

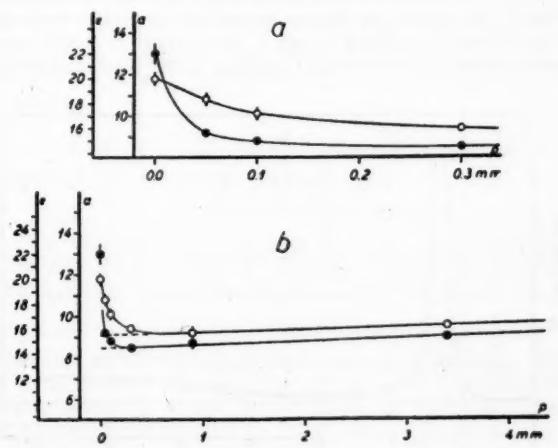

FIG. 2. Most frequent deflections of fission fragments *vs.* pressure of argon in the deflection chamber. Open and full circles refer to the light and heavy fragments, respectively.

in uranium, and the deflections for a pressure ~1 mm or argon correspond to the equilibrium charges in argon. The rate of decrease of the deflections for increasing pressure between 0 and 0.5 mm is determined by the rate with which the charges decrease due to capture of electrons. The cross sections estimated from the curves are in rough agreement with theory; they are of the order of magnitude 10^{-16} cm².

The curves are not horizontal for pressures above 1 mm. Since, as was shown by direct measurements, the charge varies in the beginning of the range very nearly proportional to the velocity, the increase of the deflection can only be caused by an increase of e with increasing pressure. The increase is rather small but safely outside the limits of error; it is found for both fragments in a number of gases investigated. An attempt has been made to follow the increase of the charges up to higher pressures. The rate of increase is found to be markedly smaller for $p > 10$ mm of argon. It is planned to examine the charges at much higher pressures.

The experiments reveal a marked difference between the mechanism of electron capture and loss in solid and gaseous materials. In particular, the dependence of the mean charge on gas pressure shows that excited states of the fragment ions with lifetimes comparable with intervals between successive collision play an essential part in the phenomenon. A theoretical treatment of electron capture and loss with special reference to these points will be given in a paper by N. Bohr and J. Lindhard to appear in the *Communications of the Danish Academy of Science*. Also, a detailed paper on the present experiments with a closer discussion of the observations will be published shortly.

[1] N. O. Lassen, Kgl. Danske Vid. Sels. Math.-fys. Medd. **23**, nr. 2 (1945).
[2] N. O. Lassen, Phys. Rev. **68**, 142 (1945).
[3] N. O. Lassen, Phys. Rev. **75**, 1762 (1949).
[4] N. O. Lassen, Kgl. Danske Vid. Sels. Math.-fys. Medd. **25**, nr. 11 (1949).

Improved Map of the Solar Spectrum between 9 and 10μ*

J. H. SHAW, R. M. CHAPMAN,† AND J. N. HOWARD
Mendenhall Laboratory of Physics, Ohio State University, Columbus, Ohio
July 24, 1950

DURING the mapping program of the infra-red solar spectrum being carried out at the Ohio State University the 9 to 10μ region has recently been investigated with a 3600-line/inches replica echelette grating and the apparatus described in a previous communication.[1] Figure 1 is a composite diagram of the best records so far obtained, the most prominent absorption in this region being a band of ozone, the center of which occurs near 9.58μ. Comparison with the solar spectrum taken by Adel[2] in this region shows that many lines have now been resolved into doublets.

A weak band of carbon dioxide near 9.4μ partially overlaps the ozone band and the frequencies of the rotational lines of the band have been measured in the laboratory by Barker and Adel.[3] Many of these lines have also been observed in the solar spectrum by Adel,[4] who found a maximum absorption of eight percent for the strongest lines in spectra taken in December, 1940 at Flagstaff, Arizona.

The observations taken at Columbus, Ohio, with a solar altitude of 60° show a maximum absorption of 20 percent for the strongest lines. Comparison of CO_2 lines in our solar spectrum, in regions where there are no other obscuring lines, with the laboratory data of Barker and Adel show a small (0.2 cm^{-1}) systematic difference in frequency. In Fig. 1 this difference has been added to the values of Barker and Adel and the frequencies thus obtained are indicated by arrows, the lengths of the arrows giving the relative intensities of the lines.

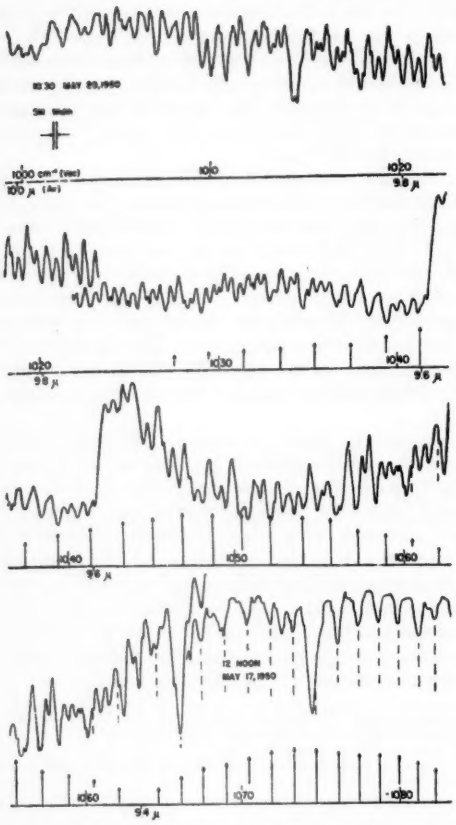

FIG. 1. The ozone band at 9.6μ in the solar spectrum.

It is not yet known whether other bands contribute to the absorption in this region or whether the structure, apart from the comparatively weak CO_2 lines, is entirely due to ozone.

* This work was supported in part by contract between the U. S. Air Force and the Ohio State University Research Foundation, through sponsorship of the Geophysical Research Directorate, Air Force Cambridge Research Laboratories, Air Materiel Command.

† Now at the A. F. Cambridge Research Laboratories, Cambridge, Massachusetts.

[1] R. M. Chapman and J. H. Shaw, Phys. Rev. **78**, 71 (1950).
[2] A. Adel, Astrophys. J. **94**, 451 (1941).
[3] E. F. Barker and A. Adel, Phys. Rev. **44**, 195 (1933).
[4] A. Adel, Astrophys. J. **94**, 379 (1941).

Neutron Scattering Resonances of Lithium*

ROBERT K. ADAIR†
University of Wisconsin, Madison, Wisconsin
July 21, 1950

IT has been noted that lithium, in contrast to most elements, scatters slow neutrons with a positive phase shift or a negative scattering length.[1] Since such behavior may be associated with the presence of a virtual level near threshold, it seemed interesting to search for such a level by measuring the total neutron cross section of lithium as a function of energy.

The cross section was determined in a manner similar to that described for sodium.[2] Measurements were made from 20 to 1400 kev with a neutron energy spread of about 20 kev. Elastic scattering is presumed to be the only process contributing appreciably to the cross section. The cross section near an isolated resonance for the scattering of neutrons with unit orbital angular momentum to form a compound state of spin J will then equal:

$$[(2J+1)/2(2I+1)](4\pi/k^2)\sin^2\delta_{lJ}$$

where

$$\delta_{lJ}=\tan^{-1}(\Gamma_{lJ}/E_r-E)+\varphi_l$$

is the neutron phase shift. Γ_{lJ} is the width of the resonance and E_r is the resonance energy. I is the spin of the target nucleus and k is the neutron wave number. φ_l is equal to the phase shift associated with hard sphere scattering. This will be equal to $-ka$ for $l=0$ where a is the nuclear radius and will be negligible in this experiment for higher l-values. The total cross section is then equal to the sum over l and J values of these partial cross sections.

Figure 1 shows the total cross section of lithium. Since the spin of Li^7 is $\frac{3}{2}$ of the peak cross section should equal $[(2J+1)/8]4\pi k^{-2}$ times the isotopic abundance of Li^7 (92.5 percent). The height of the 270-kev peak is then only compatible with $J=2$. If the peak were the result of the interaction of S-neutrons a dip should be observed, either before or after the peak, due to interference between resonance scattering and background scattering. Following Wigner[3] it is convenient to write the width Γ of a level as $\Gamma_l=2k\gamma^2T_l$ where T_l is the centrifugal potential barrier for l-neutrons. The reduced width, γ^2, is then energy independent. The width of the 270-kev level was measured to be 45 kev. If the resonance were caused by D neutrons the reduced width would be greater than $3\hbar^2/2ma$ where m is the mass of the neutron. This violates a completeness relation of Wigner.[3] These considerations lead us to attribute the peak to the interaction of P neutrons with Li^7 to form an excited state of Li^8 with spin 2. The reduced width of this level is then $(\Gamma/2k)[(ka)^2+1]/(ka)^2$, or $3.5\cdot10^{-13}$ Mev cm. Because of the centrifugal barrier for P-neutrons this level will have no effect on the low energy cross section.

This 270-kev resonance coincides with a peak in the $Li^6(n,\alpha)$ cross section.[4] It seems possible that some of the alpha-particles contributing to this peak are the result of the $Li^7(n,\gamma)Li^8$ reaction, where Li^8 decays with a half-life of 0.87 sec. to excited states of Be^8 which immediately break up into two alpha-particles.[5]

The rise in cross section to 1.6 barns at 1400 kev is explained as being mainly due to a broad elastic scattering resonance. The shape of a broad level is complicated by the variation of Γ and φ_l with energy as well as by the $1/E$ dependence of the cross section [Eq. (1)]. A qualitative fit to the experimental results could be obtained only by attributing the rise to the resonant interaction of S-neutrons to form a state of spin 2 in Li^8 at a neutron energy of about 1.15 Mev. Inelastic scattering to the 480-kev excited state of Li^7 would tend to reduce the observed cross section. The results are best fitted by assuming the inelastic scattering width is small. The width at resonance of this level was taken as 2.4 Mev, leading to a reduced width, $\Gamma/2k$ of $5.6\cdot10^{-13}$ Mev cm. Taking the binding energy[6] of a neutron to Li^7 as 2.03 Mev, these levels lie 2.27 and 3.03 Mev above the ground state.

The S-wave resonance will have a large influence on the scattering at low energies. In this connection it is convenient to speak of the coherent scattering length l, the average of $-\delta/k$, over isotopes and spin orientations. Using Eq. (2) for δ and neglecting

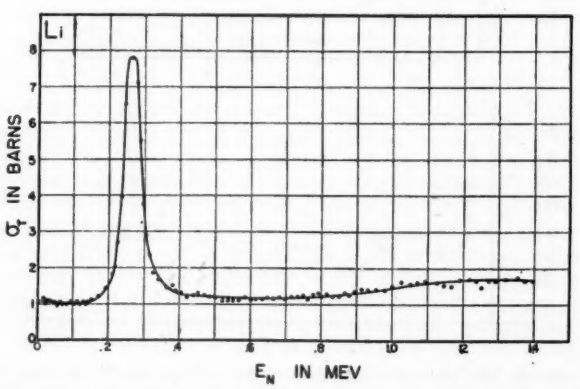

FIG. 1. Total neutron cross section of lithium as a function of neutron energy.

the contribution of Li^6, the scattering length of lithium at zero energy equals $\frac{1}{2}(a-\gamma^2/E_r)$, or $-0.7\cdot10^{-13}$ cm which is numerically of only qualitative significance because of the uncertainty in estimating the parameters γ^2 and E_r and the approximation involved in using the single level resonance theory.

* This work was supported by the AEC and by the Wisconsin Alumni Research Foundation.
† AEC Predoctoral Fellow.
[1] E. Fermi and L. Marshall, Phys. Rev. 71, 666 (1947).
[2] Adair, Barschall, Bockelman, and Sala, Phys. Rev. 75, 1124 (1949).
[3] E. P. Wigner, Am. J. Phys. 17, 99 (1949).
[4] J. M. Blair *et al.*, quoted by Goldsmith, Ibser, and Feld, Rev. Mod. Phys. 19, 259 (1947).
[5] W. F. Hornyak and T. Lauritsen, Phys. Rev. 77, 160 (1950).
[6] Rumbaugh, Roberts, and Hafstad, Phys. Rev. 54, 657 (1938).

Nuclear Dipole Vibrations*

HELMUT STEINWEDEL AND J. HANS D. JENSEN
Institut für theoretische Physik, Universität Heidelberg, Germany
AND
PETER JENSEN
Physikalisches Institut, Universität Freiburg, Germany
July 10, 1950

RESONANCES recently observed by several authors[1] in (γ, x) processes at γ-energies $\hbar\omega\cong20$ Mev have been interpreted by Goldhaber and Teller[1] as dipole vibrations due to collective motion of all protons relative to all neutrons inside the nucleus. Goldhaber and Teller treated in detail a very simplified model assuming periodic displacement of a rigid proton sphere relative to a rigid neutron sphere. However it seemed worth while to discuss the more plausible model, mentioned only shortly by these authors, of an interpenetrating motion of the proton fluid with density $\rho_p(r,t)$, and neutron fluid with density $\rho_n(r,t)$, under the condition of constant total density $\rho_0=\rho_p+\rho_n$, and fixed nuclear radius $R=r_0A^{\frac{1}{3}}$. This model, besides representing a case of a peculiar hydrodynamics, does not require any arbitrary parameters.

The "symmetry-energy term" in the expression for the nuclear binding energy[2] per nucleon: $K\cdot(Z-N)^2/A^2$, with $K\cong20$ Mev, can be interpreted as $K\cdot(\rho_p-\rho_n)^2/\rho_0^2$ because of the short range of nuclear forces. By multiplication with ρ_0 we obtain an energy density:

$$\epsilon(\rho_p-\rho_n)=\rho_0\cdot K(\rho_r-\rho_n)^2/\rho_0^2=K\cdot(2\rho_p-\rho_0)^2/\rho_0, \tag{1}$$

which is a function only of the local density-difference. This term is to be inserted into the Lagrangian L of hydrodynamics,

$$L=\int dV\{M[\rho_p\dot{\phi}_p+\rho_n\dot{\phi}_n]-\tfrac{1}{2}M\rho_p(\mathrm{grad}\phi_p)^2 +\rho_n(\mathrm{grad}\phi_n)^2]-\epsilon(\rho_p-\rho_n)\} \tag{2}$$

with M the nucleonic mass. From $\delta\int Ldt=0$ follows Euler's equation for the relative velocity $\mathbf{v}=(\mathbf{v}_p-\mathbf{v}_n)=-(\mathrm{grad}\phi_p-\mathrm{grad}\phi_n)$:

$$M\dot{\mathbf{v}}/dt=-(\partial^2\epsilon/\partial\rho_p^2)\ \mathrm{grad}\rho_p=-(8K/\rho_0)\ \mathrm{grad}\rho_p, \tag{3}$$

together with the continuity equation

$$\dot{\rho}_n=-\dot{\rho}_p=\mathrm{div}\{(\rho_p\rho_n/\rho_0)\mathbf{v}\}. \tag{4}$$

In the customary way we have linearized the equations by omitting quadratic terms in v, $\mathrm{grad}\rho_p$, and $\dot{\rho}_p$. The velocity of propagation of relative density disturbances turns out to be

$$u=[(ZN/A^2)8K/M]^{\frac{1}{2}}\cong c/5. \tag{5}$$

Combined with the boundary condition $v_r\equiv0$, implying $\partial\rho_p/\partial r\equiv0$, at $r=R$, Eqs. (3) and (4) have been solved by Lord Rayleigh.[3] Dipole vibrations of type $\rho_p=(Z/A)\rho_0+y(r)\cos\vartheta\cdot\exp(i\omega t)$ exist with lowest eigenfrequency

$$\hbar\omega_0=2.08\cdot\hbar u/R=(4ZN/A^2)^{\frac{1}{2}}\cdot60\cdot A^{-\frac{1}{3}}\ \text{(in Mev)}. \tag{6}$$

For comparison with experimental data see Fig. 1.

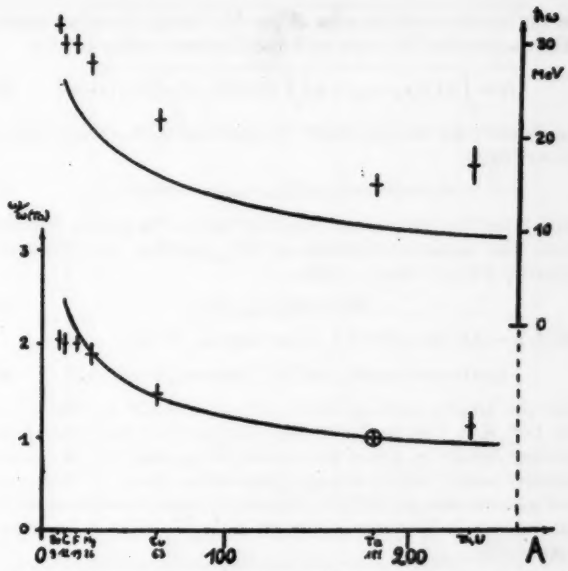

FIG. 1. Abscissa: atomic number; ordinate: resonance frequency for (γ, x). Upper curve: absolute values $\hbar\omega_0$ (in Mev); crosses experimental values. Lower curve: relative values, $\omega_0:\omega_0(\mathrm{Ta})$.

It is easy to include in the formalism the effects of radiative damping and of damping by dissipation of collective motion into disordered motion (heating by friction[1]) followed by nucleon emission. We introduce the radiation width Γ_r,

$$\hbar\Gamma_r/2mc^2=(2NZm/3AM)(e^2/\hbar c)(\hbar\omega/2mc^2)^2 \tag{7}$$

(m=electronic mass), the total width Γ which must be taken from experiments, and the phase angle φ between incident field strength and induced nuclear dipole moment, defined by $\mathrm{tg}\varphi=\Gamma\omega/(\omega^2-\omega_0^2)$. In this motion the total cross section σ is

$$\sigma=4\pi(e^2/2mc^2)^2(NZm/AM)(e^2/\hbar c)(2mc^2/\hbar\Gamma)\sin^2\varphi, \tag{8}$$

and the scattering cross section is $\sigma_r=\sigma\Gamma_r/\Gamma$. For the integrated total cross section we obtain:

$$(\hbar/2mc^2)\int\sigma d\omega=2\pi^2(e^2/2mc^2)^2\cdot(NZm/AM)(\hbar c/e^2) \tag{9}$$

which is one-half of the corresponding value given by Goldhaber and Teller for the rigid sphere model.

* See also: J. H. D. Jensen and P. Jensen, Zeits. f. Naturforsch. 5a, 343 (1950), and H. Steinwedel and J. H. D. Jensen, Zeits. f. Naturforsch. (to be published).
[1] M. Goldhaber and E. Teller, Phys. Rev. 74, 1048 (1948); R. D. Present, Phys. Rev. 77, 355 (1950); J. S. Levinger and H. A. Bethe, Phys. Rev. 78, 115 (1950).
[2] N. Bohr and J. A. Wheeler, Phys. Rev. 56, 426 (1939).
[3] Lord Rayleigh, *Theory of Sound* (The Macmillan Company, New York, 1894), second edition, Chapter 17.

Proton Density Variation in Nuclei

HELMUT STEINWEDEL AND MICHAEL DANOS
Institut für theoretische Physik, Universität Heidelberg, Germany
July 10, 1950

A VERY simple estimate of the variation of proton density ρ_p inside the nucleus is afforded by the assumption that the "symmetry-energy term" in the expression for the nuclear binding energy per nucleon:

$$K\cdot(Z-N)^2/A^2,\quad\text{with}\quad K\cong20\ \text{Mev},$$

should be understood as resulting from an energy density

$$\epsilon(\rho_p-\rho_n)=K\cdot(\rho_p-\rho_n)^2/\rho_0=K(2\rho_p-\rho_0)^2/\rho_0, \tag{1}$$

as proposed by Steinwedel, Jensen, and Jensen in the preceding letter. This assumption should be a good approximation at least

for the heavier nuclei because of the short range of nuclear forces. When combining this term with the Coulomb energy to give

$$H=\int dV\epsilon(\rho_p-\rho_n)+\tfrac{1}{2}e^2\int dVdV'\rho_p(\mathbf{r})\rho_n(\mathbf{r}')/|\mathbf{r}-\mathbf{r}'| \quad (2)$$

we obtain from $\delta H=0$, under the condition $\rho_p+\rho_n=\rho_0=3/4\pi r_0^3$ ($r_0=e^2/2mc^2$),

$$\partial\epsilon/\partial\rho_p=(4K/\rho_0)(2\rho_p-\rho_0)=-e\Psi_p(r), \quad (3)$$

$\Psi(r)$ being the electrostatic potential due to the proton distribution. The Laplacian derivate of (3), together with Poisson's equation $\Delta\Psi_p=-4\pi e\rho_p$, yields

$$(8K/4\pi e^2\rho_0)\Delta\rho_p=\rho_p. \quad (4)$$

With $\Lambda=(8K/4\pi e^2\rho_0)^{\frac{1}{2}}=7.3\cdot r_0$ the solution of (4) is

$$\rho_p(r)=\text{const.}\sinh(r/\Lambda)/(r/\Lambda)\cong\text{const.}\{1+\tfrac{1}{6}(r/\Lambda)^2\}. \quad (5)$$

For the density ratio $\rho_p(A^{\frac{1}{3}}r_0):\rho_p(0)=1+A^{\frac{1}{3}}/320$ we find:[1] 1.12 for U^{238}, resp. 1.08 for Xe^{130}, resp. 1.04 for Ca^{48}. Variation of the nuclear density ρ_0 inside the nucleus (compressibility of nuclear matter) would slightly enlarge those ratios. However there does not seem to exist any reliable estimate of nuclear compressibility;[2] at any rate it is so small that the ratio (5) will not be altered appreciably.

[1] For detailed discussion see: M. Danos and H. Steinwedel, Sitzber. Heidelberg. Akad. Wiss. Math. natur. Klasse (to be published).
[2] Compare E. Feenberg, Rev. Mod. Phys. 19, 239 (1947).

The Acceleration of Dust Grains by Supernovae

BERTRAM WOLFE, P. MC.R. ROUTLY,* A. S. WIGHTMAN, AND L. SPITZER, JR.
Princeton University, Princeton, New Jersey
July 20, 1950

IT has been suggested by Spitzer[1] that the pressure of radiation from supernovae might accelerate dust grains in the galaxy and thus generate heavy cosmic-ray particles. The present letter reports an investigation of several effects which much reduce the maximum grain velocities, and which make it unlikely that this proposed process can in fact produce many of the observed heavy cosmic-ray particles.

Spitzer's paper made the following simplifying assumptions. (a) Radiation pressure on a spherical grain of radius b equals $\pi b^2/c$ times the radiative flux, where c is the speed of light. (b) The effect of the grain velocity on the acceleration is negligible. (c) The supernova luminosity L is constant with time after the outburst. (d) The absorptivity of the grain for the supernova radiation equals the grain's absorptivity in the infra-red.

With assumptions (a) to (c) a potential relative to infinity can be defined, giving for the potential energy V of a grain at an initial distance r_0 from the supernova

$$V=Lb^2/4cr_0. \quad (1)$$

We now examine the validity of these assumptions.

(1) Assumption (a) should be correct to within a factor[2] of about 2 provided that $2\pi b$ is not less than the wave-length of maximum radiative flux from the supernova, and provided also that the index of refraction of the grain for supernova radiation is not close to unity. In any case, assumption (a) will not greatly underestimate the radiation pressure.

(2) The acceleration of a grain at high velocity is diminished by the reduction in the incident photon flux, the Doppler shift of the photons, and the relativistic increase of the grain's mass. When these effects are taken into account, but assumptions (a) and (c) retained, the limiting kinetic energy, T, in units of its rest mass, for a grain which started from rest at a distance r_0 from the supernova is given by

$$T+2T^2+\tfrac{8}{3}T^3+\tfrac{8}{3}(T^3+2T)^{\frac{1}{2}}=Lb^2/4c^3mr_0; \quad (2)$$

m is the rest mass of the grain. The energy found from Eq. (2) is plotted in Fig. 1; the dashed line represents Eq. (1). For an energy E of 1 Bev per nucleon the value of Lb^2/r_0 found from (2) is seven times as great as that found from (1).

(3) The radiation curve of the supernova in all frequencies may, in the absence of definite information, be taken as the observed curve[3] for photographic radiation. If r_0 is sufficiently great, v is determined by direct integration of $L(t)$, neglecting the change in r. Numerical integration of the equation of motion and graphical interpolation were used to find v in intermediate cases. Results are given in Table I for a supernova effective temperature of 10^{5}°K, about the highest value now contemplated,[4] for a corresponding[4] value of 2×10^{43} ergs/sec. for L and for a grain radius of 5×10^{-7} cm, which is about the smallest value for which assumption (a) is valid and which yields the greatest velocity. The grain mass m has been computed for a density of 4.5 g/cm³.

TABLE I. Energies attained by grains near supernova (dependence of acceleration on velocity neglected).

γ	r_0(cm)	E(Bev/nucleon)
0.01	1.35×10^{16}	1.15
1.0	1.35×10^{17}	1.66×10^{-3}
100	1.35×10^{18}	1.38×10^{-7}

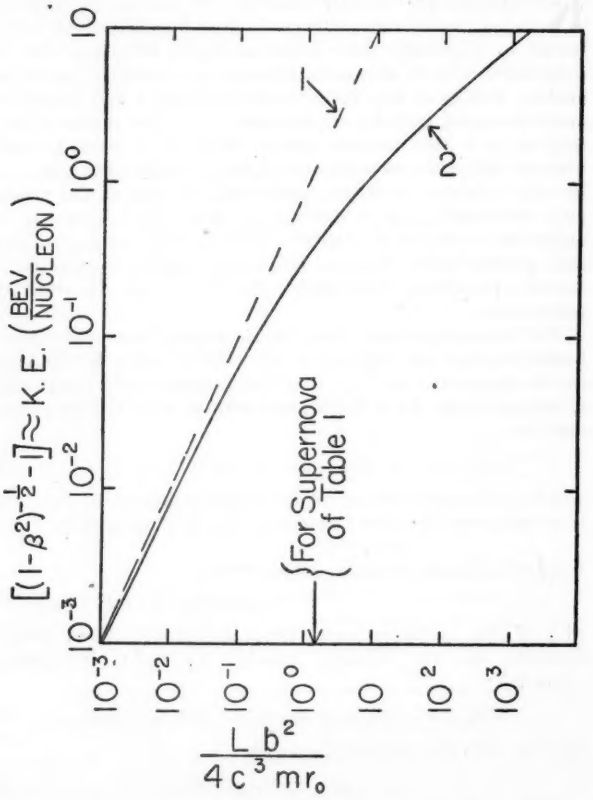

FIG. 1. Kinetic energy of the grain under assumption (c) (constant supernova radiation): curve 1 with neglect of velocity effects—see Eq. (1); curve 2 with full account of velocity effects—see Eq. (2); L is the supernova luminosity, b the radius and m the mass of the dust grain, c the velocity of light, and r_0 the initial distance of the grain from the supernova.

(4) The temperature of the grain is determined not only by the amount of radiation present but also by the absorptivities of the grain in the far ultraviolet, where the supernova radiates, and in the infra-red, where the grain radiates. Information on these absorptivities is lacking, and the results in Table I have been computed for three different values of γ, the ratio of absorptivities in the ultraviolet and infra-red, respectively. The value of r_0 is

then found on the condition that the grain temperature is at most 1000°K.

To obtain more precise results one must correct assumptions (b) and (c) simultaneously. This is necessary only for low values of γ, since only then do the grains acquire sufficient energy to make velocity corrections to the force important. We have merely obtained an upper bound: for the extremely low value $\gamma=0.01$, the final kinetic energy, T, <300 Mev/nucleon. Even this bound is probably too high; a low value of γ is likely to be accompanied by an index of refraction very near unity in the ultraviolet, which would modify assumption (a) and reduce the energy attained. Moreover, the low value of r_0 associated with a low γ decreases the volume in which grains are accelerated, and would make it more difficult, on the basis of the proposed mechanism, to account for the observed flux of the cosmic-ray particles.

* Special Scholar of the Canadian National Research Council.
[1] L. Spitzer, Jr., Phys. Rev. **74**, 583 (1950).
[2] H. C. van de Hulst, *Optics of Spherical Particles* (J. F. Dunwaer and Zonen, Amsterdam, 1946).
[3] An average curve for supernovae of Type 1 was constructed from data supplied informally by R. Minkowski.
[4] F. L. Whipple, Proc. Am. Phil. Soc. **81**, 253 (1939).

Superconductivity of Columbium Nitride

D. B. Cook, M. W. Zemansky,* and H. A. Boorse†
Pupin Physics Laboratories, Columbia University,‡ New York, New York
July 20, 1950

A RECENT investigation of the superconducting properties of columbium[1] included the nitriding of columbium powder and the observation of superconducting transitions of the nitride. Thin ribbons of columbium had been nitrided by Andrews and co-workers[2] and had been observed in zero-field transitions near 15°K. It is the purpose of this note to report on magnetic field transitions of columbium nitride from the superconducting to the normal state over a range from zero to 10,000 oersteds. It was decided to investigate powder specimens in view of the difficulty of interpreting magnetic field data on ribbons, and because nitrided films on columbium cylinders tend to flake off. Fine wires were also found to be unsuitable since they disintegrated after being nitrided.

The powder of 200-mesh particle size was nitrided in prefired Alundum boats in an Alundum combustion tube which was first evacuated and then filled with an atmosphere of Airco "prepurified" nitrogen. An annular, molybdenum-wound hydrogen furnace was used to provide high temperatures which were measured with the aid of a Leeds and Northrup optical pyrometer.

Two batches of nitrided powder were prepared: the first (A) in 1 atmos. of nitrogen at 1300°C for 3 hr., the second (B) in 1.6 atmos. of nitrogen at 1450°C for 5 hr. By measuring the gain in weight, powder A was found to contain a nitrogen content of 12.8 percent; powder B, 11.1 percent. Samples of each batch were studied by an x-ray diffraction camera and the cubic NaCl structure, observed by other investigators, was verified. We are indebted to Mr. J. K. Roros of the Metallurgy Department of Columbia University for making the x-ray analysis.

The powder samples were sealed into glass tubes filled with helium at a low pressure. Thermal conduction to the cryostat[1] was provided by a copper rod sealed through the glass. Two capsule shapes were used, cylindrical and spherical, both of 10 mm i.d., the cylinder being 16 mm long. Smaller cylinders of inside diameter 3 mm and inside length 20 mm were also used in survey experiments.

The two batches of columbium nitride powder gave similar results on a large number of zero-field transition tests. The half-value of the transition occurred at 15.2°K for material A, and at 15.0°K for material B. The transitions from the normal to the superconducting state began at 16.2°K and ended at 13.5°K for sample A and at 12.2°K for sample B. Powder A, with a somewhat narrower zero-field transition, gave more interpretable results in a transverse magnetic field than did B.

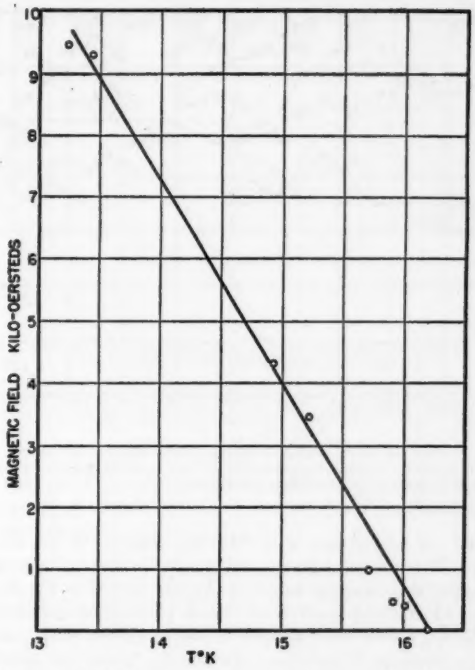

FIG. 1. Magnetic fields necessary to restore the normal state in CbN.

The $H-T$ curve for A is shown in Fig. 1, where the temperature T_0 corresponding to $H=0$ is taken as 16.2°K rather than 15.2°K, the half-value temperature. The slope of this curve was very close to 3300 oersteds/deg. Similar experiments for powder B gave inconclusive results at temperatures lower than 14.8°K, and the indicated dH/dT appeared to be of the order of 6000 oersteds/deg.

* The City College of New York.
† Barnard College, Columbia University.
‡ Assisted by the ONR.
[1] Cook, Zemansky, and Boorse, Phys. Rev. (to be published).
[2] Andrews, Milton, and De Sorbo, J. Opt. Soc. Am. **36**, 518 (1946).

Nuclear Isomerism and Shell Structure

R. D. Hill
Physics Department, University of Illinois, Urbana, Illinois*
July 26, 1950

THAT nuclear isomers occur preponderantly in regions of "magic" nucleon numbers has been cited as evidence for theories of nuclear shell structure.[1] The following note is concerned mainly with the examination of experimental isomeric data for level trends as a function of nuclear structure.

A table of known isomers arranged in ascending order of odd nucleon number shows, apart from the well-known[2] fact that the odd Z-even N and even Z-odd N types are concentrated at the ends of the fourth (N or $Z=50$) and fifth (N or $Z=82$) nuclear shells, that the only isomers occurring at the beginnings of the shells are of the odd Z-odd N type. Since, according to Mayer's[3] theory of shell structure, levels of sufficiently high angular momentum differences also occur at the beginnings of shells, it is not unlikely that isomers should exist there. But in order to explain the presence of odd Z-odd N types only, it might be necessary to postulate stronger odd proton-odd neutron coupling in a newly developing shell.

The most favorable data for studying level trends are located at the end of the fifth shell for even Z-odd N isomers. The transitions here are of multipole order (Λ) equal to five, followed in a number of cases by $\Lambda=2$ transitions. The levels involved will be

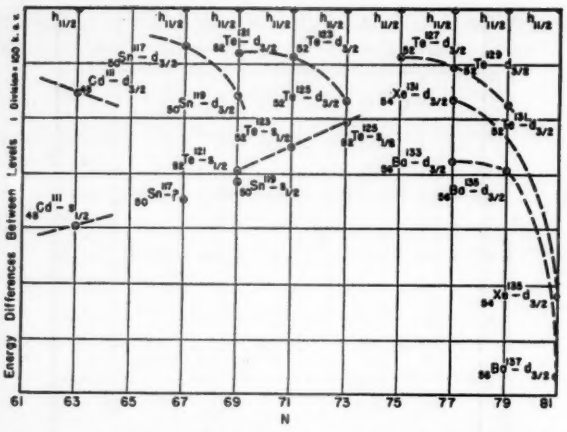

FIG. 1. Plot of level positions against odd neutron numbers for the even-odd isomers of the fifth nuclear shell. Only isomers exhibiting internally converted gamma-ray transitions are shown.

assumed, in accordance with Mayer's theory, to be $h_{11/2}$, $d_{3/2}$, and $s_{1/2}$. The observed energy differences between the levels as a function of odd neutron numbers, N, are plotted in Fig. 1. There appear to be definite level trends which are summarized as follows: (1) The $s_{1/2}$ levels, for constant Z, rise in energy with respect to the $h_{11/2}$ levels as N increases. (2) The $d_{3/2}$ levels, for constant Z, fall in energy with respect to the $h_{11/2}$ levels as N increases. The energy separations, for $81 \geqslant N \geqslant 75$, appear, very roughly, to vary inversely as $(82-N)$. (3) There is a step-like discontinuity in the $d_{3/2}$ level trend where the $d_{3/2}$ and $s_{1/2}$ levels cross. (4) For $81 \geqslant N \geqslant 75$, and constant N, the separations between $h_{11/2}$ and $d_{3/2}$ levels increase with Z.

In their analysis of nuclear shell structure, Feenberg and Hammack have considered the movement of nuclear energy levels. Following Elsasser they postulated that levels of comparatively low angular momenta, with nodes inside the nucleus,

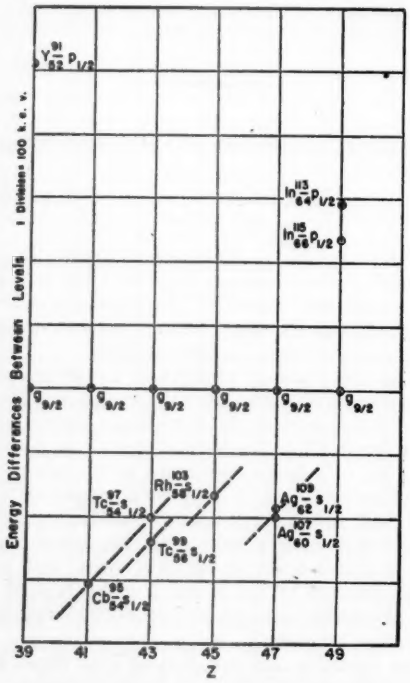

FIG. 2. Plot of level positions against odd proton numbers for the known odd-even isomers of the fourth nuclear shell. Only isomers exhibiting internally converted gamma-ray transitions are shown.

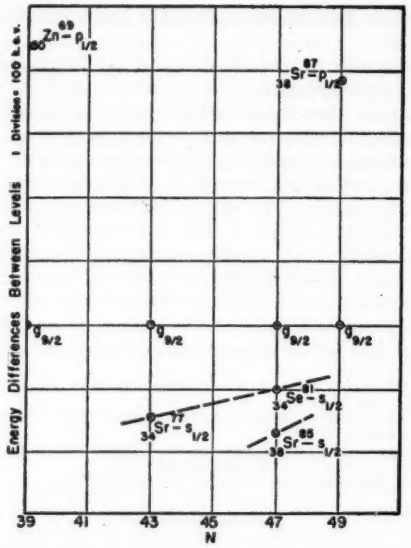

FIG. 3. Plot of level positions against odd neutron numbers for known even-odd isomers of the fourth nuclear shell. Only isomers exhibiting internally converted gamma-ray transitions are shown.

move to higher energy values as high angular momentum nucleons are added to form heavier nuclei. That the levels do move is supported by the experimental evidence of Fig. 1, but the level trends are not entirely in agreement with the predicted behavior. It would appear that, whereas the $s_{1/2}$ levels move correctly upward, the $d_{3/2}$ levels move downward with increasing addition of $h_{11/2}$ neutrons. Moreover, if the step-like displacement of the $d_{3/2}$ level is due to the filling of the $s_{1/2}$ level, the movement should be downward instead of upward.

At the end of the fourth nuclear shell the available data are still fragmentary. In this region there is also the confusion[2] between the $\Lambda=5$ and $\Lambda=4$ transitions. A value of $\Lambda=5$ is consistent on Mayer's theory with transitions between the $p_{1/2}$ and $g_{9/2}$ levels, but in order to explain the $\Lambda=4$ transitions as well it seems necessary to accept a level arrangement such as Feenberg and Hammack's in which transitions between $g_{9/2}$ and $s_{1/2}$ levels may also occur. It is probable that the $\Lambda=5$ transition is associated with the ground-state spin of 9/2 and the $\Lambda=4$ transition with a spin of 1/2.

The energy differences between $g_{9/2}$ and $p_{1/2}$, and between $g_{9/2}$ and $s_{1/2}$ levels are plotted against values of Z and N, respectively, in Figs. 2 and 3. Lacking complete information, especially about the spins of the ground states, these plots are somewhat arbitrary but follow, nevertheless, the accepted multipole order values. Although the evidence from these plots is meager, it does support an upward trend of the $s_{1/2}$ levels with respect to the $g_{9/2}$. This is in agreement with the central elevation theory of nuclear potential wells and with the trend already observed in the fifth shell for $s_{1/2}$ levels.

* Research program sponsored in part by joint ONR and AEC contracts.

[1] E. Feenberg, Phys. Rev. **75**, 320 (1949); E. Feenberg and K. C. Hammack, Phys. Rev. **75**, 1877 (1949); L. W. Nordheim, Phys. Rev. **75**, 1894 (1949).

[2] E. Feenberg, Phys. Rev. **77**, 771 (1950); M. G. Mayer, Phys. Rev. **78**, 16 (1950).

Scattering of Protons by Carbon*

W. D. WHITEHEAD†
University of Virginia, Charlottesville, Virginia
July 18, 1950

THE angular dependence of the ratio of the elastic proton scattering cross section for carbon to the classical scattering cross section has been determined at 2.0, 2.25, 2.50, and 2.75 Mev using the pressurized Van de Graaff generator at the Department

of Terrestrial Magnetism. The protons scattered from a thin carbon target on a silver leaf backing were counted with an argon-filled proportional counter biased to count only those protons near the end of their range. The ratio of the number scattered by carbon to the number scattered by silver determined the ratio of the cross sections except for a constant multiplying factor due to the difference in the number of carbon nuclei and silver nuclei. Since the ratio of cross sections was determined the target thicknesses were not determined, but both targets were thin; and since both targets were bombarded at the same time the geometrical factors cancel. The protons scattered from the two different nuclei can be resolved because of the difference of the recoil energy of the nuclei.

Number *vs.* range curves were determined at 55°, 90°, 132.5°, and 160° in the laboratory system for bombarding energies of 2.5 and 2.75 Mev and at 90°, 132.5°, and 160° for energies of 2.0 and 2.25 Mev (Fig. 1). The area under a peak minus a fixed area determined by the channel width of the detecting system, which is a function of the effective counter and depth and the bias of the system, is proportional to the intensity. The channel width is defined here as the intercept of the curve of *widths of the proton peaks at half-maximum vs. range in air* at zero range. The slope of this curve is very nearly the slope of the range straggling curve computed for widths at half-maximum.[1] The area under the peaks was measured with a planimeter; several independent measurements were made for each area and the ratio of the average values was used.

The half-widths due to straggling and channel width were assumed to add as the sum of the squares then the ratio of areas was corrected for channel width by multiplying by

$$[(\sigma_{\text{obs}}^2-\sigma_{\text{ch}}^2/\sigma_{\text{obs}}^2)_C{}^{\frac{1}{2}}(\sigma_{\text{obs}}^2/\sigma_{\text{obs}}^2-\sigma_{\text{ch}}^2)_{\text{Ag}}{}^{\frac{1}{2}}]$$

where σ_{obs} is the observed width at half-maximum and σ_{ch} is the channel width. The ratio of the areas was also transformed to the carbon center-of-mass system, assuming that the silver scattering is classical.

The corrected area ratios *vs.* angle in the carbon center-of-mass system are shown in Fig. 2. The dotted line is[2] $R(\phi)$ at 2.5 Mev for S-wave scattering, with δ_0 at 125° as determined by Heitler[2] *et al.*, normalized to 0.1 at 60°. The error of ±10 percent consists principally of the statistical counting errors, errors in area measurement, and errors in measuring the widths at half-maximum. Except for the 2.0-Mev curve the curves all show a definite tendency to decrease at the larger angles and this probably means that the P wave is becoming effective. More precise curves are necessary if the P-wave and S-wave components are to be determined accurately.

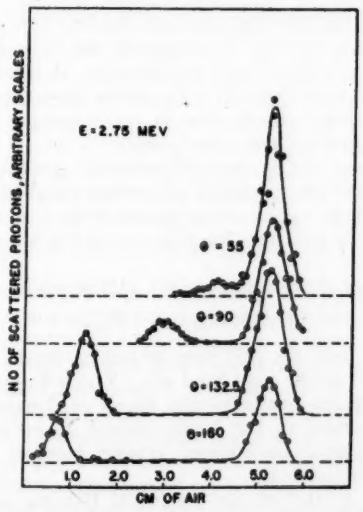

FIG. 1. Family of number *vs.* range curves for different angles for a thin carbon target on a silver leaf backing at 2.75 Mev. The long-range group is due to silver and the large scale has been shifted so that this group has the same range at all angles. The number scales are different for each angle so that the curves can be plotted on the same graph.

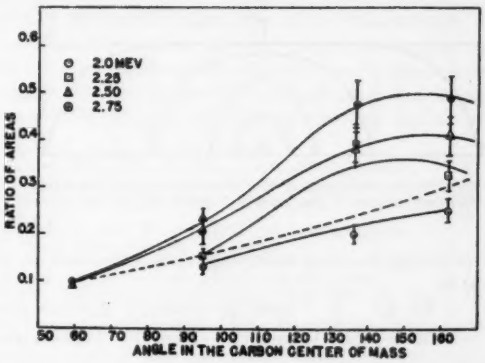

FIG. 2. The ratio S of the areas under the peaks *vs.* angle in the carbon center-of-mass system. Dotted line is $R(\phi)$ for $\delta_0=125°$ at 2.5 Mev. See reference 2.

* Work done as AEC Predoctoral Fellow, 1948–49.
† Now at Bartol Research Foundation, Swarthmore, Pennsylvania.
[1] M. S. Livingston and H. Bethe, Rev. Mod. Phys. 9, 285 (1937).
[2] Heitler, May, and Powell, Proc. Roy. Soc. 190, 180 (1947).

Note on the Hall Potential Across an Inhomogeneous Conductor

J. VOLGER
Philips Research Laboratories, N. V. Philips' Gloeilampenfabrieken, Eindhoven, Netherlands
March 27, 1950

IT seems that no formula has been given yet for the Hall potential as a function of the positional coordinates within a conductor of given shape. This can easily be done, however, with the help of potential theory, in the following case (which also may be of interest with respect to inhomogeneous conductors).

Let us consider a thin plate of *homogeneous* conducting material, perpendicular to B, the magnetic induction in the y direction. The relations between the components of E and i are:

$$E_x/\rho=(A_H\cdot B/\rho)i_z+i_x \quad \text{and} \quad E_z/\rho=i_z-(A_H\cdot B/\rho)i_x,$$

where ρ is the resistivity of the material and A_H its Hall coefficient. The y-components of E and i are ignored. We know E to be the negative gradient of a potential function φ, which must obey the Laplace equation $\Delta\varphi=0$. We assume that the solution of this equation can be written as a power series in A_HB/ρ, the zero-order term of course being the potential for $B=0$. The first-order term, which we shall call φ_{Hall} is obtained as a solution of the Laplace equation under the following conditions.

We suppose the plate to have the usual *rectangular* form, with current electrodes along two opposite sides ($x=0$ and $x=l$) and Hall probes facing each other somewhere along the other two sides ($z=-\frac{1}{2}b$ and $z=+\frac{1}{2}b$). Furthermore, we suppose the electrodes to be made of fairly well-conducting material, as is generally used, and we ignore the Hall effect in it. Then φ_{Hall} must be approximately zero along $x=0$ and $x=l$, respectively, and therefore the current must have a z-component there. We further assume, however, that in our sample the ratio A_HB/ρ is very small and hence that the current still flows sufficiently homogeneously in the x direction, so that along $z=-\frac{1}{2}b$ and $z=+\frac{1}{2}b$ we have $\partial\varphi_{\text{Hall}}/\partial z=A_HJB/bd$, in which J is the total current through the sample, d its thickness in the y direction. $\partial\varphi_{\text{Hall}}/\partial z$, abruptly becoming zero at the edges, can be developed in a Fourier series in the usual way.

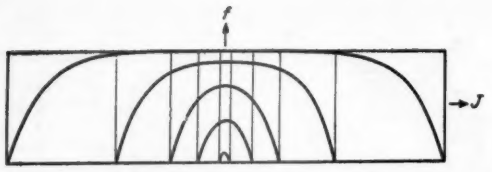

FIG. 1. f-values as a function of the position of the Hall sondes for some different shapes of the sample ("ideal" current electrodes).

The potential function satisfying these conditions is readily found to be

$$\varphi_{\text{Hall}}=A_H\frac{BJ}{d}\cdot\frac{4}{\pi}\sum_1^\infty\frac{1}{(2k-1)}\frac{\sinh[(2k-1)\pi z/l]}{\cosh[(2k-1)\pi b/2l]}\cdot\frac{\sin[(2k-1)\pi x/l]}{[(2k-1)\pi b/l]}.$$

The Hall potential between the probes A and B (on $z=+\frac{1}{2}b$ and $z=-\frac{1}{2}b$, respectively) is:

$$(A)\quad(B)$$
$$\varphi_{\text{Hall}}-\varphi_{\text{Hall}}=V_{\text{Hall}}=A_H(BJ/d)f(b/l,\,x/b),$$

in which f depends on the ratio of the length to the width of the sample and of the position of the probes along its sides. Some values of f are given in Table I. These results, which include

TABLE I. Values of the function $f(b/l,\,x/b)$.

x/l \ l/b	0.1	0.5	1.0	2.0	4.0	∞
00	0	0	0	0	0	0
0.125	0.04	0.20	0.39	0.62	0.83	1.00
0.250	0.06	0.30	0.56	0.82	0.98	1.00
0.500	0.075	0.37	0.68	0.94	1.00	1.00

those of Isenberg *et al.*[1] are plotted in Fig. 1. We determined experimentally the values of f for $x/l=0.5$, using samples with l/b values of about 0.5, 1, 2, and 8. We found them to be in agreement with the theory. When the problem of the Hall potential is treated in this way, no so-called "einge-prägte Kräfte" nor electrostatic charges are introduced, as was done by Isenberg. It is sufficient to consider the resistivity of the material as a tensor.

Thus no appreciable Hall potential can be built up in the sample if the current electrodes are placed close to each other. Perrier,[2] in suggesting such an arrangement, has not taken into account this fact and therefore his suggestion pointing to very high Hall voltages is incorrect.

This point of view may be of some importance for the study of *inhomogeneous conductors*. Let us consider a material consisting of highly conducting grains separated by thin layers of lower conductivity, and let the picture in Fig. 2 be a consistent model of this situation. The macroscopic resistivity is to a good approximation: $\bar{\rho}=\rho_1+(l_2/l_1)\rho_2$. The most interesting case occurs if the third term dominates the second. Let this be so. Then approximately $i_1:i_2=l_1:l_2$, where i_1 and i_2 are the *mean* values of the components of the current densities in the direction of J. Now we

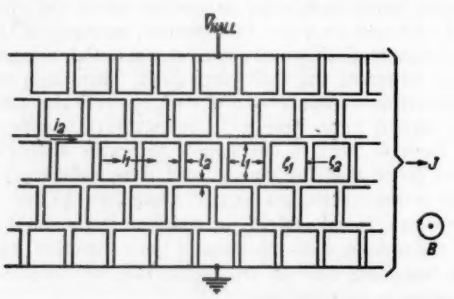

FIG. 2. A model for an inhomogeneous conductor.

have in each grain a Hall voltage of about $A_H^{(1)}l_1i_1B$ and in each longitudinal layer likewise $A_H^{(2)}l_2i_2B$, but in each perpendicular layer the Hall voltage cannot be higher than $0.75(l_2/l_1)A_H^{(2)}l_1i_1B$. We have used here the value of f for the middle of the layer and in the limit for small l_2, assuming that the conducting grains may be considered as electrodes for the layer, as was done above. We suppose $A_H^{(2)}>A_H^{(1)}$.

For the sample as a whole we obtain approximately (with c being of the order of magnitude unity):

$$\bar{A}_H=A_H^{(1)}+c(l_2/l_1)^2\cdot A_H^{(2)}.$$

Generally $\bar{A}_H$ will not be very different from $A_H^{(1)}$; $\bar{\rho}$ on the other hand can be much greater than ρ_1. This means that, if the Hall effect and the resistivity of such an inhomogeneous conductor is to be explained in terms of electron density and mobility, no conclusion as to the mobility either in the highly conducting grains or in the badly conducting layers may be drawn.

We have in fact found in some samples of semiconducting materials very low values of the mobility, which, however, could be explained in the manner given.

[1] Isenberg, Russell, and Greene, Rev. Sci. Inst. 19, 685 (1948).
[2] A. Perrier, Helv. Phys. Acta 19, 410 (1946).

The Thermodynamics of Liquid Helium of He^3—He^4 Solutions

O. K. RICE
Department of Chemistry, University of North Carolina, Chapel Hill, North Carolina
July 26, 1950

THE thermodynamics of liquid helium on the basis of the two-fluid theory of He II has been considered independently by Gorter[1] and the writer.[2] Though using different methods these treatments are in many respects similar. We differ, however, in one rather fundamental point. I assumed zero enthalpy of mixing of normal and superfluid, which allowed me to set the partial molal enthalpy of superfluid[3] $\bar{H}_{4s}$ equal to zero. I then obtained an approximate expression for the partial molal entropy $\bar{S}_{4s}$, which arises from an entropy of mixing of normal and superfluid, to be expected from the picture I developed in which the superfluid is separated from the normal fluid in ordinary space as well as momentum space.

On the other hand, Gorter based all his applications on Tisza's[4] assumption that the total molal entropy is equal to the molal entropy of normal fluid times its mole fraction. This is equivalent to $\bar{S}_{4s}=0$, or no entropy of mixing. On this basis $\bar{H}_{4s}$ must be finite; in fact, $-\bar{H}_{4s}/T$ will be given by an expression very similar to that found by me for $\bar{S}_{4s}$, and it plays much the same role in the theory, namely that of stabilizing the mixtures of normal and superfluid below the λ-point.

Either assumption is thermodynamically possible. We wish here to consider the possibility of distinguishing between them experimentally by means of the change of the λ-temperature T_λ with pressure or with mole fraction x_3 of He^3 in a mixture of the isotopes.

If $\bar{S}_{4s}=0$, we obtain instead of Eq. (25) of reference 2 (1949)

$$dp/dT_\lambda=S_\lambda/(V_\lambda-\bar{V}_{4n,\lambda}) \qquad (1)$$

which differs from Eq. (25) only by lacking the factor $r/(r+1)$ (roughly 0.85) on the right-hand side [$\bar{V}_{4n,\lambda}\equiv\bar{V}_{2,\lambda}$ of Eq. (25)]. This would upset the previously found good agreement with experiment somewhat, but hardly enough to be conclusive in view of the uncertainties involved. It offers, however, a possibility for future investigation.

The effect of He^3 on the λ-point of He^4 has recently been investigated theoretically[5-7] and experimentally.[8,9] Assuming $\bar{H}_{4s}=0$, and assuming that He^3 and normal He^4 form an ideal solution, with He^3 insoluble in superfluid,[10] Engel and Rice showed that

$$dT_\lambda/dx_3=-RT_\lambda^2/\bar{H}_{4n,\lambda}(1-x_3) \qquad (2)$$

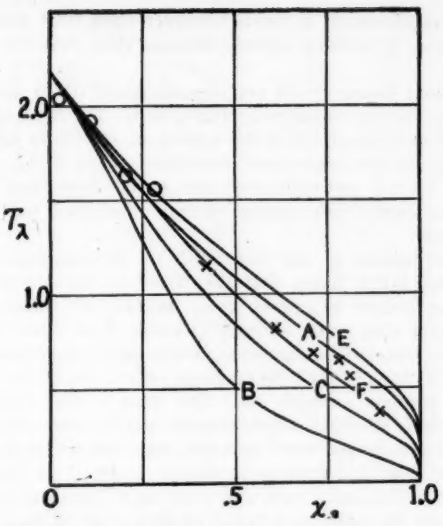

FIG. 1. Effect of He^3 on the λ-point of He^4 under various assumptions.

where it follows from $\bar{H}_{4s}=0$ that $\bar{H}_{4n,\lambda}=H_{4n}{}^0$, the latter being the enthalpy of *pure normal* He^4 at T_λ (metastable and unobtainable if $T\lambda<T\lambda_0$).

For the case $\bar{S}_{4s}=0$ we obtain

$$dT_\lambda/dx_3=-RT_\lambda/\bar{S}_{4n,\lambda}(1-x_3). \tag{3}$$

Since we assume always that $x_{4s}=0$ at T_λ for any given x_3 and that normal He^4 and He^3 form an ideal solution, $\bar{S}_{4n,\lambda}=S_{4n}{}^0-R\ln x_4$, where $x_4=1-x_3$, and Eq. (3) becomes

$$dT_\lambda/dx_4=RT_\lambda[x_4(S_{4n}{}^0-R\ln x_4)]^{-1}. \tag{4}$$

$S_{4n}{}^0$ like $H_{4n}{}^0$ cannot be measured below $T\lambda_0$. If we guess with Tisza that $S_{4n}{}^0=\text{constant}=S\lambda_0$, the integral of Eq. (4) is

$$RT\lambda\ln x_4=S\lambda_0(T\lambda-T\lambda_0). \tag{5}$$

This is identical with Eq. (34) of de Boer and Gorter[7] and curve B of Daunt and Heer.[9] The relationship between x_4 and $T\lambda$ is determined by $S\lambda_0$ and $T\lambda_0$, and is not clear to me how curve E of Daunt and Heer differs from curve B.

$S_{4n}{}^0$ is probably not exactly constant. If the specific heat is given by[6] $C_{p,4n}=aT$, so that $S_{4n}{}^0=S\lambda_0-a(T\lambda_0-T)$ we obtain

$$RT\lambda\ln x_4=S\lambda_0(T\lambda-T\lambda_0)+\tfrac{1}{2}a(T\lambda-T\lambda_0)^2. \tag{6}$$

This reduces to Eq. (5) if $a=0$.

In Fig. 1 we show curves calculated using $S\lambda_0=1.59$ cal. mole^{-1} deg.$^{-1}$ and $H\lambda_0=2.95$ cal. mole^{-1}. Of three curves for $\bar{H}_{4s}=0$, curve A has $H_{4n}{}^0$ and hence $S_{4n}{}^0$ constant ($a=0$), and curve C has $C_{p,4n}=aT$ with $a=0.725$ cal. mole^{-1} deg.$^{-2}$ (which makes $S_{4n}{}^0=0$ at 0°K); curve B has $C_{p,4n}$ constant for temperatures near $T\lambda_0$, then falling off to give $S_{4n}{}^0=0$ at 0°K. These are the curves of Engel and Rice[6] except for trivial differences in the parameters. Curves E and F are for $\bar{S}_{4s}=0$, with $a=0$ and 0.725, respectively.

The experimental points shown agree almost exactly with curve F. If it is believed that $S_{4n}{}^0$ should be zero at 0°K this might be supposed to be evidence in favor of taking $\bar{S}_{4s}=0$. The points are too close to curve A to allow much probability of $S_{4n}{}^0$ going to zero if $\bar{H}_{4s}=0$ is taken as the basis of the calculations, though perhaps it is not excluded. (Note the difference between curves B and C for both of which $S_{4n}{}^0$ goes to zero.) However, we have such a hazy idea of what normal He^4 should be like below the λ-point that we really cannot say whether its entropy should approach zero or not, and we have noted that Tisza assumed it to be constant. Furthermore, we must remember that the curves are based on the assumption that normal He^4 and He^3 form an ideal solution, which may not be strictly true. Therefore it appears that these data cannot help us to decide whether to take $\bar{H}_{4s}=0$ or $\bar{S}_{4s}=0$. However, extremely accurate measurements of dT_λ/dx_3 for very dilute solutions of He^3 might serve to resolve the question, for in this case all the quantities are known and there is a definite though small difference between Eqs. (2) and (3).

[1] C. J. Gorter, Physica **15**, 523 (1949).
[2] O. K. Rice, Phys. Rev. **76**, 1701 (1949); **78**, 182 (1950).
[3] Subscripts: $4n$ refers to normal He^4, $4s$ to superfluid, 3 to He^3; λ means "at the λ-point;" λ_0 "at the λ-point of pure He^4." In general, the notation as in reference 2.
[4] L. Tisza, Phys. Rev. **72**, 838 (1947), and earlier papers.
[5] J. W. Stout, Phys. Rev. **76**, 864 (1949).
[6] O. G. Engel and O. K. Rice, Phys. Rev. **78**, 55 (1950).
[7] J. de Boer and C. J. Gorter, Physica **16**, 225 (1950).
[8] Abraham, Weinstock, and Osborne, Phys. Rev. **76**, 864 (1949), see circles, Fig. 1.
[9] J. G. Daunt and C. V. Heer, Phys. Rev. **79**, 46 (1950), see crosses, Fig. 1.
[10] Taconis, Beenakker, Nier, and Aldrich, Physica **15**, 733 (1949).

A Mixed Shower of Nuclear Origin

M. S. SINHA*
Bose Research Institute, Calcutta, India
July 3, 1950

IT has been noticed recently by several investigators that showers containing both soft and penetrating particles are definitely produced. The origin of many of these showers is not electromagnetic, and has been attributed by Rossi[1] to some nuclear interaction by particles other than ordinary mesons. As an example of this kind of shower a photograph has been reproduced by Rossi (see Fig. 3d of reference 1) in which a shower is produced with two separate cones whose axes are inclined at an angle of about 20°.

We reproduce herewith (Fig. 1) a photograph of a shower in which the axes of the two cones emerging from a point in the third lead plate (thickness 1 cm) are separated by an angle of about 180°. This is most unusual and a shower of this type has not so far come to our notice. A burst produced in a gas, previously observed by the author,[2] contained particles emitted in all directions, but few in the upward direction.

A fourfold coincidence counter system, two above and two below the chamber triggered the expansion of the cloud chamber, which had 10 cm of Pb above it and a total of 4 cm inside. The experiment was being performed to record showers of nuclear origin, produced in the lead placed above the lead plates inside the chamber serving to distinguish between the nature of the particles constituting the shower. The shower in Fig. 1 could not

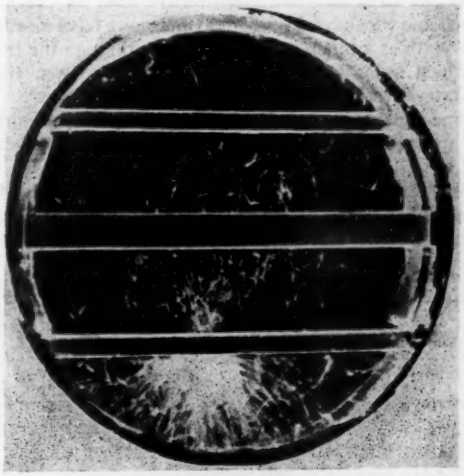

FIG. 1. Photograph of a mixed shower with two cones whose axes are separated by 180°.

be produced either by a primary soft particle or by the cascade process for the following reasons:

(1) Any highly energetic soft particle capable of producing so many (more than 200) particles would have surely multiplied long before in the thickness of lead of 13 cm that it had to cross before it reached the third lead plate inside the chamber.

(2) This high multiplication in such a short range (less than two radiation units) is almost impossible by the cascade process.

(3) A cone of a shower produced in a direction opposite to the direction of the incident particle is not possible in a cascade process.

The shower is therefore due to some explosive process which has taken place just inside the upper surface of the third lead plate. The production of particles in almost all directions and particularly a copious number in the upward direction indicates a time lag between the incidence of the initiating particle and the occurrence of the explosion.

The nature of the particles constituting the shower is difficult to determine. The occurrence of one or two heavy nuclei inside the downward cone cannot be detected. It is, however, clear that most of the particles emitted in the upward direction are soft and of low energies as they could not penetrate the second lead plate (thickness 2 cm). Among the particles emanated in the downward direction, there are some very straight and thin tracks which appear to be highly energetic and penetrating.

We believe this picture to be unmistakable evidence of the production of soft and penetrating particles in one act by the nuclear interaction of an incident particle with a lead nucleon. There are three particles entering the chamber from above; but none of these seem to be the originator of the shower and nothing can be said with certainty about the initiating particle except that it is definitely not electronic in nature.

The author is indebted to Dr. D. M. Bose for very helpful discussions on this photograph.

* Now at the Massachusetts Institute of Technology, Cambridge, Massachusetts.

[1] B. Rossi, Rev. Mod. Phys. 21, 104 (1949).
[2] M. S. Sinha, Phys. Rev. 64, 248 (1943).

Study of High Polymers by Nuclear Magnetism*
I. Line Widths at Room Temperature

L. V. HOLROYD, B. A. MROWCA, AND E. GUTH
University of Notre Dame, Notre Dame, Indiana
July 10, 1950

QUALITATIVE observations on nuclear magnetism in rubber-like high polymers have been reported by Alpert.[1] Recently, we have obtained quantitative data on the magnetic resonance line widths of various polymers. We have also followed the line width as a function of temperature through the transition range which separates the soft, rubbery state from the hard, glassy state. (See following Letter to the Editor.)

The line widths, in gauss, at room temperature, obtained in a field of approximately 7000 gauss at about 30 Mc, are shown in Table I.

The width of 0.19 gauss represents the line width due to magnetic field inhomogeneity, determined by obtaining the line width for a water sample. Both unvulcanized natural rubber and GR-S may have, therefore, a width narrower than 0.19 gauss. The GR-S signal is perhaps slightly broader than that for natural rubber.

TABLE I. Line widths.

Sample	Unvulcanized	Vulcanized	Carbon black loaded 30%	Carbon black loaded 50%
Natural rubber	≤0.19	≤0.19	≤0.19	
GR-S	≤0.19	0.27	0.57	0.67
Hycar OS-10	0.38	0.51	0.57	
Butyl rubber	0.38	0.42	0.91	
Polyethylene	0.57			
Plexiglas (at 103°C)	1.2			
S-polymer 30	1.5			
S-polymer 50	1.9			
S-polymer 75	5.8			

GR-S and Hycar OS-10 are approximately 70/30 and 50/50 butadiene styrene co-polymers respectively. The *S*-polymers 30, 50, GR-S and Hycar OS-10 are approximately 70/30 and 50/50 butadiene styrene co-polymers respectively. The *S*-polymers 30, 50, and 75 are isobutylene-styrene co-polymers, the number giving the approximate styrene content. Plexiglas is polymethylmetacrylate.

The narrowness of the line width for unvulcanized natural rubber and GR-S shows that the "free" rotation of molecules containing proton groups is about as fast in these rubbery materials as that of the protons in water. This "free" rotation must take place with a frequency much higher than that of the r-f field (30 Mc), so that the magnetic interaction of the "freely" rotating protons averages out. One expects that vulcanizing (cross linking of flexible long chains) and loading with carbon black will impede the "free" rotation, thus broadening the line as observed. One also expects increasing amounts of styrene to impede "free" rotation more and more, again broadening the line as observed in going from GR-S to Hycar OS-10 and from *S*-polymer 30 to 50 and 75. The large line widths for the *S*-polymers indicate that the "free" rotation is slowed down to a frequency comparable to that of the r-f field of 30 Mc. It seems that the method of nuclear magnetism is the first one to prove ***directly*** the existence of "free" rotation in polymers, a concept which was previously inferred ***indirectly*** from other phenomena and which forms the basis of the statistical network theory of rubber elasticity.

* Supported in part by the ONR.

[1] N. L. Alpert, Phys. Rev. 75, 398 (1949).

Study of High Polymers by Nuclear Magnetism*
II. Line Widths through Transition Temperatures

B. A. MROWCA, L. V. HOLROYD, AND E. GUTH
University of Notre Dame, Notre Dame, Indiana
July 10, 1950

THE polymers investigated (see preceding Letter to the Editor) exhibit in a certain temperature region a transition from the soft rubbery state to a hard, glassy state. The line width was found to increase with decreasing temperature through this transition region. For natural rubber this increase in line width was not large. However, the signal weakens so much as one approaches the transition region (−70°C) that accurate measurements of line width or shape are precluded. Since natural rubber is known to crystallize, it seems reasonable to attribute these results to crystallization or a related process which suppresses the rotation of molecular groups in a major fraction of the material. This would drastically broaden the contribution of these groups to the resonance line and correspondingly weaken it; the observed sharp resonance line would then be due to a relatively

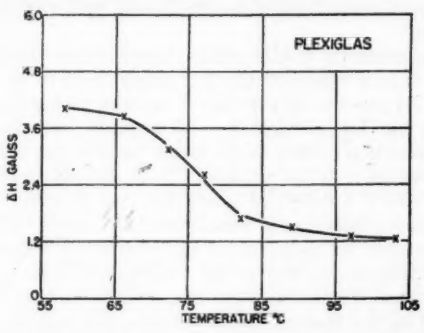

FIG. 1. Line width as a function of temperature for polymethylmetacrylate.

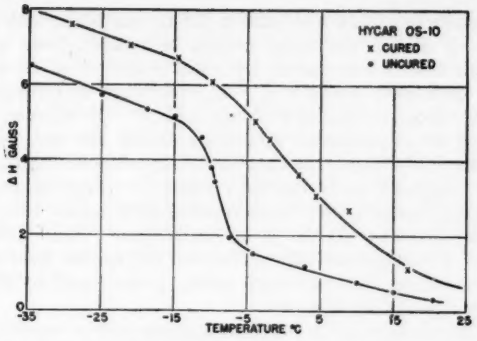

FIG. 2. Line width as a function of temperature for cured and uncured Hycar OS-10.

few groups with rotation still unhindered, and would be superposed on a broad "background" due to the rest of the groups. This interpretation is being checked experimentally. For Hycar OS-10 and Plexiglas, known not to crystallize, it was possible to study the line width as a function of the temperature through the transition region. The results are presented in Figs. 1 and 2.

The curve of Fig. 1 for the unvulcanized Hycar OS-10 shows a change in line width that is surprisingly sharp for a material so inhomogeneous and irregular.[1] It seems plausible to consider the change as a three-step process. As one lowers the temperature, the first step is an initial increase of the line width; it may be associated with a gradual decrease of the free volume of the molecules, which interferes with the relative motion of adjacent chain segments. The second step is a sudden increase in line width which suggests an abrupt cessation of some type of motion, presumably the rotation of molecular groups. The third step, a further gradual increase of the line width, may be connected with a gradual stopping of the sliding of adjacent segments past each other. Conversely, starting at low temperatures, "holes" must first be created for motion of the segments, before free rotation in the segments can set in.

The whole three-step transition must be due to short-range forces involving near neighbors only. The suddenness of the second step suggests that it is due to a cooperative effect, such as the formation of domains in which molecular rotations are impeded, but which are too small for detection by x-ray spot diagrams. One must expect an abrupt change in the elastic properties of the material to result from such a suppression of rotations. One must also expect that curing will interfere with group rotation, but even more with the formation of cooperative domains, just as it interferes with the crystallization of natural rubber. Thus one can understand the larger initial line width and the absence of abrupt changes in ΔH observed in cured Hycar OS-10.

The line-width transition for Plexiglas, shown in Fig. 2, is more gradual. The initial line width is considerably higher here than for unvulcanized Hycar OS-10. One would expect this from the polar character of Plexiglas. The broadness of the transition resembles that of the vulcanized Hycar OS-10. Not only is the "second step" in the transition broad, but the initial and final steps are quite gradual. Comparison of unvulcanized Hycar OS-10 and Plexiglas shows clearly that the transition is qualitatively the same for all long-chain polymers. Quantitatively, however, wide differences can occur. The second step for Hycar OS-10 may be a cooperative phenomenon while that for Plexiglas may be compatible with a non-cooperative transition.—The above interpretation of Figs. 1 and 2 is very tentative, and awaits checking by further experimental and theoretical work.

We are indebted to Professor H. M. James (Purdue University) for stimulating discussions on the interpretation of our results.

* Supported in part by the ONR.

[1] For transitions in simpler compounds, see N. L. Alpert, Phys. Rev. 75, 398 (1949); H. S. Gutowsky and G. E. Pake, J. Chem. Phys. 18, 162 (1950).

On the Nature of a Soldered Contact on a Semiconductor

JACQUES I. PANTCHECHNIKOFF
Radio Corporation of America, RCA Laboratories Division, Princeton, New Jersey

May 29, 1950

WHEN studying the rectifying properties of semiconductors, it is customary to neglect the behavior of the "non-rectifying contact" which consists of a large area soldered contact. Measurements[1] made on germanium crystals to which connections were made through two soldered contacts of considerably different area showed no rectification, thus clearly indicating that the lack of rectification is a property of the nature of the contact and not of its geometry.

The following experiment was performed to verify the assumption that the soldered contact is effectively a gradual transition from a metal to a semiconductor. Metal atoms diffuse into the semiconductor during soldering, their concentration being greatest near the surface through which they have diffused.

A small soldered region ($<10^{-4}$ cm²) on an N-type germanium crystal was etched repeatedly, removing electrolytically about 1000 atomic layers at a time. The purpose of this etch was to expose successively regions having a decreasing density of metallic impurities.

Forward and back currents were measured (at 1.5 volts) through a tungsten probe contacting each new surface at the same location and with an identical pressure. The ratio of forward to back currents was plotted on a logarithmic scale as a function of depth (Fig. 1). The resulting relation below a 100 to 1 rectification ratio agrees with the above assumption. Above 100, the experimental rectification ratio shows the fluctuation which is usually found when probing the surface of a germanium crystal.

The following interpretation attempts to explain a mechanism responsible for this result. When metallic atoms are introduced in a semiconductor, new energy levels, which were forbidden before the addition of metallic atoms, are made available locally. The number of new allowed energy states is proportional to the concentration of these metallic impurities. The presence of new allowed energy states effectively reduces locally the energy gap and brings the Fermi level closer to the filled band. Eventually, as the concentration of metallic atoms becomes large enough,

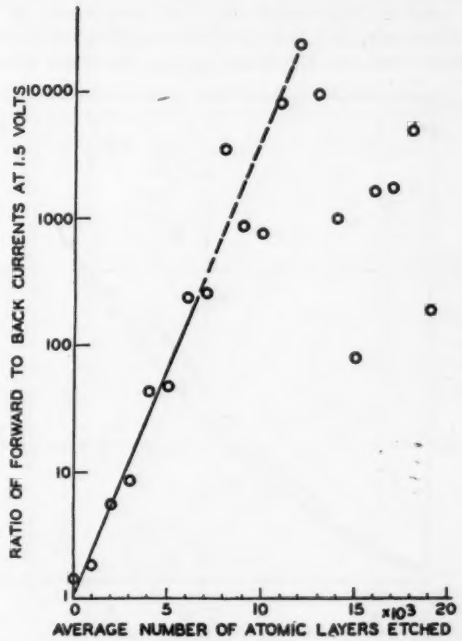

FIG. 1. Forward and back currents through a soldered region.

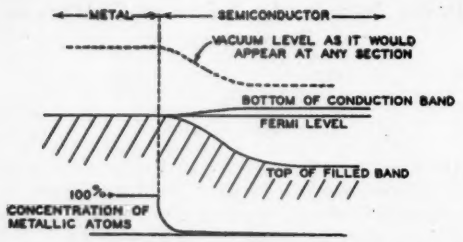

FIG. 2. Proposed energy level diagram at a contact.

the forbidden band shrinks out of existence and the Fermi level occupies the same position as in a metal, as is illustrated in Fig. 2. Since there is no thin barrier layer at such a metal-semiconductor transition, no rectification should be expected. According to Fig. 2, if some energy gap exists at the semiconductor surface, a rectifying barrier would be formed at the contact (vertical dashed line); the rectification should then depend on the barrier height.

Thus, a soldered contact to a semiconductor forms a smooth transition between a metal and the semiconductor. The energy gap in the latter may be shrunk in such a fashion that there is no barrier layer, so that rectification cannot take place.

I wish to thank Drs. D. O. North and A. Rose for their discussions and comments.

[1] H. B. Law, RCA Laboratories Division (unpublished).

Atomic Heat of Indium at Liquid Helium Temperatures

J. R. CLEMENT AND E. H. QUINNELL
Naval Research Laboratory, Washington, D. C.
July 26, 1950

THE atomic heat of indium has been measured in the normal and the superconducting states. For the superconducting state the data extend from 2.3°K through the transition, 3.368°K. The data obtained with the sample in a magnetic field of 250 gauss, sufficient to suppress superconductivity, extend from 1.7°K to 4.3°K. Figure 1 presents the unsmoothed data of two single experimental runs.

There exist no calorimetric data for comparison. However, Daunt, Horseman, and Mendelssohn[1] and Misener[2] have calculated values of ΔC, the difference between the atomic heat in the superconducting state and that in the normal state, and γ, the coefficient of the electronic specific heat term, from critical magnetic field measurements. Preliminary analysis of our calotimetric data gives $\gamma = 4.0 \times 10^{-4}$ cal./mole/deg.[2] as compared to 3.5×10^{-4} found by Daunt *et al.* and 3.6×10^{-4} by Misener.

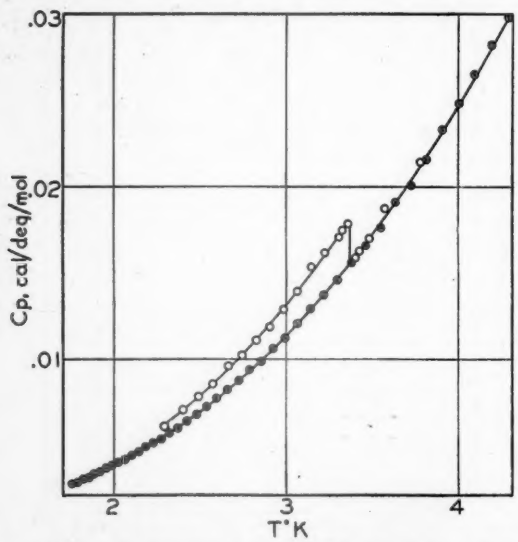

FIG. 1. Atomic heat of normal and superconducting indium. ⊙: Specimen in an applied magnetic field of 250 gauss. ○: No applied magnetic field.

Owing to experimental difficulties during the run with no magnetic field present, the data in the superconducting state are not so conclusive as is desirable. Tentative values of ΔC were calculated, however, and found to be slightly higher than those obtained by either Daunt *et al.* or Misener. These data also indicate a temperature dependence for the specific heat of the superconducting electrons more nearly proportional to T^3 than to T^4 as reported by Misener.

Additional data and a complete analysis will be reported in a forthcoming article.

[1] Daunt, Horseman, and Mendelssohn, Phil. Mag. **27**, 754 (1939).
[2] A. D. Misener, Proc. Roy. Soc. **174**, 262 (1940).

The Thermoelectromotive Force of Tin at the Superconducting-Normal Junction

R. T. WEBBER AND M. C. STEELE
Naval Research Laboratory, Washington, D. C.
July 21, 1950

MEASUREMENTS recently published by Steele[1] of the thermoelectromotive forces existing in tin at the superconducting-normal junction were in strong disagreement with the values previously published by Keesom and Matthijs.[2] Steele's technique of measurement employing a uniform magnetic field and a single superconducting-normal junction differed in several respects from the method of Keesom in which a magnetic field made sharply non-uniform by a shield of superconducting lead provided two superconducting-normal junctions at different temperatures.

Since the Keesom method would appear to allow a more direct determination of the temperature of the superconducting-normal junctions, it was felt desirable to repeat this experiment in an attempt to resolve the conflicting results. We therefore constructed an apparatus consisting of a single loop of spectroscopically pure tin wire mounted so that half the loop passed through the core of a hollow lead cylinder 25 cm long.

The apparatus was mounted vertically in a uniform longitudinal magnetic field supplied by a liquid-nitrogen-cooled solenoid. The liquid helium bath was adjusted so that about half of the lead shield was immersed.

To assure the needed temperature gradient, a heater and carbon thermometer were attached to the tin inside the lead shield at a point about 5 cm from its upper end.

Copper wires were attached to the ends of the tin loop and were brought out of the flask to a Perkin-Elmer amplifier which served to measure the voltages. Both copper-tin junctions were outside of the lead shield and were placed in close proximity in the liquid helium bath to minimize any thermoelectromotive forces from this source.

By supplying power to the heater, the upper end of the tin loop was raised to a temperature above the normal transition point, 3.72°K, the lower end of the loop being at the temperature of the bath. In the absence of a magnetic field there then existed a superconducting-normal junction in each branch of the tin loop, both junctions being at 3.72°K. The application of a magnetic field of about 300 gauss destroyed the superconductivity of those parts of the tin wire which were not shielded. Under these conditions, a hot superconducting-normal junction (3.72°K) was located in the field-free region inside the shield, and a cold superconducting-normal junction, at the temperature of the bath, occurred near where the tin wire emerged from the lower end of the shield. The temperature of this cold junction was determined

by measurement of the vapor pressure of the bath. The measurement of the thermoelectromotive force consisted in a determination of the difference in voltages before and after application of the magnetic field. By this procedure, any extraneous thermoelectromotive forces in the circuit were canceled.

It was observed that when the power applied to the heater was not sufficient to keep the hot junction well inside the shield, this junction occurred in the part of the tin wire emerging from the top of the shield where a strong field gradient exists. This junction was then at some temperature between 3.72°K and the bath temperature and resulted in the observed electromotive force being too low.

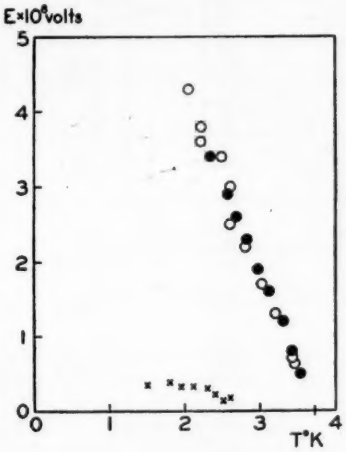

FIG. 1. Thermoelectromotive force of the superconducting-normal junction of tin as a function of temperature; ○ these data, ● Steele (reference 1), × Keesom and Matthijs (reference 2).

The values of thermoelectromotive forces determined in this way are shown in Fig. 1 and compared with the results of Steele and of Keesom and Matthijs. All values of E shown in Fig. 1 are relative to the thermoelectromotive force of the superconducting-normal junction at the transition temperature (3.72°K) which was set equal to zero. The agreement with the results of Steele is excellent. The data of Keesom are lower by a factor of approximately ten.

Further work is in progress and will be reported at a later date.

[1] M. C. Steele, Phys. Rev. **78**, 308 (1950).
[2] W. H. Keesom and C. J. Matthijs, Physica **5**, 437 (1938).

Decay of Hg^{197}

H. FRAUENFELDER, O. HUBER, A. DE-SHALIT,* AND W. ZÜNTI
Physikalisches Institut der Eidg. Technischen Hochschule, Zürich, Switzerland

April 4, 1950

PREVIOUS measurements[1,2] have indicated that Hg^{197} exists in two isomeric states Hg^{197} (23 hr.) and Hg^{197} (65 hr.) decaying independently by K-capture into Au^{197}. About 96 percent of the transitions of Hg^{197} (23 hr.) are associated with a cascade of two strongly converted gamma-rays γ_1 and γ_2 with energies $E_1=164$ and $E_2=133$ kev. The half-life of the intermediate state[3,4] and the angular correlation of the successive conversion electrons[5] have been measured recently.

To determine the conversion coefficients of these gamma-rays and especially the ratio N_K/N_L, we measured the spectrum (Fig. 1) of the conversion lines of Hg^{197} with a magnetic lens spectrometer.[6] Thin sources were prepared with the previously described evaporation technique.[5]

The lines designated as 164_K, 164_L, 164_M, and 133_K, 133_L, 133_M are the conversion lines of γ_1 and γ_2, respectively. From the accurately determined $(K-L)$, and especially $(K-M)$ differences, we must conclude that these gamma-rays are converted in Hg

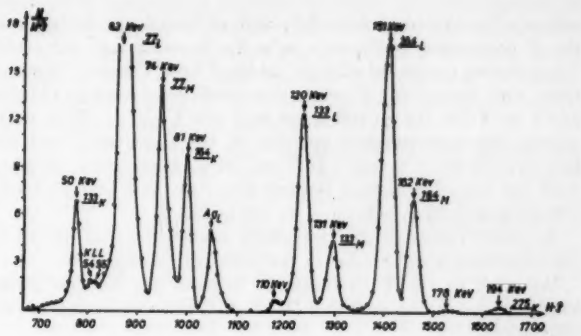

FIG. 1. Spectrum of the conversion electrons from Hg^{197}. The counter window is 1.30 mg/cm² mica and the thickness of the source and backing is 0.25 mg/cm².

and not, as previously assumed, in Au. The complete interpretation of Fig. 1 is listed in Table I.

TABLE I. Interpretation and intensity ratios of the measured lines of Hg^{197}.

Decaying nucleus	Conversion lines	Converted in	Energy of γ-ray in kev	N_K	N_L	N_{M+N} [c]
Hg^{197} (23 hr.)	$164_{K,L,M}$	Hg	$E_1=164$	100	223	100
	$133_{K,L,M}$	Hg	$E_2=133$	71	181	62
	$275_{K,L}$ [b]	Au	$E_3=275$	4.8	1.4	
Hg^{197} (65 hr.)	$77_{L,M}$	Au	$E_4=77$		680	190
Hg^{197} (23 and 65 hr.)	KLL		Auger electrons			
Cd^{107} (6.7 hr.)[a] (contamination)	Ag_L		Ag_K masked by 77_L			

[a] Bradt, Gugelot, Huber, Medicus, Preiswerk, Scherrer, and Steffen, Helv. Phys. Acta **20**, 153 (1947).
[b] See reference 2.
[c] The ratios $N_K:N_L:N_M$ are corrected for absorption in the counter window.

In addition, we measured the decay curve of the 77_L and 77_M conversion electrons in the spectrometer. They both show a genetic relation between Hg^{197} (23 hr.) and Hg^{197} (65 hr.), namely, except for four percent that decays by K-capture to Au^{197*} (7.4 sec.),[2] the Hg^{197} (23 hr.) decays by an isomeric transition to Hg^{197} (65 hr.). If the spectrometer measurements $N_{133}{}^{tot}/N_{164}{}^{tot}=0.73$ are combined with counter coincidence results, the conversion coefficients of γ_1 and γ_2 can be determined. We find the

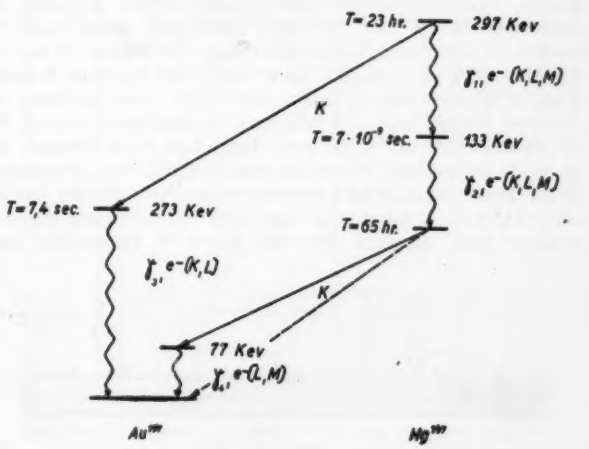

FIG. 2. Decay scheme of Hg^{197}.

values $\kappa_1^{tot}=N_e/(N_e+N_\gamma)\sim 0.9_5$ and $\kappa_2^{tot}\sim 0.7_0$, or in terms of the K-conversion coefficients $\alpha_1^K=N_K/N_\gamma\sim 4.5$ and $\alpha_2^K\sim 0.53$. These values, compared with the tables of Rose, Goertzel, Spinard, Harr, and Strong[7] for K-conversion coefficients seem to indicate $\Delta I=5$ or 4 for the γ_1-transition and $\Delta I=2$ for γ_2. With these values, the corresponding energies of the transitions, and the half-lives 23 hr. of γ_1 and 7.10^{-9} sec. for γ_2, a good fit is obtained with the lines for nuclear isomers given by Axel and Dancoff.[8] The proposed decay scheme is shown in Fig. 2.

Accurate values of the conversion coefficients and details of the experiments will appear in the *Helvetica Physica Acta*.

We wish to thank Professor P. Scherrer for his continuous kind support of this work and Dr. D. C. Peaslee for many helpful discussions.

* Hebrew University, Jerusalem.
[1] G. Friedlander and C. S. Wu, Phys. Rev. **63**, 227 (1943).
[2] Huber, Steffen, and Humbel, Helv. Phys. Acta **21**, 192 (1948).
[3] F. K. McGowan, Phys. Rev. **77**, 138 (1950).
[4] M. Deutsch and W. E. Wright, Phys. Rev. **77**, 139 (1950).
[5] Frauenfelder, Walter, and Zünti, Phys. Rev. **77**, 557 (1950).
[6] W. Zünti, Helv. Phys. Acta **21**, 179 (1948).
[7] Rose, Goertzel, Spinrad, Harr, and Strong (privately circulated report).
[8] D. Axel and S. M. Dancoff, Phys. Rev. **76**, 892 (1949).

Electron Spectrum* of Pa^{233}

H. B. KELLER† AND J. M. CORK
University of Michigan, Ann Arbor, Michigan
AND
Argonne National Laboratory, Chicago, Illinois
July 27, 1950

THE protoactinium used in this investigation was derived from the 23-min. Th^{233} which was produced in the Oak Ridge pile by neutron capture in stable thorium. It was kindly made available to us by Dr. M. H. Studier of the Argonne National Laboratory.

The existence of a 27.4-day activity in protoactinium was first proposed by Meitner, Strassman, and Hahn;[1] it was later questioned by Hahn and Strassman,[2] and assigned to an isotope of zirconium. The final assignment to an isotope of protoactinium of mass number 233 was made and verified by other investigators.[3] Haggstrom[4] and Levy[5] have both previously investigated the conversion spectra and the beta-continuum using a 180° constant radius-type beta-spectrometer. Both found the end point of the beta-spectrum masked by conversion electrons but estimated it to be about 200 kev. Fulbright[6] proposed a beta-component with end point about 700 kev.

In the present investigation, a permanent magnet-type photographic beta-spectrometer was employed. Field strengths of approximately 200 and 600 gauss were used, which made it possible to cover continuously the energy range from 19 kev to 1.5 Mev. The photographic plates used were Eastman Kodak, Type NTB with emulsions 25μ thick. They were processed in Eastman Kodak Type D-8 developer for maximum contrast. In all, 46 conversion and three weak Auger lines were observed, all of which are confined to energies less than 411 kev. Absorption of the gamma-rays in lead revealed no gamma-radiation harder than 400 kev. Absorption in beryllium and aluminum gives a beta-end point agreeing with that found by Haggstrom[4] and Levy;[5] no trace of a harder beta-component such as that reported by Fulbright[6] was found.

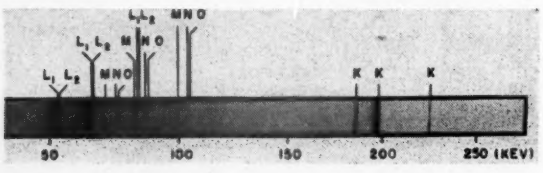

FIG. 1. Predominant lines in the low energy conversion spectrum of Pa^{233}.

TABLE I. Interpretation of the conversion spectrum of Pa^{233}.

Electron energy	Proposed interpretation	Energy sum (kev)	Gamma-energy (kev)
23.5	M^1I,II,III	28.9	
24.6	$M_{IV}{}^1$	28.9	
27.5	N^1	28.9	
28.5	O^1	28.9	28.9
19.6	$L_{II}{}^2$	40.6	
35.2	M^2I,II,III	40.6	
39.1	N^2	40.5	40.6
36.3	$L_I{}^3$	58.1	
37.1	$L_{II}{}^3$	58.1	58.1[a]
53.8	$L_I{}^4$	75.6	
54.7	$L_{II}{}^4$	75.7	
70.2	M^4I,II,III	75.6	
74.3	N^4	75.7	
75.3	O^4	75.7	75.7
65.2	$L_I{}^5$	87.0	
66.1	$L_{II}{}^5$	87.1	
81.7	M^5I,II,III	87.1	
85.7	N^5	87.1	
86.8	O^5	87.2	87.1
82.6	$L_I{}^6$	104.4	
83.5	$L_{II}{}^6$	104.5	
99.0	M^6I,II,III	104.4	
103.2	N^6	104.6	
104.1	O^6	104.5	104.5
156.6	K^7	272.6	
250.9	L^7	272.7	272.6
185.6	K^8	301.6	
279.6	L^8	301.4	
296.1	M^8	301.5	301.5
197.5	K^9	313.5	
291.3	L^9	313.1	
307.5	M^9	312.9	
311.5	N^9	312.9	313.1
226.6	K^{10}	342.6	
320.2	L^{10}	342.0	
336.0	M^{10}	341.4	
340.1	N^{10}	341.5	342.0
260.6	K^{11}	376.6	
354.5	L^{11}	376.4	376.5
283.8	K^{12}	399.8	
378.1	L^{12}	399.9	
394.6	M^{12}	400.0	399.9
300.4	K^{13}	416.4	
394.6	L^{13}	416.4	
411.0	M^{13}	416.4	416.4
88.8	Auger L_I	110.6	$K-M$
93.4	Auger L_I	115.2	$K-N$
108.8	Auger M	114.2	$K-N$

[a] M or N lines could not be seen because of interferences of the very strong lines at 53.8 and 54.7 kev.

Since Pa^{233} decays by beta-emission, the $K-L-M$ x-ray differences employed in determining the energy of the gamma-rays will be characteristic of uranium. In the low energy portion of the spectrum, where the resolution of the instrument used is greatest, the L shell fine structure can be resolved into two components whose separation is 0.8 kev. It is important to mention, however, that no conversion could be detected in the L_{III} sub-shell. A photographic reproduction of the low energy spectrum appears in Fig. 1; the observed electron lines along with their interpretation is summarized in Table I. No satisfactory interpretation could be found for the line at 139.5 kev. It was consequently deleted from Table I. All gamma-rays listed fit well into the proposed level scheme of Fig. 2. While no claim to uniqueness for such a scheme is possible at this time, it is to be noted, however, that all possible transitions were observed with two exceptions. The least energetic of these is dotted in on the level scheme, since it is necessary to the scheme if it is to be

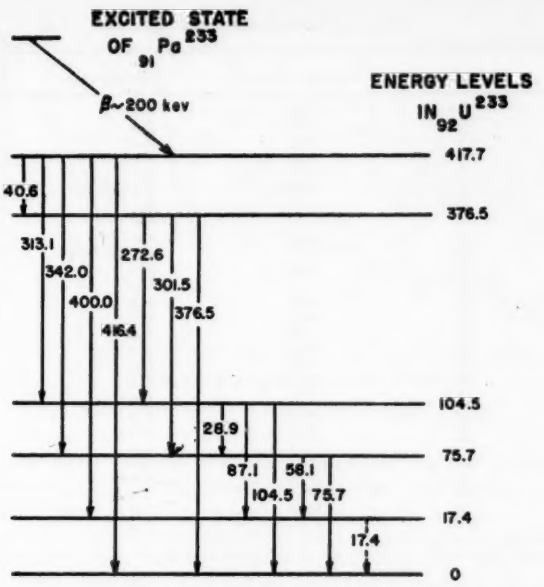

FIG. 2. Proposed level scheme (kev) for U^{233} following beta-emission from Pa^{233}.

self-consistent. Unfortunately, this gamma-ray lies below the lower detection limits of the apparatus.

The facilities of the Argonne National Laboratory were kindly put at our disposal for this work.

* This investigation was made possible by the joint support of the ONR and AEC.

† Phoenix Project Fellow, University of Michigan.

[1] Meitner, Strassman, and Hahn, Zeits. f. Physik **109**, 538 (1938).
[2] O. Hahn and F. Strassman, Naturwiss. **28**, 543 (1940).
[3] Seaborg, Gofman, and Kennedy, Phys. Rev. **59**, 321 (1941); Grosse, Booth, and Dunning, Phys. Rev. **59**, 322 (1941).
[4] E. Haggstrom, Phys. Rev. **59**, 322 (1941).
[5] P. W. Levy, Phys. Rev. **72**, 352 (1947).
[6] H. W. Fulbright, P.P.R. CP-1954 (August 1944, unpublished).

Superfluidity and Thermomechanical Effect in the Absorbed Helium II Film

EARL LONG AND LOTHAR MEYER
Institute for the Study of Metals, University of Chicago, Chicago, Illinois
July 7, 1950

DURING measurements on the adsorption of He gas below 2.19°K, in which the formation of the Rollin film from the unsaturated vapor was indicated,[1] the observed speed of approach to equilibrium suggested that superfluidity occurs even in the adsorbed film, without the presence of bulk liquid. This was investigated by measuring the rate of flow through superleaks, in the manner previously described for liquid HeII,[2] except that the superleaks were usually connected to a copper-stainless steel chamber containing 75 g of adsorbent (Fe_2O_3), the assembly being one of considerable heat capacity. Several different leak geometries were used, either 0.013- or 0.008-cm diameter×2.5-cm long Pt wires sealed into Pyrex glass, or a leak made by pressing together two optically flat stainless steel circular plates of 1 cm diameter, the bottom plate having a central exit hole of 0.08 cm diameter. The widths of the leaks were determined by gas flow measurements at the helium boiling point; they varied from 1 to 9×10^{-5} cm. The onset of superfluidity could be established by measuring the quantity of He passing through the leaks in a given time as a function of the temperature T and the saturation P/P_0, P being the pressure in the adsorption system, and P_0 the vapor pressure of the liquid.

Superfluidity does indeed occur in the adsorbed films, and in a rather striking manner. The temperature at which superflow is observed is not only a function of P/P_0 (i.e., the number of adsorbed layers), but is also determined by the pressure difference (Δp) across the superleak. With a small pressure difference across the leak ($\Delta p \ll P$), it is found that superflow occurs at all saturations above $P/P_0 \sim 0.15$, corresponding to $1\frac{1}{2}$ statistical layers, at all temperatures[3] below 2.186°K.

These results suggest that superfluidity occurs (within our accuracy of ±0.002°) at the λ-temperature of the bulk liquid, independent of the number of layers adsorbed, i.e., that the temperature at which the properties of HeII appear is independent of the number of layers.[4] This could be confirmed by a simple experiment. The adsorption system was loaded with a certain P/P_0 at HeII temperatures, and was slowly warmed; the saturation stayed substantially constant up to the normal λ-point, then changed practically discontinuously when passing the λ-point. The effect has been observed down to $P/P_0=0.35$, and is especially conspicuous at $P/P_0>0.95$ (more than 30 layers adsorbed). The pressure difference between the adsorption system and the bath (~3 cm on a differential oil manometer) disappears abruptly when warming through the λ-point, and reappears again on cooling back to the HeII region. These results suggest the possibility that the transition HeII—HeI becomes first order in the adsorbed layers.

The superflow is extremely sensitive to the slight fluctuations of the bath temperature. A normal rate of flow from the adsorption system to the collection system could be either greatly *increased* or even *reversed* by raising or lowering the bath temperature by a few ten-thousandths of a degree.

A typical experiment is shown in Fig. 1, for a system at 2.173°K and $P/P_0=0.26$ (~2 adsorbed layers), in which the bath vapor pressure variation (dotted curve) and the change of pressure in the collection system (solid curve) are plotted against time. The

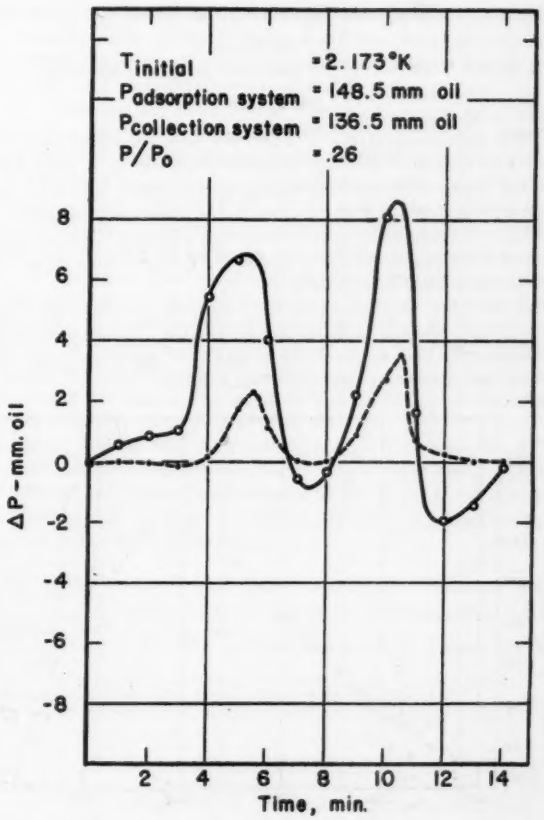

FIG. Variations of the bath vapor pressure and the pressure change in the collection system.

bath temperature was deliberately varied periodically, the resulting pressures (and temperatures) being read on differential oil manometers. A trend of the solid curve toward increasing pressures means superflow *out of*, and toward decreasing pressures superflow *into*, the adsorption system.

The observed flow behavior is presumably due to the inability of the adsorption system to stay in phase with the fluctuations of the bath temperature, so that a temperature gradient is set up across the leak. It is indeed almost impossible to thermostat the bath sufficiently well to prevent the effect. The phenomenon is completely analogous to the fountain effect in bulk liquid HeII, and these preliminary measurements show that the thermomechanical effect here observed is of the same order of magnitude as in the bulk liquid.

Measurements are being continued to establish, if possible, the order of the transition HeII—HeI in adsorbed films, and in particular to measure accurately the thermomechanical effect in adsorbed layers in order to determine $\Delta P/\Delta T$ for comparison with the theory of the fountain effect in liquid HeII.

[1] E. Long and L. Meyer, Phys. Rev. **76**, 440 (1949).
[2] Giauque, Stout, and Barieau, J. Am. Chem. Soc. **61**, 654 (1939); Osborne, Weinstock, and Abraham, Phys. Rev. **75**, 988 (1949).
[3] However, with vacuum initially at the exit of the leak, superflow is detected only at temperatures lower than the normal λ-point, the "onset" temperature being a function of P/P_0, and ranging from 1.40°K at $P/P_0=0.50$ to 2.03°K for $P/P_0=0.95$. This result is probably related to the fact that under these conditions the pressure near the exit of the leak is far lower than the equilibrium pressure for 1½ layers. However, all the leaks gave, with a given saturation, exactly the same sharp "onset" temperature, with or without the presence of adsorbent at the inlet of the leak.
[4] This is not inconsistent with the specific heat data of H. P. R. Frederikse, Physica **XV**, 860 (1949). Frederikse evidently measured the specific heat at substantially constant amount adsorbed, due to the use of a closed vessel of small dead-space volume, whereas the present experiments are performed at constant pressure.

Gamma-Spectrum of Ta^{182}

F. E. O'Meara
NEPA Division, Fairchild Engine and Airplane Corporation, Oak Ridge, Tennessee
July 3, 1950

THE gamma-spectrum of Ta^{182} has been examined in a thin lens beta-spectrometer. A preliminary survey in 1949 using the Oak Ridge National Laboratory spectrometer indicated that there were numerous gamma-rays in the interval from 0.325 to 1.13 Mev where none had previously been reported.[1] The spectrum has now been examined again on the NEPA spectrometer and 27 electron lines have been found.

The tantalum was prepared by irradiation in the Oak Ridge pile and then allowed to decay for six months. A piece of uranium approximately 100 mg/cm² thick was used as a radiator. The counter had a conventional mica end window.

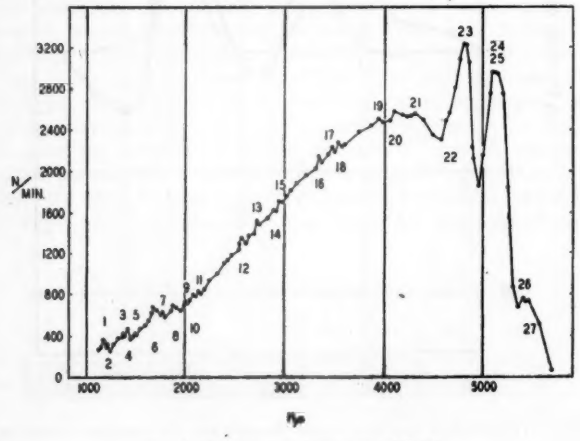

FIG. 1. Gamma-ray spectrum of Ta^{182}.

TABLE I. Electron lines from Ta^{182}.

Line No.	Energy (kev)	Identification
1	109	K_1
2	117	K_2
3	145	K_3
4	153	K_4
5	165	K_5
6	205	K_6 and L_1
7	227	K_7
8	247	K_8
9	277	K_9
10	297	K_{10} and L_4
11	306	K_{11}
12	411	K_{12}
13	450	K_{13}
14	492	K_{14}
15	509	K_{15}
16	613	K_{16}
17	648	K_{17}
18	665	K_{18}
19	777	K_{19}
20	820	K_{20}
21	878	K_{21}
22	971	L_{21}
23	1018	K_{22}
24	1100	K_{23}
25	1116	K_{24} and L_{22}
26	1189	L_{23}
27	1204	L_{24}

Figure 1 shows the electron spectrum obtained. Table I lists the electron lines, their energies, and identification. Table II lists the gamma-rays and their energy. It is quite possible that some of the low energy lines may be L shell lines from gamma-rays whose K shell lines were too low in energy to be observed.

TABLE II. Observed gamma-rays.

Gamma-ray No.	Energy from K	L (Mev)
1	0.224	0.227
2	0.232	
3	0.260	
4	0.268	
5	0.280	
6	0.320	0.319
7	0.342	
8	0.362	
9	0.392	
10	0.412	
11	0.421	
12	0.526	
13	0.565	
14	0.607	
15	0.624	
16	0.728	
17	0.763	
18	0.780	
19	0.892	
20	0.935	
21	0.993	0.993
22	1.133	1.138
23	1.215	1.211
24	1.231	1.226

[1] Beach, Peacock, and Wilkinson, Phys. Rev. **76**, 1585 (1949).

Radioactivity of Ni^{59} and Ni^{63}

H. W. Wilson
Department of Natural Philosophy, University of Glasgow, Scotland
July 6, 1950

A PREVIOUS communication[1] described an investigation by the proportional counter technique of the long-lived activity of nickel after pile irradiation. This was first undertaken to examine the positron activity ascribed to Ni^{59} by Segrè,[2] Rosenfeld[3] and others. Our experiments failed to reveal this activity but a soft negative β^--activity of upper energy limit 63±2 kev was shown to belong to Ni^{63}. The form of the spectrum was compared with Fermi theory.

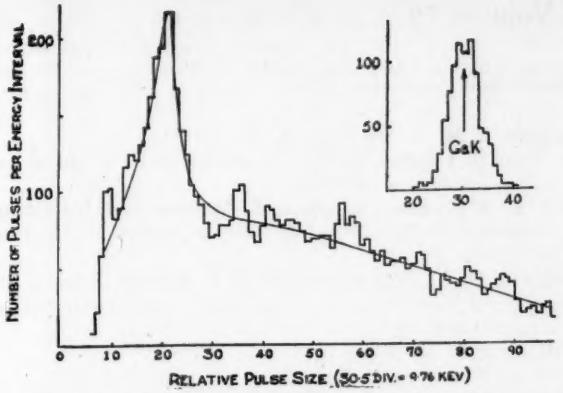

FIG. 1. Pulse-height spectrum for particles to about 30.5 kev.

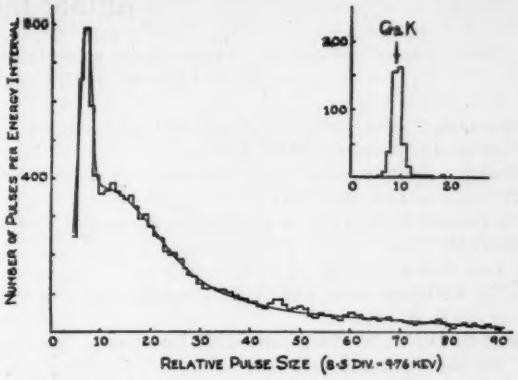

FIG. 2. Pulse-height spectrum for particles to about 100 kev.

In the paper referred to above it was noted that no evidence of positrons, K x-radiations or Auger electrons could be detected. Since the isotope Ni^{59} is expected to decay by K-capture and/or emission of positrons the failure of the very sensitive search led to the conclusion that the lifetime of Ni^{59} was very long. The alternative possibility that the neutron capture cross section of Ni^{58} was very small did not seem to be likely.[4]

To extend the investigations, a sample of pure nickel oxide (free of iron and cobalt) was irradiated for two months in the thermal region of a pile and then a portion was carefully purified as described previously;[1] i.e., by precipitating any active cobalt, with non-active carrier, using α-nitroso-β-naphthol; precipitating nickel with dimethylglyoxime and finally by converting the nickel to nickel carbonyl. The nickel from the carbonyl vapor was then deposited on a hot aluminum foil which was thereafter inserted into the central region of a proportional counter, pressed against the cathode. (The diameter of the counter was 6 cm and the active length 15 cm. It was filled with 2 atmospheres of argon and 10 cm of methane.) The counting rate was 34,000/min. and it was quickly shown by the examination of the β-spectrum emitted from this source, that this rate was almost entirely due to Ni^{63}. Next the source was covered with an aluminum foil, of thickness 1 mil, sufficient to absorb all the β-radiation of Ni^{63}. The counting rate of the counter was now reduced, within the statistical fluctuations, to the background value ($\sim$350/min.) but nevertheless it was thought desirable that the energy spectrum of the pulses should be examined carefully. The results for two different energy ranges, are shown in Fig. 1 and Fig. 2. The first extends to $\sim$30 kev and the second to $\sim$100 kev. A peak is clearly seen in both histograms. It is superposed on the spectrum of the counter background. The K-capture radiation of Ge^{71} giving rise to the x-rays of Ga^{71}, was used as a calibrator (inset figures). The radiation was filtered with Perspex of a thickness sufficient to equalize the intensities of the K_α and K_β x-rays (slightly resolved in Fig. 1). Taking the mean value of these radiations as 9.76 kev, the energy corresponding to the peak observed on the spectra is calculated to be 6.9$\pm$0.3 kev. Now the energy of the K_α x-ray of cobalt is 6.93 kev. The nearly perfect agreement between these values strongly supports the view that this radiation is due to Ni^{59}, decaying by K-capture to Co^{59} and emitting the x-radiations of cobalt.

This radiation from Ni^{59} is of very low intensity. The counting rate (corresponding to the integral under the peak of Fig. 1 not including background) was 22/min. Allowing for the efficiency of the counter and its solid angle of 2π, this corresponds to 49 disintegrations/min. in a source weighing approximately 17.3 mg. This low activity is, no doubt, one of the reasons why the radiation has escaped detection hitherto. The proportional counter technique is possibly unique in its ability to reveal and give accurately the energy of a radiation of such low intensity and energy.

The extremely long life calculated for this isotope is of interest. If the cross section of Ni^{58} from which Ni^{59} is formed by slow neutron irradiation, is taken as 1 barn, the half-life is calculated to be 1.8×10^5 years. The main uncertainty is in the cross-section value. Ross and Story[4] state that the absorption cross section for nickel is between 4.2 and 4.6 barns for thermal neutrons and is mainly due to Ni^{58}. If this is so the half-life is $\sim8\times10^5$ years.

Our estimate of the life of Ni^{63} is much less than that given by Seaborg and Perlman;[5] i.e., 300 years. On the basis of a cross section of 0.51 barn[2] for Ni^{62}, a life of 2.1 years is obtained. The cross section of Ni^{62} may be doubtful and no figures for its cross section could be found elsewhere in the literature. In fact, very little work appears to have been done on the cross sections of the nickel isotopes although Seren *et al.*[6] give the cross section of Ni^{64}, leading to the 2.6-hour isotope Ni^{65} on slow neutron bombardment, as 1.96 barns.

In a recent letter, Thomas and Kurbatov[7] described a search for photons emitted by long-lived nickel isotopes and also, by cloud chamber, for the continuous spectrum of Ni^{63}. They found evidence of the former but not of the latter activity. On the other hand, our experiments with carefully purified nickel show that a relatively intense β-emission of Ni^{63} is accompanied by a weak K-capture emission of Ni^{59}, the ratio of the disintegration rates being $\sim$1200:1. It is difficult to understand their failure to observe the relatively much stronger activity of Ni^{63}. We have ourselves observed no γ-rays corresponding to their values (either for Ni^{59} or Ni^{63}) but our work showed that very thorough chemical purification is necessary to eliminate spurious radiations. Further work is proceeding on the lifetimes and activities of the nickel isotopes with a source of higher activity.

I should like to take this opportunity of thanking Dr. S. C. Curran for his continued interest and help in these investigations, and also to record my indebtedness to Sir J. D. Cockcroft and the Ministry of Supply, A.E.R.E., Harwell, England for the preparation of radioactive nickel.

[1] H. W. Wilson and S. C. Curran, Phil. Mag. 40, 631 (1949).
[2] Segrè Isotope Chart, 1947.
[3] L. Rosenfeld, *Nuclear Forces* (North-Holland Publishing Company, Amsterdam, 1948), Vol. 1, p. 506.
[4] M. Ross and J. S. Story, Reports on Progress in Physics, 12, 296 (1948–1949).
[5] G. T. Seaborg and I. Perlman, Rev. Mod. Phys. 20, 596 (1948).
[6] Seren, Friedlander, and Turkel, Phys. Rev. 72, 894 (1947).
[7] D. G. Thomas and J. D. Kurbatov, Phys. Rev. 77, 151 (1950).

Author Index to Volume 79

References with (A) are to abstracts of papers presented at meetings of the American Physical Society, and those with (T) designate title only. References with (L) are to Letters to the Editor.

Abragam, A. Paramagnetic resonance and hyperfine structure in the iron transition group—534(L)
Ackerman, Eugene. Maximum pressure for cavitation in biological suspensions—231(A)
Adair, Robert K. Neutron scattering resonances of lithium—1018(L)
—— (see Peterson, R. E.)—218(A), 935
——, **C. K. Bockelman, and R. E. Peterson.** Nuclear energy levels in lead—218(A)
Adams, G. D., D. W. Kerst, and C. S. Robinson. Performance of 300-Mev betatron—208(A)
Adler, Fred P. and Henry Margenau. Electron conductivity and mean free paths—970
Ageno, M., M. Chiozzotto, and R. Querzoli. Scintillations in liquids and solutions—720(L)
Ajzenberg, F. (see Bashkin, S.)—238(A)
—— (see Johnson, V. R.)—187(L), 239(A)
Albrecht, H. O. (see Mandeville, C. E.)—1010(L)
Alburger, David E. Beta-ray spectrum of K^{40}—236(A)
—— (see Sunyar, A. W.)—181(L)
Alexander, B. H. (see Dawson, M. H.)—217(A)
Allen, A. J. (see Sun, K. H.)—3, 197(A)
Allen, K. W. (see Almqvist, E.)—209(A)
—— (see Sanders, J. H.)—238(A)
——, **E. Almqvist, J. T. Dewan, T. P. Pepper, and J. H. Sanders.** T+T reaction: I. Energy distribution of the α-particles—238(A)
Allred, J. C. and Louis Rosen. *D-P* scattering for 10.4-Mev deuterons—227(A)
Almqvist, E. (see Allen, K. W.)—238(A)
—— (see Sanders, J. H.)—238(A)
——, **K. W. Allen, J. T. Dewan, T. P. Pepper, and J. H. Sanders.** 200-kv accelerator with gas recovery system—209(A)
Almy, G. M. (see Diven, B. C.)—242(A)
Anderson, C. D. (see Seriff, A. J.)—204(A)
Anderson, G. (see Freier, P. S.)—206(A)
Anderson, P. W. Antiferromagnetism. Generalizations of the Weiss molecular field theory of antiferromagnetism—705
—— Antiferromagnetism. Theory of superexchange interaction—350
Anderson, Roy S. (see Burkhalter, James H.)—224(A), 651
Anslow, Gladys A. Origin of the weak absorption in the near ultraviolet spectra of hydrogen-bridged amides and alcohols—234(A)
—— (see Shea, Ruth C.)—234(A)
Apker, L. A. and E. Taft. Photoelectric emission from *F*-centers in KI—964
Argo, H. V. (see Jarvis, G. A.)—929
Arnold, W. R. Angular correlation in the reaction $F^{19}(p,\alpha)O^{16*}$-$(\gamma)O^{16}$—170(L)
Arroe, O. H. Hyperfine structure and isotope shift in barium—836
—— On the nuclear spin of Mo^{95} and Mo^{97}—212(A)
Ascoli, Giulio. Relation between π- and μ-meson production spectra in the atmosphere—812
Ashkin, A. (see DeWire, J. W.)—210(A)
Ashkin, J., T. Auerbach, and R. Marshak. Note on a possible annihilation process for negative protons—266
Auerbach, T. (see Ashkin, J.)—266
Austin, George E. (see Fundingsland, O. T.)—232(A)
Avery, R., C. H. Blanchard, and R. G. Sachs. Velocity dependent nuclear interactions—220(A)
Axel, P. (see Saur, A. J.)—237(A)
Baggett, L. M. (see Bame, S. J., Jr.)—415(A)
—— **and S. J. Bame, Jr.** Measurements from a magnetic lens pair spectrometer—415(A)
Bak, B., E. Stenberg Knudsen, E. Madsen, and J. Rastrup-Andersen. Preliminary analysis of the microwave spectrum of ketene—190(L)
Baldwin, G. C., F. I. Boley, and H. C. Pollock. Angular distribution and intensity of 70-Mev x-rays from various targets—210(A)
Ball, Anne F. (see Douglas, T. B.)—202(A)
—— (see Ginnings, D. C.)—202(A)
Bame, S. J., Jr. (see Baggett, L. M.)—415(A)
—— **and L. M. Baggett.** Magnetic lens pair production gamma-ray spectrometer—415(A)
Band, William. Condensation phenomena in a clustering Bose-Einstein gas—871
—— Debye modes and superconductivity—739(L)
—— Non-equilibrium phenomena in a Bose-Einstein gas. Part II. Heat transfer—589
—— Superconductivity and Debye modes—1005(L)
Barbour, Ian and Lawrence Greene. Emulsion studies of cosmic-ray stars produced in metal foils—406(L)
Bardeen, J. Theory of infra-red absorption in silicon and germanium—216(A)
—— Zero-point vibrations and superconductivity—167(L)
Barnothy, J. M. and M. Forro. Coincidence efficiency of gamma-rays—199(A)
Barr, E. Scott. Infra-red absorption spectra of some vegetable oil and related compounds—416(A)
—— (see McGehee, F. M., Jr.)—416(A)
Barrett, J. H. Upper limit on the cross section for the scattering of neutrinos—907(L)
Barschall, H. H. (see Henkel, R. L.)—218(A)
—— (see Peterson, R. E.)—218(A), 593, 935
Bartholomew, G. A. (see Kinsey, B. B.)—218(A)
——, **B. B. Kinsey, and W. H. Walker.** Neutron capture-radiation from heavy elements—218(A)
Barton, H. M., Jr. Average electron density measurements by low angle x-ray scattering—211(A)
Bashkin, S. (see Richards, H. T.)—239(A)
——, **F. Ajzenberg, C. P. Browne, Gerson Goldhaber, M. J. W. Laubenstein, and H. T. Richards.** Yield of He^3 and scattered protons from Li^6+P—238(A)
Bass, Robert E. Stability of systems and general principles—201(A)
Bateson, W. O. and Ernest Pollard. Protons from the deuteron bombardment of Co^{59}—241(A)
Batzel, Roger E. and Glenn T. Seaborg. Fission of medium weight elements—528(L)
Bay, Z. New type of high speed coincidence circuit—233(A)
Beach, L. A. (see DeWire, J. W.)—210(A)
Beams, J. W. (see Smith, E. C.)—222(A)
Beard, G. B., J. L. Levy, W. A. Nierenberg, and R. W. Pidd. Design of magnet ends and straight sections for a racetrack synchrotron—209(A)
Bearden, J. A. and Guenter Schwarz. Precision evaluation of h/e by x-rays—674
Beckett, C. W. (see Taylor, W. J.)—234(A)
Belcher, H. V. (see Bestul, A. B.)—223(A)
Belinfante, F. J. Self-energy of moving free electron—201(A)
Bell, Ely E. (see Jones, Robert)—1004(L)
Bell, P. R. (see Cassidy, J. M.)—418(A)
—— (see Francis, J. E., Jr.)—418(A)
—— **and Judith M. Cassidy.** Measurement of the gamma-ray energy of K^{40}—173(L)

—— **and W. H. Jordan.** Gamma-rays from Po-Be neutron source and the excited state of C^{12}—392(L)
Bell, R. E. and L. G. Elliott. Gamma-rays from the reaction $H^1(n,\gamma)D^2$ and the binding energy of the deuteron—282
—— **and R. L. Graham.** Erratum: measurement of a 1.6×10^{-9}-sec. half-life in Yb^{170}—194(L)
Benedict, W. S. and E. K. Plyler. Spectrum of water vapor in the region of 2.7μ—234(A)
Bennett, Willard H. Rapid scanning mass spectroscope—222(A)
Berger, Martin J. (see Groetzinger, Gerhart)—228(A), 454
Bergmann, Peter G. (see Goldberg, Joshua)—225(A)
——, **Robert Penfield, Ralph Schiller, and Henry Zatzkis.** Equations of motion in the covariant canonical formulism—201(A)
Bergström, Ingmar and Sigvard Thulin. On the decay of Xe^{133m}—538(L)
—— **and Sigvard Thulin.** On the isomerism of Kr^{85}—537(L)
Berlin, T. H. (see Thomsen, John S.)—203(A)
Berlman, Isadore B. 1.0-Mev energy level in C^{13}—411(L)
Bernardini, G., G. Cortini, and A. Manfredini. On nuclear evaporation in cosmic rays and the absorption of the nucleonic component. II—952
Besdin, D. J. Diamagnetism of free electrons—417(A)
Bestul, A. B. and H. V. Belcher. Degradation of different molecular weight polyisobutylenes on shearing in solution—223(A)
Bethe, H. A., L. M. Brown, and M. C. Walske. Stopping power of *K*-electrons—413(L)
Beyster, J. R. and M. L. Wiedenbeck. Beta-gamma- and gamma-gamma-angular correlation experiments on Sb^{124}—169(L)
—— **and M. L. Wiedenbeck.** Beta-gamma-angular correlation experiments—728(L)
—— **and M. L. Wiedenbeck.** Gamma-gamma-correlation experiments—411(L)
Bezmann, Irving J. (see Johnston, Herrick L.)—235(A)
Biondi, Manfred A. Ambipolar diffusion in neon—733(L)
Birge, Raymond T. Bohr formula for the Rydberg constant—193(L); Erratum—1005(L)
Birkhoff, Robert D., Earl E. Hays, and S. A. Goudsmit. Energy loss of million-volt electrons—199(A)
Bitter, F. (see Brossel, J.)—225(A)
Blair, J. Morris and J. R. Wallace. Total neutron cross section of vanadium from 10 to 1000 kev—28
Blanchard, C. H. (see Avery, R.)—220(A)
Bleakney, W. and D. R. White. Diffraction of shock waves around, and surface pressures on, two-dimensional objects—546(A)
Bleil, D. F. (see Trounson, E. P.)—226(A), 542(L)
—— **and R. K. Wangsness.** Interpretation of magnetic resonance absorption in antiferromagnetic materials—227(A)
Bloch, Felix. Recent developments of nuclear induction—234(T)
Blocker, Wade, Robert Kenney, and Wolfgang K. H. Panofsky. Transition curves of 330-Mev bremsstrahlung—419
Bloembergen, N. and W. C. Dickinson. On the shift of the nuclear magnetic resonance in paramagnetic solutions—179(L)
Bloom, Stanley (see Margenau, Henry)—213(A)
Bockelman, C. K. (see Adair, R. K.)—218(A)
—— (see Peterson, R. E.)—593, 218(A)
Bohm, David (see Ford, K. W.)—746(L)
—— (see Pines, David)—232(A)
—— **and E. P. Gross.** Effects of plasma boundaries in plasma oscillations—992
Boley, F. I. (see Baldwin, G. C.)—210(A)
—— (see Pratt, W. W.)—208(A)
Bollinger, Lowell M. Measurements on cosmic radiation far underground—207(A)
Bonner, T. W. (see Whaling, Ward)—258
——, **J. W. Butler, and J. R. Risser.** Excitation levels in B^{10}—240(A)
Boorse, H. A. (see Cook, D. B.)—212(A), 1021(L)
—— **and J. G. Dash.** New method for measuring film transport in liquid He II—734(L)
—— **and J. G. Dash.** Transport rates of the liquid He II film over various surfaces—1008(L)
Borkowski, C. J. Proportional and scintillation counters—414(T)
Bothe, W. and H. Thurn. Shape of the Rossi curve—544(L)
Bouricius, G. M. B. (see Shoemaker, F. C.)—228(A)
Boyd, G. E. (see Ketelle, B. H.)—242(A)
Boyd, J. E. (see Kent, C. F.)—417(A)
Boyer, Keith (see Gove, Harry)—241(A)
—— **and Harry Gove.** Elastic and inelastic scattering of 14-Mev deuterons—228(A)
Bozorth, R. M. Atomic moments of ferromagnetic alloys—887(L)
—— **and J. G. Walker.** Domain structure of a cobalt-nickel crystal—888(L)
Bradner, Hugh, D. J. O'Connell, and B. Rankin. On the relative production of π^+- and π^--mesons by neutrons—720(L)
Branscomb, Lewis M. Anomalous molecular rotation and the temperature of the upper atmosphere—619
Branyan, C. E. (see Cork, J. M.)—238(A), 889(L), 938
—— (see Rutledge, W. C.)—237(A)
Breit, G. Fierz and Kopfermann-Brix explanation of the spectroscopic odd-even isotope shift staggering—891(L)
Brentano, J. C. M. and D. H. Davis. Electrical properties of semiconductors with macroscopic discontinuities—216(A)
Bridge, H. S. (see Rediker, R. H.)—206(A)
Brinkman, J. A. and C. Kikuchi. Hyperfine structure and nuclear specific heat of copper—226(A)
Brode, Robert B. (see Merkle, T. C., Jr.)—926
Brody, James K. (see Fred, Mark)—212(A)
Brolley, J. E., Jr., J. H. Coon, and J. L. Fowler. Neutron-proton scattering at 27 Mev—227(A)
Brooks, Franklin C. On the theory of van der Waals forces—200(A)
Brosi, A. R. (see Zeldes, H.)—901(L)
——, **H. Zeldes, and B. H. Ketelle.** $Argon^{39}$ beta-spectrum—902(L)
Brossel, J., P. Sagalyn, and F. Bitter. Optical detection of radiofrequency resonance—225(A)
Brow, Jeanne E. (see Schwertz, F. A.)—223(A)
Brown, H. (see Martinson, O.)—178(L)
Brown, Harrison S. Cosmic abundances of nuclear species—414(T)
Brown, L. M. Asymptotic expression for the stopping power of *K*-electrons—297
—— (see Bethe, H. A.)—413(L)
Brown, Sanborn C. (see Varnerin, Lawrence J., Jr.)—946
Browne, C. P. (see Bashkin, S.)—238(A)
Broyles, A. A. and M. H. Hull. Effect of assumed range of tensor force on the neutron-proton interaction—247
—— **and B. Kivel.** Lower bounds on the range of the neutron-proton interaction—418(A)
Brueckner, K. A. Production of mesons by photons—641
—— **and K. M. Watson.** Production of neutral mesons by photons—187(L)
Bruner, Joseph A. and Lawrence M. Langer. Beta-disintegration of Sc^{44}—236(A)
—— **and Lawrence M. Langer.** Radioactivity of $scandium^{44}$—606
Buechner, W. W. (see Strait, E. N.)—240(A)
—— (see Van Patter, D. M.)—900(L)
—— **and D. M. Van Patter.** Energy levels in B^{11} from the $B^{10}(d,p)B^{11*}$ reaction—240(A)
——, **D. M. Van Patter, E. N. Strait, and A. Sperduto.** Proton groups from $B^{11}(d,p)B^{12}$—262

Bunker, Merle E., Robert Canada, and Allan C. G. Mitchell. Radiations from Os^{185}, Os^{191}, and Os^{193}—610
Bupp, Lamar P. (see Scott, Allen B.)—341, 346
Burgus, W. H., J. D. Knight, and R. J. Prestwood. Radiations of Zr^{97} and Nb^{97}—104
Burgy, M. T. (see Hughes, D. J.)—227(A)
Burkhalter, James H., Roy S. Anderson, William V. Smith, and Walter Gordy. Fine structure of the microwave absorption spectrum of oxygen—651
——, **R. S. Anderson, W. V. Smith, and W. Gordy.** Microwave absorption spectrum of oxygen at low pressures—224(A)
Burns, G. Preston. Equation of the magnetic threshold curve for indium—211(A)
Burstein, E. (see Oberly, J. J.)—217(A)
—— **and J. J. Oberly.** Nature and properties of trapped holes in the alkali halides—217(A)
—— **and J. J. Oberly.** Nature of trapped hole color centers in the alkali halides—903(L)
Busser, J. (see Chance, B.)—244(A)
Butler, J. W. (see Bonner, T. W.)—240(A)
—— (see Whaling, Ward)—414(A)

Callen, Herbert B. Polaron states in ionic crystals—533(L)
Cameron, A. G. W. (see Millar, C. H.)—182(L)
Campbell, Edward C. (see Goodrich, Max)—418(A)
Canada, Robert (see Bunker, Merle E.)—610
Carnes, Elmer B. Vibrations produced by water flowing through a constricted elastic tube—416(A)
Cartwright, W. F. (see Wilcox, H. A.)—198(A)
Case, K. M. Singular potentials—220(A)
—— **and A. Pais.** On high energy nucleon-nucleon scattering—185(L)
Cassidy, Judith M. (see Bell, P. R.)—173(L)
—— **and P. R. Bell.** Long-lived cadmium activities—418(A)
Castellan, G. W. and F. Seitz. Transition from insulating to metallic behavior in semiconducting silicon—216(A)
Chamberlain, Owen, R. F. Mozley, J. Steinberger, and C. Wiegand. Measurement of the positive π-μ-decay lifetime—394(L)
—— **and Clyde Wiegand.** Proton-proton scattering at 340 Mev—81
Chance, Britton. Low frequency fluctuations in the tungsten-lamp-photo-cell system—233(A)
——, **J. Busser, and F. C. Williams.** Fast multiplying circuit—244(A)
Chang, Chia-hua (see Cook C. Sharp)—244(A)
Chang, Chieh-Chien (see des Clers, Bertrand)—547(A)
Chang, W. Y. Further experiments on slow μ-mesons stopped at thin Al foils—205(A)
Chao, C. Y., A. V. Tollestrup, W. A. Fowler, and C. C. Lauritsen. Low energy alpha-particles from fluorine bombarded by protons—108
Chapman, R. M. (see Shaw, J. H.)—1017(L)
Charpie, R. A. (see Sun, K. H.)—3, 197(A)
Cheng, Lin-sheng and J. D. Kurbatov. Radiations emitted by Sr 85—237(A)
Chew, Geoffrey F. Inelastic scattering of high energy neutrons by deuterons and the neutron-neutron interaction—219(A)
Chiozzotto, M. (see Ageno, M.)—720(L)
Chow, R. H. (see More, K. R.)—208(A)
Christian, R. S. and H. P. Noyes. Proton-proton interaction—85
Chu, T. C. New radioactive isotopes of iridium—582
Clark, G. W. and L. B. Snoddy. Production of high current electron pulses by a resonant cavity accelerator—232(A)
Clark, J. S. (see Getting, I. A.)—208(A)
Clay, J. and H. F. Jongen. Solar flare of November 19, 1949 and cosmic rays—908(L)
Cleland, Marshall R. (see Jastram, Philip S.)—243(A)
——, **Wilfred R. Konneker, and A. L. Hughes.** Pair production by electrons—229(A)
Clement, J. R. and E. H. Quinnell. Atomic heat of indium at liquid helium temperatures—1028(L)
Cocconi, G. Extensive air showers and total cosmic radiation—1006(L)
—— **and V. Cocconi Tongiorgi.** Intensity and lateral distribution of the *N*-component in the extensive showers of the cosmic radiation—730(L)
——, **V. Cocconi Tongiorgi, and M. Widgoff.** Cascades of nuclear disintegrations induced by the cosmic radiation—768
Coester, F. and J. M. Jauch. On the role of the subsidiary condition in quantum electrodynamics—201(A)
Cohen, V. W., W. D. Knight, T. Wentink, Jr., and W. S. Koski. Nuclear magnetic resonance of Sb^{121} and Sb^{123}—191(L)
Coles, D. K., W. E. Good, and R. H. Hughes. Microwave spectrum of methyl cyanide and its isotopic modifications—224(A)
Collins, Thomas L. Nuclear magnetic moment of Sb^{121}—226(A)
Conn, William M. Coating method based on the use of electrically "exploded" wires—213(A)
Conversi, Marcello. Experiments on cosmic-ray mesons and protons at several altitudes and latitudes—749
Cook, C. Sharp (see Ter-Pogossian, Michel)—244(A)
—— **and Chia-hua Chang.** Measurements of the relative transmission of beta-particles through thin zapon windows—244(A)
Cook, D. B., M. W. Zemansky, and H. A. Boorse. Superconductivity of columbium nitride—1021(L)
——, **M. W. Zemansky, and H. A. Boorse.** Superconducting properties of columbium—212(A)
Coomes, E. A., R. J. Munick, and W. B. La Berge. Effect of patch fields on Schottky deviations—233(A)
Coon, J. H. (see Brolley, J. E., Jr.)—227(A)
Cooper, C. D. and H. Sponer. Absorption spectra of the xylene vapors in the near ultraviolet—235(A)
Cooper, D. I., D. H. Frisch, C. L. Storrs, Jr., and C. J. Strumski. Small electrostatic generator—208(A)
Corak, W. S. (see Wexler, Aaron)—737(L)
Cork, Bruce. Energy dependence of proton-proton scattering over the interval of 19 to 32 Mev—227(A)
——, **Lawrence Johnston, and Chaim Richman.** Proton-proton scattering at 31.8 Mev, proportional counter method—71
Cork, J. M. (see Keller, H. B.)—1030(L)
—— (see Rutledge, W. C.)—237(A)
——, **W. C. Rutledge, C. E. Branyan, A. E. Stoddard, and J. M. LeBlanc.** Energy levels associated with Se^{75}—889(L)
——, **W. C. Rutledge, A. E. Stoddard, C. E. Branyan, and J. M. LeBlanc.** Radioactivity from enriched isotopes of cadmium—938
——, **W. C. Rutledge, A. E. Stoddard, C. E. Branyan, and J. LeBlanc.** Radioactivity in enriched cadmium isotopes—238(A)
Corrsin, L. Remarks on the infra-red spectrum of deuteronaphthalene—235(A)
Corruccini, Robert J. Effect of heat treatment on the electrical properties of platinum—202(A)
Corson, Dale R. and Margaret R. Keck. Electron track grain densities in nuclear emulsions—209(A)
Cortini, G. (see Bernardini, G.)—952
Courant, H. W. J. (see Williams, R. W.)—207(A)
Cowan, E. W. (see Seriff, A. J.)—204(A)
Craig, D. S. (see Richards, H. T.)—239(A)
Crawford, J. H., Jr. and K. Lark-Horovitz. Thermal equilibrium in neutron-irradiated semiconductors—889(L)
Crawley, Clyde B. (see Wineland, W. C.)—416(A)
Critchfield, C. L., E. P. Ney, and Sophie Oleksa. Electrons in cosmic rays—402(L)

Crown, J. C. Flow of a gas characterized by the Beattie-Bridgeman equation of state and variable specific heats. Part II. Shock waves—229(A)
Crymes, Morita (see Straley, Joseph W.)—416(A)
Cuffey, William H. Coincidence studies of the disintegration of Sc^{44}—180(L)
Czyzak, S. J. (see Reynolds, D. C.)—543(L)

Dailey, Benjamin P. (see Sharbaugh, A. Harry)—189(L)
Dale, B. M. (see Sorensen, B. N.)—1007(L)
Danforth, W. E. and F. H. Morgan. Electrical resistance of thoria—142
Danos, Michael (see Steinwedel, Helmut)—1019(L)
Dash, J. G. (see Boorse, H. A.)—734(L), 1008(L)
Daunt, J. G. and C. V. Heer. Lambda-temperatures of solutions of He^3 in He^4 below 1°K—46
Davis, D. H. (see Brentano, J. C. M.)—216(A)
Davis, W. O. (see Staker, W. P.)—207(A)
Dawson, M. H. and B. H. Alexander. Metallographic study of germanium point contact rectifiers—217(A)
DeBenedetti, S. (see Konneker, W. R.)—210(A)
de Launay, Jules. On the isotope effect in superconductors 398(L)
DeLord, J. (see Dresden, M.)—211(A)
der Mateosian, E. (see Miskel, J. A.)—193(L)
—— **and M. Goldhaber.** Question of isomerism in Ca^{49}—192(L)
des Clers, Bertrand and Chieh-Chien Chang. Aerodynamic behavior and interaction of supersonic and subsonic axially symmetric flows—547(A)
de-Shalit, A. (see Frauenfelder, H.)—1029(L)
Deutsch, Martin and Arne Hedgran. Radioactivity of Hf^{181}—400(L)
Dewan, J. T. (see Allen, K. W.)—238(A)
—— (see Almqvist, E.)—209(A)
—— (see Sanders, J. H.)—238(A)
DeWire, J. W., A. Ashkin, and L. A. Beach. Pair spectrometer for high energy x-rays—210(A)
Dibeler, Vernon H. (see Mohler, Fred L.)—223(A)
——, **E. J. Wells, Jr., and R. M. Reese.** Mass spectra of $C^{13}O_2$ and $C^{13}O$—223(A)
Dickinson, W. C. (see Bloembergen, N.)—179(L)
Dieke, G. H. (see Robertson, Harry S.)—232(A)
Diggins, J. L. Investigation of the efficiency of a simple diffuser for supersonic wind tunnels—229(A)
Dijkstra, L. J. and C. Wert. Effect of inclusions on coercive force of iron—979
Diven, B. C. and G. M. Almy. Photo-disintegration of Ag and Al—242(A)
Donahue, D. (see Richards, H. T.)—239(A)
Doughty, J., K. Lark-Horovitz, L. M. Roth, and B. Shapiro. Structure of lead sulfide films—203(A)
Douglas, T. B. (see Ginnings, D. C.)—202(A)
——, **Anne F. Ball, and D. C. Ginnings.** Heat capacity of liquid mercury between 0° and 450°C—202(A)
Dow, W. G. (see Early, H. C.)—186(L)
Drell, S. D. Non-perturbation calculation of the nucleon-meson coupling constant—220(A)
Dresden, M. (see Reed, Ronald L.)—200(A)
—— **and J. DeLord.** Bloch's theorem and superconductivity—211(A)
Duckworth, Henry E. and Richard S. Preston. Masses of Si^{28}, Si^{29}, Mn^{55}, Fe^{56}, Ni^{58}, Pd^{110}, Cd^{110}, Cd^{112}, Cd^{116}, and Sn^{116}—402(L)
——, **Richard S. Preston, and Karl S. Woodcock.** Masses of Si^{30}, Co^{59}, Ni^{60}, Zr^{90}, Mo^{96}, and Mo^{100}—188(L)
——, **Karl S. Woodcock, and Richard S. Preston.** Packing fraction curve in the neighborhood of the magic number $n=50$—198(A)
Duffield, R. B., L. Hsiao, and E. N. Sloth. Radioactivities of Nb^{99}, Ta^{185}, and W^{185}, and the relative (γ,n) and (γ,p) cross sections of Mo^{100}—1011(L)
DuMond, J. W. M. High precision methods for absolute determination of nuclear energy levels—210(T)
Dunlap, W. C. Some properties of high resistivity *P*-type germanium—286
Dunnington, F. G. (see Garfunkel, M. P.)—211(A)
—— (see Hemenway, C. L.)—887(L)
Dwight, K. (see Winckler, J. R.)—656

Early, H. C. and W. G. Dow. Supersonic wind at low pressures produced by arc in magnetic field—186(L)
Eisner, E. (see Hamermesh, M.)—888(L)
Ekstein, H. and T. Gilbert. Mechanism of remagnetization in an initially saturated ferromagnet—214(A)
Elliot, J. O., S. H. Liebson, and C. F. Ravilious. Variation of the decay time of the fluorescence of anthracene and stilbene with temperature—393(L)
Elliott, L. G. (see Bell, R. E.)—282
Elsasser, Walter M. Hydromagnetic equations—183(L)
Elston, A. W. (see Lord, J. J.)—540(L)
Elton, L. R. B. Effect of nuclear structure on the elastic scattering of fast electrons—412(L)
Emeleus, K. G. (see Sayers, N. D.)—166(L)
Ener, Cavid. Relative velocities of ultrasonic waves in liquids by spark shadow photography—231(A)
Engelkemeir, D. W. (see Freedman, M. S.)—897(L)
Erginsoy, Cavid. Neutral impurity scattering in semiconductors—1013(L)
Estermann, I. and A. Foner. Magnetoresistance of germanium samples between 20° and 300°K—365

Failla, G. (see Gross, W.)—209(A)
Fairbank, Henry A. (see Lynton, Ernest A.)—735(L)
——, **Ernest A. Lynton, and C. T. Lane.** Rollin film creep rate in He^4 and He^3-He^4 mixture—211(A)
Falk, C. E. Angular distribution of neutrons from 15-Mev deuterons on thick cyclotron targets—219(A)
Falkoff, David L. and G. E. Uhlenbeck. On the beta-gamma-angular correlation—334
—— **and G. E. Uhlenbeck.** On the directional correlation of successive nuclear radiations—323
Fan, C. Y. On the origin of the cosmic radiation—912(L)
Fan, H. Y. (see Johnson, V. A.)—899(L)
Faris, F. E. and Byron T. Wright. Results of 12.4-Mev proton-proton scattering at 90°—577
Farrar, R. T. (see Liebson, S. H.)—733(L)
Faulkner, J. E. (see Shoemaker, F. C.)—228(A)
Feingold, A. M. and E. P. Wigner. Effect of tensor forces on the level structure of Li^6 and Li^7—221(A)
Feldman, David (see Yang, C. N.)—972
Feuer, Paula and Hubert M. James. Perturbed periodic wave equation in three dimensions—216(A)
Fillmore, Franklin L. (see Panofsky, Wolfgang K. H.)—57
Finkelnburg, Wolfgang. Spectroscopic and extrapolated ionization potentials of atoms and ions—213(A)
Finkelstein, R. and M. Rudermann. Non-linear spinor fields—220(A)
Fisher, L. H. (see Kachickas, G. A.)—232(A)
Fisk, C. B. (see Salant, E. O.)—184(L), 184(L)
——, **J. Hornbostel, E. O. Salant, and J. E. Smith.** Energetic stars at different latitudes—205(A)
Fitzpatrick, J. A. and W. J. Thaler. Barium titanate coaxial cable for the production of a short duration spark—231(A)
Fletcher, C. H. Diffraction of a shock wave through a small angle—546(A)
Flowers, John W. (see Hatchett, Cresswell)—417(A)
Foldy, L. L. (see Osborn, R. K.)—795
—— (see Sachs, R. G.)—221(A)

Folsom, R. G. and S. A. Schaaf. Some experiments in the field of rarefied gas dynamics—546(T)
Foner, A. (see Estermann, I.)—365
Foner, S. (see Heine-Geldern, R.)—230(A)
——, **E. M. Pugh, R. Heine-Geldern, and E. C. Mutschler.** III. Kerr cell photography of high speed phenomena—instrumentation—230(A)
Forbush, Scott E., Thomas B. Stinchcomb, and Marcel Schein. Extraordinary increase of cosmic-ray intensity on November 19, 1949—501
Ford, K. W. and D. Bohm. Nuclear size resonances—746(L)
Forro, M. (see Barnothy, J. M.)—199(A)
Fowler, J. L. (see Brolley, J. E., Jr.)—227(A)
Fowler, W. A. (see Chao, C. Y.)—108
Fowler, W. B. Altitude dependence of neutron production by cosmic-ray particles—178(L)
Francis, J. E., Jr., P. R. Bell, and J. C. Gundlach. Single-channel differential pulse-height analyzer—418(A)
Frank, F. C. and W. T. Read, Jr. Multiplication processes for slow moving dislocations—722(L)
Frankel, Sherman (see Stump, Robert)—243(A)
Franzen, W., R. Peelle, and R. Sherr. Measurement of particle energies with scintillation counters—209(A)
——, **R. W. Peelle, and R. Sherr.** Measurement of proton energies with scintillation counters—742(L)
Frauenfelder, H., O. Huber, A. de-Shalit, and W. Zünti. Decay of Hg^{197}—1029(L)
Fred, Mark, Frank S. Tomkins, and James K. Brody. Spectrum of He^3 I—212(A)
Freedman, M. S. (see Smaller, B.)—940
—— **and D. W. Engelkemeir.** Radiations of Ce^{141} and Pa^{233}—897(L)
——, **A. H. Jaffey, and F. Wagner, Jr.** Spectrometer and coincidence studies of Np^{238}—410(L)
Freier, George D., L. Rosen, and T. F. Stratton. Excited nuclear state of Be^7—239(A)
——, **T. F. Stratton, and L. Rosen.** Excited nuclear state of Be^7—721(L)
Freier, P. S. (see Ney, E. P.)—206(A)
——, **E. P. Ney, J. Naugle, and G. Anderson.** Nighttime flux of heavy nuclei—206(A)
Frenkiel, F. N. Statistical analysis of turbulence data with computing machines—229(A)
Friedlander, G. (see Sunyar, A. W.)—181(L)
Friedman, Abraham S. (see Johnston, Herrick L.)—235(A)
—— (see White, David)—235(A), 235(A)
Frisch, D. H. (see Cooper, D. I.)—208(A)
Fröhlich, H. Theory of the superconducting state. I. Properties at the absolute zero of temperature—845
—— **and F. Seitz.** Notes on the theory of dielectric breakdown in ionic crystals—526
Fry, William F. Low energy electrons at the end of μ-meson tracks—893(L)
Fuchs, M. and E. S. Lennox. Effect of the nuclear charge and of interference on calculated β-γ-correlations—221(A)
Fuller, E. G. Photo-disintegration of deuterium by 4.5- to 20.3-Mev x-rays—303
Fundingsland, O. T. and George E. Austin. Magnetically controlled ambipolar diffusion—232(A)
Furst, Milton (see Kallmann, Hartmut)—857
Furukawa, G. T., R. E. McCoskey, R. S. Jessup, and R. A. Nelson. Thermal properties of diphenyl ether—223(A)

Gaerttner, E. R. and M. L. Yeater. On the identification of the predominant photo-nuclear disintegrations in nitrogen and oxygen—401(L)
Gallagher, C. J. Anode phenomena in high current arcs—231(A)
Galt, J. K. (see Yager, W. A.)—214(A)
——, **B. T. Matthias, and J. P. Remeika.** Properties of single crystals of nickel ferrite—214(A), 391(L)
Gamow, G. and C. Longmire. Problem of red giants and cepheid variables—743(L)
Gangnes, A. V. (see Van Allen, J. A.)—51
Garelli, C, M. and G. Wataghin. Cosmic rays underground—718(L)
Garfunkel, M. P. (see Serin, B.)—211(A)
——, **F. G. Dunnington, and B. Serin.** Resistance minima in metals at low temperatures—211(A)
Garstens, Martin A. Nuclear magnetic resonance in metallic hydrides—397(L)
Geiger, Felix E., Jr. Isotope shift in Pb II—212(A)
Geschwind, S., H. Minden, and C. H. Townes. Microwave measurements on the stable selenium isotopes in OCSe—226(A)
Getting, I. A., J. S. Clark, J. E. Thomas, Jr., I. G. Swope, and M. L. Sands. Operation of the M.I.T. 350-Mev electron synchrotron—208(A)
Ghiorso, A. (see Hagemann, French)—435
—— (see Street, K., Jr.)—530(L)
Gierer, A. and K. Wirtz. On the theory of supersonic absorption—906(L)
Gilbarg, David. Existence and limit behavior of the one-dimensional shock layer—547(A)
Gilbert, T. (see Ekstein, H.)—214(A)
Ginnings, D. C. (see Douglas, T. B.)—202(A)
——, **T. B. Douglas, and A. F. Ball.** Heat capacity of sodium between 0° and 900°C.—202(A)
Gliessman, J. R. (see Hung, C. S.)—726(L)
Gold, Louis. On the theory of beta-brass structure—202(A)
Goldberg, Joshua and Peter G. Bergmann. Radiofrequency transitions in a tapered electric field—225(A)
Goldberger, M. L. Electric processes involved in deuteron reactions—221(A)
Goldhaber, Gerson (see Bashkin, S.)—238(A)
Goldhaber, M. Recent work on nuclear isomers—242(T)
—— (see der Mateosian, E.)—192(L)
—— (see Miskel, J. A.)—193(L)
—— (see Sunyar, A. W.)—181(L)
Goldman, J. E. Magnetostriction in magnetic alloys with preferred crystal orientation—215(A)
—— (see Plotkin, H. H.)—215(A)
Goldstein, Herbert. On the lower levels of He^5—740(L)
Goldstein, L. (see Parzen, P.)—190(L), 231(A)
—— **and D. Sweeney.** On the scattering of slow neutrons by solid helium—218(A)
Goldwasser, E. L. (see Merkle, T. C., Jr.)—926
Good, W. E. (see Coles, D. K.)—224(A)
Goodrich, Max and Edward C. Campbell. Radiation from short-lived tantalum isomer—418(A)
Gordy, Walter (see Burkhalter, James H.)—224(A), 651
—— (see Kessler, Myer)—54
—— (see Sheridan, John)—224(A), 513
—— (see Trambarulo, Ralph)—224(A)
—— (see Williams, Quitman)—225(A)
—— **and John Sheridan.** Microwave spectra of the methyl mercuric halides—224(A)
Gottleib, Melvin B. (see Hartzler, Alfred J.)—204(A)
—— **and Alfred J. Hartzler.** Large cloud chamber for the study of penetrating showers—204(A)
——, **A. J. Hartzler, and Marcel Schein.** On the particles initiating high energy penetrating showers—741(L)
Goudsmit, S. A. (see Birkhoff, Robert D.)—199(A)
Gove, Harry (see Boyer, Keith)—228(A)
—— **and Keith Boyer.** Energy spectrum and differential cross sections of (d,p) reactions using 14-Mev deuterons—241(A)
Grabner, Ludwig (see Hughes, Vernon)—314, 829
—— **and Vernon Hughes.** Radiofrequency spectrum of $K^{39}F$ by the electric resonance method—819
Gráf, T. Electron capture/beta-decay ratio in K^{40}—1014(L)
Graham, R. L. (see Bell, R. E.)—194(L)

Greene, Lawrence (see Barbour, Ian)—406(L)
Gregory, B. P. (see Tinlot, J. H.)—205(A)
—— **and J. H. Tinlot.** Production of high energy photons in nuclear interactions of cosmic rays—205(A)
Griffith, G. L., M. E. Remley, and P. G. Kruger. Interaction of 12- to 13-Mev neutrons with deuterons—443
Griffith, Wayland C. Relaxation times for exchange of vibrational energy in gas molecules—235(A)
—— Transonic flow measurements—546(A)
Groetzinger, Gerhart, Lewis B. Leder, Fred L. Ribe, and Martin J. Berger. Study of electron-electron scattering—228(A), 454
—— **and Fred L. Ribe.** Multiple scattering of the particles producing the "positive tracks" appearing near beta-ray emitters—904(L)
Gross, E. P. (see Bohm, D.)—992
Gross, W. and G. Failla. New method of radioactivity measurement—209(A)
Guier, William H. and James H. Roberts. Energy levels in C^{12} from Be^{9} (α,n) C^{12}—719(L)
Guillaud, Charles, W. A. Yager, F. R. Merritt, and C. Kittel. Ferromagnetic resonance in manganese ferrite and the theory of the ferrites—181(L)
Gundlach, J. C. (see Francis, J. E., Jr.)—418(A)
Guth, E. (see Holroyd, L.)—1026(L)
—— (see Mrowca, B. A.)—1026(L)
Guttman, Lester (see Stout, J. W.)—396(L)

Hagemann, French. Properties of Tl^{209}—534(L)
——, **L. I. Katzin, M. H. Studier, G. T. Seaborg, and A. Ghiorso.** $4n+1$ radioactive series: the decay products of U^{233}—435
Hager, Charles (see Hatfield, T. N.)—418(A)
Hall, Harvey. On the evaluation of the Fermi β-distribution function—745(L)
Hall, Theodore. Ratio of cross sections for electron capture and electron loss by proton beams in metals—504
Halpern, J. (see Sher, R.)—241(A)
Halter, J. (see Hamouda, I.)—539(L)
Hamermesh, M. and E. Eisner. Spin of the neutron—888(L)
Hamouda, I., J. Halter, and P. Scherrer. Scattering of 3.27-Mev neutrons by deuterons in the Wilson chamber—539(L)
Hanau, Richard. Recombination of positive ions and electrons—417(A)
Hanna, S. S. (see Neuendorffer, J. A.)—239(A)
Hanson, A. O. (see Lyman, E. M.)—228(A)
—— (see Palevsky, H.)—242(A)
Hansson, Ingvar F. E. Photo-disintegration of the deuteron—909(L)
Harkins, William D. Special and magic numbers as factors in nuclear stability and abundance—724(L)
Harris, G. G. (see Rau, R. Ronald)—206(A), 915
Harris, S. P. Neutron scattering cross sections of the noble gases—219(A)
——, **C. O. Muehlhause, and G. E. Thomas.** Low energy neutron resonance scattering and absorption—11
Harrison, F. B. and G. T. Reynolds. Spectral emission from scintillation solutions and crystals—745(L)
Hart, Edward W. (see Watson, Kenneth M.)—918
Hartman, C. D. (see Molnar, J. P.)—1015(L)
Hartsough, Walter, Milton Hill, and Wilson M. Powell. Deuterons bombarded by 90-Mev neutrons—219(A)
Hartzler, Alfred J. (see Gottlieb, Melvin B.)—204(A), 741(L)
—— **and Melvin B. Gottlieb.** Cloud-chamber observations of showers at an altitude of 11,500 ft.—204(A)
Harvey, J. A. Energy levels in lead, bismuth, and thallium—241(A)
Hatchett, Cresswell and John W. Flowers. Production of high currents electrical discharges over long paths—417(A)
Hatfield, T. N., Fred Morris, and Charles Hager. Phase spectrum in pulse analysis—418(A)
Hauptman, H. and J. Karle. Crystal structure problem—204(A)
Hayden, Richard J. (see Inghram, Mark G.)—271
Haynes, S. K. and D. A. Thomas. Medium resolution lens spectrometer for beta-ray energies from 1 kev to 4.5 Mev—414(T)
Hays, Earl E. (see Birkhoff, Robert D.)—199(A)
Hayward, Raymond W. Beta-spectra of Zn^{65} and Cu^{62}—541(L)
—— Beta-spectrum of Sn^{125}—409(L)
—— Sn^{117} isomeric activity—542(L)
Hazen, W. E. (see Randall, C. A.)—905(L)
Hedgran, Arne (see Deutsch, Martin)—400(L)
Heer, C. V. (see Daunt, J. G.)—46
Hein, R. E. and A. F. Voigt. Radioactive isotopes of gadolinium—783
Heine-Geldern, R. (see Foner, S.)—230(A)
—— (see Pugh, E. M.)—230(A)
——, **E. M. Pugh, and S. Foner.** I. Kerr cell photography of high speed phenomena—detonation and shock phenomena—230(A)
Hemenway, C. L. and F. G. Dunnington. New determination of h/e—887(L)
Hemmendinger, A. (see Jarvis, G. A.)—929
Henderson, Joseph E. (see Miller, Charles E.)—206(A), 459
Henkel, R. L. and H. H. Barschall. Fast neutron capture cross section of Al^{27} as a function of energy—218(A)
Henry, A. F. Zeeman effect in O_2—213(A)
Hereford, Frank L. Correlation between the polarization states of annihilation quanta—228(A)
Herzfeld, Karl F., Emanuel Maxwell, and Russell B. Scott. Isotope effect and lattice properties in superconductivity—911(L)
Hess, David C. (see Inghram, Mark G.)—271
Heybey, W. Solution of Lagrange's problem of interior ballistics by means of its characteristic lines—229(A)
Heydenburg, N. P. (see Whitehead, W. D.)—99
Hibdon, C. T. Neutron cross section at 120 ev and 345 ev—747
—— **and C. O. Muehlhause.** Negative energy neutron resonance in Cl^{35}—44
—— **and C. O. Muehlhause.** Neutron scattering resonance in Cl^{35} at -73 ev—219(A)
Hicks, Harry G. (see Wilkinson, Geoffrey)—815
Hill, David L. Fission of liquid drop nuclear model—197(A)
Hill, Milton (see Hartsough, Walter)—219(A)
Hill, R. D. Decay of Au^{199}—413(L)
—— Nuclear isomerism and shell structure—1021(L)
—— (see Mihelich, J. W.)—781
—— **and J. W. Mihelich.** Successive neutron capture in gold—275
Hipple, J. A. Recent developments in precision mass-spectroscopy and the present status of the method of magnetic resonance—197(T)
Hirschfelder, J. O. and J. L. Magee. Erratum: range-energy relations for protons in substances containing C, H, O, A, and Xe—1005(L)
Hofstadter, R. (see McIntyre, J. A.)—208(A)
—— **and J. A. McIntyre.** Gamma-ray measurements with NaI(Tl) crystals—389(L)
Holden, R. B. (see Taylor, W. J.)—234(A)
Holroyd, L. V. (see Mrowca, B. A.)—1026(L)
——, **B. A. Mrowca, and E. Guth.** Study of high polymers by nuclear magnetism. I. Line widths at room temperature—1026(L)
Holstein, T. Pressure broadening of spectral lines—744(L)
Holt, R. B. High speed spectroscopic and electron-density measurements on gas-discharge plasmas—197(T)
—— (see McClure, B. T.)—232(A)
Hopkins, John I. Electron energy studies with the anthracene scintillation spectrometer—415(A)

Hornbostel, J. (see Fisk, C. B.)—205(A)
—— (see Salant, E. O.)—184(L), 184(L)
Hornig, D. F. (see Lohman, J. B.)—235(A)
Houston, W. V. and N. Muench. Electromagnetic forces on a superconductor—967
Howard, J. N. (see Shaw, J. H.)—1017(L)
Howard, Raydeen (see Smith, William V.)—132
—— **and William V. Smith.** Microwave collision diameters—225(A)
—— **and William V. Smith.** Microwave collision diameters I. Experimental—128
Howe, Robert M. Investigation of a low pressure mercury arc—231(A)
Hrostowski, Henry J. (see Scott, Allen B.)—346
Hsiao, C. (see Seriff, A. J.)—204(A)
Hsiao, L. (see Duffield, R. B.)—1011(L)
Huber, O. (see Frauenfelder, H.)—1029(L)
Huddleston, C. M. (see Mei, J. Y.)—19, 237(A), 237(A), 429, 1010(L)
Hudson, Ralph P. Superconductivity in tin-germanium "alloys"—883(L)
Hughes, A. L. (see Cleland, Marshall R.)—229(A)
Hughes, D. J., M. T. Burgy, and G. R. Ringo. Coherent neutron-proton scattering by liquid mirror reflection—227(A)
Hughes, J. V. Velocity of electromagnetic waves and the dielectric constant of dry air—222(A)
Hughes, R. H. (see Coles, D. K.)—224(A)
Hughes, Vernon (see Grabner, Ludwig)—819
—— **and Ludwig Grabner.** Energy levels, selection rules, and line intensities for molecular beam electric resonance experiments with diatomic molecules—829
—— **and Ludwig Grabner.** Radiofrequency spectrum of $Rb^{85}F$ and $Rb^{87}F$ by the electric resonance method—314
Huizenga, J. R., L. B. Magnusson, O. C. Simpson, and G. H. Winslow. Neutron binding energies—908(L)
Hulburt, E. O. (see Johnson, M. H.)—222(A), 802
Hull, M. H. (see Broyles, A. A.)—247
Hulm, J. K., B. T. Matthias, and E. A. Long. Ferromagnetic Curie point in $KTaO_3$ at very low temperatures—885(L)
Hulthén, Lamek. Neutron-proton capture and coherent scattering amplitudes—166(L)
—— **and P. O. Olsson.** Remarks on the variational method for scattering problems—531(L)
Hung, C. S. Theory of resistivity and Hall effect at very low temperatures—727(L)
—— **and J. R. Gliessman.** Resistivity and Hall effect of germanium at low temperatures—726(L)
—— **and V. A. Johnson.** Resistivity of semiconductors containing both acceptors and donors—535(L)
Hurst, G. S. and R. H. Ritchie. Flat response proportional counter for fast neutrons—415(A)
Hyde, Earl K. (see Jaffey, Arthur H.)—280
Hylleraas, Egil and S. Skavlem. On the magnetic shielding in He and H_2—117

Infeld, L. (see Scheidegger, A. E.)—201(A)
Inghram, Mark G., Richard J. Hayden, and David C. Hess. U^{235} fission yields in the rare-earth region—271
Inglis, D. R. (see Neuendorffer, J. A.)—239(A)
Isaacs, P. (see Martinson, O.)—178(L)
Isenberg, Irvin. Ionization of hydrogen in metals—736(L)
—— Virial theorem and the variation principle—737(L)

Jacques, J. R. and H. A. Jarrell. Observations of the effect of temperature on the luminescence of an alpha-particle excited Wurtzite phosphor—418(A)
Jaffey, Arthur H. (see Freedman, M. S.)—410(L)
—— **and Earl K. Hyde.** Half-life of Pa^{232}—280
James, Hubert M. (see Feuer, Paula)—216(A)
—— **and Guy W. Lehman.** Potential fluctuations in homogeneous semiconductors—216(A)
Jarrell, H. A. (see Jacques, J. R.)—418(A)
Jarvis, G. A., A. Hemmendinger, H. V. Argo, and R. F. Taschek. Reaction constants for $T^3(p,n)He^3$—929
Jastram, Philip S., W. Konneker, and Marshall R. Cleland. Doubtful decay of Au^{198}—243(A)
Jastrow, Robert. On charge independence and high energy scattering—389(L)
Jauch, J. M. (see Coester, F.)—201(A)
Jaynes, Edwin T. Displacement of oxygen in $BaTiO_3$—1008(L)
—— **and E. P. Wigner.** Electronic theory of ferroelectrics—213(A)
Jehle, Herbert. Quantum-mechanical resonance between identical big molecules—200(A)
Jennings, B. (see Sun, K. H.)—3, 197(A)
Jensen, E. N. (see Laslett, L. Jackson)—412(L)
——, **L. J. Laslett, R. T. Nichols, and W. W. Pratt.** Disintegration of Yb^{169}—243(A)
Jensen, J. Hans D. (see Steinwedel, Helmut)—1019(L)
Jensen, Lyle (see Johnston, Herrick L.)—235(A)
Jensen, Peter (see Steinwedel, Helmut)—1019(L)
Jessup, R. S. (see Furukawa, G. T.)—223(A)
Johansson, Stig. Beta-decay of Ag^{111} and spin-orbit coupling in Cd^{111}—896(L)
Johnson, F. S. (see Watanabe, K.)—217(A)
Johnson, M. H. and E. O. Hulburt. Diffusion in the ionosphere—222(A), 802
Johnson, R. A. (see McClure, B. T.)—232(A)
Johnson, V. A. (see Hung, C. S.)—535(L)
—— **and H. Y. Fan.** Temperature dependence of the energy gap in germanium from conductivity and Hall data—899(L)
—— **and K. Lark-Horovitz.** Electronic mobility in germanium—409(L)
—— **and K. Lark-Horovitz.** Theoretical Hall coefficient expressions for impurity semiconductors—176(L)
Johnson, V. R. (see Richards, H. T.)—239(A)
——, **F. Ajzenberg, and M. J. Wilson Laubenstein.** Neutron spectrum for protons on Be^9—187(L)
——, **M. J. W. Laubenstein, and F. Ajzenberg.** Neutron spectrum from proton bombardment of beryllium—239(A)
Johnston, Herrick L. (see Smith, A. Lee)—728(L)
—— (see Taylor, W. J.)—234(A)
—— (see White, David)—235(A), 235(A), 236(A)
——, **Irving J. Bezmann, Thor Rubin, Lyle Jensen, David White, and Abraham S. Friedman.** Gaseous data of state for hydrogen between 1 and 200 atmos. from 20 to 300°K—235(A)
Johnston, Lawrence (see Cork, Bruce)—71
Jones, Emily W. and Joseph W. Straley. Coriolis perturbation in methane—417(A)
Jones, Ernest A. (see Woltz, Patricia J. H.)—416(A)
Jones, Robert and Ely E. Bell. 2.7μ bands of carbon dioxide—1004(L)
Jongen, H. F. (see Clay, J.)—908(L)
Jordan, W. H. (see Bell, P. R.)—392(L)
Jossem, E. L. and L. G. Parratt. Versatile precision bent crystal focusing vacuum x-ray spectrometer—210(A)
Jungerman, J. Fission excitation functions for charged particles—198(A), 632

Kachickas, G. A. and L. H. Fisher. Formative time lags of spark breakdown in oxygen—232(A)
Kahn, F. D. On the origin of the sodium *D* lines during twilight—167(L)
Kallmann, Hartmut and Milton Furst. Fluorescence of solutions bombarded with high energy radiation (energy transport in liquids)—857

Kantrowitz, Arthur. Nucleation in very rapid vapor expansions—547(A)
Karle, J. (see Hauptman, H.)—204(A)
Karplus, Robert and Maurice Neuman. Scattering of light by light—220(A)
Katzin, L. I. (see Hagemann, French)—435
Kaufmann, S. G. (see Shoemaker, F. C.)—228(A)
Keck, J. C., M. Stearns, and R. R. Wilson. Search for gamma-rays from nuclei exposed to synchrotron radiation—199(A)
Keck, Margaret R. (see Corson, Dale R.)—209(A)
Keller, H. B. and J. M. Cork. Electron spectrum of Pa^{233}—1030(L)
Keller, William E. (see Smith, A. Lee)—728(L)
Kelly, E., C. Leith, E. Segrè and C. Wiegand. Experiments on n-p scattering with 260-Mev neutrons—96
Kelly, Edward J. Equivalence theorems for meson-nucleon couplings—399(L)
Kenney, Robert (see Blocker, Wade)—419
Kent, C. F. and J. E. Boyd. Probability distributions of the resultants of two or more vibrations—417(A)
Kerst, D. W. (see Adams, G. D.)—208(A)
—— **and G. A. Price.** Yields of photo-neutrons with calorimetrically measured 320-Mev bremsstrahlung—725(L)
Kessler, Karl G. Hyperfine structure of Ni^{61}—167(L)
Kessler, Myer, Harold Ring, Ralph Trambarulo, and Walter Gordy. Microwave spectra and molecular structures of methyl cyanide and methyl isocyanide—54
Ketelle, B. H. (see Brosi, A. R.)—902(L)
—— (see Zeldes, H.)—901(L)
——, **C. M. Nelson, and G. E. Boyd.** Radiations of Sn^{123} and Sn^{125}—242(A)
Kiepenheuer, K.O. Cosmic rays as the source of general galactic radio emission—738(L)
Kikuchi, C. (see Brinkman, J. A.)—226(A)
Kikuchi, Ryoichi. Method of approximation for cooperative phenomena—718(L)
Kilpatrick, John E. Note on the vapor pressure of He^3, He^4 solutions—529(L)
Kimura, Motoharu. Thermal neutron scattering by ammonium chloride—544(L)
Kinnear, J. K. (see More, K. R.)—208(A)
Kinsey, B. B. (see Bartholomew, G. A.)—218(A)
——, **G. A. Bartholomew, and W. H. Walker.** Neutron capture γ-rays from Mg, Si, P, and K—218(A)
Kittel, C. Theory of magnetic dispersion in ferrites—214(A)
—— (see Guillaud, Charles)—181(L)
Kivel, B. (see Broyles, A. A.)—418(A)
Klein, Martin J. and Robert S. Smith. Thin ferromagnetic films—214(A)
Klick, Clifford C. Luminescence of color centers in alkali halides—894(L)
Knight, J. D. (see Burgus, W. H.)—104
Knight, W. D. (see Cohen, V. W.)—191(L)
Knipp, J. K. Ionization yields of heavy particles—197(A)
Knudsen, E. Stenberg (see Bak, B.)—190(L)
Koehler, J. S. and E. Salkovitz. Dislocation model of a kink band—202(A)
Koehler, W. C., E. O. Wollan, and C. G. Shull. Coherent neutron scattering cross sections of nickel and its isotopes—395(L)
Kolsky, H. G., T. E. Phipps, Jr., N. F. Ramsey, and H. B. Silsbee. Radiofrequency spectrum of H_2 in a magnetic field—883(L)
Kondaiah, Evani. Disintegration of Ru^{103}—891(L)
Konneker, Wilfred R. (see Cleland, Marshall R.)—229(A)
—— (see Jastram, Philip S.)—243(A)
——, **S. DeBenedetti, and F. K. McGowen.** Versatile delayed coincidence circuit— 210(A)
Kopecek, J. T. (see Lockenvitz, Arthur E.)—417(A)
Kopfermann, Hans. Isotope shift in atomic spectra of heavy elements—212(T)
Koski, W. S. (see Cohen, V. W.)—191(L)
—— **and C. O. Thomas.** Scintillation spectra of some organic crystals—217(A)
Kraushaar, W. L. (see Williams, R. W.)—207(A)
Kruger, P. G. (see Griffith, G. L.)—443
Krumbein, A. D. Anomalous effect observed in self-quenching counters containing neon—910(L)
Kubitschek, Herbert E. Detection of positron-conjoint nuclear gamma-radiation—23
Kuhn, T. S. Application of the W.K.B. method to the cohesive energy of monovalent metals—515
—— **and J. H. Van Vleck.** Simplified method of computing the cohesive energies of monovalent metals—382
Kurbatov, J. D. (see Cheng, Lin-sheng)—237(A)
—— (see Sorensen, B. N.)—1007(L)
Kusch, P. (see Prodell, A. G.)—1009(L)

La Berge, W. B. (see Coomes, E. A.)—233(A)
Ladenburg, R. and P. Watchell. Interferometric studies of laminar and turbulent boundary layers along a flat plate in supersonic flow—548(A)
Lafferty, J. M. Boride cathodes—1012(L)
Lamb, Willis E., Jr. and Robert C. Retherford, Fine structure of the hydrogen atom. Part I—549
Lane, C. T. (see Fairbank, Henry A.)—211(A)
—— (see Reynolds, Joseph M.)—405(L)
Langer, Lawrence M. (see Bruner, Joseph A.)—236(A), 606
—— (see Moffat, R. D.)—237(A)
——, **R. D. Moffat, and H. C. Price, Jr.** Further investigation of the radioactivity of Sb^{124}—808
Laquer, Henry L. and William E. McGee. Techniques for measuring sound velocities and elastic constants—202(A)
Lark-Horovitz, K. (see Crawford, J. H., Jr.)—889(L)
—— (see Doughty, J.)—203(A)
—— (see Johnson, V. A.)—176(L), 409(L)
Laslett, L. Jackson (see Jensen, E. N.)—243(A)
——, **E. N. Jensen, and A. Paskin.** First forbidden beta-spectra and the beta-spectrum of Sr^{90}-Y^{90}—412(L)
Lassen, N. O. Total charges of fission fragments in gaseous and solid media—1016(L)
Latter, Richard. Finite Wiener-Hopf equations—199(A)
Laubenstein, M. J. Wilson (see Bashkin, S.)—238(A)
—— (see Johnson, V. R.)—187(L), 239(A)
Lauritsen, C. C. (see Chao, C. Y.)—108
Lax, Benjamin. Electromagnetic waves in bounded magneto-ionic media—222(A)
Lax, Melvin. Removal of degeneracy in any order—200(A)
Leachman, R. B. Ionization yields of fission fragments—197(A)
LeBlanc, J. M. (see Cork, J. M.)—238(A), 889(L), 938
—— (see Rutledge, W. C.)—237(A)
Leder, Lewis B. (see Groetzinger, Gerhart)—228(A), 454
Lees, L. Hypersonic flow—546(T)
Lehman, Guy W. (see James, Hubert M.)—216(A)
Leighton, R. B. (see Seriff, A. J.)—204(A)
Leith, C. (see Kelly, E.)—96
Leitner, Alfred and R. D. Spence. Effect of a finite ground-plane on antenna radiation—199(A)
Lennox, E. S. (see Fuchs, M.)—221(A)
Lepore, Joseph V. Polarization of neutrons and protons by scattering—137
Levinstein, Henry (see Marple, D. T. F.)—223(A)
Levy, J. L. (see Beard, G. B.)—209(A)
Liebson, S. H. (see Elliot, J. O.)—393(L)
—— **and R. T. Farrar.** Temperature characteristics of naphthalene-anthracene mixtures—733(L)
Lin, T. C. Effect of variable viscosity and thermal conductivity on the high speed plane Couette flow of a semirarefied gas—547(A)
Linsley, J. (see Ney, E. P.)—206(A)

Lipkin, H. J. and M. G. White. Scattering of positrons and electrons by nuclei—892(L)
Lippmann, B. A. Variational principles for scattering processes. II. Scattering of slow neutrons by parahydrogen—481
—— **and Julian Schwinger.** Variational principles for scattering processes. I—469
Litovitz, T. A. Ultrasonic absorption in glycerol—230(A)
Lockenvitz, Arthur E. and J. T. Kopecek. Specific ionization of air by 10- to 45-kev hydrogen particles—417(A)
Lohman, J. B. and D. F. Hornig. Infra-red spectrum of crystalline hydrogen sulfide—235(A)
Long, Earl A. (see Hulm, J. K.)—885(L)
—— **and Lothar Meyer.** Superfluidity and thermomechanical effect in the adsorbed helium II film—1031(L)
Longmire C. (see Gamow, G.)—743(L)
Lord, J. J., A. W. Elston, and Marcel Schein. Large fluctuation in the rate of production of nuclear disintegrations following a solar flare—540(L)
Low, W. (see Townes, C. H.)—198(A)
—— **and C. H. Townes.** Effect of Fermi resonance on rotation-vibration interaction in OCS and OCSe—224(A)
Lundquist, G. A. Electronic method for determining gas liquefaction in shock tubes by light scattering—230(A)
Lyman, E. M., A. O. Hanson, and M. B. Scott. Elastic scattering of 16.5-Mev electrons—228(A)
Lynton, Ernest A. (see Fairbank, Henry A.)—211(A)
—— **and Henry A. Fairbank.** Velocity of second sound in mixtures of He^3 and He^4—735(L)

Madansky, Leon and Franco Rasetti. Attempt to detect thermal energy positrons—397(L)
Madsen, E. (see Bak, B.)—190(L)
Magee, J. L. (see Hirschfelder, J. O.)—1005(L)
Magnusson, L. B. (see Huizenga, J. R.)—908(L)
Mandeville, C. E. (see Swann, C. P.)—240(A), 598
—— **and H. O. Albrecht.** Detection of scintillations from crystals with a photo-sensitive Geiger-Müller counter—1010(L)
—— **and E. Shapiro.** Radiations from cerium $(144)\xrightarrow{\beta^-}$praseodymium $(144)\xrightarrow{\beta^-}$neodymium (144)—243(A)
—— **and E. Shapiro.** Some characteristics of the 11-day neodymium (147)—391(L)
—— **and C. P. Swann.** Neutrons from the disintegration of C^{13} by deuterons—787
Manfredini, A. (see Bernardini, G.)—952
Mann, L. G. (see Saur, A. J.)—237(A)
Many, Abraham. Low terms of Ti II—531(L)
Margenau, Henry (see Adler, Fred P.)—970
—— **and Stanley Bloom.** Pressure broadening of spectral lines and frequency modulation—213(A)
Marple, D. T. F. and Henry Levinstein. Sitting time of molecules on a hot wire detector—223(A)
Marshak, R. E. (see Ashkin, J.)—266
—— **and A. S. Whitman.** Absorption of π^--mesons by protons—220(A)
Martin, D. (see Richards, H. T.)—239(A)
Martin, Don S., Jr. (see Moses, Alfred J.)—467
Martinson, O., P. Isaacs, H. Brown, and I. W. Ruderman, Rise times of voltage pulses from photo-multipliers—178(L)
Marton, L., J. A. Simpson, and A. Van Bronkhorst. Fringe field observations of domains—215(A)
Matthias, B. T. (see Galt, J. K.)—214(A), 391(L)
—— (see Hulm, J. K.)—885(L)
—— (see Yager, W. A.)—214(A)
Maxwell, Emanuel. Superconductivity of Sn^{124}—173(L)
—— (see Herzfeld, Karl F.)—911(L)
Maxwell, L. R. (see Trounson, E. P.)—226(A), 542(L)
May, J. (see Smaller, B.)—940
Mayburg, Sumner. Effect of pressure on the low frequency dielectric constant of ionic crystals—203(A), 375
Mays, John M. (see Sharbaugh, A. Harry)—189(L)
McClure, B. T., R. A. Johnson, and R. B. Holt. Electron removal in helium afterglows—232(A)
McClure, G. W. and M. A. Pomerantz. Ionization chamber bursts at very high altitudes—911(L)
McCoskey, R. E. (see Furukawa, G. T.)—223(A)
McDaniel, B. D. (see Walker, R. L.)—242(A)
McFee, Raymond H. Temperature variation of properties of photo-sensitive lead sulfide films—203(A)
McGee, William E. (see Laquer, Henry L.)—202(A)
McGehee, F. M., Jr. and E. Scott Barr. Infra-red absorption spectrum of tung oil—416(A)
McGowan, F. K. 5.7×10^{-9}-sec. isomeric state in $_{77}Ir^{191}$—404(L)
—— (see Konneker, W. R.)—210(A)
McIntyre, J. A. (see Hofstadter, R.)—389(L)
—— **and R. Hofstadter.** Gamma-ray spectrometer based on the Compton effect—208(A)
McKeehan, L. W. Ferromagnetic block—739(L)
—— Physical theory of ferromagnetic domains—747(L)
McMahon, Allen J. and Bruno Rossi. Altitude and latitude dependence of bursts in a lead-shielded ion chamber—205(A)
McMillan, Edwin M. Origin of cosmic rays—498
Mc.R. Routly, P. (see Wolfe, Bertram)—1020(L)
Mei, J. Y., C. M. Huddleston, and Allan C. G. Mitchell. Disintegration of Ru^{103}—237(A)
——, **C. M. Huddleston, and Allan C. G. Mitchell.** Disintegration of ruthenium 103 and palladium 103—429
——, **C. M. Huddleston, and Allan C. G. Mitchell.** Gamma-rays of Ag^{105} and Ag^{106}—1010(L)
——, **Allan C. G. Mitchell, and C. M. Huddleston.** Disintegration of As^{72}—19
——, **Allan C. G. Mitchell, and C. M. Huddleston.** Radiations from As^{72} and As^{71}—237(A)
Menzel, D. H. How to write scientific papers—234(T)
Merkle, T. C., Jr., E. L. Goldwasser, and Robert B. Brode. Intensity and masses of cosmic-ray particles—926
Merritt, F. R. (see Guillaud, Charles)—181(L)
—— (see Yager, W. A.)—214(A)
Metzger, Franz. Internal conversion of the gamma-rays from Rh^{106}—398(L)
Meyer, Lothar (see Long, Earl)—1031(L)
Mezzetti, L. and R. Querzoli. On the production of penetrating showers in lead and carbon—168(L)
Mihelich, J. W. (see Hill, R. D.)—275
—— **and R. D. Hill.** Radioactive isomers of Sn^{117} and Sn^{119}—781
Millar, C. H. and A. G. W. Cameron. Ejection of Li^8 nuclei by gamma-rays—182(L)
Miller, B. L. Optimum parameters for particle acceleration by TM 010 cylindrical cavities—209(A)
Miller, Charles E., Joseph E. Henderson, David S. Potter, and Jay Todd. Analysis of the cosmic radiation at 3.4 kilometers into its proton and meson components—206(A)
——, **Joseph E. Henderson, David S. Potter, Jay Todd, Jr., and A. William Wotring.** Magnetic cloud-chamber analysis of cosmic rays at 3.4 kilometers—459
Millsaps, K. Oscillations of magnetic suspensions—418(A)
Minden, H. (see Geschwind S.)—226(A)
Miskel, John A. Genetic relationship in Ag^{110}—403(L)
——, **E. der Mateosian, and M. Goldhaber,** Question of isomerism in Ti^{51}—193(L)
Mitchell, Allan C. G. (see Bunker, Merle E.)—610
—— (see Mei, J. Y.)—19, 237(A), 237(A), 429, 1010(L)
Miyatake, O. (see Yasaki, T.)—740(L)
Moffat, R. D. (see Langer, L. M.)—808
—— **and L. M. Langer.** Disintegration of Ga^{66}—237(A)

Mohler, Fred L., Vernon H. Dibeler, E. J. Wells, Jr., and R. M. Reese. Mass spectra of isotopic hydrogen molecules—223(A)
Molnar, J. P. and C. D. Hartman. Induced absorption bands in MgO crystals—1015(L)
Montgomery, C. G., D. D. Montgomery, and J. A. Northrop. Penetration of particles associated with cosmic-ray stars—293
Montgomery, D. D. (see Montgomery, C. G.)—293
Moon, M. L. (see Waggoner, M. A.)—236(A)
——, **M. A. Waggoner, and A. Roberts.** Internal conversion coefficients of Sc^{46}—905(L)
More, K. R., R. H. Chow, J. K. Kinnear, and S. B. Woods. Radiofrequency ion source for electrostatic generator—208(A)
Morgan, F. H. (see Danforth, W. E.)—142
Morris, Fred J. Dielectric properties of selenium—418(A)
—— (see Hatfield, T. N.)—418(A)
Moses, Alfred J. and Don S. Martin, Jr. Evidence for the formation of Ce^{139} by an n-γ-reaction—467
Moss, T. S. Changes in the activation energy of tellurium—1011(L)
Mozley, R. F. (see Chamberlain, O.)—394(L)
Mrowca, B. A. (see Holroyd, L. V.)—1026(L)
——, **L. V. Holroyd, and E. Guth.** Study of high polymers by nuclear magnetism. II. Line widths through transition temperatures—1026(L)
Muehlhause, C. O. Capture γ-ray multiplicity—219(A)
—— Neutron capture gamma-ray multiplicity—277
—— On spin dependent nuclear "radii"—1002(L)
—— (see Harris, S. P.)—11
—— (see Hibdon, C. T.)—44, 219(A)
Muench, N. (see Houston, W. V.)—967
Munick, R. J. (see Coomes, E. A.)—233(A)
Murakawa, K. Note on the revision of the hyperfine structure of the spectrum of mercury—536(L)
Murphy, E. J. Alternating current conduction in ice—396(L)
—— Hydrogen bond energy from a.c. conduction data on ice—203(A)
Mutschler, E. C. (see Foner, S.)—230(A)
—— (see Pugh, E. M.)—230(A)

Nabarro, F. R. N. Restriction of prismatic punching to a limited class of crystals—894(L)
Nagamatsu, Henry J. Results of recent hypersonic flow research in the Army Ordnance-California Institute of Technology hypersonic wind tunnel—546(T)
Naugle, J. (see Freier, P. S.)—206(A)
Nechaj, J. F. (see Sun, K. H.)—3, 197(A)
Nelson, C. M. (see Ketelle, B. H.)—242(A)
Nelson, R. A. (see Furukawa, G. T.)—223(A)
Nethercot, A. H., Jr. and C. W. Peters. Pressure shift of the inversion frequency of ammonia—225(A)
Neuendorffer, J. A., D. R. Inglis, and S. S. Hanna. Angular yield of deuterons and alphas from the proton bombardment of Be^9—239(A)
Neuman, Maurice (see Karplus, Robert)—220(A)
Newell, G. F. Crystal statistics of a two-dimensional triangular Ising lattice—876
Ney, E. P. (see Critchfield, C. L.)—402(L)
—— (see Freier, P. S.)—206(A)
——, **J. Linsley, and P. S. Freier.** Daytime azimuthal effect for heavy nuclei—206(A)
Nichols, R. T. (see Jensen, E. N.)—243(A)
—— (see Pratt, W. W.)—208(A)
Nier, Alfred O. Redetermination of the relative abundances of the isotopes of neon, krypton, rubidium, xenon, and mercury—450
—— (see Roberts, T. R.)—198(A)
Nierenberg, W. A. (see Beard, G. B.)—209(A)
Nieset, Robert T. Role of physics in biology—414(T)
Northrop, J. A. (see Montgomery, C. G.)—293
Noyes, H. P. (see Christian, R. S.)—85

Oberly, J. J. (see Burstein, E.)—217(A), 903(L)
—— **and E. Burstein.** Photo-conductivity of trapped electrons in the alkali halides—217(A)
O'Connell, D. J. (see Bradner, Hugh)—720(L)
Oleksa, Sophie (see Critchfield, C. L.)—402(L)
Olsson, P. O. (see Hulthén, L.)—531(L)
O'Meara, F. E. Gamma-spectrum of Ta^{182}—1032(L)
Orr, J. B. U^{235} in thucholite—401(L)
Osborn, J. A. Susceptibility measurements using the moment balance—214(A)
Osborn, R. K. and L. L. Foldy. Phenomenological theory of exchange currents in nuclei—795
Ovadia, J. (see Saur, A. J.)—237(A)

Page, Lorne A. and W. M. Woodward. Electron-electron scattering—228(A)
Pai, S. I. Axially symmetrical jet mixing of a compressible fluid—547(A)
Pais, A. (see Case, K. M.)—185(L)
—— **and G. E. Uhlenbeck.** On field theories with non-localized action—145
Palevsky, H. and A. O. Hanson. Photo-neutron thresholds for Pb^{206}, Pb^{207}, Pb^{208}—242(A)
Panetti, M. and G. Wataghin. Cosmic-ray intensity in the upper atmosphere—177(L)
Panofsky, Wolfgang K. H. (see Blocker, Wade)—419
—— **and Franklin L. Fillmore.** Scattering of protons by protons near 30 Mev, photographic method—57
Pantchechnikoff, Jacques I. On the nature of a soldered contact on a semiconductor—1027(L)
Parratt, L. G. (see Jossem, E. L.)—210(A)
Parzen, P. and L. Goldstein. Current fluctuations in a d.c. gas discharge plasma—190(L), 231(A)
Paskin, A. (see Laslett, L. Jackson)—412(L)
Pearlstein, E. A. and R. B. Sutton. Mobility of electrons and holes in diamond—907(L)
—— **and R. B. Sutton.** Some phenomena in diamond gamma-ray counters—217(A)
Pecjak, F. A. (see Sun, K. H.)—3, 197(A)
Peelle, R. W. (see Franzen, W.)—209(A), 742(L)
Pekeris, C. L. Zero-point energy of helium—884(L)
Pell, E. M. and D. H. Tomboulian. Interface absorption by evaporated aluminum films at 130 angstroms—210(A)
Pellam, John R. Thermal Rayleigh disk in liquid helium II—212(A)
Penfield, Robert (see Bergmann, Peter G.)—201(A)
—— **and Henry Zatzkis.** Conservation laws in Einstein's theory of gravitation with electromagnetic field—201(A)
Pensak, L. Electron bombardment induced conductivity in selenium—171(L)
Pepper, T. P. (see Allen, K. W.)—238(A)
—— (see Almqvist, E.)—209(A)
—— (see Sanders, J. H.)—238(A)
Perkin, J. L. Angular distribution of protons from the $B(\alpha,p)C,C^*$ reaction—175(L)
Perkins, J. F. and A. W. Solbrig, Jr. Empirical method for calculating electron orbits and line shapes for a point source of electrons in a thick-lens beta-ray spectrometer—415(A)
Perlman, I. and T. J. Ypsilantis. Consistency of nuclear radii of even-even nuclei from alpha-decay theory—30
Peshkin, Murray. Scattering of mesons by nucleons—221(A)
Peters, C. W. (see Nethercot, A. H., Jr.)—225(A)
Peterson, R. E. (see Adair, R. K.)—218(A)
——, **R. K. Adair, and H. H. Barschall.** Nuclear energy levels in lead isotopes—935
——, **R. K. Adair, H. H. Barschall, and C. K. Bockelman.** Nuclear energy levels in sulfur—218(A)

——, **H. H. Barschall, and C. K. Bockelman.** Investigation of nuclear energy levels in sulfur—593
Peterson, Vincent Z. Mesons produced in proton-proton collisions—407(L)
Petritz, R. L. and A. J. F. Siegert. On the theory of noise in semiconductors—215(A)
Phillips, G. C. Excitation curves for $B^{10}(d,p)B^{11}$—240(A)
Phipps, T. E., Jr. (see Kolsky, H. G.)—883(L)
Pickup, E. and L. Voyvodic. Emission of neutral radiation in cosmic-ray stars—899(L)
Pidd, R. W. (see Beard, G. B.)—209(A)
Pierce, J. R. Physical aspects of postwar microwave amplifiers—197(T)
Pines, David and David Bohm. Role of plasma oscillations in the description of electron interactions—232(A)
Pirani, F. A. E. and A. Schild. On the quantization of Einstein's gravitational field equations—986
Plotkin, H. H. and J. E. Goldman. Effect of tension on magnetic properties in iron-cobalt—215(A)
Plyler, E. K. (see Benedict, W. S.)—234(A)
Pochapsky, T. E. and S. L. Quimby. Temperature variation of the compressibility of molten sodium—892(L)
Pollard, Ernest (see Bateson, W. O.)—241(A)
Pollock, H. C. (see Baldwin, G. C.)—210(A)
Pomerantz, M. A. (see McClure, G. W.)—911(L)
Porter, Fred T. (see Ter-Pogossian, Michel)—244(A)
Poss, H. L. Note on angular asymmetries in (γ,n) reactions—539(L)
Post, R. F. Decay time and efficiency of a liquid scintillator—735(L)
Potter, David S. (see Miller, Charles E.)—206(A), 459
Pound, R. V. Nuclear electric quadrupole interactions in crystals—685
Powell, Wilson M. (see Hartsough, Walter)—219(A)
Powers, Ruth I. and A. F. Voigt. Half-life of strontium^{90}—175(L)
Pratt, W. W. (see Jensen, E. N.)—243(A)
——, **F. I. Boley, and R. T. Nichols.** Ring focusing in a thin lens magnetic spectrometer—208(A)
Preston, Richard S. (see Duckworth, Henry E.)—188(L), 198(A), 402(L)
Prestwood, R. J. (see Burgus, W. H.)—104
Price, G. A. (see Kerst, D. W.)—725(L)
Price, H. C., Jr. (see Langer, L. M.)—808
Pritchard, Benjamin S. (see Sharbaugh, A. Harry)—189(L)
Proctor, W. G. On the magnetic moments of Tl^{203}, Tl^{205}, Sn^{115}, Sn^{117}, Sn^{119}, Cd^{111}, Cd^{113}, and Pb^{207}—35
Prodell, A. G. and P. Kusch. On the hyperfine structure of hydrogen and deuterium—1009(L)
Pugh, E. M. (see Foner, S.)—230(A)
—— (see Heine-Geldern, R.)—230(A)
——, **R. Heine-Geldern, and E. C. Mutschler.** II. Kerr cell photography of high speed phenomena—metal jet charges—230(A)

Querzoli, R. (see Ageno, M.)—720(L)
—— (see Mezzetti, L.)—168(L)
Quimby, S. L. (see Pochapsky, T. E.)—892(L)
Quinnell, E. H. (see Clement, J. R.)—1028(L)

Racah, G. and N. Zeldes. On the spins of Li^6 and B^{10}—1012(L)
Rainwater, James. Nuclear energy level argument for a spheroidal nuclear model—432
Ramsey, Norman F. Nuclear magnetic moment of scandium^{45}—1010(L)
—— (see Kolsky, H. G.)—883(L)
Randall, C. A., N. Sherman, and W. E. Hazen. Absorption of penetrating cosmic rays underground—905(L)
Rankin, B. (see Bradner, Hugh)—720(L)
Rasetti, Franco (see Madansky, Leon)—397(L)
Rastrup-Andersen, J. (see Bak, B.)—190(L)
Rau, R. Ronald and G. G. Harris. Preliminary results of a cloud-chamber study of the cosmic radiation at an altitude of 90,000 feet—206(A)
—— **and G. G. Harris.** Wide angle sprays produced by cosmic radiation—915
Ravilious, C. F. (see Elliot, J. O.)—393(L)
Read, W. T., Jr. (see Frank, F. C.)—722(L)
Reber, Grote. Galactic radio waves—234(T)
Rediker, R. H. and H. S. Bridge. Absorption measurements on cosmic-ray particles producing nuclear interactions at 10,600 feet—206(A)
Redman, W. C. Angular distributions of ground-state protons from $B^{10}+D$—6
Reed, Ronald L. and M. Dresden. Uncertainty principle for an arbitrary number of variables—200(A)
Reese, R. M. (see Dibeler, V. H.)—223(A)
—— (see Mohler, Fred L.)—223(A)
Remeika, J. P. (see Galt, J. K.)—214(A), 391(L)
Remley, M. E. (see Griffith, G. L.)—443
Retherford, Robert C. (see Lamb, Willis E., Jr.)—549
Reynolds, C. A. (see Serin, B.)—211(A)
Reynolds, D. C. and S. J. Czyzak. Single synthetic zinc sulfide crystals—543(L)
Reynolds, G. T. (see Harrison, F. B.)—745(L)
Reynolds, John H. Mass spectrometric investigation of branching in Cu^{64}, Br^{80}, Br^{82}, and I^{128}—789
—— Mass spectrometric investigation of branching in neutron inducer activities—243(A)
—— New long-lived krypton activity—886(L)
Reynolds, Joseph M. and C. T. Lane. Superconducting bismuth alloys—405(L)
Ribe, Fred L. (see Groetzinger, Gerhart)—228(A), 454, 904(L)
Rice, O. K. Thermodynamics of liquid helium and of He^3-He^4 solutions—1024(L)
Richards, H. T. (see Bashkin, S.)—238(A)
——, **S. Bashkin, D. S. Craig, D. Donahue, V. R. Johnson, and D. Martin.** Yield of scattered protons from Li^7—239(A)
Richardson, J. E. Neutrons from the disintegration of C^{13} by deuterons—415(A)
Richardson, John M. Irreversibility and the statistical mechanical derivation of the equations of hydrodynamics—200(A)
Richman, Chaim (see Cork, Bruce)—71
—— (see Wilcox, H. A.)—198(A)
Riddell, R. J., Jr. On the notion of pressure in a canonical ensemble—200(A)
Ridgway, S. L. Beta-gamma-angular correlation in Rb^{86}, Au^{198}—243(A)
Ring, Harold (see Kessler, Myer)—54
Ringo, G. R. (see Hughes, D. J.)—227(A)
Rink, F. J. Radiofrequency positive ion source—414(A)
Risser, J. R. (see Bonner, T. W.)—240(A)
Ritchie, R. H. (see Hurst, G. S.)—415(A)
Roberts, A. (see Moon, M. L.)—905(L)
—— (see Waggoner, M. A.)—236(A)
Roberts, James H. (see Guier, William H.)—719(L)
Roberts, T. R. and Alfred O. Nier. Ca^{40}-A^{40} mass difference and the radioactivity of K^{40}—198(A)
Robertson, Harry S. and G. H. Dieke. Electrical oscillations in spark discharges—232(A)
Robinson, C. S. (see Adams, G. D.)—208(A)
Rosen, Louis (see Allred, J. C.)—227(A)
—— (see Freier, George D.)—239(A), 721(L)
Rosenbluth, M. N. High energy elastic scattering of electrons on protons—615
Rossi, Bruno (see McMahon, Allen J.)—205(A)
Roth, L. M. (see Doughty, J.)—203(A)
Rubin, Thor (see Johnston, Herrick L.)—235(A)
Ruderman, I. W. (see Martinson, O.)—178(L)
Rudermann, M. (see Finkelstein, R.)—220(A)

Rutledge, W. C. (see Cork, J. M.)—238(A), 889(L), 938
——, **A. E. Stoddard, C. E. Branyan, J. LeBlanc, and J. M. Cork.** 282-day radioactivity in silver 110—237(A)
Ryan, Alden H. Paramagnetic resonance in single crystals of the manganous halides—226(A)

Sabin, R. (see Winckler, J. R.)—656
Sachs, R. G. (see Abery, R.)—220(A)
—— **and L. L. Foldy.** Scattering of gamma-rays by protons—221(A)
Sáenz, A. W. On time-independent integrals of motion of the one-body problem in Dirac theory—1004(L)
Sagalyn, P. (see Brossel, J.)—225(A)
Salam, Abdus. Differential identities in three-field renormalization problem—910(L)
Salant, E. O. (see Fisk, C. B.)—205(A)
——, **J. Hornbostel, C. B. Fisk, and J. E. Smith.** Latitude effects for stars. I. Production rates and prong distributions—184(L)
——, **J. Hornbostel, C. B. Fisk, and J. E. Smith.** Latitude effects for stars. II. Shower particles—184(L)
Salkovitz, E. (see Koehler, J. S.)—202(A)
Sanders, J. H. (see Allen, K. W.)—238(A)
—— (see Almqvist, E.)—209(A)
——, **K. W. Allen, E. Almqvist, J. T. Dewan, and T. P. Pepper.** T+T reaction: II. Energy distribution of the neutrons—238(A)
Sands, M. L. (see Getting, I. A.)—208(A)
Saur, A. J., P. Axel, L. G. Mann, and J. Ovadia. Beta-spectrographic investigation of Ru^{103} and Rh^{103m}—237(A)
Sawyer, G. A. and M. L. Wiedenbeck. Decay constants of K^{40}—490
Sayers, N. D. and K. G. Emeleus. Wave-length of the trans-auroral line of oxygen—166(L)
Schaaf, S. A. (see Folsom, R. G.)—546(T)
Scharff-Goldhaber, G. (see Sunyar, A. W.)—181(L)
Scheidegger, A. E. and L. Infeld. Gravitational radiation and motion—201(A)
Schein, Marcel (see Forbush, Scott E.)—501
—— (see Gottlieb, M. B.)—741(L)
—— (see Lord, J. J.)—540(L)
Scherrer, P. (see Hamouda, I.)—529(L)
Schild, A. (see Pirani, F. A. E.)—986
Schiller, Ralph (see Bergmann, Peter G.)—201(A)
Schwarz, Guenter (see Bearden, J. A.)—674
Schwertz, F. A. and Jeanne E. Brow. Diffusivity of water vapor in some common gases—223(A)
Schwinger, Julian (see Lippmann, B. A.)—469
Scott, Allen B. and Lamar P. Bupp. Equilibrium between *F*-centers and higher aggregates in KCl—341
——, **Henry J. Hrostowski, and Lamar P. Bupp.** Paramagnetism of color centers in KCl—346
Scott, M. B. (see Lyman, E. M.)—228(A)
Scott, Russell B. (see Herzfeld, Karl F.)—911(L)
Seaborg, Glenn T. (see Batzel, Roger E.)—528(L)
—— (see Hagemann, French)—435
—— (see Street, K., Jr.)—530(L)
Segrè, E. (see Kelly, E.)—96
Seitz, Frederick. Generation of vacancies by dislocations—1002(L)
—— Note on the theory of resistance of a cubic semiconductor in a magnetic field—372
—— On the formation of dislocations from vacancies—890(L)
—— On the nature of V-centers in the alkali halides—529(L)
—— Prismatic dislocations and prismatic punching in crystals—723(L)
—— Spiral prismatic dislocations and the origin of slip bands—1003(L)
—— (see Castellan, G. W.)—216(A)
—— (see Fröhlich, H.)—526
Seriff, A. J., R. B. Leighton, C. Hsiao, E. W. Cowan, and C. D. Anderson. On the new unstable cosmic-ray particles—204(A)
Serin, B. (see Garfunkel, M. P.)—211(A)
——, **C. A. Reynolds, and M. P. Garfunkel.** Experiment with alternating currents on tin superconductors. II—211(A)
Shamos, M. H. (see Zar, Jacob L.)—207(A)
Shapiro, B. (see Doughty, J.)—203(A)
Shapiro, E. (see Mandeville, C. E.)—243(A), 391(L)
Sharbaugh, A. Harry, Benjamin S. Pritchard, Virginia G. Thomas, John M. Mays, and Benjamin P. Dailey. Microwave rotational spectrum and structure of bromogermane—189(L)
Shaw, J. H., R. M. Chapman, and J. N. Howard. Improved map of the solar spectrum between 9 and 10μ—1017(L)
Shaw, R. Explicit representation of the flow in the region of interaction of two arbitrary simple waves in one-dimensional compressible fluid flow—547(A)
Shea, Ruth C. and Gladys A. Anslow. Effect of aging and of heat treatment on the infra-red and ultraviolet spectra of urea—234(A)
Sher, R., J. Halpern, and W. E. Stephens. Formation of N^{17} by gamma-ray bombardment of O^{18}—241(A)
Sheridan, John (see Gordy, Walter)—224(A)
—— **and Walter Gordy.** Microwave spectrum of methyl bromo-acetylene—224(A)
—— **and Walter Gordy.** Nuclear quadrupole moment of N^{14} and the structure of nitrogen trifluoride from microwave spectra—513
Sheriff, Robert E. and Dudley Williams. Nuclear magnetic moment of scandium^{45}—175(L)
Sherman, N. (see Randall, C. A.)—905(L)
Sherr, R. (see Franzen, W.)—209(A), 742(L)
Shockley, W. Effect of magnetic fields on conduction—"tube integrals"—191(L)
—— Fundamental processes of magnetization shown by movies—215(T)
Shoemaker, F. C., J. E. Faulkner, S. G. Kaufmann, and G. M. B. Bouricius. Scattering and capture of protons by aluminum—228(A)
Shull, C. G. (see Koehler, W. C.)—395(L)
Siegel, Keeve M. Incompressible, ideal, subsonic flow past an infinite cone—229(A)
Siegert, A. J. F. (see Petritz, R. L.)—215(A)
Silsbee, H. B. (see Kolsky, H. G.)—883(L)
Simon, Albert. Bremsstrahlung in high energy nucleon-nucleon collisions—573
Simpson, J. Arol. Quantitative field mapping by the electron optical shadow method—215(A)
—— (see Marton, L.)—215(A)
Simpson, O. C. (see Huizenga, J. R.)—908(L)
Singer, S. F. (see Van Allen, J. A.)—206(A)
Sinha, M. S. Mixed shower of nuclear origin—1025(L)
Sitte, K. On penetrating showers and meson production—204(A)
Skavlem, S. (see Hylleraas, Egil)—117
Skinner, W. C. and F. G. Slack. Ultrafiltration experiments with silver membranes—417(A)
Slack, F. G. (see Skinner, W. C.)—417(A)
Sloth, E. N. (see Duffield, R. B.)—1011(L)
Smaller, B., J. May, and M. Freedman. Scintillation studies on potassium iodide—940
Smelt, R. Recent research at the Naval Ordnance Laboratory on hypersonic flow—546(T)
Smith, A. Lee, William E. Keller, and Herrick L. Johnston. Infra-red spectra of condensed oxygen and nitrogen—728(L)
Smith, D. F., M. Tidwell, and D. V. P. Williams. Microwave spectrum of BrCl—1007(L)
Smith, E. C. and J. W. Beams. High constant speed rotating mirror—222(A)

Smith, J. E. (see Fisk, C. B.)—205(A)
—— (see Salant, E. O.)—184(L), 184(L)
Smith, Robert S. (see Klein, Martin J.)—214(A)
Smith, William V. (see Burkhalter, James H.)—224(A), 651
—— (see Howard, Raydeen R.)—128, 225(A)
—— **and Raydeen Howard.** Microwave collision diameters II. Theory and correlation with molecular quadrupole moments—132
Snoddy, L. B. (see Clark, G. W.)—232(A)
Snyder, Hartland S. Quantum field theory—520
Solbrig, A. W., Jr. (see Perkins, J. F.)—415(A)
Solomon, A. K. Half-life of sodium 24—403(L)
Sorensen, B. N., B. M. Dale, and J. D. Kurbatov. Disintegration scheme of scandium^{46}—1007(L)
Spence, R. D. (see Leitner, Alfred)—199(A)
Sperduto, A. (see Buechner, W. W.)—262
—— (see Van Patter, D. M.)—900(L)
Spetner, L. M. (see Williams, R. W.)—207(A)
Spitzer, L., Jr. (see Wolfe, Bertram)—1020(L)
Sponer, H. (see Cooper, C. D.)—235(A)
Squire, Charles F. Recent research in low temperature physics—414(T)
Staker, William P. and W. O. Davis. Latitude dependence of atmospheric neutrons at high altitudes—207(A)
Stearns, M. B. (see Keck, J. C.)—199(A)
—— (see Walker, R. L.)—242(A)
Steele, M. C. (see Webber, R. T.)—1028(L)
Steinberger, J. (see Chamberlain, O.)—394(L)
Steinwedel, Helmut and Michael Danos. Proton density variation in nuclei—1019(L)
——, **J. Hans D. Jensen, and Peter Jensen.** Nuclear dipole vibrations—1019(L)
Stephens, W. E. (see Sher, R.)—241(A)
Stevens, V. J. Hypersonic research facilities at the Ames Aeronautical Laboratory—546(T)
Stevens, W. H. (see Yaffe, L.)—893(L)
Stever, H. G. Effect of thermal radiation on hypersonic flow in wind tunnels and free flight—546(T)
Stinchcomb, Thomas B. (see Forbush, Scott E.)—501
Stix, T. (see Winckler, J. R.)—656
Stoddard, A. E. (see Cork, J. M.)—238(A), 889(L), 938
—— (see Rutledge, W. C.)—237(A)
Stone, Orville. Electron injection gun for the M.I.T. 350-Mev synchrotron—209(A)
Storrs, C. L., Jr. (see Cooper, D. I.)—208(A)
Storruste, A. Neutron-induced radioactivity in palladium—193(L)
Stout, J. W. and Lester Guttman. Meissner effect in superconducting alloys of indium and thallium—396(L)
Strait, E. N. (see Buechner, W. W.)—262
—— (see Van Patter, D. M.)—900(L)
——, **D. M. Van Patter, and W. W. Buechner.** Ground state of B^{12} from the $B^{11}(d,p)B^{12}$ reaction—240(A)
Straley, Joseph W. (see Jones, Emily W.)—417(A)
—— **and Morita Crymes.** Liquid prism photoelectric Raman spectrograph—416(A)
Stratton, T. F. (see Freier, George D.)—239(A), 721(L)
Strauch, Karl. Isomerism in Co^{58}—487
—— Nuclear reactions induced by high energy x-rays—241(A)
Street, K., Jr., A. Ghiorso, and G. T. Seaborg. Isotopes of americium—530(L)
Strumski, C. J. (see Cooper, D. I.)—208(A)
Studier, M. H. (see Hagemann, French)—435
Stump, Robert and Sherman Frankel. β-γ-angular correlation measurements—243(A)
Sturrock, P. A. Theorem on the focusing of electron beams in magnetic fields of certain "mirror" symmetry, with two corollaries, one on the fringe effect—215(A)
Sugarman, Nathan. Photo-fission of bismuth—532(L)
Sun, K. H., R. A. Charpie, F. A. Pecjak, B. Jennings, J. F. Nechaj, and A. J. Allen. Delayed neutrons from U^{238} and Th^{232} fission—3, 197(A)
Sunyar, A. W., D. Alburger, G. Friedlander, M. Goldhaber, and G. Scharff-Goldhaber. Isomerism in Pb^{204} and "memory" in angular correlation—181(L)
Sutton, R. B. (see Pearlstein, E. A.)—217(A), 907(L)
Swann, C. P. (see Mandeville, C. E.)—787
—— **and C. E. Mandeville.** Nuclear energy levels in nitrogen (14) and aluminum (27)—240(A)
——, **C. E. Mandeville, and W. D. Whitehead.** Neutrons from the disintegration of the separated isotopes of magnesium by deuterons—598
Swann, W. F. G. On certain matters pertaining to electrets—213(A)
Sweeney, D. (see Goldstein, L.)—218(A)
Swenson, C. A. Liquid-solid transformation in helium near absolute zero—626
Swift, C. J. Extrapolation of the geomagnetic potential—222(A)
Swope, I. G. (see Getting, I. A.)—208(A)

Taft, E. (see Apker, L. A.)—964
Tamor, Stephen. Absorption of π^--mesons by deuterons—221(A)
Taschek, R. F. (see Jarvis, G. A.)—929
Taylor, H. S. Adsorption, catalysis, and the physics of surfaces—197(T)
Taylor, W. J., C. W. Beckett, J. Y. Tung, R. B. Holden, and H. L. Johnston. Raman and infra-red spectra of pentaborane—234(A)
Temmer, G. M. Scattering of 250-Mev protons from nucleons within nuclei—227(A)
Ter-Pogossian, Michel, Fred T. Porter, and C. Sharp Cook. System for the study of short-lived radioactive gases—244(A)
Terrell, James. Pair spectrometer investigation of high energy gamma-rays—415(A)
—— Pair spectrum of gamma-rays from polonium-beryllium—239(A)
Thaler, W. J. (see Fitzpatrick, J. A.)—231(A)
Thirring, W. Quantization of higher order equations—703
Thomas, C. O. (see Koski, W. S.)—217(A)
Thomas, D. A. (see Haynes, S. K.)—414(T)
Thomas, G. E. (see Harris, S. P.)—11
Thomas, J. E., Jr. (see Getting, I. A.)—208(A)
Thomas, Virginia G. (see Sharbaugh, A. Harry)—189(L)
Thomsen, John S. and T. H. Berlin. Phase transition due to dipole interaction in a simple cubic crystal—203(A)
Thulin, Sigvard (see Bergström, Ingmar)—537(L), 538(L)
Thurn, H. (see Bothe, W.)—544(L)
Tidwell, M. (see Smith, D. F.)—1007(L)
Ting, Yu, Roy C. Weidler, and Dudley Williams. Effective g-values of various paramagnetic ions—226(A)
Tinlot, J. H. (see Gregory, B. P.)—205(A)
—— **and B. P. Gregory.** Cross sections for nuclear collisions of protons and π-mesons—205(A)
Tiomno, J. (see Yang, C. N.)—495
Todd, Jay, Jr. (see Miller, Charles E.)—206(A), 459
Tollestrup, A. V. (see Chao, C. Y.)—108
Tomboulian, D. H. (see Pell, E. M.)—210(A)
Tomkins, Frank S. (see Fred, Mark)—212(A)
Tongiorgi, V. Cocconi (see Cocconi, G.)—730(L), 768
Tousey, R. (see Watanabe, K.)—217(A)
Townes, C. H. (see Geschwind, S.)—226(A)
—— (see Low, W.)—224(A)
—— **and W. Low.** Evidence from nuclear masses on proposed closed shells at 20 nucleons—198(A)
Trambarulo, Ralph (see Kessler, Myer)—54
—— **and Walter Gordy.** Microwave spectra and molecular constants of CD_3NC and CD_3CN—224(A)

Trounson, E. P., D. F. Bleil, and L. R. Maxwell. Magnetic resonance absorption in chromium sesquioxide—226(A)
——, **D. F. Bleil, R. K. Wangsness, and L. R. Maxwell.** Magnetic resonance in antiferromagnetic materials near the Curie temperature—542(L)
Truesdell, C. Vorticity averages—229(A)
Tung, J. Y. (see Taylor, W. J.)—234(A)

Uhlenbeck, G. E. (see Falkoff, David L.)—323, 334
—— (see Pais, A.)—145

Van Allen, J. A. and A. V. Gangnes. On the azimuthal asymmetry of cosmic-ray intensity above the atmosphere at the geomagnetic equator—51
—— **and S. F. Singer.** Total primary cosmic-ray energy at the geomagnetic equator—206(A)
Van Asselt, Robert and Dudley Williams. Further studies of infra-red absorption by homopolar diatomic molecules—1016(L)
Van Bronkhorst, A. (see Marton, L.)—215(A)
Van Patter, D. M. (see Buechner, W. W.)—240(A), 262
—— (see Strait, E. N.)—240(A)
——, **A. Sperduto, E. N. Strait, and W. W. Buechner.** Magnetic analysis of the $B^{10}(p,\alpha)Be^{7}$ reaction—900(L)
Van Tuyl, A. H. On nearly glancing reflection of weak shocks—230(A)
Van Vleck, J. H. (see Kuhn, T. S.)—382
Varnerin, Lawrence J., Jr. and Sanborn C. Brown. Microwave determinations of average electron energies and the first Townsend coefficient in hydrogen—946
Villars, F. On the energy-momentum tensor of the electron—122
Voigt, A. F. (see Hein, R. E.)—783
—— (see Powers, Ruth I.)—175(L)
Volger, J. Note on the Hall potential across an inhomogeneous conductor—1023(L)
von Dardel, Guy. Precision determination of the half-life of radium *C'*—734(L)
Voyvodic, L. (see Pickup, E.)—899(L)

Waggoner, M. A. (see Moon, M. L.)—905(L)
——, **M. L. Moon, and A. Roberts.** Internal conversion coefficients in Co^{60}—236(A)
Wagner, F., Jr. (see Freedman, M. S.)—410(L)
Walker, J. G. (see Bozorth, R. M.)—888(L)
Walker, R. L. Gamma-ray spectra from B^{10}, B^{11}, and Be^{9} under proton bombardment—172(L)
——, **B. D. McDaniel, and M. B. Stearns.** Neutron yields from photo-disintegration by 17.6-Mev gamma-rays—242(A)
Walker, W. H. (see Bartholomew, G. A.)—218(A)
—— (see Kinsey, B. B.)—218(A)
Wallace, J. R. (see Blair, J. Morris)—28
Walske, M. C. (see Bethe, H. A.)—413(L)
Wangsness, R. K. (see Bleil, D. F.)—227(A)
—— (see Trounson, E. P.)—542(L)
Wannier, G. H. Antiferromagnetism. The triangular Ising net—357
Wantuch, Ernest. Neutron-deuteron scattering at 4.5 and 5.5 Mev—729(L)
Ward, J. C. Convergent non-linear field theory—406(L)
Wataghin, G. (see Garelli, C. M.)—718(L)
—— (see Panetti, M.)—177(L)
Watanabe, K., F. S. Johnson, and R. Tousey. Constant quantum efficiency of some luminescent materials in the vacuum ultraviolet—217(A)
Watchell, P. (see Ladenburg, R.)—548(A)
Watson, Kenneth M. (see Brueckner, K. A.)—187(L)
—— **and Edward W. Hart.** On the use of the Tomonaga intermediate coupling method in meson theory—918
Watson, W, W. (see Zucker, A.)—241(A)
Waymouth, J. F., Jr. Deterioration of oxide-coated cathodes under low duty-factor operation—233(A)
Webber, R. T. and M. C. Steele. Thermoelectromotive force of tin at the superconducting-normal junction—1028(L)
Wei, J. P. N. Narrow air showers of cosmic rays. II. Absorption measurements—670
Weidler, Roy C. (see Ting, Yu)—226(A)
Weimer, David. Supersonic flow in a shock tube—546(A)
Weimer, Paul K. Photo-conductivity in amorphous selenium—171(L)
Weinstein, M. S. and W. C. Wineland. Transmission and reflection of ultrasonic waves from a solid plate in water—416(A)
Wells, E. J., Jr. (see Dibeler, V. H.)—223(A)
—— (see Mohler, Fred L.)—223(A)
Welton, T. A. Photo-alpha-reactions in light nuclei—241(A), 399(L)
Wentink, T., Jr. (see Cohen, V. W.)—191(L)
Wentzel, Gregor. μ-pair theories and the π-meson—710
Wert, C. A. Diffusion coefficient of C in α-iron—601
—— (see Dijkstra, L. J.)—979
Wexler, Aaron and W. S. Corak. Superconductivity of vanadium—737(L)
Whaling, Ward and T. W. Bonner. Disintegration of Li^{6} by deuterons—258
—— **and J. W. Butler.** Neutrons from the bombardment of Li^{6} by deuterons—414(A)
White, D. R. (see Bleakney, W.)—546(A)
White, David. Second virial coefficients of non-polar binary gas mixtures—236(A)
—— (see Johnston, Herrick L.)—235(A)
——, **Abraham S. Friedman, and Herrick L. Johnston.** Forces of interaction in a solution of two non-polar gases: hydrogen and nitrogen—235(A)
——, **Abraham S. Friedman, and Herrick L. Johnston.** Intermolecular force constants for hydrogen and for nitrogen—235(A)
—— **and Herrick L. Johnston.** Intermolecular force constants for helium and for deuterium—236(A)
White, M. G. (see Lipkin, H. J.)—892(L)
Whitehead, M. N. (see Wilcox, H. A.)—198(A)
Whitehead, W. D. Low energy neutron spectrum from $Li^{7}(d,n)Be^{8}$—393(L)
—— Neutrons from the disintegration of Li^{7} by deuterons—239(A)
—— Scattering of protons by carbon—1022(L)
—— (see Swann, C. P.)—598
—— **and N. P. Heydenburg.** Proton groups from the deuteron bombardment of aluminum, sodium, and manganese—99
Whitman, A. S. (see Marshak, R. E.)—220(A)
Widgoff, M. (see Cocconi, G.)—768
Wiedenbeck, M. L. (see Beyster, J. R.)—169(L), 411(L), 728(L)
—— (see Sawyer, G. A.)—490
Wiegand, Clyde (see Chamberlain, Owen)—81, 394(L)
—— (see Kelly, E.)—96
Wightman, A. S. (see Wolfe, Bertram)—1020(L)
Wigner, E. P. (see Feingold, A. M.)—221(A)
—— (see Jaynes, E. T.)—213(A)
Wilcox, H. A., W. F. Cartwright, C. Richman, and M. N. Whitehead. Technique for measuring meson production cross sections in the forward direction—198(A)
Wilkinson, Geoffrey. Note on 11.5-day Tl^{202}—1014(L)
—— **and Harry G. Hicks.** Radioactive isotopes of the rare earths. III. Terbium and holmium isotopes—815
Wilkinson, Michael K. Crystallographic variations in field emission from single tungsten crystals—233(A)
Williams, D. V. P. (see Smith, D. F.)—1007(L)
Williams, Dudley (see Sheriff, Robert E.)—175(L)
—— (see Ting, Yu)—226(A)
—— (see Van Asselt, Robert)—1016(L)

Williams, F. C. (see Chance, B.)—244(A)
Williams, Quitman and Walter Gordy. Microwave spectrum of bromoform and phosphorus tribromide—225(A)
Williams, R. W., L. M. Spetner, W. L. Kraushaar, and H. W. J. Courant. Cloud chamber triggered by internal scintillation counter—207(A)
Wilson, H. W. Radioactivity of Ni^{59} and Ni^{63}—1032(L)
Wilson, Richard. Cross-over transitions in Ir^{194}, Ag^{110}, Cs^{134}—1004(L)
Wilson, Robert R. Monte Carlo calculations of showers in lead—204(A)
—— (see Keck, J. C.)—199(A)
Winckler, J. R., T. Stix, K. Dwight, and R. Sabin. Directional and latitude survey of cosmic rays at high altitudes—656
Wineland, W. C. (see Weinstein, M. S.)—416(A)
—— **and Clyde B. Crawley.** Theory of models of acoustical systems—416(A)
Winslow, G. H. (see Huizenga, J. R.)—908(L)
Wirtz, K. (see Gierer, A.)—906(L)
Witmer, Enos E. Integral relationships between atomic and nuclear quantities—198(A)
Wolfe, Bertram, P. Mc.R. Routly, A. S. Wightman, and L. Spitzer, Jr. Acceleration of dust grains by supernovae—1020(L)
Wollan, E. O. (see Koehler, W. C.)—395(L)
Woltz, Patricia J. H. and Ernest A. Jones. Some new measurements on the infra-red and Raman spectra of SiF_4—416(A)
Wood, E. A. (see Yager, W. A.)—214(A)
Woodcock, Karl S. (see Duckworth, Henry E.)—188(L), 198(A)
Woods, S. B. (see More, K. R.)—208(A)
Woodward, W. M. (see Page, Lorne A.)—228(A)
Wotring, A. William (see Miller, Charles E.)—459
Wright, Byron T. (see Faris, F. E.)—577
Wright, S. Courtenay. Li^8 splinters from nuclear bombardments—838
Wrinch, Dorothy. Vector functions for uniform spheres and spherical shells—203(A)
Yadoff, Oleg. On the state of conductivity created in a liquid isolator under the action of an electric dispersive field—223(A)
Yaffe, L. and W. H. Stevens. Reaction $C^{14}(n,\gamma)C^{15}$—893(L)
Yager, W. A. (see Guillaud, Charles)—181(L)
——, **J. K. Galt, F. R. Merritt, E. A. Wood, and B. T. Matthias.** Ferromagnetic resonance in single crystals of nickel ferrite—214(A)
Yagoda, Herman. Emulsion chamber—a new photographic tool for the study of ionizing particle tracks—207(A)
Yang, C. N. and David Feldman. S-matrix in the Heisenberg representation—972
—— **and J. Tiomno.** Reflection properties of spin ½ fields and a universal Fermi-type interaction—495
Yasaki, T. and O. Miyatake. Note on asymmetric fission—740(L)
Yeater, M. L. (see Gaerttner, E. R.)—401(L)
York, Herbert. Gamma-rays from nuclear collisions—207(T)
Ypsilantis, T. J. (see Perlman, I.)—30
Yu, Yi-Yuan. Breaking of waves by an opposing current—546(A)

Zar, Jacob L. and M. H. Shamos, On the zenith angle and energy dependence of mesons at sea level—207(A)
Zatzkis, Henry (see Bergmann, Peter G.)—201(A)
—— (see Penfield, Robert)—201(A)
Zeldes, H. (see Brosi, A. R.)—902(L)
——, **B. H. Ketelle, and A. R. Brosi.** Radiations of krypton^{85}—901(L)
Zeldes, N. (see Racah, G.)—1012(L)
Zemansky, M. W. (see Cook, D. B.)—212(A), 1021(L)
Zilsel, P. R. Liquid helium II: the hydrodynamics of the two-fluid model—309
Zucker, A. and W. W. Watson. Concentration of argon 36 and study of the $A^{36}(d,p)A^{37}$ reactions—241(A)
Zünti, W. (see Frauenfelder, H.)—1029(L)

Analytic Subject Index to Volume 79

References with (A) are to abstracts of papers presented at meetings of the American Physical Society. References with (L) are to Letters to the Editor.

Absorption of radiation
Infra-red absorption in Si and Ge, J. Bardeen—216(A)
By KCl, *F*-centers and aggregates, Allen B. Scott and Lamar P. Bupp—341
Acoustics
Models, theory, W. C. Wineland and Clyde B. Crawley—416(A)
Transmission, reflection of ultrasonic waves, M. S. Weinstein and W. C. Wineland—416(A)
Ultrasonic absorption in glycerol, T. A. Litovitz—230(A)
Velocities of ultrasonic waves in liquids, David Ener—231(A)
Aerodynamics (see also **Hydrodynamics**)
Axially symmetric flows, Bertrand des Clers and Chieh-Chien Chang—547(A)
Alloys (see **Crystalline state**)
Astrophysics
Hydromagnetic equations, Walter M. Elsasser—183(L)
Red giants and cepheid variables, G. Gamow and C. Longmire—743(L)
Na *D* lines during twilight, origin, F. D. Kahn—167(L)
Source of galactic radio emission, cosmic rays, K. O. Kiepenheuer—738(L)
Wave-length of transauroral line of oxygen, N. D. Sayers and K. G. Emeleus—166(L)
Atmosphere (see **Meteorology**)
Atomic structure (see also **Energy states of atoms; Spectra**)
Fine structure of hydrogen atom, Willis E. Lamb, Jr. and Robert C. Retherford—549

Biophysics
Cavitation in biological suspensions, Eugene Ackerman—231(A)
Bremsstrahlung (see also **Radiation**)
In nucleon-nucleon collisions, Albert Simon—573
Transition curves, Wade Blocker, Robert Kenney, and Wolfgang K. H. Panofsky—419
Broadening of spectral lines
Of ammonia lines, Raydeen R. Howard and William V. Smith—128
Broadening and frequency modulation, Henry Margenau and Stanley Bloom—213(A)
Inversion frequency of ammonia, A. H. Nethercot, Jr. and C. W. Peters—225(A)
Microwave collision diameters, Raydeen R. Howard and William V. Smith—225(A)
Pressure broadening, T. Holstein—744(L)

Cold emission (see **Field currents**)
Conductivity, electrical (see **Electrical conductivity and resistance; Discharge of electricity in gases**)
Constants, physical standards
Atomic and nuclear quantities, integral relationships, Enos E. Witmer—198(A)
h/e, C. L. Hemenway and F. G. Dunnington—887(L)
h/e by x-rays, J. A. Bearden and Guenter Schwarz—674
Rydberg constant, Raymond T. Birge—193(L); Erratum—1005(L)
Cosmic radiation
Absorption at 10,600 ft., R. H. Rediker and H. S. Bridge—206(A)
Annihilation process for negative protons, J. Ashkin, T. Auerbach, and R. Marshak—266
Azimuthal asymmetry above atmosphere, primary radiation, J. A. Van Allen and A. V. Gangnes—51
Bursts at very high altitudes, G. W. McClure and M. A. Pomerantz—911(L)
Bursts in lead-shielded chamber, altitude and latitude dependence, Allen J. McMahon and Bruno Rossi—205(A)
Cascades of nuclear disintegrations, G. Cocconi, V. Cocconi Tongiorgi, and M. Widgoff—768
Cloud chamber at 90,000 ft., R. Ronald Rau and G. G. Harris—206(A)
Coincidence efficiency of gamma-rays, J. M. Barnothy and M. Forro—199(A)
Cross sections for collisions of protons and π-mesons, J. H. Tinlot and B. P. Gregory—205(A)
Directional and latitude survey, high altitudes, J. R. Winckler, T. Stix, K. Dwight, and R. Sabin—656
Dust grains, acceleration by supernovae, Bertram Wolfe, P. Mc.R. Routly, A. S. Wightman, and L. Spitzer, Jr.—1020(L)
Electrons at end of μ-meson tracks, William F. Fry—893(L)
Electrons in primaries, C. L. Critchfield, E. P. Ney, and Sophie Oleksa—402(L)
Emulsion chamber, ionizing particle tracks, Herman Yagoda—207(A)
Extensive air showers, G. Cocconi—1006(L)
Fluctuation in rate of production of nuclear disintegrations following solar flare, J. J. Lord, A. W. Elston, and Marcel Schein—540(L)
Heavy nuclei, azimuthal effect, E. P. Ney, J. Linsley, and P. S. Freier—206(A)
Heavy nuclei, nighttime flux, P. S. Freier, E. P. Ney, J. Naugle, and G. Anderson—206(A)
Intensity increase and solar activity, Scott E. Forbush, Thomas B. Stinchcomb, and Marcel Schein—501
Latitude effects for stars, production rates, E. O. Salant, J. Hornbostel, C. B. Fisk, and J. E. Smith—184(L)
Latitude effects for stars, shower particles, E. O. Salant, J. Hornbostel, C. B. Fisk, and J. E. Smith—184(L)
Magnetic cloud chamber at 3.4 km, Charles E. Miller, Joseph E. Henderson, David S. Potter, Jay Todd, Jr., and A. William Wotring—459
Mesons and protons at sea level, T. C. Merkle, Jr., E. L. Goldwasser, and Robert B. Brode—926
Mesons and protons at several altitudes and latitudes, Marcello Conversi—749
μ-mesons stopped in Al foils, W. Y. Chang—205(A)
Narrow air showers, J. P. N. Wei—670
N-component in extensive showers, G. Cocconi and V. Cocconi Tongiorgi—730(L)
Neutron production, altitude dependence, W. B. Fowler—178(L)
Neutrons at high altitudes, latitude dependence, W. P. Staker and W. O. Davis—207(A)
Nuclear evaporation, absorption of nucleonic component, G. Bernardini, G. Cortini, and A. Manfredini—952
Origin, Edwin M. McMillan—498; C. Y. Fan—912(L)
Particles associated with stars, penetration, C. G. Montgomery, D. D. Montgomery, and J. A. Northrop—293
Particles initiating penetrating showers, M. B. Gottlieb, A. J. Hartzler, and Marcel Schein—741(L)
Penetrating showers and meson production, K. Sitte—204(A)
Penetrating showers, cloud-chamber study, Melvin B. Gottlieb and Alfred J. Hartzler—204(A)
Penetrating showers in Pb and C, L. Mezzetti and R. Querzoli—168(L)

Cosmic radiation (continued)
Photons of high energy, B. P. Gregory and J. H. Tinlot—205(A)
π- and μ-meson production, Giulio Ascoli—812
Primary energy at geomagnetic equator, J. A. Van Allen and S. F. Singer—206(A)
Proton and meson components at 3.4 km, Charles E. Miller, Joseph E. Henderson, David S. Potter, and Jay Todd—206(A)
Shape of Rossi curve, W. Bothe and H. Thurn—544(L)
Shower of nuclear origin, M. S. Sinha—1025(L)
Showers at 11,500 ft., cloud chamber, Alfred J. Hartzler and Melvin B. Gottlieb—204(A)
Showers in lead, Monte Carlo calculations, Robert R. Wilson—204(A)
Solar flare, J. Clay and H. F. Jongen—908(L)
Source of galactic radio emission, K. O. Kiepenheuer—738(L)
Stars at different latitudes, C. B. Fisk, J. Hornbostel, E. O. Salant, and J. E. Smith—205(A)
Stars in metal foils, Ian Barbour and Lawrence Greene—406(L)
Stars, neutral radiation, E. Pickup and L. Voyvodic—899(L)
Underground absorption, C. A. Randall, N. Sherman, and W. E. Hazen—905(L)
Underground measurements, Lowell M. Bollinger—207(A)
Underground rays, C. M. Garelli and G. Wataghin—718(L)
Unstable particles, A. J. Seriff, R. B. Leighton, C. Hsiao, E. W. Cowan, and C. D. Anderson—204(A)
In upper atmosphere, M. Panetti and G. Wataghin—177(L)
Wide angle sprays, R. Ronald Rau and G. G. Harris—915
Zenith angle and energy of mesons at sea level, Jacob L. Zar and M. H. Shamos—207(A)

Cross section, measurements, theory (see also **Scattering of electrons, mesons, neutrons, protons, and ions**)
Annihilation process for negative protons, J. Ashkin, T. Auerbach, and R. Marshak—266
Collision diameters of molecules, William V. Smith and Raydeen Howard—132
Collision diameters of NH_3 and other gases, Raydeen Howard and William V. Smith.—128
Of (d,p) reactions, Harry Gove and Keith Boyer—241(A)
Fast neutron capture in Al^{27}, R. L. Henkel and H. H. Barschall—218(A)
Of Au, neutron capture, R. D. Hill—413(L)
Of Kr ^{80} for neutron absorption, John H. Reynolds—886(L)
$Li^6(d,p)Li^7$ reactions, Ward Whaling and T. W. Bonner—258
Of Mo^{100}, (γ,n) and (γ,p) reactions, R. B. Duffield, L. Hsiao, and E. N. Sloth—1011(L)
Neutron-proton capture, Lamek Hulthén—166(L)
n-p scattering, E. Kelly, C. Leith, E. Segrè, and C. Wiegand—96
Neutron resonance in Cl^{35}, C. T. Hibdon and C. O. Muehlhause—44, 219(A)
Neutron resonance scattering and absorption, S. P. Harris, C. O. Muehlhause, and G. E. Thomas—11
Neutrons in Pb, R. E. Peterson, R. K. Adair, and H. H. Barschall—935
Neutrons in noble gases, S. P. Harris—219(A)
For 120- and 345-ev neutron, C. T. Hibdon—747
Of Ni, coherent neutron scattering, W. C. Koehler, E. O. Wollan, and C. G. Shull—395(L)
For p-p scattering, Bruce Cork, Lawrence Johnston, and Chaim Richman—71; Owen Chamberlain and Clyde Wiegand—81
Proton-proton scattering, energy dependence, Bruce Cork—227(A)
Protons and π-mesons, J. H. Tinlot and B. P. Gregory—205(A)
Ratio for electron capture and electron loss, Theodore Hall—504
Scattering of neutrinos, J. H. Barrett—907(L)
$T^3(p,n)He^3$ reaction, constants, G. A. Jarvis, A. Hemmendinger, H. V. Argo, and R. F. Taschek—929
Of Va for neutrons, J. Morris Blair and J. R. Wallace—28

Crystal structure
Beta-brass structure, Louis Gold—202(A)
Dislocations, formation from vacancies, Frederick Seitz—890(L)
Displacement of oxygen in $BaTiO_3$, Edwin T. Jaynes—1008(L)
Inequalities in structure factors, H. Hauptman and J. Karle—204(A)
Lead sulfide films, J. Doughty, K. Lark-Horovitz, L. M. Roth, and B. Shapiro—203(A)
Multiplication processes for dislocations, F. C. Frank and W. T. Read, Jr.—722(L)
Perturbed period wave equation, three dimensions, Paula Feuer and Hubert M. James—216(A)
Prismatic dislocations, Frederick Seitz—723(L), 1003(L)
Prismatic punching, F. R. N. Nabarro—894(L)
Statistics of two-dimensional triangular Ising lattice, G. F. Newell—876
Vacancies generated by dislocations, Frederick Seitz—1002(L)
Vector functions for spheres and spherical shells, Dorothy Wrinch—203(A)

Crystalline state
Absorption bands in MgO crystals, J. P. Molnar and C. D. Hartman—1015(L)
Activation energy of Te, T. S. Moss—1011(L)
Antiferromagnetism, superexchange interaction, P. W. Anderson—350
Cohesive energies and compressibility of monovalent metals, T. S. Kuhn and J. H. Van Vleck—382
Cohesive energy of monovalent metals, W.K.B. method, T. S. Kuhn—515
Cooperative phenomena, entropy, Ryoichi Kikuchi—718(L)
Dielectric breakdown in ionic crystals, theory, H. Fröhlich and F. Seitz—526
Dielectric constant of ionic crystals, Sumner Mayburg—375
Diffusion of C in α-iron, C. A. Wert—601
Energy gap in Ge, temperature dependence, V. A. Johnson and H. Y. Fan—899(L)
F-centers and higher aggregates in KCl, Allen B. Scott and Lamar P. Bupp—341
Hall potential across an inhomogeneous conductor, J. Volger—1023(L)
High resistivity P-type germanium, W. C. Dunlap—286
Hydrogen bond energy, conduction data on ice, E. J. Murphy—203(A)
Infra-red absorption in Si and Ge, J. Bardeen—216(A)
Ionization of H in metals, Irvin Isenberg—736(L)
Isotope effect on transition temperature, Karl F. Herzfeld, Emanuel Maxwell, and Russell B. Scott—911(L)
Kink band in single crystal, J. S. Koehler and E. Salkovitz—202(A)
Mobility of electrons and holes in diamond, E. A. Pearlstein and R. B. Sutton—907(L)
Neutral impurity scattering in semiconductors, Cavid Erginsoy—1013(L)
Nickel ferrite, properties of crystals, J. K. Galt, B. T. Matthias, and J. P. Remeika—391(L)
Nuclear electric quadrupole interactions, R. V. Pound—685
Paramagnetism of color centers in KCl, Allen B. Scott, Henry J. Hrostowski, and Lamar P. Bupp—346

Phase transition, cubic crystal, John S. Thomsen and T. H. Berlin—203(A)
Photo-sensitive lead sulfide films, Raymond H. McFee—203(A)
Polaron states in ionic crystals, Herbert B. Callen—533(L)
Polymers, nuclear magnetism, L. Holroyd, B. A. Mrowca, and E. Guth—1026(L); B. A. Mrowca, L. V. Holroyd, and E. Guth—1026(L)
Scintillation spectra of organic crystals, W. S. Koski and C. O. Thomas—217(A)
Scintillations from crystals, photon counters, C. E. Mandeville and H. O. Albrecht—1010(L)
Single synthetic zinc sulfide crystals, D. C. Reynolds and S. J. Czyzak—543(L)
Soldered contact on semiconductor, Jacques I. Pantchechnikoff—1027(L)
Thermal equilibrium in *N*-irradiated semiconductors, J. H. Crawford, Jr. and K. Lark-Horovitz—889(L)
Trapped hole color centers in alkali halides, E. Burstein and J. J. Oberly—903(L)
Trapped holes in alkali halides, E. Burstein and J. J. Oberly—217(A)
V-centers in alkali halides, Frederick Seitz—529(L)

Diamagnetism (see **Magnetic properties**)
Dielectric constants (see **Dielectrics and dielectric properties**)
Dielectrics and dielectric properties
Constant of ionic crystals, effect of pressure, Sumner Mayburg—203(A), 375
Of dry air, velocity of waves, J. V. Hughes—222(A)
Of nickel ferrite, single crystals, J. K. Galt, B. T. Matthias, and J. P. Remeika—214(A), 391(L)
Of Se, F. J. Morris, 418(A)
Diffusion
Of C in α-iron, C. A. Wert—601
In ionosphere, M. H. Johnson and E. O. Hulburt—802
Water vapor in common gases, F. A. Schwertz and Jeanne E. Brow—223(A)
Discharge of electricity in gases
Anode phenomena in high current arcs, C. J. Gallagher—231(A)
Current fluctuations in plasma, P. Parzen and L. Goldstein—231(A)
Diffusion in ionosphere, M. H. Johnson and E. O. Hulburt—802
Diffusion in neon, Manfred A. Biondi—733(L)
Electron conductivity, mean free paths, Fred P. Adler and Henry Margenau—970
Electron energies, microwave determinations, Townsend coefficient in H_2, Lawrence J. Varnerin, Jr. and Sanborn C. Brown—946
Electron removal in He afterglows, B. T. McClure, R. A. Johnson, and R. B. Holt—232(A)
Formative time lags of spark, G. A. Kachickas and L. H. Fisher—232(A)
High current electron pulses in resonant cavity, G. W. Clark and L. B. Snoddy—232(A)
High currents over long paths, Cresswell Hatchett and John W. Flowers—417(A)
Low pressure Hg arc, Robert M. Howe—231(A)
Magnetically controlled diffusion, de-ionization, O. T. Fundingsland and George E. Austin—232(A)
Oscillations in spark, Harry S. Robertson and G. H. Dieke—232(A)
Plasma boundaries and oscillations, D. Bohm and E. P. Gross—992
Plasma fluctuations, P. Parzen and L. Goldstein—190(L)
Plasma oscillations, electron interactions, David Pines and David Bohm—232(A)
Recombination of ions, Richard Hanau—417(A)
Wind produced by arc in magnetic field, H. C. Early and W. G. Dow—186(L)
Disintegration and excitation of nucleus (see also **Photodisintegration; Radioactivity; Cross sections, measurements, theory**)
Of Al, Na, Mn by *d*, proton groups, W. D. Whitehead and N. P. Heydenburg—99
Angular correlation in $F^{19}(p,\alpha)O^{16*}(\gamma)O^{16}$, W. R. Arnold—170(L)
$A^{36}(d,p)A^{37}$ reactions, A. Zucker and W. W. Watson—241(A)
Of As^{75}, J. Y. Mei, Allan C. G. Mitchell, and C. M. Huddleston—19
Of Be^7, excited state, George D. Freier, T. F. Stratton, and L. Rosen—721(L)
Beta-gamma- and gamma-gamma-angular correlation in Sb^{124}, J. R. Beyster and M. L. Wiedenbeck—169(L)
Beta-gamma-angular correlation, David L. Falkoff and G. E. Uhlenbeck—334
β-γ-correlations, effect of nuclear charge, M. Fuchs and E. S. Lennox—221(A)
Of B^{10} by *d*, angular distributions of protons, W. C. Redman—6
$B^{10}(p,\alpha)Be^7$ reaction, D. M. Van Patter, A. Sperduto, E. N. Strait, and W. W. Buechner—900(L)
Branching in neutron inducer activities, mass spectrometric investigation, John H. Reynolds—243(A)
Of C^{13} by *d*, neutrons, J. E. Richardson—415(A)
Cascades of nuclear disintegrations, G. Cocconi, V. Cocconi Tongiorgi, and M. Widgoff—768
Deuterons and alphas from protons on Be^9, J. A. Neuendorffer, D. R. Inglis, and S. S. Hanna—239(A)
Directional correlation of successive radiations, David L. Falkoff and G. E. Uhlenbeck—323
Energy levels in B^{11}, W. W. Buechner and D. M. Van Patter—240(A)
Excitation curves for $B^{10}(d,p)B^{11}$, G. C. Phillips—240(A)
Excitation levels in B^{10}, T. W. Bonner, J. W. Butler, and J. R. Risser—240(A)
Excited state of Be^7, Geo. D. Freier, L. Rosen, and T. F. Stratton—239(A)
Of F by *p*, alpha-particles, C. Y. Chao, A. V. Tollestrup, W. A. Fowler, and C. C. Lauritsen—108
Formation of M^{17} in $O^{18}(\gamma,p)N^{17}$, R. Sher, J. Halpern, and W. E. Stephens—241(A)
Gamma-rays from $Be^9(\alpha n,\gamma)C^{12}$, James Terrell—239(A)
Gamma-rays from B^{10}, B^{11}, and Be^9, proton bombardment, R. L. Walker—172(L)
Gamma-rays from $H^1(n,\gamma)D^2$, binding energy of deuteron, R. E. Bell and L. G. Elliott—282
Gamma-rays from Po-Be neutron source, P. R. Bell and W. H. Jordan—392(L)
Ground state of B^{12}, E. N. Strait, D. M. Van Patter, and W. W. Buechner—240(A)
He^3 and P from Li^6+P, S. Bashkin, F. Ajzenberg, C. P. Browne, Gerson Goldhaber, M. J. W. Laubenstein, and H. T. Richards—238(A)
Of Li^6 by *d*, neutrons, Ward Whaling and J. W. Butler—414(A)
$Li^6(d,p)Li^7$ reactions, cross sections, Ward Whaling and T. W. Bonner—258
Li^8 ejected by gamma-rays, C. H. Millar and A. G. W. Cameron—182(L)
Li^8 splinters from nuclear bombardments, S. Courtenay Wright—838
Low energy neutrons from $Li^7(d,n)Be^8$, W. D. Whitehead—393(L)
Neutron capture γ-ray multiplicity, C. O. Muehlhause—219(A), 277
Neutron capture γ-rays, Mg, Si, P, and K, B. B. Kinsey, G. A. Bartholomew, and W. H. Walker—218(A)

Disintegration and excitation of nucleus (continued)
Neutron capture-radiation, heavy elements, G. A. Bartholomew, B. B. Kinsey, and W. H. Walker—218(A)
Neutron spectrum from proton bombardment of Be, V. R. Johnson, M. J. W. Laubenstein, and F. Ajzenberg—239(A)
Neutrons from $Be^{9}(p,n)B^{9}$, V. R. Johnson, F. Ajzenberg, and M. J. Wilson Laubenstein—187(L)
Neutrons from $C^{13}(d,n)N^{14}$, C. E. Mandeville and C. P. Swann—787
Neutrons from deuteron bombardment of Mg isotopes, C. P. Swann, C. E. Mandeville, and W. D. Whitehead—598
Neutrons from $Li^{7}(d,\alpha)He^{5}$, $He^{5}\rightarrow\alpha+n$, W. D. Whitehead—239(A)
Proton groups from $B^{11}(d,p)B^{12}$, W. W. Buechner, D. M. Van Patter, E. N. Strait, and A. Sperduto—262
Protons from $B(\alpha,p)C,C^{*}$, J. L. Perkin—175(L)
Protons from deuteron on Co^{59}, W. O. Bateson and Ernest Pollard—241(A)
Reaction constants for $T^{3}(p,n)He^{3}$, G. A. Jarvis, A. Hemmendinger, H. V. Argo, and R. F. Taschek—929
T+T reaction, energy of α-particles, K. W. Allen, E. Almqvist, J. T. Dewan, T. P. Pepper, and J. H. Sanders—238(A)
T+T reaction, energy of neutrons, J. H. Sanders, K. W. Allen, E. Almqvist, J. T. Dewan, and T. P. Pepper—238(A)
$T(T,2n)He^{4}$ reaction, dineutron (no author)—238(A)
Twelve-Mev neutrons with deuterons, G. L. Griffith, M. E. Remely, and P. G. Kruger—443

Dynamics
Oscillations of magnetic suspensions, K. Millsaps—418(A)

Elasticity
Compressibility of molten Na, T. E. Pochapsky and S. L. Quimby—892(L)
Dislocations, formation from vacancies, Frederick Seitz—890(L)
Multiplication processes for dislocations, F. C. Frank and W. T. Read, Jr.—722(L)
Prismatic dislocations, Frederick Seitz—723(L), 1003(L)
Sound velocities and elastic constants, Henry L. Laquer and William E. McGee—202(A)
Vacancies generated by dislocations, Frederick Seitz—1002(L)

Electrets
Charge and decay time, W. F. G. Swann—213(A)

Electrical conductivity and resistance
At absolute zero, H. Fröhlich—845
A.c. conduction in ice, E. J. Murphy—396(L)
Bloch's theorem and superconductivity, M. Dresden and J. DeLord—211(A)
Conductivity created in a liquid, action of electric dispersive field, Oleg Yadoff—223(A)
Of cubic semiconductor in magnetic field, Frederick Seitz—372
Dielectric breakdown in ionic crystals, theory, H. Fröhlich and F. Seitz—526
Electronic mobility in Ge, V. A. Johnson and K. Lark-Horovitz—409(L)
Forces on a superconductor, W. V. Houston and N. Muench 967
Ge point contact rectifiers, M. H. Dawson and B. H. Alexander—217(A)
Hall effect, resistivity, C. S. Hung and J. R. Gliessman—726(L); C. S. Hung—727(L)
Hall potential across an inhomogeneous conductor, J. Volger—1023(L)
High resistivity *P*-type germanium, W. C. Dunlap—286
Of ice, hydrogen bond energy, E. J. Murphy—203(A)
Of In and Th alloys, Meissner effect, J. W. Stout and Lester Guttman—396(L)
Induced in Se by electron bombardment, L. Pensak—171(L)
Insulating to metallic behavior in silicon, G. W. Castellan and F. Seitz—216(A)
Isotope effect in superconductors, Jules de Launay—398(L)
Magnetic fields and conduction—"tube integrals," W. Shockley—191(L)
Magnetic threshold curve for In, G. Preston Burns—211(A)
Magnetoresistance of germanium, I. Estermann and A. Foner—365
N-irradiated semiconductors, J. H. Crawford, Jr. and K. Lark-Horovitz—889(L)
Noise in semiconductors, R. L. Petritz and A. J. F. Siegert—215(A)
Of Pt, heat treatment, Robert J. Corruccini—202(A)
Potential fluctuations in semiconductors, Hubert M. James and Guy W. Lehman—216(A)
Resistance minima at low temperatures, M. P. Garfunkel, F. G. Dunnington, and B. Serin—211(A)
Of semiconductors containing both acceptors and donors, C. S. Hung and V. A. Johnson—535(L)
Semiconductors with macroscopic discontinuities, J. C. M. Brentano and D. H. Davis—216(A)
Soldered contact on semiconductor, Jacques I. Pantchechnikoff—1027(L)
Superconducting Bi alloys, Joseph M. Reynolds and C. T. Lane—405(L)
Superconducting properties of Cb, D. B. Cook, M. W. Zemansky, and H. A. Boorse—212(A)
Superconductivity and Debye modes, William Band—739(L), 1005(L)
Superconductivity and zero-point vibrations, J. Bardeen—167(L)
Superconductivity in Sn-Ge "alloys," Ralph P. Hudson—883(L)
Superconductivity of columbium nitride, D. B. Cook, M. W. Zemansky, and H. A. Boorse—1021(L)
Superconductivity of vanadium, Aaron Wexler and W. S. Corak—737(L)
Of thoria, W. E. Danforth and F. H. Morgan—142
Tin superconductors, alternating currents, B. Serin, C. A. Reynolds, and M. P. Garfunkel—211(A)
Of Sn^{124}, superconductivity, Emanuel Maxwell—173(L)

Electrodynamics (see **Electromagnetic theory**)

Electromagnetic theory (see also **Quantum electrodynamics**)
Conservation laws, electromagnetic field, Robert Penfield and Henry Zatzkis—201(A)
Hydromagnetic equations, Walter M. Elsasser—183(L)
Magnetic shielding in He and H_2, Egil Hylleraas and S. Skavlem—117
Oscillations of magnetic suspensions, K. Millsaps—418(A)
Velocity of waves, dielectric constant of dry air, J. V. Hughes—222(A)
Waves in bounded magneto-ionic media, Benjamin Lax—222(A)

Electron optics
Focusing of beams in fields of "mirror" symmetry, P. A. Sturrock—215(A)

Electrons in metals
Ionization of H in metals, Irvin Isenberg—736(L)

Energy states of nucleus (see **Disintegration and excitation of nucleus; Nuclear structure**)

Errata
Bohr formula for Rydberg constant, Raymond T. Birge—1005(L)
Measurement of a 1.6×10^{-9}-sec. half-life in Yb^{170}, R. E. Bell and R. L. Graham—194(L)
Range-energy relations for protons in substances containing C, H, O, A, and Xe, J. O. Hirschfelder and J. L. Magee—1005(L)

Excitation of nuclei (see **Disintegration and excitation of nucleus; Nuclear structure**)

Ferroelectric phenomena
Curie point in $KTaO_3$, J. K. Hulm, B. T. Matthias, and E. A. Long—885(L)
Electronic theory, E. T. Jaynes and E. P. Wigner—213(A)
Field currents
Emission from single tungsten crystals, Michael K. Wilkinson—233(A)
Field theory (see also **Quantum electrodynamics**)
Convergent non-linear field theory, J. C. Ward—406(L)
Equivalence theorems for meson-nucleon couplings, Edward J. Kelly—399(L)
With non-localized action, A. Pais and G. E. Uhlenbeck—145
Renormalization, differential identities, Abdus Salam—910(L)
Tomonaga coupling method in meson theory, Kenneth M. Watson and Edward W. Hart—918
Films, properties of
By electrically "exploded" wires, William M. Conn—213(A)
Ferromagnetic films, Martin J. Klein and Robert S. Smith—214(A)
Structure of lead sulfide, J. Doughty, K. Lark-Horovitz, L. M. Roth, and B. Shapiro—203(A)
Fission of nucleus (see also **Disintegration and excitation of nucleus**)
Asymmetric fission, T. Yasaki and O. Miyatake—740(L)
Delayed neutrons from U^{238} and Th^{232}, K. H. Sun, R. A. Charpie, F. A. Pecjak, B. Jennings, J. F. Nechaj, and A. J. Allen—3, 197(A)
Excitation functions for charged particles, J. Jungerman—198(A), 632
Ionization yields of fragments, R. B. Leachman—197(A)
Of medium weight elements, Roger E. Batzel and Glenn T. Seaborg—528(L)
Photo-fission of Bi, Nathan Sugarman—532(L)
Quantum field theory, Hartland S. Snyder—520
Total charges of fragments in gaseous and solid media, N. O. Lassen—1016(L)
Yields in rare earths, Mark G. Inghram, Richard J. Hayden, and David C. Hess—271
Fluid dynamics (see also **Aerodynamics; Hydrodynamics**)
Analysis of turbulence data, F. N. Frenkiel—229(A)
Compressible fluid flow, R. Shaw—547(A)
Flow past an infinite cone, Keeve M. Siegel—229(A)
Interior ballistics, expansion of gases in cylinder, W. Heybey—229(A)
Jet mixing of compressible fluid, S. I. Pai—547(A)
Shock layer, existence ahd limit behavior, David Gilbarg—547(A)
Vorticity averages, C. Truesdell—229(A)
Fluorescence
Of anthracene and stilbene, decay time and temperature, J. O. Elliot, S. H. Liebson, and C. F. Ravilious—393(L)
Liquid scintillator, efficiency, R. F. Post—735(L)
Of potassium iodide, impurities, B. Smaller, J. May, and M. Freedman—940
Scintillation solutions, spectral emission, F. B. Harrison and G. T. Reynolds—745(L)
Scintillations in liquids and solutions, M. Ageno, M. Chiozzotto, and R. Querzoli—720(L)
Of solutions bombarded with radiation, Hartmut Kallmann and Milton Furst—857
Temperature characteristics of napthalene-anthracene, S. H. Liebson and R. T. Farrar—733(L)

Geophysics
Extrapolation of geomagnetic potential, C. J. Swift—222(A)

Hall effect
In impurity semiconductors, V. A. Johnson and K. Lark-Horovitz—176(L)
At low temperatures, C. S. Hung and J. R. Gliessman—726(L); C. S. Hung—727(L)
Magnetoresistance of germanium, I. Estermann and A. Foner—365
P-type germanium, W. C. Dunlap—286
Resistance of cubic semiconductor in magnetic field, Frederick Seitz—372
Helium, liquid
Film transport in liquid He II, H. A. Boorse and J. G. Dash—734(L)
Lambda-temperatures of He^3 in He^4, J. G. Daunt and C. V. Heer—46
Liquid-solid transformation near absolute zero, C. A. Swenson—626
Non-equilibrium phenomena in Bose-Einstein gas, heat transfer, William Band—589
Rollin film creep, Henry A. Fairbank, Ernest A. Lynton, and C. T. Lane—211(A)
Superfluidity and thermomechanical effect, Earl Long and Lothar Meyer—1031(L)
Thermal Rayleigh disk in He II, John R. Pellam—212(A)
Thermodynamics, He^3-He^4 solutions, O. K. Rice—1024(L)
Transport rates, H. A. Boorse and J. G. Dash—1008(L)
Vapor pressure of He^3, He^4 solutions, John E. Kilpatrick—529(L)
Velocity of second sound in mixtures of He^3 and He^4, Ernest A. Lynton and Henry A. Fairbank—735(L)
Zero-point energy, C. L. Pekeris—884(L)
High voltage tubes and machines (see **Methods and instruments**)
Hydrodynamics
Breaking of waves by opposing current, Yi-Yuan Yu—546(A)
Of He II, two-fluid model, P. R. Zilsel—309
Hydromagentic equations, Walter M. Elsasser—183(L)
Vibrations due to water flowing through elastic tube, Elmer B. Carnes—416(A)
Hyperfine structure (see also **Nuclear moments and spin**)
Of Cu, J. A. Brinkman and C. Kikuchi—226(A)
Of hydrogen and deuterium, A. G. Prodell and P. Kusch—1009(L)
In iron transition group, A. Abragam—534(L)
Isotope shift in Ba, O. H. Arroe—836
Of Hg, K. Murakawa—536(L)
Of Ni^{61}, Karl G. Kessler—167(L)

Ionization
By heavy particles, J. K. Knipp—197(A)
Specific ionization in air, Arthur E. Lockenvitz and J. T. Kopecek—417(A)
Ionization potentials
Spectroscopic determination, Wolfgang Finkelnburg—213(A)
Ionosphere
Diffusion in ionosphere, M. H. Johnson and E. O. Hulburt—222(A)
Isomers, nuclear (see also **Nuclear structure; Radioactivity**)
In Ca^{49}, E. der Mateosian and M. Goldhaber—192(L)
In Co^{58}, Karl Strauch—487
Of $^{77}Ir^{191}$, F. K. McGowan—404(L)
Of Kr^{86}, Ingmar Bergström and Sigvard Thulin—537(L)
In Pb^{204}, "memory" in angular correlation, A. W. Sunyar, D. Alburger, G. Friedlander, M. Goldhaber, and G. Scharff-Goldhaber—181(L)
Of Sn^{117}, J. W. Mihelich and R. D. Hill—781
In Ti^{51}, J. A. Miskel, E. der Mateosian, and M. Goldhaber—193(L)
Of Xe^{133}, Ingmar Bergström and Sigvard Thulin—538(L)

Isotopes
Of americium, K. Street, Jr., A. Ghiorso, and G. T. Seaborg —530(L)
Ca^{40}-A^{40} mass difference, T. R. Roberts and Alfred O. Nier —198(A)
Masses of Si^{28}, Si^{29}, Mn^{55}, Fe^{56}, Ni^{58}, Pd^{110}, Cd^{110}, Cd^{112}, Cd^{116}, and Sn^{116}—Henry E. Duckworth and Richard S. Preston—402(L)
Masses of Si^{30}, Co^{59}, Ni^{60}, Zr^{90}, Mo^{96}, and Mo^{100}, Henry E. Duckworth, Richard S. Preston, and Karl S. Woodcock—188(L)
Packing fraction, $n=50$ neutrons, Henry E. Duckworth, Karl S. Woodcock, and Richard S. Preston—198(A)
Relative abundances of Ne, Kr, Rb, Xe, and Hg, Alfred O. Nier—450
Of Se, S. Geschwind, H. Minden, and C. H. Townes—226(A)
U^{235} in thucholite, J. B. Orr—401(L)

Kinetic theory
Condensation in clustering Bose-Einstein gas, William Band—871
Data of state for hydrogen, Herrick L. Johnston, Irving J. Bezmann, Thor Rubin, Lyle Jensen, David White, and Abraham S. Friedman—235(A)

Liquids (see also **Hydrodynamics; Helium, liquid**)
Fluorescence, energy transport, Hartmut Kallmann and Milton Furst—857
Nucleation in vapor expansions, Arthur Kantrowitz—547(A)
Supersonic absorption, A. Gierer and K. Wirtz—906(L)
Low temperature phenomena (see also **Helium, liquid**)
Atomic heat of In, J. R. Clement and E. H. Quinnell—1028(L)
Lambda-temperatures of He^3 in He^4, J. G. Daunt and C. V. Heer—46
Luminescence
Color centers in alkali halides, Clifford C. Klick—894(L)
Efficiency in vacuum ultraviolet, K. Watanabe, F. S. Johnson, and R. Tousey—217(A)

Magnetic properties (see also **Nuclear moments and spin; Crystal structure; Magnetic resonance absorption**)
Antiferromagnetism, field theory, P. W. Anderson—705
Antiferromagnetism, superexchange interaction, P. W. Anderson—350
Antiferromagnetism, triangular Ising net, G. H. Wannier—357
Atomic moments of ferromagnetic alloys, R. M. Bozorth—887(L)
Coercive force of iron, inclusions, L. J. Dijkstra and C. Wert—979
Diamagnetism of free electrons, D. J. Besdin—417(A)
Dispersion in ferrites, C. Kittel—214(A)
Domains in cobalt-nickel crystal, R. M. Bozorth and J. G. Walker—888(L)
Ferromagnetic block, L. W. McKeehan—739(L)
Ferromagnetic domains, L. W. McKeehan—747(L)
Ferromagnetic films, Martin J. Klein and Robert S. Smith —214(A)
Fringe field of domains, L. Marton, J. A. Simpson, and A. Van Bronkhorst—215(A)
Magnetostriction, crystal orientation, J. E. Goldman—215(A)
Of manganese ferrite, Charles Guillaud, W. A. Yager, F. R. Merritt, and C. Kittel—181(L)
Of nickel ferrite, single crystals, J. K. Galt, B. T. Matthias, and J. P. Remeika—214(A), 391(L)
Of KCl, paramagnetism of color centers, Allen B. Scott, Henry J. Hrostowski, and Lamar P. Bupp—346
Remagnetization in saturated ferromagnet, H. Ekstein and T. Gilbert—214(A)
Tension and properties of iron-cobalt, H. H. Plotkin and J. E. Goldman—215(A)
Magnetic resonance absorption (see also **Nuclear moments and spin**)
In antiferromagnetic materials interpretation, D. F. Bleil and R. K. Wangsness—227(A)
In antiferromagnetic materials near Curie temperature, E. P. Trounson, D. F. Bleil, R. K. Wangsness, and L. R. Maxwell—542(L)
Of Sb^{121} and Sb^{123}, V. W. Cohen, W. D. Knight, T. Wentink, Jr., and W. S. Koski—191(L)
In chromium sesquioxide, E. P. Trounson, D. F. Bleil, and L. R. Maxwell—226(A)
In manganese ferrite, Charles Guillaud, W. A. Yager, F. R. Merritt, and C. Kittel—181(L)
In metallic hydrides, Martin A. Garstens—397(L)
Of paramagnetic ions, Yu Ting, Roy C. Weidler, and Dudley Williams—226(A)
Shift of nuclear resonance in paramagnetic solutions, N. Bloembergen and W. C. Dickinson—179(L)
In single crystals of manganous halides, Alden H. Ryan—226(A)
In single crystals of nickel ferrite, W. A. Yager, J. K. Galt, F. R. Merritt, E. A. Wood, and B. T. Matthias—214(A)
Magnetostriction (see **Magnetic properties**)
Mass ratios (see **Isotopes**)
Mass spectroscopy
Ca^{40}-A^{40} mass difference, T. R. Roberts and Alfred O. Nier —198(A)
Of $C^{13}O_2$ and $C^{13}O$, V. H. Dibeler, E. J. Wells, Jr., and R. M. Reese—223(A)
Isotopic hydrogen molecules, Fred L. Mohler, Vernon H. Dibeler, E. J. Wells, Jr., and R. M. Reese—223(A)
Packing fraction, $n=50$ neutrons, Henry E. Duckworth, Karl S. Woodcock, and Richard S. Preston—198(A)
Rapid scanning mass spectroscope, Willard H. Bennett—222(A)
Mean over-all life (see **Radioactivity**)
Mechanics, quantum—atomic structure and spectra
Magnetic shielding in He and H_2, Egil Hylleraas and S. Skavlem—117
Mechanics, quantum—general
Properties of spin $\frac{1}{2}$ fields, C. N. Yang and J. Tiomno—495
Quantization of Einstein's gravitational field equations, F. A. E. Pirani and A. Schild—986
Quantization of higher order, W. Thirring—703
Quantum field theory, Hartland S. Snyder—520
Removal of degeneracy, Melvin Lax—200(A)
Resonance between identical big molecules, Herbert Jehle—200(A)
S-matrix in Heisenberg representation, C. N. Yang and David Feldman—972
Singular potentials, K. M. Case—220(A)
Time-independent integrals of motion in Dirac theory, A. W. Sáenz—1004(L)
Uncertainty principle for number of variables, Ronald L. Reed and M. Dresden—200(A)
Variational principles for scattering processes, B. A. Lippmann and Julian Schwinger—469
Virial theorem and variation principle, I. Isenberg—737(L)
Mechanics, quantum—nuclear
n-p interaction, lower bounds of range, A. A. Broyles and B. Kivel—418(A)
Nucleon-meson coupling constant, S. D. Drell—220(A)
Velocity dependent nuclear interactions, R. Avery, C. H. Blanchard, and R. G. Sachs—220(A)
Mechanics, statistical
Antiferromagnetism, triangular Ising net, G. H. Wannier—357

Equations of hydrodynamics, derivation, John M. Richardson—200(A)
Non-equilibrium phenomena in Bose-Einstein gas, heat transfer, William Band—589
Pressure in canonical ensemble, R. J. Riddell, Jr.—200(A)
Mesons (see also **Cosmic radiation**)
Absorption of π^--mesons by deuterons, Stephen Tamor—221(A)
Absorption of π^--mesons by protons, R. E. Marshak and A. S. Whitman—220(A)
Cross sections for collisions of protons and π-mesons, J. H. Tinlot and B. P. Gregory—205(A)
Decay lifetime of positive π-μ, O. Chamberlain, R. F. Mozley, J. Steinberger, and C. Wiegand—394(L)
Electrons at end of μ-meson tracks, William F. Fry—893(L)
Meson-nucleon couplings, Edward J. Kelly—399(L)
μ-mesons stopped in Al foils, W. Y. Chang—205(A)
μ-pair theories and the π-meson, Gregor Wentzel—710
Neutral mesons produced by photons, K. A. Brueckner and K. M. Watson—187(L)
π- and μ-meson production spectra, Giulio Ascoli—812
Production by photons, K. A. Brueckner—641
Production cross sections, H. A. Wilcox, W. F. Cartwright, C. Richman, and M. N. Whitehead—198(A)
Production of π^+ and π^- by neutrons, Hugh Bradner, D. J. O'Connell, and B. Rankin—720(L)
In proton-proton collisions, Vincent Z. Peterson—407(L)
Tomonaga coupling method in meson theory, Kenneth M. Watson and Edward W. Hart—918
Metals (see **Crystalline state**)
Meteorology
Molecular rotation and temperature of upper atmosphere, Lewis M. Branscomb—619
Methods and instruments
Absorption technique for γ-rays from position emitters, Herbert E. Kubitschek—23
Anthracene scintillation spectrometer, John I. Hopkins—415(A)
Bent crystal x-ray spectrometer, E. L. Jossem and L. G. Parratt—210(A)
Betatron performance, G. D. Adams, D. W. Kerst, and C. S. Robinson—208(A)
Cloud chamber, large, Melvin B. Gottlieb and Alfred J. Hartzler—204(A)
Cloud chamber triggered by internal scintillation counter, R. W. Williams, L. M. Spetner, W. L. Kraushaar, and H. W. J. Courant—207(A)
Cylindrical cavities, optimum parameters, B. L. Miller—209(A)
Delayed coincidence circuit, W. R. Konneker, S. De-Benedetti, and F. K. McGowan—210(A)
Diamond gamma-ray counters, E. Pearlstein and R. B. Sutton—217(A)
Differential pulse-height analyzer, J. E. Francis, Jr., P. R. Bell, and J. C. Gundlach—418 (A)
Diffuser for supersonic wind tunnels, J. L. Diggins—229(A)
Discharges over long paths, Cresswell Hatchett and John W. Flowers—417(A)
Electron injection gun for synchrotron, Orville Stone—209(A)
Electron orbits, line shapes in β-ray spectrometer, J. F. Perkins and A. W. Solbrig, Jr.—415(A)
Electron track densities in emulsions, Dale R. Corson and Margaret R. Keck—209(A)
Electrostatic generator, D. I. Cooper, D. H. Frisch, C. L. Storrs, Jr., and C. J. Strumski—208(A)
Emulsion chamber, ionizing particle tracks, Herman Yagoda—207(A)
Fast multiplying circuit, B. Chance, J. Busser, and F. C. Williams—244(A)
Fermi β-distribution, evaluation, Harvey Hall—745(L)
Field mapping by the electron optical shadow, J. Arol Simpson—215(A)
Films by electrically "exploded" wires, William M. Conn—213(A)
Finite Wiener-Hopf equations, Richard Latter—199(A)
Fluctuations in tungsten-lamp-photo-cell system, Britton Chance—233(A)
Gamma-ray measurements with NaI(T1) crystals, R. Hofstadter and J. A. McIntyre—389(L)
Gamma-ray spectrometer, Compton effect, J. A. McIntyre and R. Hofstadter—208(A)
Gas liquefaction in shock tubes by light scattering, G. A. Lundquist—230(A)
Gas recovery system, accelerator, E. Almqvist, K. W. Allen, J. T. Dewan, T. P. Pepper, and J. H. Sanders—209(A)
High speed coincidence circuit, Z. Bay—233(A)
Ion source for electrostatic generator, K. R. More, R. H. Chow, J. K. Kinnear, and S. B. Woods—208(A)
Liquid scintillator, efficiency, R. F. Post—735(L)
Magnet ends and sections for synchrotron, G. B. Beard, J. L. Levy, W. A. Nierenberg, and R. W. Pidd—209(A)
Magnetic lens pair production spectrometer, L. M. Baggett and S. J. Bame, Jr.—415(A); S. J. Bame, Jr. and L. M. Baggett—415(A)
Molecules on hot wire detector, sitting time, D. T. F. Marple and Henry Levinstein—223(A)
Monoenergetic neutron source, V. R. Johnson, F. Ajzenberg, and M. J. Wilson Laubenstein—187(L)
Operation of 350-Mev electron synchrotron, I. A. Getting, J. S. Clark, J. E. Thomas, Jr., I. G. Swope, and M. L. Sands—208(A)
Optical detection of radiofrequency resonance, J. Brossel, P. Sagalyn, and F. Bitter—225(A)
Pair spectrometer, J. W. DeWire, A. Ashkin, and L. A. Beach—210(A)
Particle energies with scintillation counters, W. Franzen, R. Peelle, and R. Sherr—209(A)
Phase spectrum in pulse analysis, T. N. Hatfield, Fred Morris, and Charles Hager—418(A)
Photography of detonation and shock phenomena, R. Heine-Geldern, E. M. Pugh, and S. Foner—230(A)
Photography of high speed phenomena, S. Foner, E. M. Pugh, R. Heine-Geldern, and E. C. Mutschler—230(A)
Photography of metal jet charges, E. M. Pugh, R. Heine-Geldern, and E. C. Mutschler—230(A)
Photo-multipliers, rise times of pulses, O. Martinson, P. Isaacs, H. Brown, and I. W. Ruderman—178(L)
Potassium iodide, scintillation studies, B. Smaller, J. May, and M. Freedman—940
Proportional counter for fast neutrons, G. S. Hurst and R. H. Ritchie—415(A)
Proton energies with scintillation counters, W. Franzen, R. W. Peelle, and R. Sherr—742(L)
Radioactivity measurement, new method, W. Gross and G. Failla—209(A)
Radiofrequency source, F. J. Rink—414(A)
Rapid scanning mass spectroscope, Willard H. Bennett—222(A)
Ring focusing magnetic spectrometer, W. W. Pratt, F. I. Boley, and R. T. Nichols—208(A)
Rotating mirror, high constant speed, E. C. Smith and J. W. Beams—222(A)
Scintillation solutions, spectral emission, F. B. Harrison and G. T. Reynolds—745(L)
Scintillations in liquids and solutions, M. Ageno, M. Chiozzotto, and R. Querzoli—720(L)
Self-quenching counters, anomalous effect, A. D. Krumbein—910(L)
Short duration spark, J. A. Fitzpatrick and W. J. Thaler—231(A)

Methods and instruments (continued)
Short-lived radioactive gases, Michel Ter-Pogossian, Fred T. Porter, and C. Sharp Cook—244(A)
Sound velocities and elastic constants, Henry L. Laquer and William E. McGee—202(A)
Susceptibility measurements, moment balance, J. A. Osborn —214(A)
Temperature characteristics of naphthalene-anthracene, S. H. Liebson and R. T. Farrar—733(L)
Thermal Rayleigh disk in He II, John R. Pellam—212(A)
Synchrotron beam standardizing, Wade Blocker, Robert Kenney, and Wolfgang K. H. Panofsky—419
Ultrafiltration with Ag membranes, W. C. Skinner and F. G. Slack—417(A)
Variational method for scattering problems, L. Hulthén and P. O. Olsson—531(L)
Microwaves (see also **Electromagnetic theory; Spectra, microwave**)
Analysis of ketene, B. Bak, E. Stenberg Knudsen, E. Madsen, and J. Rastrup-Andersen—190(L)
From 15-Mev deuterons on thick targets, angular distribution, C. E. Falk—219(A)
Photo-sensitive Geiger-Müller counter, scintillations, C. E. Mandeville and H. O. Albrecht—1010(L)
Molecular structure and constants (see also **Spectra, molecular; Raman spectra**)
Of bromogermane, A. Harry Sharbaugh, Benjamin S. Pritchard, Virginia G. Thomas, John M. Mays, and Benjamin P. Dailey—189(L)
Of CD_3NC and CD_3CN, Ralph Trambarulo and Walter Gordy—224(A)
Collision diameters, quadrupole moments, William V. Smith and Raydeen Howard—132
Of methane, coriolis perturbation, Emily W. Jones and Joseph W. Straley—417(A)
Of methyl cyanide and methyl isocyanide, Myer Kessler, Harold Ring, Ralph Trambarulo, and Walter Gordy—54
Molecular beam electric resonance with diatomic molecules, Vernon Hughes and Ludwig Grabner—829
Of pentaborane, W. J. Taylor, C. W. Beckett, J. Y. Tung, R. B. Holden, and H. L. Johnston—234(A)
Relaxation times for exchange of vibrational energy, Wayland C. Griffith—235(A)

Necrology
John Torrence Tate—1
Neutrino (see also **Radioactivity; Scattering of electrons, mesons, neutrons, protons, and ions**)
Scattering cross section, J. H. Barrett—907(L)
Neutrons
Dineutron, T(T,2n)He^4 reaction (no author)—238(A)
At high altitudes, latitude dependence, W. P. Staker and W. O. Davis—207(A)
From Li^6, energy, Ward Whaling and J. W. Butler—414(A)
From $Li^7(d,n)Be^8$, low energy, W. D. Whitehead—393(L)
Polarization by scattering, Joseph V. Lepore—137
Proton bombardment of Be, V. R. Johnson, M. J. W. Laubenstein, and F. Ajzenberg—239(A)
Spin, M. Hamermesh and E. Eisner—888(L)
From U^{238} and Th^{232} fission, K. H. Sun, R. A. Charpie, F. A. Pecjak, B. Jennings, J. F. Nechaj, and A. J. Allen—3, 197(A)
Nuclear moments and spin (see also **Hyperfine structure**)
Of Sb^{121}, Thomas L. Collins—226(A)
Of Sb^{121} and Sb^{123}, V. W. Cohen, W. D. Knight, T. Wentink, Jr., and W. S. Koski—191(L)
Of deuteron, quadrupole moment, A. A. Broyles and M. H. Hull—247
g-values of paramagnetic ions, Yu Ting, Roy C. Weidler, and Dudley Williams—216(A)
Of Mo^{95} and Mo^{97}, O. H. Arroe—212(A)
Quadrupole interactions in crystals, R. V. Pound—685
Of Sc^{45}, Robert E. Sheriff and Dudley Williams—175(L)
Of Sc^{45}, Norman F. Ramsey—1010(L)
Of Se isotopes, S. Geschwind, H. Minden, and C. H. Townes—226(A)
Shift of nuclear resonance in paramagnetic solutions, N. Bloembergen and W. C. Dickinson—179(L)
Spins of Li^6 and B^{10}, G. Racah and N. Zeldes—1012(L)
Of T1, Sn, Cd, and Pb, W. G. Proctor—35
Nuclear spectra (see also **Disintegration and excitation of nucleus**)
Of Au^{199}, R. D. Hill and J. W. Mihelich—275
Beta-spectrum of A^{39}, A. R. Brosi, H. Zeldes, and B. H. Ketelle—902(L)
Cross-over transitions in Ir^{194}, Ag^{110}, Cs^{134}, Richard Wilson—1004(L)
Gamma-rays of Ag^{105} and Ag^{106}, J. Y. Mei, C. M. Huddleston, and Allan C. G. Mitchell—1010(L)
Gamma-spectrum of Ta^{182}, F. E. O'Meara—1032(L)
Of Np^{238}, M. S. Freedman, A. H. Jaffey, and F. Wagner, Jr. —410(L)
Photo-alpha-reactions in light nuclei, T. A. Welton—399(L)
Of Pa^{233}, β-spectrum, H. B. Keller and J. M. Cork—1030(L)
Nuclear structure (see also **Disintegration and excitation of nucleus; Radioactivity; Nuclear spectra**)
Of Al, C. P. Swann, C. E. Mandeville, and W. D. Whitehead—598
Of A^{37}, A. Zucker and W. W. Watson—241(A)
Binding energy of deuteron, R. E. Bell and L. G. Elliott—282
Of C^{12}, P. R. Bell and W. H. Jordan—392(L)
Closed shells at 20 nucleons, C. H. Townes and W. Low—198(A)
Dipole vibrations, Helmut Steinwedel, J. Hans D. Jensen, and Peter Jensen—1019(L)
Exchange currents, in nuclei, R. K. Osborn and L. L. Foldy —795
Isomerism and shell structure, R. D. Hill—1021(L)
Isotope shift staggering, G. Breit—891(L)
Of Kr^{86}, Ingmar Bergström and Sigvard Thulin—537(L)
Levels in C^{12} from $Be^9(\alpha,n)C^{12}$, William H. Guier and James H. Roberts—719(L)
Levels in lead isotopes, R. E. Peterson, R. K. Adair, and H. H. Barschall—935
Levels in N^{14} and Al^{27}, C. P. Swann and C. E. Mandeville—240(A)
Levels in Pb, R. K. Adair, C. K. Bockelman, and R. E. Peterson—218(A)
Levels in Pb, Bi, and Th, J. A. Harvey—241(A)
Levels in S, R. E. Peterson, R. K. Adair, H. H. Barschall, and C. K. Bockelman—218(A)
Levels in S, R. E. Peterson, H. H. Barschall, and C. K. Bockelman—593
Liquid drop model, fission, David L. Hill—197(A)
Lower levels of He^5, Herbert Goldstein—740(L)
Neutron binding energies, J. R. Huizenga, L. B. Magnusson, O. C. Simpson, and G. H. Winslow—908(L)
Of N^{15}, energy levels, J. E. Richardson—415(A)
Nuclear size resonances, K. W. Ford and D. Bohm—716(L)
1.0-Mev level in C^{13}, Isadore B. Berlman—411(L)
Packing fraction and magic number $n=50$, Henry E. Duckworth, Karl S. Woodcock, and Richard S. Preston—198(A)
Protxn density variation, Helmut Steinwedel and Michael Danos—1019(L)
p-p interaction, R. S. Christian and H. P. Noyes—85
Radii of even-even nuclei from alpha-decay theory, I. Perlman and T. J. Ypsilantis—30
Radiofrequency spectrum of H_2, H. G. Kolsky, T. E. Phipps, Jr., N. F. Ramsey, and H. B. Silsbee—883(L)

Of Se^{75}, J. M. Cork, W. C. Rutledge, C. E. Branyan, A. E. Stoddard, and J. M. LeBlanc—889(L)
Special and magic numbers, abundance, William D. Harkins—724(L)
Spheroidal nuclear model, James Rainwater—432
Spin dependent, C. O. Muehlhause—1002(L)
Tensor forces, level of Li^6 and Li^7, A. M. Feingold and E. P. Wigner—221(A)

Packing fraction (see **Isotopes**)
Pair production
By electrons, Marshall R. Cleland, Wilfred R. Konneker, and A. L. Hughes—229(A)
Philosophy of physics
Stability of systems and general principles, Robert E. Bass —201(A)
Phosphorescence
Of Wurtzite, temperature effects, J. R. Jacques and H. A. Jarrell—418(A)
Photoconductivity
In amorphous Se, Paul K. Weimer—171(L)
Lead sulfide films, temperature variation, Raymond H. McFee—203(A)
Photoelectric emission from *F*-centers, L. Apker and E. Taft—964
Trapped electrons in alkali halides, J. J. Oberly and E. Burstein—217(A)
Trapped holes in alkali halides, E. Burstein and J. J. Oberly —217(A)
V-centers in alkali halides, Frederick Seitz—529(L)
Photodisintegration
Alpha-reactions in light nuclei, T. A. Welton—241(A)
Angular asymmetries in (γ,n) reactions, H. L. Poss—539(L)
Of deuterium by 4.5- to 20.3-Mev x-rays, E. G. Fuller—303
Of deuteron, Ingvar F. E. Hansson—909(L)
Energy for various reactions, Karl Strauch—241(A)
Of Mo^{100}, (γ,n) and (γ,p) reactions, R. B. Duffield, L. Hsiao, and E. N. Sloth—1011(L)
Neutron thresholds for Pb^{206}, Pb^{207}, Pb^{208}, H. Palevsky and A. O. Hanson—242(A)
Neutron yields from 32 elements, R. L. Walker, B. D. McDaniel, and M. B. Stearns—242(A)
In N and O, predominant disintegrations, E. R. Gaerttner and M. L. Yeater—401(L)
Of Ag and Al, B. C. Diven and G. M. Almy—242(A)
Yields of photo-neutrons, 320-Mev bremsstrahlung, D. W. Kerst and G. A. Price—725(L)
Photoelectric evect and properties; cells
Emission from *F*-centers, L. Apker and E. Taft—964
Photography (see also **Methods and instruments**)
Electron track densities in emulsions, Dale R. Corson and Margaret R. Keck—209(A)
Emulsion chamber, ionizing particle tracks, Herman Yagoda —207(A)
Polymerization, properties of polymers
Degradation on shearing in solution, A. B. Bestul and H. V. Belcher—223(A)
Line widths at room temperature, L. Holroyd, B. A. Mrowca, and E. Guth—1026(L)
Line widths through transition temperatures, B. A. Mrowca, L. V. Holroyd, and E. Guth—1026(L)
Positrons
Thermal energy positrons, Leon Madansky and Franco Rasetti—397(L)
Probability
Distributions of resultants of vibrations, C. F. Kent and J. E. Boyd—417(A)
Protons
Polarization by scattering, Joseph V. Lepore—137
Quantum electrodynamics (see also **Field theory**)
Energy-momentum tensor of the electron, F. Villars—122
Quantum field theory, Hartland S. Snyder—520
S-matrix in Heisenberg representation, C. N. Yang and David Feldman—972
Self-energy of free electron, F. J. Belinfante—201(A)
Subsidiary condition, F. Coester and J. M. Jauch—201(A)
Time-independent integrals of motion in Dirac theory, A. S. Sâenz—1004(L)

Radio (see also **Ionosphere**)
Antenna radiation, finite ground-plane, Alfred Leitner and R. D. Spence—199(A)
Radioactivity (see also **Disintegration and excitation of nucleus; Nuclear spectra**)
Of Sb^{124}, L. M. Langer, R. D. Moffat, and H. C. Price, Jr.— 808
Of Sb^{124} beta-gamma- and gamma-gamma-angular correlation, J. R. Beyster and M. L. Wiedenbeck—169(L)
Of americium, K. Street, Jr., A. Ghiorso, and G. T. Seaborg —530(L)
Of As^{72} and As^{71}, J. Y. Mei, Allan C. G. Mitchell, and C. M. Huddleston—237(A)
Beta-disintegration of Sc^{44}, A. Bruner and M. Langer— 236(A)
Beta-gamma-angular correlation, J. R. Beyster and M. L. Wiedenbeck—728(L)
β-γ-angular correlation, in scintillation counters, Robert Stump and Sherman Frankel—243(A); S. L. Ridgway— 243(A)
Of Cd, J. M. Cassidy and P. R. Bell—418(A)
Of Cd isotopes, J. M. Cork, W. C. Rutledge, A. E. Stoddard, C. E. Branyan, and J. LeBlanc—238(A); 938
Of C^{15}, L. Yaffe and W. H. Stevens—893(L)
Of Ce^{139} formed by n-γ reaction, Alfred J. Moses and Don S. Martin, Jr.—467
Of Ce^{141} and Pa^{233}, M. S. Freedman and D. W. Engelkemeir—897(L)
Of Ce^{144} and Pr^{144}, C. E. Mandeville and E. Shapiro—243(A)
Of Co^{60}, internal conversion, M. A. Waggoner, M. L. Moon, and A. Roberts—236(A)
Coincidence efficiency of gamma-rays, J. M. Barnothy and M. Forro—199(A)
Of Cu^{64}, Br^{80}, Br^{82}, and I^{128}, branching ratio, John H. Reynolds—789
Fermi β-distribution, evaluation, Harvey Hall—745(L)
Of Gd, R. E. Hein and A. F. Voigt—783
Of Ga^{66}, R. D. Moffat and L. M. Langer—237(A)
Gamma-gamma-correlations, J. R. Beyster and M. L. Wiedenbeck—411(L)
Gamma-ray measurement with NaI(Tl) crystals, R. Hofstadter and J. A. McIntyre—389(L)
γ-rays from nuclei exposed to photons, J. C. Keck, M. Stearns, and R. R. Wilson—199(A)
γ-rays pair spectrometer study, James Terrell—415(A)
Of Au, R. D. Hill and J. W. Mihelich—275
Of Au^{198}, Philip S. Jastram, W. Konneker, and Marshall R. Cleland—243(A)
Of Au^{199}, R. D. Hill—413(L)
Of Hf^{181}, Martin Deutsch and Arne Hedgran—400(L)
Half-life of radium C′, Guy von Dardel—734(L)
Half lives of 61^{147} and Sm^{151}, Mark G. Inghram, Richard J. Hayden, and David C. Hess—271
Internal conversion of Sc^{46}, M. L. Moon, M. A. Waggoner, and A. Roberts—905(L)
Of Ir, T. C. Chu—582
Of Ir^{194}, Ag^{110}, Cs^{134}, Richard Wilson—1004(L)
Kr^{81}, new long-lived activity, John H. Reynolds—886(L)
Of Kr^{85}, H. Zeldes, B. H. Ketelle, and A. R. Brosi—901(L)
Of Hg^{197}, H. Frauenfelder, O. Huber, A. de-Shalit, and W. Zünti—1029(L)

Radioactivity (continued)
Of Nd, C. E. Mandeville and E. Shapiro—391(L)
Of Np^{238}, M. S. Freedman, A. H. Jaffey, and F. Wagner, Jr.—410(L)
Of Nb^{99}, Ta^{185}, and W^{185}, R. B. Duffield, L. Hsiao, and E. N. Sloth—1011(L)
Of Ni^{59} and Ni^{63}, H. W. Wilson—1032(L)
Of Os^{185}, Os^{191}, and Os^{193}, Merle E. Bunker, Robert Canada, and Allan C. G. Mitchell—610
Of Pd^{111}, A. Storruste—193(L)
Polarization states of annihilation quanta, Frank L. Hereford—228(A)
"Positive tracks" near β-ray emitters, Gerhart Groetzinger and Fred L. Ribe—904(L)
Positron-conjoint gamma-radiation detection, Herbert E. Kubitschek—23
Of K^{40}, T. R. Roberts and Alfred O. Nier—198(A); G. A. Sawyer and M. L. Wiedenbeck—490
Of K^{40}, beta-ray spectrum, David E. Alburger—236(A)
Of K^{40}, decay constant, B. Smaller, J. May, and M. Freedman—940
Of K^{40}, gamma-ray energy, P. R. Bell and Judith M. Cassidy—173(L)
Of K^{40}, electron capture/beta-decay ratio, T. Gráf—1014(L)
Of Pa^{232}, half-life, Arthur H. Jaffey and Earl K. Hyde—280
Of Rh^{106}, internal conversion, Franz Metzger—398(L)
Of Ru^{103}, J. Y. Mei, C. M. Huddleston, and Allan C. G. Mitchell—237(A); Evani Kondaiah—1010(L)
Of Ri^{103} and Rh^{103m}, A. J. Saur, P. Acel, L. G. Mann, and J. Ovadia—237(A)
Of Ru^{103}, Pd^{103}, and Rh^{103}, J. Y. Mei, C. M. Huddleston and Allan C. G. Mitchell—429
Of Sc^{44}, Joseph A. Bruner and Lawrence M. Langer—606
Of Sc^{44}, coincidence studies, William H. Cuffey—180(L)
Of Sc^{46}, decay scheme, B. N. Sorensen, B. M. Dale, and J. D. Kurbatov—1007(L)
Short-lived radioactive gases, Michel Ter-Pogossian, Fred T. Porter, and C. Sharp Cook—244(A)
Of Ag^{105} and Ag^{106}, J. Y. Mei, C. M. Huddleston, and Allan C. G. Mitchell—1010(L)
Of Ag^{110}, W. C. Rutledge, A. E. Stoddard, C. E. Branyan, J. LeBlanc, and J. M. Cork—237(A)
Of Ag^{110}, genetic relationship, John Miskel—403(L)
Of Ag^{111}, Cd^{111} and In^{111}, decay scheme, Stig Johansson—896(L)
Of Na^{24}, half-life, A. K. Solomon—403(L)
Of Sr^{85}, Lin-sheng Cheng and J. D. Kurbatov—237(A)
Of Sr^{90}, Ruth I. Powers and A. F. Voigt—175(L)
Of Sr^{90}-Y^{90}, first-forbidden beta-spectra, L. Jackson Laslett, E. N. Jensen, and A. Paskin—412(L)
Of Ta isomer, Max Goodrich and Edward C. Campbell—418(A)
Of Tb and Ho, Geoffrey Wilkinson and Harry G. Hicks—815
Of Tl^{202}, Geoffrey Wilkinson—1014(L)
Of Tl^{209}, French Hagemann—534(L)
Of Sn^{117} isomeric activity, Raymond W. Hayward—542(L)
Of Sn^{117}, isomers, J. W. Mihelich and R. D. Hill—781
Of Sn^{123} and Sn^{125}, B. H. Ketelle, C. M. Nelson, and G. E. Boyd—242(A)
Of Sn^{125}, beta-spectrum, Raymond W. Hayward—409(L)
Of Xe^{133m}, Igmar Bergström and Sigvard Thulin—538(L)
Of Yb^{169}, E. N. Jensen, L. J. Laslett, R. T. Nichols, and W. W. Pratt—243(A)
Of Yb^{170} half-life, erratum, R. E. Bell and R. L. Graham—194(L)
Of Zn^{65} and Cu^{62}, Raymond W. Hayward—541(L)
Of Zr^{97} and Nb^{97}, W. H. Burgus, J. D. Knight, and R. J Prestwood—104

Raman spectra
Of SiF_4, Patricia J. H. Woltz and Ernest A. Jones—416(A)

Range of particles
Asymptotic expression for stopping power of *K*-electrons, L. M. Brown—297
β-particles through zapon windows, C. Sharp Cook and Chia-hua Chang—244(A)
Ionization by heavy particles, J. K. Knipp—197(A)
Of million-volt electrons, Robert D. Birkhoff, Earl E. Hays, and S. A. Goudsmit—199(A)
Range-energy relations for protons in C, H, O, A, and Xe, erratum, J. O. Hirschfelder and J. L. Magee—1005(L)
Stopping power of *K*-electrons, H. A. Bethe, L. M. Brown, and M. C. Walske—413(L)

Relativity
Conservation laws, electromagnetic field, Robert Penfield and Henry Zatzkis—201(A)
Covariant canonical formulism, Peter G. Bergmann, Robert Penfield, Ralph Schiller, and Henry Zatzkis—201(A)
Gravitational radiation and motion, A. E. Scheidegger and L. Infeld—201(A)
Quantization of Einstein's gravitational field equations, F. A. E. Pirani and A. Schild—986

Scattering of electrons, mesons, neutrons, protons, and ions (see also **Cross section, measurements, theory**)
Asymptotic expression for stopping power of *K*-electrons, L. M. Brown—297
Capture of protons by Al, F. C. Shoemaker, J. E. Faulkner, S. G. Kaufmann, and G. M. B. Bouricius—228(A)
Coherent neutron-proton scattering, liquid mirror, D. J. Hughes, M. T. Burgy, and G. R. Ringo—227(A)
d-p for 10.4-Mev deuterons, J. C. Allred and Louis Rosen—227(A)
Deuterons by 90-Mev neutrons, Walter Hartsough, Milton Hill, and Wilson M. Powell—219(A)
Elastic scattering of electrons on protons, M. N. Rosenbluth—615
Electric processes in deuteron reactions, M. L. Goldberger—221(A)
Electron-electron scattering, Lorne A. Page and W. M. Woodward—228(A); Gerhart Groetzinger, Lewis B. Leder, Fred L. Ribe, and Martin J. Berger—228(A), 454
Of fast electrons, elastic scattering, nuclear structure, L. R. B. Elton—412(L)
Of 14-Mev deuterons, elastic and inelastic, Keith Boyer and Harry Gove—228(A)
High energy neutrons by deuterons, neutron-neutron interaction, Geoffrey F. Chew—219(A)
High energy nucleon-nucleon scattering, K. M. Case and A. Pais—185(L)
High energy scattering, charge independence, Robert Jastrow—389(L)
Of mesons by nucleons, Murray Peshkin—221(A)
Neutron cross sections for noble gases, S. P. Harris—219(A)
n-d scattering at 4.5 and 5.5 Mev, Ernest Wantuch—729(L)
n-p scattering at 27 Mev, J. E. Brolley, Jr., J. H. Coon, and J. L. Fowler—227(A)
n-p at 260 Mev, E. Kelly, C. Leith, E. Segrè, and C. Wiegand—96
Neutron-proton interaction, range of tensor force, A. A. Broyles and M. H. Hull—247
Neutron resonance in Cl^{35}, C. T. Hibdon and C. O. Muehlhause—44, 219(A)
Neutron resonances, S. P. Harris, C. O. Muehlhause, and G. E. Thomas—11
Neutron resonance of lithium, Robert K. Adair—1018(L)
Of neutrons by *S*, R. E. Peterson, H. H. Barschall, and C. K. Bockelman—593

Neutrons from thick targets, angular distribution, C. E. Falk—219(A)
Of Ni coherent neutron scattering, W. C. Koehler, E. O. Wollan, and C. G. Shull—395(L)
Of positrons and electrons by nuclei, H. J. Lipkin and M. G. White—892(L)
Proton-proton at 90°, F. E. Faris and Byron T. Wright—577
p-p at 31.8-Mev proportional counter method, Bruce Cork, Lawrence Johnston, and Chaim Richman—71
p-p at 340 Mev, Owen Chamberlain and Clyde Wiegand—81
p-p near 30 Mev, Wolfgang K. H. Panofsky and Franklin L. Fillmore—57
p-p, theory, R. S. Christian and H. P. Noyes—85
Protons by carbon, W. D. Whitehead—1022(L)
Protons from Li^7, H. T. Richards, S. Bashkin, D. S. Craig, D. Donahue, V. R. Johnson, and D. Martin—239(A)
Protons from nucleons within nuclei, G. M. Temmer—227(A)
Of 16.5-Mev electrons, elastic, E. M. Lyman, A. O. Hanson, and M. B. Scott—228(A)
Slow neutrons by parahydrogen, variational principles, B. A. Lippmann—481
Slow neutrons by solid helium, L. Goldstein and D. Sweeney—218(A)
Spin dependent nuclear "radii," C. O. Muehlhause—1002(L)
Thermal neutron scattering by NH_4Cl, Motoharu Kimura—544(L)
Of 3.27-Mev neutrons by deuterons, I. Hamouda, J. Halter, and P. Scherrer—539(L)
Variational method for scattering problems, L. Hulthén and P. O. Olsson—531(L)
Variational principles for scattering processes, B. A. Lippmann and Julian Schwinger—469

Scattering of radiation (see also **Raman spectra**)
Of CD_3NC and CD_3Cn, Ralph Trambarulo and Walter Gordy—224(A)
Gamma-rays by protons, R. G. Sachs and L. L. Foldy—221(A)
Of light by light, Robert Karplus and Maurice Neuman—220(A)

Semiconductors (see **Electrical conductivity and resistance**)

Shock waves
Characterized by Beattie-Bridgeman equation of state, J. C. Crown—229(A)
Diffraction around two-dimensional objects, surface pressures, W. Bleakney and D. R. White—546(A)
Diffraction through small angle, C. H. Fletcher—546(A)
Gas liquefaction in shock tubes by light scattering, G. A. Lundquist—230(A)
Glancing reflection, A. H. Van Tuyl—230(A)
Photography of detonation and shock phenomena, R. Heine-Geldern, E. M. Pugh, and S. Foner—230(A)
Photography of metal jet charges, E. M. Pugh, R. Heine-Geldern, and E. C. Mutschler—230(A)

Solid state (see **Crystalline state**)

Spark discharge (see **Discharge of electricity in gases**)

Specific heat
Of Cu, nuclear, J. A. Brinkman and C. Kukuchi—226(A)
Of diphenyl ether, G. T. Furukawa, R. E. McCoskey, R. S. Jessup, and R. A. Nelson—223(A)
Of Hg between 0° and 450°C, T. B. Douglas, Anne F. Ball, and D. C. Ginnings—202(A)
Of Na between 0° and 900°C, D. C. Ginnings, T. B. Douglas, and A. F. Ball—202(A)

Spectra, absorption (see also **Absorption of radiation**)
Of condensed O_2 and H_2, A. Lee Smith, William E. Keller, and Herrick L. Johnston—728(L)
Of crystalline hydrogen sulfide, L. B. Lohman and D. F. Hornig—235(A)
Of deuteronaphthalene, L. Corrsin—235(A)
Of homopolar diatomic molecules, infra-red, Robert Van Asselt and Dudley Williams—1016(L)
Of SiF_4, Raman spectra, Patricia J. H. Woltz and Ernest A. Jones—416(A)
Of tung oil, infra-red, F. M. McGehee, Jr. and E. Scott Barr—416(A)
Of vegetable oil compounds, infra-red, E. Scott Barr—416(A)
Of xylene vapors, C. D. Cooper and H. Sponer—235(A)

Spectra, atomic
Of He^3 I, Mark Fred, Frank S. Tomkins and James K. Brody—212(A)
Isotope shift in Ba, O. H. Arroe—836
Isotope shift in Pb II, Felix E. Geiger, Jr.—212(A)
Low terms of Ti II, Abraham Many—531(L)
Rydberg constant, Bohr formula, Raymond T. Birge—193(L); Erratum—1005(L)
Spin of Mo^{95} and Mo^{97}, O. H. Arroe—212(A)

Spectra, general
Molecular rotation and temperature of upper atmosphere, Lewis M. Branscomb—619
Radiofrequency spectrum of $K^{39}F$, Ludwig Grabner and Vernon Hughes—819
Of scintillation solutions, F. B. Harrison and G. T. Reynolds—745(L)
Scintillation spectra of organic crystals, W. S. Koski and C. O. Thomas—217(A)
Na *D* lines during twilight, F. D. Kahn—167(L)
Solar spectrum, map, J. H. Shaw, R. M. Chapman, and J. N. Howard—1017(L)
Transauroral line of oxygen, N. D. Sayers and K. G. Emeleus—166(L)

Spectra, microwave
Absorption of O_2, J. H. Burkhalter, R. S. Anderson, W. V. Smith, and W. Gordy—224(A)
Of BrCl, D. F. Smith, M. Tidwell and D. V. P. Williams—1007(L)
Of bromogermane, A. Harry Sharbaugh, Benjamin S. Pritchard, Virginia G. Thomas, John M. Mays, and Benjamin P. Dailey—189(L)
Of $ChBr_3^{79}$, $CHBr_3^{81}$, and PBr^{81}, Quitman Williams and Walter Gordy—225(A)
Collision diameters from pressure broadening, Raydeen R. Howard and William V. Smith—128
Of ketene, B. Bak, E. Stenberg Knudsen, E. Madsen, and J. Rastrup-Andersen—190(L)
Of methyl bromo-acetylene, John Sheridan and Walter Gordy—224(A)
Of methyl cyanide and methyl isocyanide, Myer Kessler, Harold Ring, Ralph Trambarulo, and Walter Gordy—54
Of methyl cyanide, isotopic modifications, D. K. Coles, W. E. Good, and R. H. Hughes—224(A)
Of methyl mercuric halides, Walter Gordy and John Sheridan—224(A)
Microwave collision diameters, Raydeen R. Howard and William V. Smith—225(A)
Of N^{14}, structure of NF_3, John Sheridan and Walter Gordy—513
Optical detection of radiofrequency resonance, J. Brossel, P. Sagalyn, and F. Bitter—225(A)
Of oxygen, fine structure, James H. Burkhalter, Roy S. Anderson, William V. Smith, and Walter Gordy—651
Of $Rb^{85}F$ and $Rb^{87}F$, Vernon Hughes and Ludwig Grabner—314
Selenium isotopes in OCSe, S. Geschwind, H. Minden, and C. H. Townes—226(A)
Transitions in an inhomogeneous electric field, Joshua Goldberg and Peter G. Bergmann—225(A)

Spectra, molecular (see also **Molecular structure and constants**)
Of CO_2, 2.7μ bands, Robert Jones and Ely E. Bell—1004(L)

Spectra, molecular (continued)
Of hydrogen-bridged amides and alcohols, Gladys A. Anslow—234(A)
Of methane, coriolis perturbation, Emily W. Jones and Joseph W. Straley—417(A)
Of pentaborane, W. J. Taylor, C. W. Beckett, J. Y. Tung, R. B. Holden, and H. L. Johnston—234(A)
Rotation-vibration interaction in OCS and OCSe, W. Low and C. H. Townes—224(A)
Of urea, effect of aging and of heat treatment, Ruth C. Shea and Gladys A. Anslow—234(A)
Of water vapor in region of 2.7μ, W. S. Benedict and E. K. Plyler—234(A)
Spectroscopy, technique
Photoelectric Raman spectrograph, Joseph W. Straley and Morita Crymes—416(A)
Spinor fields
Non-linear spinor fields, R. Finkelstein and M. Rudermann —220(A)
Statistical mechanics (see **Mechanics, statistical**)
Superconductivity (see **Electrical conductivity and resistance**)
Supersonics (see also **Shock waves**)
Absorption theory, A. Gierer and K. Wirtz—906(L)
Axially symmetric flows, Bertrand des Clers and Chieh-Chien Chang—547(A)
Flow in shock tube, David Weimer—546(A)
Flow measurements, Wayland C. Griffith—546(A)
Laminar and turbulent boundary layers, R. Ladenburg and P. Watchell—548(A)
Plane Couette flow of semirarefied gas, T. C. Lin—547(A)

Thermionic emission; Emitting surfaces
Boride cathodes, J. M. Lafferty—1012(L)
Deterioration of oxide-coated cathodes, J. F. Waymouth, Jr.—233(A)
Molecules on hot wire detector, sitting time, D. T. F. Marple and Henry Levinstein—223(A)
Schottky deviations, patch fields, E. A. Coomes, R. J. Munick, and W. B. La Berge—233(A)
Thermodynamics
Of liquid helium and of He^3-He^4 solutions, O. K. Rice—1024(L)
Thermoelectric effects
Thermoelectromotive force of Sn, R. T. Webber and M. C. Steele—1028(L)
Transmutation (see **Disintegration and excitation of nucleus**)

Ultrasonics (see **Acoustics**)
Uncertainty principle (see **Quantum mechanics-general**)

Van der Waals forces
Theory, Franklin C. Brooks—200(A)
Vapor pressure
Of He^3, He^4 solutions, John E. Kilpatrick—529(L)
Virial coefficient
Data of state for hydrogen, Herrick L. Johnston, Irving J. Bezmann, Thor Rubin, Lyle Jensen, David White, and Abraham S. Friedman—235(A)
Force constants for helium and for deuterium, David White and Herrick L. Johnston—236(A)
Force constants for H_2 and for N_2, David White, Abraham S. Friedman, and Herrick L. Johnston—235(A)
Of non-polar binary gas mixtures, David White—236(A)
Solution of two non-polar gases, David White, Abraham S. Friedman, and Herrick L. Johnston—235(A)

X-rays, absorption, diffraction, scattering, reflection, refraction, and polarization
Interface absorption by evaporated films, E. M. Pell and D. H. Tomboulian—210(A)
Low angle scattering, electron density measurements, H. M. Barton, Jr.—211(A)
X-rays, emission
Angular distribution 70-Mev x-rays, G. C. Baldwin, F. I. Boley, and H. C. Pollock—210(A)
X-rays, tubes, apparatus
Bent crystal spectrometer, E. L. Jossem and L. G. Parratt—210(A)

Zeeman effect
In O_2, A. F. Henry—213(A)

THE

PHYSICAL REVIEW

Series — NUMBER 6

SEPTEMBER 15, 1950

g

d for the

PHYSICAL SOCIETY

the

STITUTE OF PHYSICS

New York, N. Y.

PH

A journal of experimen

Published by the American Institute of Physics
for the
AMERICAN PHYSICAL SOCIETY

Officers

President

I. I. RABI
Columbia University
New York, New York

Vice-President

C. C. LAURITSEN
California Institute of Technology
Pasadena, California

Secretary

K. K. DARROW
Bell Telephone Laboratories
Office:
Columbia University
New York 27, New York

Treasurer

G. B. PEGRAM
Columbia University
New York 27, New York

Local Secretary
for the Pacific Coast

J. KAPLAN
University of California at Los
Angeles
Los Angeles, California

Managing Editor

E. L. HILL
University of Minnesota
Minneapolis, Minnesota

The Physical Review is pu

Entered as second-class matter March

Acceptance for mailing at special rate of postage

VIEW

established by E. L. Nichols in 1

BOARD OF EDITORS

Associate Editors

W. E. LAMB, JR.
H. G. HERB
J. BARDEEN

should be submitted to the
Minnesota. The author
charge of $8 per page which
Instructions will be sent with
concerning papers in the process
the Publication Manager, American
New York 22, New York.

Subscription Price

Back Numbers

complete year is available:
1949: $30.00
$27.00
to July, 1929;
July, 1929–December, 1941;
January, 1942–December, 1946;
January, 1947–December, 1948;
thereafter.

and orders for back numbers should
Physics, 47 East 55 Street, New York

members of the American
the Treasurer; in the case of other
physics.

Department, Cornell University, Ithaca,

at Williamson Printing Service, Lancaster, Pennsylvania.
Office at Lancaster, Pennsylvania, under the Act of
section 34.40, P. L. & R. of 1942, authorized